# MINERALOGY AND GEOCHEMISTRY OF THE GEMSTONES AND THE GEMSTONE-BEARING PEGMATITES IN SHIGAR VALLEY OF SKARDU NORTHERN AREAS OF PAKISTAN

By

**MUHAMMAD HASSAN**

A thesis submitted to the National Centre of Excellence in Geology, University of Peshawar in partial fulfillment of the requirement for the Degree of Doctor of Philosophy in Geology

NATIONAL CENTRE OF EXCELLENCE IN GEOLOGY

UNIVERSTIY OF PESHAWAR

**Session 2007**

## *APPROVED BY*

*(External Examiner)*
*Dr. Said Rahim Khan*
*Deputy Director*
*Geoscience Advance Research Laboratories*
*Geological Survey of Pakistan*
*Islamabad*

*(Supervisor)*
*Prof. Dr. M. Tahir Shah*
*NCE in Geology*
*University of Peshawar*

*(Co-Supervisor)*
*Dr. Tahseenullah Khan*
*Deputy Director*
*Geoscience Advance Research Laboratories*
*Geological Survey of Pakistan*
*Islamabad*

*Prof. Dr. M. Asif Khan (T.I)*
*Director*
*NCE in Geology*
*University of Peshawar*

**DEDICATED TO MY PARENTS**

*For their Love, Support and Prayers throughout my Academic Carrier*

## Acknowledgement

First, I would like to thank Almighty Allah, who always helped me whenever I feel that. By this way, it was HE, WHO helped me a lot during all this research work and with His kindness all of the steps of my research work completed smoothly and in time. During whole of the research period, whenever I felt any problem, I prayed for the solution and He solved that.

Secondly, I am grateful to the authorities of my parent institution, "University of Sindh, Jamshoro", who granted me study leave for the completion of Ph. D work. They not only granted study leave but also gave scholarship to meet the expenditure during my stay in the Peshawar.

Thirdly, I expressed my great gratitude to my Supervisor Prof. Dr. M. Tahir Shah. Honestly speaking, it was he who always very kind to me and always helped me, whenever I needed his help. During whole of this research work, as I recall my memory that there was not a single day when I went to him for some discussion and he said that I have no time. Besides, he always pushed me and asked about the progress that what is going on. So for this reason, I always tried to accomplish all my assignments within time to the best of my ability. He always helped me in the analytical work and sent my study samples abroad to his friends and generated data for my research work. Moreover, his moral support was always with me. I will always pray for him and his family

My Co- Supervisor Dr. Tahseenullah Khan, Deputy Director, Geoscience Advance Research Laboratory, Geological Survey of Pakistan is also equally acknowledged because he is the man who selected such a nice and interesting topic for my Ph. D work. He also helped me a lot and always gave me his fruitful suggestions whenever I needed. Moreover, during his stay in Japan he also produced mineral chemistry data, especially of gemstones.

I am also very thankful to Prof. Dr. Muhammad Arif, Dept. of Geology for generating data especially mineral chemistry of pegmatites during his stay in the University of Leicester, UK. He also provided related literature and guided me in regard to the genesis of gemstones. Dr. Irshad Ahmed also helped a lot, especially for the qualitative analysis of gemstones on XRD and he spent even months with me to identify the gemstones on their XRD pattern.

I am also very thankful to Prof. Dr. M. Asif Khan, Director, National Centre of Excellence in Geology for his valuable suggestions to interpret the chemical data in the regional perspective especially from tectonic point of view. So many times, I took his personal books and other relevant literature to interpret my data. I will also pray and remember Late Prof. Dr. Syed Hamidullah for his encouragement and sweet words that he always said when I met him and for his efforts that he did for the strengthen of this Centre. Moreover, all the other faculty members of this Centre and the Department of Geology are also equally acknowledged for their moral support. I am very obliged to Dr.

P. Cerny, University of Manitoba, Australia, for providing me the most relevant literature, which has improved my research to greater extent.

All the laboratory incharges of this centre are also equally acknowledged for their support and cooperation during the analytical work in a very friendly environment. Especial thanks are to Mr. Liaqat Ali, Mr. Razzaq, Mr. Tariq, Mr.Iqbal and Mr, Zahoor. All the other academic and administrative staff of the Centre were very kind and supportive for which I am thankful to them. All the Library Staff of the Centre is also highly acknowledged because they always provide every information that I needed. I can also not forget Muhammad Khan (Driver), the driver, who helped me a lot during the field and gave me a company as a friend. I will call this gentleman as driver-cum- geologist because of his curiosity to obtain the geological information.

I will also remember Mr Kafayatt Ullah, Mr Syed Zahid Shah and Prof. Dr. Naimatullah Khattak for their valuable and fruitful suggestions and discussions. I can also not forget my other friends including Mr. Hamid Rehman, Shah Faisal Shinwari, Shafique Ahmed Junejo, Dr. Imdadullah Siddique and M. Hanif Lakho for their moral support and company during my stay in Peshawar.

All the faculty members (both present and former) of the Centre for Pure and Applied Geology, University of Sindh, Jamshoro are equally acknowledged because of their support and encouragement during my stay in Peshawar. Special thanks are to Prof. Dr. L. B. Bozdar, who always encouraged me for higher studies. Dr. Amanullah Laghari will always remain in my prayers because he is the man who helped and guided me a lot to take admission in this Centre. I can also not forget the sympathies of Mr. Saeed Ahmed Bablani and Mrs. Humaira Dars. These kind persons looked after all of the academic and financial matters at the University of Sindh, Jamshoro for me. I will never forget the kindnesses and sympathies of Mrs. Humaira Dars and her family members, especially her mother. Drs. A. D. Memon, M. A. Baryar, A. A. Memon, S. A. Soomro, S. A. Solangi and I. A. Brohi are also highly acknowledged for their moral support from time to time. It will be injustice to forget Prof. Dr. Parveen A. Usmani, Director Centre for Pure and Applied Geology, University of Sindh, Jamshoro, because it was she who fully supported me during the last stages of my thesis work.

I will always pray for all of my family members, especially my parents for their love, support and scarifies during whole of my academic carrier. Special thanks are to my wife because her all kinds of support during our stay in Peshawar.

In the end, I will always keep all of those well-wishers in my prayers, who encouraged and helped me both financially and morally, especially during my studies in the college and university.

## LIST OF CONTENTS


| | |
|---|---|
| List of Figures | i |
| List of Plates | iii |
| List of Tables | vi |
| Abstract | viii |

**CHAPTER ONE INTRODUCTION PAGE #**

| | |
|---|---|
| General Statement | 1 |
| Pegmatites in Northern areas of Pakistan | 3 |
| Location and Accessibility | 4 |
| Aims and Objectives | 5 |
| Previous Work | 5 |

**CHAPTER TWO REGIONAL GEOLOGY**

| | |
|---|---|
| General Statement | 7 |
| Regional tectonic setting of the Karakoram Mountains | 10 |
| Divisions of the Karakoram Block | 12 |
| Karakoram Axial Batholith | 13 |
| Western Karakoram Batholith | 14 |
| Hunza Karakoram Batholith | 15 |
| Karakoram Batholith: (The Baltoro-Biafo-Hushe areas) | 19 |
| Eastern Karakoram Batholith | 22 |
| Tirich Mir Zone | 23 |
| Southern Sedimentary Belt | 23 |
| Northern Sedimentary Belt | 24 |
| Kohistan-Ladakh island arc | 25 |
| Intraoceanic stage of crustal growth | 26 |
| Yasin Group | 27 |
| Chalt volcanic Group | 28 |
| Gilgit Formation | 30 |
| Kamila Amphibolite Belt | 31 |
| Intrusive rock units | 33 |
| Mafic and ultramafic complexes | 33 |
| Sapat and Jijal Complexes | 33 |
| Chilas Complex | 34 |
| Intermediate to felsic intrusions | 36 |
| Continental-margin stage of crustal growth | 37 |

Kohistan Batholith 37
Dir Group 39
Main Karakoram Thrust 41
Main Mantle Thrust 42
Indian Plate 44
Tethyan Himalayas 45
High Himalayas 46
Lesser Himalaya 47
Sub-Himalayas 48
Himalayan fore deep 49

**CHAPTER THREE GEOLOGY OF THE SHIGAR VALLEY (STUDY AREA)**

Major stratigraphic units 54
Rock units south of the Main Karakoram Thrust 55
Katzarah Formation 55
Bauma-Harel Formation 56
Rock units north of the Main Karakoram Thrust 57
Daltumbore Formation 57
Dassu Gneiss 58
Other igneous rocks of the study area 59
Igneous intrusions north of Main Karakoram Thrust 60
Igneous intrusions south of Main Karakoram Thrust 60
Deformed and metamorphosed intrusions of first stage 61
Undeformed intrusion of second stage 61
Mafic dikes of third stage 62
Metamorphism in the Shigar valley 62
Metamorphism south of the Main Karakoram Thrust 63
Metamorphism north of the Main Karakoram Thrust 64
Pegmatites of the Shigar valley area 65

**CHAPTER FOUR METHODOLOGY**

Field methodology 75
Collection of rock samples 75
Laboratory methodology 77
Preparation of thin-sections 77
Crushing and pulverizing of rock samples 78
Preparation of stock solutions 78
Stock Solution A: using acid digestion method 78
Stock solution B: using sodium hydroxide fusion method 79
Determination of major and minor oxides 80

Determination of $SiO_2$ 80
Determination of $Al_2O_3$ 81
Determination of $TiO_2$ 82
Determination of $P_2O_5$ 82
Determination of total iron as $Fe_2O_3$ 83
Determination of CaO and MgO 84
Determination of $Na_2O$ and $K_2O$ 85
Determination of MnO 86
Determination of loss on ignition by using gravimetric method 86
Qualitative analysis of gemstones 87
Preparation of the sample 87
Mineral analysis by Electron Probe microanalyzer 87
Scanning Electron Microscope and preparation of samples 89

**-CHAPTER FIVE MEGA AND MICROSCOPIC FEATURES OF PEGMATITES**

General Statement 91
Gem-bearing pegmatites 91
Gem-barren pegmatites 92
Gem-bearing pegmatites 92
Muscovite-schorl-beryl-garnet pegmatites 92
Megascopic features 92
Microscopic features 93
Muscovite-schorl pegmatites 95
Megascopic features 95
Microscopic features 96
Gem-barren pegmatites 97
Biotite ± garnet ± muscovite pegmatites 97
Megascopic features 97
Microscopic features 97
Muscovite-biotite ± garnet pegmatites 98
Megascopic features 98
Microscopic features 99
Shengus and Indus-Gilgit Confluence pegmatites 100
Megascopic features 100
Microscopic features 101
Host Rocks 102
Megascopic features of the Dassu biotite gneiss 103
Microscopic features of the Dassu biotite gneiss 103

**CHAPTER SIX** **MINERAL CHEMISRTY**


General statement 153
Mineral Phases of the Shigar Valley Pegmatites 153
Plagioclase 153
Alkali Feldspar 156
Muscovite 156
Biotite 158
Tourmaline 160
Garnet 162
Zircon 164
Apatite 166
Fluorite 168
Chlorite 168
Mineral phases of the Indus-Gilgit Confluence and Shengus Pegmatites 169
Plagioclase 170
Alkali feldspar 171
Biotite 172
Epidote 173
Allanite 174
Apatite 176
Chlorite 176
Zircon 177
Ilmenite 178
Magnetite 179
Gemstones of the Shigar valley pegmatites and their mineral chemistry 180
Topaz 180
Garnet 182
Beryl 183
Schorl-foitite 186
Zoisite 188
Axinite 189
Fluorite 190
Apatite 191
Clinozoisite 192
Economics of the Gemstones of the Shigar Valley area 193
Exploration and evaluation of gemstones 195
Mining of the gemstones 195
Lapidary work 196

**CHAPTER SEVEN** **WHOLE ROCK GEOCHEMISTRY**

Major element characteristics and classification 265
Trace element characteristics and tectonic environments 270
Characteristics of the Rare Earth Elements 273
Possible source of magma for the Shigar valley pegmatites 274
Collisional leucogranites and the Shigar valley pegmatites 277
Chemical characteristics of Indus-Gilgit confluence pegmatites 278

**CHAPTER EIGHT** **DISCUSSIONS**

Leucogranites 313
Himalayan leucogranites 314
Models and causes for the generation of the Himalayan leucogranites 315
Classification of the Himalayan leucogranites 316
Shigar valley pegmatites and other post-collisional leucogranites and pegmatites 317
Baltoro Plutonic Unit: the possible parent magma of the Shigar valley pegmatite 318
Comparison of the Shigar valley Pegmatites with the Hunza valley leucogranite 321
Classification of the Shigar valley pegmatites 325
Causes of zonation and Shigar valley pegmatites 329
Trace element fractionation 335
Petrogenesis of Shigar valley pegmatites 336
Li-bearing source rock and Shigar valley pegmatites 345
Mechanics of pegmatite intrusion 347

**CHAPTER NINE** **CONCLUSIONS** 358

**REFERENCES** 362

## LIST OF FIGURES


| FIGURES | | PAGE |
|---|---|---|
| 1.1 | Location map of the Shigar valley, northern areas of Pakistan | 7 |
| 2.1 | Map of Central Asia showing the location of Western Himalaya, Karakoram, Hindu Kush and Pamir Mountain ranges (after Searle, 1991) | 50 |
| 2.2 | Simplified geological sketch map of the Central Karakorum between Skardu and K-2 showing the three main sub-divisions of the Karakoram block | 51 |
| 2.3 | Geological map of the Kohistan (after Tahirkheli and Jan, 1979; Coward et al.,19 | 52 |
| 2.4 | Geological map of the Himalaya and Karakoram showing major lithotectonic units (after Searle, 1991) | 53 |
| 2.5 | Regional Geological map of the Karakoram Plate | 53-i |
| 2.6 | Cretaceous-Tertiary time chart showing radiometeric dates for the Pakistan Himal Nanga Parbat, Kohistan, Hunza and Baltoro karakoram (after Searle et al., 1999) | 53-ii |
| 2.7 | Geological map of the Kohistan (modified after Sweatman et al., 1995) | 53-iii |
| 3.1 | Geological map of the Shigar valley (after Hanson, 1986; 1989) | 69 |
| 3.2 | Map showing location of the pegmatite dykes and veins in the Shigar valley, N. Pakistan | 71 |
| 4.1 | Map showing location of samples in Shigar valley | 90 |
| 6.1 | X-ray powder diffraction pattern and data of the garnet from a pegmatite, Yuno, Shigar valley | 255 |
| 6.2 | X-ray powder diffraction pattern and data of the beryl (var. aquamarine) from a pegmatite, Dassu, Shigar valley | 256 |
| 6.3 | X-ray powder diffraction pattern of the tourmaline (var. schorl-foitite) from a pegmatite, Kashmol, Shigar valley | 257 |
| 6.4 | X-ray powder diffraction pattern and data of the epidote (var. zoisite) from Alchuri, Shigar valley area | 258 |
| 6.5 | X-ray powder diffraction pattern and data of the axinite (var. ferroaxinite) from Alchuri, Shigar valley area | 259 |
| 6.6 | X-ray powder diffraction pattern and data of the fluorite from Kashmol mine, Shigar valley | 260 |
| 6.7 | X-ray powder diffraction pattern and data of the apatite (var. dahlite) from Yuno mine, Shigar valley | 261 |
| 6.8 | X-ray powder diffraction pattern and data of the epidote (var. clinozoisite) from Yuno mine, Shigar valley | 262 |
| 6.9 | Map showing gemstone occurrences in the Shigar valley | 263 |
| 7.1 | Plot showing classification of the studied pegmatites | 281 |
| 7.2 | Feldspar normative plot showing classification of the studied pegmatites (after O' Connor, 1965 and Barker, 1979) | 281 |
| 7.3 | Harker-type binary diagrams for the Shigar valley pegmatites | 282 |
| 7.4 | Binary diagrams of the Shengus and the Indus-Gilgit Confluence pegmatites | 285 |
| 7.5 | Classification of Shigar valley pegmatites on the basis of Shands Index (after Maniar and Piccoli, 1989) | 288 |

| | | |
|---|---|---|
| 7.6 | $SiO_2$ vs. $Al_2O_3$ plot for the Shigar valley and Indus Confluence Pegmatites (after Maniar & Piccoli, 1989) | 289 |
| 7.7 | FeO (t) / FeO (t) + MgO vs. $SiO_2$ diagram for the pegmatites from Shigar valley, Shengus and Indus-Gilgit confluence (after Maniar & Piccoli, 1989) | 289 |
| 7.8 | Nb vs.Y discrimination diagram for the Shigar valley, Shengus and Indus Confluence pegmatites (after Pearce et al., 1984) | 290 |
| 7.9 | Rb vs.(Y + Nb) discrimination diagram for the Shigar Valley, Shengus and Indus-Gilgit confluence pegmatites (after Pearce et al., 1984) | 291 |
| 7.10 | SiO2 vs.Rb diagram for the Shigar valley, Indus-Gilgit confluence and the Shengus pegmatites (after Pearce et al., 1984). | 292 |
| 7.11 | Primitive mantle-normalized spidergram for the different groups of the Shigar valley pegmatites (after Sun and Mac-Donald, 1989) | 293 |
| 7.12 | Chondrite-normalized REE patterns for the different groups of the Shigar valley pegmatites (after Sun and Mac-Donald, 1989) | 294 |
| 7.13 | Primitive mantle-normalized spidergram for the post-collisional pegmatites of the Shengus and Shigar valley (after Sun and Mac-Donald, 1989) | 295 |
| 7.14 | Comparative spider diagrams for the post-collisional pegmatites o f the Indus Confluence and Shigar valley (after Sun and Mac-Donald, 1989) | 296 |
| 7.15 | Chondrite-normalized spiderdiagram for the Shigar valley and the Shengus pegmatite (after Sun and Mac-Donald, 1989) | 297 |
| 7.16 | Chondrite-normalized spiderdiagram for the Shigar valley and the Indus Confluence pegmatites (after Sun and Mac-Donald, 1989) | 298 |
| 8.1 | Harker-type binary diagrams showing comparison of Shigar valley pegmatites and Baltoro and Hunza granitoid rocks | 349 |
| 8.2 | Primitive mantle-normalized spidergram for the Baltoro Plutonic Unit and the Shigar valley pegmatites (after Sun and Mac-Donald, 1989) | 352 |
| 8.3 | Primitive mantle-normalized spidergram for the leucogranites of the Baltoro Plutonic Unit and the Shigar valley pegmatites (after Sun and Mac-Donald, 1989) | 352 |
| 8.4 | Chondrite-normalized REE - patterns of the different lithologies of the BPU along wi Shigar valley pegmatites (after Sun and Mac-Donald, 1989) | 353 |
| 8.5 | Primitive mantle-normalized spidergram for the Shigar valley pegmatites and the Sumayar leucogranite (after Sun and Mac-Donald, 1989) | 353 |
| 8.6 | Chondrite-normalized REE pattern for the Shigar valley pegmatites and Sumayar pluton (after Sun and Mac-Donald, 1989) | 354 |
| 8.7 | Primitive mantle-normalized spidergram for the leucogranites of the Hunza Plutonic Complex and the Shigar valley pegmatites (after Sun and Mac-Donald, 1989) | 354 |
| 8.8 | Chondrite-normalized REE - patterns for the different lithologies of the post-collisior Hunza Plutonic Complex (after Sun and Mac-Donald, 1989) | 355 |
| 8.9 | Rb vs. Sr plot for different zones of the Shigar valley pegmatites | 356 |
| 8.10 | $K_2O$ vs. $Na_2O$ plot for wall zone and intermediate zone of the Shigar valley pegmatite | 356 |
| 8.11 | $K_2O$ vs. Rb plot for the wall zone and intermediate zone of the Shigar valley pegmati | 357 |
| 8.12 | Rb vs. Ba plot for tourmaline-rich and biotite-rich types of the pegmatites from the Shigar valley | 357 |

## LIST OF PLATES


| PLATES | | PAGE |
|---|---|---|
| 3.1 | An outcrop near the Kashmol village, where pre-collision metamorphosed mafic dykes sills are exposed | 70 |
| 3.2 | Zoned pegmatite showing sharp contact with the host augen-biotite gneisses, at Dassu | 72 |
| 3.3 | Pegmatite dyke about 5 feet thick intruding the para-gneisses near Goyungo mine | 73 |
| 3.4 | Horizontal, unzoned and simple pegmatite dyke within the Dassu biotite gneiss near the village of Baha | 74 |
| 5.1 | Photograph showing a pegmatite mine at Baha (Dassu) | 107 |
| 5.2 | Photograph showing a zoned gem-bearing pegmatite at Dassu | 107 |
| 5.3 | Coarse-grained pegmatite dyke mined for aquamarine, topaz, fluorite etc | 108 |
| 5.4 | Coarse-grained pegmatite dyke at Baha (Dassu), mined for aquamarine, topaz etc | 108 |
| 5.5 | Photomicrograph showing microperthite texture in the Kashmol pegmatites | 109 |
| 5.6 | Photomicrograph showing saussuritization of plagioclase in a pegmatite at Dassu | 109 |
| 5.7 | Photomicrograph showing bending or kinking in the plagioclase which is slightly bent or kinked | 110 |
| 5.8 | Microphotograph showing large cleavable sheets of muscovite in a zoned pegmatite at Dassu | 110 |
| 5.9 | Photomicrograph showing alteration in the upper part of the muscovite flake | 111 |
| 5.10 | Photomicrographs showing euhedral tourmaline crystals | 112 |
| 5.11 | Plane polarized light | 112 |
| 5.12 | Photomicrographs showing euhedral to subhedral tourmaline crystals | 113 |
| 5.13 | Plane polarized light | 113 |
| 5.14 | Photomicrographs showing an euhedral and zoned tourmaline crystal in the | 114 |
| 5.15 | pegmatites at Goyungo | |
| 5.16 | An euhedral to subhedral and zoned tourmaline crystal at Mungo | 115 |
| 5.17 | Plane polarized light | 115 |
| 5.18 | Photomicrographs showing small euhedral garnet crystals as inclusion in the plagioclase and orthoclase grains | 116 |
| 5.19 | Plane polarized light | 116 |
| 5.20 | Photomicrograph showing alignment of euhedral tourmaline crystals | 117 |
| 5.21 | Photomicrograph showing partial saussuritization of plagioclase | 119 |
| 5.22 | Photomicrograph showing small tabular and euhedral to subhedral plagioclase cryst | 119 |
| 5.23 | Photomicrograph showing cross-cutting relationship within a tabular plagioclase feldspar | 120 |
| 5.24 | Photomicrograph showing micrographic texture and vague albite twinning | 120 |
| 5.25 | Photomicrograph showing euhedral to subhedral, equigranular and fresh-looking quartz crystals in pegmatites near Sildi | 121 |
| 5.26 | Photomicrograph showing displacement and bending within plagioclase | 121 |

| | | |
|---|---|---|
| 5.27 | Large fresh and cleavable sheets of muscovite in pegmatites of Gone area | 122 |
| 5.28 | Plane polarized light | 122 |
| 5.29 | Photomicrograph showing overgrowth within muscovite grains in pegmatites at Kashmol area | 123 |
| 5.30 | Photomicrograph showing quartz crystals and iron-leaching along micro-fractures in the mafic minerals | 124 |
| 5.31 | Plane polarized light | 124 |
| 5.32 | A subhedral-anhedral tourmaline crystal, iron-leaching and fresh quartz crystals | 125 |
| 5.33 | Plane polarized light | 125 |
| 5.34 | Photomicrograph showing alteration of orthoclase to sericite, kaolinite and muscovite. Euhedral and fractured grain of garnet is also present | 127 |
| 5.35 | Plane polarized light | 127 |
| 5.36 | Photomicrograph showing alteration of orthoclase to sericite and kaolinite | 128 |
| 5.37 | A plagioclase crystal with perfect albite twinning as inclusion is present within the orthoclase | 128 |
| 5.38 | Photomicrograph showing perthite intergrowth of albite and microcline | 129 |
| 5.39 | Photomicrograph of highly-fractured garnet crystal occurs as inclusion within the orthoclase | 129 |
| 5.40 | Iron leaching along the micro fractures near the opaque phases | 130 |
| 5.41 | Plane polarized light | 130 |
| 5.42 | Medium-grained pegmatite having disseminated grains of garnet | 132 |
| 5.43 | Displacement of the pegmatite dyke due to the local faulting within Para-gneisses | 132 |
| 5.44a,b | Photomicrograph showing partially altered orthoclase. Well twinned plagioclase grains can also be noticed | 133 |
| 5.45 | Photomicrograph showing partial to complete saussuritization of plagioclase | 134 |
| 5.46 | Photomicrograph showing microperthitic texture between orthoclase and plagiocla: | 134 |
| 5.47 | Photomicrograph showing vermiculitic texture in orthoclase | 135 |
| 5.48 | Photomicrograph showing partial alteration of orthoclase and plagioclase | 135 |
| 5.49 | Photograph showing complex network of pegmatite dykes and veins | 137 |
| 5.50 | Photograph showing three simple pegmatite dykes exposed near Shengus | 137 |
| 5.51 | Photograph showing pegmatite dykes, exposed on the left side of the Indus River near Shengus along the Gilgit-Skardu road | 138 |
| 5.52 | Photograph showing numerous parallel pegmatite dykes and veins exposed at the confluence of Indus and Gilgit rivers | 138 |
| 5.53 | Photomicrograph showing microperthite texture in pegmatites of Shengus area | 139 |
| 5.54 | Photomicrograph showing euhedral plagioclase, altered orthoclase, anhedral quartz and muscovite flakes | 139 |
| 5.55 | Photomicrograph showing euhedral to subhedral garnet in extinction position and are scattered throughout the slide | 140 |
| 5.56 | Plane polarized light | 140 |
| 5.57 | Photomicrograph showing cross-hatched twinning in microcline in the Indus-Gilgit Confluence pegmatites | 141 |

| | | |
|---|---|---|
| 5.58 | Plane polarized light | 141 |
| 5.59 | Photomicrograph showing tabular fashion in microcline | 142 |
| 5.60 | Plane polarized light | 142 |
| 5.61 | Photomicrograph showing large flakes of muscovite and small euhedral garnets | 143 |
| 5.62 | Plane polarized light | 143 |
| 5.63 | Photomicrograph showing prismatic plagioclase having partial alteration along marg | 145 |
| 5.64 | Plane polarized light | 145 |
| 5.65 | Photomicrograph showing granophyric texture | 146 |
| 5.66 | Plane polarized light | 146 |
| 5.67 | Photomicrograph showing preferred orientation of biotites in Dassu biotite orthogneiss at Mungo | 147 |
| 5.68 | Photomicrograph showing cross-cutting and overgrowth relationships within biotites | 148 |
| 5.69 | Plane polarized light | 148 |
| 5.70 | Photomicrograph showing field of view that is mostly covered with biotites, in which overgrowth and cross-cutting relationships are very prominent | 149 |
| 5.71 | Plane polarized light | 149 |
| 5.72 | Iron-leaching or alteration near the mafic phase | 150 |
| 5.73 | Plane polarized light | 150 |
| 5.74 | Photomicrograph showing small euhedral zircon crystals | 151 |
| 5.75 | Plane polarized light | 151 |
| 5.76 | Photomicrograph showing partial to complete alteration of alkali-feldspar into kaolinite, sericite, epidote in the Dassu gneiss at Nyit, Braldu valley | 152 |
| 6.1 | Colorless and transparent crystal of topaz from Kashmol pegmatite | 246 |
| 6.2 | Zoned pegmatite near Dassu containing garnet and schorl | 246 |
| 6.3 | A reddish-brown garnet (small grain) from Yuno pegmatite, Shigar valley | 247 |
| 6.4 | Colorless to pale-blue and transparent aquamarine crystals, Shigar valley | 247 |
| 6.5 | Two light blue-colored aquamarine crystals along with schorl in coarse-grained pegmatite near Dassu | 248 |
| 6.6 | Black-coloured tourmaline (Schorl) from Kashmol pegmatite, Shigar valley | 248 |
| 6.7 | Two zoisite crystals from Alchuri, Shigar valley area | 249 |
| 6.8 | Brown colored axinites from the Alchuri, Shigar valley | 249 |
| 6.9 | A zoned and coarse-grained pegmatite near Yuno, Shigar valley | 250 |
| 6.10 | Three light-green to dark-green fluorites collected from the pegmatite mines Kashmol area, Shigar valley | 250 |
| 6.11 | Light-green colored fluorite crystal (2cm across) from Yuno mine, Shigar valley | 251 |
| 6.12 | An aggregate of light-pink colored apatite crystals from Yuno mine, Shigar valley | 251 |
| 6.13 | An aggregate of light-pink colored apatite, fluorite, garnet and large books of muscovite crystals from Yuno mine, Shigar valley | 252 |
| 6.14 | Clinozoisite-epidote minerals in the greenschists, Alchuri, Shigar valley | 253 |
| 6.15 | Light brown-greenish brown clinozoisites (epidote) from Alchuri, Shigar valley | 254 |
| 6.16 | An aggregate of dark brown clinozoisite from the Hashupa, Shigar valley | 254 |

## LIST OF TABLES


| 'ABLE | | PAGE |
|---|---|---|
| 5.1 | Modal composition of gem-bearing pegmatites from different localities of the Shigar valley | 105 |
| | a. Muscovite-schorl-beryl-garnet pegmatites | 105 |
| | b. Muscovite-schorl pegmatite | 118 |
| 5. 2 | Modal composition of gem-barren pegmatites from different localities of the Shigar valley | 126 |
| | a. Biotite ± garnet ± muscovite pegmatites | 126 |
| | b. Muscovite-biotite ± garnet pegmatites | 131 |
| 5.3 | Modal composition of Shengus and Indus-Gilgit Confluence pegmatites | 136 |
| 5.4 | Modal composition of the host rocks of pegmatites from different localities of the Shigar valley | 144 |
| 6.1 | Electron Probe Micro analyses of various minerals from the pegmatites of Shigar vall | 198 |
| 6.2 | Electron Probe Micro analyses of various minerals from the Shengus pegmatites | 213 |
| 6.3 | Electron Probe Micro analyses of various minerals from the Indus-Gilgit Confluence pegmatites | 215 |
| 6.4 | Scanning electron microscope analyses of the various gemstones from the Shigar valle pegmatites | 232 |
| 6.5 | Electron Probe Micro analyses of various gemstones from pegmatites and other rocks from different localities of the Shigar valley | 233 |
| 6.6 | XRD data of the Shigar valley gemstones with three major d - values | 245 |
| 7.1 | Major element chemical analyses along with C. I. P. W. norms of muscovite-schorl beryl-garnet pegmatite sub-class of Shigar valley | 299 |
| 7.2 | Major element chemical analyses along with C. I. P. W. norms of muscovite-schorl pegmatite sub-class of Shigar valley | 301 |
| 7.3 | Major element chemical analyses along with C. I. P. W. norms of biotite ± garnet ± muscovite pegmatite sub-class of Shigar valley | 302 |
| 7.4 | Major element chemical analyses along with C. I. P. W. norms of muscovite biotite ± garnet pegmatite sub-class of Shigar valley | 303 |
| 7.5 | Major element chemical analyses along with C. I. P. W. norms of the Indus-Gilgit Confluence and the Shengus pegmatites | 304 |
| 7.6 | Trace and rare earth element chemical analyses of muscovite-schorl-beryl-garnet pegmatite sub-class of Shigar valley | 305 |
| 7.7 | Trace and rare earth element chemical analyses of muscovite-schorl pegmatite sub-class of Shigar valley | 307 |

TABLE PAGE


7.8 Trace and rare earth element (ppm) analyses of the biotite ± garnet ± muscovite pegmatite sub-class from the Shigar valley 308

7.9 Trace and rare earth element (ppm) analyses of muscovite – biotite ± garnet pegmatite sub-class of the Shigar valley 309

7.10 Trace and rare earth element data (ppm) of the Indus-Gilgit Confluence and Shengus pegmatites 310

## *ABSTRACT*

*The granitic-pegmatites of the northern areas of Pakistan are well-known for hosting of various types of gemstones such as the aquamarine, topaz, bi-and tri-colored tourmalines, apatite, fluorite etc. The Shigar valley pegmatites are also one of these that hold a variety of gemstones. This valley is about 32 km northeast of Skardu, the head-quarter of Baltistan, northern Pakistan and it provides a route to K2 mountains.*

*Both meta-igneous and meta-sedimentary rocks of the Asian plate and Kohistan-Ladakh island arc, are exposed in the Shigar valley. The Main Karakoram Thrust is passing through the center of this valley, separating the meta-sediments of the Asian plate from the meta-igneous and meta-sediments of Kohistan-Ladakh island arc. Multiphase metamorphism and deformation has occurred in this area, therefore, the meta-sediments to the north of the Northern Suture are collectively known as the "Karakoram Metamorphic Complex". The grade of metamorphism varies from greenschist to amphibolite grade facies. Besides, the multiphase metamorphism and deformation, igneous intrusions of both the pre-and post-collisions are also exposed in the valley. The last phase of post-collisional igneous intrusion is present in the form of leucogranites and gem-bearing pegmatites (the focus of present study).*

*The pegmatitic rocks need special attention to understand their petrogenesis because these are of dual nature. They occur either the off shoots of near by plutonic bodies or separate magmatic pulses due to direct anataxis. There are series of different processes involving the emplacement of plutonic units, the formation of pegmatites and their host gemstones and the rare element-bearing minerals. The present study is being carried out to understand the petrogenetic evolution of the Shigar valley pegmatites and the formation of different types of gemstones in these pegmatites.*

*A reconnaissance fieldwork was carried out in the study area and the samples were collected from different pegmatite bodies for petrographic, geochemical studies and mineral chemistry. On the basis of field features and petrographic studies, the pegmatites*

*of the Shigar valley are broadly classified into two types: gem-bearing and gem-barren pegmatites. The gem-bearing pegmatites are generally zoned having three or four zones, while the gem-barren pegmatites are simple both in mineralogy and internal structure. Symmetrical zoning is the common feature of the gem-bearing zoned pegmatites, while some of the dykes exhibit asymmetrical zoning. Besides this, on the basis of presence or absence or the relative proportion of the accessory mineral phases, these pegmatites are further classified into four sub-classes. These four sub-classes are: 1. muscovite-schorl-beryl-garnet pegmatites, 2. muscovite-schorl pegmatites, 3. biotite ± garnet ± muscovite pegmatites and 4. muscovite-biotite ± garnet pegmatites.*

*The petrographic and mineral chemistry data of the studied rocks and gemstones indicate that no rare element-bearing mineral phases have been identified in these pegmatites. This suggests that these pegmatites belong to the miarolitic pegmatite class instead of rare element pegmatite class. The gemstones found in the Shigar valley are mainly aquamarine, topaz, fluorite, apatite, tourmaline, axinite, zoisite and clinozoisite etc. Field study suggests that all the gemstones are not of pegmatitic origin but some of them, such as axinites, zoisites, and clinozoisites are either metasomatic or metamorphic in origin. It is also noticed that the gemstones of pegmatitic origin are mostly found either at the core-margin zone or in the intermediate zone of the zoned pegmatites. In case of internal evolution of the Shigar valley pegmatites, grain size increases from the margin towards core, which indicates that the crystallization starts from margin towards core. The presence of vugs/cavities of the gemstones near the core zone also supports the above crystallization sequence.*

*The geochemical data of the studied pegmatites shows that these pegmatites are mostly peraluminous and granitic in character. The major, trace and rare earth element characteristics of these pegmatites exhibit that these belong to the post-collisional tectonic settings. Keeping in view the results obtained for the studied pegmatites and the prevailed models for the generation and propagation of granitic pegmatites, it is evident that these pegmatites have been formed by the direct anataxis of a meta-sedimentary protolith instead of being the off shoots either of Baltoro or Mango Gusar plutons, which*

*are exposed to the northeast of the Shigar valley. On the basis of radiometric dates for the host rocks of the Shigar valley pegmatites, it is concluded that the Shigar valley pegmatites are not older than 5 Ma. This is in correspondence with the youngest leucogranites of the High Himalayas, which are generally of 5-10 Ma. The Shigar valley pegmatites share many characteristics with the other post-collisional leucogranites of the High Himalayan and Trans-Himalayan regions. Like the post-collisional leucogranites of High Himalayas, the Shigar valley pegmatites also have tourmaline as a ubiquitous mineral phase, suggesting a similar source rock for these pegmatites. In addition, the presence of topaz, fluorite and apatite in the Shigar valley pegmatites indicates that the source rock was rich in boron, fluorine, chlorine, water and other volatiles. Moreover, the absence of lithium and rare-metal bearing mineral phases in the pegmatites of Shigar valley indicates that the source rock might have been depleted in these metals.*

# CHAPTER 1

## INTRODUCTION

### General Statement

Northern areas of Pakistan are composed of three mountain ranges, i.e., the Karakoram, the Hindu Kush, and the High Himalayas. These world-famous mountain ranges are the manifestation of the northward drift of the Indian plate and its ultimate collision with the southern continental margin of the Asian plate (including micro Karakoram Plate).

These mountain ranges are comprised of crystalline rocks (both igneous and metamorphic) containing certain economically important minerals and gemstones. Among these rocks, the granitic pegmatites, formed in the late stages of the crystallizing magma and also due to the anataxis of the continental crust into the collisional tectonic settings, are the main focus of the present study. The word pegmatite is a textural term and dependant on the composition of other major rock suits; therefore, it has various types, e.g. dioritic-pegmatites, gabbroic- pegmatites, syenitic-pegmatites, granitic-pegmatites etc. Among these, the syenitic and granitic-pegmatites are the most common. The granitic-pegmatites are economically important because these contain certain rare-metals and minerals and a variety of gemstones in most parts of the world (Laurs et al., 1998; Baker, 1998; Ćerný, 1982; Ćerný, 1991a). For example, in case of rare-metals and minerals the pegmatites have been mined or being mined world over for the occurrence of tantalum, niobium, beryllium, lithium, cerium, cesium, uranium, lanthanum, yttrium, tungsten, tin etc (Ćerný, 1982a, b; Ćerný, 1991a; Ćerný, and Simpson, 1977; Foord, et al., 1986). From gemological point of view, the pegmatites are the most important host for a variety of high quality gemstones, such as pale-blue aquamarine, colorless to yellow topaz, bi to tri-colored tourmalines, emerald, morganite, goshenite, fluorite, garnet, manganotantalite etc.

Pegmatites are broadly classified into simple and complex pegmatites on the basis of their mineralogy. The complex or zoned pegmatites are further classified into various types or classes on the basis of presence or absence of certain rare-metals and gemstones. In addition to this, the zoned or complex pegmatites are also classified as symmetrical or asymmetrical depending on the repetition of their border zone. In this regard, various classification schemes have been proposed (Cameron et al., 1949; Jahns, 1955; Herrera, 1969; Ćerný, 1991a; Foord, et al., 1986), however the classification scheme of Ćerný, (1982) is very useful.

Pegmatites are generally formed as dykes, veins, sheets, and sills and intrusive either into their parental plutons or at their margins or even into the surrounding country rocks, almost of metamorphic terranes. There is always a close relationship between the pegmatites and the aplites, commonly found together but pegmatites without aplites are also found. The proportion of aplites in the pegmatites is small but these are always associated with the pegmatites either at their margins as thin layers or in the core zone due to the rupturing of cavities or releasing of internal pressure, resulting in the fast cooling of the remaining volatile-rich magma (Laurs et al., 1998).

The gem-bearing pegmatites are generally zoned and have three tor four internal zones of variable sizes, textures, and mineral assemblages. From margin to core, these zones are: thin aplitic border zone, the wall zone, intermediate zone and the core zone (Cameron et al., 1949; Jahns, 1955; Herrera, 1969; Ćerný, 1982a, b; Ćerný, 1991a; Foord, et al., 1986). The alkali-feldspar, plagioclase and quartz are the essential mineral constituents of all these zones, but these always occur in variable proportions and textures in the different zones (e.g. the percentage and crystal size of quartz increases from border zone to core zone). Moreover, some of the zones are either rich in plagioclase feldspar or in the K-feldspar along with quartz (Jahns, 1955; Jahns, 1982; Herrera, 1969; Ćerný, 1982a, b; Foord, et al., 1986; Jolliff et al., 1992; London, 1996).

## Pegmatites in the Northern Areas of Pakistan

Northern areas of Pakistan are famous amongst minerals and gems collectors of the world for the occurrence of high quality gemstones and mineral specimen. Most of the gemstone-bearing pegmatites are well exposed because of their resistance to erosion, making leucocratic wall-like projections extending across with smooth and rugged slopes.

The pegmatites in northern areas of Pakistan occur within amphibolite to granulite grade facies schists and gneisses. The amphibolites in the region extend from Hunza River in the northwest to the Shigar River near Dassu to the southeast (Laurs et. al., 1998). Besides these two localities, the pegmatites are also present at the Garam Chasma in the western Karakoram and the Hushe and Masherbrum regions of the Karakoram metamorphic complex (Searle, 1991). The granitic-pegmatites are also exposed in the Indo-Pakistan continental plate in the Haramosh Massif at Dache, Khaltaro, Shengus and Stak Nala and in the Asian plate near Nagar, Hunza and Dassu of Shigar valley. However, gem- bearing pegmatites have not yet been reported in the Kohistan island arc.

The gemstone-bearing pegmatites in the Indo-Pakistan and Asian Plates are mostly young with cooling ages less then 10 Ma (Laurs et al., 1998) and are undeformed except near the margins of the Haramosh massif, where they are sheared locally. Generally they form swarms of parallel to sub-parallel, locally anastomosing discordant dykes and lenses of nearly concordant sills. They attain thickness up to several meters. Although individual dykes more then 3000m long have been mapped near Drot in Haramosh Massif and also in Dassu area (Kazmi et al., 1985; Laurs et al., 1998). The abundance of tourmaline and topaz in these pegmatites suggest that these are rich in boron and fluorine.

The pegmatites with cavities containing precious stones occupy a specific geological position amongst the gigantic pegmatite occurrences in the Himalayan and the Karakoram mountain ranges. These pegmatites are known for their primary pockets,

which are large chambers, rounded or ovoid in shape and are found tightly packed with gem-crystals, and some-times surrounded by light-pink or white clay material. The general principle is that the larger the pocket, the larger will be the crystals found (London, 1986, 1992). All these gem-bearing pockets of pegmatites are mined for aquamarine, tourmaline, topaz, quartz, fluorite and many other gems.

Pakistan is world-famous for its wonderful gemstones such as the emeralds of Swat, the topaz of Katlang (Mardan) and northern areas, rubies of Hunza and Azad Kashmir, aquamarines of Sumaiyar and Nagar, tourmaline of Stak Nala and the peridots of Sapat, Naran, Kohistan. The Shigar valley of Skardu is producing some beautiful gemstones, which could not be explored in detail because of remoteness and rugged topography.

## Location and Accessibility

The Shigar valley is the gateway for most of the expeditions to the highest peaks of the Karakoram Range including the K2 (8611m), the second highest peak of the world. The Shigar valley falls in the Survey of Pakistan toposheets Nos. 43 M/10, 43 M/11 and partly in 43M/6 at a scale of 1:50,000. It lies between latitude 35° 15′ - 35° 45′ N and longitude 75° 30′- 75° 45′ E and covers about 400 $km^2$. The Shigar valley is about 32 km northeast of Skardu, the headquarter of Baltistan, which is about 800 km from Islamabad, the capital of Pakistan and 200 km from Gilgit, the headquarter of Northern areas of Pakistan (Fig. 1.1). It is accessible from Islamabad and Peshawar by the world-famous Karakoram Highway (KKH) via Gilgit-Skardu road. The KKH is a metalled and all weather road, but temporary road blocks are common due to rock sliding and mud flows.

Two rivers, the Braldu and the Basha join the Shigar River near Mungo or Haiderabad villages. Shigar River runs nearly north-south and joins the mighty Indus River near Skardu. The Shigar valley is accessible by a metalled road from Skardu to the proper Shigar town and then the main valley is generally accessible by a Jeepable non-metalled road.

## Aims and Objectives

The proposed research is being carried out to attain the following aims and objectives:

- To prepare a geological map of the area having gemstone prospects.

- To conduct mineralogical and geochemical studies for the possible variation in the different types of Shigar valley pegmatites, their genesis and to identify the processes involved in the formation of various types of gemstones in these pegmatites.

- To explore the economic potential of the pegmatites of the Shigar valley, including the lower reaches of the Braldu and the Basha rivers for gemstones and rare earth elements.

## Previous Work

The Shigar valley and the surrounding areas have been investigated considerably in the past for the tectono-metamorphic evolution of the region (Searle et al., 1986; Searle et al., 1989; Searle and Tirrul, 1991; Searle, 1991; Brookfield, 1980). Desio (1963; 1964; 1979) carried out preliminary work in this region. Tahirkheli (1967) carried out a reconnaissance survey in the Shigar valley for the investigation of radioactive minerals. Searle et al., (1986), Searle (1991) and Searle and Tirrul (1991) have discussed the structural and thermal evolution of the Karakoram Metamorphic Complex (KMC) and differentiated various rock formations exposed in the KMC. Allen and Chamberlain (1991) worked on the Dassu gneiss in the Shigar valley. Parrish and Tirrul (1989) have dated certain rocks of the KMC by using U-Pb Zircon technique. Bertrand et al. (1988) worked on the Karakoram gneisses in the Braldu-Baltoro valleys of the KMC. Rolland et al. (2000) reported Middle Cretaceous back-arc basin formation and studied its evolution along the Asian Plate margin in Shigar valley and the surrounding areas. Hanson (1986;

1989) mapped the Shigar valley with emphasis to study the bedrock geology and demarcate the Northern Suture in this area. In addition to this, Punjab University Expedition team (1985) has also described the geology of Shigar valley and given petrographic studies of various rocks.

As far as gem-bearing pegmatites are concerned, Middlemiss and Parshad, (1918) reported the aquamarine for the first time in the pegmatites. Later on, Kazmi et al. (1985) and Kazmi and O' Donoghue (1990) carried out preliminary work on some pegmatitic bodies of the Shigar valley. However, no detailed mineralogical and geochemical studies so for have been carried out on these pegmatites.

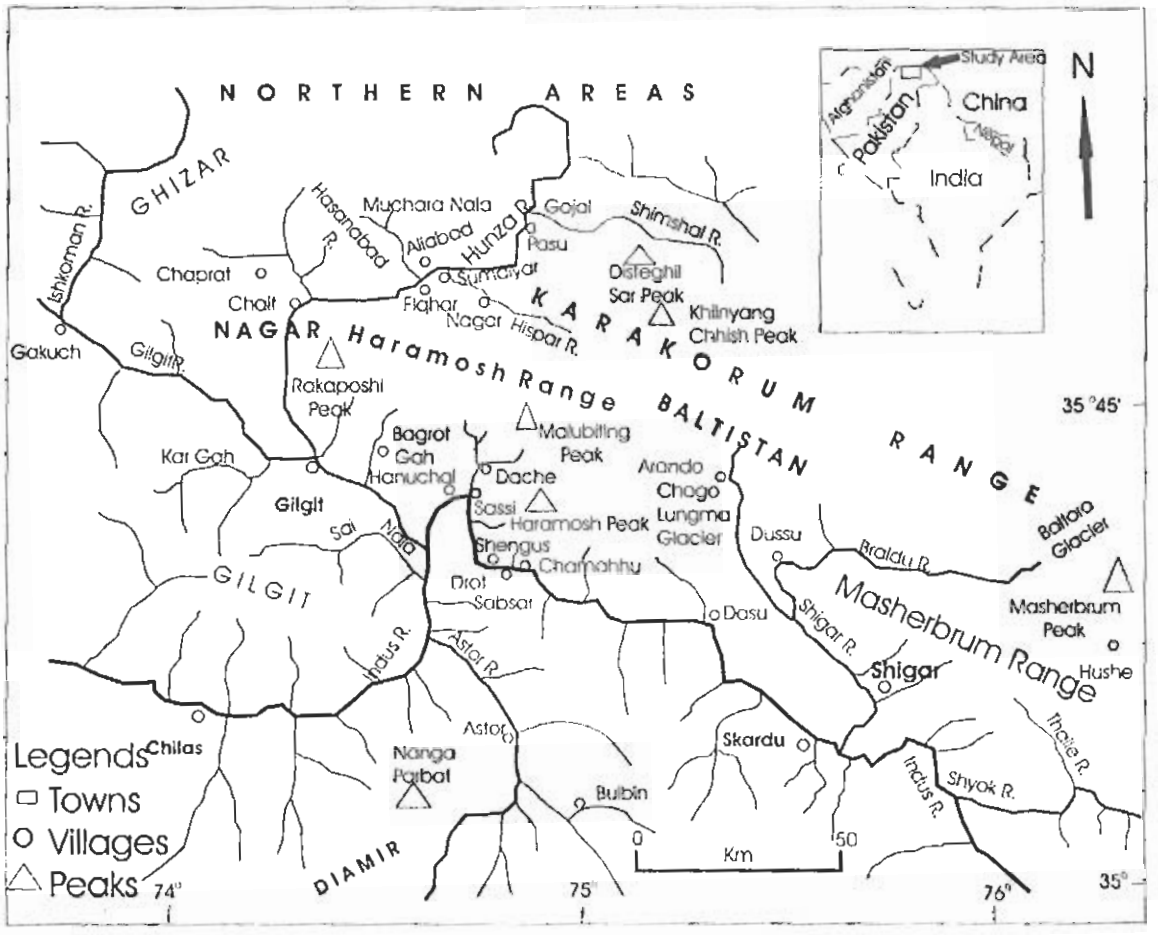


**Fig. 1. 1.** Location map of the Shigar valley, northern areas of Pakistan.

# CHAPTER 2

## REGIONAL GEOLOGY

### General introduction

The northern Pakistan is consisted of three geological domains, entirely different from each other. From north to south these are: Asian plate (including the micro Karakoram plate), the Kohistan-Ladakh island arc and the Indian plate. All the major and minor geological processes, which had occurred in Indo-Pakistan sub-continent since 130 Ma and also active at present, are related to the separation of Indian plate from the eastern Gondwanaland, its drifting towards north, subduction beneath the Tethys oceanic crust and finally its collision with the Asian plate. On the basis of some magnetic anomalies, it is estimated that Indian plate moved northward at a rate of about 3-5 cm/year between 130-80 m.y. (Johnson et al., 1976). Then from 80 m.y. India moved at an average rate of 15-25 cm/year relative to Australia and Antarctica (Powel, 1979; Patriat and Achache, 1984). The extensive extrusion of Deccan Trap basalts occurred between 65-60 m.y. during the fast northward drift of Indian Plate (Duncan and Pyle, 1988).

The development of Indian Ocean to the south and squeezing of Tethys ocean to the north began at ~ 130 m.y. ago due to the northward drift of Indian Plate (Johnson et al., 1976). Intra-oceanic subduction generated a series of volcanic arcs (Kohistan-Ladhakh, Nuristan, Kandhar) during the Cretaceous times forming back-arc basin at the southern margin of the Eurasia (Searle, 1991; Treloar andIzatt, 1993). This back-arc basin closed at about 100-90 Ma and as a result Kohistan-Ladakh island arc collided with Eurasia along the southern margin of the Karakoram plate and formed an Andean-type continental margin after accretion (Petterson andWindly, 1985).

Subsequent northward drift and subduction of Indian plate resulted in complete consumption of the leading oceanic edge of the Indian plate and its eventual collision

with the Kohistan-Ladakh arc. The abrupt slowing down of India's northward movement between 50-55 m.y. is attributed to this collision (Powell, 1979; Le Fort, 1975; Klootwijk et al., 1992). At about 50 m.y. ago the northward drift of India was slowed down due to its collision with Kohistan arc and the closure of Neo-Tethys in Tibet and Karakoram (Patriat and Achache, 1984). The new palaeomagnetic data show that the abrupt slowing down of India from 18-19.5 cm/year to 4.5 cm/year occurred at ~55 Ma (Klootwijk et al., 1992). After crossing the equator, the initial contact between northwestern greater India and Asia was established at about 65 m.y. (Klootwijk et al., 1992). The Indian Plate has steadily rotated counter- clock wise since 55 m. y. Coupled with the separation of Arabian plate from Africa about 20 m.y. ago, this rotation caused closure of Katawaz and Seistan basins, collision of various crustal blocks in Iran-Afghanistan region, convergence in Balochistan and formation of the Balochistan fold and thrust belt (Powel, 1979).

The India-Eurasia collision produced the Great Himalayas some 2500 km long along the Indian plate margin (Le Fort, 1975). The timing of collision is constrained by extensive emplacement of ophiolites along the Waziristan and Chaman Transform Fault in Waziristan, Muslim Bagh, Zhob and Lasbela areas (Gansser, 1964; Le Fort, 1975). Along these sutures, the lower middle Eocene marine sediments are found. Siwaliks are the product of Himalayan uplift, which directly overlie the Eocene limestones and contains debris of both Asian and Indian terranes (Le Fort, 1975).

As the present thesis area lies partly in Karakoram plate and partly in Kohistan - Ladakh island arc, therefore, it is important to describe these terranes and their main lithotectonic units in detail to know about the regional set up. In addition, igneous rocks of these two terranes are described in more detail relative to the meta-sediments rocks because of the nature of the present work. So, in this chapter the major lithotectonic units of the Karakoram Range, the Kohistan-Ladakh island arc and partly the Indian plate are described in detail.

## Regional tectonic setting of the Karakoram Mountains

The Karakoram range is approximately 700 km long and up to 100-150 km wide, running in an arcuate shape along the northern border of Afghanistan, Pakistan, India and the southern borders of the Tadjkistan and Khirkizia, and Chinese Turkestan "now known as Xinjiang Province" (Searle, 1991). It is a wild, treacherous and beautiful landscape, thinly populated and truly deserves the title of "Roof of the World" (Searle, 1991). Four of the world's highest (8000m) mountains- K2, Broad Peak, Gasherbrum 11 and Hidden Peak- encircle the upper corries of the Baltoro glacier, whilst a veritable ocean of 7000 peaks spreads all along the Karakoram Range.

According to Burrard and Hyden (1908), the Karakoram Range originates from near Rudok and Aling Kangri (7314m) in Tibet and extends up to Afghanistan. According to them, "the Karakoram and Hindu Kush mountain ranges of are different sections of the same crustal fold; the eastern portion of the fold is known as the Karakoram Range, and the western portion as the Hindu Kush Range.

Searle (1991) in his monumental book on Karakoram Mountains has shown the Karakoram to extend from Lake Pangong up to Afghanistan (Fig. 2.1). According to him, the Karakoram Range merges into the Hindu Kush range and includes many high mountains, notably the Tirich Mir (7690m) and Noshaq (7485m).

In this regard Kazmi and Jan (1997), on the basis of tectonics, geology, structure and orographic continuity, pointed out that the Karakoram-Hindu Kush Mountains comprise one complex mountain arc and that there is no clear geomorphic or geological feature, which divides this. It is rather a continuous chain of mountain ranges. The northern confines of the Karakoram-Hindu Kush Mountains are not so well defined on physiographic maps or the land sat imageries. The valleys of Yarkand, the Dangabash and the Amu (Oxus) rivers indicate the approximate northward extension of this mountain range (Fig. 2.1).

The Karakoram Range lies along a critical juncture in the tectonics of the central Asia. The Karakoram Range in the west can be correlated on geological evidence with the Hindu Kush and the southern Pamirs (Searle, 1991; Kazmi and Jan, 1997). Regionally on its north and northeast are the Tarim basin and the Tien Shan Mountain ranges, while eastward, the Lhasa block of southern Tibet bound it. The Kohistan-Ladakh island arc and the Indian plate are present to the south of Karakoram Range.

The Karakoram mountain belt marks the northern limit of northward dipping continental crustal slabs with intermediate-depth seismicity. Along the Karakoram and the mountain ranges to the south, most of the post-collisional thrusts dip towards north, and the thrusts and folds show a southward vergence. To the north of the Karakoram in the central and northern Pamirs, the folds and thrusts verge to the north and dip southward with intermediate-depth seismicity. All the mountain ranges to the north and east of Karakoram Range, including the northern Pamirs, the Tien Shan and the Kun Lun, show evidence of major Paleozoic orogeny, although these were strongly reactivated during the India-Asia collision. No major Late Paleozoic deformation is recorded in the Karakoram and the Himalayan ranges to the south (Matsushita and Huzita, 1965; Molnar, 1988; Searle, 1991; Kazmi and Jan, 1997).

The Karakoram terrane can be correlated with the Lhasa block of south Tibet. Both terranes have Carboniferous to Jurassic marine sedimentary successions and are intruded by subduction-related Andean-type batholiths. Though, the pre-collisional history of both the terranes is similar, but still major differences exist in their post-collision thermal, magmatic, structural and uplift histories. The southern Karakoram is completely dominated by post-collision regional metamorphism, massive crustal melt batholiths and extremely rapid recent uplift-erosion and exhumation rates. Up to 7000m of vertical exposure between mountain top and valley bottom in the Karakoram compares to a maximum of around 1500-2000m in the Tibetan Plateau, which in most areas is remarkably flat despite a mean elevation of about 5 km (For details see Matsushita and Huzita, 1965; Patriat and Achache, 1984; Molnar, 1988; Searle, 1991; Kazmi and Jan, 1997).

These spectacular topographic and structural differences between the Karakoram and the southern Tibet might be explained by the fact that the Karakoram lies immediately north of the western syntaxis of the Himalayas. Northwest-southeast striking thrust faults and folds in the western Himalayas swing around to north-south striking structures in the Nanga-Parbat-Haramosh massif, which could be interpreted as a massif northward-projecting promontory of the indenting Indian crust. This promontory may have caused greater amounts of crustal shortening, crustal subduction, uplift, erosion, and exhumation in the Karakoram than in the south Tibet Plateau. These processes in turn might have caused the more widespread regional high-grade metamorphism and crustal anataxis in the Karakoram (Matsushita and Huzita, 1965; Patriat and Achache, 1984; Molnar, 1988; Petterson et al., 1990b; Searle, 1991; Kazmi and Jan, 1997).

**Divisions of the Karakoram Block**

Searle (1991) divided the entire Karakoram Range and a part of the Hindu Kush range into the following geographic domains:

1. Western Karakoram (Chitral- Yasin),
2. Hunza Karakoram,
3. Northern Karakoram,
4. Eastern Karakoram (Siachen-Nubra-Ladakh),
5. Karakoram Metamorphic Complex,
6. Karakoram batholith (Baltoro-Biafo-Hushe areas).

However, Kazmi and Jan (1997) divided the entire Karakoram Range into the following four tectonostratigraphic divisions:

1. Karakoram Axial Batholith,
2. Tirich Mir Zone,
3. Southern Sedimentary belt,
4. Northern Sedimentary belt.

For the sack of simplicity, the classification scheme of Kazmi and Jan (1997) is followed to understand the regional scenario and tectonic set up of the Karakoram Range. It will be helpful to perceive the possible genesis of the gem-bearing pegmatites of the Shigar Valley. In addition to this as the topic of thesis is concerned with magmatic rocks especially the collisional granitoids, so for this reason the magmatic rocks of the Karakoram terrane are described in some detail relative to other lithologies.

**Karakoram Axial Batholith**

The central part following the axis of the Karakoram Range is composed of granitic rocks of pre- and post-collision and is known as Karakoram Axial Batholith (Ivanac et al., 1956 and Desio, 1979) (Figs. 2.1, 2. 2 and 2. 5). The high mountain peaks including K2 of the Karakoram Range are composed of these rocks. This belt extends for 600 km from southwest of Drosh to west of Pangong Lake and attains a width of up to 30 km. This is a composite batholith with many plutons, dykes and veins of variable composition emplaced over a time span of exceeding 100 m.y. The plutons in the Karakoram Axial batholith from west to east are: Buni Zom, Zagor-Umalsit-Ghamu Bar, Dobargar-Darkot, Hunza and Baltoro plutons. They range in age from Jurassic to Miocene (Searle et al., 1986, 1989; Searle, 1991). Along the northern margin of the Karakoram Axial batholith, near Baroghil Pass, there are small out crops of Pre-Ordovician granites. The granitic rocks and the surrounding sedimentary sequence have been metamorphosed to varying extent during the three main thermo-tectonic events and a later retrograde phase (Searle and Fryer, 1986; Searle et al., 1986; Rex et al., 1988; Searle et al., 1989; Searle and Tirrul, 1991; Searle, 1991). The Karakoram batholith divides the region into a northern and southern sedimentary belt. The western part of the region, the Tirich Mir Zone is separated from the main body of the Karakoram belt by the Tirich Mir fault (Kazmi and Jan (1997). The Karakoram batholith is composed of the pre-collision subduction-related plutonism as well as syn-collision or post-collision crustal melting (Searle and Fryer, 1986; Rex et al., 1988; Searle et al., 1989; Searle and Tirrul, 1991; Searle, 1991).

The Karakoram Axial Batholith is composed of simple and complex plutonic bodies of pre-and post-collision. These are well exposed due to the rapid uplift and erosion of this terrain, while the plutonic bodies of earliest magmatic episodes are metamorphosed to various grades. These plutons display major differences in age, chemical and mineralogical composition and tectono-metamorphic history (Debon et al., 1987). Following Searle (1991), the Karakoram batholith is here described in western, eastern, northern and Hunza sections of the Karakoram Range.

**A) Western Karakoram Batholith**

In the western Karakoram, the main Karakoram batholith splits into two prominent elongate plutons: the northern Darkot Pass (Dobargar) plutonic unit and the southern Ghamu Bar (Zagar-Umalsit) plutonic unit (Fig. 2. 2). The Darkot Pass unit appears to connect eastwards with the Batura unit and Hunza plutonic complex, with a southern branch exposed north of the village of Ishkuman. The Ghamu Bar unit is exposed in the upper Yasin valley north and west of the village of Umalsit. In addition to these, the western-most exposure of the Karakoram Axial batholith is the Kesu-Bunizom pluton, extends from Mastuj to Kesu and beyond, a distance of more than 100 km. The Jurassic-Cretaceous Darkot Pass unit includes a wide range of composition from quartz-monzodiorite to leucogranite, which are part of the northern branch of the Karakoram batholith. They intrude the Devonian limestones and marbles of the Darkot group. The Darkot Pass granites are strongly deformed and in places have a blastomylonitic texture (Debon et al., 1987). The southwestward extension of the Darkot Pass unit extends up to the village of Mastuj along the Yarkhun River.

The Ghamu Bar Unit forms the southern branch of the Karakoram batholith in the western Karakoram and is also exposed in the Darkot group along the Yasin River valley north of Umalsit. It shows a wide variety of granitic compositions, but is dominantly composed of medium-fine grained porphyritic granite (Debon et al., 1987). Several north dipping leucocratic dykes occur, similar to the Hunza dyke complex. The Ghamu-Bar

unit is intruded into the Carboniferous-Permian pelitic sediments and is strongly deformed along its southern contact with mylonites (Searle, 1991).

Geochemically, the dark medium-grained granites belong to the cafemic association with trends intermediate between calc-alkaline and sub-alkaline (Debon et al., 1987). The Ghamu-Bar unit is composed mostly of peraluminous biotite granite-adamalites. Both of these units exhibit calc-alkaline trends and REE patterns similar to the northern Kohistan granodiorite plutons and the Hunza plutonic complex (Debon et al., 1987; Searle, 1991).

Although the U-Pb radiometric data is lacking but the rocks of these units have been dated by other radiometric methods. The deformed porphyritic granites of the Darkot Pass unit have a Rb-Sr whole rock age of 111 ± 6 Ma with a low $^{87}Sr / ^{86}Sr$ initial ratio of 0.7044 whereas the leucogranites have an isochron age of 109 ± 4 Ma (Debon et al., 1987) (Fig. 2, 6). Two K-Ar hornblende ages of 199 ± 10 Ma and 83 ± 4 Ma have been obtained from the southwestern part of the Darkot pass granite along the Yarkhun valley (Debon et al., 1987). The Zagar-Umalsit pluton east of the Mastuj has a K-Ar biotite age of 77 ± 3 Ma. Debon et al. (1987) reported poorly constrained Late Paleozoic Rb-Sr ages with $^{87}Sr / ^{86}Sr$ initial ratios around 0.7051 and 0.7048 for the Ghamu-Bar pluton.

**B) Hunza Karakoram Batholith**

Along the Hunza valley section, the Karakoram Batholith consists of four distinct plutonic units. These are: Hunza plutonic complex (HPC), the Batura plutonic unit, the Sumayar pluton and the leucogranite dyke swarms. The Hunza plutonic complex contains rocks ranging from quartz diorite to granite, but granodiorite is the most predominant. About 2 km wide mixing zone occurs in the southern part of the HPC (Crawford, 1988). This zone shows a complicated mixture of rock types, notably quartz diorite and granodiorite, feldspar megacrystic granite and pegmatitic lecogranitic sweats containing

garnet and biotite. This zone could be interpreted either as the result of mixing of an acid and basic magma, or as a magmatic migmatite (Searle, 1991).

A network of aplitic sheets composed of granodiorite-monzogranite, emanate from the mixing zone on both sides. The aplite sheets are 10-30 m wide and often have pegmatitic rims rich in garnet and muscovite. The sheets intrude the granodiorite and are cut by the later Hunza lecogranitic dykes (Crawford, 1988; Searle, 1991; Fraser et al., 2001). The Hunza dyke complex consists of a co-magmatic suit of monzogranite, granodiorites and leucogranites. The leucogranitic complex form a dense anastomosing network intruding the southern deformed part of the batholith and the sillimanite grade metamorphic rocks of the Karakoram Metamorphic Complex (KMC) to the south. The dykes vary from veins of a few centimeters to several meters wide massive dykes, which can make up to 40 % of the rock by volume. The leucogranitic dykes are very similar to the large dyke swarms associated with the Masherbrum complex and the Baltoro plutonic unit further east (Searle et al., 1989). They are often layered with the aplitic centers and pegmatitic margins and characterized by sharp intrusive contacts. Many pegmatitic dykes show mineral zonation with garnet-muscovite rich centers and biotite rich margins (Searle, 1991). In addition, the leucogranitic sheets over 100m thick are exposed in Nagar and Aliabad areas. Besides, granodiorite sheets are also present at Hasanabad and Bar in Hunza valley section (Kazmi and Jan, 1997).

The Batura plutonic unit for the first time was described by Schneider (1957) around the Upper Batura glacier. It consists of undeformed biotite-hornblende granodiorite and granites. Two samples from the Batura plutonic unit have Rb-Sr isochron age of 63 ± 2 and 42 ± 5.6 Ma (Debon et al., 1987; Debon et al., 1996). The Batura unit is similar to the northern granodiorite of the Hunza plutonic complex except that the latter contains no biotite. This subalkaline and ferriferous association is dominated by light-colored meta- aluminous and slightly peraluminous rocks with low initial $^{87}Sr / ^{86}Sr$ ratios (0.7050 -0.7056). It has apparently originated from a mantle source with small crustal contamination, through a two stage melting process (Debon et al., 1996).

The Sumayar pluton is an isolated leucogranite pluton exposed south of Nagar and north of Diran, intruding the metasediments of the KMC. It is a large homogenous body characterized by sharp intrusive contacts and is approximately 4 km wide. A small contact metamorphic aureole of hornfels surrounds the pluton, which is structurally analogous to the Mango Gusar and Chingkiang-La plutons south of the Baltoro glacier (Searle et al., 1989). The Sumayar pluton cuts regional schistosity and thrust-related structures in the metamorphic complex. The Sumayar pluton is the one in Karakoram leucogranites which contains abundant tourmaline (> 2% modal). The presence of tourmaline and Mn-rich garnet rims in the Sumayar pluton reflects the chemistry of the crustal melt, that suggests a shallow level emplacement "12-15 km depth" (Searle, 1991; Fraser et al., 2001).

Geochemically, the various plutonic units along the Hunza valley have been studied by Debon et al. (1987) and more extensively by Crawford, 1988; Crawford and Windley, 1990; Crawford and Searle, 1993. The granodiorites of the Hunza plutonic complex show a typical calc-alkaline, Andean-type trend with a subduction related geochemical signature (Brown et al., 1984; Thomson et al., 1984). Although the HPC consists of a number of different magmatic pulses, the geochemistry suggests that they are formed either through fractionation or by similar source regions. The REE patterns of the Batura plutonic unit are very similar to the HPC, except that they show a slightly greater Eu anomaly (Debon et al., 1987). The geochemistry of the pre-collision granitoids of the HPC, combined with Sr-Nd isotopic signatures, suggests an origin similar to calc-alkaline Andean-type batholiths, which are related to the subduction of oceanic crust beneath the active continental margin (Crawford, 1988; Searle, 1991).

The geochemical patterns of the Hunza dykes and the Baltoro plutonic unit are very similar. Although the monzogranites and the leucogranites of the Hunza dykes show a considerable scatter in the spidergrams but bulk of the data show similar trends and plot in the same fields as to the BPU and. The only difference is that along the Hunza valley section no massive pluton of batholithic- scale like the Baltoro is present. The Hunza dyke complex is probably closely related to the Masherbrum injection complex along the

southern margin of the Baltoro Plutonic Unit (Searle, 1991). The geochemistry of the Nagar and Sumayar leucogranites is entirely different from the HPC and more closely similar to the High Himalayan leucogranites typified by the Manaslu-type leucogranite (Le Fort, 1981; Le Fort et al., 1987).

In case of geochronology, the U-Pb zircon age for the HPC is 95 ± 5 Ma (Le Fort et al., 1983b), which is similar to U-Pb ages of 101 ± 2 Ma from the Ladakh batholith to the south (Scharer et al., 1984b) and 103 ± 3 Ma (Honegger et al., 1982). In case of Batura unit, Debon et al. (1987) have documented Rb-Sr whole rock ages of 45 ± 7 and 43 ± 3 Ma with initial $^{87}Sr / ^{86}Sr$ ratios ranging from 0.7040 to 7056. This age is very close to the India-Asia collision and might represent the youngest subduction-related phase of magmatism in the Karakoram batholith. The K-Ar mica ages for the Hunza dyke complex ranges from 16.9 to 2.7 Ma (Debon et al., 1987) and from 25 to 4 Ma (Searle et al., 1989; Treloar et al., 1989). The Hunza Plutonic Complex aplite sheets have a lower $^{87}Sr / ^{86}Sr$ ratio (0.7065) and a higher $^{143}Nd / ^{144}Nd$ ratio (0.51252) than the Hunza dykes (Crawford, 1988) and slightly older K-Ar ages. The isotopic and field data support the contention that they represent two different magma sources. However, their similarity in mineralogy, trace elements and REE patterns indicate a similar petrogenetic history (Searle, 1991).

Searle (1991) has also described another belt of pre-collision plutons in the northern part of the Hunza valley. In this section he has described the pre-collision plutons of Khunjrab and Sost. According to Debon and Le Fort (1982) classification scheme, these plutons are granodiorite and monzogranite in composition and have mineralogy similar to that of HPC. Two K-Ar biotite ages of 107 and 105 ± 5 suggest that they are of a similar age as that of the Hunza plutonic complex and the northern Kohistan-Ladakh granitoids. Arc-related magmatism was, therefore, active along at least one and probably two linear belts in the Karakoram, corresponding with Andean-type magmatism in the Kohistan and Ladakh areas, south of Shyok Suture (Searle, 1991).

**C) Karakoram Batholith: (The Baltoro-Biafo-Hushe areas)**

This area stretches from the Snow lake-Hispar in the west to the Siachen Glacier and Khapalu in the east (Figs. 2.1 and 2. 7). Several large and small plutons have been reported from this area. East of the Hushe valley, the Karakoram batholith is represented by a composite magmatic unit consisting of three major components termed as the Kande Plutonic Complex (KPC) (Searle et al., 1989). The oldest lithologic unit of this complex is the foliated diorite or amphibolite containing abundant biotite or hornblende. These early intrusive phases of the batholith are similar to the deformed hornblende-biotite granodiorites of the Hushe Complex, which have K-Ar hornblende ages of 208 ± 8 Ma and 163 ± 7 Ma (Searle et al., 1989), and $^{40}Ar$ / $^{39}Ar$ ages of 140 ± 5 and 146 ± 11 Ma. This early magmatic phase is subjected to a regional low-pressure metamorphism of andalusite-grade indicating to be related to the early subduction-related components of the Karakoram batholith. The most widespread lithologic unit in the Hushe valley is a biotite ± hornblende tonalite to granodiorite and K-feldspar porphyritic granite. The third and youngest lithologic unit is the garnet, two-mica leucogranite that is associated with a large injection complex of dykes and veins.

The Muztagh Tower unit crops out just to the north of the Baltoro plutonic unit. It consists of deformed and strongly foliated tonalitic to granodioritic gneisses. The mineralogy and geochemistry and deformation style of the Muztagh Tower unit suggest that the rocks are equivalent to hornblende-bearing granodiorites of the Hunza Plutonic Complex (HPC) to the west (Debon et al., 1987; Crawford, 1988; Rex et al., 1988). The Muztagh Tower gneisses from Biange have $^{40}Ar$ / $^{39}Ar$ plateau ages of 76 ±1.6 Ma, and three K-Ar hornblende ages spanning 82-73 ± 3 Ma, confirming the above interpretation (Searle et al., 1989; 1990).

The biotite-hornblende gneisses of Lobsang peak and the Muztagh Tower (7273m) have been intruded by a network of garnet-two mica leucogranite dykes of Miocene age. These dykes are very similar to the leucogranite dykes intruding the Masherbrum Complex and the Baltoro granite and have a common late stage origin

(Crawford and Searle, 1992). The geochemistry of the Muztagh Tower gneisses shows a distinctive calc-alkaline, subduction-related signature similar to the HPC and of Andean-type tectonic settings (Rex et al., 1988).

The major part of the Karakoram batholith in the central Karakoram east of the Snow Lake and along the Baltoro glacier consists of a massive monzogranite to garnet-two mica leucogranitic intrusion of batholithic dimension and is known as Baltoro Plutonic Unit (BPU) (Searle et al., 1989; Searle, 1991; Fraser et al., 2001). In the central Karakoram it is approximately 10-20 km wide and extends at least 100 km along the strike from the Snow Lake area in the west to the Chogolisa and K6- K7 massifs around the Charakusa glacier in the east (Searle, 1991). The BPU was described by Desio and Zanettin (1970) in some detail and after that Searle et al. (1986, 1989) and Rex et al. (1988) mapped the Baltoro glacier transect and described the lithology, geochemistry and isotope chemistry. The monzogranites of the BPU consists of quartz-plagioclase-K-feldspar-biotite ± muscovite ± garnet with accessory sphene, zircon, apatite, monazite, allanite, thorite and opaque minerals. Hornblende is generally absent and tourmaline is present in a very few isolated patches, showing strong contrast to the Higher Himalayan granites (Searle, 1991).

The leucogranites of the BPU are characterized by the presence of garnet, muscovite and biotite. Accessory minerals are less abundant than in the monzogranites, and allanite, sphene and opaque minerals have not been noticed. Besides, muscovite is the most dominant mica. Garnet is particularly abundant and has a composition ranging from almandine to Mn-rich spessartine. Garnets frequently form linear or planar stringers, particularly in the latter pegmatitic dykes, indicating some sort of magmatic flow. Tourmaline is very rare. Aquamarine (Beryl) is occasionally present as megacrystic, pale-blue, euhedral-subhedral crystals (Searle, 1991).

Pegmatite and aplite dykes are normally of leucogranitic composition but have variable textures, morphology, and size. Garnet, muscovite, and biotite are ubiquitous, with grain size variation and magmatic flow textures forming some prominent banding.

Unlike the Higher Himalayan leucogranitic dyke swarms, tourmaline is practically absent within the Baltoro pegmatite-aplite dykes. The fluid phase associated with leucogranitic dyke emplacement in the BPU was, therefore, notably depleted in volatiles such as boron (Searle, 1991).

Geochemically, all the components of the BPU are mildly peraluminous. The leucogranite and the younger dykes and sills are depleted in most elements with respect to the monzogranites, except Rb, K, and the HREEs. Geochemistry and field data suggest that the leucogranites are related to the monzogranites, derived by fractional crystallization. Searle, (1991) concluded that the BPU granites appear essentially to be the lower crustal melts promoted and contaminated by a mantle input.

Parrish and Tirrul (1989) have reported U-Pb Zircon age of 21 ± 0.5 Ma from the BPU, and suggested that the emplacement age of the BPU was Miocene. Both zircon and monazite contain a significant proportion of inherited radiogenic Pb, suggesting that the magma source was ultimately derived from Pre-Cambrian crust. The crystallization and high temperature cooling ages of the BPU are very similar to the U- Pb ages of High Himalayan leucogranites south of the Indus Suture Zone. Two samples from the Karakoram Metamorphic Complex along the Biafo glacier have very similar Pb isotopic characteristics and it is possible that similar high-grade metamorphic rocks in the lower crust may provide a suitable source for the Baltoro granite (Searle, 1991).

The Masherbrum Complex is exposed along the southern margin of the BPU and consists of rafts and blocks of biotite-hornblende orthogneisses, biotite-rich paragneiss and layered calc-silicate marbles. It is intruded by massive leucogranite sheets and garnet -two micas pegmatite-aplite lecogranitic dykes. The schists have a K-Ar hornblende age of 77 ± 3 Ma similar to that of the Muztagh Tower Unit) and the pegmatites have an Rb / Sr isochron age of 14.1 ± 2.1 Ma.

Two plutons occur outside of the BPU. These are the Mango Gusar and the Chinkang-La plutons (Fig. 2. 2). The Mango Gusar pluton is a medium-grained stock of two micas leucogranite. This undeformed pluton cross-cuts the syn-metamorphic deformation fabrics and has a U-Pb Zircon age of 37 ± 0.8 Ma (Searle et al., 1989; Searle, 1991; Fraser et al., 2001). The smaller Chingkang-La pluton is pyroxene-hornblende-sphene-biotite ± muscovite granite with fluorite in the miarolitic cavities. Its K-Ar hornblende age is 34 ± 1 Ma (Kazmi and Jan, 1997; Searle, 1991).

**D) Eastern Karakoram Batholith**

The earliest observations on the Karakoram granites from the eastern Karakoram were made by De Terra (1932), Dainalli (1934), Wyss (1940) and Norin (1946). According to them half of the collected samples are biotite granites, with the remainder being two-mica granites or biotite-hornblende granites. Norin (1946) noted that the field relationships indicate a close association between various types of granites in the Karakoram, and that the older granodiorites had been subjected to strong dynamic regional metamorphism. The younger granodiorites in the Mawaz-Kangri area show no trace of internal deformation. Quartz porphyry dykes and acid intrusives intruding Jurassic limestones are formed on the northern side of the Saser Pass (Wyss, 1940). The field relationships appear to be very similar to the Broad Peak quartz diorites in the Baltoro glacier area.

Karakoram batholith is less studied in the Indian Karakoram and in this regard the studies are only confined to a narrow zone along the length of the Nubra and Shyok valleys. Srimal et al. (1987) described the batholith as composite with at least two major components, a Jurassic to early Cretaceous 'I-type', and Miocene 'S-type' granite. Lamprophyre dykes have been reported from several localities in the Aghil Range and eastern Karakoram. Norin (1946) documented that these lamprophyre dykes are common all across the Karakoram and Aghil Ranges.

## Tirich Mir Zone

The Tirich Mir Zone is largely comprised of the Arkari Formation (Jurassic?), which mainly consists of dark gray phyllites with subordinate quartzites and marbles. Southward it is intruded by numerous stocks and sills of leucogranites, metamorphosed under the amphibolite grade facies. Several elongated granitic plutons are exposed northwest of the Reshun Fault, along the Afghanistan-Pakistan border. These include Kafirstan-Garam Chasma and Tirich Mir plutons (Fig. 2. 5). Searle (1991) considered these plutons as part of the eastern Hindu Kush, making the Reshun Fault as a dividing line between the Karakoram and Hindu Kush. The eastern margin of the Garam Chasma (Hot Springs) pluton consists of undeformed two-mica granite with garnet and tourmaline has an intrusive contact with garnet leucogranite pegmatites intruding the surrounding country rocks (Calkins et al., 1981; Pudsey et al., 1985). Two K-Ar biotite ages of 20 ± 1 and 19 ± 1 Ma on the Garam Chasma granite indicate a young cooling history (Zafar et al., 2000). The Tirich Mir and the Kafirstan plutons consist mainly of biotite granodiorite and plagioclase augen gneiss (Buchroithner, 1985). The Kafirstan granite has a K-Ar biotite cooling ages of 48 ± 2 Ma and the Tirich Mir granite has an older K-Ar biotite age of 117 ± 5 Ma (Searle, 1991; Kazmi and Jan, 1997).

## Southern Sedimentary Belt

The Southern Sedimentary Belt forms an arcuate, north-verging belt of highly deformed and metamorphosed metasediments thrust southward on to the Kohistan-Ladakh sequence along the Shyok Suture Zone or (MKT) (Figs. 2. 2, 2. 3 and 2. 5). In the western part of the belt, between Chitral town and Mastuj, Late Paleozoic to Tertiary rocks are exposed. The Darkot group is the oldest sedimentary unit and it consists of slates, schists and quartzites intercalated with crystalline limestones (Fig. 2.3). Ivanac et al. (1956) have reported Carboniferous to Permian fossils from this unit. It has been intruded by granites and is unconformably overlain by the Tertiary (?) Reshun Formation (Pudsey et al., 1985). The Reshun Thrust Fault juxtaposes the Paleozoic sequence of the Northern Sedimentary Belt over the Reshun Formation and truncates the western part of

the Southern Sedimentary Belt (Kazmi and Jan 1997). In the region between Mastuj and Hunza, the Southern Sedimentary Belt is almost entirely comprised of the Darkot Group (Fig. 2. 3). Large plutons of the Karakoram batholith intrude the Darkot Group.

The Southern Sedimentary Belt or the rocks to the south of the Karakoram batholith and north of the Shyok Suture Zone or Main Karakoram Thrust (MKT) are collectively known as the Karakoram Metamorphic Complex (KMC) in the central Karakoram and in the Hunza valley section (Figs. 2. 2 and 2. 5) (Searle et al., 1989; Searle, 1991). Earlier, Desio (1964; 1979) divided these rocks into Dumordu, Ganchen, and Askole Groups. These rocks are lithologically diverse, showing a polyphase deformation and metamorphism and a long and complex tectonic history. As in many metamorphic areas of the KMC, there is insufficient sedimentological and palaeontological data to define the stratigraphy of the area and only a loose definition of units as opposed to 'formations' are used for the KMC (Searle, 1991).

The rocks of this complex have been studied in several places. The rocks of the Darkot Group in the western Karakoram display only low-grade metamorphism (Ivanac et al., 1956; Pudsey et al., 1985); while in the Hunza, central and eastern Karakoram, the rocks are metamorphosed up to the sillimanite-grade facies (Searle et al., 1989; Searle, 1991). The major units included in the KMC are: the Hushe Complex, the Dumordu Unit, the Ganchen Unit, the Askole Amphibolite, the Panma ultramafic-mafic unit, Dassu Gneiss and the Darkot Group.

**Northern Sedimentary Belt**

The Northern Sedimentary Belt extends westwards from Shaksgam through Upper Hunza and Chapursan valleys up to the Baroghil Pass. It then turns southwards and follows the Yarkhun valley. The Sost unit, the Misgar unit and the southerly Gujhal unit are the three main tectonostratigraphic units in the Upper Hunza region, and are separated by two major faults, i.e., Upper Hunza reverse fault and the Northern fault (Gaetani et al., 1990). Limestones, shales, and sandstones are the main lithologies of

these units and are Permian to Cretaceous in age (Zanchi, 1993; Gaetani et al., 1995). The prominent feature of the Northern Sedimentary Belt is the black carbonaceous shale, which overlies the KAB. It has been variously named as Pasu shale, Shimshal shale, Singhie shale, Baltoro shale, and Rimo shale in the different areas, where the Northern Sedimentary belt is exposed (Kazmi and Jan, 1997). The Tas Kupruk unit, the Karambar unit, the Baroghil unit and the axial units are the main tectonostratigraphic units of the Baroghil region and these are of Early Paleozoic age. The metasedimentary sequence exposed south of the Baroghil Pass, is intruded by Pre-Ordovician Ishkarwaz granite that was recognized for the first time by Le Fort et al., (1994) and Kazmi and Jan (1997) have proposed a name Chikar Formation (after Chikar village) for this sequence of the Baroghil unit. At the base of the sedimentary sequence, there is a conglomerate bed rich in chert followed by arkosic sandstones with brachiopods. Tongiorgi et al. (1994) and Le Fort et al. (1994) called this sequence as Baroghil sediments. But Tahirkheli (1982) named it Baroghil Formation. The Northern Sedimentary Belt continues southwestwards up to Chitral and beyond (Fig. 2. 5 and 2. 7). In this region it is apparently confined to a narrow belt between the Tirich and Reshun faults. In this region the Reshun Fault juxtaposes the Paleozoic sequence of the northern belt over the Cretaceous rocks of the Southern Sedimentary Belt (Kazmi and Jan, 1997).

## Kohistan-Ladakh island arc

The Kohistan-Ladakh island arc terrane formed due to the northward drift of India and the subsequent subduction of Neotethys Oceanic crust during Late Jurassic and Cretaceous time (Searle et al., 1987; Searle, 1991). The Kohistan-Ladakh Island Arc (KLIA) consists of a variety of volcanic, plutonic and subordinate sedimentary rocks that have been deformed and metamorphosed to varying degrees. The Nanga Parbat-Haramosh Massif (NPHM), a north-south trending promontory of the Indian plate divides the Kohistan from the Ladakh. The terrane to the east of the NPHM is the Ladakh while the western terrane is known as Kohistan (Fig. 2. 5). The two suture zones mark the northern and southern boundaries of the KLIA. In the north, the MKT marks its northern

while the southern boundary of the KLIA is marked by the Main Mantle Thrust (MMT) (Tahirkheli and Jan, 1979; Coward et al., 1982; 1986; and Bard, 1983).

As KLIA terrane was developed as a result of northward intraoceanic subduction of Neo-Tethys and it matured into a well-developed intraoceanic island arc for about 30-40 Ma (Khan et al., 1993). Then the terrane got accreted to the southern margin of the Karakoram Plate at the site of Shyok Suture Zone about 90 Ma ago (Petterson andWindley, 1985; Coward et al., 1986; Treloar et al., 1989). It was then intruded by a major batholith in an Andean-type continental margin setting until about 55 Ma ago when it was obducted onto the Indian plate at the site of the Indus Suture Zone.

The preliminary classification of the Kohistan terrane, based on the work of Tahirkheli et al. (1979), Bard et al. (1980) and Coward et al. (1982; 1986) is still applicable to it. The major contributions in understanding the mutual relationship between the various lithotectonic units of Kohistan are made by Ghazanfar et al. (1991), Sullivan et al. (1993), Khan et al. (1993), Jan et al. (1993), Khan, (1994) Khan et al. (1994), and Khan (1997). Petterson and Windley (1985) and Coward et al. (1986) have described two stages for the crustal growth of the Kohistan terrane, i.e., initially in an intraoceanic setting between ~120-90 Ma and then as an Andean type continental margin until the 50 Ma Kohistan-Indian collision. In this way the lithotectonic units of the Kohistan terrane are described below according to the above-mentioned classification.

### A) Intraoceanic stage of crustal growth

The major lithotectonic units of the intraoceanic stage of crustal growth of Kohistan are listed and described below:

1. Yasin Group: Late-Early Cretaceous,
2. Chalt Volcanic Group: Early Cretaceous,
3. Gilgit formation ?: Jurassic-Early Cretaceous,
4. Kamila Amphibolite Unit: Jurassic-Early Cretaceous,
5. Intrusive rock units.

**Yasin Group:** A group of sediments comprising sandstone, fossiliferous shaly limestone and conglomerate unconformably overlying a succession of volcanics near the village of Yasin was for the first time reported by Hayden (1914) and Ivanac et al. (1956) named these sediments and volcanics collectively as Yasin Group (Fig. 2.3). Tahirkheli (1979; 1982) used the term Yasin Group only for the sedimentary rocks and included the volcanic component into his Chalt Volcanic Group. Pudsey et al. (1985) and Pudsey (1986) divided the Yasin sediments into two units: the Lower sedimentary unit (~ 1 km thick) and the Upper fine-grained unit (up to 2 km thick). In the Ishkuman valley, the Yasin Group is composed mostly of slates, silty quartzites and conglomerates, while the limestone is missing here. In the Hunza valley, the Yasin group comprises mainly of terrigeneous clastics and volcaniclastics in the form of distal turbidites and slates with massive graywakes are predominant in the lower part.

Tectonically, the stratigraphy of the Hunza valley is repeated in the Jaglot area and is comprised of slates, with a thick marble horizon in the middle. South of the Shyok Suture Zone in the Chitral area, Pudsey et al. (1985) recognized a succession of volcanics and sediments, which they divided into Gawuch Formation at the base, Purit Formation in the middle and Drosh Formation on the top. The Bauma-Harel and the Burji Formations of Desio (1963; 1978) are the equivalents of the Yasin Group in the Baltistan area and the Katzarah Formation is present in the central part of these two formations. The Bauma-Harel Formation is mostly composed of volcanoclastic sediments, interbedded with slates, phyllites, carbonates and conglomerates. This formation was mapped in detail by Hanson (1986, 1989) along the Shigar valley area. Tahirkheli (1982) reported Lower Cretaceous fossils from this formation and on the basis of these fossils he considered that the Bauma-Harel Formation is the eastern continuity of the Yasin Group in the Baltistan.

Casnedi and Ebblin (1977) have described a sequence of volcanic and sedimentary rocks south of the Skardu and they named it "Shigarthang Sedimentary Group", but later on Desio (1978) considered it as a continuation of his Burji Formation.

It is suggested that the Bauma-Harel Formation to the north of the Katzarah Formation and the Burji Formation to the south, are tectonic repetition of a sequence, similar to Chalt Volcanic Group and the overlying Yasin Group. Lithologic resemblance and age similarities support this correlation.

**Chalt Volcanic Group:** The Chalt Volcanic Group forms an arcuate belt more than 350 km long and is the oldest volcanic group exposed in northern Kohistan and western Karakoram (Fig. 2. 3). It has been variously named as the Greenstone Complex (Ivanac et al., 1956), Turmik Formation (Desio, 1963; 1964; Desio et al., 1985; Zanettin, 1964), and Rakaposhi Volcanic Group (Tahirkheli, 1982; Petterson et al., 1990a). The volcanics comprise a diverse group of rocks. They range from basalt to andesite, dacite and rhyolite flows, agglomerate, tuff, and volcanic breccia locally interbedded with Yasin Group Sediments. These volcanics have been metamorphosed to green schist and epidote-amphibolite grade facies (Kazmi and Jan, 1997). The grade of metamorphism decreases westwards from high green schist- amphibolite in Hunza to low green schist in Ishkuman. Petterson et al. (1990a) and Petterson and Windly (1991) presented detailed geochemistry of the Chalt volcanics and identified island arc tholeiite and calc-alkaline rocks with compositions ranging between basaltic komatiite, bonanite and high Mg-andesite to calc-alkaline basalt, andesite, and dacite-rhyolite. Khan et al. (1993, 1995) concluded that the high Mg-type eastern volcanics (Chalt proper) were emplaced before the deposition of the Yasin Group (Aptian-Albian) in a back arc basin setting.

The Drosh Volcanics occur in a thin belt to the south of Shyok Suture in the southwest of Chitral are the western extension of the Chalt Volcanic Group (Pudsey et al., 1985; Pudsey, 1986). They are well exposed on the roadside south of Drosh and in the Lower Shishi valley. In the Shandur Pass area in north central part of the terrane, two types of the volcanics are recognized (Pudsey, 1986; Khan and Coward, 1990; Sullivan et al., 1993). South of the Shyok Suture Zone in the Shandur Pass area, and along the Ghizar River valley, another sequence of low-grade, flat lying or gently north-dipping metavolcanic rocks, named Shamran Volcanic Group are also present (Pudsey et al., 1985). These share many characteristics with the Utror Volcanics including the Ar-Ar

Plateau age of 58 ± 1 Ma on a hornblende bearing basaltic andesite (Treloar et al., 1989). The Shamran sequence contains flows of basalt, andesite, and abundant rhyolite. Acidic lavas and tuffs are finely bedded and intercalated with shaly sediments suggesting their simultaneously eruption and deposition. Locally, there are pillow lavas, chert bands, volcanic breccia and agglomerates. Pudsey et al. (1985) considered the Shamran Volcanics as older than the Yasin Group sediments, while Sullivan et al. (1993) correlated Shamran Volcanics with those of Dir Volcanics on the basis of close compositional resemblance and an Ar-Ar age spectra of 58 Ma (Treloar et al., 1989).

Bauma-Harel Formation is the eastern extension of the Chalt Volcanic Group into Baltistan (Desio, 1963; Hanson, 1989). This unit consists of volcanoclastic sediments interbedded with shales, phyllites, carbonates and conglomerates, and the overlying Yasin Sedimentary Group. The volcanics of the Bauma-Harel Formation are also locally known as Shigar volcanics (Punjab Univ. Expd., 1985). Turritellid gastropods of Lower Cretaceous age are reported from this unit by Hanson (1986, 1989). Along the northeastern termination of the Nanga Parbat Spur, the Askore amphibolite in the Indus valley, between Tungas and the confluence with the Turmik valley may be the continuation of the Chalt Volcanic Group (Le Fort et al., 1995). The equivalent of Chalt volcanics in the Ladakh is the Dras volcanic Group (Wadia, 1937; Honegger et al., 1982).

Khan et al. (1994) have described a thick sequence of pillowed basalts, massive basalts, agglomerates and tuffs and named it as "Gashu Confluence Volcanics". This sequence is the equivalent of the Chalt Volcanic Group in the interior of Kohistan, south of the Gilgit. These volcanics have been metamorphosed from green schist up to amphibolite-facies. Khan et al. (1993, 1994) believed that these volcanics are the tectonic repetition of the Chalt Volcanic Group at the limbs of the Gilgit anticline and Jaglot syncline of the Coward et al. (1987). The probable equivalents of the Chalt Volcanic Group in the Dir and Swat areas are the Mankial metavolcanics of Sullivan et al. (1993). As the overlying Yasin Group have yielded Albian-Aptian fossils, so on this basis the minimum age of the Chalt Volcanic Group is constrained to be Albian-Aptian (Desio, 1963; Pudsey et al., 1986).

**Gilgit Formation:** Metasediments in the form of paragneisses, migmatites and schists have been reported in the Kohistan terrane, but they were always considered either localized or anomalous. A group of metasediments exposed to the south of Gilgit was considered as the "stratigraphically lowest metasediments" in the Kohistan terrane Coward et al. (1987). Khan et al. (1994; 1996) studied these metasediments in detail in terms of their stratigraphic relations and were formally classified as the Jaglot Group. The stratigraphic unit forming the basal part of the Jaglot Group is termed as Gilgit Formation, which comprises a sequence of medium to high-grade paragneisses, migmatites, schists, quartzites and calc-silicates.

The Gilgit Formation is regionally metamorphosed under sillimanite grade facies, as evident by the presence of index minerals like biotite, garnet, kyanite, and sillimanite. The top-most unit of the Gilgit Formation is biotite-schist grading downward into garnetiferous schists, kyanite and sillimanite gneisses. In the deeper levels the paragneisses have undergone anataxis, giving rise to migmatites (Khan, 1997). As said, the Gilgit Formation is overlain by the Gashu-Confluence Volcanics (Khan, 1994; Khan et al., 1994; Khan et al., 1996), which are regionally equitable to the Chalt Volcanic Group of Petterson and Windley (1991). The basal contact of the Gilgit Formation is not exposed at least in the east-central Kohistan. Screens and xenoliths of biotite-schists and paragneisses belonging to the Gilgit Formation are frequently found in the Chilas Complex, particularly near its upper contact (Khan, 1988; Khan and Jan, 1992), indicating that the metasediments of the Gilgit Formation are older than the Chilas Complex.

The equivalent rocks of the Gilgit Formation are also reported from the Baltistan and north of Deosai in the form of metasediments called Katzarah Formation. The sediments are metamorphed under sillimanite grade facies (Desio, 1978; Tahirkheli, 1982; Hanson, 1989). The high-grade pelitic assemblage of the Katzarah Formation has a close compositional similarity with the Gilgit Formation and occupies the same stratigraphic position at the base of a volcano-sedimentary succession resembling Chalt Volcanic Group and Yasin Group of metasediments. In the west, rocks equivalent to

Gilgit Formation are exposed in the Kandia, Swat, and Dir valleys. In the Kandia valley, these metasediments are poorly described and an isolated outcrop of high-grade rocks overly epidotic-amphibolites of the Kamila belt (Yamamoto, 1993).

**Kamila Amphibolite Belt:** A linear belt of amphibolites about 10-40 km wide occurs south of the Chilas Complex and north of the MMT (Figs. 2. 3 and 2. 7). This belt has been variously named but presently it is known as Kamila Amphibolite Belt or Kamila Shear Zone. Upper Swat Hornblendic Group and the Kohistan Basic Complex are the former names of the Kamila Amphibolite belt assigned by Martin et al. (1962) and Jan and Kempe (1973) respectively. These amphibolites have also been referred to as the southern amphibolites (Jan, 1979; Bard et al., 1980) or, more commonly the Kamila Amphibolite Belt (Tahirkheli and Jan, 1979; Coward et al., 1982, 1986; Jan, 1988). Despite several detailed studies in various parts of the belt (Jan, 1988; Chaudhry et al., 1974; Ahmed and Chaudhry, 1976; Khan, 1988; Khan and Thirlwall, 1988), the nature of the Kamila amphibolite has remained ambiguous. Miller et al. (1991), on the basis of their work in the Indus valley suggested that the Kamila amphibolite belt is nothing but a stack of basic plutons. Likewise, there are differences in opinion regarding the origin of this belt. The Kamila belt represents the oceanic basement for the intrusion of the Kohistan island arc (Tahirkheli et al., 1979; Bard et al. 1980), whereas Coward et al. (1986); Jan (1988); Khan and Coward (1990), Miller et al. (1991); Shah and Majid (1992) suggested a subduction-related origin for this belt.

The Kamila amphibolite belt comprises a complex assemblage of lithologies but the fine to medium-grained and the medium to coarse-grained amphibolites are the most predominant. Fine to medium-grained amphibolites are predominant rock type in the eastern part of the belt, while the medium to coarse-grained amphibolites are predominant in the central and western part of the belt, especially along the Indus, Swat and Panjkora valleys. The fine-medium grained amphibolites are commonly foliated and include both banded and homogeneous varieties (Jan, 1979, 1988, Khan et al., 1993). The fine to medium-grained amphibolites are mainly volcanic while the medium to coarse-grained amphibolites are plutonic in origin (Kazmi and Jan, 1997; Shah et al., 1992). Due

to tectonism, the mafic flows with pillow structures are often stretched and can be observed locally in the entire extension of the belt (Dir, Swat, Buto, and Thak valleys). This supports the concept that the fine to medium-grained amphibolites in the Kamila belt are derived from the basic volcanics (Kazmi and Jan, 1997). Subordinate sedimentary rocks like amphibole-bearing quartzites, marbles, calc-silicates, and biotite & garnet paragneisses are also associated with the banded amphibolites. Locally a network of dykes and veins of tonalite-trondhjemite composition of variable thickness, intrude the Kamila amphibolite. These bodies are common along the tectonic contact with the Chilas complex. The probable origin of these acidic dykes and veins is the partial melting of the Kamila amphibolites (Khan, 1997).

The genesis of the metaplutonic amphibolites is relatively simpler. The homogeneous, foliated and banded variety of the amphibolite is derived from basic plutonic rocks. The banding is largely after the primary igneous layering but shearing has also contributed to banding in some cases. There is controversy over the tectonic setting of the Kamila amphibolites. As Jan, (1988; 1990); Shah et al., (1992); Khan and Thirlwall, (1990) have suggested that the amphibolites generally have island arc-type calc-alkaline to tholeiitic chemistry. While Khan et al. (1993), based on a reconnaissance survey of the entire belt suggested the presence of both E-type MORB and subduction related calc- alkaline mafic rocks in the Kamila belt.

Although the equivalent rocks of the Kamila amphibolite are absent from the eastern and central parts of the Kohistan north of Chilas Complex but in the West (e.g. Panjkora valley) a sequence of amphibolites does occur to the north of the Chilas Complex. This additional belt of the amphibolites was termed as the "Northern amphibolites" (Chaudhry et al., 1974) or the "Northern amphibolite belt" (Bard et al., 1980). The $^{40}Ar / ^{39}Ar$ hornblende cooling ages of 83-80 Ma (Treloar et al., 1989) suggest that the deformation and metamorphism occurred prior to the collision and suturing of the Indian Plate with the Kohistan island arc along the MMT.

**Intrusive rock units:** Like the volcanic phases of intraoceanic setting in Kohistan, several phases of intrusion of intraoceanic stage of development are also marked within the Kohistan terrane. Broadly, two types of plutonic phases are distinguished depending on their composition. They are:

a) Mafic and ultramafic complexes,
b) Intermediate to felsic intrusions.

The mafic and ultramafic complexes were emplaced into the Kamila amphibolite, while the felsic intrusions intruded and emplaced both within the Kamila amphibolite as well as in the presumably overlying younger tectonostratigraphic units like the Gilgit Formation and Chalt volcanics (Khan, 1997).

**a) Mafic and ultramafic complexes**

**Sapat and Jijal Complexes:** The southern margin of the Kohistan island arc is marked by a number of ultramafic-mafic rocks, probably ophiolitic assemblages (Figs. 2. 3 and 2. 7). These include the Tora Tiga, part of the Shangla, lower Jijal, and the Sapat and Babusar Complexes (Jan et al., 1993; Khan et al., 1993; Searle et al., 1999). The Jijal Complex is an ultramafic to mafic plutonic body exposed in the hanging wall of the MMT in the Indus valley. It is spreaded over 150 $km^2$ area and is a fault-bounded tectonic wedge (Jan, 1977, Jan and Howie, 1981). The Jijal complex represents the deepest part of the Kohistan arc terrane in southern Kohistan. It is composed of two main units, a lower ultramafic unit comprising of dunites, websterites, and clinopyroxenites and the upper unit consisting predominantly of garnet granulites (Jan and Howie, 1981; Miller et al., 1991). The Jijal complex is well exposed on either side of the KKH between Jijal and Patan. However, similar garnet granulites are also exposed at Khawżakhela in the Lower Swat valley.

There is great controversy over the origin of garnet granulites. As Jan and Howie (1981) considered the metamorphic origin for the garnet granulites while Ringuette et al. (1999) suggested a magmatic origin. But Searle et al. (1999) described a solution of this

controversy at some extent. Themobarometry based on the garnet-clinopyroxene exchange reaction and the garnet-quartz-clinopyroxene-plagioclase net transfer reaction give pressure temperature (P-T) conditions of 750-1150$^0$C and 12-19 Mpa (Miller et al., 1991; Ringuette et al., 1999). These high P-T conditions suggest post magmatic metamorphism at very high pressure granulite grade facies. Searle et al. (1999) suggested that it could be the result of the subduction of earlier lower crustal arc-related rocks to the depth of at least 45 km along the MMT under conditions of high temperature and pressure. The radiometric dates of 91 ± 6.3 to 114 ± 3.9 Ma have been documented for the garnet granulite by Coward et al. (1986); Yamamoto and Nakamura (1996) and Sano et al. (1996) but it is not clear, whether these reflect the age of metamorphism or magmatism.

The Sapat Complex in the southeastern Kohistan consists of dunites, peridotites, pyroxenites, and chromite-rich layers, passing upward into troctolites/metagabbros (Jan et al., 1993; Kazmi and Jan, 1997). Minor bodies of ultramafic and amphibolites at Babusar are the eastern continuation of the Sapat Complex (Ahmed and Chaudhry, 1976; Khan and Thirlwall, 1988; Ghazanfar et al., 1991). The complex has an exposed width of ~ 10 km in the southern Kohistan owing to the repetition through folding. The Sapat Complex contains spinel with high Cr similar to the Jijal Complex, suggesting closer affinity with the latter but different from the Chilas Complex (Jan et al., 1993). There is a possibility that the Pattan and the Kayal Complexes of Miller et al. (1991) are the westward continuations of the Sapat Complex in the Indus valley. The Khawzakhela body of troctolites and gabbros in the lower Swat valley (Jan and Karim, 1995) and Tora Tigga ultramafic-mafic complex in Dir (Jan et al., 1983) may be the westward continuation of the Sapat Complex (Khan, 1997).

**Chilas Complex:** The Chilas Complex is a large body of mafic and ultramafic rocks extending from Nanga Parbat to eastern Afghanistan (Fig. 2. 3). Similar rocks also occur on the eastern flank of the Nanga Parbat (Misch, 1949) and in Kargil, Ladakh (Rai and Pandi, 1982). This complex has been studied in some detail, at least petrographically (Jan et al., 1984; Khan, 1988; Khan et al., 1989; 1993; Khan and Jan, 1992). The rocks in the

complex are mainly gabbronorites with minor intrusive bodies of ultramafic rocks including dunites, hurzburgites, pyroxenites, anorthosites and troctolites, (Khan et al., 1989, 1993). The body is internally coherent and attains a maximum width of ~ 40 km in the central part. Locally, the gabbronorites are layered and contain websterites-anorthosites layers. Most of the Chilas Complex is undeformed, and the margins show faulted contacts with the surrounding amphibolites of the Kamila Amphibolite Complex and the intrusive contact with the metasediments of the Gilgit Complex. Rafters of the latter are enclosed as large xenolithic blocks within the Chilas Complex suggesting that the Chilas Complex is younger than the Gilgit Formation (Khan, 1988; Searle et al., 1991; Khan and Jan, 1992; Khan, 1994 and Khan et al., (1994). Westward in the Swat and Dir valleys, the complex appears to be emplaced at a stratigraphic horizon well below the upper contact of the Kamila amphibolite with the Peshmal schists. Searle et al. (1999) have described that the Chilas Complex was not emplaced at the same time in the magma chamber and had several pulses of magma over time. Khan et al. (1989; 1993) interpret the Chilas gabbronorites as representing the magma chamber at the base of the Kohistan arc or as an intrusion during intraoceanic rifting in a back arc basin. Treloar et al. (1996) concluded that the Chilas Complex was intruded after suturing of the Kohistan with the Karakoram plate to the north.

On the basis of mineral and whole-rock geochemistry Khan et al. (1989; 1993) reported that the rocks are calc-alkaline composition in composition and suggested an island arc / back-arc setting for the Chilas Complex. The P-T conditions of formation have been estimated at 750-850°C and 5-6.5 kbars and such conditions prevail in a sub-arc magma chamber at the base of the crust (Jan and Howie, 1980). The age of the Chilas Complex gabbronorites is given by a 84 ± 0.5 Ma from upper Swat (Zeitler and Chamberlain, 1991).

**b) Intermediate to felsic intrusions:** Rocks of intermediate to felsic composition of intraoceanic setting are reported from the Kohistan arc and in this regard the Thak Granitoid Sheets and Matam Das trondhjemite are of importance. Khan (1997) described plutonic rocks of intermediate to felsic composition from the valleys of Niat, Thak and Thor valleys to the south of the Chilas, which are intruded into the Kamila Amphibolites and vary in thickness from a meter to hundreds of meters (Khan, 1994; 1997). In addition to this, the composition of these bodies is also variable and in the Thak valley at least five varieties of intermediate plutonic rocks are observed near the village of Loshi. The sheets are foliated, suggesting their intrusion prior to the deformation of the Kamila amphibolites (Khan 1994, 1997).

Petterson and Windley (1985) distinguished a pluton from the northern Kohistan about 20 km upstream in the Hunza valley in the Matam Das, Jutal, and Nomal areas (Petterson et al., 1990). This pluton is mainly composed of trondhjemites with minor gabbros and norites, displaying a penetrative fabric. These deformed plutons are metamorphosed and intrude both the Chalt volcanics and the Gilgit Formation. Peterson and Windley (1985) have reported an age of 102 Ma for the Matam Das trondhjemite on the basis of whole- rock Rb-Sr isochron. The age of deformation event responsible for the penetrative fabric in these rocks was determined to be earlier than 75 Ma on the basis of Ar-Ar dating of a cross-cutting suite of undeformed basic dykes. Coward et al. (1986) concluded that it was the accretion of the Kohistan terrane with the Karakoram microplate, which caused the penetrative deformation of the Matam Das and related plutons. The equivalents of the Matam Das Pluton are missing in the Dir and Swat areas (Sullivan et al., 1993). Thus it may be concluded that only a minor component of the Kohistan batholith in the form of Madam Das trondhjemite was intruded during the intraoceanic phase development of the Kohistan terrane. Besides, (Jan and Khan, 1983) have reported some highly deformed tonalites from the upper swat, which may be the equivalents of the Matam Das pluton (Khan, 1994; 1997).

**B) Continental-margin stage of crustal growth**

The intraoceanic Kohistan terrane accreted with the southern margin of the Karakoram-Eurasia plate sometime between 100 and 75 Ma (Petterson and Windley, 1985; Coward et al., 1986). As no subduction-related magmatism in the Karakoram batholith has been reported younger than 95 Ma, which indicates the closing of subduction along the Shyok Suture. However, at the southern margin of the accreted Kohistan-Karakoram-Eurasia, the southern segment of the Neotethys continued subduction. Kohistan batholith, Barual Banda Slate, and Utror Volcanic Formation are the three lithologies in the Kohistan terrane that are related with this stage of crustal growth.

**Kohistan Batholith:** The Trans-Himalayan intrusive belt spreads over 2700 km length between Afghanistan and Burma. The Kohistan batholith is also a part of this belt. The Kohistan batholith is the main unit of the Kohistan magmatic-arc and constitutes a 300 km long and up to 60 km wide belt to the west of the Nanga Parbat-Haramosh Massif (Figs. 2. 3 and 2. 7) (Ganssar, 1964; Kazmi and Jan, 1997). Ivanac et al. (1956), Tahirkheli and Jan (1979) and Jan et al. (1981) identified a major belt of granitic rocks in the northern part of the Kohistan terrane, which was later on named as the Kohistan Batholith by Petterson and Windley (1985) and Coward et al. (1986). The Kohistan batholith is a composite and consists of numerous large and small plutons, plugs, dykes and sheets emplaced over a time span of some 75 Ma. A wide range of rocks constituting the batholith include gabbros, hornblendites, diorites, quartz-diorites, adamalites, granodiorite, granite, tonalite, trondhjemite, aplite and pegmatite etc (Kazmi and Jan, 1997). Except for a minor component, e.g., Matam Das, Jutal, Nomal, North Gilgit Ridge, and Upper Swat; the Kohistan batholith comprises of undeformed or mildly deformed intermediate to felsic plutonic rocks. Large-scale fold structures in the Gilgit Formation, Chalt volcanics and the Yasin sediments are intruded by the Kohistan batholith, which indicates that the emplacement of the batholith is subsequent to the accretion of the Kohistan terrane with the southern margin of the Karakoram Plate (Khan et al., 1993; Searle and Khan, 1996).

The Kohistan batholith has been studied in detail in the Chilas-Gilgit-Hunza transect (Petterson and Windley, 1985; 1986; Petterson et al., 1990b; Khan, 1994; Khan et al., 1994; Ivanac et al., 1956; George et al., 1993), in the Dir and Swat valleys (Jan and Mian, 1971; Chaudhry et al., 1974; Jan and Asif, 1983; Shah and Ihtisham, 2002), while east of the Nanga Parbat Haramosh Massif, the batholith has been studied by (Wadia, 1937; Zanettin, 1964; Desio 1963; Hanson, 1989). In the Chilas-Gilgit-Hunza transect, the main body of the Kohistan Batholith is known as Gor pluton (Khan, 1994; Khan et al., 1994). This body is ~ 60-70 km long and 30 km wide, occupying the drainage divide between the Indus and Gilgit rivers. The Gor pluton is a coherent mass of mainly quartz-diorite composition. Petterson and Windley (1985; 1986; 1991) and Petterson et al. (1990b) defined three main stages of granite emplacement based on the regional geological mapping, petrology and Rb/Sr dating. Stage-1 granites are the early bimodal sequence of gabbro-diorites and trondhjemite-tonalites, deformed by a Late Cetaceous deformation episode, such as the Matam Das pluton, which has a poorly constrained Rb/Sr isochron age of 102 ±12 Ma with an initial Sr isotope ratio of 0.7039 (Petterson and Windley, 1985). Besides, disrupted basic dykes are present and form a minor component of this phase. No U-Pb zircon or monazite ages have been reported from the Kohistan granites, although two U-Pb zircon ages of 101 ± 2 and 103 ± 2 Ma have been reported from the western Ladakh sector of the Trans-Himalayan batholith (Honegger et al., 1982; Scharer et al., 1984a).

Approximately two-thirds of the plutons within the Kohistan batholith are undeformed and post-date the deformation associated with the closure of the Shyok Suture. These plutons comprise a series of medium to high K-gabbros, diorites, granodiorites and granites with minor basic dykes (Peterson and Windley, 1985; 1991). Stage two intrusions are more acidic granodiorites and granites. These include the plutons of Gakuch, Gupis, Yasin, Pingal, Naz Bar, Gilgit, Shriot, and possibly Laikot, Donger in Swat and Warai in Dir (Petterson 1985; Kazmi and Jan, 1997; Searle, et al., 1999). Some of the plutons have been dated by various geochronological methods and the radiometric data fall mostly in the range of 78-40 Ma. Shirot and Gilgit granitoids have been dated by Rb/Sr methods and the ages for these plutons are 40 ± 6 Ma and 54 ± 4 Ma respectively

(Petterson and Windley, 1985). The K-Ar hornblende ages range from 61 to 53 Ma and biotite ages from 61 to 40 Ma (Treloar et al., 1989). Debon et al. (1987) obtained Rb-Sr age of 59 ± 2 Ma on the Gindai pluton near Gupis, with a Sr initial ratio of 0.7042. This age, together with hornblende Ar/Ar ages, such as the 61 ± 1 Ma age from the Gupis pluton, showing a flat plateau, may be regarded as reasonably accurate intrusions ages for the plutons west of the Gilgit (Searle, 1991). A suit of undeformed hornblende + plagioclase basic dykes, the Jutial dykes, cuts across the earlier deformed granodiorites of the Matam Das pluton and the Albian-Aptian Chalt Volcanics. The Jutial dykes have a hornblende $^{40}Ar$ / $^{39}Ar$ age of 75 ± 1 Ma (Treloar et al., 1989), which constrains the youngest timing of closure of the MKT (Searle et al., 1999).

The third and final plutonic stage of the Kohistan batholith is represented by swarms of garnet-biotite-muscovite-tourmaline leucogranite dykes and sheets that intrude all other components of the batholith. These leucogranite sheets are particularly well exposed along the confluence of the Indus and Gilgit rivers. Here the sheets and dykes are dipping at low angles to the north and constitute up to 30-40 % of the exposure, although elsewhere in Kohistan they are completely missing. Petterson and Windley (1985) distinguished the Indus confluence acid sheets from the Parri acid sheets, which are located ~ 15 km southeast of Gilgit. The latter are thicker (30-40 m thick) and tend to be more garnet and muscovite rich. The Indus confluence acid dykes and sheets have a poorly constrained Rb-Sr whole rock isochron age of 34 ± 14 Ma with an Sr initial ratio of 0.7045, and the Parri acid sheets have an isochron age of 29 ± 8 Ma, with an Sr initial ratio of 0.7052 (Petterson and Windley, 1985).

**Dir Group:** Tahirkheli (1979) described a belt composed of slates and volcanic rocks and called it as "Dir Group" (Fig. 2. 3). This belt is ~ 15-20 km wide and more than 120 km long stretching in a NE-SW trend across the Dir and Swat valleys in western Kohistan (Tahirkheli and Jan, 1979). On the basis of palaeontological and radiometric evidences the rocks have been assigned a Late Paleocene-Early Eocene age (Kakar et al., 1971; Treloar et al., 1989; Sullivan et al., 1993). The rocks of the Dir Group unconformably overlie a deep erosion surface cut into the Kohistan batholith and its host

rocks (Kamila amphibolite, Gilgit Formation, and Chalt Volcanic Group). First of all Tahirkheli (1979) divided this group into two units and Sullivan et al. (1993) also retained them. The two units are: Barual Banda Slate Formation (BBSF) and the Utror Volcanic Formation (UVF). The BBSF was studied in detail by Sullivan (1992) for systematic sedimentology and stratigraphy. The formation is ~ 3 km thick and comprises 30-70m thick basal succession of conglomerates, breccia and pebbly sandstone, overlain by ~2500m thick succession of thinly bedded-laminated sandstone, siltstone and mudstone. Limestone is interbedded in the Dir area and has yielded an abundant fauna of Actinocyclina, Discocyclina, and Nummulites atacicouss (Sullivan et al., 1993). A distal turbidite nature for the BBSF has been deduced by Sullivan et al., (1993). According to the previous workers, the BBSF was deposited in an elongated arc-parallel extensional fore-arc basin at the margin of the Kohistan-Karakoram continental margin.

The overlying UVF has a tectonic basal contact with the underlying BBSF along the Dir Thrust (Tahirkheli, 1982; Sullivan et al., 1993). The Dir Volcanic Group, consisting of the Utror volcanic, overlying the BBSF, represents the roof zone of the Kohistan batholith and is the youngest of the three volcanic belts. The volcanic rocks display a coherent chemical variation from basalt to rhyolite resulting from fractional crystallization (Shah et al., 1992). Volcanism was predominantly explosive with up to 1000 m of ash and agglomerate breccia. Flow-banded rhyolites and ignimbrites are common. The volcanics are dated as Paleocene to Early Eocene on the basis of Foraminifera found in interbedded sediments (Searle, 1991).

Incompatible element abundances are typically calc-alkaline in the basalt-andesite range, but are lower in the rhyolites, probably as a result of fractionation of accessory phases such as apatite, zircon, allanite, and ilmenite (Shah et al., 1992). Two $^{40}Ar$ / $Ar^{39}$ ages are available for the UVF. Treloar et al. (1989) presented a $^{40}Ar$ / $Ar^{39}$ age of 55 ± 2 Ma for a hornblende separated from an andesite. In contrast, an age of 70 ± 9 Ma was obtained for a hornblende from an andesite by Hamidullah and Onstat (1993). The northern contact of the Dir Group is faulted with the northern plutons of the Kohistan batholith (Khan, 1997).

## Northern Suture or Main Karakoram Thrust

The Northern Suture Zone separates the Cretaceous-Tertiary rocks of the Kohistan-Ladakh Arc from the Late Paleozoic metasediments of the Karakoram plate (Figs. 2.2 and 2. 3). It is variously known as the Northern Suture or Main Karakoram Thrust (MKT) in the Kohistan terrane, while in Ladakh area, it is known as the Shyok Suture Zone after the Shyok River. The Northern suture or the MKT developed in Late Cretaceous due to the collision of the Kohistan-Ladakh terrane with the southern margin of the micro-Karakoram Plate (Tahirkheli et al., 1982; Coward et al., 1986). This conclusion is based on: (1) Aptian-Albian fauna from the limestones of the Yasin Formation (Pudsey et al., 1986), (2) structural evidence like the folding of the volcanics and the sediments of the Kohistan-arc associated with the suture (Coward et al., 1986), and (3) 100 Ma and 80-85 Ma ages respectively for deformed granitoids in the Kohistan batholith and undeformed basic dykes cross-cutting them (Petterson and Windley, 1985; Treloar et al., 1989).

Several ophiolitic melanges have been reported throughout the length of the Northern Suture Zone from Chitral up to Khaplu and beyond. In the Chitral area, the melange consists of slates with interbedded conglomerate, sandstone, and blocks of volcanic greenstone, limestone, red shale and serpentine. This melange zone separates the Karakoram plate from the Kohistan arc (Pudsey et al., 1985). Here the melange is 3 km wide in the lower Shishi valley and 2 km wide at Harchin. It is reduced to a fault zone only 150 m wide in Naz Bar area. It comprises volcanic rocks with some sediments (Shamran Volcanic group, Drosh, Purit, and Gawuch Formation) intruded by phyric diorites, tonalites and granites. The volcanic rocks and the sediments dip towards north and have a horizontal lineation, suggesting that the Suture Zone in its western parts experienced an oblique collision (Khan, 1997).

The Northern Suture Zone along the Hunza valley is more complex and exposed around Chalt village. Here a melange zone is approximately 500 m wide and locally known as "Maium melange". It consists of serpentinite, volcanic, quartzose sandstone,

and limestone conglomerate blocks in a graphitic shale matrix locally containing biotite and chloritoid (Pudsey et al., 1985; Pudsey, 1986). The Northern Suture in the Hunza (Coward et al., 1982) and Baltistan (Rex et al., 1988) initially constituted a north- dipping thrust zone. This was steepened to sub-vertical during collision at the northern suture and was subsequently cut by the south moving Main Karakoram Thrust in Baltistan (Rex et al., 1988), which may be equivalent to the Hunza shear zone found in the hanging wall of the Northern Suture in Hunza (Coward et al., 1986).

The petrographic and the structural features of the ophiolitic melange in the Skardu-Khaplu area were described by Brookfield (1980). In the Skardu area, Zanettin (1964) and Hanson (1986; 1989) reported serpentinites, amphibolites, basalts, chlorite schists (with or without epidote or actinolite), marbles, greenschists, phyllites and gneisses. The basal contact of the melange here is a southwesterly directed-thrust. Below this occur muscovite-chloritoid schists showing isoclinal folding with axial planes dipping steeply NE (related to the southward emplacement of the melange zone). In the northeastern side of the confluence of the Hushe and Shyok rivers, a typical ophiolitic melange, containing fragments of serpentinite, pyroxenites, red and black chert, porphyritic basalt, dacite, rhyolite, gabbro and marble are present (Kazmi and Jan, 1997; Brookfield, 1980).

### The Indus Suture Zone/Main Mantle Thrust

The Indus Suture Zone defines the zone of collision between the Indian plate to the south and the Karakoram-Lhasa terranes to the north, and can be traced for over 2000 km from Kohistan and Ladakh eastwards across southern Tibet. It is variously named in different terranes: in Pakistan it is known as Main Mantle Thrust (MMT) (Tahirkheli et al., 1979; Bard, 1983); in the Ladakh Himalaya, it is called as the Indus Suture Zone (Ganssar, 1964; Searle, 1986; Thakur and Sharma, 1983) and in the southern Tibet it is known as the Yarlung-Tsangpo Suture (Allegre et al., 1984). The Indus Suture Zone also separates the Cretaceous Kohistan-Ladakh Arc from the Indian plate and the Lhasa block. It contains a wide variety of rocks ranging from Late Precambrian pelites and Cambrian

granites (Le Fort et al., 1980) to Paleozoic-Mesozoic sediments mostly in a highly deformed and metamorphosed state. Several melanges occur locally in a complex thrust zone (Kazmi et al., 1984), some of which bear blueschist facies assemblages (Shams, 1980), together with piemontite schists and serpentinites. The 200 $km^2$ Jijal-Pattan complex contains high-pressure plagioclase-bearing and plagioclase free garnet granulites and meta-ultramafic rocks. The ultra-mafic rocks are dominated by diopsides and minor dunites, websterites,wherlites and pyroxinites metamorphosed at 800-850°C and 8-12 kbars (Jan and Howie, 1981; Yamamoto, 1993). These high pressure assemblages may represent sub-island arc metamorphism, prior to collision (Khan, 1997).

The Indus Suture Zone in Ladakh consists essentially of three major linear thrust belts, namely the Lamayuru Complex, the Nindam-Dras volcanic group, and the Indus Mollase Group. These are separated by the major fault zones or ophiolitic melange belts and show a complex structural history (Searle et al., 1987). The Lamayuru Complex consists shales, sandstones and limestones with unknown radiolarian cherts and is Late Triassic to Jurassic in age (Fuchs, 1977). The Dras volcanic Group is a thick sequence of clinopyroxene, hornblende, and plagioclase phyric basalts, andesites and dacites with minor amounts of tholeiitic pillow lavas (Honegger et al., 1982). The Dras volcanics have been interpreted as Jurassic to Early Cretaceous island arc volcanic sequence erupted above a north dipping subduction zone within Tethys, prior to collision (Searle, 1991). A major ophiolitic melange (Shergol melange) separates the Nindam-Dras rocks to the southwest, and includes sheets or blocks of crossite and glaucophane-bearing blueschists (Searle et al., 1987; Honegger et al., 1989). These blueschists are interpreted as subduction zone metamorphic rocks formed at high pressure and low temperature along the north dipping subduction zone on the footwall of Dras volcanic sequence. Similar high-pressure blue-schists and granulites (Shangla and Jijal Complexes) crop out along the hanging wall of the Main Mantle Thrust in southern Kohistan (Coward et al., 1986).

The youngest marine sediments found along the Indus Suture Zone in the Ladakh and southern Tibet are the Lower Eocene limestones containing Nummulites. After the early Eocene, the sedimentation along the suture zone took place in the form of

continental mollase (Brookfield and Andrews-Speed, 1984). The change from marine to continental sedimentation at the Lower-Middle Eocene boundary (ca. 50 Ma) records the time of closing of Tethys along the Indus Suture Zone (Searle, 1986; Searle et al., 1988). This also requires that obduction of ophiolitic complexes southwards on to the Indian passive continental margin, such as the Spontang ophiolites in Zanskar, and the Kiogar-Alangta ophiolite of Tibet must have occurred prior to the early Eocene closing of Tethys (Searle et al., 1987). The Indus Group mollase sediments unconformably overlie the Ladakh batholith along the northern margin of the Indus Suture Zone (Searle, 1991).

To the west of Ladakh, the Indus Suture Zone is embayed northwards by the Nanga Parbat syntaxis, almost up to the Northern Suture Zone. Thus the Nanga Parbat antiformal structure separates the Ladakh terrane of the arc in the east from the Kohistan part in the west. This structure is developed from that part of the Indian Plate, which was initially subducted below the arc terrane and then uplifted to dissect the arc since the past 7 Ma (Smith et al., 1992). Palaeomagnetic studies in the Indian ocean indicate that the main continental collision of the Indian and Asian plates occurred from 55 Ma to 50 Ma (Klootwijk, 1979; Powell, 1979; Patriat and Acache, 1984). Closure of the Indus Suture at ca. 50 Ma is also constrained on the stratigraphic, structural and isotopic evidences (Searle, 1991; Searle et al., 1987).

## Indian Plate

The rock units exposed south of the MMT or Indus-Tsangpo Suture Zone are included into the Indian Plate. Rocks of the Indian plate along the entire length of the Indus-Tsangpo Suture Zone are highly deformed and metamorphosed relative to the rocks away from the MMT to the south. Indian plate rocks south of MMT have been described under the domain of Himalayas and the Himalayan orogeny is the result of the continental collision between the Indian and Eurasian plates. The Himalayas form a 2,500 km long and 160-400 km wide mountain belt comprising a series of en-echelon mountain ranges with extensive intervening valleys. The Himalayas have been formed along the

northern margin of the Indian plate and this zone is mostly covered by a nearly complete Phanerozoic sedimentary sequence up to the Eocene (Kazmi and Jan, 1997).

The continental crust along the Indus-Tsangpo Suture Zone in High Himalayas and Tibetan plateau is between 50 to 80 km thick, which is twice to the normal crustal thickness. This feature has been attributed to the continued under-thrusting and underplating of India beneath Asia (Molnar, 1988; Kazmi and Jan, 1997). Powell and Conaghan (1973) and Le Fort (1975) have proposed different models for this anomaly. Although these models provide logical basis for the classification of the Himalayas into various tectonostratigraphic units but here we follow the scheme of Kazmi and Jan (1997) to describe the geology and tectonics of the Himalayas for the Indian plate rocks. Actually, the classification or subdivisions of the Himalayas described by Kazmi and Jan (1997) are the morphotectonostratigraphic subdivisions of the Himalayas proposed by Burrard and Hyden (1908), Burrard and Heron (1934) and Ganssar (1964). Major thrust zones separate various tectonostratigraphic units of the Himalayas of the Indian plate from one another, as the High Himalayas and the Lesser Himalayas are separated from each other by the Main Central Thrust (MCT). The major tectonostratigraphic units of the Himalayas from north to south are:

1. Tethyan Himalayas,
2. High Himalayas,
3. Lesser Himalayas,
4. Sub-Himalayas,
5. Himalayan Foredeep.

**Tethyan Himalayas**

To the north and south, the Tethyan Himalayas are bounded by the Indus-Tsangpo Suture Zone and a northward dipping normal Trans-Himadri Fault respectively (Valdiya, 1989). The Trans-Himadri Fault is a Late-Tertiary gravity collapse structure with several tens of kilometers movement. A thick sequence of Late Precambrian, Paleozoic and Mesozoic fossiliferous Tethyan sediments was deposited on the northern

with several tens of kilometers movement. A thick sequence of Late Precambrian, Paleozoic and Mesozoic fossiliferous Tethyan sediments was deposited on the northern passive continental margin of the Indian Plate and along the southern edge of the Tibet (Thakur 1981; Gaetani et al., 1985). The sequence is stratigraphically divided into the Palaeozoic (Lahoul Super Group) and the Mesozoic (Zanskar Super Group), and is separated by the Permian Panjal Traps or Panjal Volcanic Group (Searle, 1991). The Panjal Trap rocks are the continental flood basalts formed during the Carboniferous-Permian riftings, which evolved into the passive margin of the Neo-Tethys during Mesozoic (Searle et al., 1987). Following extensive rifting and out pouring of the Panjal Traps, the northern continental margin of the India subsided rapidly, resulting in the formation of a thick sequence of limestone to the west (Zanskar and Spiti areas), shale and sandstone in the center (Kumaon), and sandstone, shale and limestone in the east (Nepal-Bhutan) (Fig. 2. 4). The Zanskar shelf-slope sediments are largely missing in the Pakistan sector of the Himalaya, where the Kohistan arc terrane is thrust directly onto the metamorphic rocks of the High Himalayan Zone (Searle et al., 1987; Searle, 1991). Evidence for early Palaeozoic basement comes from the 514 Ma (Rb-Sr) age from the Mansehra granites (Le Fort et al., 1980), which intrudes the Hazara slates and correlates with the intrusions of the similar age reported in the Tibet, Afghanistan and High Himalaya of northwest India.

**High Himalayas**

The High Himalayan Range lies south-southwest of the Zanskar Shelf Sediments and is a zone of Pre-Cambrian, Paleozoic and Mesozoic rocks metamorphosed during the climax of Himalayan deformation in the Mid-Tertiary. It includes many of the highest peaks along the Himalaya and stretches at least from Nanga Parbat in the west to the Mishmi Hills along the northern frontier of India and Burma (Fig. 2. 4). The High Himalayan Zone or the Tibetan slab (Le Fort, 1975) is bounded to the south and southwest by the Main Central Thrust (MCT) and to the north and north-east by a northward dipping normal fault (the Trans-Himadri fault) that down throws the sediments

The relationship between deformation and metamorphism is very complex in the High Himalaya. Pre-Himalayan metamorphism and deformation is documented from the Pakistan sector and the Zanskar, although this is largely over printed by the strong deformation and metamorphism since collision. The rocks forming major part of the High Himalayan Zone are the metapelites, amphibolites, marbles, quartzites, ortho-and paragneisses and migmatites. Metamorphic isograds have been mapped out on reconnaissance scale in Pakistan, Zanskar, Central Nepal and Darjeeling-Sikkim (Treloar et al., 1989; Searle et al., 1988).

The metamorphism and deformation is certainly polyphase, but peak metamorphism appears to have occurred at different times along the High Himalayan chain. Metamorphic isograds appear to cut across early structures, but are themselves folded around giant southwest or south verging recumbent folds along the hanging wall of Main Central Thrust. Several deformation phases have been recognized prior to, during and after peak metamorphism. Post metamorphic thrusting of a 'right way up' metamorphic sequence has been described from Pakistan by Treloar et al. (1989). However, along most of the length of the High Himalaya, metamorphic isograds are inverted, and appear to be related directly to the Main Central thrust (Le Fort, 1975; 1981; Searle, 1991).

**Lesser Himalaya**

The Lesser Himalayas are bounded to the north by the Main Central Thrust and to the south by the Main Boundary Thrust (MBT) (Gansser, 1964) (Fig. 2. 4). It is comprised of a pile of Late Proterozoic gneisses and Paleozoic- Mesozoic sediments (slates, phyllites, quartzites, limestones, sandstones, and flysch). The Mesozoic succession suggests a shelf origin, thickening towards north. These rocks have been overthrust by high-grade gneisses originating from the High Himalaya (Thakur, 1981; Sinha, 1981). In Pakistan the Hazara slates were deformed and metamorphosed prior to the intrusion of cordierite-bearing granites, such as the Mansehra pluton, which has been dated as of 514 Ma (Le Fort et al., 1983a).

A belt of cordierite-bearing granites extends along the length of the Lesser Himalayas structurally above the Main Central Thrust (Le Fort et al., 1980, 1983a). They include the Mansehra, Swat and related plutons in Pakistan, the Dalhousie, Lansdowne, Mandi, and Chor plutons in India, and the Palung and Simchar plutons in Nepal. The Palung granite, south of the Khatmandu has a U-Pb age of 470 ± 4 Ma (Scharer and Allegre, 1983). The Lesser Himalayan granites are peraluminous, but also contain igneous and metasedimentary inclusions (Searle, 1991). Metamorphism in the Lesser Himalayan thrust sheets is low- medium grade and the rocks are composed usually of chlorite, biotite, and garnet-bearing assemblages. Thrusts are difficult to map owing to poor exposure and dense vegetation cover in the Himalayan foot-hills (Searle, 1991).

**Sub-Himalayas**

The Himalayan foot hills, south of the MBT form the Sub-Himalayan Zone from Punjab to Assam. These hills are comprised of a narrow belt of folded Neogene mollase-type sediments (Siwaliks). These unmetamorphosed Siwalik sediments records the unroofing of the Himalayas. Southward the folded Siwalik sequence is covered by the Indo-Gigantic alluvium. The Siwalik Group consists of fluvial conglomerates, arkoses, siltstones and shales that were deposited in a fore deep along the southern margin of the mountain chain. Sedimentation started some 20-15 Ma ago (Johnson et al., 1985) with detritus dominated by High Himalayan lithologies, where the rapid uplift was followed by fast erosion (Cerveny et al., 1989).

The Himalayan Frontal Fault (HFF) or the Salt Range Thrust (SRT) is the southern most thrust zone along the foothills of Salt and Trans-Indus Himalayan Ranges. This fault comprises a series of en-echlon faults, which run parallel to the strike of the hills between Punjab and Assam (Nakata, 1989; Gee, 1989). This thrust is mostly covered by alluvium and fanglomerates (Kazmi and Jan, 1997). However, at places the thrust is exposed and where the Paleozoic rocks are thrust over the Neogene or Quaternary deposits of the Jhelum plain (Gee, 1989).

**Himalayan Fore Deep**

South of the Salt Range Thrust (SRT), the Himalayan Foredeep occupies the gently sloping continental platform. The basement of this is comprised of Archean and Proterozoic metamorphic and plutonic rocks of the Indian plate. It contains a series of upwarps, intervening depressions, horst and graben structures, defined by geophysical surveys. The Indus sedimentary basin covers the western part of the Foredeep, while the Gangetic plain covers the northern part. The Indus basin contains a thick prism of westward sloping Pre-Cambrian to Holocene sediments, which peter out eastwards. In the upwarp zones, the bedrock crops out at shallow depths (e.g., Shahpur-Delhi buried ridge, Jacobabad-Khairpur high, Khandh Kot-Mari high). Southward and westward, the sedimentary cover in the Indus basin thickens to more than 5,000 m, while the Gangetic Plain is up to 1700 m thick and is underlain by the Siwaliks mollase (Kazmi and Jan, 1997).

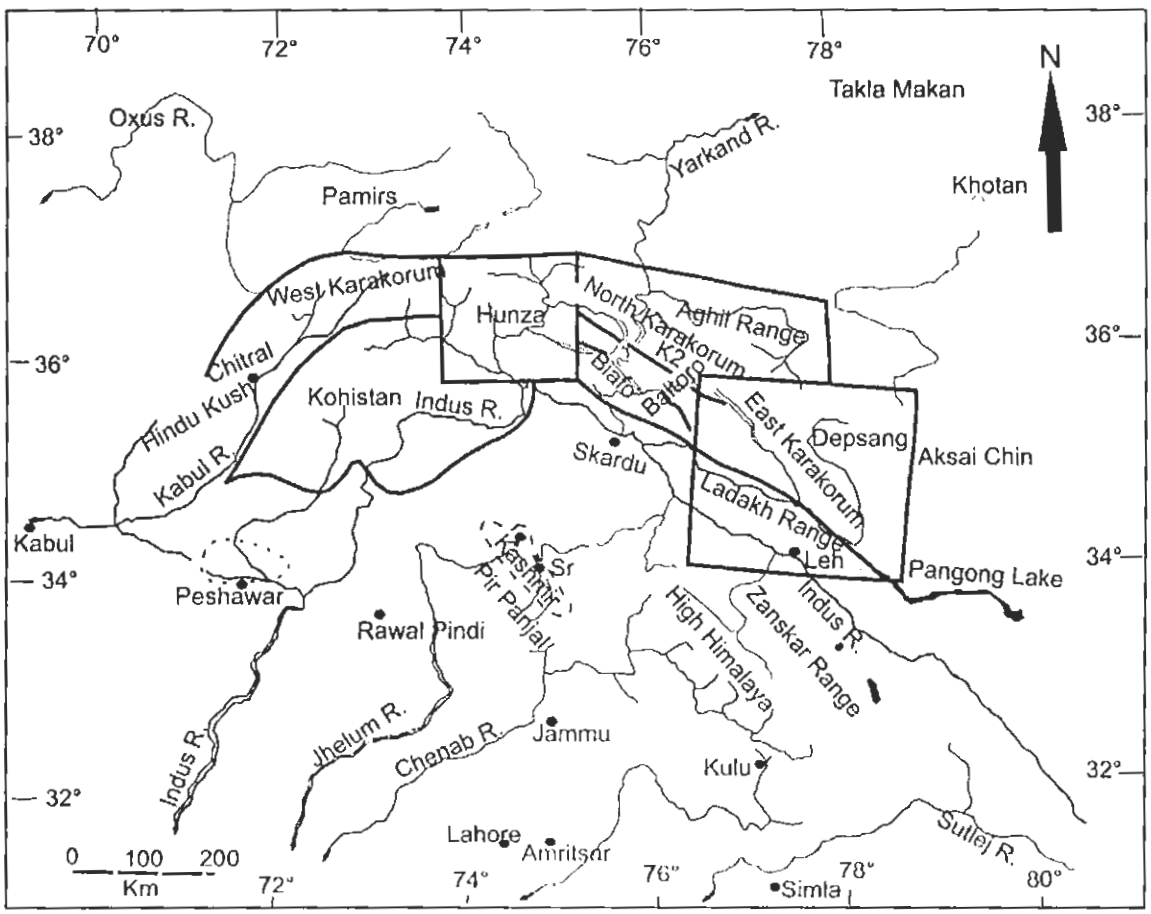


**Fig. 2. 1.** Map of Central Asia showing the location of Western Himalaya, Karakoram, Hindu Kush, and Pamir mountain ranges. The thick dark lines are the geographic subdivisions of the Karakoram Mountain Range (after Searle, 1991).

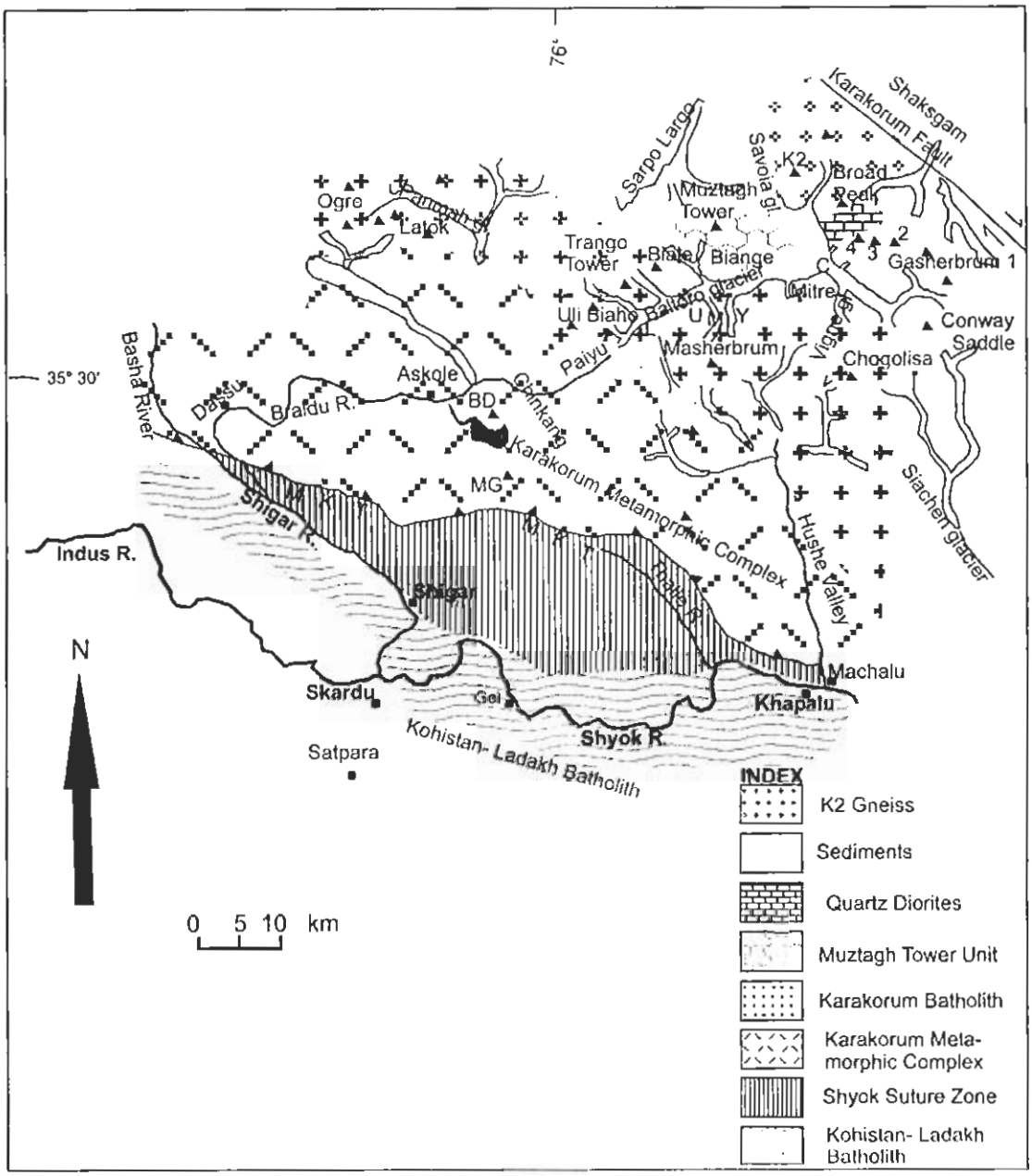


**Fig. 2. 2.** Simplified geological sketch map of the Central Karakoram between Skardu and K-2, showing the three main subdivisions of the Karakoram Terrain: the northern terrain, the Karakoram batholith and the Karakoram metamorphic Complex.

Key: MKT: Main Karakoram Thrust; BD: Bakhor Das; MG: Mungo Gusar; L: Liliwa camp site; U: Urduks; M: Mundo Glacier; Y: Yermanando Glacier; C: Concordia; BL: Brianta Glacier; 1-4 Nos: Gasherbrum Peaks (after Searle, 1991)

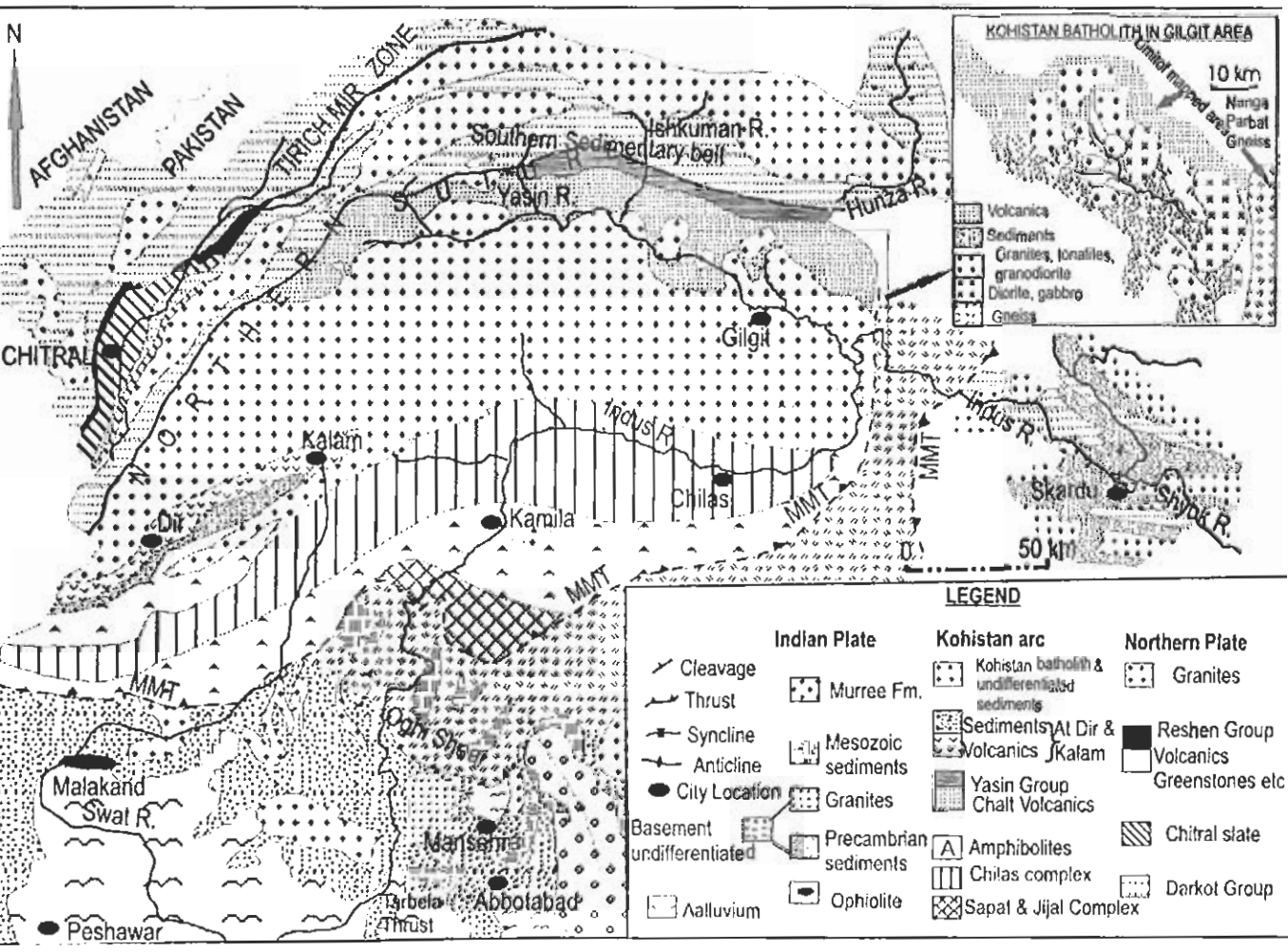


**Fig. 2. 3.** Geological map of Kohistan (after Tahirkheli and Jan, 1979; Coward et al., 1986).

Inset shows detail of the Kohistan Batholith in the Gilgit area (after Petterson, 1985; Searle, 1991).

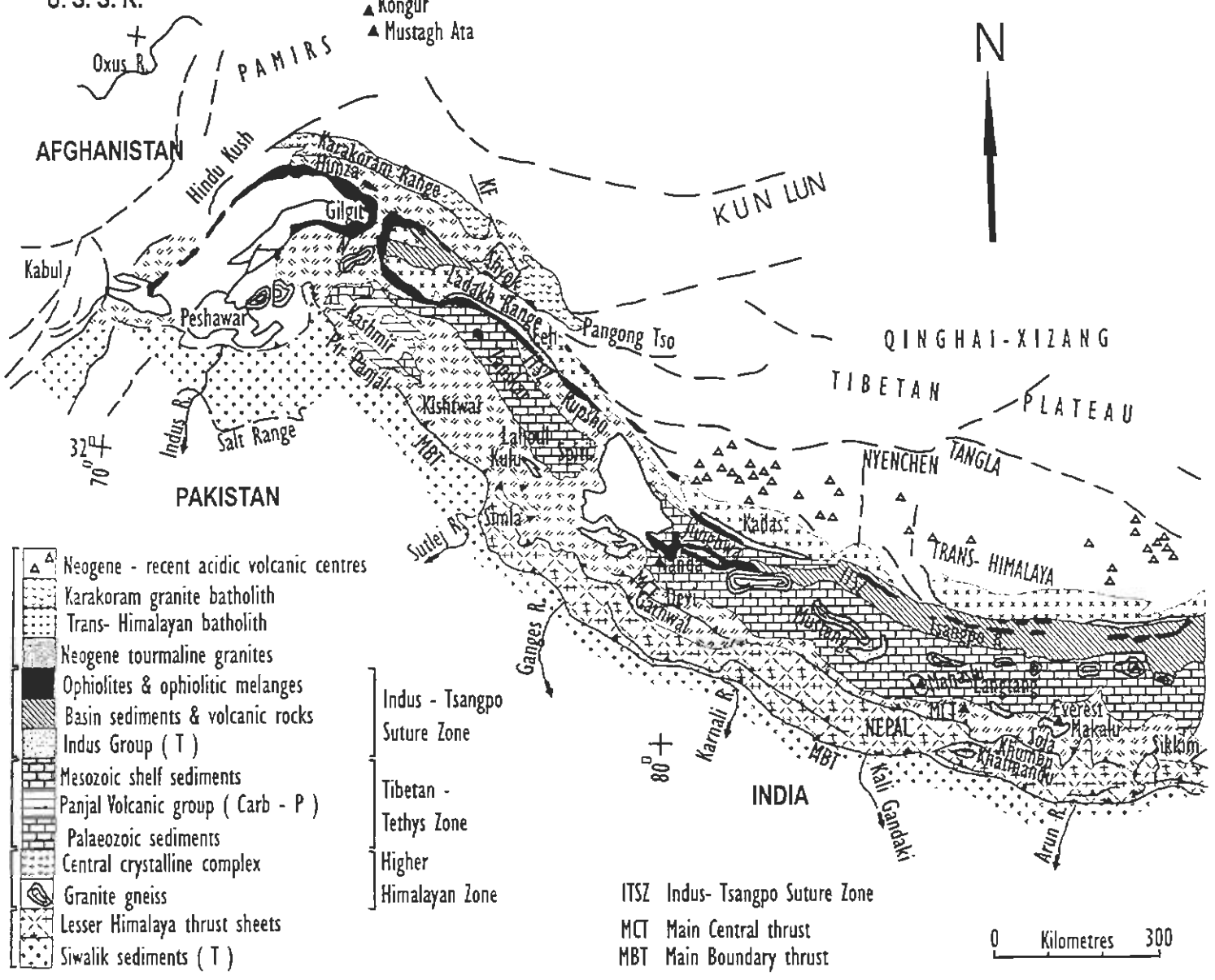


**Fig. 2. 4.** Geological map of the Himalaya and Karakoram showing location of major lithotectonic units (after Searle, 1991).

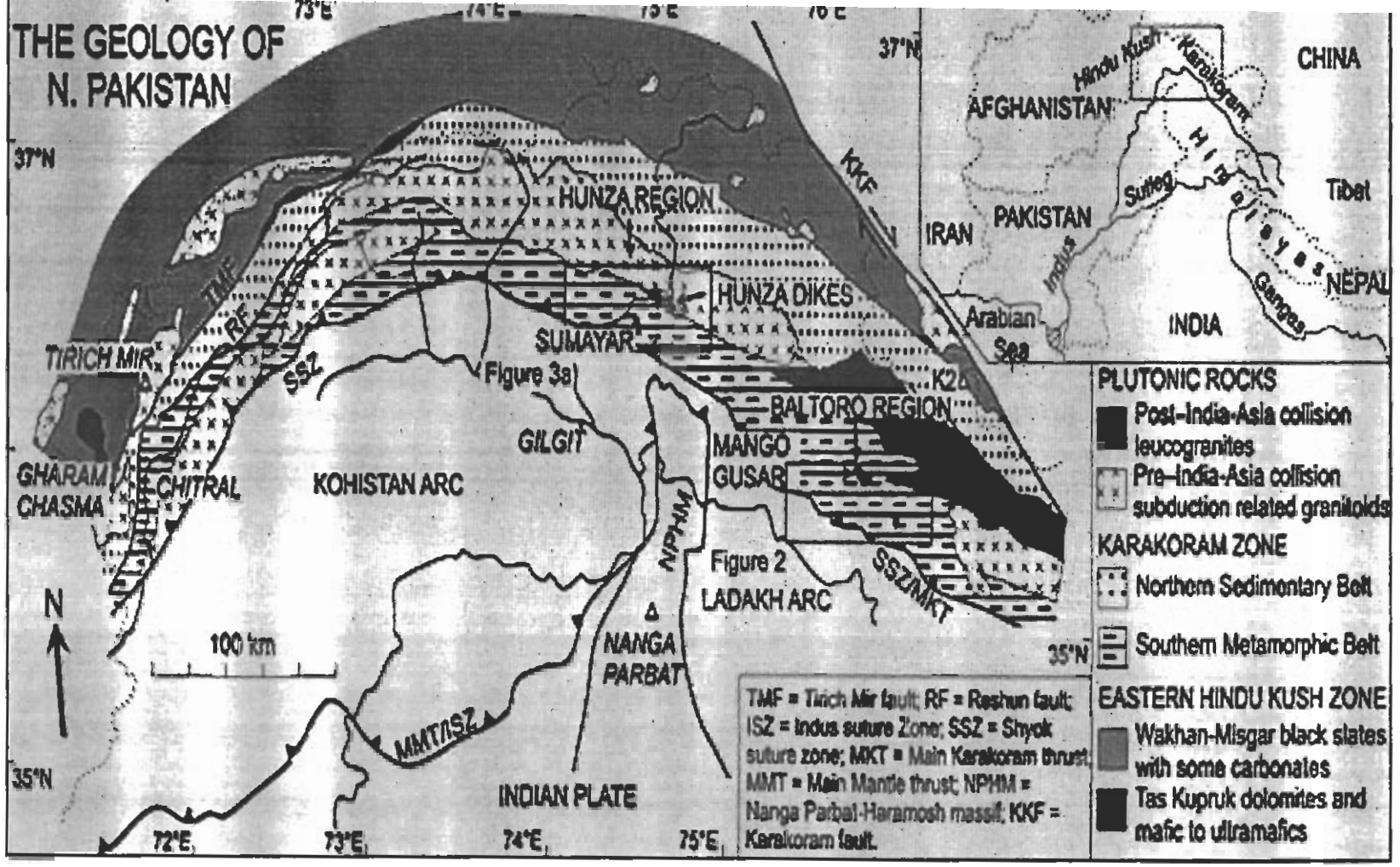


Fig. 2.5. Regional geological map of the Karakoram Plate. Note that Karakoram Strike Slip Fault bounds the plate in its east and Shyok Suture Zone (Main Karakoram Thrust) in the south. The Tirich Mir Fault (TMF) divides the plate into the Karakoram Block in the south and Eastern Hindukush Block in the north (After Fraser et al., 2001; Gaetani, 1997; Searle and Khan, 1996).

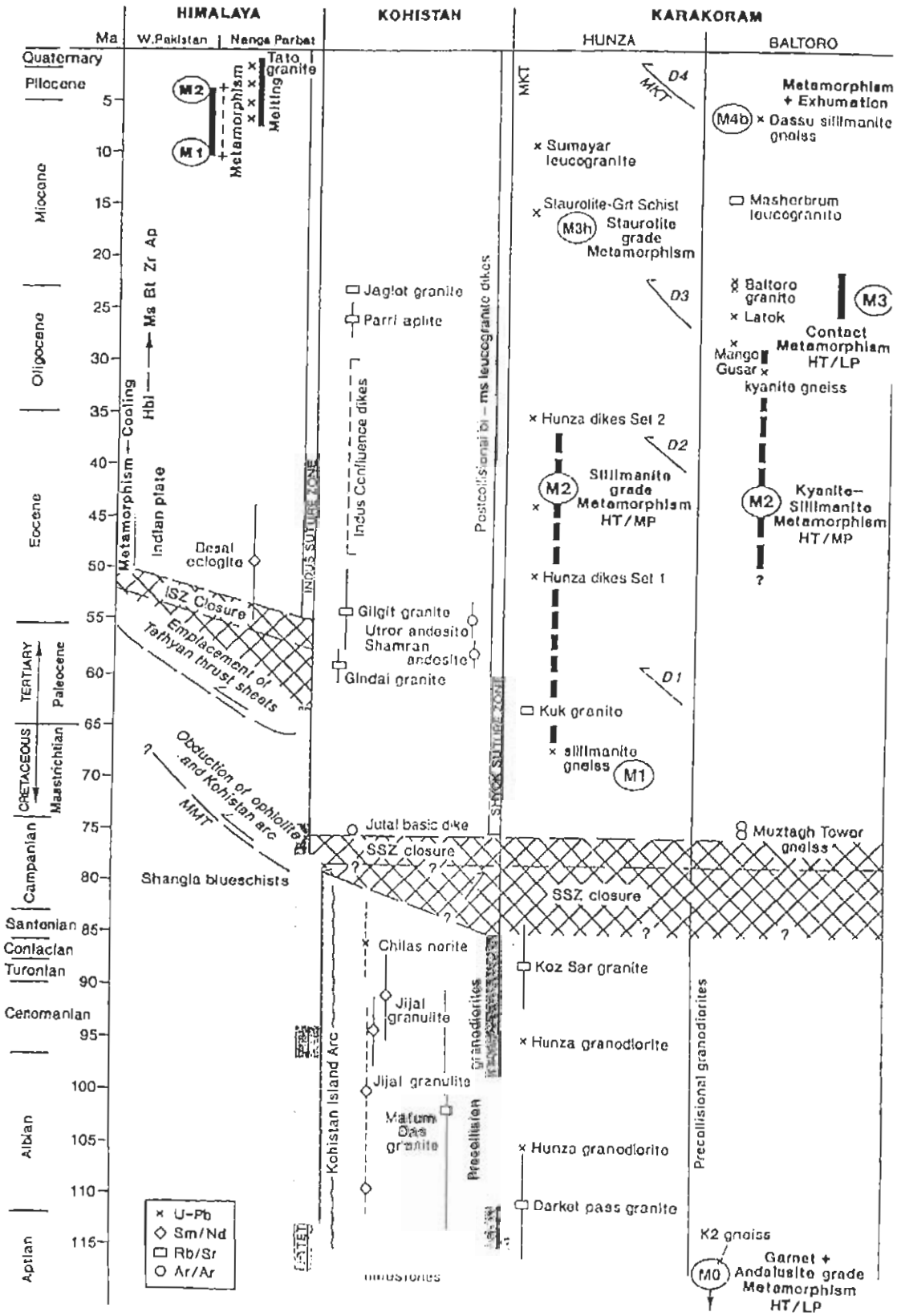


Fig. 2. 6. Cretaceous-Tertiary time chart showing all reliable radiometric dates for the Pakistan Himalaya including Nanga Parbat, Kohistan and the Hunza and Baltoro Karakoram (after Searle et al., 1999).

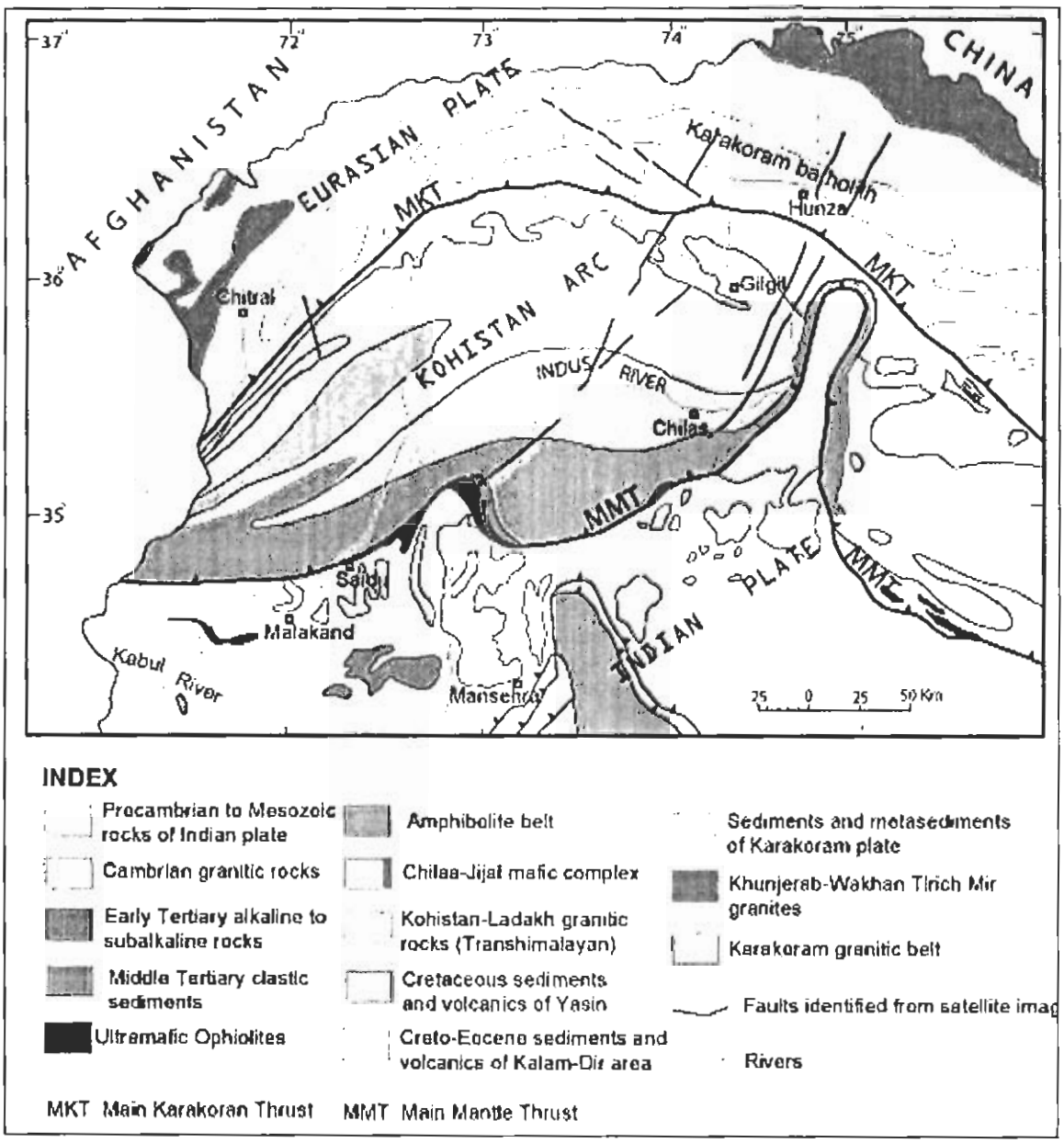


Fig. 2. 7. Geological map of the Kohistan (modified after Sweatman et al,. 1995)

# CHAPTER 3

## GEOLOGY OF THE SHIGAR VALLEY (STUDY AREA)

From the structural and tectonic point of view, the Shigar valley is situated partly on the northern end of the Kohistan-Ladakh island arc and partly on the southern edge of the Asian plate. The Northern Suture or the Main Karakoram Thrust (MKT) is passing through the center of the valley and separates the metasediments of the Asian plate from the volcanoclastic rocks of the Kohistan-Ladakh island arc (Fig. 3.1). The oldest rock unit exposed in the study area is the Daltumbore Formation of Carboniferous age that belongs to the Asian plate (Hanson, 1989). Considerable work has been done in the study area from structural, tectonic, and metamorphic point of view and as a result various lithologic units have been recognized. In this regard, the previous work has already been described in chapter one.

As far as the magmatic activity is concerned, the plutons both of pre-and post-collision have intruded the Kohistan-Ladakh island arc and also the Asian plate. The grade of metamorphism in the Shigar valley varies from chlorite to the amphibolite grade facies. In this chapter the general geology of the Shigar valley is discussed in detailed which is the focus of the present study.

### Major Stratigraphic units

The main stratigraphic units exposed in the Shigar valley area are the Bauma-Harel Formation, Katzarah Formation, Daltumbore Formation and the Dassu Gneiss. Besides, plutonic bodies of both pre and post-collision are also present. These units are briefly described as below.

**Rock units south of the Main Karakoram Thrust**

**Katzarah Formation:** This formation is composed of high-grade metasediments exposed around the Skardu and in the lower Shigar valley. The Katzarah Formation for the first time was described by Desio (1963; 1964) and then Zanettin (1964). They divided the Katzarah Formation into four units namely the Tsordas gneiss, the Skoyo gneiss, the Askore amphibolite and the Katzarah schist but following Tahirkheli (1982) and Cronin (1982); all these units were put together by Hanson (1986; 1989) and he called them as the Katzarah Formation. The maximum thickness of this formation is about 1500m.

The Katzarah Formation consists of quartz-plagioclase-biotite schists, sillimanite schists, gneisses, amphibolites, and granofelses with abundant calc-silicate minerals. These rocks are dark to brownish-gray in color, hard and resistant. Towards the northeast of this unit, the marble beds ranging in size from 5 to 50 m thick (Fig. 3.1) are exposed along the northern side of the Shigar-town (Hanson, 1986; 1989). A large part of the unit is a hornfels baked by intrusions, which are related to the Ladakh batholith. In addition to this, certain other dykes and sills of varying chemistry are also exposed in this unit along the lower reaches of the Shigar river (Hanson, 1986). Regional metamorphic grade in the formation is generally in the garnet and sillimanite grade facies. Sillimanite and K-feldspar-bearing rocks occur along the Indus river below Kachura. Complex fold structures on local scale are common in this unit. However, interlayered marbles and schists on the northeastern side of the unit near the contact with the Bauma- Harel Formation have a fairly uniform northwest strike and steep northeast dip (Hanson, 1989). Le Fort et al. (1995) suggests that the Askore amphibolites of the Katzarah Formation may have been derived from Dras volcanics (probably Dras-1 volcanics of Roberston and Degnon, 1994).

The age of this formation is unknown as it is devoid of fossils, however, Hanson (1986) assumed Cretaceous age for this formation on the basis of lithological correlation.

**Bauma-Harel Formation:** The name Bauma-Harel Formation was used by Desio (1963; 1964), because it is well exposed in the Bauma-Harel Lungma in the Shigar valley (Fig. 3.1). This formation mainly consists of volcaniclastic metasediments that have been metamorphosed under chlorite-epidote greenschist grade facies. The greenschists are interbedded with slates, phyllites and minor carbonate layers. Multi-colored conglomerate containing clasts of red and black shale, white marble and greenschist are exposed in the Bauma-Harel and Skoro Lungma areas. As the greenschists are composed of chlorite + epidote + albite + quartz and calcite, it is suggested that these rocks may have been derived from basic igneous rocks (Hanson, 1986).

The Bauma-Harel Formation also crops out on the right side of the Shigar valley to the northwest of the Gulab Pur and Tissar villages (Fig. 3. 1). Here the greenschists are interlayered with biotite-schists and thick bedded marble but here the grade of metamorphism is slightly higher. The Katzarah Formation is in contact with the Bauma-Harel Formation in southwest, while in the northeast in the Shigar valley it is bounded by the MKT (Fig. 3. 1). It's average thickness is about 9 km . Bedding in the Bauma-Harel Formation has a fairly uniform attitude. It is striking northwest and dipping 60 to 80° northeast while minor isoclinal folds are also common.

A group of greenschists and metavolcanics occurs all along to the south of MKT and north of Kohistan-Ladakh Island Arc (KLIA) (Tahirkheli, 1979; 1982; Brookfield, 1980; Pudsey, 1986). This unit starts from Chitral in the west and reaches up to the east of Skardu and is differently named by various workers. The greenschists of the Bauma-Harel Formation are correlated with the Rakaposhi Volcanic Group of Tahirkheli (1982). However, previously this group of rocks was as 'Greenstone Complex' (Ivanac et al., 1956). The metavolcanics of the Shigar valley are also locally known as Shigar volcanics (Punjab Univ. exped., 1985). In the west, the metavolcanics of the Shigar valley are also comparable with the Chalt volcanics and the Gawuch Formation (Hanson, 1989).

The Bauma-Harel Formation has been assigned Cretaceous age on the basis of fossils (Hanson, 1986). Tahirkheli (1982) reported lower Cretaceous Globotrunca fossils

near the Tissar village in the Shigar valley and Thaninasteria fossils in the greenschists of the Ghizar valley west of the Gilgit. Besides, Pudsey et al., (1985) have reported Orbitolina in Chitral, and Pudsey (1986) assigned Aptian-Albian age to the Yasin Group sediments. In addition to this, Hanson (1986; 1989) documented Turritellid gastropods of Cretaceous age from the shale beds in the upper part of the Bauma-Harel Formation in the Shigar valley.

**Rock units north of the Main Karakoram Thrust**

**Daltumbore Formation:** Daltumbore Formation is the oldest rock unit in the study area and it is mostly composed of interbedded layers of slates and marbles along with schists, phyllites, and amphibolites (Fig. 3. 1). Hanson (1989) named this formation after the type locality Daltumbore Lungma. However, in (1986) he has also used the Baltit Group of Stauffer (1968) for this rock unit in the Shigar valley area. But Desio (1963; 1964; 1979) included these rocks into the Dumordu Formation. Before this, Ivanac et al. (1956) included all the metasedimentary rocks south of the Karakoram Axial Batholith and north of MKT into his Darkot Group and extended it in the east as far as the Shigar valley and in the west to the vicinity of Mastuj in Chitral. Tahirkheli (1982) has also retained the Baltit Group of Stauffer (1968) for the metasedimentary rocks of the Asian platform north of MKT and he also included the Chitral Slates into the Baltit Group. Searle (1991) included all the metasedimentary rocks of the southern sedimentary belt (i.e., between MKT and Karakoram Axial Belt) into "Karakoram Metamorphic Complex", especially the terrain from the Hunza-Hushe valleys in the central Karakoram. This formation is in faulted contact southward along the Northern Suture with the Bauma-Harel Formation of Kohistan-Ladakh island arc and the grade of metamorphism increases northwestward along the strike. Desio (1963; 1964) and Zanettin (1964) have mapped the Shigar valley area and classified the rocks of the Daltumbore Formation into three lithologic units following the grade of metamorphism. These rock units are: the Skoro Lungma slates, the Daltumbore micaschists and the Askore amphibolites. Here the individual beds can be traced for at least 10 km along the strike and are mapable. This is the reason that Hanson (1989) proposed the name 'Daltumbore Formation' for the Baltit Group of Stauffer

(1968) and the three units of Desio (1963; 1964) in the northwest side of the Shigar valley area. The beds in the Daltumbore Formation are folded into a large anticline and syncline. The cores of which are visible above the Sildi village. Minor isoclinal folds are also common in the Daltumbore Formation and the facing directions are uncertain in the unit. But Hanson (1986; 1989) has reported graded bedding with facing directions towards northeast in the Lower Skoro Lungma area. Hanson (1986) has reported the out crop thickness of Daltumbore Formation as ~ 7 km in the stduy area. However, the original thickness of the unit is difficult to measure and it may be more than as reported (See Desio, 1964; Searle et al., 1986).

Brookfield and Gupta (1984) have reported Permian brachiopods, crinoids, and bryozoans in limestone beds in the Upper Bauma-Harel Lungma above the confluence with the Yaltsa Lungma. Tirrul (1987) and Chamberlain and Allen (1987) have reported Mississippian conodonts, also from a limestone bed in the upper Bauma-Harel Lungma and horn corals from the Thalle valley that may be of Devonian. So according to Hanson (1986), this fossil record indicates a Permo-Carboniferous age for the Daltumbore Formation and is also consistent with the Permo-Carboniferous Darkot Group of Ivanac et al., (1956).

**Dassu Gneiss:** The Dassu gneiss (named by Desio 1963; 1964) is granodioritic augen gneiss occurring in the upper part of the Shigar valley and in the lower part of the Braldu valley around the village of Dassu (Fig. 3.1). The Dassu gneiss is making a domal structure and gneiss domes of this kind also occur in several other places of the KMC (Allen and Chamberlain, 1991; Searle, 1991; Le Fort et al., 1995). Dassu felsic gneiss is mainly composed of two-feldspar, quartz, biotite, and muscovite with garnet, tourmaline, apatite, hornblende, and zircon as accessories. It intrudes the schists and marbles of the Daltumbore Formation almost just above Kashmol village and contains xenoliths of host marble, which have been altered to diopside-grossular granofelses. Above Kashmol village, the gneiss is in contact with some metamorphosed sills belonging to the meta-igneous series of pre-collision intrusions. It is, therefore, clear that the Dassu gneiss is younger than the metamorphosed dykes, sills, and the Daltumbore Formation. Several

pegmatite and leucogranite dykes and veins are common in this gneiss. In the Shigar valley area, the host rock of almost all the gem-bearing pegmatites is the Dassu augen-gneiss. The gneiss is strongly foliated, but it exhibits an igneous texture in thin sections and the mica and quartz grains show no kinking or undulatory extinction. The foliation may be a flow structure rather than a deformation structure. If so, it is probable that the Dassu gneiss is late or post-tectonic. Searle (1991) has reported a plateau age of 7.3 ± 0.2 Ma on a sample from Dassu gneiss. This age is identical to the $^{40}Ar$ / $^{39}Ar$ age spectra from the Baltoro monzogranite and it is clear that the BPU and the KMC have followed a similar cooling history since the Late Miocene. In addition to this, Searle, (1991) has reported K-Ar biotite ages of 7.1 ± 0.28 and 4.69 ± 0.19 Ma on two samples from Dassu orthogneiss. These ages indicate extremely young cooling, uplift, and exhumation (Searle, 1991). The Dassu gneiss dome crops out along the hanging wall of the MKT and the cooling ages show that uplift on the thrust continued until Pliocene times (Searle, 1991; Fraser et al., 2001). Hanson (1989) referring Barbara Barreiro reported an inherited age of ~1 b.y. using U-Pb isotope studies on zircons from the Dassu gneiss.

## Other igneous rocks of the study area

Several igneous rocks of pre-and post-collision in the form of small plutons, dykes, and sills are exposed in the study area on either side of the Northern Suture or MKT. The earlier phases of these intrusions have been deformed and metamorphosed to various grades, while the younger phases are undeformed and unmetamorphosed. Igneous intrusions north of the Main Karakoram Thrust have been assigned to the Karakoram batholith, while the intrusions south of the MKT have been assigned to the Kohistan-Ladakh batholith. In addition to this, Searle (1989; 1991) collectively called the metamorphic rocks of the central Karakoram between MKT and Karakoram Axial Batholith as Karakoram Metamorphic Complex (KMC). Multiphase metamorphism and deformations have occurred into the KMC. These igneous intrusions occurring on either side of the MKT in the study area are described below.

**Igneous intrusions north of Main Karakoram Thrust (MKT):** The metamorphosed igneous rocks exposed north of the MKT in the study area are mostly gabbro to granodiorite in composition and the dykes and sills of this stage have intruded the sediments of the Palaeozoic Daltumbore Formation. Such rocks are prominently exposed in the Lungma between Alchuri and Sildi villages, where these intrude the country rocks lit par lit. Besides, several metamorphosed mafic dykes and sills are exposed both north and south of Kashmol village (Plate. 3.1). These rocks are metamorphosed and variably foliated. Some of the foliations are due to the laminar flow, indicated by elongate xenoliths that are parallel to the walls of the sills. However, metamorphic minerals in the sills are also oriented parallel to the country rock foliations, this is true for platy and prismatic minerals (micas and amphiboles). This indicates that the rocks were emplaced before the major metamorphism and deformation in the region, and, hence, before the closure of the Northern Suture. Two prominent metamorphosed sills intruding a marble bed are well exposed in the Daltumbore Lungma and in the Lungma east of Hurchus village (Hanson, 1986, 1989).

The meta-igneous rocks in the Shigar valley north of the MKT may be related to the earlier phases of magmatism that is reported from Hushe Complex in the east and the Hunza Plutonic Complex (HPC) and the Darkot Group in the west (see Tahirkheli, 1982; Searle, 1991; Kazmi and Jan, 1997).

**Igneous intrusions south of Main Karakoram Thrust (MKT:** Igneous intrusions of various episodes south of the MKT in the study area, are part of the Kohistan-Ladakh Batholith. These intrusions originated in three stages. The intrusions of the first stage have been metamorphosed and deformed; those of second stage have been sheared and hydrothermally altered in places, while those of third stage are generally mafic dykes which intrude both the intrusions of earlier two stages (Hanson, 1986, 1989). However, this last stage of intrusion is also affected to some extent by a few minor late stage faults (Hanson, 1986). These three stages are described below:

a) **Deformed and metamorphosed intrusions of first stage:** Rocks of this stage are exposed near the Shigar village. The main body is a biotite tonalite that extends from Shigar village across the river to the southeast base of the Marshakala Peak. The foliation in these rocks is generally parallel to the foliation of the wall rocks. This indicates that the pluton was pretectonic and was deformed at the same time as the metasediments. Hanson (1989) had correlated this pretectonic pluton with the 100 m.y. old Nomal pluton near Gilgit described by Petterson and Windley (1985) and Debon et al. (1987). The tonalite near the Shigar village is mainly composed of quartz, plagioclase, and biotite, but it contains abundant secondary epidote with other calc-silicate minerals and garnet occurring in places. These rocks also contain irregularly shaped pods of quartz and calc-silicates that are apparently due to contact metamorphism of calcareous inclusions engulfed by the tonalite.

b) **Undeformed intrusion of second stage:** Rocks of this stage occur all around the Skardu basin and are also exposed at some localities within the Shigar valley. This magmatic phase has intruded the Katzarah and Burji Formations. These intrusive bodies are the off shoots of the main Ladakh batholith of the Deosai plateau to the south, and probably have a similar Eocene age (Searle, 1991; Hanson, 1986). The rocks range from hornblendites to granites, with the dominant minerals (i.e., quartz, two feldspars, biotite, and hornblende). No pyroxenes are found in these rocks. These rocks are non-foliated and most are unaltered except for the presence of some minor secondary epidote and sericite (Hanson, 1986).

In the Shigar valley, a mafic complex (about 2 km diameter) of this stage consisting of hornblendites and hornblende diorites is exposed at Strongdokma La south of the Shigar village (Fig. 3.1). This complex is completely surrounded by granodiorite and granite and is probably an autolith of cumulate or a restitic phase that was carried to its present position by felsic magma (Hanson, 1986; 1989). In places, such as the upper southwestern side of the Shigar valley and at the mouth of the Skoro Lungma, these younger intrusions have been sheared and hydrothermally altered. This indicates that

faulting continued after this younger intrusive stage, even though the major deformation occurred earlier.

c) **Mafic dykes of third stage:** Several mafic dykes of the last stage cut the plutons of the earlier two stages as well as the structures of the Katzarah Formation. These dykes of basaltic to andesitic composition are fine-grained, undeformed, unmetamorphosed. These are also affected by minor faults, indicating that the region was still tectonically active after their emplacement. These dykes have not been dated, and their origin is still debatable (Hanson, 1986).

Hanson (1986; 1989) classified the igneous rocks of the Shigar valley south of the Main Karakoram Thrust into I-type. They are low in aluminum and rich in Na, Ca, and Sr. Muscovite is rare, whereas biotite and hornblende are the common minerals in these rocks. According to Coward et al. (1986) and Debon et al. (1987) these plutons may have been formed due to subduction of oceanic lithosphere beneath the arc, rather than by partial melting of upper crustal or sedimentary rocks.

In addition to this, a plutonic body of tholeiitic character near the Shigar village is exposed and this body may be correlated well with the pre-tectonic Nomal pluton north of Gilgit (Hanson, 1986; 1989). In this way, it supports the theory of Debon et al., (1987) that the pretectonic intrusive phase of the KLIA was characterized by more tholeiitic rocks, compared to the calc-alkaline/subalkaline rocks of the post-tectonic phase (Searle, 1991; Kazmi and Jan, 1997).

## Metamorphism in the Shigar valley

Metamorphism in the study area is highly variable. Regional metamorphism ranges from sub-chlorite grade (sub-green schist facies) to sillimanite-K-feldspar grade (uppermost amphibolite facies, possibly as high as granulite facies). Besides, contact metamorphism is also evident in the form of hornfelses. The regional metamorphic

isograds are cut by the Main Karakoram Thrust or MKT, indicating that the regional metamorphism occurred before the closure of the suture (Hanson, 1986). The metamorphism occurred on both sides of the Northern Suture in the Shigar valley and that is described below.

**Metamorphism south of the Main Karakoram Thrust or MKT:** The highest metamorphic grades south of the Main Karakoram Thrust or MKT are near granulite grade facies and these occur in the form of a northwest-southeast trending belt. The granulite facies rocks have been characterized by the presence of four minerals (i.e., cordierite-garnet-sillimanite-K- feldspar). Hanson (1986) reported that these minerals can not be found as assemblage at one place but can be found separately in the field area. Sillimanite- bearing rocks occur all around the base of Marshakala Peak, and along the Indus river between Kachura and Basha. The sillimanite-K-feldspar assemblage occurs across the Indus river near Basha. On the right side of the Shigar valley near the village of Nielle, Hanson (1986) reported cordierite along with garnet. In addition to this, sillimanite is also present in the same out crop but K- feldspar is absent. Northwest of the high-grade metamorphic belt, the rocks retrograde from sillimanite grade to sub-chlorite grade across from Shigar village up to the Bauma-Harel Lungma (Hanson, 1986).

The heat source for this metamorphism is uncertain and even at least it may not be related to the Eocene Ladakh intrusions, as there is no spatial relation to the isograds. The field relations show that the Ladakh plutons have intruded the chlorite as well as the sillimanite grade rocks, so it is clear that the Eocene Ladakh intrusions are younger than the metamorphism. But it is probable that the metamorphism may be related to a pluton of Cretaceous age, which is exposed at the foot of Marshakala and it is also evident from the grade of metamorphism as it increases from Bauma-Harel Lungma towards Marshakala (Fig. 3. 1). But as this pluton is also a small one, so it is difficult to relate such a high-grade metamorphism to the intrusion of this pluton (Hanson, 1986). In addition to this, Searle (1991) also favours a pre-collision (India-Asia) metamorphism around the Skardu basin and relate it either with pre-collision plutonism or possibly with

the collision of the Karakoram plate with the Kohistan-Ladakh island arc along the Main Karakoram Thrust.

In addition to the regional metamorphism, contact metamorphism has also occurred in and around the Shigar valley. This contact metamorphism is related to the Eocene plutons, which are scattered throughout the Shigar valley and most of the country rocks have been baked to dense hornfels which retain little of their original foliation (Hanson, 1986; 1989).

b) **Metamorphism north of the Main Karakoram Thrust or MKT:** Isograds in the Daltumbore Formation north of the Main Karakoram Thrust run nearly perpendicular to the trace of the suture, and increase in grade to the northwest from subchlorite grade rocks in the upper Bauma-Harel Lungma to garnet grade rocks in the Daltumbore Lungma and adjacent to the Dassu Gneiss. In addition to this Hanson (1986) has also reported staurolite in the rocks between the villages of Alchuri and Sildi.

Rocks, even of higher grade have also been reported in areas adjacent to the Shigar valley. Searle et al. (1986) reported that kyanite-staurolite schists occur along the Braldu River near Askole, and that the kyanite and staurolite react to form sillimanite and muscovite further up stream towards the Karakoram Batholith (Baltoro granite). They suggest that the retrograde metamorphism had occurred along the Main Karakoram Thrust. These findings seem to be consistent with the low-grade rocks found in the eastern part of the Shigar valley (Hanson, 1986).

The heat source for such a metamorphism is not clear. Due to the post-tectonic intrusion of Dassu gneiss, the metamorphism could not be related to this intrusion. This metamorphism may be related to the pre-tectonic stages of the Karakoram Batholith, which are reported in the east of the field area in the Hushe valley region of the central Karakoram (Fig. 2. 2). However, such type of pre-collision magmatism is not present in the field area. Although the Cretaceous dykes and sills exposed in the study area are also

metamorphosed, so they must be separated from any intrusion that might cause such a regional type of metamorphism. If the metamorphism is related to the plutonism, the plutons must have been emplaced after the dykes and sills intruded in the rocks of the Shigar valley, but before the closure of the Northern Suture. Hanson (1986; 1989) following Searle et al. (1986) described a retrograde metamorphism for such isograds on a regional scale.

**Pegmatites of the Shigar valley area**

In northern areas of Pakistan, the gem-bearing pegmatites have been known from various localities of the three geological domains, such as the Karakoram, the Hindukush, and the Indian Plate (particularly the Haramosh region). The majority of the gem-bearing pegmatites are related either to the Haramosh Range of the Indian plate such as the gem-bearing pegmatites of the Stak Nala, Khaltaro, and Shingus or to the Main Karakoram Batholith such as the gem-bearing pegmatites of the Shigar valley, Hunza valley, and the pegmatites of the Masherbrum and Hushe areas.

The Shigar valley area is unique amongst the other regions of the northern Pakistan in the sense that a variety of gemstones are found mostly from the pegmatites as well as some metamorphic rocks from this valley. The pegmatites of the Shigar valley are well concentrated near the village of Mungo or Haiderabad up to Kashmol village along the Shigar river and from Dassu to Goyungo villages along the lower Braldu river (Fig. 3. 2). The pegmatites of these areas are diverse and different not only in their mineralogy but also in internal structure, texture, dimension and thickness. Majority of the pegmatites in the study area are zoned but some unzoned pegmatite dykes and veins are also noticed. Some pegmatites have symmetrical zoning (i.e., repetition of same zone on both sides of the dykes or veins) (Plate. 3. 2), while others are asymmetrical. It is the known fact that the zoned pegmatites have almost four zones but it is not necessary that four zones should always be present in any zoned pegmatite. Some pegmatites from all over the world with two or three or even 5 - 6 zones or sub-zones are also known (Cerny, 1982a,b). The pegmatites of the Shigar valley also have variable zoning. In case of zoned pegmatites,

each zone is lithologically, compositionally, and texturally different from the other zones. In some of the symmetrically zoned pegmatites (those occur near Dassu and Baha villages; Fig. 3. 2), the outer border zone is commonly fine-grained with a pronounced layering and are similar to those reported by Webber, et al. (1999) from the pegmatites of San Diego County, California and may be called as aplitic or "line-rock". About 50 - 60 pegmatite dykes (both the gem-bearing and gem-barren) are exposed into the Shigar valley area, but the exact number can not be counted due to rough topography and steep slopes.

In case of zoned-pegmatites of the Shigar valley, the four zones from margin to core are determined as: the outer aplitic zone, the wall zone with two-feldspar + two mica (mostly muscovite) + quartz, the coarse-grained intermediate zone with variable mineralogy (the zone of gem pockets or cavities) and the core zone with either massive or large euhedral quartz crystals. There is always a close relationship between pegmatites and aplites and these two leucocratic rocks almost occur together but pegmatites may also occur without aplites that are present either at the margin or core of the pegmatites (Jahns, 1953; Laurs et al., 1998). However, majority of the zoned-pegmatites in the Shigar valley are without aplitic border zone. Besides the thickness of the dykes and veins; the internal zones of these bodies are also different in thickness.

In some dykes or veins the outer aplitic border zone is about 2 to 5 cm wide, while in others it is almost absent. The major zone of the zoned pegmatites is the intermediate coarse-grained zone, which is the actual zone, in which the pockets or cavities of variable sizes and shapes are present either at the center of this zone or at the margin of the core zone, which hold various combinations of gemstones. But majority of the gem-bearing cavities or pockets are present at the core-margin zone, where euhedral crystals of various gemstones with different combinations have been crystallized. As already mentioned that the sizes of these intrusive bodies are also variable as some are from few inches to 5 feet, while others are measured up to 5 meters in thickness such as the dykes near the village of Goyungo along Braldu river (Plate 3.3). The pegmatite dykes also vary in length in the study area. These are generally 40-50 m long but in some

cases like the pegmatite dykes near the village of Haiderabad or Mungo and Baha extend up to 2 km in length (Plate 3. 4).

In addition to the aplitic-pegmatitic dykes, the leucogranitic dykes composed of two feldspars, quartz and two micas are also exposed in the study area but these leucogranitic dykes concentrate mostly near the village of Dassu and along the upstream of the Braldu river, while these are absent along the course of the Shigar river. These pegmatites are barren as for as the gemstones are concerned. The pegmatitic dykes are generally cutting the foliations of their host rocks and no visible deformation has been seen in these pegmatitic and the leucogranitic dykes, which indicate that these dykes are very young. These dykes were emplaced in the late stages after the major multiphase regional deformation and metamorphism and are, therefore, considered to be post-tectonic.

The host rocks of these pegmatitic bodies are also variable throughout the length of the Shigar valley and belong to the two different geological entities (i.e., the Karakoram block and the Kohistan-Ladakh island arc). Searle (1991) and Searle et al. (1986; 1989) included all these rocks in the Karakoram Metamorphic Complex (Fig. 2. 2). From Yuno village up to the Goyungo village, the host rock of the pegmatites is Dassu biotite orthogneiss. But from Kashmol village up to the Alchuri village, the host rocks are mainly the metasediments and metaigneous rocks of the Daltumbore and Bauma-Harel Formations (Fig. 3. 1).

As some gemstones are common in the entire Shigar valley such as beryl (aquamarine), tourmaline (schorl) but some gemstones (e.g., epidote (Zabarjad), sphene (titanite), yellow apatite, diopside, goshenite, manganotantalite) are confined to certain localities. This indicates that various geochemical processes have been involved in the formation of these gemstones within the pegmatites and it is also possible that some of gemstones may be the result of either metamorphism or contact-metasomatism in the lower Shigar valley. This is further discussed in chapter six, where the mineral chemistry and paragenesis of each gemstone along with other pegmatitic minerals is described in

detail. The gemstones such as the diopside, epidote, clinozoisite, titanite (sphene), and zoisite are being mined in the lower Shigar valley from Sildi village up to Hashupa village (Fig. 3. 2). These gemstones are present in both the magmatic as well as in the metamorphic terrains.

These gem-bearing pegmatites are being mined for aquamarine, topaz, tourmaline, fluorite, apatite by the local people and these gemstones are displayed in small shops of the Shigar valley. The exporters and mineral collectors related to the gem-industry are visiting the Shigar area for the purchase of these gemstones and export them either as polished or in a raw-form. The major source of income of the local peoples of this valley is the mining of the gemstones along with sparse agriculture.

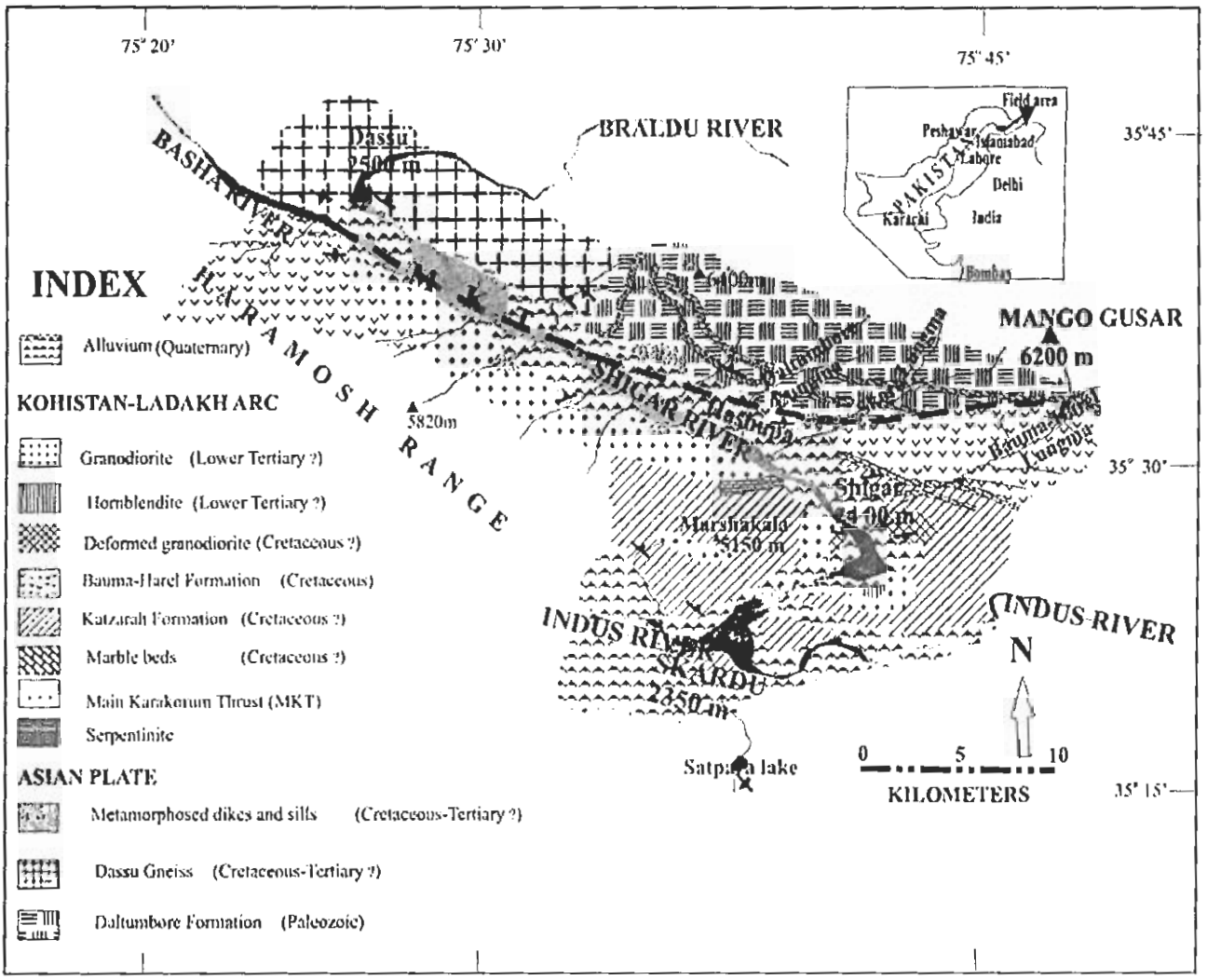


**Fig. 3. 1.** Geological map of the Shigar valley (after Hanson, 1986; 1989).

**Plate 3. 1.** An outcrop near the village of Kashmol, where metamorphosed mafic dykes and sills of pre-collision are exposed.

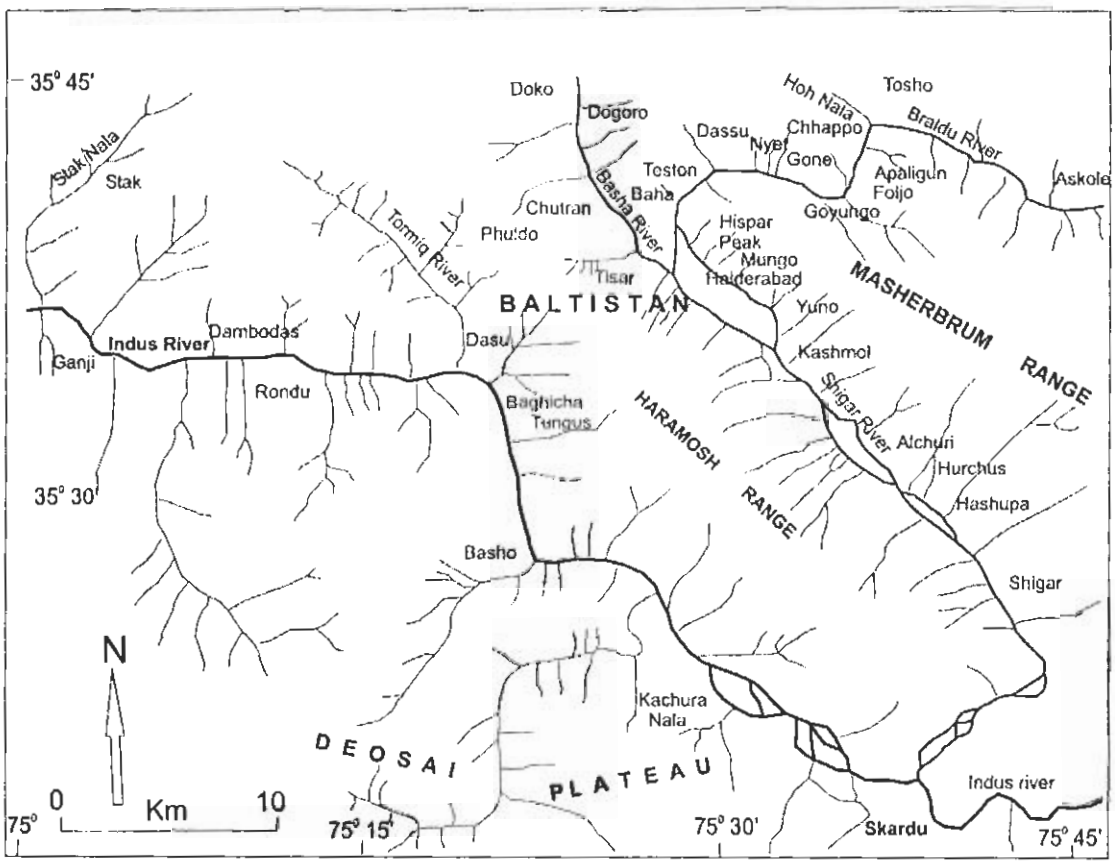


**Fig. 3. 2.** Map showing the different localities of the Shigar valley, where gem-bearing pegmatite dykes and veins are exposed.

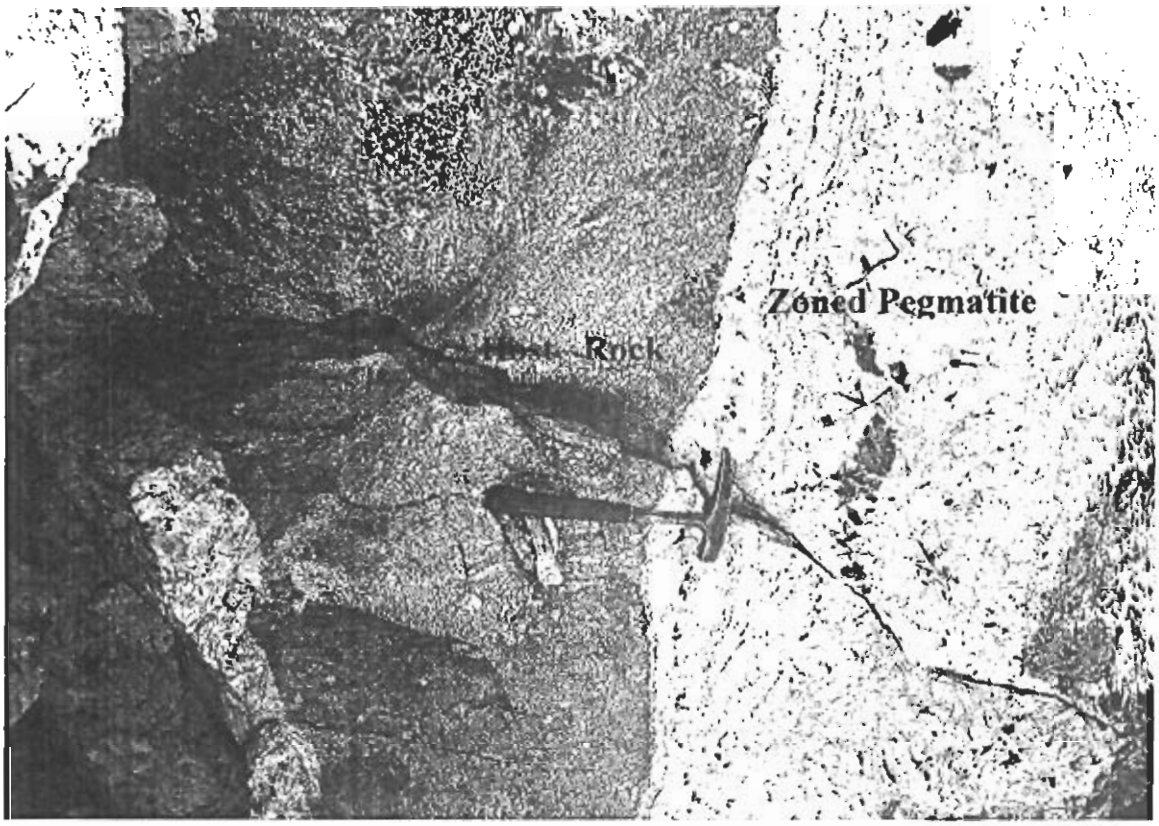


**Plate 3. 2.** Symmetrical-zoned pegmatite showing a sharp contact with the augen-biotite gneisses, the host rock at Dassu. The dyke is cross-cutting the host rock perpendicular to its foliation plane. The dyke is coarse-grained at the contact on both sides making a zone of ~ 3- 4 inches, then there is a medium-coarse grained zone of about 4 - 5 inches, again there is repetition of the coarse-grained zone at the foot wall of the dyke. Muscovite and biotite flakes of about 3-5 cm are also present as patches within this zoned pegmatite. In the hanging wall of the dyke, minute schorl crystals are aligned and making a thin layering that indicates the direction of propagation and crystallization of the dyke.

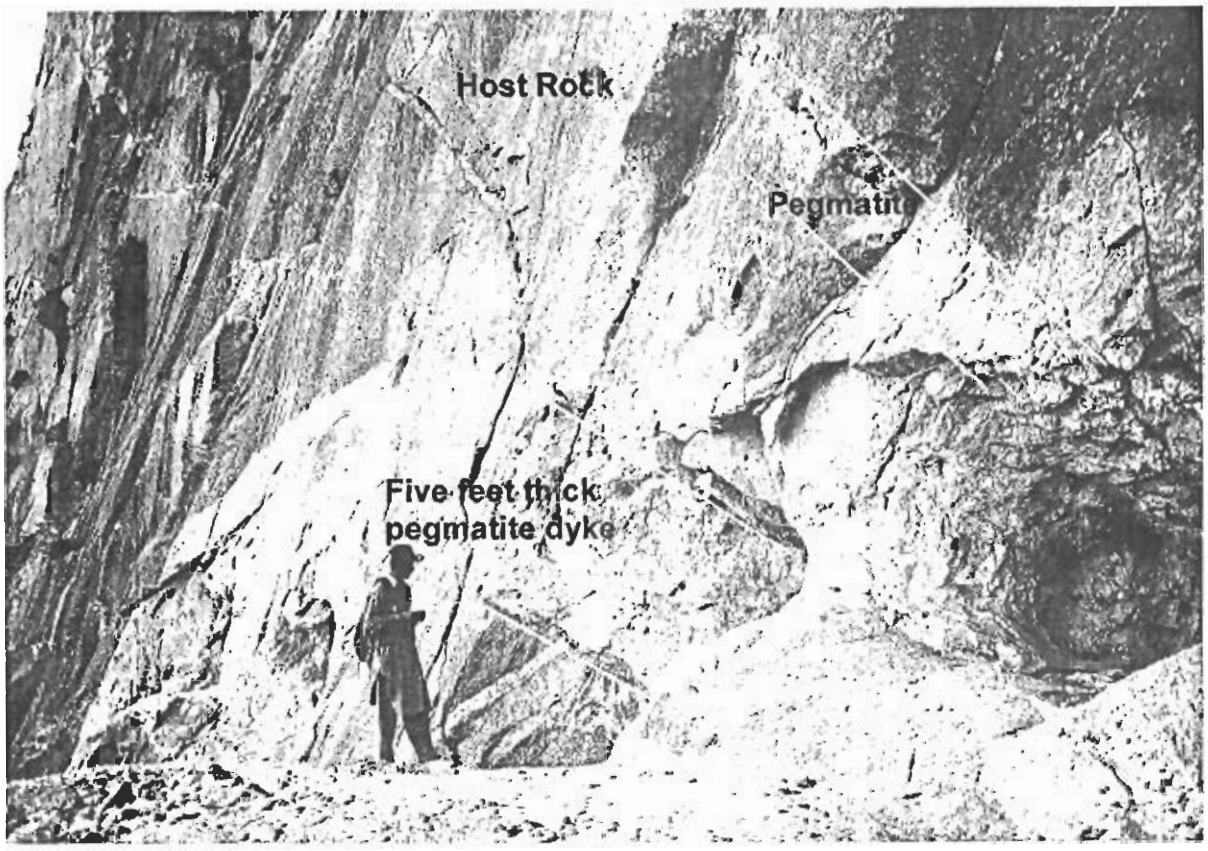


**Plate 3.3.** Photograph showing a pegmatite dyke about 5 feet thick within paragneisses near Goyungo, which has been mined and excavated for gemstones. Aquamarine, schorl, beryl, topaz and large crystals of quartz have been mined from these pegmatites. Beside the main dyke, veins of pegmatite about 2 feet are also visible.

**Plate 3. 4.** Photograph showing a horizontal, unzoned and simple pegmatite dyke within the Dassu biotite gneiss near the village of Baha. This dyke varies in thickness from 0.5 to 1.5 meter and extending for about half a km. On the surface, iron leaching close to biotite is very common.

# CHAPTER 4

## METHODOLOGY

### Field Methodology

**Collection of rock samples**

In case of zoned pegmatites, special types of sampling are required to better understand the progressive crystallization sequence of minerals and also to perceive the regional and internal zonation, textural, and mineralogical differences within the same or different bodies of pegmatite. In this regard, sampling should be done from almost every zone of the same pegmatite body while in case of regional zonation; samples should also be taken from the possible parent plutonic body to see the parent-daughter relationship. But, unfortunately this was not done in this study because of the following reasons:

- Because of the unavailability of the drilling equipments, the core sampling of the various zones was not possible to collect during field work. The collection of channel samples was also not possible because of the location of the pegmatites in the area.
- The easily accessible pegmatitic bodies in the Shigar valley are highly mined for various gemstones by the local people, so it is also difficult to get proper samples from different zones of such bodies.
- These pegmatite bodies are generally exposed in the study area where the Braldu Gorge has deeply cut the bed rocks and majority of these pegmatites are exposed at very high altitude and along almost vertical slopes, from where the collection of samples from each zone of zoned pegmatite is impossible.

So for the above-mentioned hurdles and difficulties, though the samples could not be collected from every zone of the same pegmatitic body, however every possible attempts were made to get the best and representative samples from various zones of the

pegmatites. Some of the pegmatites (e.g., Dassu pegmatite) were sampled very carefully to take the representative samples from every zone to investigate the crystallization behaviour of these zoned pegmatites. Moreover, sketch maps of some of the zoned pegmatitic bodies were also prepared on the spot.

Both the zoned as well as the unzoned pegmatite bodies are exposed in the study area. As it is generally considered that the unzoned pegmatites are not as productive both in the occurrence of gemstones as well as in the rare-metals as the zoned pegmatites, therefore, the majority of samples were collected from the zoned bodies. But some samples from the unzoned bodies were also collected to study the possible mineralogical and the geochemical differences. In order to study the internal mineralogical and textural differences, sizes of different zones and other field features of different pegmatites from different localities of the Shigar valley, photographs, sketch maps and field notes were also taken.

There is always a close relationship between the pegmatites and their host rocks, which are generally the metamorphic rocks. In certain cases, the processes of metasomatism and alteration of the host rocks do also occur either at the contact or even at a distance away from the margin. So for this purpose, samples of the host rocks were also collected from almost every sample location.

Some samples were also collected from pegmatites other than those of the Shigar valley for comparison purpose. These are about 200 km in the west of the Shigar valley and these are known as the Indus-Gilgit confluence pegmatites. These pegmatites are generally devoid of gemstones.

A total of 115 rock samples were collected during the present field work from pegmatites and their host rocks (Figure 4.1). Keeping in view the field features, sixty two (62) representative samples of both pegmatites and their host rocks were selected for petrographic, mineralogical and geochemical studies.

It is very difficult to collect the in situ gemstones from the studied pegmatites because these gemstones have been mined by the local people. However, attempts were made to collect the gemstone samples from the local people with proper identification of their location. In some cases, in situ gemstones within these pegmatites were also collected during field.

## Laboratory methodology

The selected samples have been treated with various laboratory techniques to get the best results. For this purpose, thin sections (both polished and unpolished) were prepared to show mineralogical and textural features on polarizing microscope, while the polished thin-sections (both of the gemstones and the pegmatites) were also used for mineral chemistry on the Electron Probe Micro Analyzer. For the whole rock chemistry, the rock samples were digested with acid mixtures and fusion complexes and the major and trace element analyses were performed by using atomic absorption, UV/Visible spectrophotometer. The trace element analyses were also performed on powder-pellets by using the X-Ray Fluorescence Spectrophotometer. In addition, the gemstones were also run on the X-Ray Diffractometer for the qualitative analysis. In case of gemstones, where it was difficult to identify them on X-Ray power diffraction patterns, they were analyzed on Scanning Electron Microscope for EDS. These techniques are briefly discussed in this chapter.

### Preparation of thin-sections

The rock chips of about (4 × 2 cm) were cut by a rock cutting machine and then one side of each chip was ground and polished to make a plane surface. This polished plane surface of the chip was then mounted on a glass slide of same size with an epoxy. Before mounting the rock chip on the glass slide, it was heated above 100°C on a hot plate. After mounting the rock chip on the glass slide, it was again cut on the rock cutting

machine to minimize the thickness of the chip for further process. The chip was then further ground to minimum thickness of 0.03 mm by using various sizes of the silicon carbide powder. For petrographic studies, these thin sections were then covered with cover slips using canadabalsom. For mineral chemistry, the thin sections were not covered with cover slips but these were further polished by using various size abrasive cloths on automatic polisher.

**Crushing and pulverizing of rock samples**

The rock samples were crushed in a Jaw Crusher to small size chips and then the crushed chips were pulverized in a tungsten carbide ball mill to ~ 200 mesh size. Great care was practiced to avoid the contamination during both of these two processes. The representative portion of each rock sample was taken after quatering and coning and was stored in the tight glass bottles. To remove the moisture, all the samples were kept in the oven at 110°C for overnight.

**Preparation of stock solutions**

**Stock Solution A: using acid digestion method**

The method of Jeffery and Hutcheson (1986) was used for the preparation of solution A. 0.500g of oven-dried powdered rock sample was accurately weighed in a Teflon beaker. Then 10 ml of concentrated HF and 4 ml of perchloric acid $HCLO_4$ were added and then the Teflon beaker was slowly heated on the hot plate/sand bath. After half an hour further 2 ml of $HClO_4$ were added and the Teflon beaker was continuously heated at low temperature until semi dry paste obtained at the end. Again 4 ml of $HClO_4$ and a little deionized water were added to the Teflon beaker and warm for five minutes on sand bath. Finally, the Teflon beaker was removed from the hot plate and the contents of it were then transferred to 250 ml beaker by thorough washing with deionized water until no particle is left in the crucible. Generally, the solution in the flask was crystal clean but if some precipitation was observed in the solution, the solution was again heated until

clear solution is obtained. But if there was any persistence of precipitation in the solution then about 2 ml of HCl was added and boiled. The final solution was transferred to 250 ml volumetric flask with deionized water. In this way all the samples were treated by the same procedure for the preparation of solution A. This solution was then used for the determination of all the major oxides except $SiO_2$ and $Al_2O_3$.

**Stock solution B: using sodium hydroxide fusion method**

The method of Jeffery and Hutcheson (1986) was used for the preparation of solution B. 30 g of NaOH pellets were dissolved in 100 ml deionized water and stored in a polythene bottle. 5 ml of NaOH solution was taken and added to a series of already cleaned nickel crucibles. The crucibles were kept on hot plate/sand bath at approximately 100 °C for complete dryness. These crucibles were then cooled in a desicator. Accurately weighed 0.05 g of powdered rock samples were added to each crucible. One crucible was used for the preparation of blank in which nothing was added except 5 ml NaOH solution. The crucibles were covered with lids and each crucible was heated to dull redness over a gas burner for a period of five minutes. The crucibles were swirled while hot. Deionized water (5-10ml) was added to each crucible after these are mildly cooled. The contents of each crucible were washed into 600 ml plastic beakers, which already contained 400 ml of deionized water and 10 ml of concentrated HCl. Mostly, the clear solution was obtained but if it was not clear then it was warmed until clear solution was obtained. The resulting solution was transferred to one litre volumetric flask and was made to the volume with deionized water and was stored in polythene bottles for the determination of silica and alumina.

## Determination of major and minor oxides

Among the major element oxides $SiO_2$, $Al_2O_3$, $TiO_2$, and $P_2O_5$ were determined by the spectrophotometric method (using SP-400 PYE UNICAM UV/VIS spectrophotometer), whereas, $Fe_2O_3$, CaO, MgO, MnO, $Na_2O$ and $K_2O$ were determined by atomic absorption spectrophotometric method (using AAnalyst 700 Perkin Elmer atomic absorption spectrophotometer).

### Determination of $SiO_2$

### Reagents

**Ammonium molybdate solution:** 7.5 g of ammonium molybdate was dissolved in 70 ml deionized water by adding 20 ml of $9NH_2SO_4$. The solution was made to the volume of 100 ml and was stored in a polythene bottle.

**Tartaric acid solution:** 25 g of the tartaric acid was dissolved in deionized water and was diluted to 250 ml with deionized water.

**Reducing solution:** 0.7 g of sodium sulfite ($Na_2SO_3$), 0.15 g of 1- amino -2 - naphthol - 4 - sulphonic acid and 9 g of sodium metabisulphite ($Na_2SO_2O_5$) were dissolved in 100 ml of deionized water. The solution was kept in a dark and cool place and was prepared freshly as this solution deteriorates after few days.

### Procedure

10 ml of stock solution B of each of the powdered rock sample and a blank was taken in a series of 100 ml volumetric flask. About 50 ml of deionized water was added to each flask. 2 ml of ammonium molybdate solution was added to each flask and was swirled to mix well. After exactly 10 minutes, 4 ml of tartaric acid solution was added to each flask and again swirled and mixed well. At the end 1 ml of reducing solution was added to these flasks and each flask was diluted to 100 ml with deionized water. All these

solutions were set aside for at least 30 minutes and at the end blue color solution was obtained. The silica determination was then made on the UV/Visible spectrophotometer at a wavelength of 650nm relative to the reference rock standards.

**Determination of $Al_2O_3$**

**Reagents**

**8 - hydroxyquinoline solution:** 1.25 g of the 8 - hydroxyquinoline was dissolved in 250 ml of pure grade of chloroform and was stored in a refrigerator.

**Complexing reagent:** 1 g of hydroxylamine hydrochloride ($HONH_2HCl$), 3.6 g of sodium acetate trihydrate and 0.5 g of beryllium sulphate tetrahydrate were dissolved in 50 ml of deionized water. 0.04 g of 2 - 2 dipyridyl was also dissolved in 20 ml of 0.2N HCl. Both the solutions were then mixed and diluted up to 100 ml with deionized water.

**Procedure**

5 ml of each rock sample stock solution B, three known standards and a reagent blank were taken into a series of 100 ml seperatory funnels. 5 ml of deionized water and 10 ml of complexing reagent solution were added to these funnels and mixed well. After few minutes 20 ml of 8- hydroxyquinoline solution was added to each funnel. These solutions were then shaked for about 8 minutes by an automated flask shaker. The organic layers obtained at the bottom of these solutions in the seperatory funnels were then separated into 25 ml volumetric flasks by washing the funnels with chloroform for several times. The final volume of 25 ml for each sample was made to the mark with chloroform. The yellow color extracts obtained through this process were run on the spectrophotometric for determination of $Al_2O_3$ at wavelength of 381nm relative to the reference rock standards.

**Determination of $TiO_2$**

10 ml of stock solution A from each sample and at least two certified rock standards were taken in 50 ml volumetric flask and then 15 ml of coloring reagent was added to all flasks and made up to the mark with deionized water. Similarly blank was also prepared by the same method. These solutions were then shaked and mixed well and were ready for analysis. The spectrophotometer was turn ON and set to warm up for 30 minutes. The wavelength optimization was done on the certified rock standards. A maximum peak was noticed at 445 nm. The instrument was set on a wavelength of 445 nm and was zeroed with the blank. The certified rock standards were run on the instrument and the results were calculated and compared with the certified values. After making sure that the results of the certified standards were within confidence limit, the rock solutions were then run as unknown for the concentration of $TiO_2$.

**Determination of $P_2O_5$**

**Reagents**

**Ammonium meta vanadate solution:** 0.25 g ammonium meta vanadate ($NH_4VO_3$) was dissolved in 120 ml of 33 % $HNO_3$.

**Ammonium molybdate solution:** 10 g of ammonium molybdate was dissolved in 80 ml of deionized water. Both the solutions were mixed and stored in polythene bottle. This mixture was used as vanadate molybdate reagent.

**Procedure**

10 ml of stock solution A from every sample and at least two certified standards were taken in a series of 50 ml volumetric flasks. To each flask 2 ml of vanadate molybdate reagent was added. The volume was made to the mark with deionized water. The solutions were shaked and were run on spectrophotometer as under. The spectrophotometer was turn ON and set to warm up for 30 minutes. The wavelength

optimization was done on the certified rock standards. A maximum peak was noticed at 372 nm. The instrument was set on a wavelength of 372 nm and was zeroed with the blank. The certified rock standards were run on the instrument and the results were calculated and compared with the certified values. After making sure that the results of the certified standards were within the confidence limit, the rock solutions were then run as unknown for the concentration of $P_2O_5$.

**Determination of total iron as $Fe_2O_3$**

The total iron as $Fe_2O_3$ in the studied rock samples was determined by atomic absorption spectrophotometer by using the stock solution A.

**Stock solution of 1000 ppm for Fe:** 1 g of pure iron metal was dissolved in minimum amount of HCl and was made to the volume with deionized water in one litre volumetric flask.

**Stock solution of 100 ppm:** 10 ml from 1000 ppm stock solution was taken in 100 ml volumetric flask and made to the mark with deionized water.

**Working standard solutions:** 1, 2, 4 and 8 ppm working standard solutions were prepared by taking 1, 2, 4, and 8 ml from the 100 ppm stock standard solution in a 100 ml volumetric flask and made to the volume with deionized water.

**Procedure**

The atomic absorption spectrophotometer cathode lamp was set at the wavelength of 248.3 nm and was calibrated with the iron working standard solutions of 4 and 8 ppm. The working standards 1, 2, 4 and 8 ppm were then run as unknown. After verification of accuracy, the certified standard solution was run on the machine. The results were compared with the certified values and were found within the confidence limit. After standardization of the instrument, the rest of the sample solutions were run on the atomic absorption and the concentration of iron as $Fe_2O_3$ were determined. Whenever the solutions were out of range, those solutions were diluted accordingly.

**Determination of CaO and MgO**

**Stock solution of 1000 ppm for Ca and Mg:** Stock solution of 1000 ppm for Ca and Mg was prepared by dissolving 2.497 g of $CaCO_3$ and 3.057 g of $MgCO_3$ in 1 N HCl and were diluted to one litre with deionized water in a 1000 ml volumetric flask.

**Stock solution of 100 ppm for Ca and Mg:** 10 ml from 1000 ppm stock solution was taken in 100 ml volumetric flask and made to the mark with deionized water.

**Lanthanum 5 % solution:** Lanthanum 5 % solution was prepared by dissolving 58.64 g of $La_2O_3$ dissolved in 200 ml deionized water to which 150 ml of 60 % $HClO_4$ was added. It was heated until completely dissolved. The solution was then filtered through ordinary filter paper into 1000 ml volumetric flask and the volume was made up to the mark with deionized water.

**Working standards:** 1, 2, 4, and 8 ppm working standards for Ca and Mg were prepared by taking 1, 2, 4, and 8 ml of 100 ppm standard solution in a series of 100 ml volumetric flasks. To these flasks 10 ml of lanthanum solution was added and the volume was made up to the mark with deionized water.

**Dilution of samples:** 2 ml (depending upon the expected concentration of Ca and Mg) of the stock solution A of both certified rock standards and the studied rock samples were taken in a series of 25 ml volumetric flask. 3 ml of lanthanum solution was added to each flask and the volume was made up to the mark.

**Procedure**

Atomic absorption spectrophotometer was calibrated for Ca and Mg separately at wavelength of 422 nm by using Ca and Mg cathode lamps respectively. The instrument was then calibrated and standardized with the working standards of 2 and 4 ppm. All the working standards were run as unknown and their actual concentration was verified. For further accuracy the certified rock standards were run as unknown and the results were compared. After making sure that the results of the certified standards were within the confidence limit, the studied rock sample solutions (in diluted form) were run on the

atomic absorption and the concentrations of Ca and Mg were noted for each sample. The wt. % of CaO and MgO in each sample was then calculated.

**Determination of $Na_2O$ and $K_2O$**

Both of the $Na_2O$ and $K_2O$ were determined by Atomic Absorption Spectrophotometer by using the stock solution A.

**Stock solution of 1000 ppm for Na and K:** 3.087 g of moisture free $Na_2SO_4$ and 2.228 g moisture free $K_2SO_4$ were dissolved in deionized water and the volume was made to 1000 ml in a volumetric flask. The solution was stored in a polythene bottle.
**Stock solution of 100 ppm for Na and K:** 10 ml from 1000 ppm stock solution was taken in 100 ml volumetric flask and made to the mark with deionized water.
**Working standards:** 1, 2, 4, and 8 ppm working standard were prepared by taking 1, 2, 4, and 8 ml of 100 ppm standard solution in a series of 100 ml volumetric flasks and the volume was made up to the mark with deionized water.

**Procedure**

Atomic Absorption Spectrophotometer was calibrated for Na and K separately at wavelength of 589 nm by using Na and K cathode lamps, respectively. The instrument was calibrated and standardized by working standards of 4 and 8 ppm and then the working standards were also run as unknown in order to verify the standardization of the instrument. The diluted certified rock standards were then run and the results were compared to know the accuracy of the method. The diluted solutions of the rock samples were sprayed one by one through the flame and the concentration of Na and K was noted in each sample. The wt. % of $Na_2O$ and $K_2O$ were then calculated.

**Determination of MnO**

MnO in the studied rock samples was determined by atomic absorption spectrophotometer by using the stock solution A.

**Stock solution of 1000 ppm for Mn:** 4.05 g of $MnSO_4.4H_2O$ was dissolved in 20 ml of 1 N $H_2SO_4$. It was then transferred to 1000 ml volumetric flask and was made up to the mark with deionized water.

**Stock solution of 100 ppm for Na and K:** 10 ml from 1000 ppm stock solution was taken in 100 ml volumetric flask and made to the mark with deionized water.

**Working standards:** 1, 2, 4, and 8 ppm working standards of Mn were prepared by taking 1, 2, 4, and 8 ml of 100 ppm standard solution in a series of 100 ml volumetric flasks and the volume was made up to the mark with deionized water.

**Procedure**

Atomic absorption spectrophotometer was calibrated for Mn at wavelength of 279.5 nm cathode lamp and the cathode lamp was warmed up for 10 minutes. It was then calibrated and standardized with the working standards and the certified rock standards were then run to check the accuracy of the method. After verification, samples concentration was noted. The wt. % of MnO was then calculated.

**Determination of loss on ignition by using gravimetric method**

Samples of known weight were taken in already weighed porcelain crucibles. The crucibles were kept in the furnace at 950°C for two hours. They were cooled in the desicator and weighed again. The difference in the weight was noted and the amount of ignition loss (in percent) was calculated for each sample.

## Qualitative analysis of gemstones

Various types of gemstones, collected during the fieldwork were run on the X-Ray Diffractometer in the powder form for qualitative analyses. The qualitative analysis helped in identification of different types of gemstones that can not easily be identified by their physical properties. These analyses were performed on the Riguku X-ray Diffractometer (XRD) at the National Centre of Excellence in Geology, University of Peshawar under the following operating conditions:

1. Target: Cu Kα,
2. Voltage: 35 Kv,
3. Current: 20 Ma,
4. Scanning: both step scanning and continuous scanning @ step size of 0.05 and 0.01 respectively.

**Preparation of the sample:** A small part of each gemstone was cut through a very fine diamond blade in the Gems and Gemological Institute of Pakistan (GGIP), Peshawar. That piece of gem was powdered and finally a pressed plate on glass slide was prepared and put in the sample chamber of the X-Ray Diffractometer. Then the machine was set on the above-mentioned operating conditions and all the gemstone samples were analysed step by step. The d-values and intensities of each sample were calculated by a computer program. The powdered diffraction patterns of each gemstone were also obtained and these patterns were compared with the data files of International Centre for Diffraction data (ICDD) through computer software and hence the gemstones were identified through their d-values and intensities.

## Mineral analysis by Electron Probe Micro Analyzer

The gemstones, which were selected for XRD studies were also analyzed by Electron Probe Microanalyzer for their chemistry. For this a small piece from each gemstone was cut with a very fine diamond blade in the Gems and Gemological Institute of Pakistan (GGIP), Peshawar. These small pieces or grains were mounted on glass slides

and polished in the Mineral testing Laboratory (MTL), Hayatabad, Peshawar on the automatic diamond polisher. Some 40 grains of different gemstones from different pegmatites exposed at various localities of the Shigar valley and also the gemstones of metasomatic or metamorphic origin were mounted on sixteen glass slides as grain mounts. These polished sections were made carbon-coated before fixing in the sample chamber of the machine. In addition to the gemstone polished sections, some eleven sections of pegmatites and their host rocks were also polished and analysed for the chemistry of their constituent minerals. Polished sections of the gemstones, pegmatites and their host rocks were also analysed in Japan and in the United Kingdom. In Japan, the sections were analysed on Jeol Superprobe Model JXA-8600 Electron Probe Microanalyser, using the Wavelength Dispersive System (WDS). The analyses were performed under the following operating conditions. The accelerating voltage was 15 kv and the current was in the range from 1.99E-08 to 1.210E-08 amp. Total eleven elements Si, Ti, Al, Fe, Mg, Mn, Ca, Na, K, Cr, and Ni were determined and for these the following standards were used: $CaSiO_3$ (wollastonite), $TiO_2$, $Al_2O_3$ (corundum), $Fe_2O_3$ (Hematite), MgO, MnO, $CaSiO_3$, albite, K-feldspar, $Cr_2O_3$, NiO.

The polished thin-sections of pegmatites were also analyzed on Jeol Superprobe Model JXA - 8600 for different constituent minerals (both silicates as well as the oxides) at the University of Leicester, United Kingdom. These analyses were conducted by using wavelength dispersive system under the following operating conditions: 15 Kv accessory voltage; 30 x 10-9A probe current; 20 (2 x 10) seconds peak, 10 (2 x 5) seconds negative background and 10 (2 x 5) seconds positive background counting times. The diameter of x-ray beam varied according to the type, grain size and nature (e.g. scale of compositional homogeneity) of the analyzing phase but it was mostly 5 μm for most of the silicates and oxides. The silicate phases were analyzed for all the common major and minor oxides (i.e., $SiO_2$, $TiO_2$, $Al_2O_3$, FeO, MnO, MgO, CaO, $Na_2O$, $K_2O$, $Cr_2O_3$ and NiO). In case of magnetite and ilmenite, the iron both of divalent and trivalent states was also determined. Moreover, incase of epidotes, allanites, columbites, zircons and apatites, the $ZrO_2$, $HfO_2$, $La_2O_3$, $Ce_2O_3$, $Nb_2O_5$, $Ta_2O_5$, $Y_2O_3$, $Yb_2O_3$ and $P_2O_5$ were also determined

along with the above-mentioned major and minor oxides. Besides these, Cl and F were also analyzed into fluorites, muscovites and biotites.

The following standards were used during the course of microprobe analyses: wollastonite (natural for Si and Ca); jadeite (natural for Al and Na); magnetite (natural for Fe); rhodonite (natural for Mn); MgO (synthetic for Mg); microcline (natural for K); scapolite (natural for Cl) and SrF2 (synthetic for F). Besides this, pure synthetic metals of Ni and Cr were used for nickel and chromium.

In case of pegmatites and their host rocks, the spot analyses were performed for garnet, muscovite, biotite, plagioclase, K-feldspar, tourmaline, magnetite, ilmenite, epidote, allanite, chlorite, columbite, zircon, sillimanite, clinopyroxene, and sphene. To know about the zonation and alteration within the same grain, the spot analyses were also performed from the core to the margin of some of the crystals and for this purpose mostly the garnets and biotites were selected. The total iron was determined as FeO.

**Scanning Electron Microscope and preparation of samples**

JEOL- JSM - 5910 Scanning Electron Microscope was used for EDS microanalysis. Some 22 powdered gemstone samples were analysed for the major oxides. A small portion of each sample was taken and the hubs of these samples were prepared and put in the sample chamber for microanalysis. The samples were run on 20 Kv with working distance of 15 mm as operating conditions at the Central Resource Laboratory, University of Peshawar.

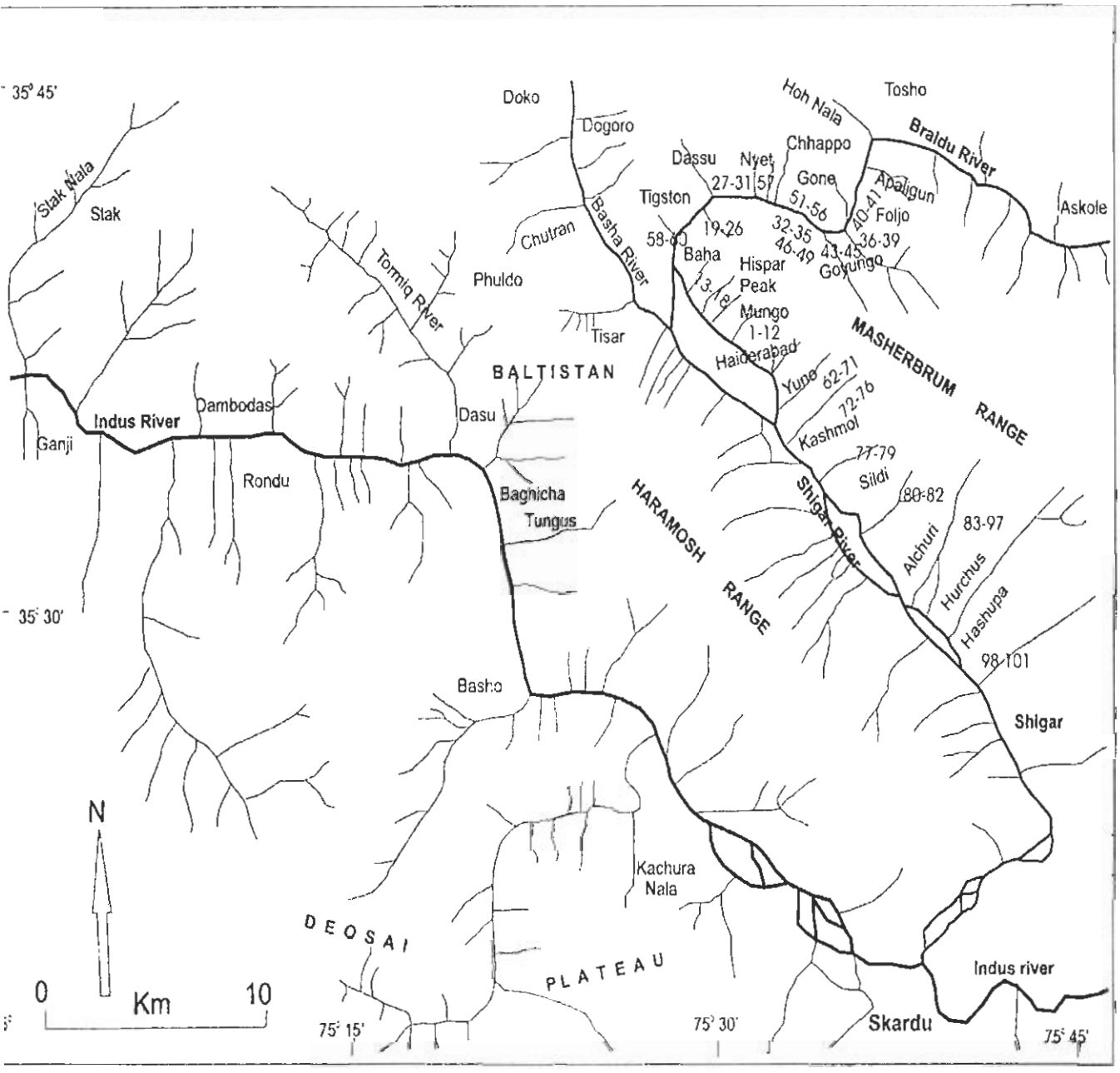


**Fig. 4. 1.** Map showing sample locations within Shigar valley (Study area).

# Chapter 5

## MEGA AND MICROSCOPIC FEATURES OF THE PEGMATITES

### General Statement

There are various classifications of pegmatites depending on their mode of occurrence, internal structure, presence or absence of gemstones, rare-metals and other accessory minerals. Therefore, the pegmatites have been classified into various classes and subclasses. The pegmatites of the Shigar valley are also variable not only in their internal structure, texture and mode of occurrence but also in their mineralogy. In case of internal structure, the Shigar valley pegmatites are both zoned and unzoned, while mineralogically, these are differentiated as gem-bearing pegmatites and gem-barren or gem-free pegmatites.

As the gem-bearing pegmatites of the Shigar valley have complex structure and internal zoning, therefore, these are considered as "complex or zoned pegmatites", while the gem-barren pegmatites are simple not only in mineralogy but also in their internal structure and texture, so these pegmatites are considered as "simple pegmatites". The major constituents of both the complex and simple pegmatites are plagioclase feldspar, alkali-feldspar, and quartz, while there is a significantly difference in the minor constituents of these two types of pegmatites. The minor constituents of the complex or zoned pegmatites are variable at different localities of the Shigar valley, while biotite and muscovite are generally the minor constituents of the simple pegmatites.

On the basis of field observations, petrographic studies, and presence or absence of accessory minerals, each of the two major classes are further divided into the following sub-classes or types.

1. **Gem-bearing pegmatites**
   a. Muscovite-schorl-beryl-garnet pegmatites,
   b. Muscovite-schorl pegmatites.

## 2. Gem-barren pegmatites

a. Biotite ± garnet ± muscovite pegmatites,

b. Muscovite-biotite ± garnet pegmatites.

These groups of pegmatites are described below in some detail on the basis of mega and microscopic studies.

### Gem-bearing pegmatites

#### a. Muscovite-schorl-beryl-garnet pegmatites

**Megascopic features:** This group of pegmatites is very coarse-grained with two feldspars and quartz as the major constituents and the main accessory minerals identified in hand specimen are muscovite, schorl and garnet (Plate 5.1). Biotite is almost absent in this sub-class of pegmatites but if present then only in traces (Table 5. 1). Megascopically, only in sample number 33 some flakes of biotite are present. These pegmatites are generally white in color due to the absence of mafic minerals especially biotite but the tourmaline is present as a minor constituent. Although the minor constituents are scattered throughout these bodies but some of the minor phases concentrate into certain parts of pegmatite and hence form clear cut zones, e.g., schorl is present in large quantity either at the border zone or in certain intermediate zones (Plate 5.2). These pegmatites are zoned and have very sharp contacts with their host rocks. The dikes are of variable sizes ranging from small veins (20-30 cm) to about 4 m thick. In these pegmatites, the coarseness is from margin to core that indicates the direction and sequence of crystallization. Besides this, the sizes of individual zones in the hanging wall and in the footwall are also of variable sizes. Mostly, the sizes of each zone in every zoned pegmatite in the footwall are of maximum thickness relative to those in the hanging wall. As there is the repetition of same zone in this group or subclass of pegmatites, therefore, these are considered as symmetrically zoned pegmatites (Plate 5.2). The samples of this group of pegmatites were taken from the different zones. In these

pegmatites the intermediate zones have pockets or cavities containing the gems in cluster and these zones are of great importance because most of the professional miners are interested in such gemstone-bearing zones (London, 1986). The relics of such type of cavities or pockets from which certain gemstones have been excavated by the local miners were also seen in the field (Plate 5. 3). The symmetrically zoned pegmatites of this sub-class have generally three or four zones, i.e., the border aplitic zone, the intermediate zone and the central quartz zone but the dikes without the central quartz zone were also observed (Plate 5. 2). In some of the dikes, it is very difficult to distinguish between the wall zone and the intermediate zone. In addition some of the pegmatites of this sub-class have also two or three intermediate zones. The aplites, which are generally associated with pegmatites and in most of the cases these are commonly present at the border zone but sometimes these may also occur in the core zone (Laurs et al., 1998). In case of pegmatites of the Stak Nala, the aplitic zone is present in the core, while the pegmatites of the Shigar valley are either without the aplite, if present, it occurs at the margin (Plate 5. 2). The sample number 32, 33, 66 were taken from those pegmatites, which are highly enriched in gemstones and at present extensive mining is going on in these pegmatites. According to local miners they have found aquamarine, topaz (colorless-light yellow), schorl, fluorite (light-green) and apatite etc from these pegmatites. Minute crystals of the above-mentioned gems were seen in the field (Plate 5.4). These gems were also collected for further analyses.

**Microscopic features:** This sub-class of pegmatites is relatively coarse-grained and inequigranular but some sections exhibit the equigranular texture. In thin sections, these pegmatites contain plagioclase (15 to 70 %), orthoclase (7 to 50 %), and quartz (20 to 35 %) as essential constituents, while tourmaline (1 to 15 %), garnet (1 to 3 %), muscovite (2 to 24 %), epidote (in traces up to 1 %), apatite (traces to 2 %), sphene (traces to 1 %), zircon (traces) and opaque (in traces up to 1 %) are present as accessories (Table 5. 1). Some orthoclase grains in sample number 66, 43 and 44 from Kashmol and Goyungo areas show microperthitic texture (Plate 5.5), indicating simultaneous crystallization of the orthoclase and the quartz. Both the feldspars of this sub-class of pegmatites are partially to highly altered. The altered products of these are sericite, muscovite, epidote,

and kaolinite (Plate 5.6). These are generally altered along the margins and micro-fractures within the grains, however, in some samples, like sample number 33 both the orthoclase and plagioclase are so highly altered and the pseudomorph of these are well noticed. Unaltered plagioclase grains are also common and exhibiting well-developed albite twinning. In some grains of orthoclase, the vermiculite texture is also seen. The crystals of plagioclase are generally tabular to bladed in shape and most of the grains are subhedral to anhedral while the orthoclase grains are mostly anhedral. In some plagioclase, bending is well noticed, which indicates that these pegmatites have gone through regional stresses as is evident in sample number 26 collected from Dassu area (Plate 5.7). In addition, overgrowths and cross cutting relationships within the plagioclase are also common in sample number 66 and 33 at Kashmol and Goyungo pegmatites respectively. Small tabular crystals of plagioclase are also present as an inclusion within the orthoclase, indicating an earlier crystallization of the plagioclase. The anorthite contents of the plagioclases are in the range of albite (An 14-18). It is usually associated with certain gemstones and is the characteristic feldspar of gem-bearing pegmatites (Laurs et al., 1998; London, 1986; Nabelek et al., 1992a). Pepper-mesh texture has also been noticed in some crystals of plagioclase in sample number 66. The quartz is subhedral-anhedral and is interlocked with plagioclase and orthoclase. Quartz also occurs as inclusion within the two feldspars, garnet and muscovite. Pressure shadow or undulose extinction is the common feature of these quartz, indicating that these pegmatites have undergone stress conditions after their formation.

In the minor constituents, muscovite is the most dominant phase with variable sizes and is ubiquitous of all the zones except of central quartz zone but at the core-margin zone large books (sheets) of muscovite are noticed. The sizes of muscovite flakes increases from the border zone towards the core-margin zone and the flakes with maximum dimension were seen in those sections, taken from the core-margin zone (Plate 5.8). The intergrowths and overgrowths are the common features of the muscovite itself but some muscovites are also intergrown with plagioclase as well as orthoclase. Muscovite also occurs as fine-grained material as alteration product along the margins and fractures of orthoclase (Plate 5.9). Euhedral to subhedral fractured grains of garnet

and tourmaline are well noticed in some of the thin sections (Plates 5.10, 5.11, 5.12 and 5.13). At places the zoned tourmalines are also present (Plates 5.14, 5.15, 5.16 and 5.17). Some of the pegmatites (sample number 29 and 43) collected from Dassu and Goyungo areas are relatively enriched in tourmaline containing about 15 % and 6 % of tourmaline respectively (Table 5. 1). In sample number 47, the overgrowth of muscovite with tourmaline was also noticed. Sporadic grains of garnet are well observed in these pegmatites. Garnet as small inclusions within the plagioclase is noticed in the pegmatites of Kashmol area (Plates 5.18 and 5.19). Euhedral-subhedral crystals of sphene and apatite are also present in traces. In sample number 32 collected from Goyungo area, the apatite up to 2 % has been found (Plate 5.20). Euhedral crystals of zircon in traces are also noticed in few thin sections. The opaque phases are found in dissemination.

As the mega and microscopic studies indicate that these pegmatites are generally devoid of biotite, or if present it is in traces, and contain the beryl, garnet, schorl, and muscovite as their main accessory minerals. These pegmatites can be considered as productive for gemstones. Majority of the pegmatites in the Shigar valley belong to this sub-class of pegmatites.

**b. Muscovite-schorl pegmatites**

**Megascopic features:** Megascopically, this group of pegmatites is coarse to medium-grained and light-gray to white on fresh surface and yellowish-brown on weathered surface. Alkali-feldspar, plagioclase, quartz and muscovite are recognizable in hand specimen. Muscovite at places occurs as 3-4 cm cleavable sheets. Garnet and schorl are generally absent in these pegmatites, if present, then in traces.

Sample number 54 was taken from pegmatites at Gone village (Fig. 4. 1), which are extensively mined for aquamarine, topaz, and quartz etc. As it was noticed in the field that pegmatites (both gem-bearing and gem-barren) are only exposed from Goyungo up to Sildi villages and are absent from Alchuri to proper Shigar town (Fig. 4. 1). Here, it is important to mention that even the pegmatites are not exposed from Alchuri to Shigar

town but were seen in the float of nalas (Lungmas) near the vicinity of these localities and sample number 81, 97, and 98 were taken from the float left by Lungmas (locally used for nalas) for the sack of comparison. So there is a possibility that the pegmatite exposures may be present far from those classic localities, which are easily accessible. It is also important to note that the pegmatites (sample number 81, 97, and 98) have many characteristics similar to that of pegmatites (sample number 54 and 74). These pegmatites may also be the potential source of certain gemstones, if accessed and explored.

**Microscopic features:** Thin section study indicates that the pegmatites of this sub-class are generally coarse-grained, however, medium-grained pegmatites are also present. These pegmatites are inequigranular with majority of the crystal outlines being subhedral to anhedral. Orthoclase (10 to 36 %), plagioclase (30 to 55 %) and quartz (25 to 30 %) are the major constituents of these pegmatites. Among the accessory minerals muscovite is the main phase and is present up to 20 % (Table 5. 1). While biotite, tourmaline, apatite, epidote, sphene and zircon are absent but, if present, are in trace amount (Table 5. 1). Opaque phase is present from trace to about 1 %. Orthoclase and plagioclase are generally fresh but at places both the phases exhibit alteration along the margin and fractures to sericite, muscovite and epidote (Plate 5. 21). In certain cases the degree of alteration is so intense that the pseudomorphs of these phases are clearly visible in the thin sections. Majority of the alkali- feldspar is orthoclase in composition; however some perthite grains are seen in some of the thin sections (Table 5.1). Plagioclase crystals are generally lath-like, tabular and mostly euhedral-subhedral (Plate 5. 22). Inclusion of quartz and muscovite within orthoclase and plagioclase are also observed in some of the sections. In section number 97, the overgrowth and cross-cutting relationships within plagioclase are also noticed (Plate 5. 23). Some of the plagioclase grains also show micrographic texture (Plate 5. 24). The majority of quartz crystals are subhedral to anhedral, however, in some cases fresh-looking euhedral grains are also noticed in the pegmatites near Sildi village (Plate 5. 25). Quartz grains in all the samples are strained and are having undulose extinction, while the plagioclase grains are exhibiting kink bending in some samples. This indicates that the pegmatites were subjected to regional stress (Plate 5. 26).

Among the accessory phases, muscovite is most dominant in this sub-class of pegmatites and its large flakes with perfect cleavage planes are prominent in thin sections of all the samples (Plates 5. 27 and 5. 28). The overgrowth and intergrowths of muscovite are also seen in some of the pegmatites of this subclass (Plate 5. 29). In some muscovites, the quartz and minute biotite flakes are seen as an inclusion. The opaque minerals are also present in traces and intensive iron-leaching is observed along the micro-fractures near the opaque phases (Plates 5. 30 and 5. 31). Garnet and tourmaline are almost absent in this group of pegmatites but some subhedral-anhedral crystals of tourmaline are observed in Kashmol area pegmatites (Plates 5. 32 and 5. 33). In addition to this, euhedral grains of zircon, apatite, and sphene are found in traces.

## Gem-barren pegmatites

### a. Biotite ± garnet ± muscovite pegmatites

**Megascopic features:** These pegmatites are medium to coarse-grained, greenish-white on fresh and grayish-yellow on weathered surfaces. Orthoclase, plagioclase, biotite and garnet can very easily be recognized in the hand specimen. Biotite is present in significant quantity, while tourmaline and muscovite are absent in these pegmatites. However, muscovite in traces is noticed in the sample collected from a pegmatite exposed at Mungo village. These pegmatites are also exposed at Haiderabad and Goyungo villages of the Shigar valley area (Fig. 4. 1).

**Microscopic features:** In thin sections, this sub-group of pegmatites has orthoclase (36 to 45 %), plagioclase (16 to 23 %) and the quartz (30 to 35 %) as the essential constituents, while biotite, garnet, muscovite, apatite, epidote, sphene, Tremolite/ actinolite and opaque minerals occur as accessories. This subgroup is microscopically distinguished from other pegmatites in having no gems and the orthoclase and quartz contents are relatively high in volume (Table 5. 2). Among the accessory minerals biotite

is present up to 10 %, while rest of the accessory minerals are generally in traces, except garnet, which in one sample (MUN- 3) reaches to 1 %.

Orthoclase and plagioclase exhibit partial to complete alteration. Orthoclase is altered along margins and fractures to sericite, kaolinite and muscovite (Plates 5. 34 and 5. 35). While the plagioclase exhibits saussuritization along the margins and cleavages (Plate 5. 36). Small tabular crystals of plagioclase are also present as inclusion in the orthoclase (Plate 5. 37), indicating an earlier crystallization of plagioclase. Anorthite contents of these plagioclases are in the range of oligoclase ($An_{15-30}$). This may be another distinction between the gem-bearing and Gem-barren pegmatites of the Shigar Valley because in the previous sub-classes (the gem-bearing group) the major plagioclase is albite in composition, while in this sub-class it is oligoclase. Intergrowth between plagioclase and microcline is observed showing perthite texture (Plate 5. 38). In some cases the plagioclase shows kink bending. The quartz is mostly subhedral to anhedral and is found as interlocked with two feldspars. In certain cases both the orthoclase and quartz grains show undulatory extinction. This suggests that the pegmatites have undergone regional stress. Besides, quartz is also present as an inclusion in both of the feldspars as well as in the highly fractured garnets. The modal composition of biotite in this sub-class of pegmatites ranges from (4 - 10 %). The garnet crystals are mostly euhedral-subhedral but certain crystals are highly fractured (Plate 5. 39). In addition to this, iron leaching was also seen in sample number 3 near the opaque phases and biotite along the micro fractures (Plates 5. 40 and 5. 41).

**b. Muscovite-biotite ± garnet pegmatites**

**Megascopic features:** The samples (MUN-1, 5 and 7) were taken from a pegmatite dike (~ 1.5 m thick) exposed at the Haiderabad or Mungo area (Fig. 4.1). In hand specimen these pegmatites are medium to coarse-grained. Alkali feldspar, plagioclase, quartz, muscovite and biotite are easily recognizable in hand specimen. Garnet crystals are also found in dissemination (Plate 5. 42). Sample number 38 and 41 were taken from the more

felsic dikes, exposed along upstream of Braldu River after the village of Goyungo. These are displaced due to local faulting (Plate 5.43).

**Microscopic features:** These pegmatites are medium to coarse-grained and inequigranular in thin sections. The major constituents of this group of pegmatites in thin sections are the orthoclase (25 to 40 %), plagioclase (15 to 40 %) and quartz (27 to 35 %), while the main accessories are biotite (2 to 8 %) and muscovite (1 to 8 %). Garnet, sphene, epidote, apatite, zircon and opaque occur in traces.

The orthoclase and plagioclase are generally subhedral to anhedral and characterized by hapidiomorphic texture. The plagioclase is oligoclase to andesine ($An_{20-30}$) in composition. Both these phases are occasionally altered to sericite, kaolinite, muscovite, and epidote along the margins and micro fractures (Plates 5. 44a and 5. 44b). The intensity of alteration varies from partial to complete in certain thin sections (Plate 5. 45). At places pseudomorphs after both orthoclase and plagioclase are noticed. Microperthitic texture is observed in some thin sections of pegmatites (Plate 5. 46). In addition, vermiculite texture is also noticed in one thin section of these pegmatites (Plate 5. 47).

The quartz crystals are mostly subhedral to anhedral and exhibiting undulation extinction interlocking with two feldspars (Plate 5. 48). Moreover quartz is also present as an inclusion in the feldspar. As these bodies are mostly leucocratic that is evidenced by the felsic mineral contents ranging from 93 to 96 % of the total constituent minerals. Large flakes of biotite and muscovite are variably distributed in these pegmatites. Some euhedral crystals of apatite and sphene are noticed in some samples. A few crystals of garnet are seen as inclusion in orthoclase, indicating that garnet is crystallized prior to the feldspar.

## Shengus and Indus-Gilgit Confluence pegmatites

In order to correlate the pegmatites of the Shigar valley with other pegmatites of different tectonic settings, few samples from two pegmatite bodies (i.e., Shengus and Indus-Gilgit confluence) from distal areas have been collected. The Shengus pegmatites are famous for the occurrence of certain gemstones, while the Indus-Gilgit Confluence pegmatites are generally free of gemstones. Samples (102 and 104) are collected from the Shengus, while rest of the samples of this group belongs to the Indus-Gilgit Confluence pegmatites. The Indus-Gilgit Confluence pegmatites at places have a unique pattern of cross-cutting dikes (Plate 5. 49), which has not been observed in the pegmatites from Shengus and Shigar valleys. The sizes of individual dikes of the Shengus pegmatites vary from (1-2 m) in thickness (Plates 5. 50 and 5. 51). At places, the Indus-Gilgit Confluence pegmatite dykes have parallel orientation (Plate 5. 52). The Shengus pegmatites are being mined for topaz, aquamarine, fluorite and schorl etc.

**Megascopic features:** In hand specimen both the Shengus and Indus-Gilgit Confluence pegmatites are coarse-grained, however, the Shengus pegmatites are coarser than the Indus-Gilgit Confluence pegmatites. The Indus-Gilgit Confluence pegmatites are simple in mineralogy and internal structure, while the Shengus pegmatites are relatively complex and zoned but the internal zoning is not as clear as is in the Shigar valley pegmatites.

In hand specimen the alkali-feldspar, plagioclase feldspar and the quartz are the essential minerals of both of these two pegmatite fields or locations but the accessory minerals are variable. In case of micas, the Indus-Gilgit Confluence pegmatites have generally equal quantity of the two common micas (muscovite and biotite). However, the Shengus pegmatites are relatively rich in muscovite. Tourmaline is generally absent in the Indus-Gilgit Confluence pegmatites, while at Shengus some of the pegmatites contain tourmaline as an accessory phase. In addition to this, garnet is the common accessory mineral of some of the dikes and veins at both of these localities. The mineralogy of these two pegmatite fields indicates that these are the simple pegmatites having no rare elements and metals.

In case of gemstones, the aquamarine, topaz, fluorite and black-colored tourmalines are being mined from the Shengus pegmatites, especially from the zoned pegmatites, while, the Indus-Gilgit Confluence pegmatites are generally gem-barren. Like the Shigar valley pegmatites, the gemstones are either present in the intermediate zone or in the core-margin zone.

**Microscopic features:** The pegmatites of the Shengus area are medium to coarse-grained and inequigranular in texture. The major constituents are plagioclase (35 to 38 %), orthoclase (25 to 27 %) and quartz (30 to 33 %) (Table 5. 3). Plagioclase is dominant over the orthoclase and is mostly oligoclase (An $_{20-30}$) in composition. Both the feldspars are partially to highly altered. The alteration products are kaolinite, sericite, muscovite and epidote. Microperthitic texture is common in some of these sections (Plate 5. 53). Some of the anhedral quartz crystals were also seen as inclusion in the microperthite. In one of the thin sections of Shengus pegmatites, a clear-cut zoning is observed. One part of which is rich in orthoclase, while the other in muscovite. No muscovite is noticed in the orthoclase rich part, whereas in the muscovite part large flakes and sheets of muscovite along with quartz are observed (Plate 5. 54). In addition, garnet and apatite are noticed in the muscovite rich part. Quartz occurs as fresh and subhedral to anhedral grains with undulose extinction. In the minor phases, some biotite is seen along with muscovite. Besides, opaque and some euhedral crystals of zircon are also observed in the Shengus pegmatites. Moreover, minute grains of tourmaline and beryl are seen in thin sections under the microscope.

The Indus-Gilgit Confluence pegmatites are mostly medium-grained but some are coarse-grained. The major mineral constituents of these pegmatites are orthoclase (10 to 70 %), plagioclase (12 to 47 %) and quartz (15 to 30 %). While biotite and muscovite are present in considerable amounts in some of the samples. Garnet, apatite, epidote, zircon and opaque are present in traces. However, one sample (ICP-107) has up to 3 % garnet (Plates 5. 55 and 5. 56). The Indus-Gilgit Confluence pegmatites contain both microcline and orthoclase as alkali-feldspar with microcline in relatively high contents as compared

to the orthoclase (Plates 5. 57 and 5. 58). These are, therefore, different from the pegmatites of Shengus and Shigar valleys, as the later are having high amount of orthoclase and negligible amount of microcline. Some of the samples of Indus-Gilgit Confluence pegmatites are so highly enriched in microcline that it reaches up to 70 % by volume (Table 5.3). Both the feldspars (alkali-feldspar and plagioclase) are generally fresh but partial alteration to kaolinite, sericite, muscovite and epidote is very common in these pegmatites. In few cases, complete alteration of these phases is also noticed, where pseudomorph after these phases is clearly visible. The plagioclase is generally oligoclase with anorthite content ranging from 15-24 %. Quartz occurs as anhedral to subhedral grains showing undulose extinction and is interlocked with feldspar grains. The inclusion of quartz and garnet within feldspar are also observed into some of the sections (Plates 5. 55, 56, 61 and 62). Moreover, like the plagioclase, microcline is also present in tabular fashion (Plates 5. 59 and 5. 60).

Tourmaline is completely absent from these pegmatites, while apatite and opaque are present in traces. The absence of tourmaline also differentiates these pegmatites from those of the Shengus and Shigar valleys pegmatites. In addition to this, few grains of zircon as inclusions are observed in some of the sections. Garnet is generally present as inclusion in feldspars.

## Host Rocks

The study of host rocks of pegmatites is also very important, because these contribute a lot in the mineralogy and chemistry of pegmatites, especially at their margin. For this purpose, samples of host rocks of pegmatites from various localities were collected to see the possible changes that might be expected at the contacts of pegmatites and host rocks. The host rock of pegmatites from Goyungo up to Kashmol is the biotite gneiss and is known as Dassu biotite gneiss (Searle, 1991), while from Sildi to downstream of Shigar river, the host rocks are gneisses, schists, marbles and metavolcanics (Fig. 3 1). The host rocks of all the gem-bearing and gem-barren

pegmatites of the Shigar valley area are Dassu biotite gneisses, therefore, megascopic and microscopic features of these gneisses are described below in detail.

**Megascopic features of Dassu biotite gneiss:** The Dassu gneiss is granodioritic augen-gneiss occurring in the upper part of the Shigar and lower part of the Braldu valleys. In hand specimen, it is composed of two-feldspar, quartz, biotite, while muscovite is present in minor quantities. Along with muscovite, garnet is also present as an accessory phase and minute garnet crystals are even visible with naked eye. Tourmaline is generally absent. Iron-leaching is the common feature of this gneiss, especially in the large biotite flakes and opaque phases. The gneiss is strongly foliated, but it still exhibits an igneous texture in thin sections. The foliation and augen-texture are the common features of the Dassu biotite gneiss. The flakey minerals are well aligned. The contact of the pegmatites with the gneisses is very sharp (Plate 3. 4) and xenoliths of gneisses are found in the pegmatites.

**Microscopic features:** The mineral assemblages observed in thin section were also seen in the field in hand specimen but some additional phases were seen in traces. Those found in traces are the apatite, sphene, epidote, opaque and zircons. Tourmaline is completely absent into these and garnet is present in traces.

The Dassu biotite gneiss is medium to coarse-grained in thin sections. The constituents of the gneisses are slightly fractured; even quartz crystals are also fractured, indicating the great stress in the area. In case of alteration, both the alkali as well as plagioclase feldspars are partially to highly altered into kaolinite, sericite, muscovite and epidote (Plates 5. 63, 5. 64 and 5. 65). The alteration is present throughout the grains, while in some sections, it is restricted either to the margin or core. Quartz and K-feldspar also shows undulose extinction that indicates greater stress in the region. In granularity, all the constituents are subhedral to anhedral but some grains of quartz, biotite and plagioclase are also euhedral. The plagioclase is mostly andesine in composition with anorthite content ranging from 20-28 %. The kink bending in plagioclase and granophyric texture is noted in alkali-feldspar (Plates 5. 66, 5. 67). Quartz occurs as

anhedral to subhedral grains but it also occurs as inclusions within the two feldspars. Sometimes, quartz inclusions are present in high intensity and, therefore, impart pepper-mesh texture in the feldspar grains. A preferred orientation of flaky minerals, especially in biotites is well noticed and is very common in every section of these gneisses (Plate 5. 68). The biotites are generally brown to greenish-brown in color under plane light and are found as minute to large flakes. The overlapping, cross cutting and overgrowths of the biotites are the common features of the Dassu gneiss (Plates 5. 69, 5. 70, 5. 71 and 5.72). In some of the sections, the volume percentage of biotites is reaching up to 25 % (Table 5. 4). Muscovite is present up to 1 % but in some sections, it reaches up to 10 % (Table 5. 4).

Among the accessory phases, euhedral crystals of apatite (up to 1 %), euhedral to subhedral garnet, epidote, sphene, zircon (Plates 5. 73, 5. 74) and opaque phases are also noticed. Iron-leaching near the opaque phases and also along the micro fractures is common in these rocks (Plates 5. 75, 5. 76).

**Table 5. 1. Modal composition (visual estimation) of the gem-bearing pegmatites from different localities of the Shigar valley.**

**a. Muscovite-schorl-beryl-garnet pegmatites**

| Section # | MUN-13 | DAS-19 | DAS-22A | DAS-22B | DAS-23 | DAS-26 | NYT-28 | NYT-29 |
|---|---|---|---|---|---|---|---|---|
| Alkali feldspar | 26 | 34 | 27 | 31 | 9 | 7 | 20 | 30 |
| Plagioclase | 40 | 18 | 38 | 36 | 60 | 70 | 25 | 25 |
| Quartz | 30 | 28 | 30 | 28 | 25 | 20 | 33 | 27 |
| Biotite | tr | tr | – | tr | – | – | – | – |
| Muscovite | 2 | 20 | 3 | 3 | 4 | 2 | 22 | 3 |
| Garnet | – | tr | tr | – | – | – | – | tr |
| Tourmaline | 1 | tr | 1 | – | 2 | – | – | 15 |
| Apatite | 1 | – | | – | tr | – | – | – |
| Epidote | – | tr | - | - | tr | 1 | tr | - |
| Sphene | – | – | – | 1 | – | – | – | – |
| Zircon | tr | – | – | – | – | – | - | – |
| Opaque | tr | tr | 1 | 1 | – | tr | – | – |
| **Total** | **100** | **100** | **100** | **100** | **100** | **100** | **100** | **100** |

**Key:-MUN = Mungo; DAS = Dassu; NYT = Nyit; GOY = Goyungo; KSH = Kashmol; GON = Gone**

(Table 5. 1 continued)

| Section # | GOY-32 | GOY-33 | GOY-43 | GOY-44 | GON-47 | KSH-62 | KSH-63 | KSH-66 | KSH-68 |
|---|---|---|---|---|---|---|---|---|---|
| Alkali feldspar | 20 | 18 | 30 | 50 | 30 | 16 | 15 | 9 | 16 |
| Plagioclase | 25 | 50 | 36 | 15 | 23 | 40 | 35 | 45 | 40 |
| Quartz | 30 | 26 | 25 | 30 | 28 | 35 | 25 | 25 | 27 |
| Biotite | – | – | – | tr | – | – | tr | – | – |
| Muscovite | 20 | 3 | 3 | 5 | 15 | 8 | 24 | 18 | 15 |
| Garnet | tr | tr | – | – | tr | tr | 1 | 3 | 1 |
| Tourmaline | 3 | 3 | 6 | | 3 | | | | 1 |
| Apatite | 2 | tr | | – | 1 | tr | tr | tr | tr |
| Epidote | – | – | - | - | - | 1 | tr | tr | tr |
| Sphene | tr | tr | – | – | – | – | – | – | – |
| Zircon | – | – | – | – | tr | – | – | tr | – |
| Opaque | – | – | – | – | – | – | tr | – | – |
| **Total** | **100** | **100** | **100** | **100** | **100** | **100** | **100** | **100** | **100** |

**GOY = Goyungo; KSH = Kashmol; GON = Gone**

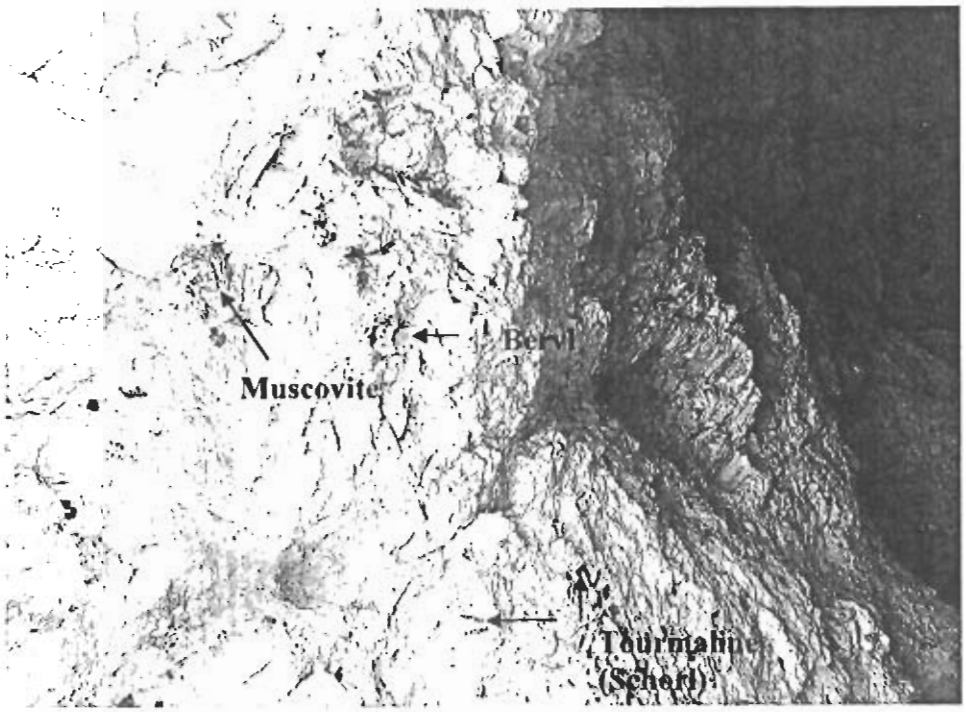


**Plate 5.1.** Photograph showing a pegmatite mine at Baha (Dassu), from where gemstones have been excavated. Small euhedral blue aquamarine, schorl and large sheets (or books) of muscovite are also visible.

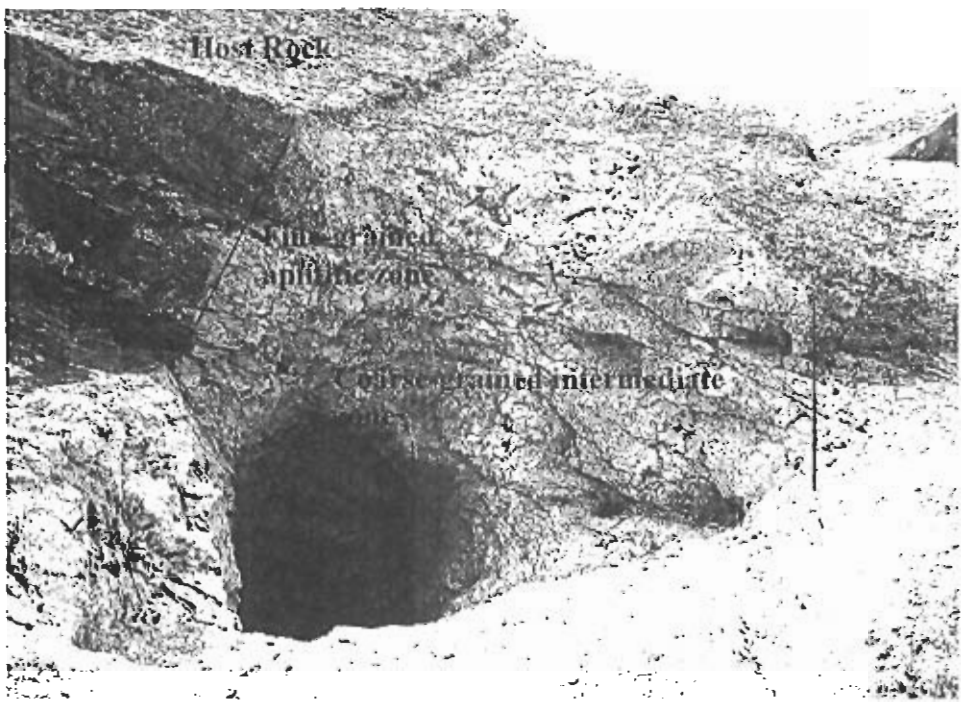


**Plate 5.2.** Photograph showing a zoned gem-bearing pegmatite at Dassu. The internal zoning is very complex and is without the central quartz zone. The border zone in the hangingwall and the footwall is fine-grained and aplitic, while three intermediate zones are rich in schorl. The host rock is Dassu biotite gneiss. As there is repetition of the same zone, therefore, this pegmatitic body can be considered as symmetrical.

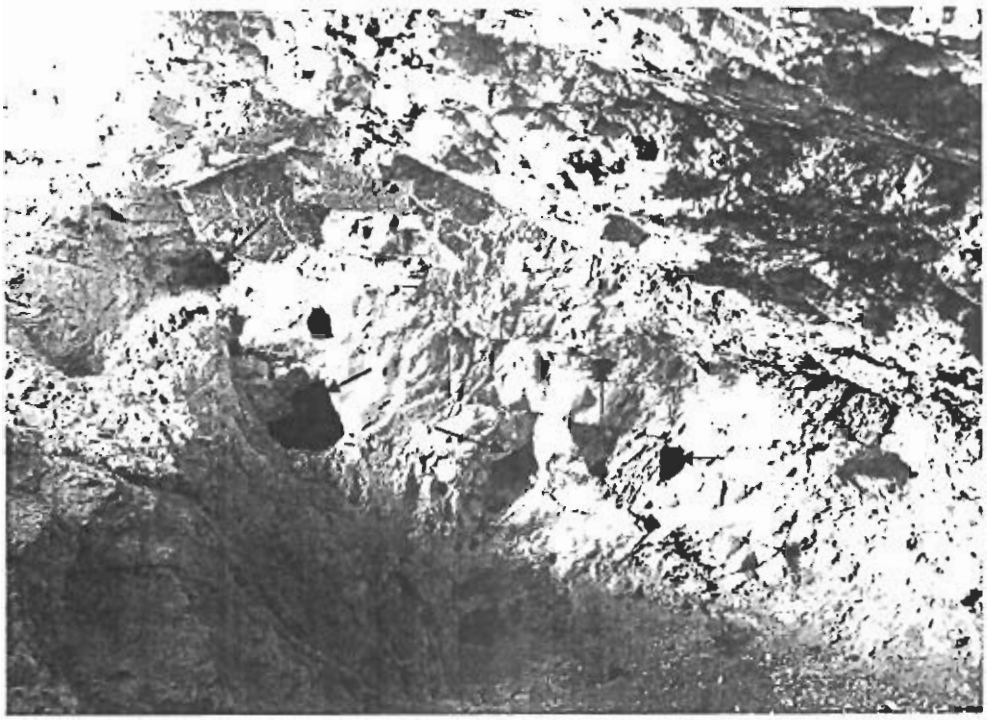

**Plate 5. 3.** Photograph of a coarse-grained pegmatite mined for aquamarine, topaz and fluorite. The cavities of different sizes are also visible.

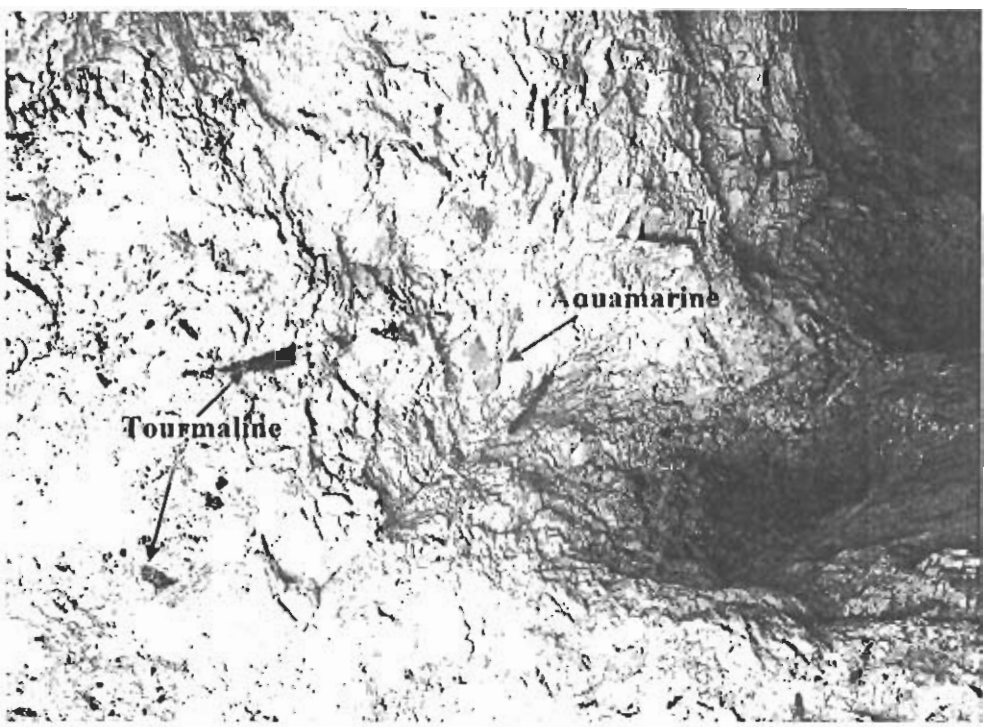


**Plate 5.4.** A coarse-grained pegmatite at Baha (Dassu), which has been extensively mined for aquamarine, topaz etc. Three light blue aquamarine crystals along with schorl are present in the coarse-grained intermediate zone.

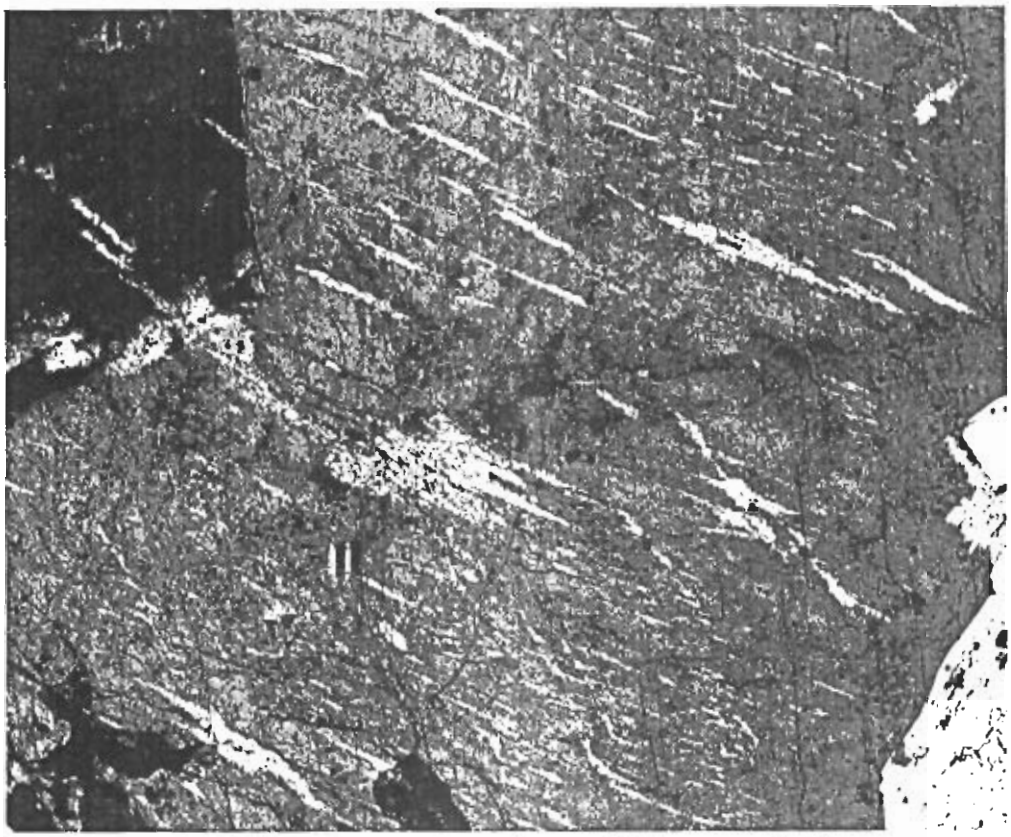

**Plate 5.5.** Photomicrograph showing microperthitic texture in the pegmatites of Kashmol area. The flakes of muscovite are also visible. (Mag: 4× / 0.1)

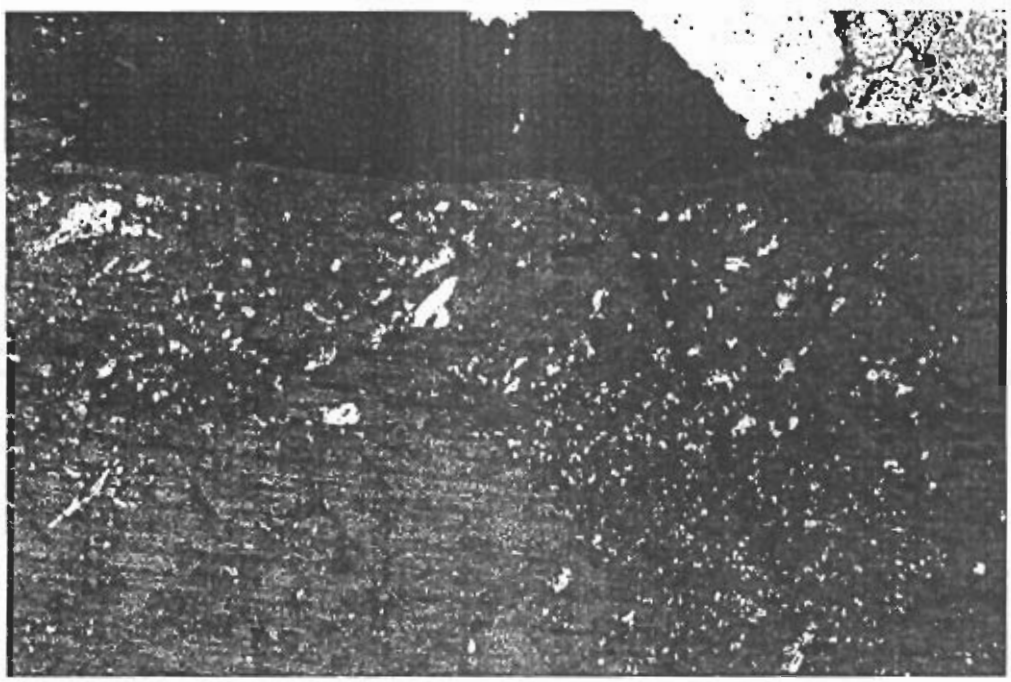

**Plate 5. 6.** Photomicrograph showing the saussuritization of plagioclase in a pegmatite at Dassu. (Mag: 4× / 0.1)

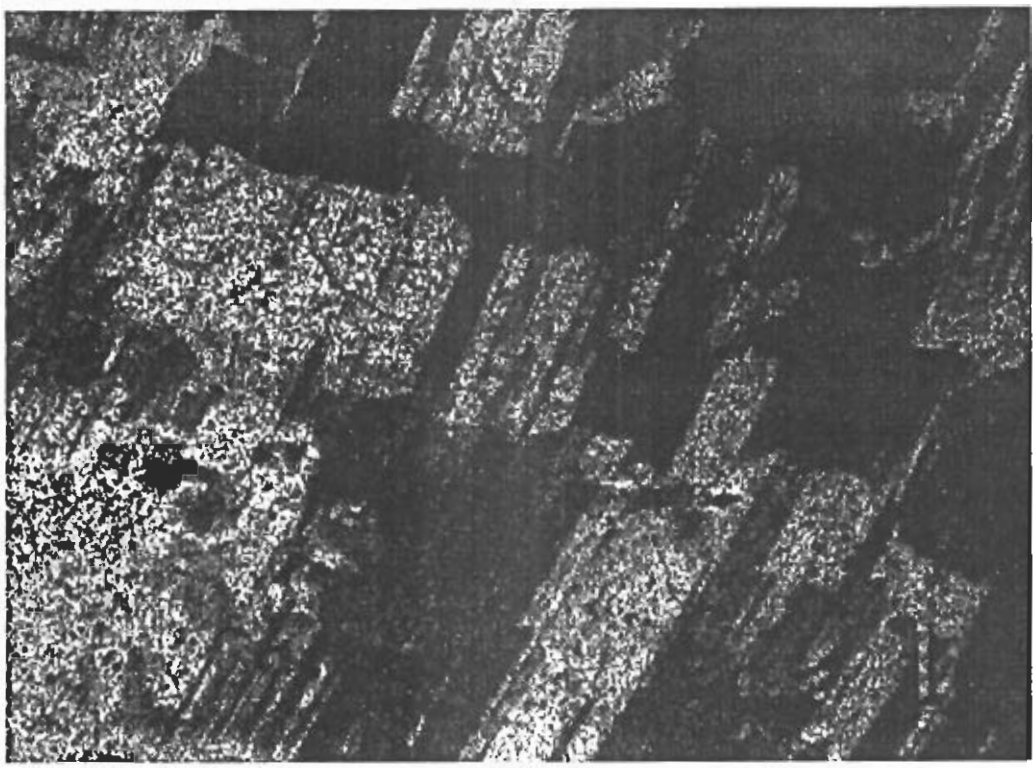

**Plate 5.7.** Photomicrograph showing kink bending in plagioclase. (Mag: 4× / 0.1).

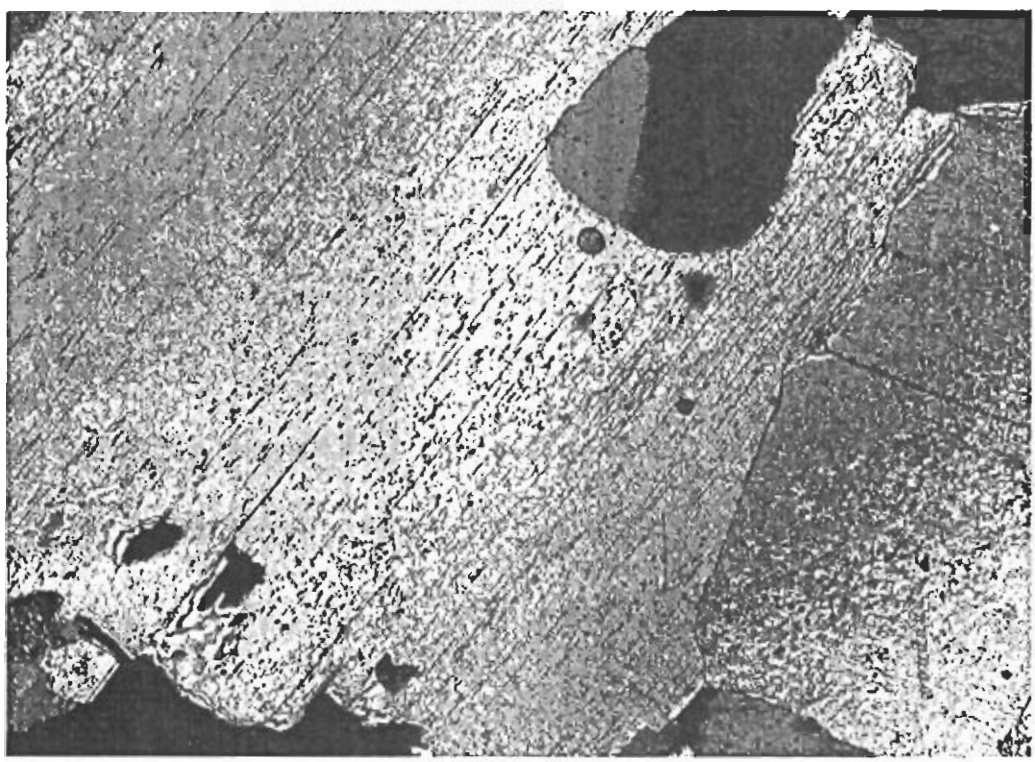

**Plate 5. 8.** Microphotograph large cleavable sheets of muscovite in a sample (DAS-19), taken from the core-margin zone of a zoned pegmatite at Dassu. (Mag: 4× / 0.1).

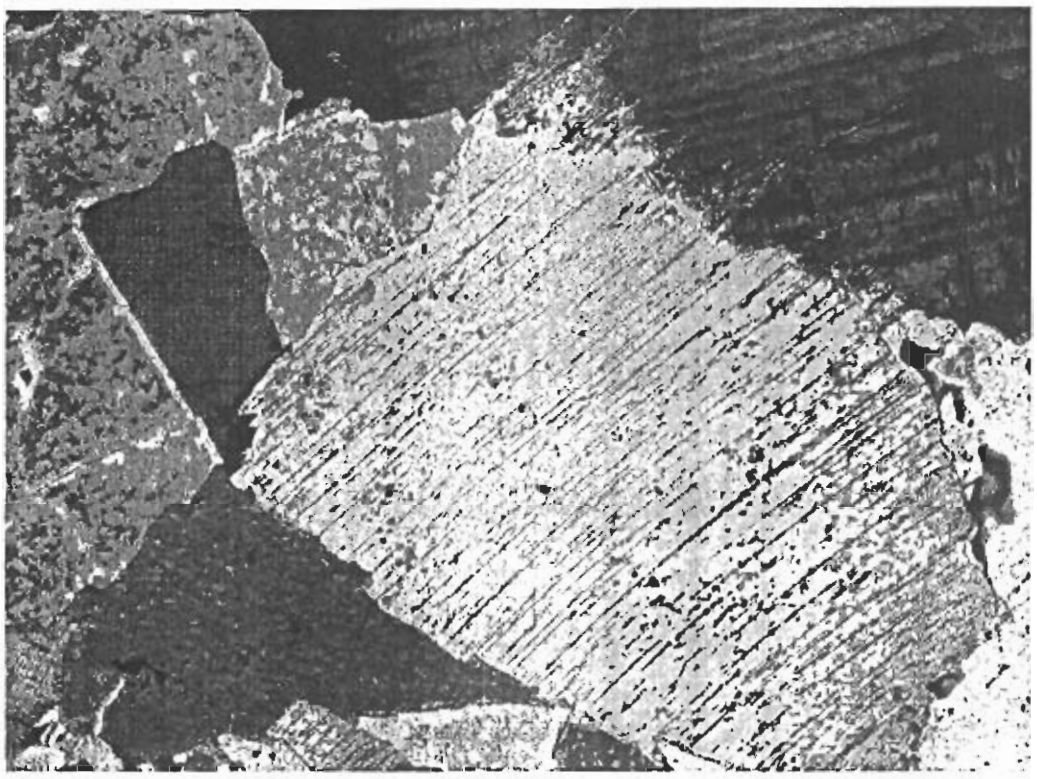

**Plate 5. 9.** Photomicrograph showing partial alteration at the upper margin of a large flake of muscovite. At the top right corner, a plagioclase with vague albite twinning may also be seen, while quartz is seen in the left side. (Mag: 4× / 0.1)

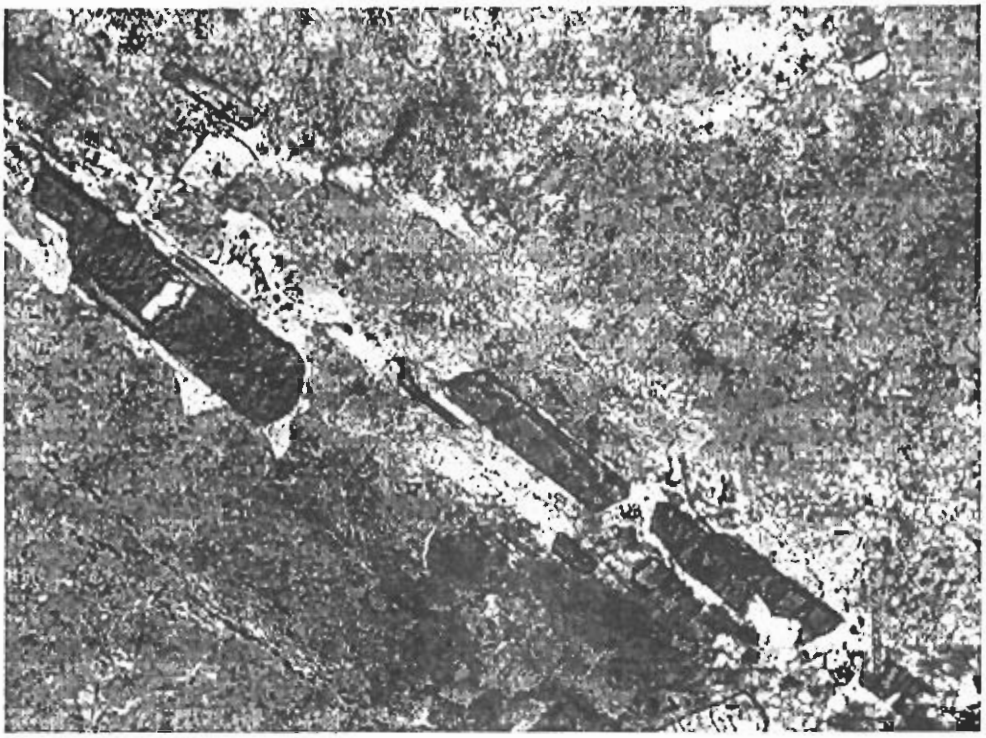

**Plate 5. 10.** Photomicrograph showing euhedral tourmaline crystals aligned in one direction and are included in orthoclase (cross light, Mag: 4× / 0.1).

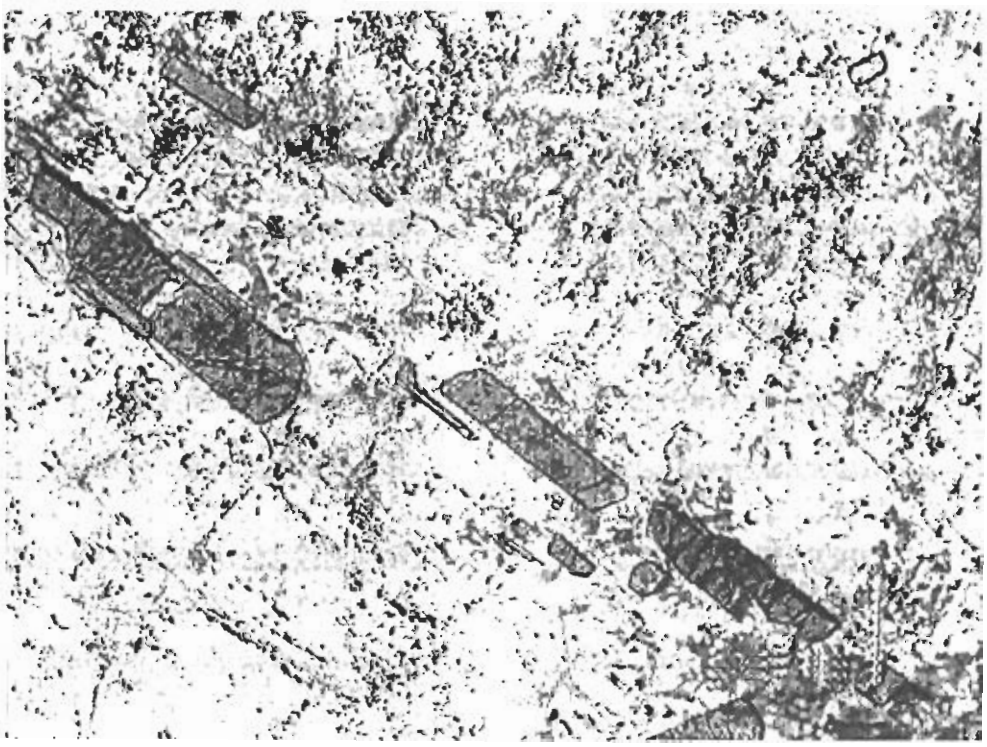

**Plate 5. 11.** Same view in the plane polarized light.

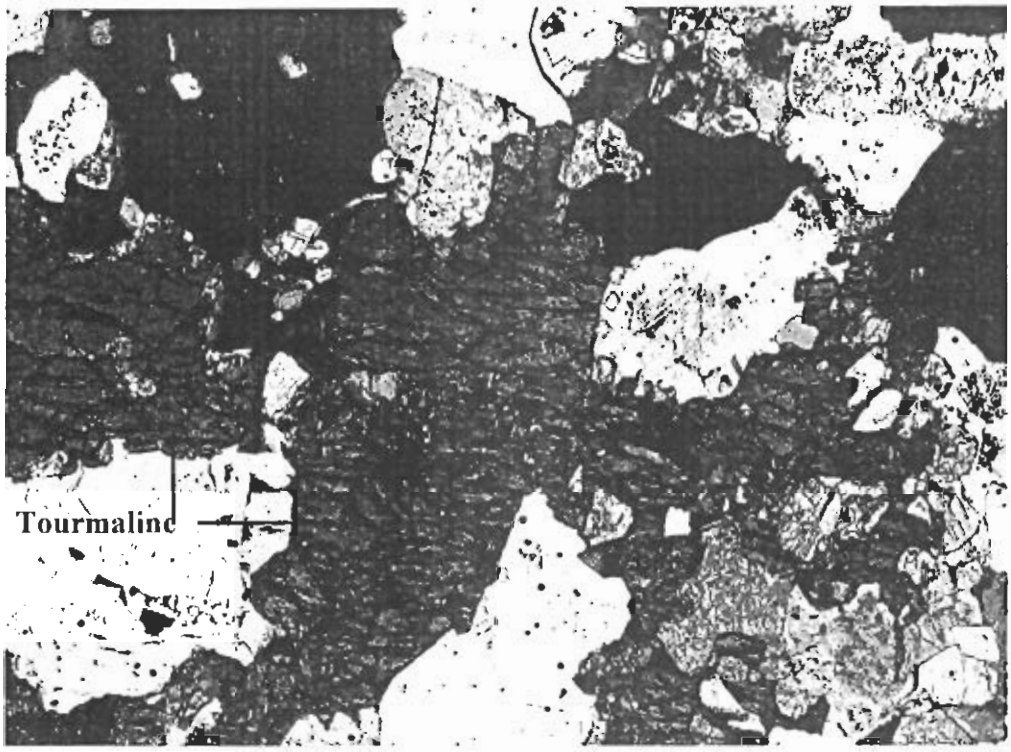


**Plate 5. 12.** Photomicrograph showing euhedral-subhedral tourmaline crystals (cross light, Mag: 4× / 0.1).

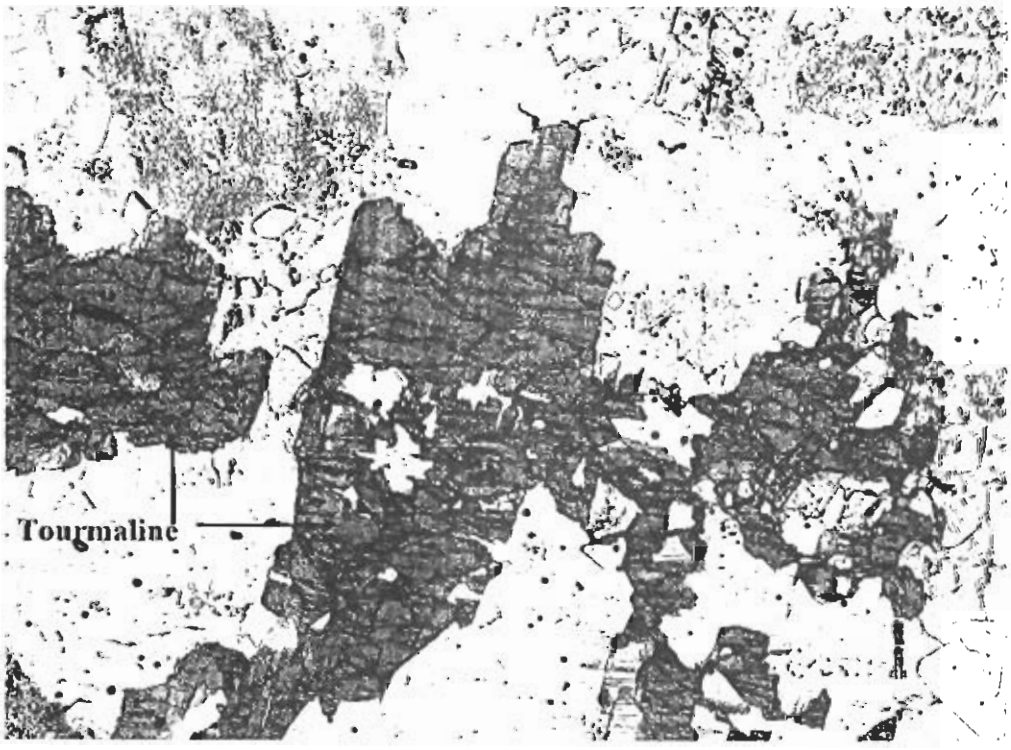


**Plate 5. 13.** Same view in the plane polarized light.

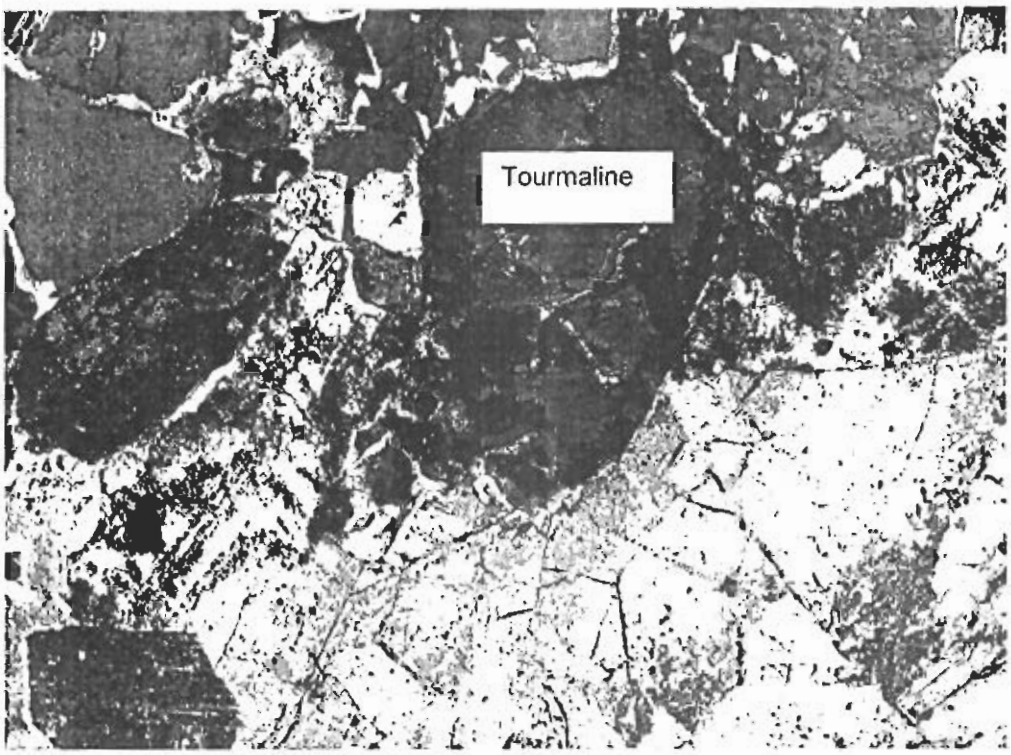


**Plate 5. 14.** Photomicrograph showing an euhedral and zoned tourmaline crystal in the pegmatites at Goyungo. The interlocking minerals are quartz and orthoclase (cross light, Mag: 4× / 0.1).

**Plate 5. 15.** Same view in plane polarized light.

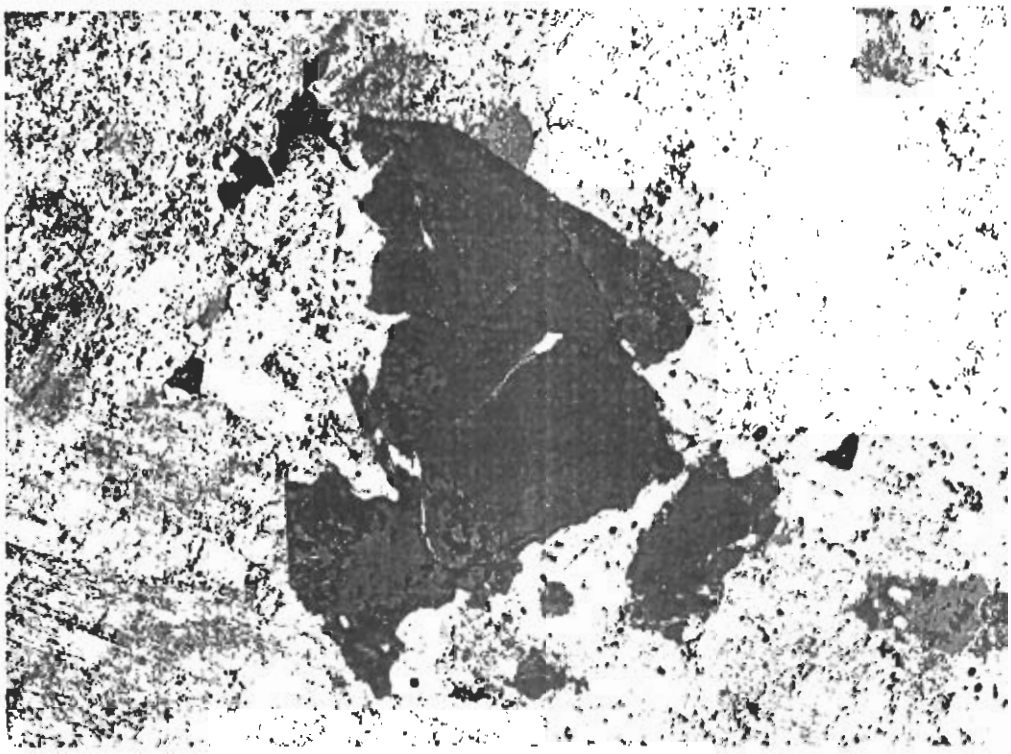

**Plate 5. 16.** Photomicrograph showing an euhedral-subhedral and zoned tourmaline crystal in the groundmass of plagioclase and orthoclase feldspar at Mungo (Hyderabad). Mag: 4× / 0.1

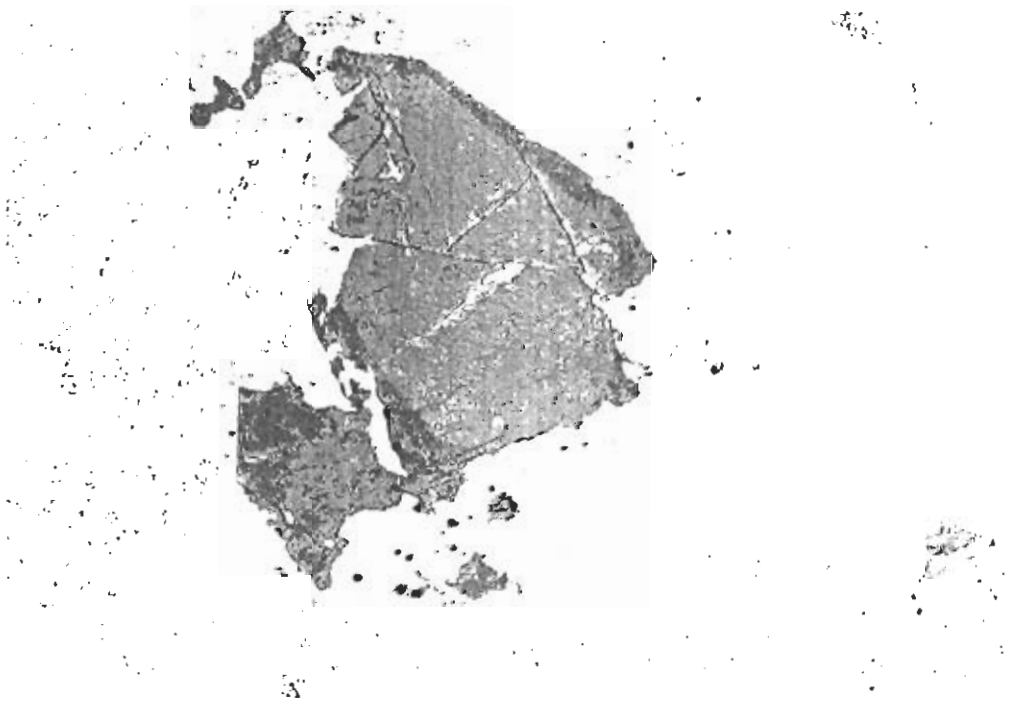

**Plate 5. 17.** Same view in plane polarized light.

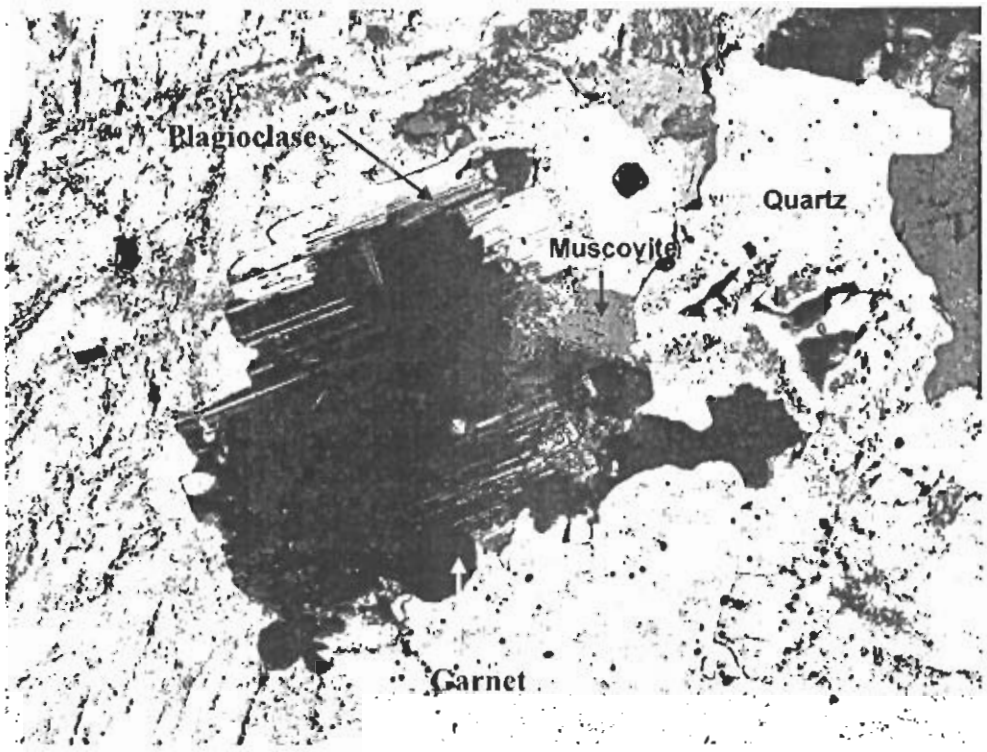


**Plate 5. 18.** Photomicrograph showing small euhedral garnet crystals present as inclusion in the plagioclase and orthoclase. Plagioclase is showing vague albite twinning, while on right quartz and two flakes of muscovite are also visible. (Mag: 4× / 0.1)

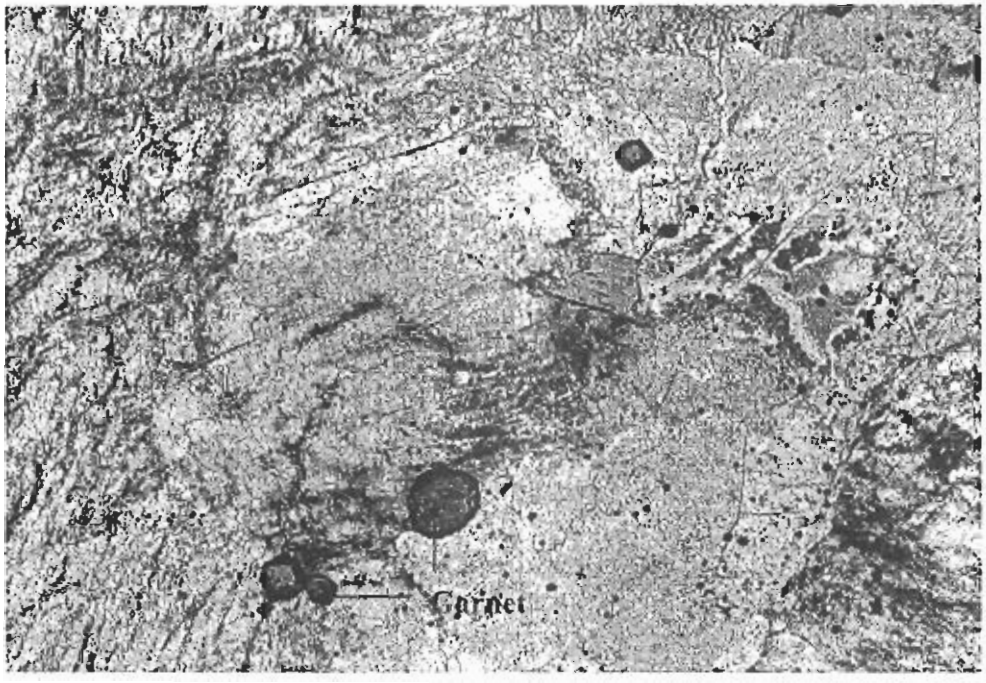


**Plate 5. 19.** Same view in plane polarized light.

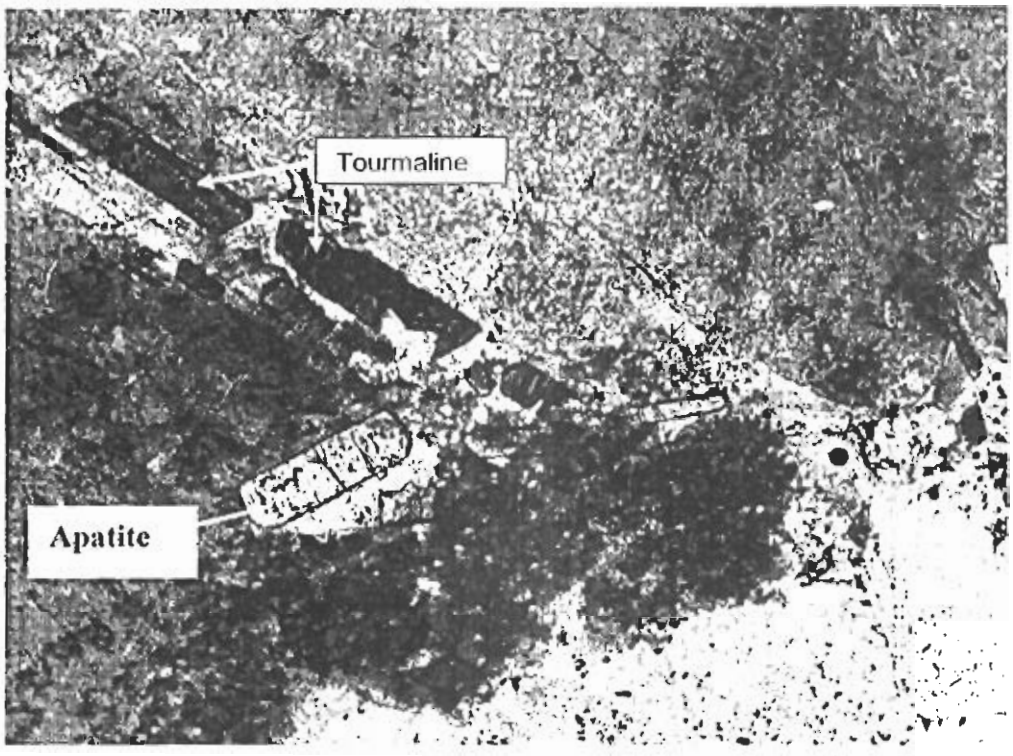


**Plate 5. 20.** Photomicrograph showing euhedral tourmaline crystals aligned in one direction in the groundmass of K- feldspar, besides some euhedral apatite crystals are also seen in the center. (Mag: 4× / 0.1)

(Table 5. 1 continued)

**b. Muscovite-schorl pegmatite**

| Section # | NYT-54 | KSH-74 | SIL-81 | ALCH-97 | HAS-98 |
|---|---|---|---|---|---|
| Alkali feldspar | 36 | 16 | 10 | 15 | 28 |
| Plagioclase | 30 | 44 | 55 | 55 | 32 |
| Quartz | 25 | 28 | 30 | 26 | 30 |
| Biotite | tr | - | – | 1 | – |
| Muscovite | 8 | 12 | 5 | 3 | 10 |
| Garnet | – | – | – | – | – |
| Tourmaline | | tr | – | – | – |
| Apatite | tr | – | tr | tr | tr |
| Epidote | tr | tr | – | tr | – |
| Sphene | tr | | – | | |
| Zircon | tr | | | | |
| Opaque | 1 | tr | tr | tr | - |
| **Total** | **100** | **100** | **100** | **100** | **100** |

**NYT = Nyit; KSH = Kashmol; SIL = Sildi; ALCH = Alchuri; HAS = Hashupa**

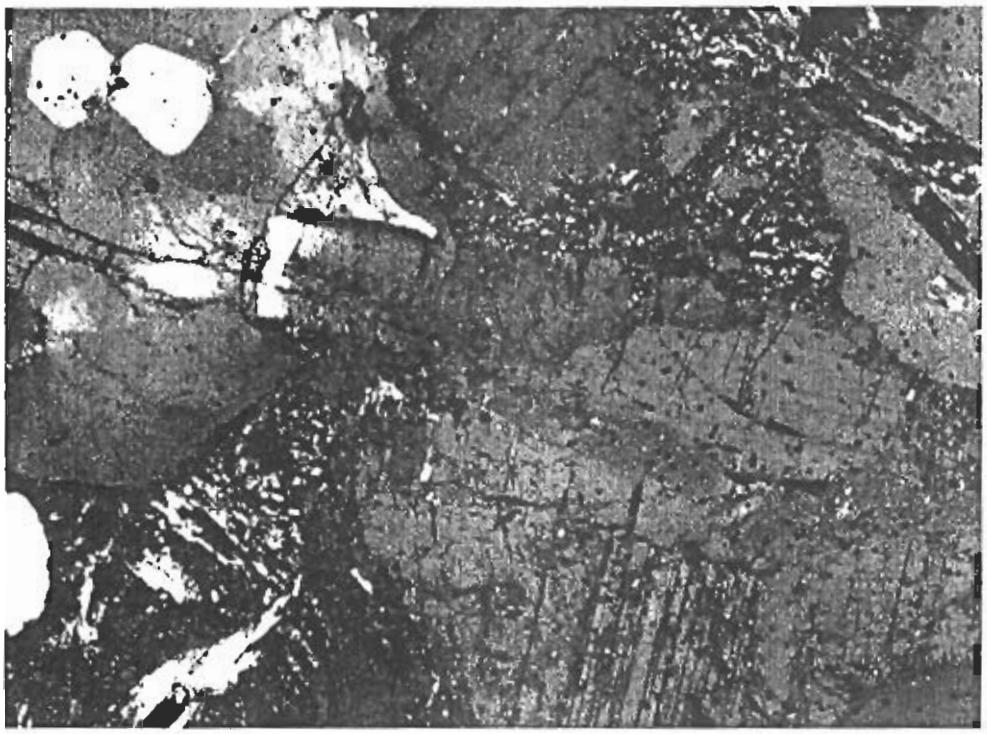

**Plate 5. 21.** Photomicrograph showing partial saussuritization of plagioclase and altered to epidote, muscovite, and sericite. Fresh looking crystals of quartz are also seen on left top corner.

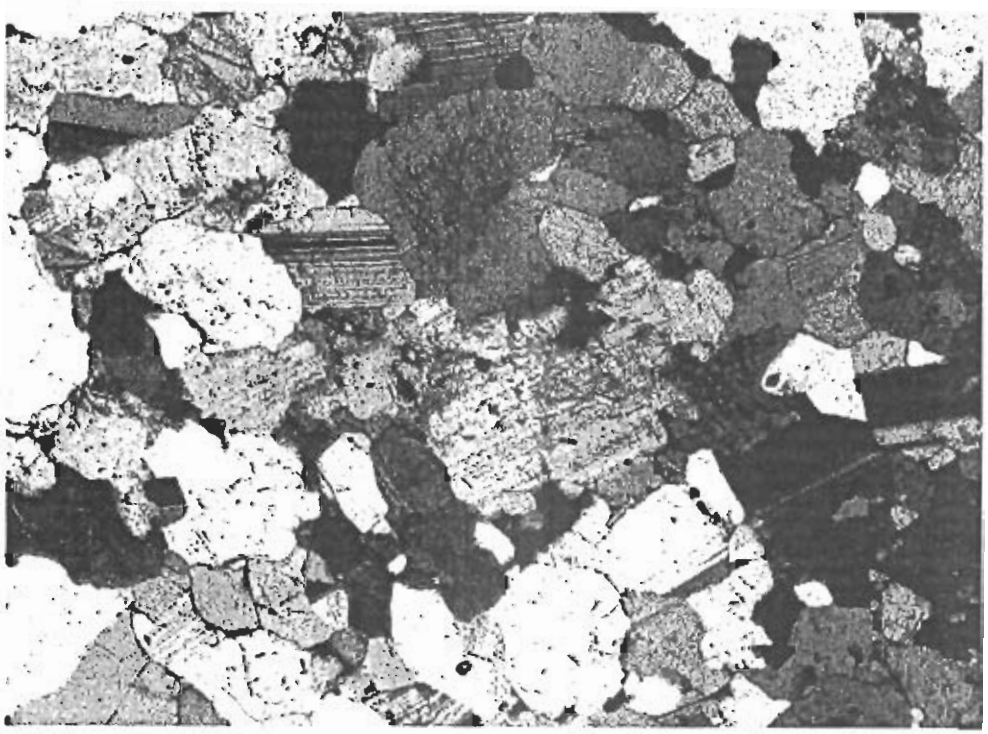

**Plate 5.22.** Photomicrograph showing small tabular and euhedral to subhedral plagioclase crystals having interlocking behaviour with quartz and orthoclase. (Mag: 4× / 0.1).

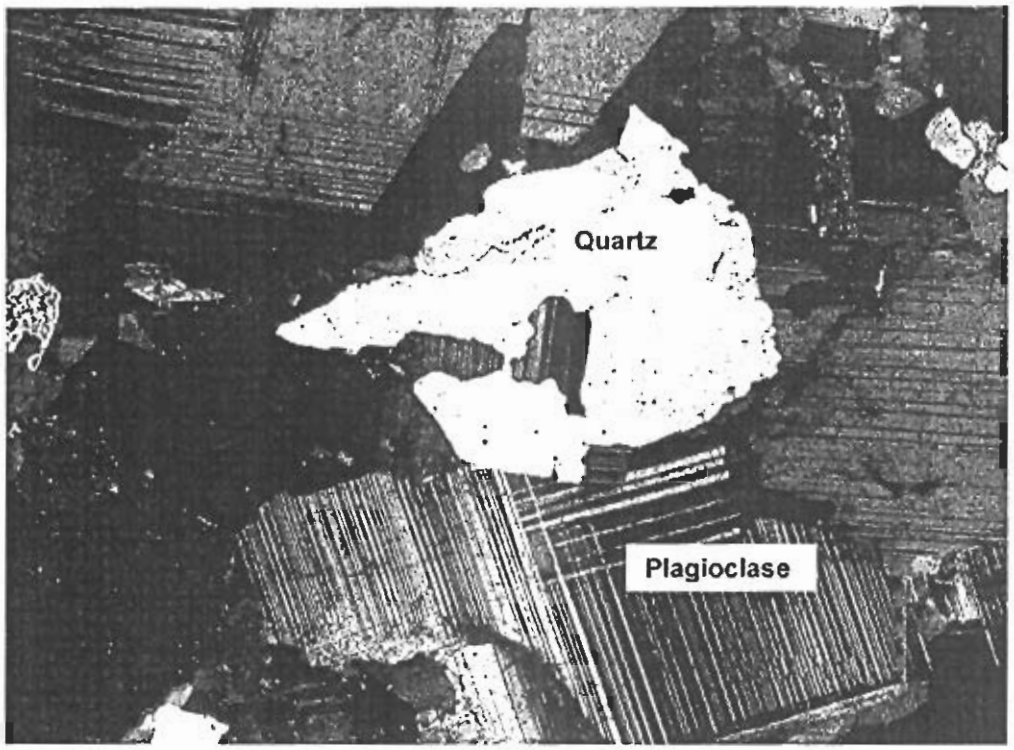


**Plate 5. 23.** Photomicrograph showing cross-cutting relationship within tabular plagioclase feldspar. Plagioclase also occurs as inclusion within the quartz.

**Plate 5. 24.** Photomicrograph showing micrographic texture and vague albite twinning. Muscovite flakes are also visible. (Mag: 4× / 0.1).

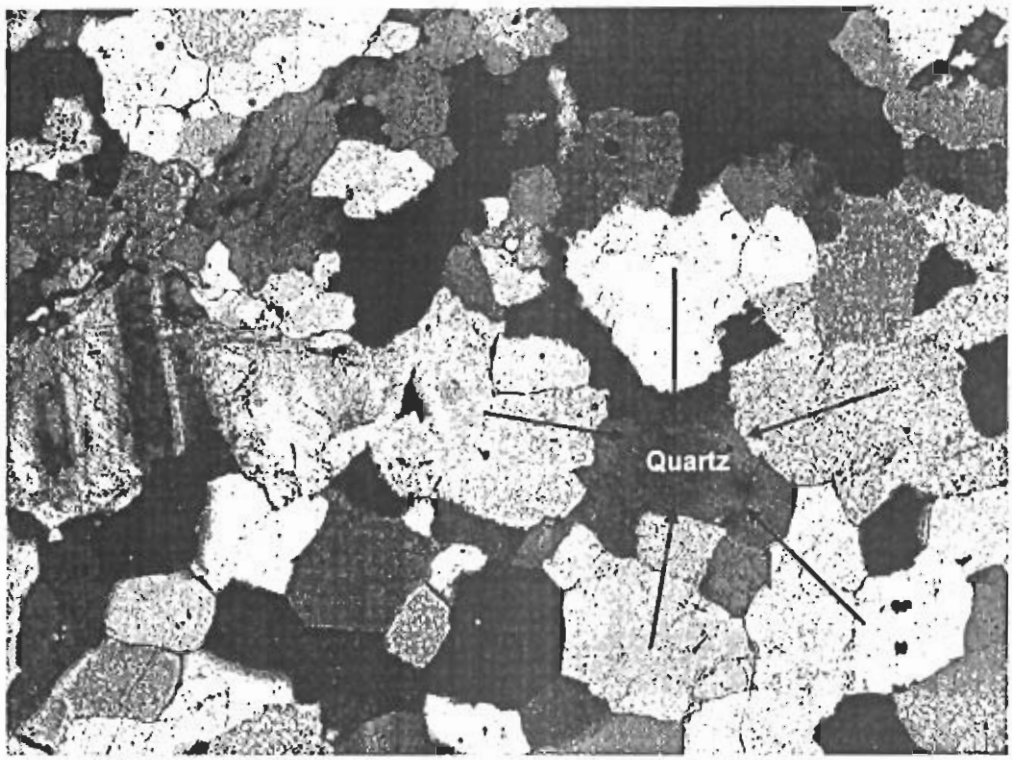


**Plate 5. 25.** Photomicrograph showing euhedral to subhedral, equigranular and fresh-looking quartz crystals in pegmatites near Sildi.

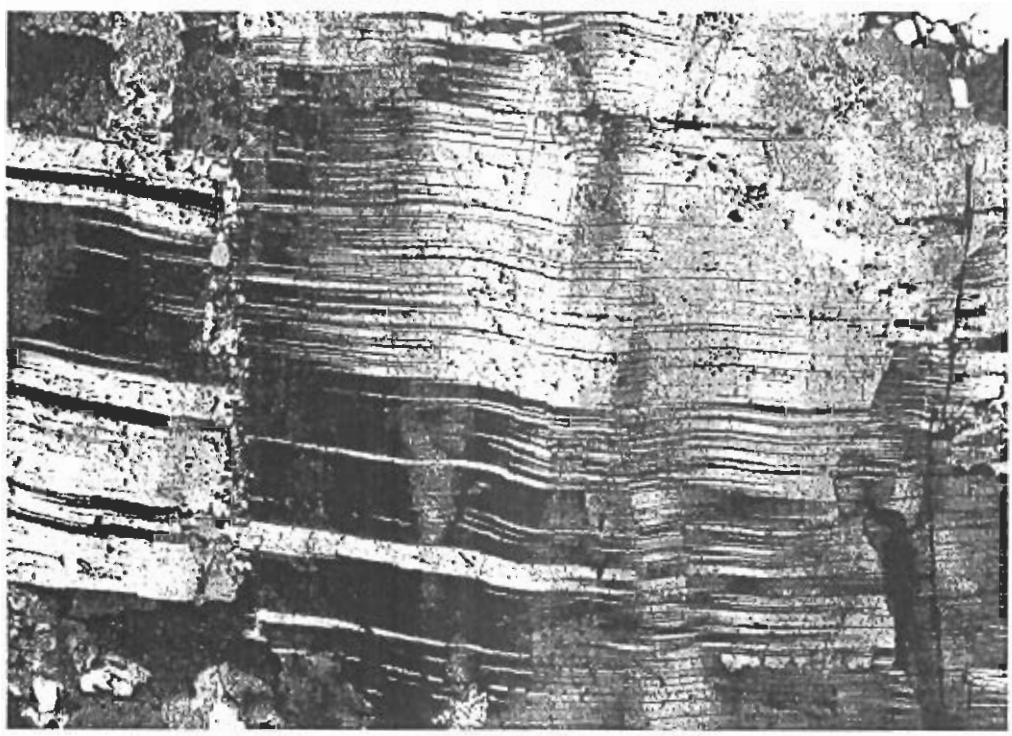

**Plate 5. 26.** Photomicrograph showing displacement and kinking in the plagioclase. A micro quartz vein is visible at left side. (Mag: 4× / 0.1)

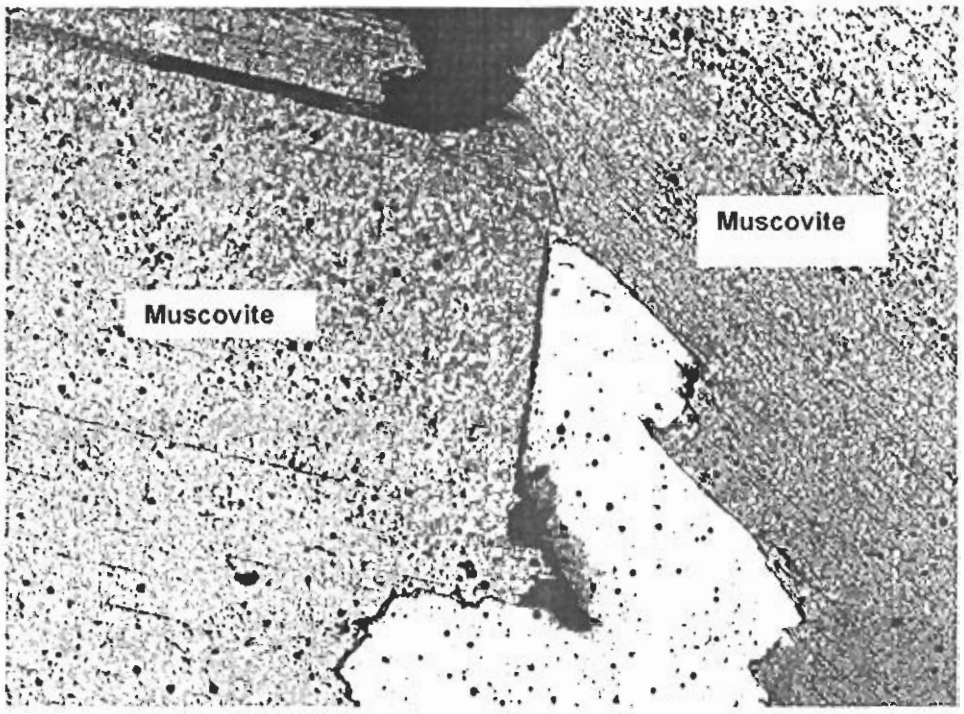


**Plate 5. 27.** Photomicrograph showing large fresh and cleavable sheets of muscovite in pegmatites of Gone area. (Mag: 4× / 0.1).

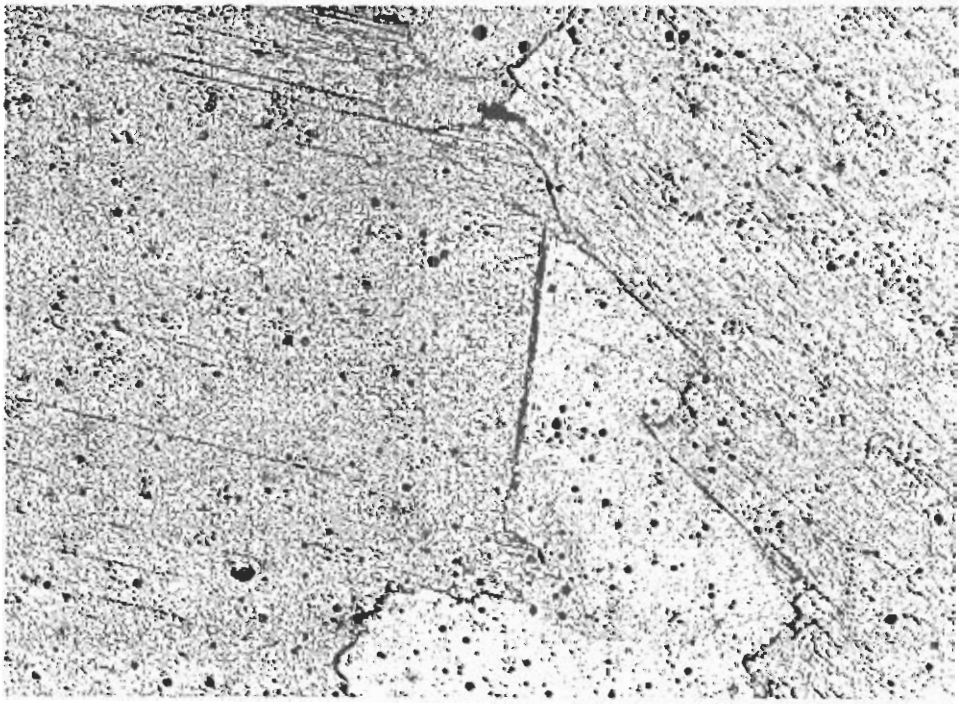

**Plate 5. 28.** Same view in plane polarized light.

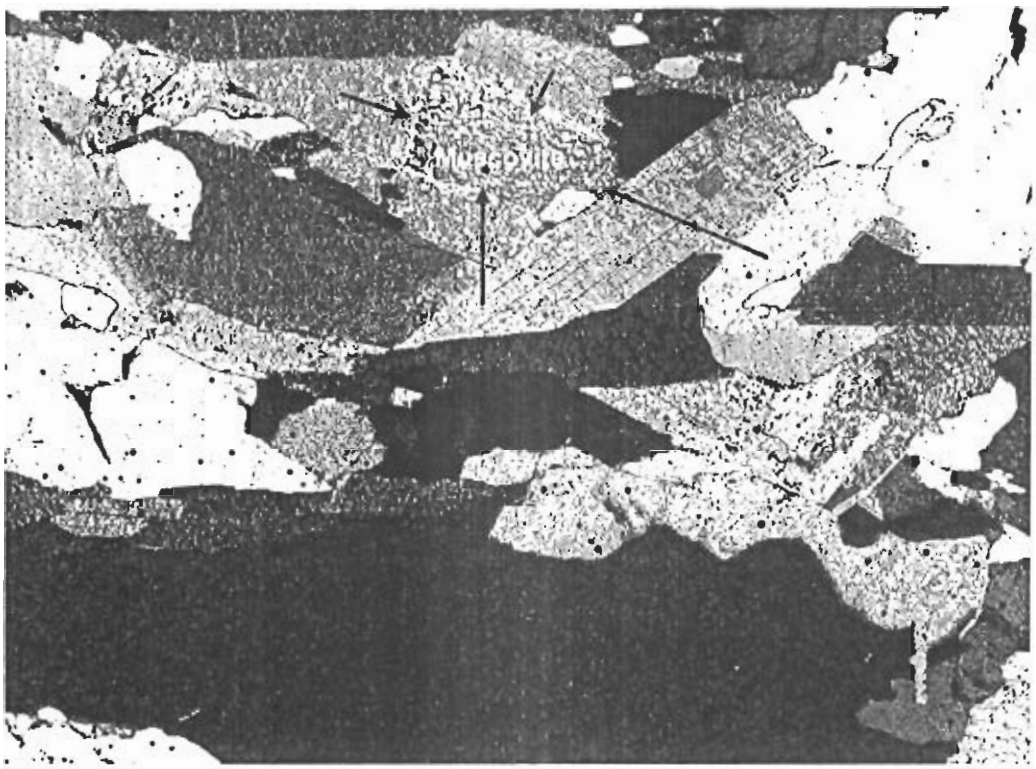


**Plate 5. 29.** Photomicrograph showing overgrowth within muscovite grains in pegmatites at Kashmol. (Mag: 4× / 0.1)

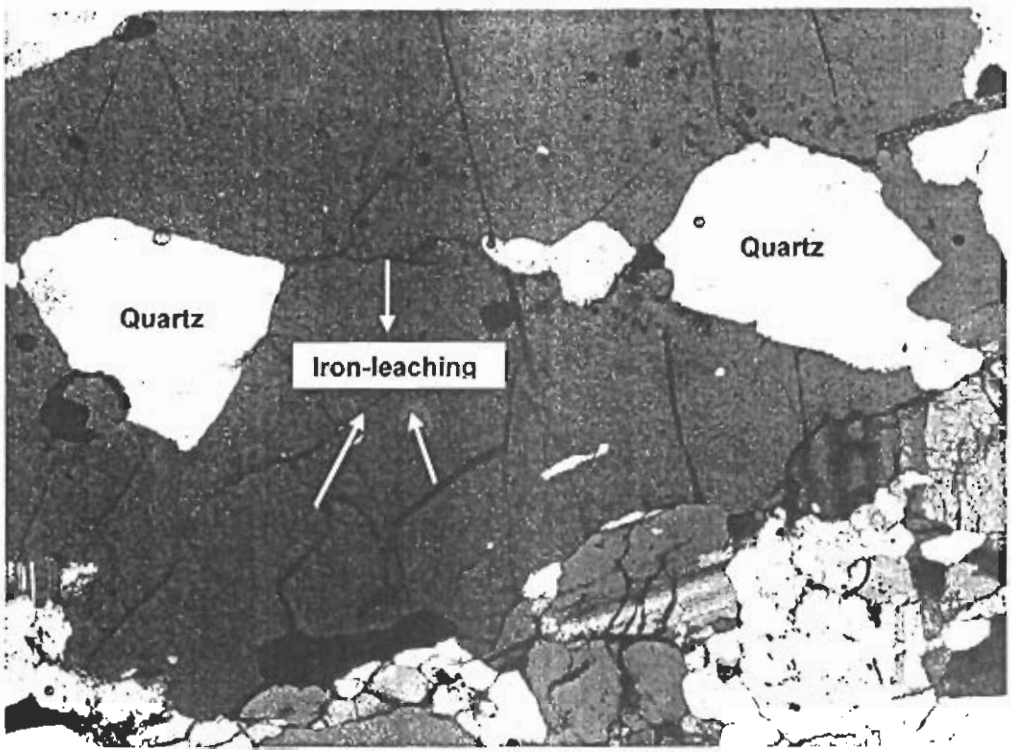


**Plate 5. 30.** Photomicrograph showing fresh looking quartz crystals, while intensive iron-leaching is seen along micro-fractures near the opaque phases.

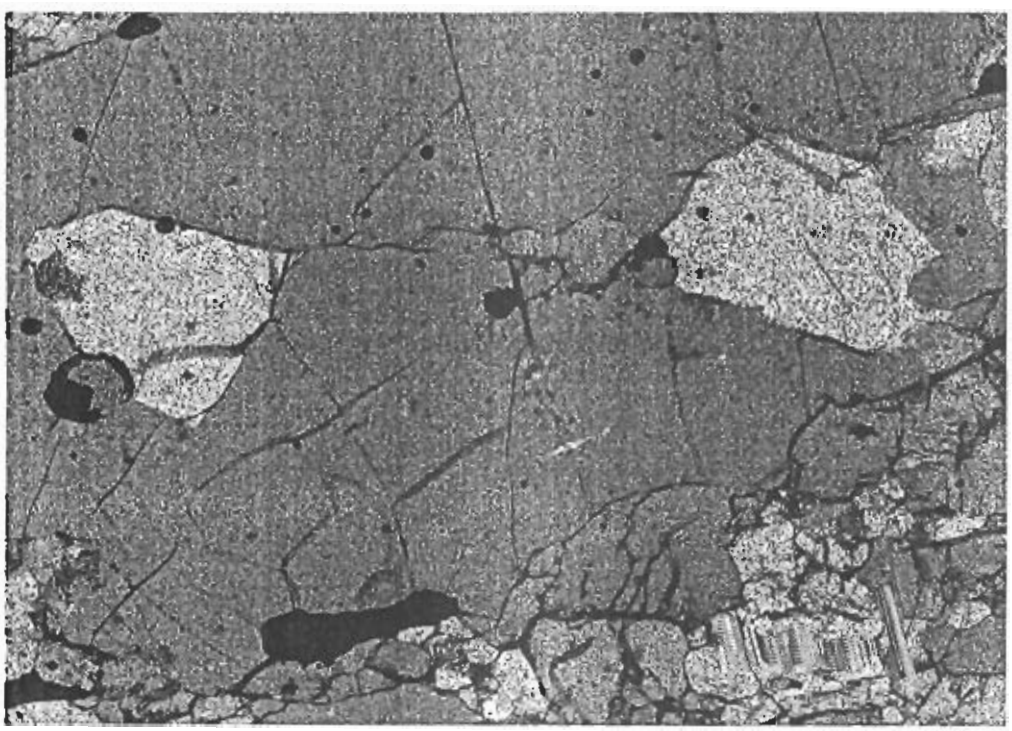

**Plate 5. 31.** Same view in plane polarized light.

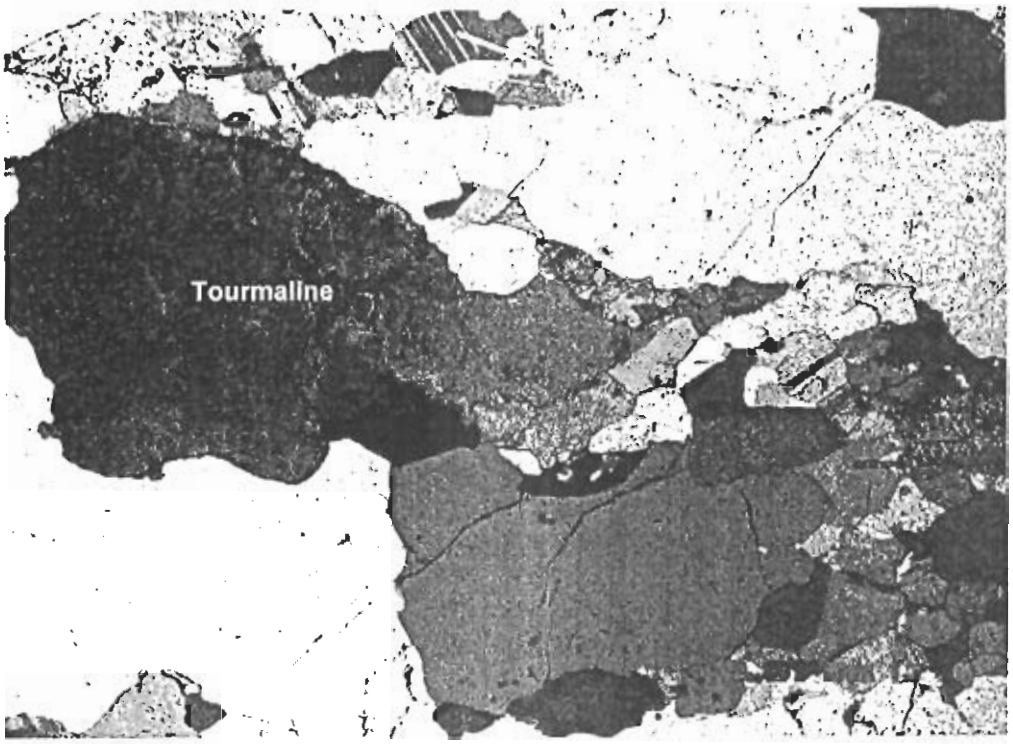


**Plate 5. 32.** Photomicrograph showing subhedral to anhedral tourmaline crystal at the left side and an euhedral plagioclase depicting Carlsbad twinning at the top, are seen. The rest field of view is covered with fresh quartz crystals. (Mag: 4× / 0.1).

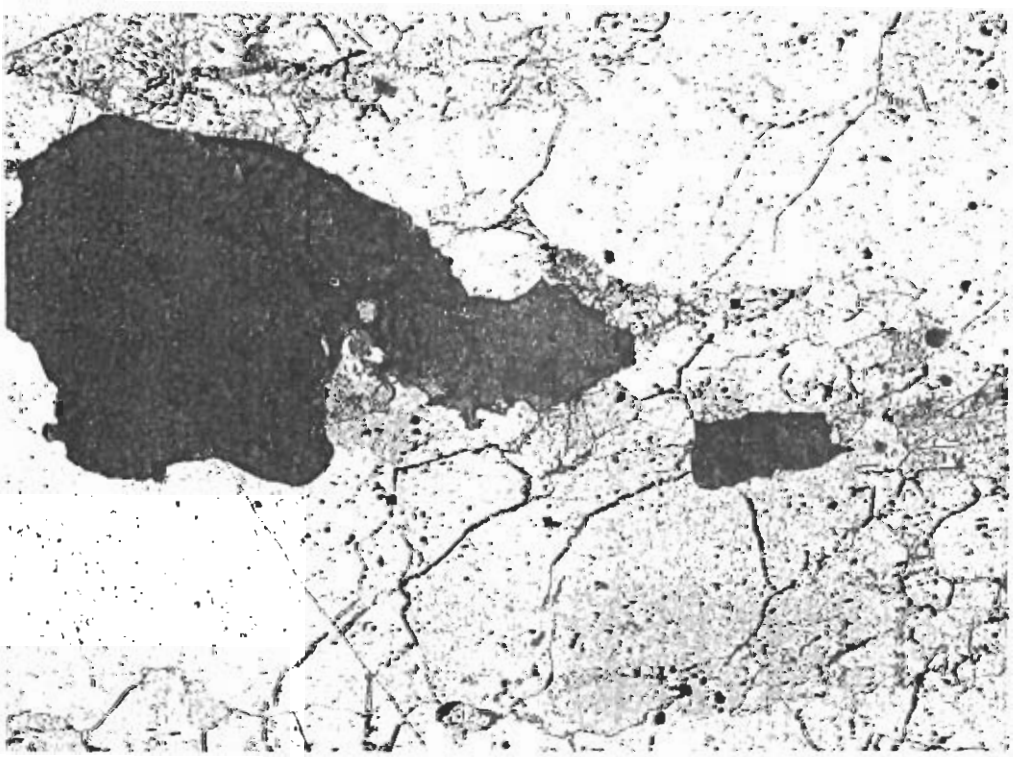

**Plate 5. 33.** Same view in plane polarized light.

**Table 5. 2. Modal composition (visual estimate) of gem-barren pegmatites from different localities of the Shigar valley.**

**a. Biotite ± garnet ± muscovite pegmatites**

| Section # | MUN-3 | MUN-6 | GON-48 |
|---|---|---|---|
| Alkali feldspar | 40 | 45 | 36 |
| Plagioclase | 18 | 16 | 23 |
| Quartz | 30 | 35 | 33 |
| Biotite | 10 | 3 | 8 |
| Muscovite | - | tr | -- |
| Garnet | | 1 | tr |
| Tourmaline | - | -- | |
| Apatite | 1 | | tr |
| Epidote | - | tr | tr |
| Sphene | 1 | tr | - |
| Tremolite / actinolite | tr | -- | - |
| Opaque | tr | – | tr |
| **Total** | **100** | **100** | **100** |

**MUN = Mungo; GON = Gone**

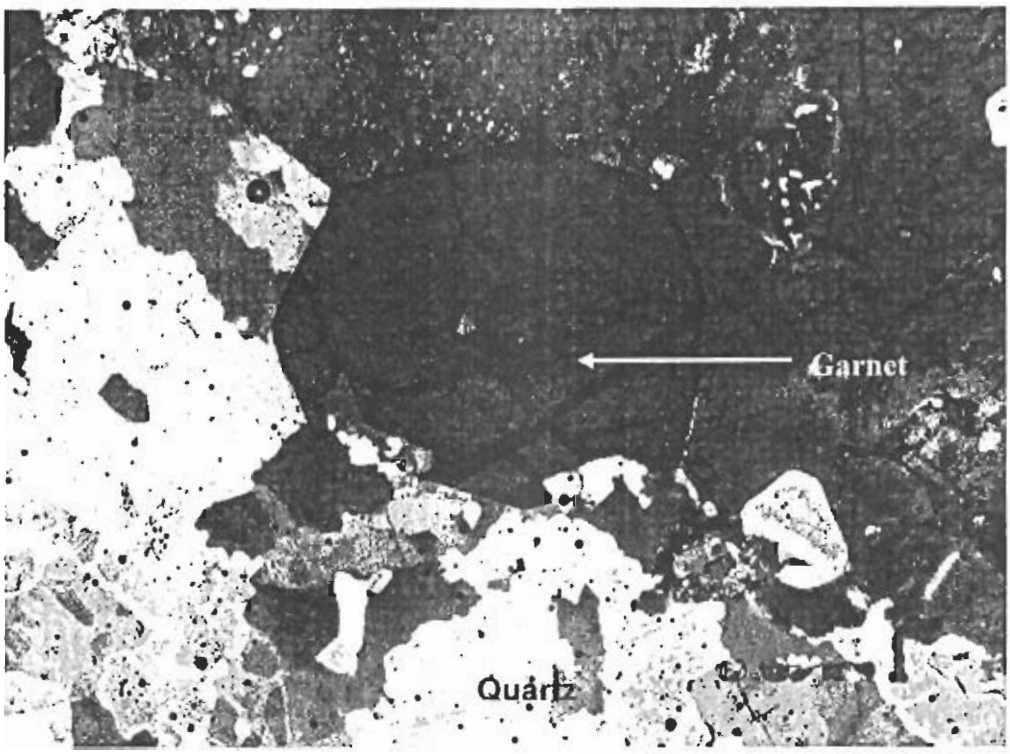


**Plate 5. 34.** Photomicrograph showing alteration of orthoclase to sericite, kaolinite and muscovite. Euhedral and fractured grain of garnet is also visible. Anhedral interlocking grains of quartz are seen in the lower part (cross light).

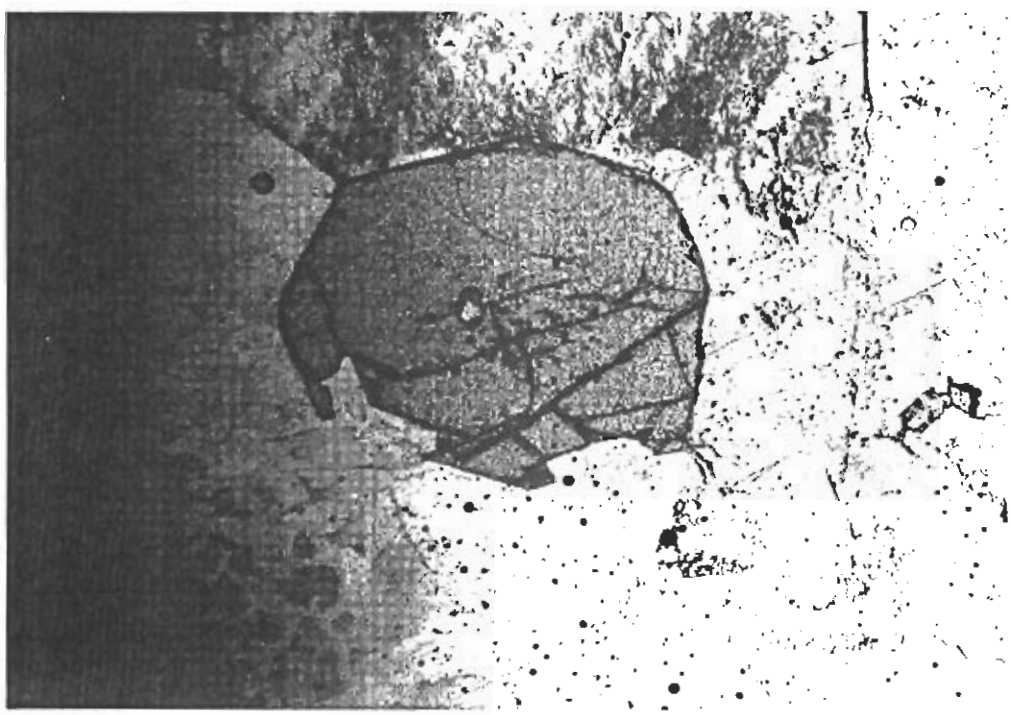

**Plate 5. 35.** Same view in plane polarized light.

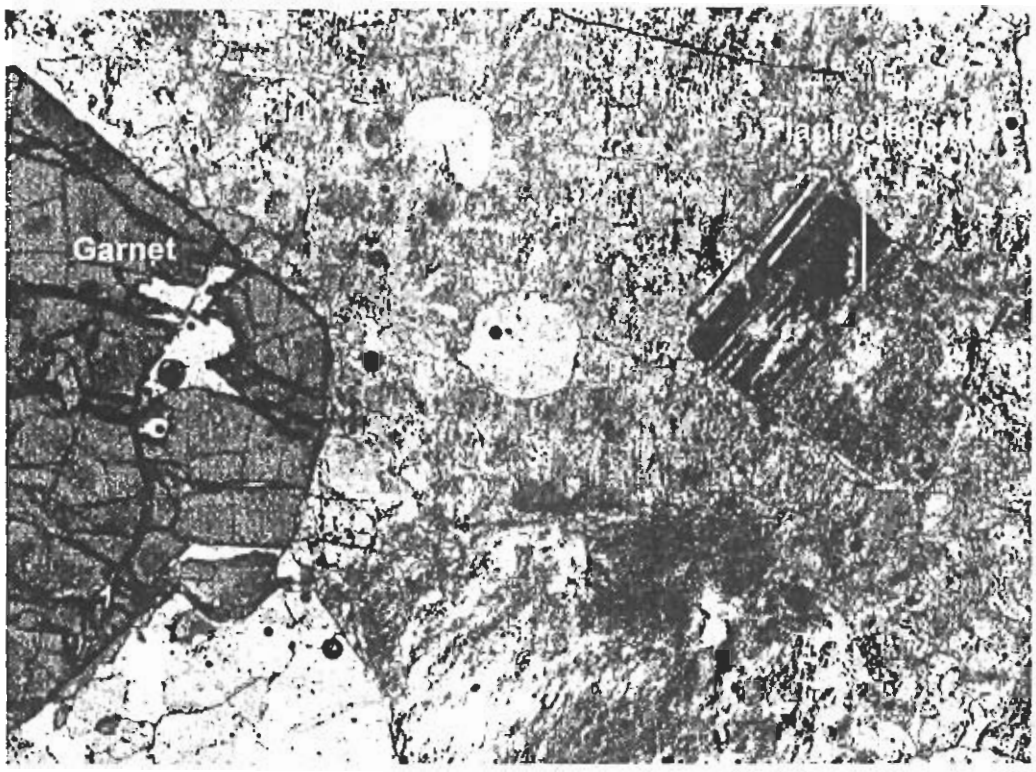


**Plate 5. 36.** Photomicrograph showing alteration of orthoclase to sericite and kaolinite. On right a highly altered and saussuritized plagioclase crystal is seen. On the extreme left a piece of fractured euhedral garnet crystal is also visible (cross light; Mag: 4× / 0.1).

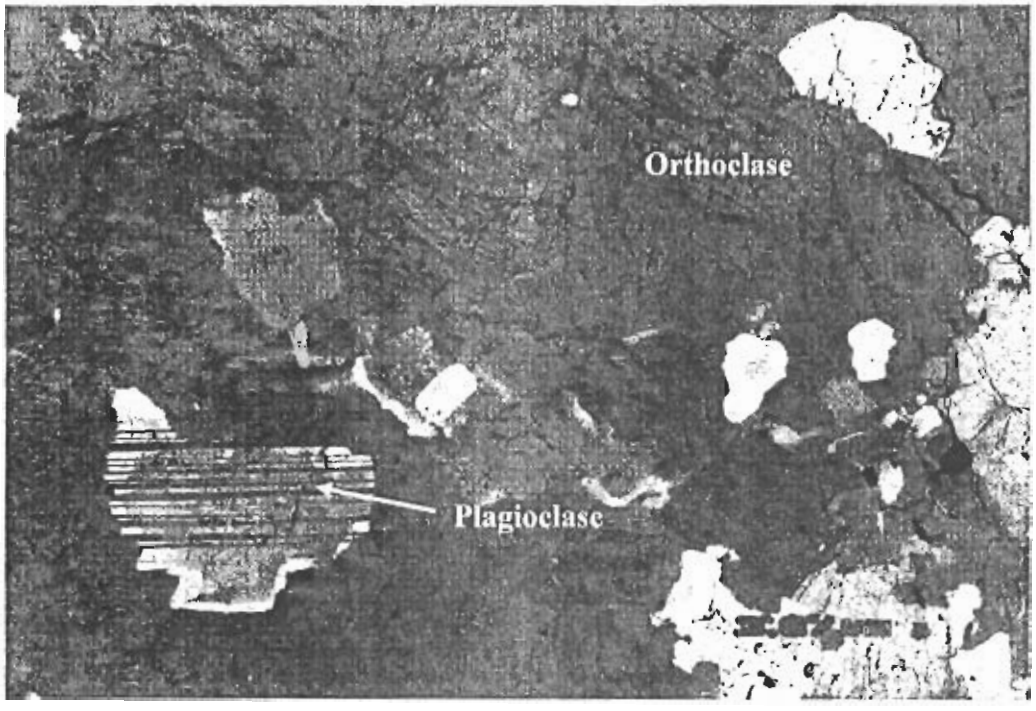


**Plate 5. 37.** Photomicrograph showing plagioclase crystal with perfect albite twinning is found as inclusion within the orthoclase.

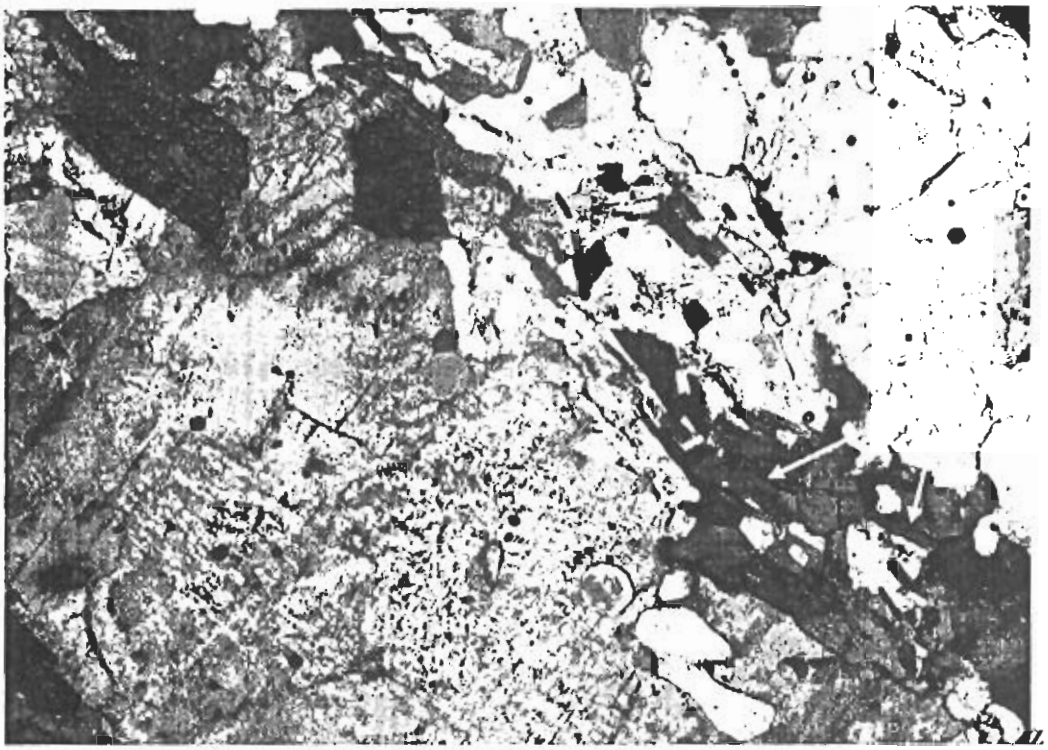

**Plate 5. 38.** Photomicrograph showing perthite intergrowth of albite and microcline. In the center, lower left and at top the biotite crystals are also visible.

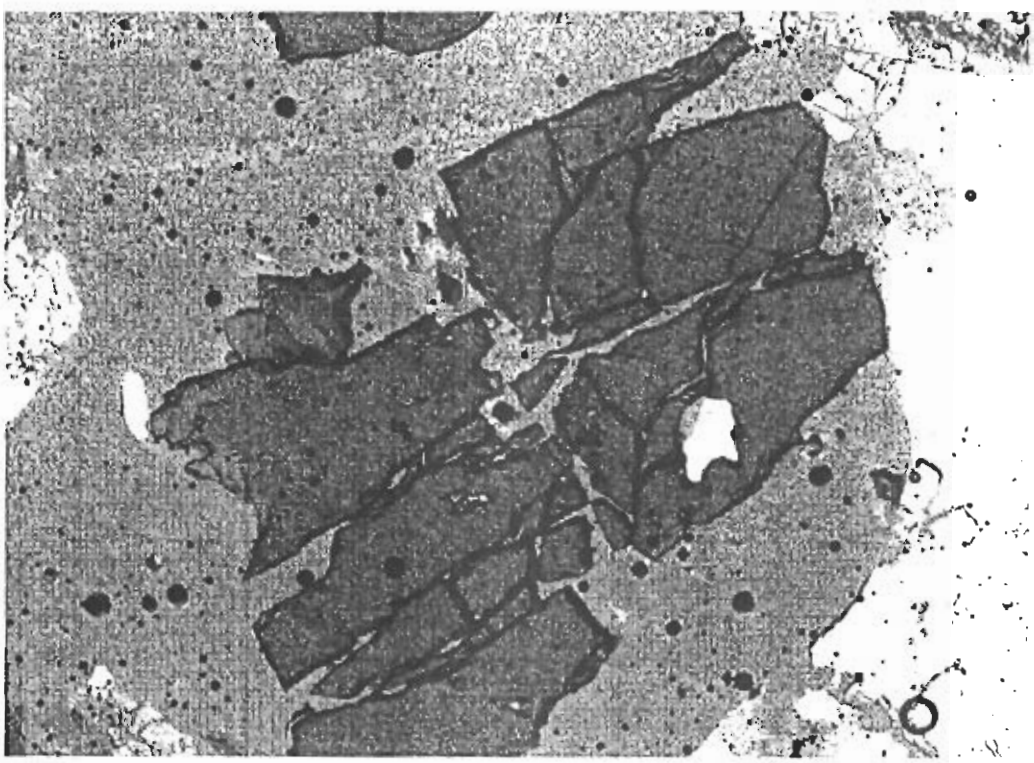

**Plate 5. 39.** Photomicrograph showing a highly-fractured garnet crystal occuring as inclusion within the orthoclase. (Mag: 4× / 0.1).

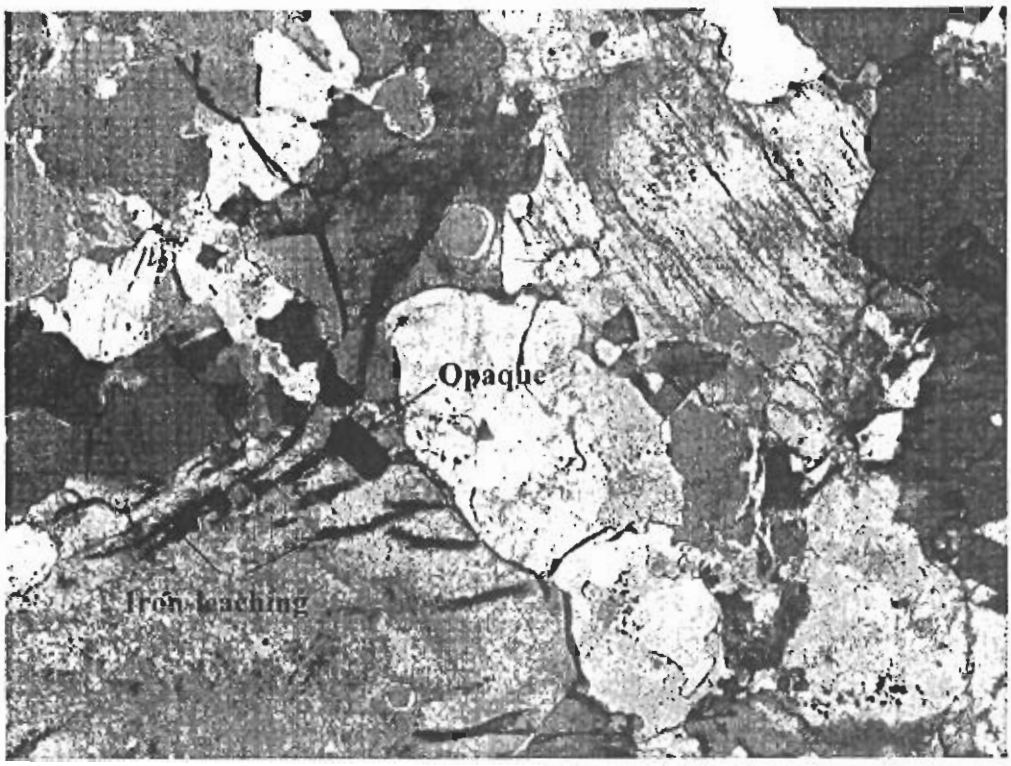


**Plate 5. 40.** Photomicrograph showing iron leaching along the micro fractures near the opaque phases. At the top an orthoclase is bent. (cross light; Mag: 4× / 0.1)

**Plate 5. 41.** Same view in plane polarized light.

(Table 5. 2 continued)

**b. Muscovite-biotite ± garnet pegmatites**

| Section # | MUN-1 | MUN-5 | MUN-7 | DAS-21 | GOY-38 | GOY-41 |
|---|---|---|---|---|---|---|
| Alkali feldspar | 26 | 25 | 30 | 42 | 38 | 40 |
| Plagioclase | 40 | 35 | 37 | 18 | 15 | 21 |
| Quartz | 27 | 35 | 26 | 33 | 32 | 34 |
| Biotite | 5 | 2 | 4 | 3 | 6 | 2 |
| Muscovite | 2 | 3 | 3 | 4 | 8 | 3 |
| Garnet | | | | | tr | tr |
| Tourmaline | | | – | | | |
| Apatite | – | | tr | – | 1 | tr |
| Epidote | | | – | tr | tr | |
| Sphene | – | – | – | – | tr | tr |
| Zircon | tr | – | – | – | | – |
| Opaque | tr | - | – | tr | tr | tr |
| **Total** | **100** | **100** | **100** | **100** | **100** | **100** |

**MUN = Mungo; DAS = Dassu; GOY = Goyungo;**

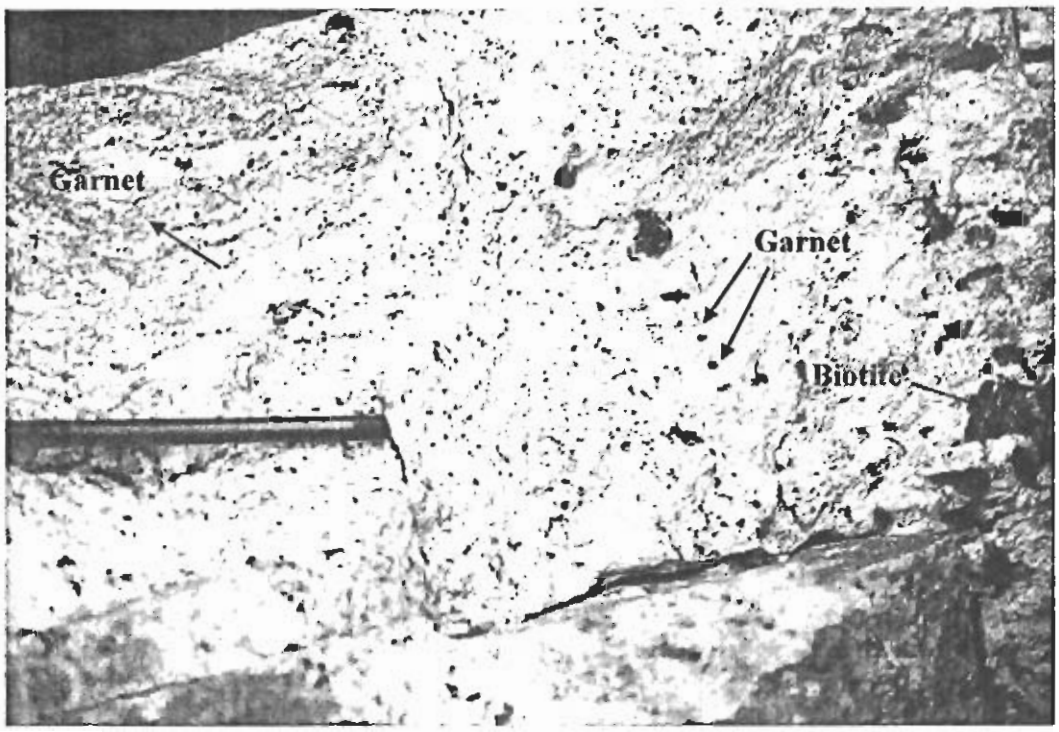


**Plate 5. 42.** Photograph showing medium-grained pegmatite having disseminated grains of garnet. The darker color patches at the right side are biotite flakes.

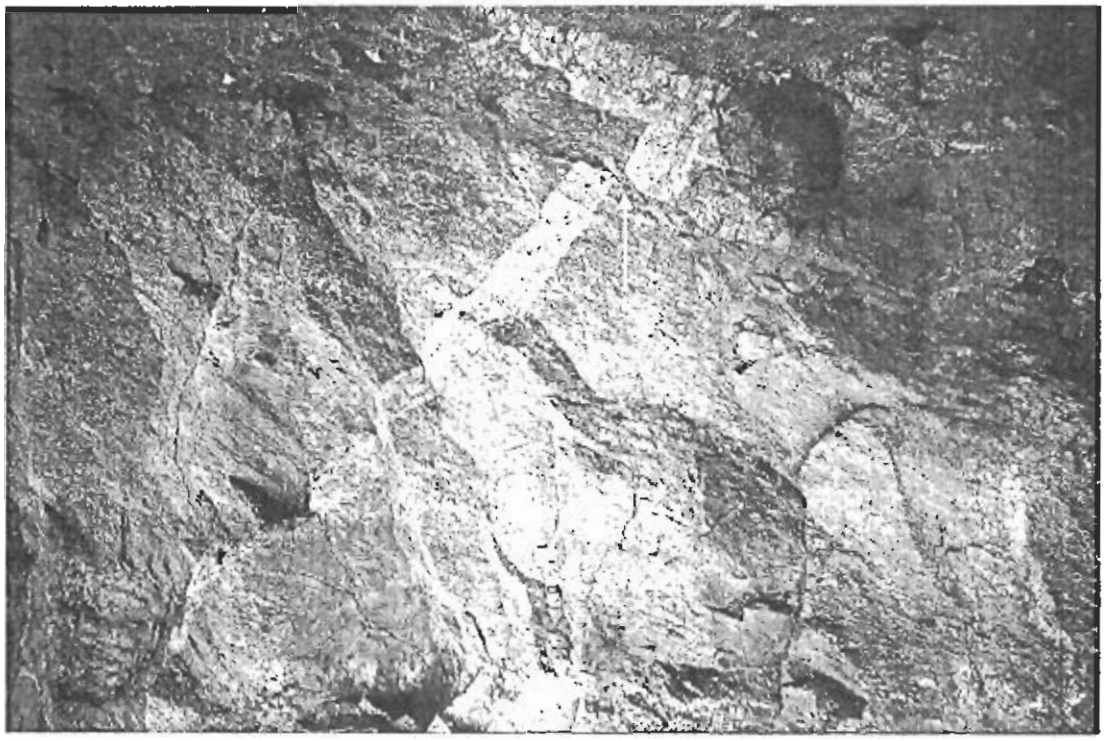

**Plate 5. 43.** Photograph showing displacement of the pegmatite dike due to the local faulting in the Para-gneisses, in the area between Goyungo and Foljo villages.

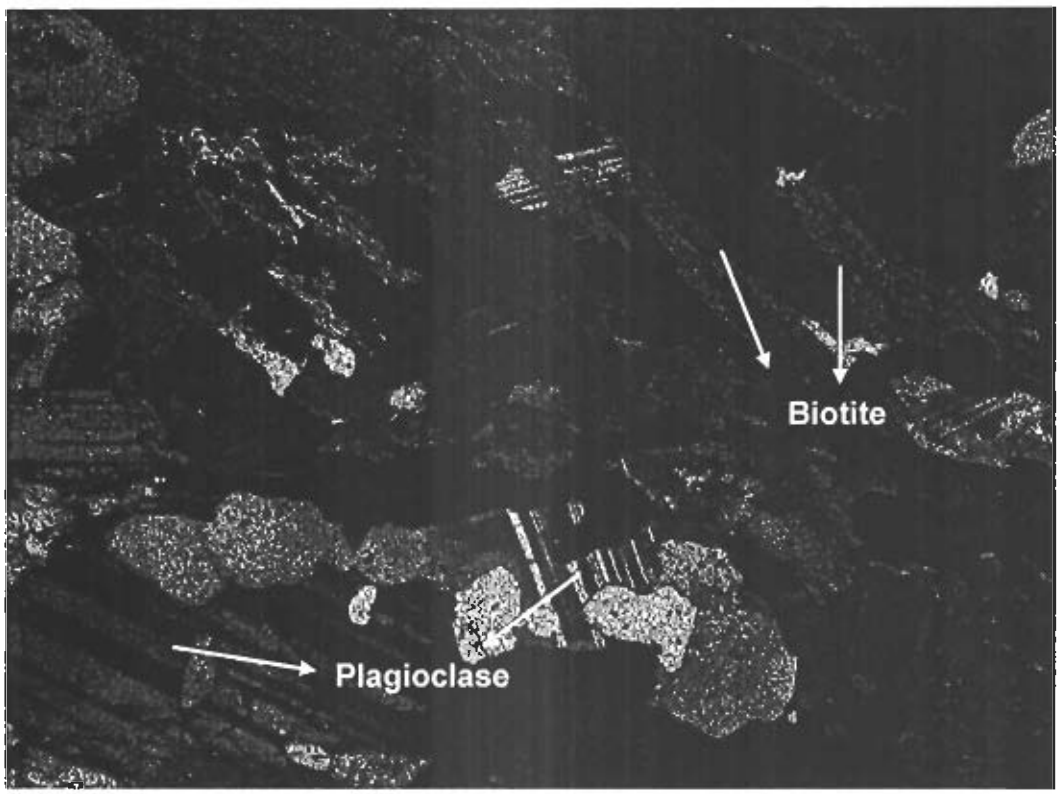


**Plate 5. 44a.** Photomicrograph showing partially altered orthoclase. Well twinned plagioclase grains can also be noticed. Overgrowth between biotite and small tabular crystals of andesine are also visible (cross light; Mag: 4× / 0.1).

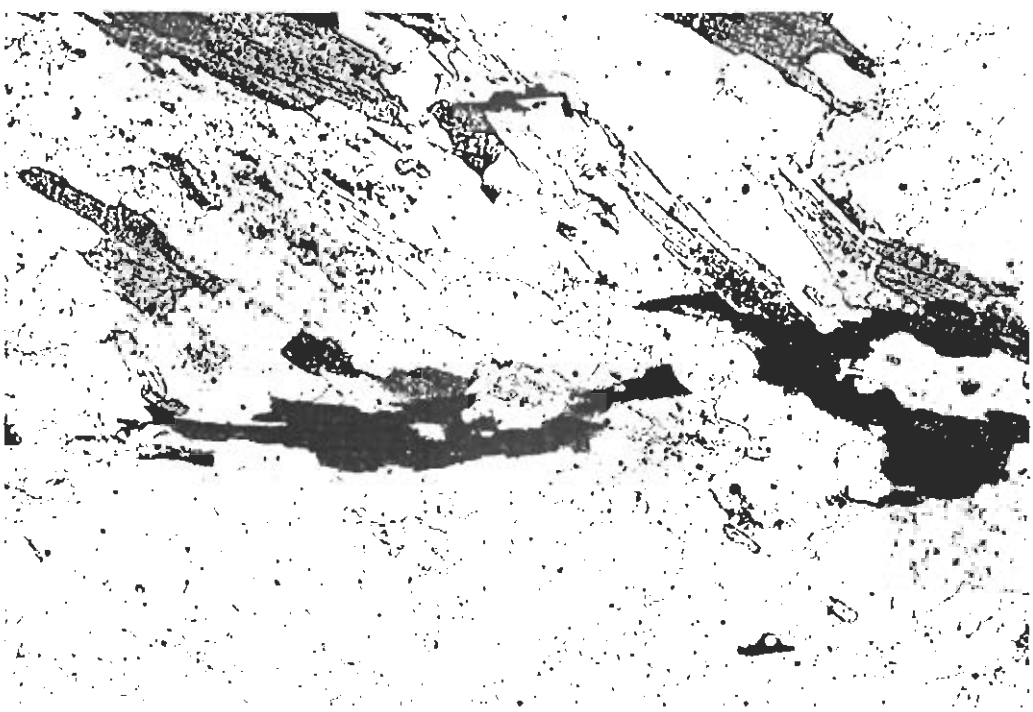

**Plate 5. 44b.** Same view in plane polarized light.

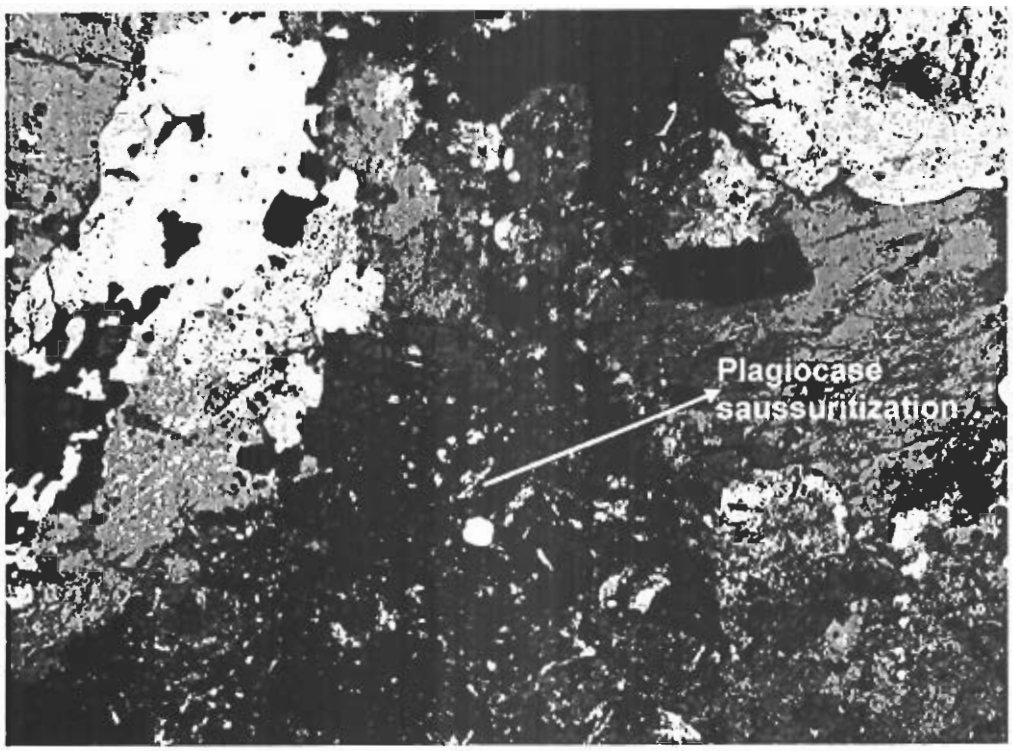


**Plate 5. 45.** Photomicrograph showing partial to complete saussuritization of plagioclase. Alteration of orthoclase to sericite, kaolinite and muscovite is also visible.

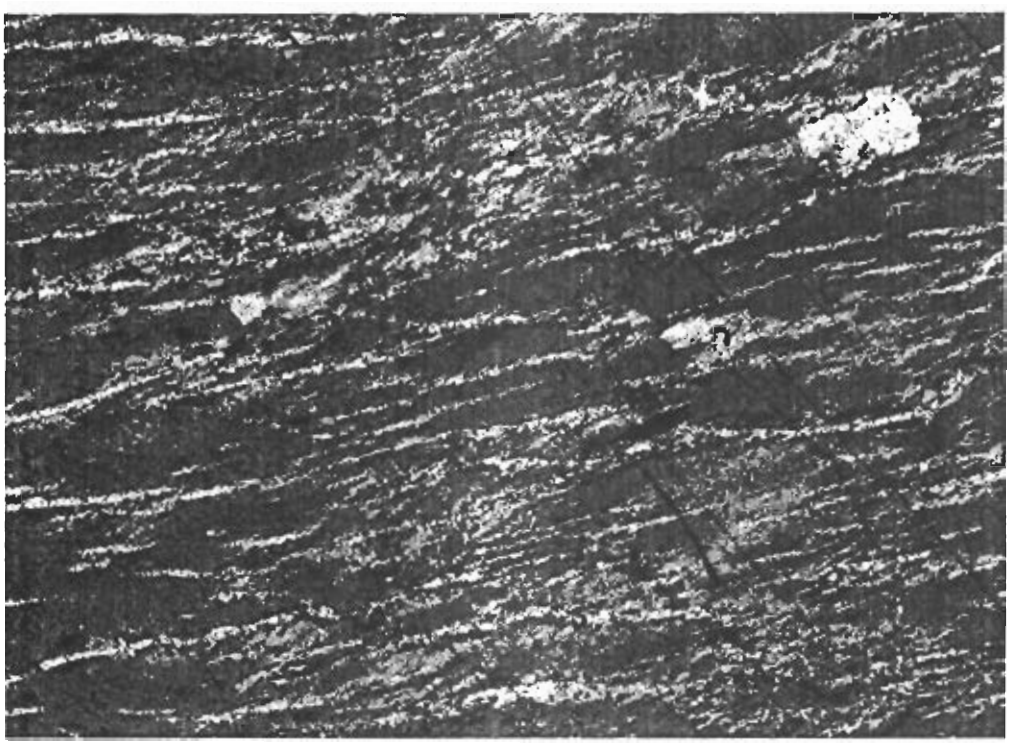

**Plate 5. 46.** Photomicrograph showing microperthitic texture between orthoclase and plagioclase, indicating simultaneous crystallization of these two phases.

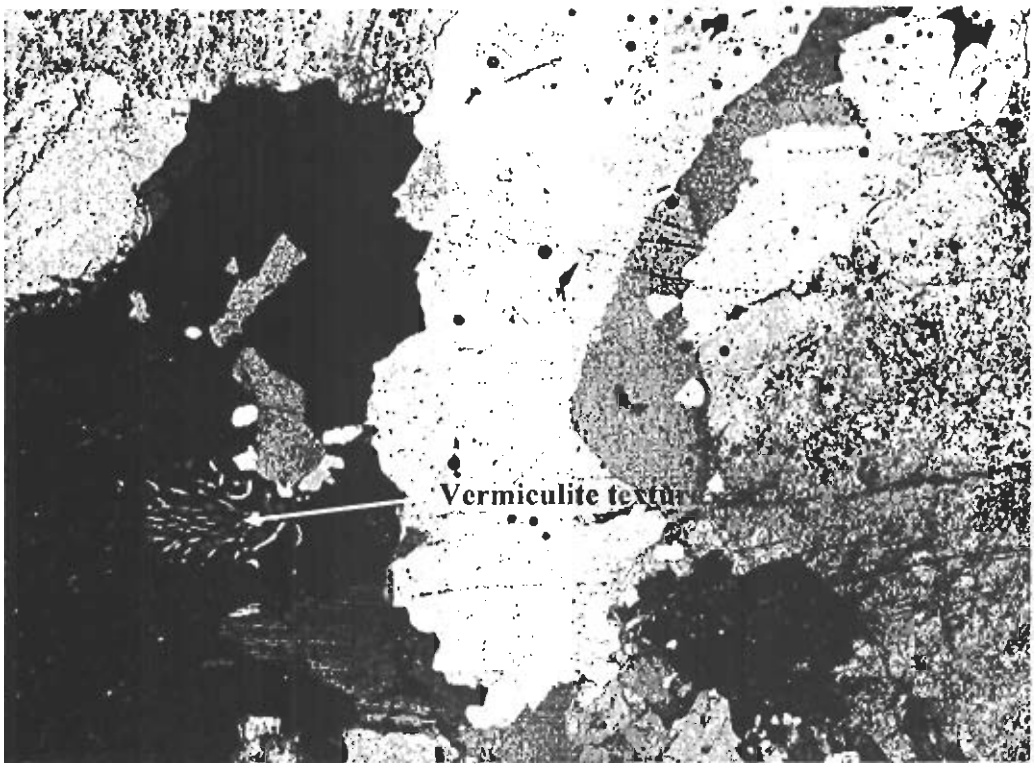


**Plate 5. 47.** Photomicrograph showing vermiculite texture in orthoclase, while on the right partial alteration of orthoclase can also be seen. (Mag: 4× / 0.1).

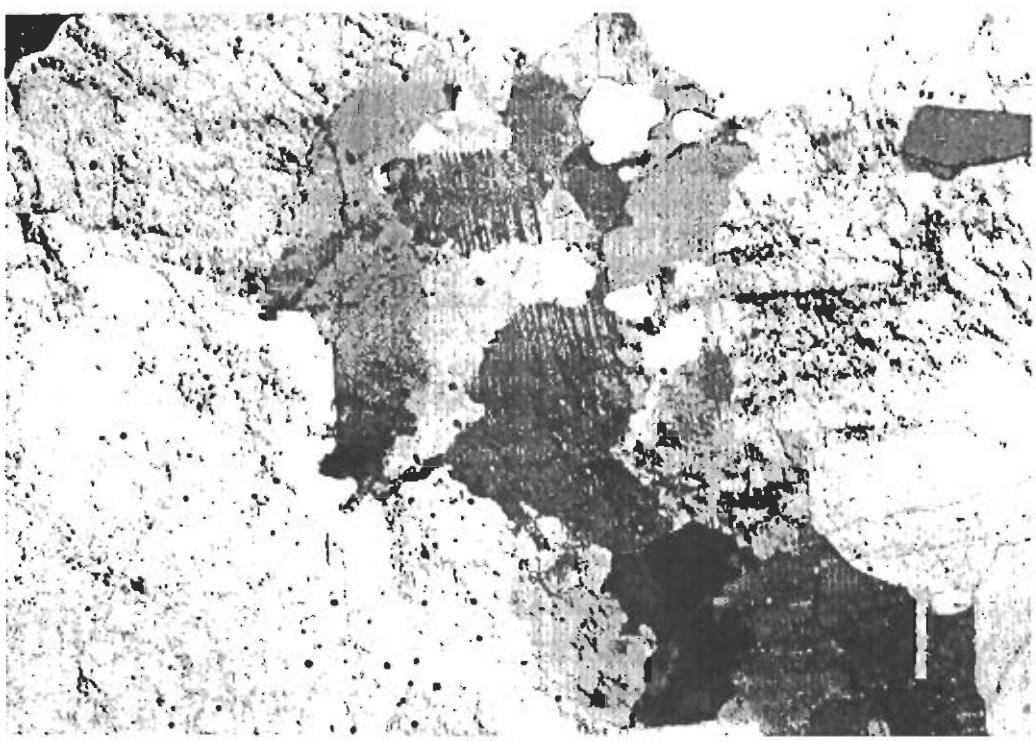

**Plate 5. 48.** Photomicrograph showing partial alteration of orthoclase and plagioclase and also the undulose extinction within quartz.

**Table 5. 3. Modal composition (visual estimate) of Shengus and Indus-Gilgit Confluence pegmatites.**

| Section # | SHN-102 | SHN-104 | ICP-107 | ICP-109 | ICP-110 | ICP- 113 | ICP |
|---|---|---|---|---|---|---|---|
| Alkali feldspar | 25 | 27 | 10 | 70 | 47 | 35 | 5 |
| Plagioclase | 36 | 35 | 47 | 12 | 30 | 31 | 2 |
| Quartz | 33 | 30 | 30 | 15 | 22 | 30 | 2 |
| Biotite | 4 | – | – | – | 1 | 2 | |
| Muscovite | 2 | 8 | 10 | 3 | tr | 2 | |
| Garnet | – | tr | 3 | tr | – | – | |
| Tourmaline | – | – | – | – | – | – | |
| Apatite | – | tr | tr | tr | tr | tr | |
| Epidote | tr | | | – | – | tr | |
| Sphene | – | | – | – | – | – | |
| Zircon | – | tr | – | – | tr | tr | |
| Opaque | tr | tr | tr | – | tr | tr | |
| **Total** | **100** | **100** | **100** | **100** | **100** | **100** | **1** |

**Key: SHN= Shengus; ICP= Indus-Gilgit Confluence pegmatites**

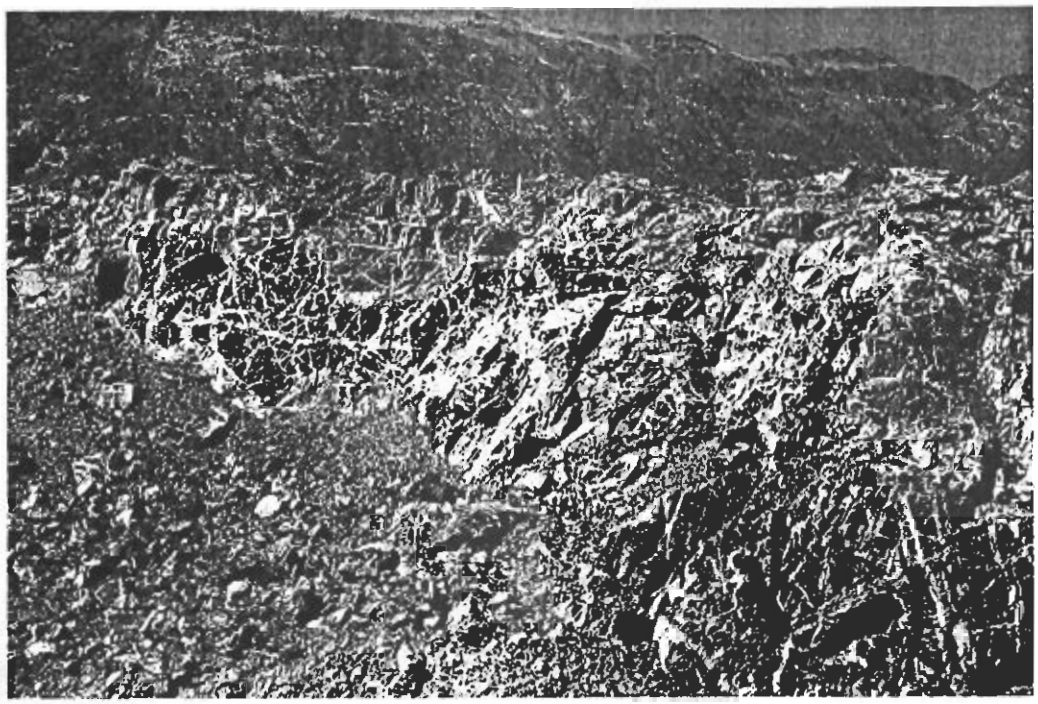

**Plate 5. 49.** Photograph showing complex network of pegmatite dyke and veins exposed at the confluence of Indus river and Gilgit river.

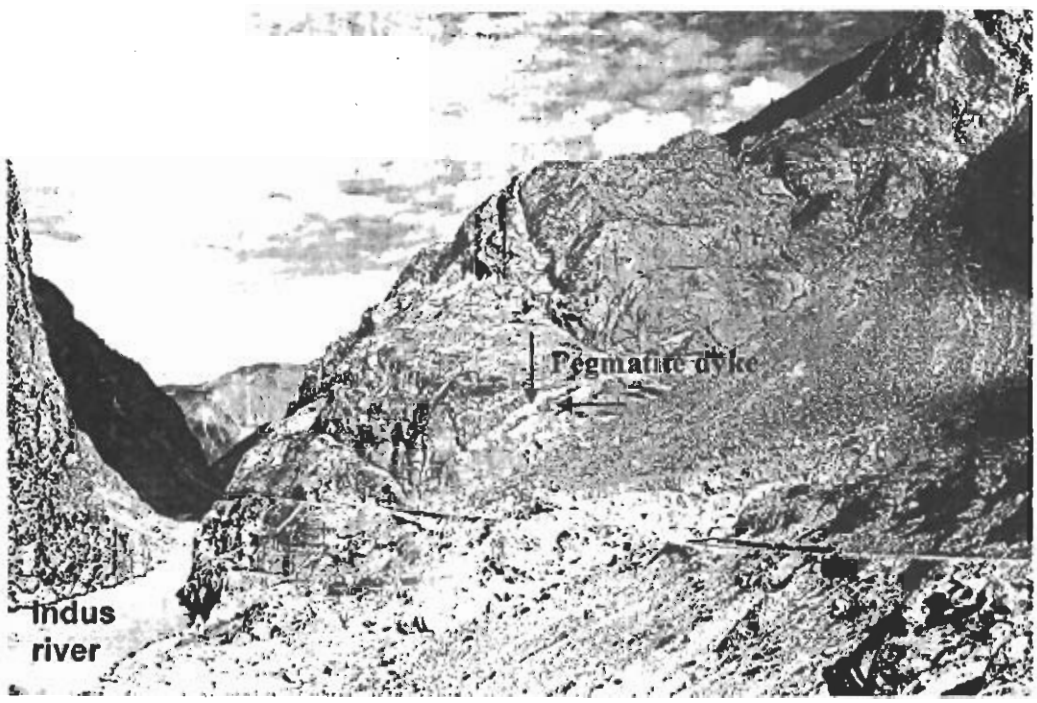


**Plate 5. 50.** Photograph showing some three simple pegmatite dyke exposed near Shengus into the Shengus Gneisses (NPHM). The Indus river is flowing down stream.

**Plate 5. 51:** Photograph showing pegmatite dykes exposed on the left side of the Indus river near Shengus along the Gilgit-Skardu road. The host rock is Shengus Gneiss.

**Plate 5. 52.** Photograph showing numerous parallel pegmatite dykes and veins, exposed at the confluence of Indus River with the Gilgit river and are known as Indus-Gilgit Confluence pegmatites. These are very simple in mineralogy as well as in zoning.

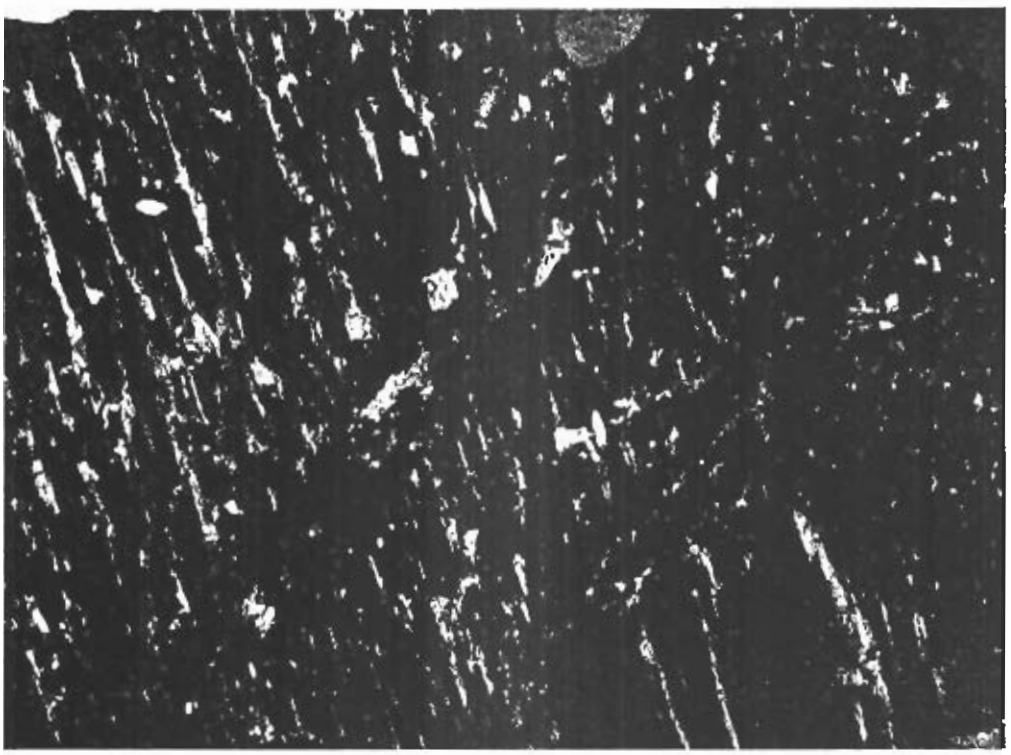

**Plate 5. 53.** Photomicrograph showing microperthite texture in pegmatites of Shengus area. In the center flakes either of muscovite or sericite can be seen.

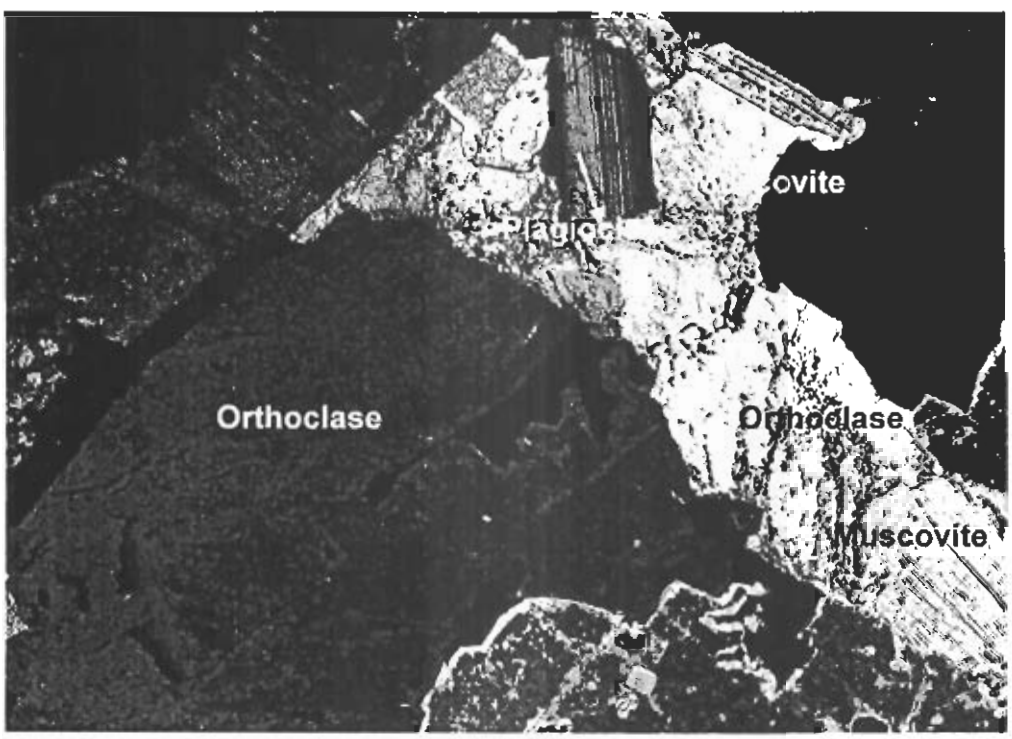


**Plate 5. 54.** Photomicrograph showing euhedral plagioclase, altered orthoclase, anhedral quartz and muscovite flakes.

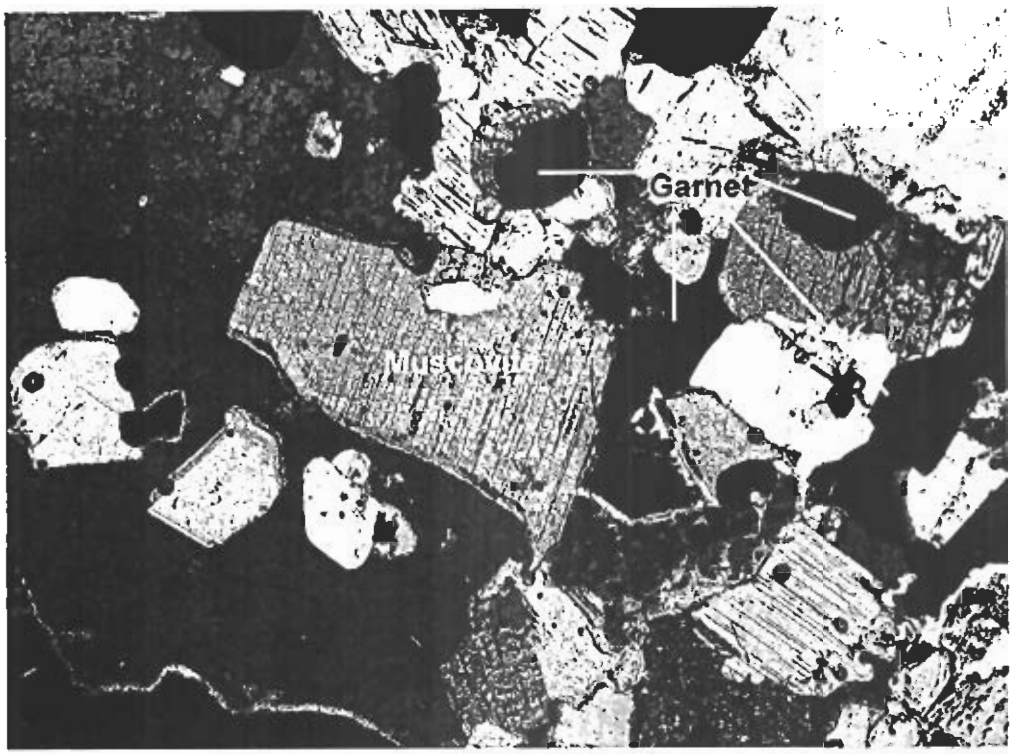


**Plate 5. 55.** Photomicrograph showing euhedral to subhedral garnet scattered throughout the slide. Large flakes of muscovite with perfect cleavages are also visible. (Mag: 4× / 0.1).

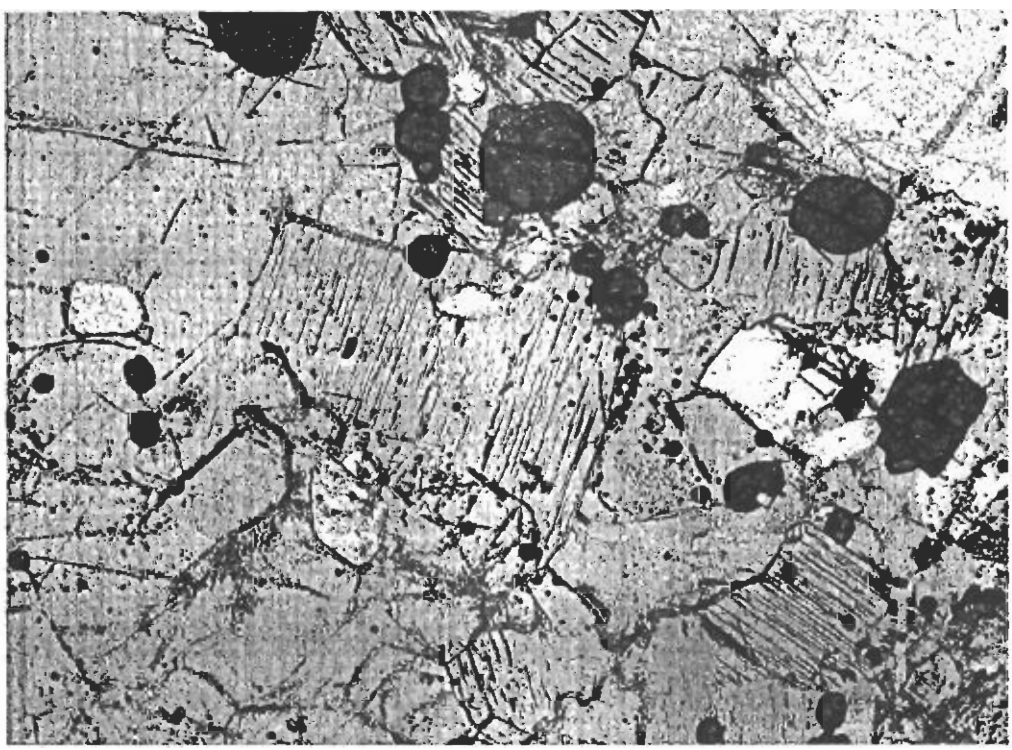

**Plate 5. 56.** Same view in plane polarized light.

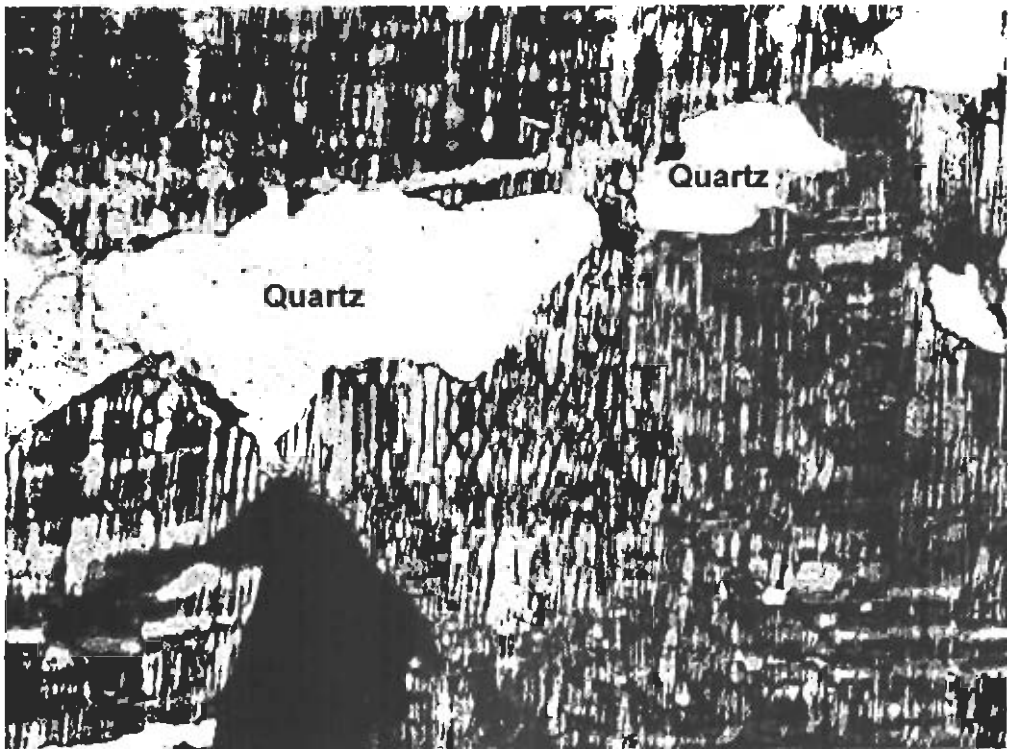


**Plate 5. 57.** Photomicrograph showing cross-hatched twinning in microcline in the Indus-Gilgit Confluence pegmatites. Such type of twinning was absent in both the Shigar as well as in Shengus pegmatites. (Mag: 4× / 0.1).

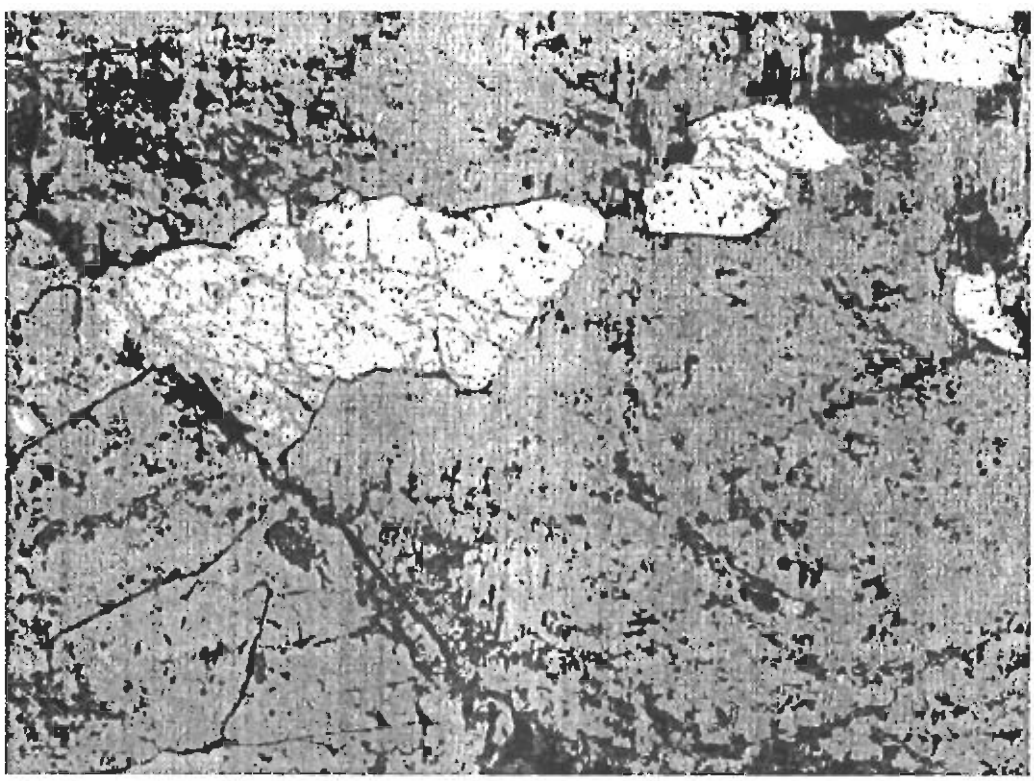

**Plate 5. 58.** Same view in plane polarized light.

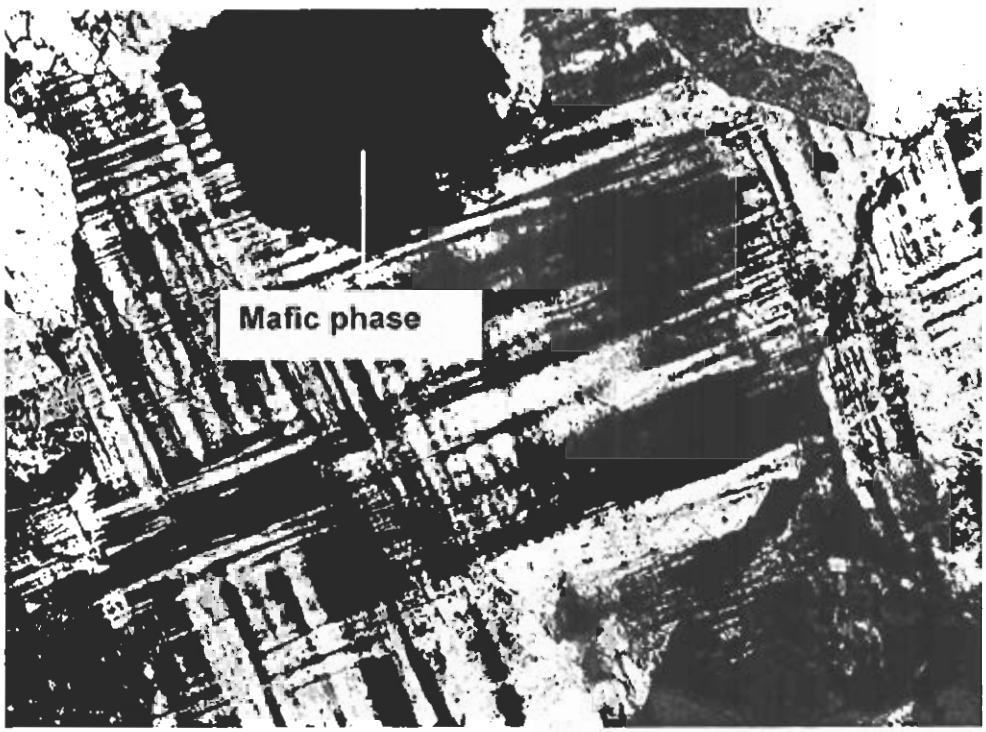


**Plate 5. 59.** Photomicrograph showing field of view mostly covered with microcline that is in tabular fashion. At the top a mafic phase, while at bottom the flakes of biotite are seen.

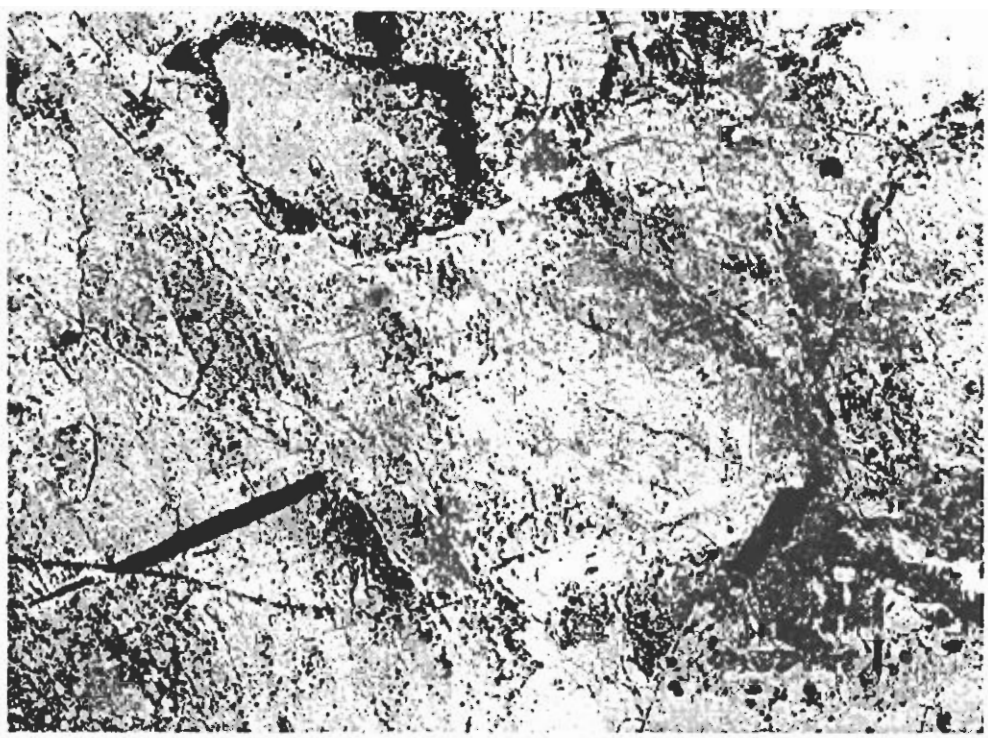

**Plate 5. 60.** Same view in plane polarized light.

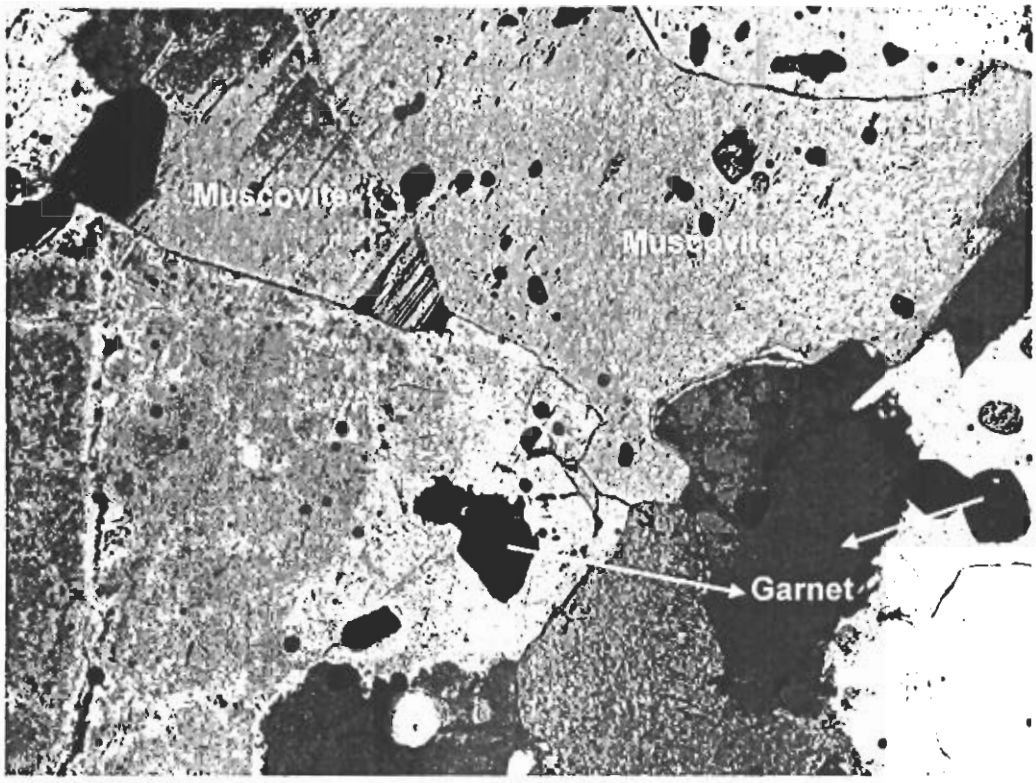


**Plate 5. 61.** Photomicrograph showing large flakes of muscovite and small euhedral garnet crystals as inclusions within feldspar. (Mag: 4×/ 0.1).

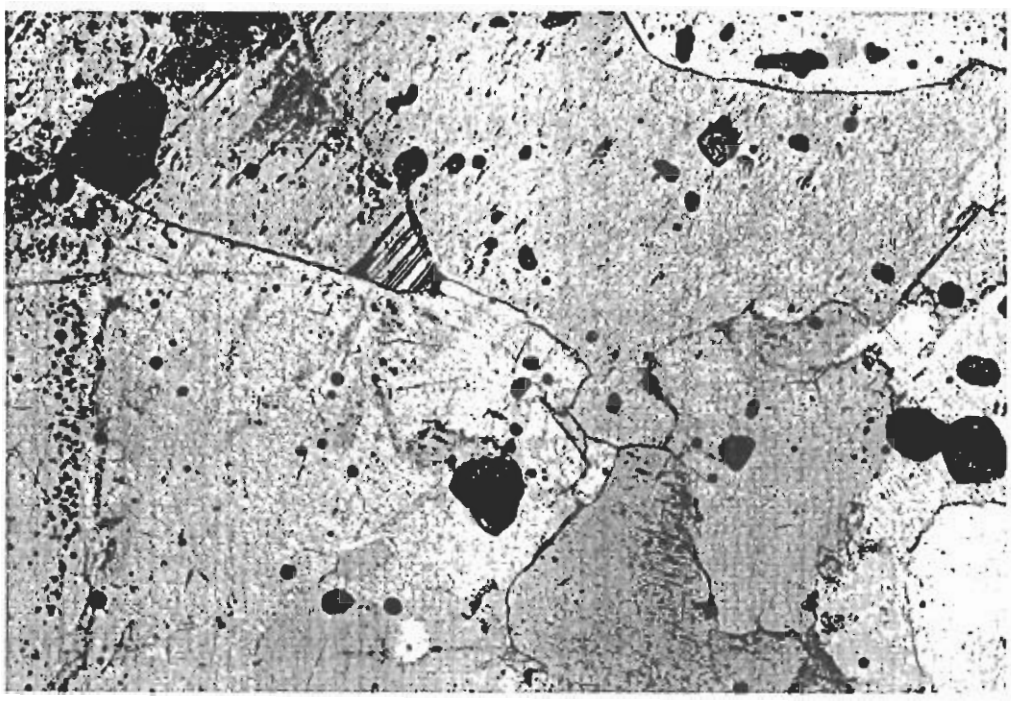

**Plate 5. 62.** Same view in plane polarized light.

'able 5. 4. Modal composition (visual estimation) of the host rocks of pegmatites from different localities of Shigar valley.

| ;ection # | MUN-4 | MUN-8 | MUN-11 | MUN-16 | DAS-22E | NYT-55 | KSH-69 |
|---|---|---|---|---|---|---|---|
| \lkali- feldspar | 45 | 40 | 28 | 25 | 10 | 30 | 15 |
| 'lagioclase | 5 | 8 | 25 | 15 | 37 | 35 | 15 |
| )uartz | 30 | 28 | 25 | 20 | 30 | 20 | 40 |
| 3iotite | 20 | 21 | 20 | 40 | 20 | 3 | 25 |
| \luscovite | tr | 1 | 1 | tr | 1 | 10 | 5 |
| 3arnet | – | – | – | tr | tr | – | tr |
| Tourmaline | – | – | – | – | – | – | – |
| \patite | – | tr | 1 | tr | 1 | 1 | – |
| 3pidote | – | 1 | – | tr | – | 1 | tr |
| 3phene | tr | tr | tr | tr | – | – | – |
| 3ircon | – | – | tr | – | tr | – | – |
| )paque | tr | 1 | tr | tr | 1 | – | tr |
| **Total** | **100** | **100** | **100** | **100** | **100** | **100** | **100** |

**Key:- MUN = Mungo; DAS = Dassu; NYT = Nyit; KSH = Kashmol**

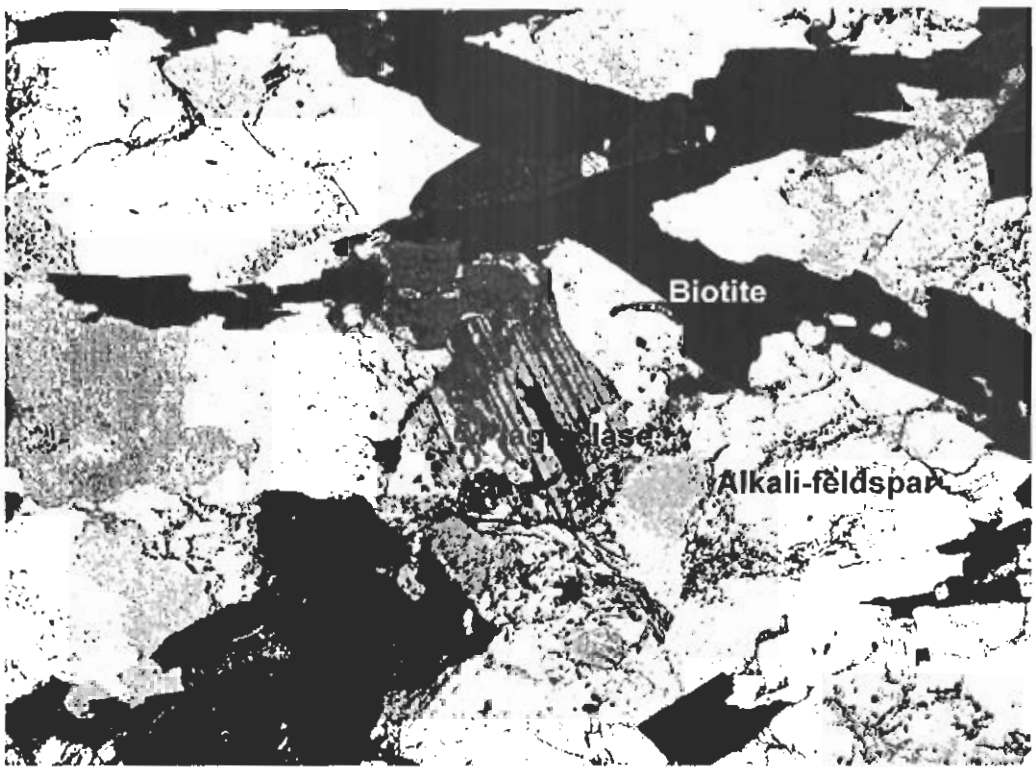


**Plate 5. 63.** Photomicrograph showing prismatic plagioclase having partial alteration along margins. Alkali-feldspar is also showing partial alteration to kaolinite, sericite and muscovite (cross light; Mag: 4× / 0.1).

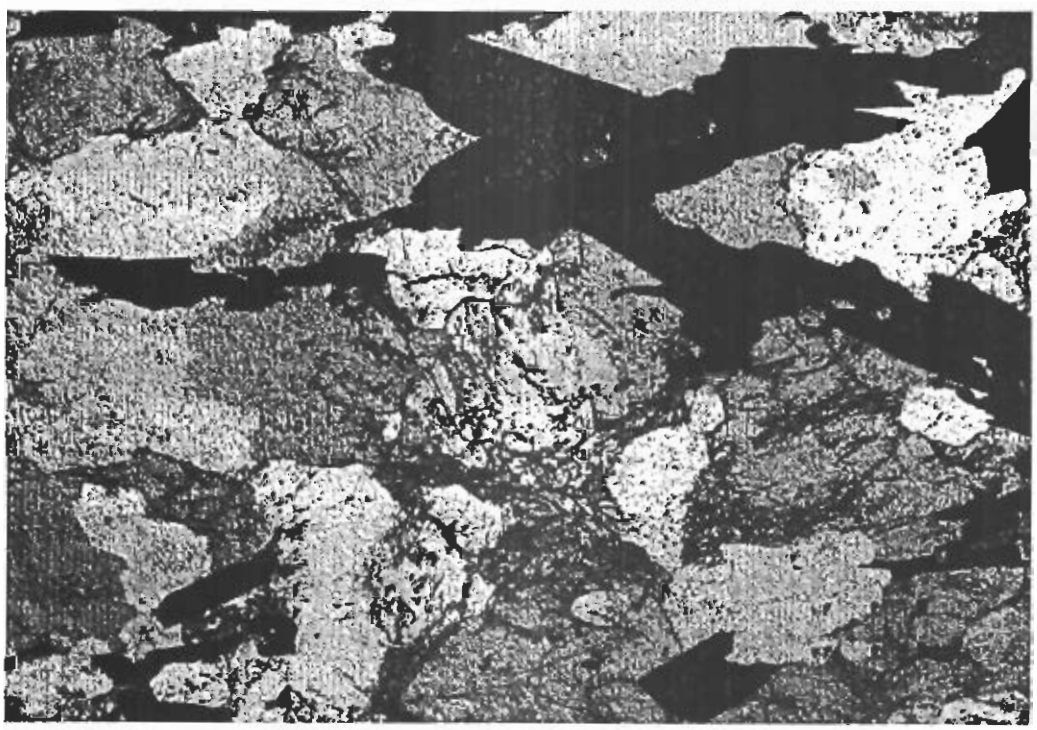

**Plate 5. 64.** Same view in plane polarized light.

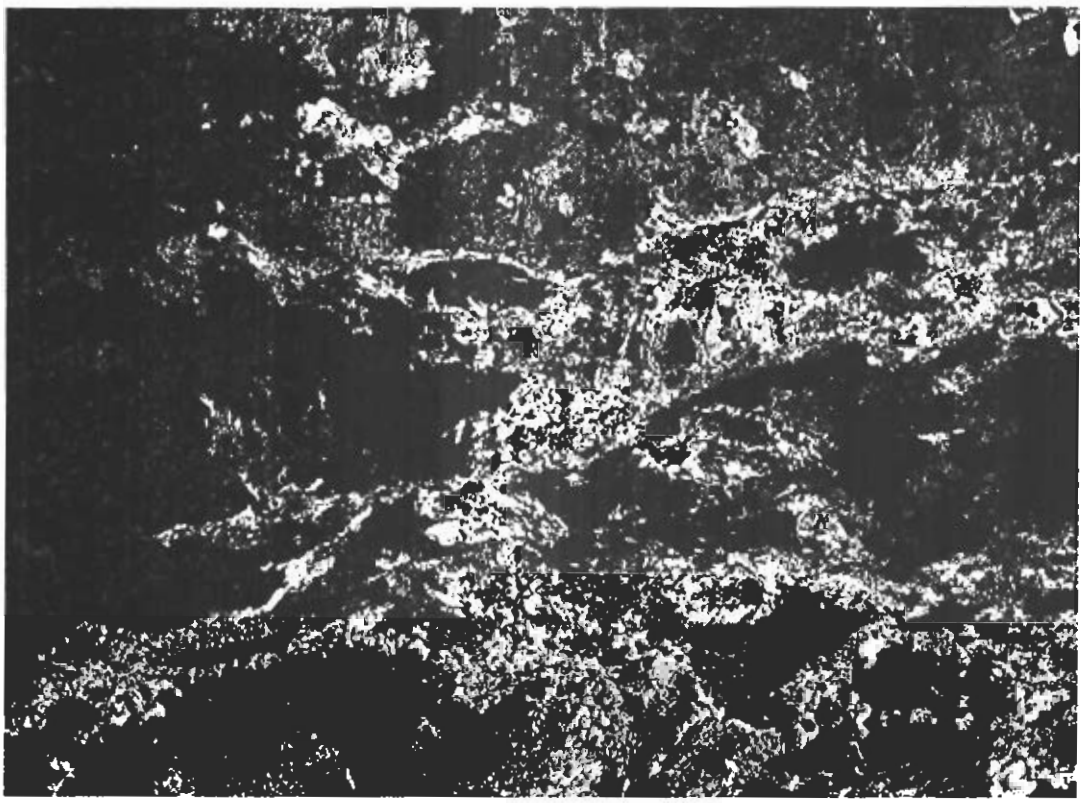

**Plate 5. 65.** Photomicrograph showing partial to complete alteration of alkali-feldspar into kaolinite, sericite and epidote in Dassu gneiss at Nyit, Braldu valley (under crossed Polar; Mag: 4× / 0.1).

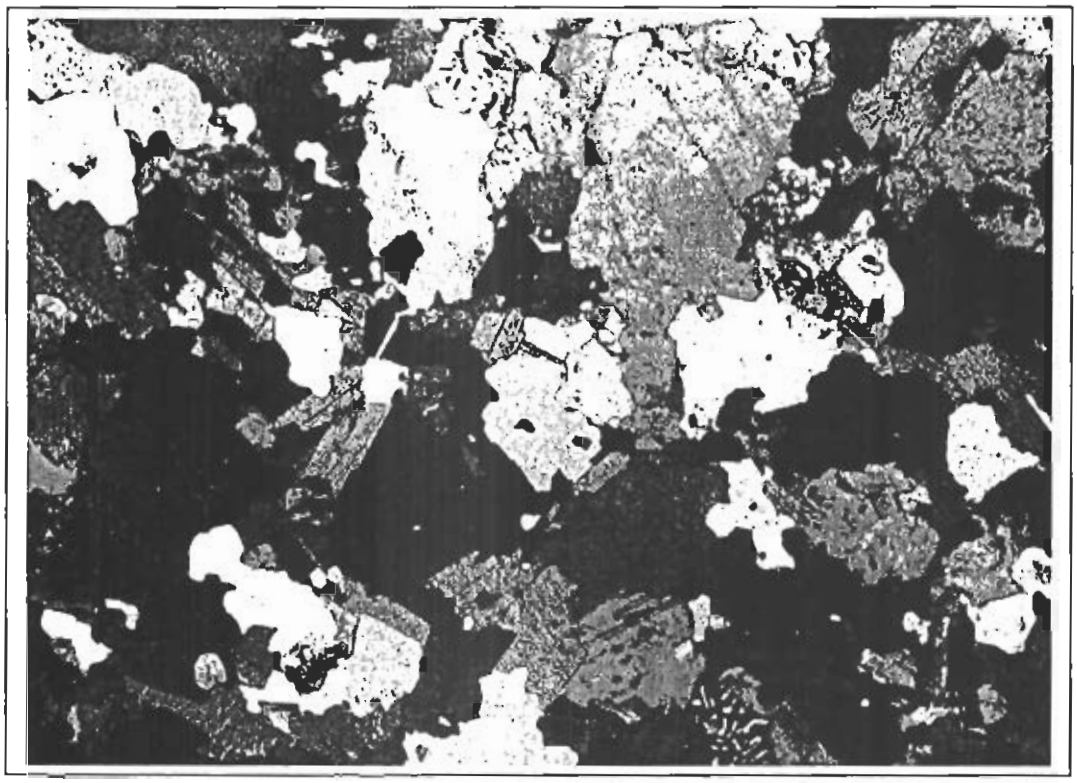

**Plate 5. 66:** Photomicrograph showing granophyric texture at right bottom, the rest field of view is covered with quartz, biotite and plagioclase. (cross light; Mag: 4× / 0.1).

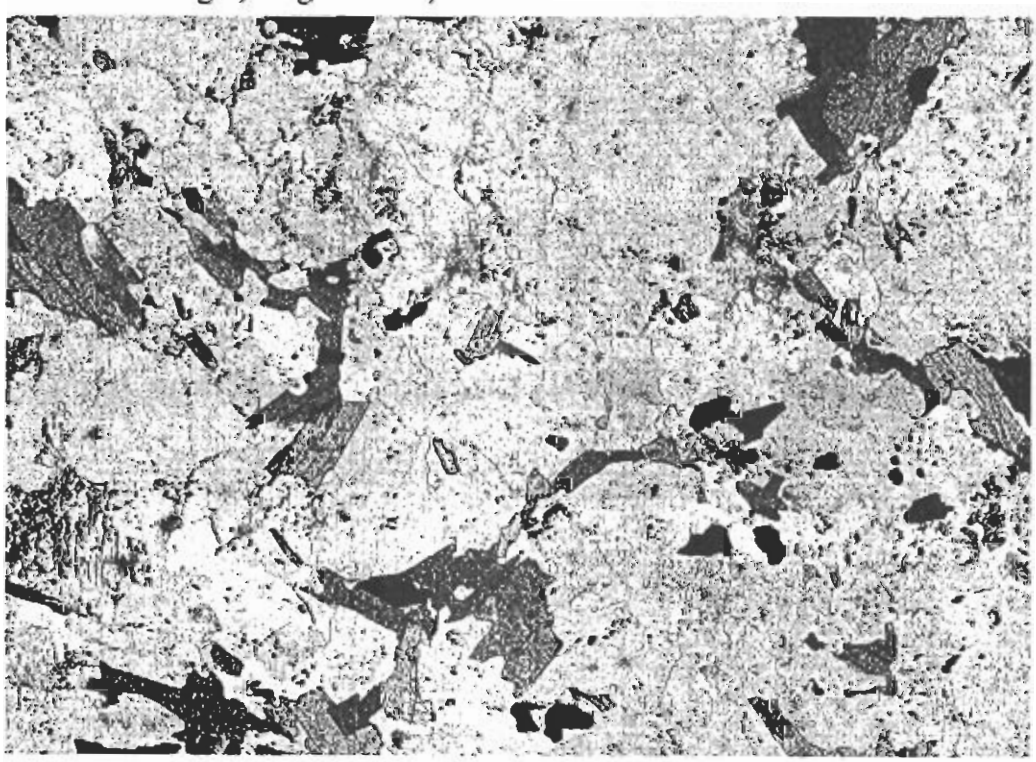

**Plate 5. 67.** Same view in plane polarized light.

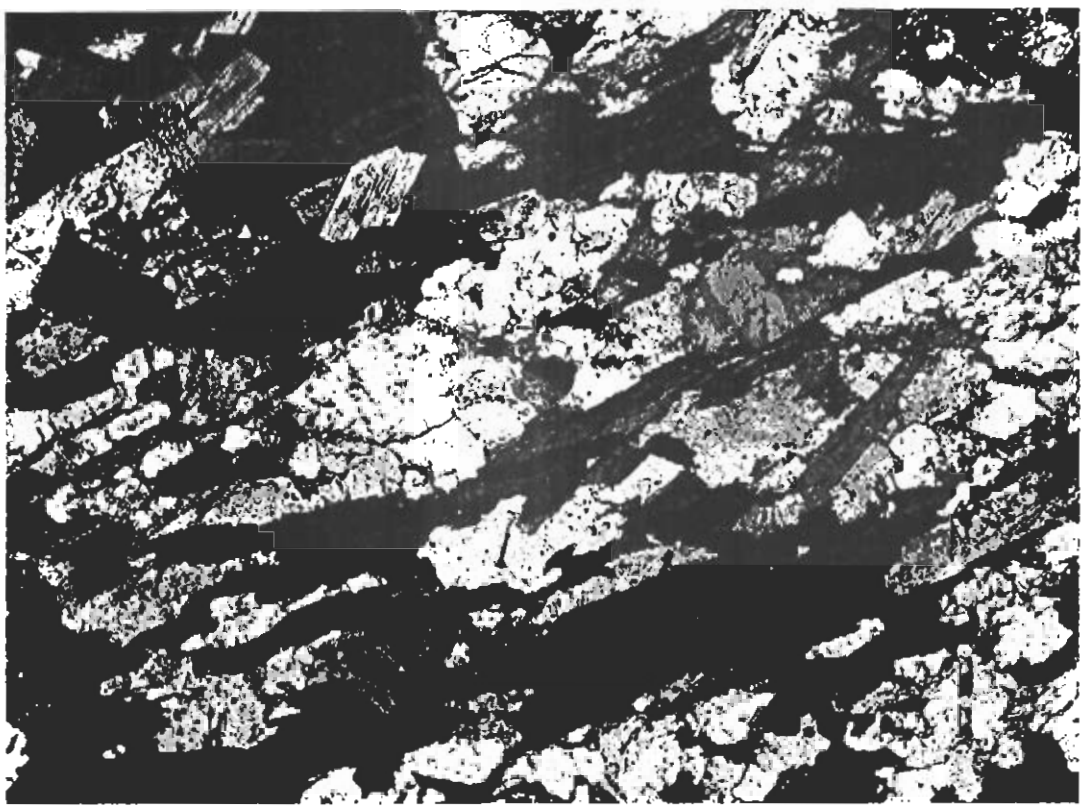

**Plate 5. 68**. Photomicrograph showing preferred orientation of biotites in Dassu biotite orthogneiss at Mungo. The interstitial mineral is quartz. (under crossed Polar; Mag: 4× / 0.1)

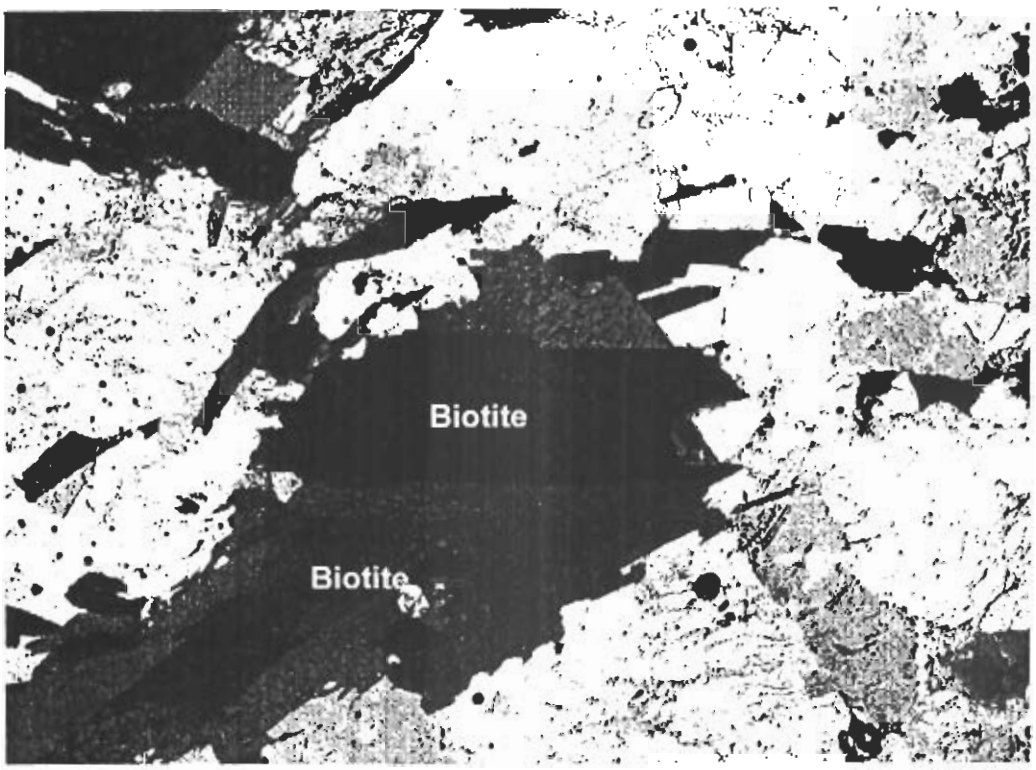


**Plate 5. 69.** Cross-cutting and overgrowth relationships within biotites, while perfect cleavages are also visible (under crossed Polar; Mag: 4× / 0.1).

**Plate 5. 70.** Same view in plane polarized light.

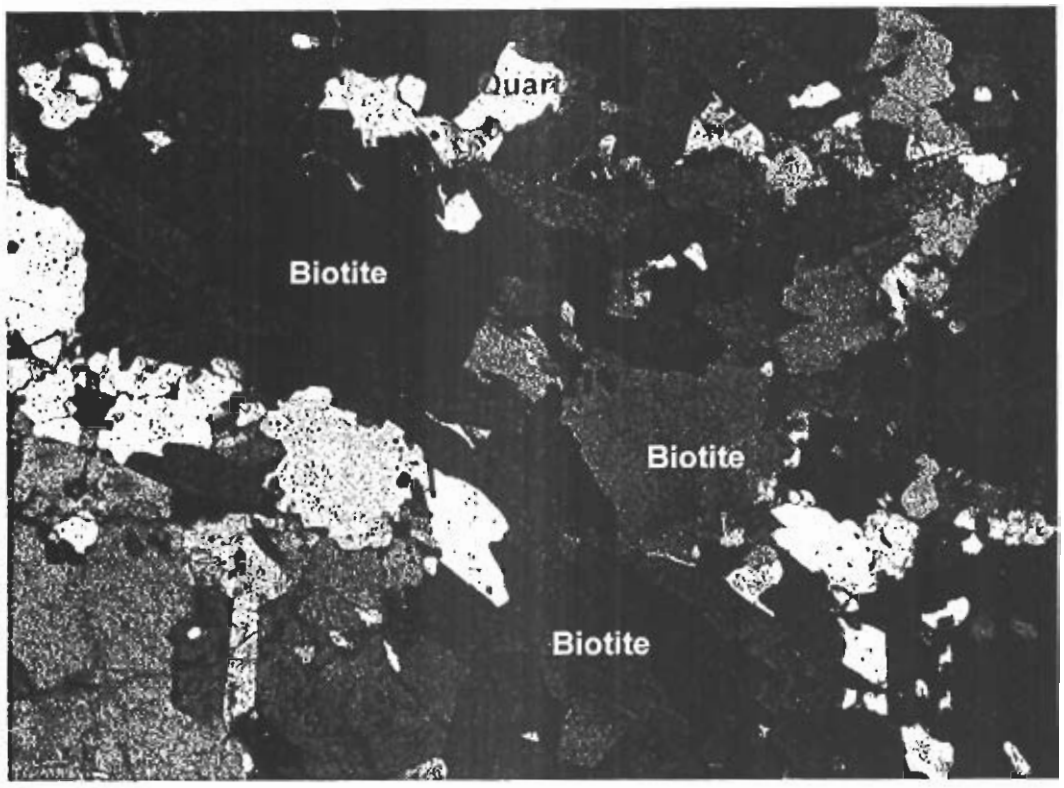


**Plate 5. 71.** Field of view is mostly covered with biotites, in which overgrowth and cross-cutting relationships are very prominent. The interlocking mineral is quartz. (under crossed Polar; Mag: 4× / 0.1).

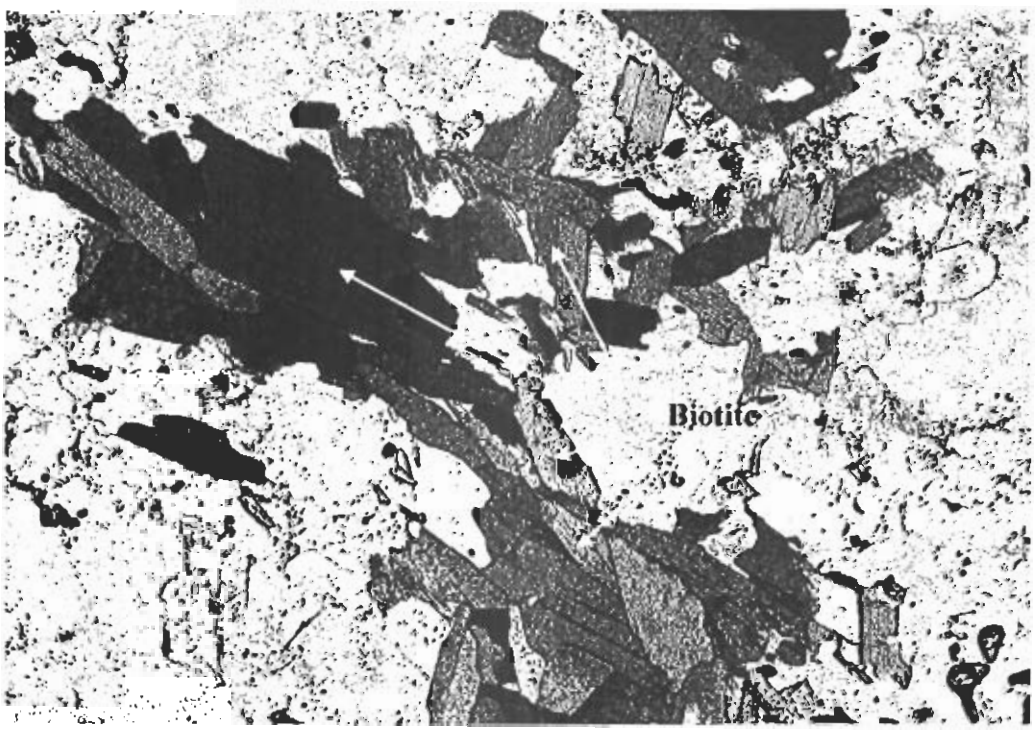


**Plate 5. 72.** Same view in plane polarized light.

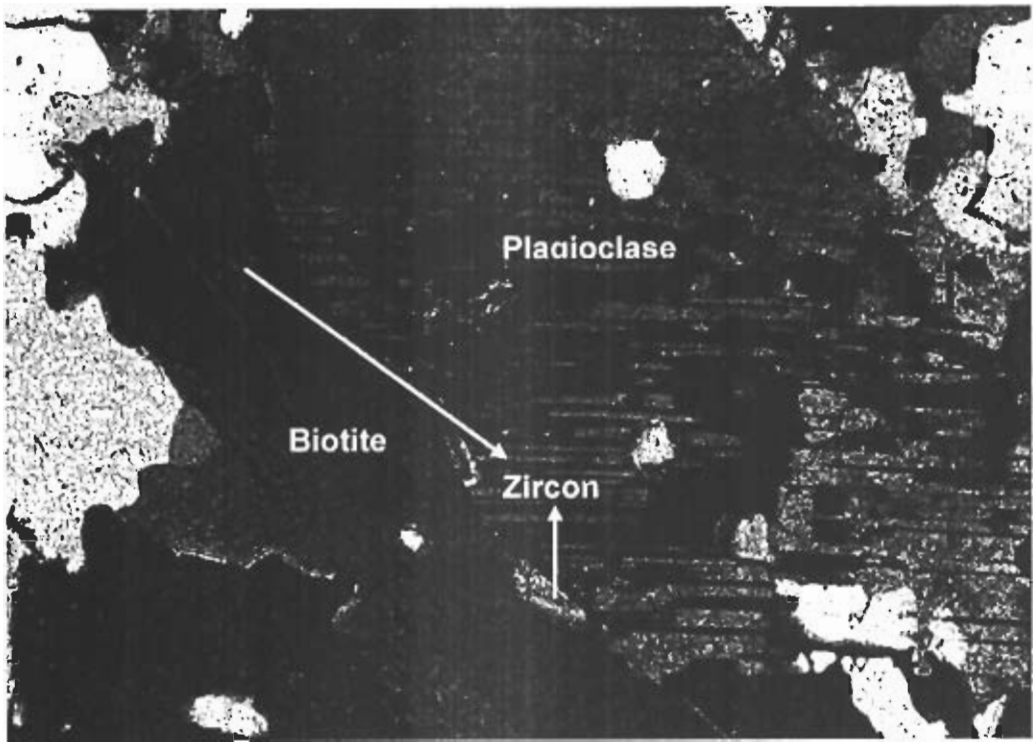


**Plate 5. 73.** Photomicrograph showing two euhedral zircon crystals are highlighted; one is present at the margin of plagioclase and biotite, while the other is within biotite. The cross-cutting behaviour of biotites is also clear. (under crossed Polar; Mag: 10× / 0.25)

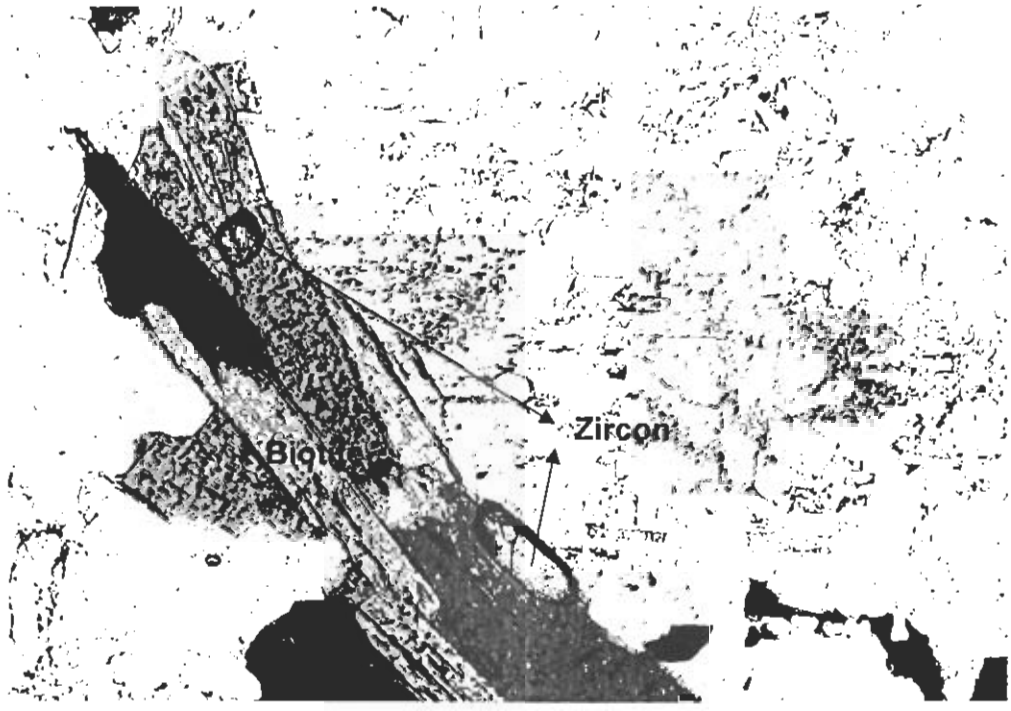


**Plate 5. 74.** Same view in plane polarized light.

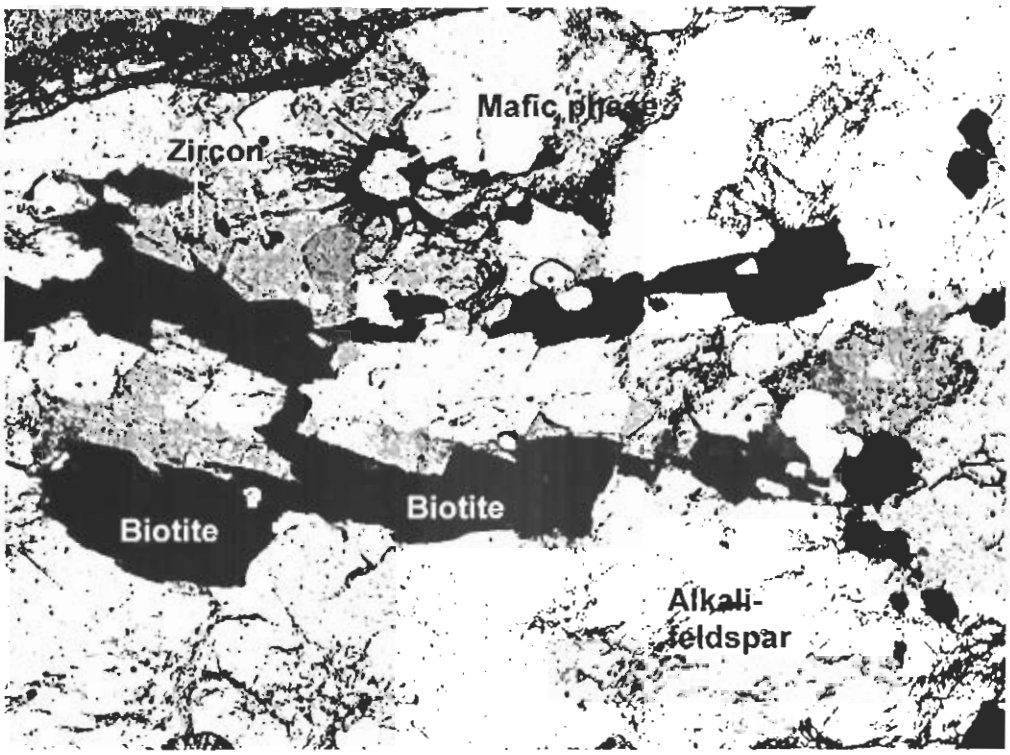


**Plate 5. 75.** Photomicrograph showing iron-leaching near the mafic phase. The dark parts are the biotites at extinction position, while the groundmass is alkali-feldspar and quartz. Three minute zircon crystals on the left side near the opaque are seen. (under crossed Polar; Mag: 4× / 0.1).

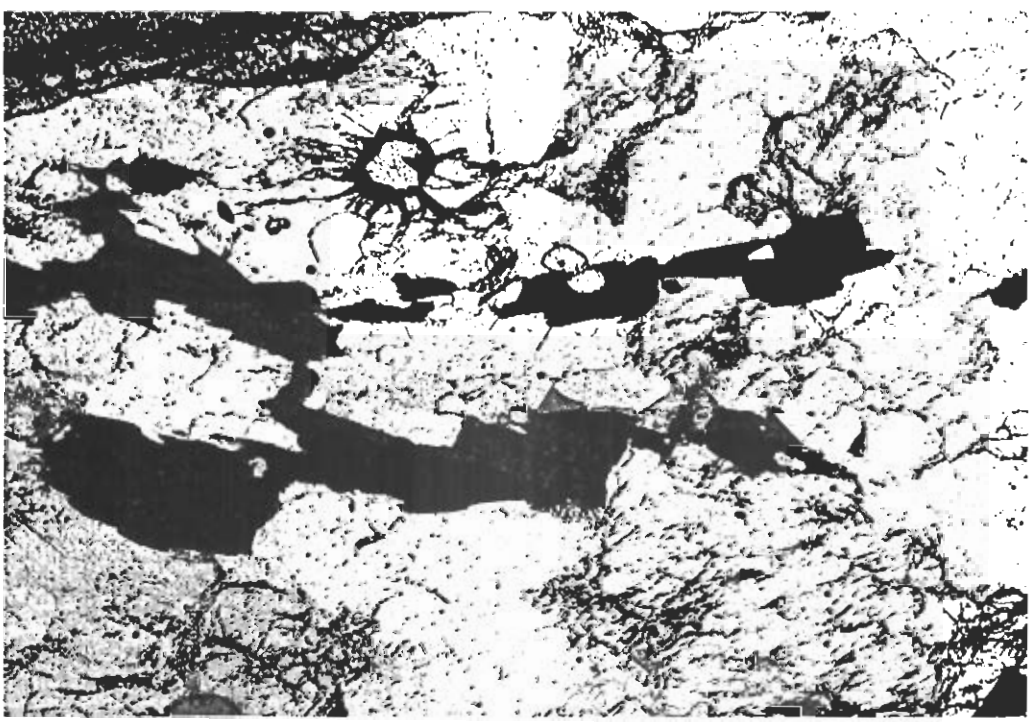

**Plate 5. 76.** Same view in plane polarized light.

# CHAPTER 6

## MINERAL CHEMISRTY

**General statement:** After careful petrographic study, various thin sections of both the gem-bearing and gem-barren pegmatites and the pegmatites of Shengus and Indus-Gilgit confluence were selected for the mineral chemistry. The detailed analytical techniques used for the determination of mineral compositions are discussed in chapter number 4. In certain rock types, only one or two kinds of gemstones are found but in pegmatite a variety of gemstones e.g., aquamarine, topaz, fluorite, different varieties of tourmaline, goshenite, morganite, garnet etc are found at a time, therefore, it is essential to conduct different analytical techniques to identify and confirm the various minerals present in these pegmatites and also to understand the type of mineralization and the processes involved in their formation. To achieve these goals and to confirm the field observations, the Electron Probe Microanalyzer, X-Ray Diffractometer, and polarizing microscope techniques were used. First of all, the polished thin sections of both pegmatites and the gemstones were studied under the polarizing microscope to identify different mineral phases, which are described in detail in chapter 5. Further, to confirm these phases, the Electron Probe Microanalyzer and X-Ray Diffractometer techniques were used.

### Mineral Phases of the Shigar Valley Pegmatites

Various phases of the Shigar valley pegmatites are described as follows:

#### Plagioclase

Plagioclase, along with quartz and alkali-feldspar are the major constituents of the granitic pegmatites (both simple and complex pegmatites). These three minerals are also present in all the zones of zoned pegmatites except the core zone, which is mainly composed of quartz. However, the proportion of these three minerals is always variable in these zones (Jahns, 1953; Černý, 1982a; Foord et al., 1986). The central core zone is

mainly composed of quartz, however, a variety of economically important minerals and gemstones are mostly associated either with the core zone or the core margin zone (London, 1986b). As far as the plagioclase is concerned, most of the granitic pegmatites are mainly composed of plagioclase, either albite or oligoclase in composition but certain pegmatites are entirely composed of albite or its variety "cleavelandite" and the proportion of oligoclase is very low (Norton and Redden, 1990). Albite is mostly associated with certain gemstones like aquamarine, topaz, schorl, fluorite and garnet (Laurs et al. 1998; Foord et al., 1986). The pure white albite itself is sometimes used as gemstone. The Shigar valley pegmatites (both zoned and unzoned and gem-bearing and gem-barren) are also mainly composed of plagioclase, alkali-feldspar and quartz.

The Electron Probe Microanalyzer analyses of plagioclases from the Shigar valley pegmatites (Table 6. 1) indicate that the plagioclase is pure albite in composition and are similar to the well known pegmatites elsewhere in the world (Jahns, 1953, 1955; Jahns and Tuttle 1963; Ćerný, 1982a and Ćerný et al., 1984). All the major oxides of the studied plagioclases are comparable but contain relatively high content of CaO (up to 2 wt. %). The cations are recalculated on the basis of 32 Oxygen and are found similar to the standard analyses of albite, especially the albites of miarolitic pegmatite class. Like the Tanco pegmatite, Bernic Lake, Manitoba (Crouse and Ćerný, 1972), the zoned pegmatites of the Shigar valley have albite as the major constituent of all the aplitic border zone, wall zone, intermediate zone, and the core zone but the proportion of orthoclase content is relatively higher as compared to albite, especially in the intermediate zone. Ćerný et al. (1984) studied the geochemical and structural characteristics of plagioclase in the Venza pegmatite, West Moravia, Czech Republic and described that the composition of the plagioclase varies according to its paragenetic position in the zoned pegmatite body. They suggested that the albite and its varieties present in different zones of a pegmatite are secondary and metasomatic in origin, while the primary plagioclase present in these zones is oligoclase that is replaced by albite in the last stages of crystallization. This is the reason that the secondary albite present in pegmatites is also known as metasomatic albite (Fleet, 2002) and the units where such type of albite is present are also known as replacement units. Other evidence for such a

paragenesis is the association of albite with rare minerals and metals that are mostly concentrated in the fluid phase and crystallized in the last stages. The late stage albite is also known as miarolitic albite because it is mostly associated with gemstones that are formed in the miarolitic cavities. In case of pegmatites of Shigar valley, no plagioclase analysis is in correspondence to the oligoclase and optically on the basis of anorthite-content it was also confirmed that the major plagioclase phase in the studied pegmatites is albite but it is not clear, either it is primary or secondary in origin. Although, it was difficult in the field to conceive and understand the metasomatic nature of albite clearly but with the help of mineral assemblages associated with albite and on the basis of optical properties it may be suggested that albite associated with gemstones is, at least, of metasomatic or secondary origin. Although, it is difficult to conclude such a paragenesis, however, some of the field features and mineral assemblages allow concluding a metasomatic origin for the albite of core zone or core-margin zone. Moreover, the albite of the border, wall and intermediate zones is primary in origin.

Linnen et al. (1992) studied a layered aplite-pegmatite body in Nong Sua intrusive complex, Thailand and have also discussed the paragenesis of pegmatites on the basis of composition of plagioclase. They suggest that if the cooling of intrusive bodies is relatively rapid following emplacement, deformation and uplift then there are chances of formation of oligoclase, but if the cooling is slow, then there are chances of recrystallization of the secondary albite. The occurrence of secondary albite in the Shigar valley pegmatites is also suggesting a slow cooling process for these pegmatites.

**Alkali Feldspar**

The Electron Probe Microanalyzer analyses of the alkali feldspar of the Shigar valley pegmatites (both zoned and simple pegmatites) are presented in Table 6. 1. The data suggest that the alkali-feldspar in these pegmatites is mostly orthoclase in composition. However, in thin section study some microperthite textures are observed. All the analyzed orthoclase grains are stoichiometrically in agreement with the standard analyses of pegmatitic orthoclase (Fleet, 2002).

In the studied alkali feldspars, the $SiO_2$ is ranging from 64.05 to 65.16, $Al_2O_3$ from 18.13 to 18.44, $K_2O$ from 14.75 to 16.34 and $Na_2O$ from 0.44 to 1.76 wt. %. All the other cations are less than 0.01 wt. %. Although iron may be present in small quantities (< 1 wt. %) in various alkali feldspars, even in the orthoclase feldspar but the studied feldspars are very poor in their iron content (0.01 to 0.14 wt. %), which supports the absence of biotite especially in the gem-bearing subclass of pegmatites of the Shigar valley. Like Fe, Mg is also a minor constituent of a great majority of alkali feldspars but it rarely exceeds 0.1 wt. %. MgO contents of 0.07 and 0.18 wt. % has been reported from orthoclase-perthite in the fluorite-bearing pegmatites (Fleet, 2002) but the feldspars of the studied pegmatites have negligible amount of MgO. The cations of these alkali feldspars are recalculated on the basis of 32 oxygen and like other standard analyses, the apfu of Si and Al of these feldspars at tetrahedral sites are in range and not less than 11.96 and 3.97 apfu respectively.

**Muscovite**

Muscovite is the main accessory mineral of gem-bearing pegmatites of Shigar valley but it is also present in gem-barren pegmatites in small quantities. It is silvery white in color with large cleavable sheets (books) and is almost common in all zones but the size and quantity increase towards the central or core zone, where large sheets of muscovite enclose various gemstones in the cavities. The common associations of muscovite are two feldspars, quartz and schorl. Field observations show that it is

commonly associated with almost all the gemstones found in the Shigar valley pegmatites.

A variety of micas (e.g., muscovite, biotite, zinnwaldite, lepidolite etc) is found in granitic pegmatites and on the basis of presence or absence of these micas, the granitic pegmatites are further classified in subtypes e.g., muscovite subtype pegmatites and lepidolite subtype pegmatites (Jahns, 1953, 1955; Černý, 1982a). In the Shigar valley pegmatites only muscovite and biotite are present and no lepidolite or zinnwaldite are noticed. The muscovites in various samples of studied pegmatites are analyzed by the Electron Probe Microanalyzer and the data is given in Table 6. 1.

In case of muscovite, various replacements and substitutions of cations may occur in tetrahedral, octahedral and interlayer positions and on the basis of presence or absence of different cations or anions, at these positions different species of muscovite may be distinguished. The interlayer cations which may occur at A-site in muscovite are K, Na, Ca, Sr, Ba, Rb, Cs. The mineral analyses of muscovites and other micas from various localities of Shigar valley are partial analyses because the total of major oxides is up to 95 wt. %. Major advances in the research on pegmatites have indicated that the rare alkali elements such as the Li, Rb, and Cs are present in the muscovites at A-sites and they may range from 1 to 5 wt. % (Černý et al., 1985). Common muscovites are also classified in certain types on the basis of presence of these rare and trace elements. As $H_2O^+$ is also the major constituent of muscovite crystal structure and ranges up to 4-5 wt. %. The EPMA results indicate that the above-mentioned rare elements are either absent or present below the detection limit of EPMA in these muscovites. If Li, Rb, and Cs contents are determined in these muscovites, then it is easy to distinguish between the gem-bearing and gem-barren pegmatites (Einfalt et al., 1995).

The mineral assemblage, texture and chemistry of studied muscovite indicate that these are primary and magmatic in origin and stoichiometrically these are pure muscovites. The $SiO_2$ and $Al_2O_3$ are in normal range, while the FeO is variable and in some flakes it is up to 8 wt. %. The muscovites of Shigar valley are chemically very

identical to the muscovites of the Himalaya mine, Mesa Grande, California (Fleet, 2002). The muscovites of both of these two fields are significantly rich in their FeO contents and belong to the 2M1 polytype. Although, the F content of the muscovites from the Shigar valley pegmatites is up to 2 wt. % (Table 6. 1) but this amount is not so significant to classify these muscovite as fluormuscovite. The muscovites of the core-margin zone are rich in F as compared to muscovites in samples taken from the border zone which indicates that the crystallization is progressive from border to core. Such type of gradational enrichment of F in different zones of zoned pegmatites is also reported by Kleck and Foord, (1999) from the George Ashley Block Pegmatites (GAB), California.

As in chapter 5, it is described that muscovite is mostly present as separate big cleavable sheets and also as small inclusions within alkali and plagioclase feldspar. Both of these types were analyzed and found as common muscovite.

**Biotite**

Biotite is a dark black colored mineral found in a variety of mafic to felsic rocks of igneous and metamorphic origin. It belongs to the trioctahedral class of mica family. This exists as a separate mineral but is also described as a biotite series of minerals (Fleet, 2002). Unlike muscovite, biotite contains no Li content but in certain cases it is present up to 1 wt. % and such biotite is known as lithian biotite. The major Li-varieties found in trioctahedral structural form of mica are zinnwaldite and lepidolite, in which $Li_2O$ is up to 5 wt. %. The interlayer cations that may be accommodated at A-site in the biotite series are K, Na, Ca, Ba, Rb, Cs, Sr, and $NH_4^+$. Na may enter and replace some of the K at A-site in the biotite isomorphous series as it is evident from some of the sodian-phlogopites from a crystalline marble in Val Malenco, Italy (Fleet, 2002). In addition, the other above-mentioned cations may also replace some of the K in the interlayers of the biotite isomorphous series and form different minerals of this isomorphous series. The substitutions and replacements within the biotite isomorphous series do not only occur at the A-sites but also in the tetrahedral, octahedral, and X-anion sites and as a result various minerals and their species are crystallized from this solid solution (Fleet, 2002).

In Shigar valley pegmatites, biotite is the main accessory mineral of the biotite ± garnet ± muscovite subclass (see chapter 5). It is also the minor constituent of the muscovite-biotite ± garnet subclass of pegmatites. However, it is generally absent in the gem-bearing class of pegmatites in the Shigar valley area but if present, it occurs in traces both in the border or wall zone and not in the intermediate or core-margin zone.

Biotite flakes of various pegmatites of the Shigar valley are analyzed by the Electron Probe Microanalyzer and the results are given in Table 6.1. The chemical composition of biotite flakes is close to the pure biotite and is generally falling in the biotite isomorphous series but some of the analyses may also qualify for other minerals of the biotite isomorphous chemical and structural series, e.g. siderophyllite, which are mostly rich in ferrous iron and poor in ferric iron and magnesium. The other major cations and anions are also in agreement with this conclusion. Titanium is also an important constituent of the biotite structural series and in the studied biotites, it ranges from 1 to 5 wt. %. There is always an increase in $Fe^{+2}$ and $Fe^{+2}$ +$Fe^{+3}$ and a decrease in Mg for the late-formed biotites (Deer et al., 1962), therefore, those biotites of the Shigar valley pegmatites, which are enriched in $Fe^{+2}$ and deficient in Mg are formed late in their paragenesis but the whole rock data and field observations do not support it. In the early studies on biotites Larsen and Draisin, (1950) concluded that the $Fe^{+2}$ content within biotites increases as the acidity of rock increases that is the reason that the biotites of the studied granitic pegmatites have higher contents of $Fe^{+2}$ relative to other rock types. In addition to this, Heinrich (1946) studied biotites of various parageneses and classified them on the basis of certain parameters. In this classification, the biotites of the granite pegmatitic affinity have high FeO; and the MgO and $Fe_2O_3$ + $TiO_2$ are less than 10 wt. %. This is consistent with the biotites from the Shigar valley pegmatites. The $Al_2O_3$ of these biotites is from 20 to 25 wt. % (Table 6.1). The fluorine in particular and chlorine in general replace some of the OH ion in the X-anions sites and the F may range from 1 to 5 wt. % in different species of the biotite series. In the studied biotites, the F-content is ranging from 0.5 to 1.5%.

The biotites of the host rock are significantly different in their chemistry from the biotites of Shigar valley pegmatites. These biotites have lower $Al_2O_3$ (up to 15 wt. %) contents and higher $TiO_2$ (up to 4 wt. %) relative to pegmatites (Table 6. 1). A distinctive difference between the biotites of pegmatite and their host rock is the higher amount of MgO in the biotites of host rock, while this cation has been generally reported up to 1 wt. % in the biotites of pegmatitic paragenesis. Therefore, the chemistry of some of the biotites from the studied pegmatites is very close to siderophyllite instead of pure biotite.

**Tourmaline**

Tourmaline is typically a mineral of granitic pegmatites, pneumatolitic veins, and some granites. Besides, it is also found in metamorphic rocks either as a product of boron metasomatism or as the result of detrital grains from the original sediment (Kleck, and Foord, 1999). The term tourmaline is not only used as a single mineral but it is also used for a group of minerals. The main compositional varieties found in this mineral group are the magnesian tourmalines or dravites, the iron tourmalines or schorl and the alkali tourmalines or elbaites. In these varieties, the Y- sites are predominantly composed of Mg, $Fe^{2+}$ and Li respectively. There is also a continuous series between dravites and schorl and between schorl and elbaite, but there appears to be an immiscibility gap between elbaite and dravites. The iron-rich varieties are generally found in the granitic rocks and belong to the schorl-elbaite series (see London, 1986; Ćerný et al., 1985; Kleck and Foord, 1999).

The tourmalines of the Shigar valley pegmatites are analyzed by using Electron Probe Microanalyzer and the results are given in Table 6.1. These tourmalines are generally the iron rich variety called schorl. The $SiO_2$ in these schorls is up to 35 wt. %, while the $Al_2O_3$, FeO and $Na_2O$ are ranging from 32 to 34 wt. %, 11.55 to 15.59 wt. % and 1.93 to 2.62 wt. % respectively. It is also evident from these analyses that some of the studied schorls are rich in MgO (1-3 wt. %). Staatz et al. (1955) have differentiated the tourmalines of border and core-margin zones of pegmatites. According to them, the tourmalines formed at the margin or border zone are Fe-rich, while those formed in the

central zone or core-margin zone are Li-rich. This may be true for those pegmatites, which are Li-rich but as the studied pegmatites are poor in their Li-contents and no mineral having appreciable amount of lithium is found. Therefore, Li-tourmalines may be absent in these pegmatites or these pegmatites are not well fractionated, especially in Li. Here, it may be added that when some of the black-colored gem-quality tourmalines (schorl) are qualitatively analyzed on XRD (Table 6. 6), it became evident that these tourmalines are very similarr to the foitite instead of schorl. Chemically, the schorl and foitite are almost identical in their Si and Al contents but the two major ions (Fe and Na) are deficient in foitite and rich in schorl. The FeO is up to 15 wt. % in schorl but in the foitite it is about 11 wt. %, the $Na_2O$ in schorl is ranging from 1 to 2 wt. %, while foitite is relatively deficient in $Na_2O$ (up to 0.75 wt. %) (Mac Donald et al., 1993; Milan and Taylor, 2000). Therefore, both the iron-rich varieties (foitite and schorl) of tourmaline are present in the pegmatites of the Shigar valley.

Various studies have shown that different types of tourmalines may be present even in a single pegmatite body (Quensel, 1956; Shearer et al., 1984). However, some specific types of tourmalines have also been reported from various pegmatites (Laurs et al., 1998). The Shigar valley pegmatites generally have schorl as a ubiquitous phase. Therefore, the studied pegmatites are broadly classified into two main categories i.e. gem-bearing and gem-barren pegmatites; the schorl is the chief minor constituent of the gem-bearing class of pegmatites, especially of muscovite-schorl-beryl-garnet subclass of pegmatites. These pegmatites are generally zoned and exposed at the various localities of the Shigar valley but are very limited in number. Field studies show that these tourmalines are mainly concentrating either at the border zone with radiating structure or are associated with the pocket or cavity zones, along with other gemstone associations. So, it indicates that these tourmalines may have been formed during the different stages of pegmatite evolution. The tourmalines present at the border zone may be formed during the main pegmatitic stages, while those associated with cavities or fracture zones may be of pneumatolytic or hydrothermal stage during the saturation of fluid phase, because minerals like topaz, fluorite, apatite are also found in these zones and are normally associated with schorl. Optically, it is observed that some of these schorls are zoned

tourmalines (Plates 5. 14, 15, 16 and 17). Quensel (1956) reported that such types of zoned tourmalines belong to the sodium replacement unit within the pegmatite body and are of pneumatolytic stage. In the pneumatolytic stage, the process of tourmalinization may occur by the introduction of boron, which attacks the common granitic minerals and as a result tourmalines are formed (Brammall and Harwood, 1925). Tourmalines are commonly associated with quartz and muscovite other than biotite (Jahns, 1953). This is consistent with the field observations that the biotite is almost absent in the gem-bearing class of pegmatites in the Shigar valley area. Besides this, it is also observed in the field that these tourmaline crystals are generally oriented towards the central core zone, which shows that the crystallization sequence of these pegmatites are progressing towards the central zone. This is in consistence with the increase in coarseness from the border zone towards the core zone and that the rupture zones or the minerals of pneumatolytic stage emanate from the core-margin zone.

**Garnet**

The minerals of the garnet group are characteristic of metamorphic rocks but these are also found in different plutonic rocks (e.g., granites, granite pegmatites, aplites) and also in acid volcanic rocks. Due to its resistant to abrasion and to chemical attack, it is also found in detrital sediments. Like certain other mineral groups, the garnet is also an isomorphous series and its end-members are pyrope, almandine, spessartine, grossular, andradite and uvarovite. Garnets having rare elements are also found e.g., goldmanite, kimzeyite, yttrogarnet but are very rare (Deer et al., 1997). Two other varieties having moderate to high titanium content are the melanite and schorlomite. Melanite is synonymously used for titanian andradite, while andraditic garnets in which Ti is greater than $Fe^{3+}$ in the octahedral position are known as schorlomite (Ito and Frondel, 1968). For the calculation of garnet mineral formula, there are various methods but the most frequently used method is of Richwood (1968), however, there are also some disadvantages of it. As in the garnet isomorphous series, no member occurs as a separate pure phase but it always caries molecules of another end-member. For this reason

Sobolov, (1965) classified the end-members of the garnet isomorphous series in the following four types and discarded the collective names 'pyralspite' and 'ugrandite'. The four types are: almandine-pyrope, almandine-spessartine, spessartine-grossular, and grossular-andradite. The members of the garnet group may also be distinguished from one another by their refractive indices, specific gravities, cell edges, and chemical data. The average proportions of the four major garnet types present in different types of rocks are calculated by Wright (1938). According to his classifications, the main garnet types present in pegmatites are almandine and spessartine in the proportion of 41.8: 47.1.

The garnets in the various types of pegmatites of the Shigar valley are analyzed by the Electron Probe Microanalyzer and the results are given in Table 6. 1. The cations are recalculated on the basis of 24 oxygen atoms, while the end-member molecules are calculated by the method of Richwood (1968) and Deer et al. (1992). The calculated end-members indicate that the garnets of the studied pegmatites are rich in almandine-spessartine molecules and are not either pure almandine or spessartine. However, pure spessartine or spessartine-almandine has been reported from various pegmatites elsewhere in the world (Strock, 1930; Hall, 1965; Gresens, 1966). The proportions of other end -members are very insignificant (Table 6. 1). The proportion of almandine is ranging from 56 to 69 mole%, while the spessartine is from 27 to 40 mole %. Almandine is the commonest species in the garnet group, and contains appreciable amounts of the spessartine with small proportion of pyrope and grossular. However, in case of granitic pegmatites, the garnets are mostly fall in almandine-spessartine molecule. According to present analyses, the garnet molecular formulas may be written as $Alm_{56-69}$ $Sp_{27-40}$ $Gro_{1.94-5.0}$ $Py_{0.03-0.11}$. In addition to pegmatites, the garnets from their host rocks (biotite gneisses) are also analyzed and the results indicate that the end-members are almandine-grossular (Table 6. 1). In these biotite gneisses, the almandine molecule is from 58 to 59 mole %, while the grossular molecule is up to 32 mole % and the spessartine is only 4 mole %. The chemical composition of garnet in the studied pegmatites is different from those of their host rocks, indicating that the garnets of both units are of different origin. As in certain metamorphic rocks, almandine acts as scavengers for manganese and as a result the proportion of spessartine molecule decreases and, therefore, the host rock have lesser

proportion (up to 4 %) spessartine (Richwood, 1968). Almandines with FeO up to 40 mole % from various metamorphic rocks have been reported and due to this high Fe-content, their molecular ratio reaches up to 86 mole % (Bostock, 1977). If the micas (especially muscovite) are poor in their MnO (0.06 - 0.08 wt. %) content either in granitic aplites or pegmatites then the manganese apparently concentrate in the residual magma until almandine-spessartine are formed (Hall, 1965). On the basis of molecular proportion of garnets, the depth of emplacement of Shigar valley pegmatites can be estimated. According to Green (1977), if the molecular proportion of spessartine is <10 mole% in a garnet than the depth of emplacement will be > 18 km and if the mole% of spessartine is >25, then the depth of emplacement will be as low as 12 km. In this regard the spessartine content of garnet from the Shigar valley pegmatites is ranging from 27 to 40 mole %; therefore, it is probable that the Shigar valley pegmatites could have been emplaced at a depth between 12 to 15 km.

**Zircon**

Zircon grains within the Shigar valley pegmatites are analyzed by the Electron Probe Microanalyzer and the results are given in Table 6. 1. The chemical composition of these zircons shows that these are pure zircon having small amounts of REEs and phosphorus (Table 6. 1). The zircons from Shigar valley pegmatites, especially those of Nyit, are relatively enriched in Y, Yb and P than the zircons of the Indus-Gilgit Confluence pegmatites (Tables 6. 1 and 6. 3). In the presence of REEs, especially yttrium group, the phosphorous may replace some of the Si and may range up to 4 wt. % (Černý and Siivola, 1980). This replacement might have taken place within the zircons of Shigar valley pegmatites which causes increase in $P_2O_5$ in these pegmatites. The presence of REE in granitic zircons is also reported by Exley (1980). Although, uranium and thorium are not detected in the studied zircons but according to Lyons (1961) these two elements are generally present in the zircons, especially from the granitic rocks. A certain amount of hafnium is always associated with zircons and it varies from one rock type to other rock type. In the studied zircons, it ranges from 2 to 5 wt. % but values as high as 39 wt. % $HfO_2$ have also been reported by Von Knorring and Hornung (1961) from a lithium

and tantalum rich pegmatites. Due to this high content of hafnium, these zircons are known as hafnian zircons. In addition to this, hafnium rich zircons have also been reported from lithium-phosphate pegmatites of the Pyrenees and the Tanco pegmatites, Manitoba (Ćerný and Siivola, 1980). Besides this, the zirconian hafnon and the hafnon end-member ($HfSiO_4$) have also been reported from Ta-bearing pegmatites of Zambezia in northern Mozambique (Correia Neves et al., 1974). It is clear from the above-mentioned examples that the hafnon rich zircons are either reported from the Li-bearing or Ta-bearing pegmatites. In contrast, the Shigar valley pegmatites are poor in these elements and no mineral rich either in Li or Ta is noticed in these pegmatites, therefore, the zircons from the Shigar valley pegmatites are poor in their hafnon content but have high values than those of the Indus-Gilgit Confluence pegmatites (Table 6. 1 and 6.3). The Hf / Zr ratio in the pegmatites is within the range of normal zircon (0.02 – 0.04), however, higher ratio (up to 0.09) is noticed in the zircons from the Shigar valley pegmatites. Vorma and Passivirta (1979) have given an average ratio of Hf / Zr as 0.023 for Finnish Rapakivi granite zircons that is based on 331 analyses and they have also concluded that Hf becomes progressively enriched as the differentiation of the granite increases. So it is concluded that the pegmatites of the Shigar valley are relatively more differentiated as compared to those of the Indus-Gilgit Confluence pegmatites (Table 6. 3). In this context, Leonova and Galibin (1963) did work on the zircons from the pegmatites and their host gneisses in the White Sea region and they noted that the Hf / Zr ratio increases from the gneiss wall rock through granitic rocks to pegmatites. In this connection the work of Lyakhovich and Shevalcyevskii (1962) played an important role for the petrogenesis of a rock type. According to them the Hf / Zr ratio increases from granite to aplite to pegmatite and they suggested that this ratio can be used for the correlation of aplites and pegmatites with the specific granite or other rock suite. In addition, the hafnium zircons have also been reported from world's famous pegmatite fields such as Karibib pegmatites of South West Africa, (Von Knorring and Hornung, 1961) and Tanco pegmatite of Bernic Lake, Manitoba (Ćerný and Siivola, 1980). In regard to the timing of crystallization of zircons, Poldervaart (1956) has suggested that the zircon is formed at later stage during the basaltic magma crystallization, while formed earlier in the case of dioritic or granitic magma crystallization but in case of alkaline

magma, it may be formed early or late in their crystallization sequence. The petrographic study of the Shigar valley pegmatites reveals that the zircons are usually present as inclusions, which indicates an early crystallization. Moreover, Murthy (1958) has also suggested that the crystallization of zircon is of short duration and is completed immediately after the emplacement of magma from its source and prior to the crystallization of other minerals.

Two analyses of zircon from the Nyit pegmatite of Shigar valley have low percentage of both the $SiO_2$ (27.71 to 28.83 wt. %) and $ZrO_2$ (51.14 to 51.93 wt. %) (Table 6. 1) but their total is less than 100 %, which indicates that some of the ions are below the detection limits of EPMA. Similar chemical compositions have also been reported from other pegmatites, where the zircon has considerable amount of the $H_2O$, $UO_3$, $ThO_2$, and $P_2O_5$ in addition to the major constituents (e.g., Hasegawa, 1957; Fujiwara et al., 1965). As these constituents are not determined in the studied zircons, so this may be the reason that total is less than 100 %.

**Apatite**

Apatite is the most common accessory mineral group found in almost all the igneous rocks. Besides, it is also found in the sedimentary and metamorphic rocks. The most common varieties found in this group are: fluorapatite, chlorapatite, hydroxylapatite, and carbonate-apatite (Deer et al., 1966). The different varieties of this group are the most abundant phosphorus-bearing minerals.

In the Shigar valley, apatites occur as gem-quality as well as mineral specimen within the gem-bearing class of pegmatites. The gem-quality apatites are described separately under the section of gemstones. Here the mineral chemistry of the minute crystals of apatites is described which are observed in thin-section study. Although, the gem-quality apatites are only present within the gem-bearing class of pegmatites, but small crystals of apatite are also noticed in the gem-barren class of pegmatites under microscope. These grains are analyzed by the Electron Probe Microanalyzer and the

results are presented in Table 6. 1. The data indicate that the total sum of cations is about 100 % without the chlorine, fluorine, carbonate and hydroxyl ions, which shows that such types of ions are either absent or in traces in these apatites (Tables 6. 1 and 6. 5). However, MnO concentration in these apatites is in significant quantity. Therefore, these apatites can be considered as manganapatite instead of either as chloro, fluoro and carbonate or hydroxyl apatites because at the A-sites some of the calcium may be replaced by Sr, Mn, Na and the REEs. However, the XRD data of the gem-quality apatites indicate that these are fluorapatite (Table 6. 6). In this respect, it may be added here that in case of apatite analyses under EPMA care must be taken because the Cl and F may be diffused under increasing duration of exposure to the electron beam as reported by Stormer et al. (1993).

The apatite in the pegmatites is mostly associated with the different varieties of the lithium-bearing minerals (i.e., lepidolite, spodumene, lithiophilite and amblygonite), beryl and tourmaline c (Cerny et al., 1985; Cerny, 1991a, b). However, the pegmatites of the Shigar valley are poor in Li- bearing minerals and, therefore, the studied apatites are associated with beryl, schorl, fluorite and muscovite.

**Fluorite**

Fluorite usually occurs as a vein mineral associated with quartz and calcite but it also occurs granites and pegmatites. It is also found in pneumatolitic deposits and in sedimentary rocks (e.g., limestones and dolomites) as a result of metasomatism. The most commercial type fluorite comes from carbonatites and other alkaline igneous rocks (Deer et al., 1966; Bill et al., 1967).

The fluorite grains of Shigar valley pegmatites are analyzed by the Electron Probe Microanalyzer and the results are given in Table 6. 1. Majority of the fluorites contains 99 % $CaF_2$ but some amounts of Si, Al, and Mg may be present either as impurities or inclusions (Saito, 1950). The Shigar valley fluorites are pure because in most of the analyses the total of $CaF_2$ is very close to 100 wt. % except of a few (Table 6.1). Some REEs have been reported from the fluorite analyses such as Y and Ce and on the basis of their presence some varieties of fluorite are also known. The mineralization of fluorite in igneous rocks (e.g., granites, syenites, pegmatites) is mainly of late stage hydrothermal origin and is having homogenization temperature $T_h$ of 450 - 550°C for its mineralization (Chang et al., (1998).

**Chlorite**

Like mica, the chlorites are a group of minerals with layered structures and resemble mica in many respects. Chlorites mainly occur in igneous rocks due to the alteration by hydrothermal action. Besides, these also occur in chlorite schists along with clay minerals and also in argillaceous sediments (Deer et al., 1966).

Chlorites of the Shigar valley pegmatites are analyzed by the Electron Probe Microanalyzer and the results are given in Table 6. 1. Chlorites are classified by various ways but the most common subdivision is on the basis of $Fe_2O_3$. According to this scheme, the chlorites are classified as oxidized ($Fe_2O_3 > 4$ wt. %) and unoxidized ($Fe_2O_3 < 4$ wt. %). Although, there is a wide range of substitutions in the layers of chlorites but

the most common replacements are of Si by Al and Mg by Al but in some of the varieties $Fe^{+2}$ may replaces the Mg. Besides, small amounts of Mn, Ni, Cr, Ti may be present in the chlorites (Deer et al., 1966).

Paragenetically, chlorite is widely distributed in the low grade metamorphic rocks and is the characteristic mineral of the greenschist facies. It is also formed by hydrothermal alteration of the primary ferromagnesian minerals in the igneous rocks. Besides, it is also a common product of weathering and found in many types of sediments. The chemical composition of chlorites of the Shigar valley pegmatites (Table 6. 1) is very close to daphnite variety, in which FeO is more than 40 wt. % and MgO is very low (Deer et al., 1966). In case of replacement and substitution, the compositions of chlorites are mostly related to that of the coexisting mineral. The high contents of iron in the studied chlorite suggest that during the hydrothermal alteration there could have been the substitution of iron in the structure of chlorite from the coexisting phases such as biotite, magnetite and ilmenite. The total of oxides is less than 100 wt. % and it is because of the absence of $H_2O^+$ molecule, which in the case of chlorites normally ranges from 12- 15 wt. %. However, $H_2O^+$ is not analyzed in these chlorites.

**Mineral phases of the Indus-Gilgit Confluence and Shengus Pegmatites**

The Indus-Gilgit Confluence pegmatites are well exposed near Jaglot, where the Gilgit river merges in the Indus river. These are gem-barren pegmatites and are very simple not only in mineralogy but also in internal structure. The mineral phases identified in these pegmatites in the hand specimen and by different analytical techniques are described below:

**Plagioclase**

The plagioclase grains of the Indus-Gilgit Confluence (ICP) and the Shengus pegmatites are analyzed by the Electron Probe Microanalyzer and the results are presented in Tables 6.2 and 6.3. Unlike the Shigar valley pegmatites, the Indus-Gilgit Confluence pegmatites are mostly composed of alkali-feldspar (especially microcline) instead of sodium-plagioclase. Although, sodium-plagioclase feldspar is also present in these pegmatites as an essential component but according to the modal composition (Table 5. 3), the proportion of alkali feldspar is greater than the plagioclase feldspar.

A prominent difference noted in the Indus-Gilgit Confluence pegmatites is the presence of oligoclase and andesine (Tables 6. 1 and 6. 3), which are not found in the Shigar valley pegmatites. The oligoclase analyses of the Indus-Gilgit Confluence pegmatites indicate that the $SiO_2$ is ranging from 61.51 to 62.52 wt. %, $Al_2O_3$ from 22.46 to 23.10 wt. %, CaO from 4.27 to 5.09 wt. %, $K_2O$ from 8.74 to 9.31 wt. %. In case of andesine the $SiO_2$ is up to 58 wt. % and the $Al_2O_3$ is up to 24.86 wt. %, while the CaO and $Na_2O$ are up to 7 wt. %. As the intrusion of ICP is very younger around some 5-10 Ma and during this time, the deformation and uplift of the Kohistan was continued (Petterson and Windley, 1985; Zeitler and Chamberlain, 1991), so there were maximum chances for the formation of oligoclase relative to albite (Linnen et al., 1992).

The Shengus pegmatites are also rich in albite but small amount of oligoclase is also observed (Tables 6. 2 and 6. 3). Although, the Shengus pegmatites are also gem-bearing but as limited number of samples are taken from this pegmatite field, so it is difficult to say that either these albites are primary or secondary in origin. As the minerals of hydrothermal origin are also found from these pegmatites, therefore, it is probable that some of the albite may be of metasomatic origin as is the case of Shigar valley pegmatites.

On the basis of internal structure, the albites are classified as high and low albites but several studies have shown that the high temperature albites are mostly found in

volcanic rocks and the low temperature albites are found in the plutonic as well as in various low grade metamorphic rocks. So the albites in the studied pegmatites especially from the Shengus pegmatites are also low temperature albites and it is confirmed on the basis of XRD data (Table 6. 6).

**Alkali feldspar**

The alkali-feldspars of both the Indus-Gilgit Confluence and Shengus pegmatites are analyzed by the Electron Probe Microanalyzer and the results are presented in Tables 6.2 and 6. 3. The alkali feldspars found in plutonic igneous rocks are mainly orthoclase, microperthite and microcline. The chemical composition of the alkali-feldspars from the Indus-Gilgit Confluence pegmatites indicates that these are microcline and microperthite in composition (Table 6. 3). All the analyzed alkali feldspars are stoichiometrically in agreement with the standard analyses given by Fleet (2002). Unlike the Shigar valley pegmatites, where the main alkali feldspar is orthoclase, the Indus-Gilgit Confluence pegmatites are rich in microcline and majority of the samples also exhibit microperthite texture. Besides this, the modal composition of plagioclase feldspar in Indus-Gilgit Confluence pegmatites is less than the Shigar valley pegmatites. The Shigar valley pegmatites are rich in plagioclase feldspar especially in albite, while the Indus-Gilgit Confluence pegmatites are rich in microcline. In the alkali feldspars, the anorthite content is generally less than 5 %.

In the studied alkali feldspars, the $SiO_2$ ranges from 62.78 to 65.20 wt. %; $Al_2O_3$ from 17.82 to 18.24 wt. %, $K_2O$ from 15.36 to 16. 49 wt. % and $Na_2O$ from 0.66 to 1.12 wt. %. Like the Shigar valley pegmatites, the alkali feldspars of Indus-Gilgit Confluence pegmatites are also very low in other cations (e.g., $Fe^{3+}$, $Fe^{2+}$, Mg, Ti, Mn) (Table 6. 3). The Si and Al contents of these feldspars at tetrahedral sites are ranging from 11.93 to 12.03 and 3.92 to 4.02 apfu respectively.

The trace elements such as Li, Ba, Sr, Rb, Cs etc may be present in significant quantities and accommodate in the structures of the alkali feldspars (especially in those

alkali feldspars, which belong to the rare element pegmatite class) but as the Indus-Gilgit Confluence pegmatites are very simple in their mineralogy as well as internal structure and, therefore, belong to the simple pegmatite class. So there are less chances for these elements to be accommodated in such type of alkali feldspar and are reported as below the detection limit.

**Biotite**

Biotite is the ubiquitous phase in the Indus-Gilgit Confluence pegmatites, while it is relatively in lesser amount in the Shengus pegmatites. The Indus-Gilgit Confluence pegmatites are unzoned, therefore, biotite flakes are disseminated through out the pegmatitic body. It is evident from Table 6.3 that the sum of the total cations of the studied biotites is less than 100 wt. %, which could be due to the fact that the $H_2O^+$ is not determined in these biotites. Some other cations such as Li, Cs, Rb may be present in significant quantities in biotites but such types of substitutions are only restricted to the rare element class of pegmatites. Therefore, there are minimum chances for such type of elements to be substituted in these biotites of the Indus-Gilgit Confluence pegmatites because these are very simple not only in mineralogy but also in the internal structure. Moreover, like the Shigar valley pegmatites, there are also a few chances for the above-said rare alkalis to be substituted in the biotites of the Shengus pegmatites because both of these pegmatite fields are of miarolitic type rather than a rare element pegmatite class.

Chemically, the studied biotites are very close to the pure biotite in the isomorphous biotite series but some major differences are also noted between these and the biotites from the Shigar valley. The main variation is that the biotites from the Shigar valley pegmatites are very poor (~ 1 wt. %) in their magnesium contents, while the biotites of Indus-Gilgit Confluence pegmatites and the Shengus pegmatites have MgO contents up to 8 wt. % and 5 wt. % respectively. $TiO_2$ is low (up to 1 wt. %) in the biotites of Shigar valley pegmatites, while it is very high (4 wt. %) in the biotites of Indus-Gilgit Confluence and the Shengus pegmatites. Conversely, the $Al_2O_3$ and FeO contents of biotites from the Shigar valley pegmatites are higher than the biotites of

Indus-Gilgit Confluence and the Shengus pegmatites. In the biotites of Shigar valley pegmatites, the $Al_2O_3$ and FeO are up to 20 and 28 wt. % respectively, while in the ICP biotites these are up to 16 and 23 wt. % and 19 and 23 wt. % in the biotites of the Shengus pegmatites. However, $SiO_2$ contents of biotites are similar in all the three types of pegmatites. Chemically, some biotites from the Shigar valley pegmatites are characterized as siderophyllite but the biotites of ICP and the Shengus pegmatites are stoichiometrically identical with the standard analyses of pure biotites. In addition to this the fluorine contents of biotites from the Shigar valley pegmatites are also slightly higher than the biotites of ICP, which shows that the pegmatitic magma of the Shigar valley area was rich in volatiles and fluids relative to the Indus-Gilgit Confluence pegmatites. Moreover, like the Shigar valley pegmatites, the Shengus pegmatites are also slightly enriched in their fluorine contents relative to the Indus-Gilgit Confluence pegmatites.

**Epidote**

The word epidote is used in dual meaning: as a separate mineral as well as a group of minerals. The main minerals occurring in this group are zoisite, clinozoisite, epidote, piemontite, and allanite. Structurally as well as chemically this group is very complex and its minerals occur in a wide variety of parageneses (Howie, and Walsh, 1982). The minerals of this group mostly occur in a variety of metamorphic rocks ranging from low grade greenschist up to high grade eclogites and glaucophanites.

The epidote grains in the pegmatites of Indus-Gilgit Confluence and Shengus are analyzed by the Electron Probe Microanalyzer and the results are given in Tables 6.2 and 6. 3. It is clear from these tables that the major cations of analyzed epidotes are in agreement with the standard analyses of epidote and there is very limited replacement of Si by Al in these epidotes as the total of Si is very close to 3 apfu (Table 6. 3). Both these phases have low variation. $SiO_2$ is ranging from 35 to 38 wt. % and the $Al_2O_3$ from 21 to 23 wt. % in these epidotes. The total of major cations is less than 100 wt. % because the $H_2O^+$ molecule is not determined, which is usually up to 3 wt. % in epidotes. The iron present in at the Y- sites in the structures of epidotes is generally $Fe^{+3}$ but $Fe^{+2}$ may also

enter and replaces Ca. In addition to this, the replacement by Mg and Mn is also relatively very small. Besides, the presence of other cations is insignificant in the analyzed epidotes. The amount of $TiO_2$ is ranging from 0.08 to 0.18 wt. % and is consistent with the standard analyses of epidote. The other ions (Sr, Cr, V, Pb) may occur variably in the structures of epidotes and on this basis certain species of epidote are also known as chromian epidote, plumbian epidote, vanadian epidote etc (Schreyer and Abraham, 1978; Willemse and Bensch, 1964). An epidote rich in $P_2O_5$ (0.42 wt. %) is also reported from glaucophane schist (Howie and Walsh (1982). But the studied epidotes are very poor in these ions especially in $Cr_2O_3$ and $P_2O_5$. In addition to this, the REE-bearing epidotes have also been reported (Deer et al., 1986). The studied epidotes are, however, have no significant amount of any REE.

**Allanite**

Unlike the epidote and its other members, which are mostly found in metamorphic rocks of various grades having different parageneses, the allanite is generally found in many granites, granodiorites, syenites and also in pegmatites. It may also be present in gneisses, schists and also as a detrital mineral in sedimentary rocks. Certain REEs are also present in allanites in considerable quantities and the XRD patterns change with the increase of rare earth elements as is suggested by Kumskova and Khostova (1964). A coupled replacement of $Ca^{2+}$ $Fe^{3+}$ $\leftrightarrow$ $REE^{3+}$ + $Fe^{2+}$ may occur between the epidotes and the allanites. The allanites are the only members of the epidote group, in which ferrous iron is present as an essential constituent along with REEs. Further more, the allanites are the only minerals that have maximum amount of Ce (Smith et al., 1957). Due to the presence of radioactive elements, allanites have also been used for the age determination (Rao et al., 1979).

The minute allanite grains (visible in high magnification) present in the Indus-Gilgit Confluence pegmatites, have been analyzed by the Electron Probe Microanalyzer and the results are given in Table 6. 3. Like the epidotes, the $H_2O^+$ content of the allanites is also not determined, therefore, the total sum of oxides is less than 100 wt. %. In

addition, the allanites are analyzed by two methods, in one, only common major cations are analyzed, while in the other REEs along with certain trace elements are also analyzed to determine their concentration. As even after the inclusion of REEs, the total of oxides is much less than 100 wt. %, which again indicates that the analyses are not complete and still there are some elements present in these allanites, which may be below the detection limits.

In these allanites the $SiO_2$ is ranging from 31 to 34 wt. % (Table 6. 3) with apfu 3.01 to 3.11, $Al_2O_3$ from 17 to 19 wt. %, FeO from 12.07 to 13.47 wt. %, CaO 14.77 to 18.67 wt. %, MnO 0.30 to 0.86 wt. %. The REE and other trace elements present in significant quantities in the structures of allanites are generally Ce, La, Y, Nd, Pb, Sr, V (Frondel, 1964). Ce, La and Y are, however, ubiquitous in allanites. In the studied allanites, the $Ce_2O_3$ is ranging from 5 - 6 wt. % and $La_2O_3$ from 2.69 to 3.3 wt. % (Table 6. 3). Frondel (1964) documented the relative abundances of REEs present in the allanites and concluded that the Ce is always greater than La and the Ce: La ratio is generally 2:1. Such type of relationship is also true for the allanites of the Indus-Gilgit Confluence pegmatites (Table 6. 3). Although thorium and uranium are also present in the majority of allanites and variably ranges from traces up to about 5 wt. % (Rao et al., 1979) but in the studied allanites, these were not determined. Vainstein et al., (1956) reported that allanites occurring in pegmatites are poorer in La and Ce than those found in granites. However, the allanites found in hydrothermal veins are strongly enriched in La (Frondel, 1964). In addition to this, allanites having Be, P, Ge and F in considerable quantities have been reported worldwide (Rao et al., 1979) but in the allanites of the Indus-Gilgit Confluence pegmatites (Table 6. 3) except phosphorus, no other elements have been determined and the phosphorous content in these allanites is very low.

The process of metamictization is common in the allanites because of the presence of radioactive elements in their structure. Due to the bombardment of alpha particles, destruction occurs within the internal structure of allanites and as a result daughter elements are formed and some of the elements partially or completely removed from the allanite structure (Rao et al., 1979). When the process of metamictization

occurs, allanite changes its color from greenish-brown to orange-brown (Deer et al., 1986). The total sum of oxides is less than 100 wt. % in the studied allanites (Table 6. 3), it may be due to this process that some of the elements are completely or partially removed from the allanite structure. Allanites are also classified as metamict and non-metamict. The metamict varieties are mostly isotropic in character and can be distinguished by the presence of anastomosing cracks, which are produced by radioactive elements (Rao et al., 1979).

**Apatite**

The apatite grains of Indus-Gilgit Confluence and Shengus pegmatites are analyzed by the Electron Probe Microanalyzer and the results are presented in Table 6.3. The data show that the total sum of cations is close to 100 wt. % without the determination of chlorine, fluorine, carbonate and hydroxyl ions; which shows that such types of ions are either absent or in traces in these apatites (Tables 6. 2 and 6. 3). The apatites of Shengus pegmatites contain MnO up to1.27 wt. % and are, therefore, characterized as manganapatites. Sr, Ba, Mn, Na and the REEs may be present in significant quantities in the structures of apatites and on this basis certain varieties of apatite have been recognized. The present studies show that the apatites from the Indus-Gilgit Confluence pegmatites can not be further classified as these are very poor in these cations except the apatites from the Shengus pegmatites, where the MnO is in considerable quantity, and is classified as manganapatites. The analyses of these apatites (Table 6. 2) show that the studied apatites are also poor in La to Yb elements.

**Chlorite**

Chlorite occurring as an alteration product in the Indus-Gilgit Confluence and Shengus pegmatites is analyzed by the Electron Probe Microanalyzer and the results are given in Tables 6. 2 and 6. 3. There is a wide range of substitutions in the chlorites but the most common replacements and substitutions are of Si and Mg by Al. But in some of

the varieties $Fe^{+2}$ may also be substituted for Mg. In addition to these major substitutions, small amounts of Mn, Ni, Cr, Ti etc may also be present in the chlorites.

Chlorite is widely distributed in the low-grade metamorphic rocks and is also the characteristic mineral of the greenschist grade facies. It is also found in the igneous rocks due to the hydrothermal alteration of primary ferromagnesian minerals. The results of analyzed chlorites from the Indus-Gilgit Confluence pegmatites are slightly different from the Shigar valley pegmatites (Table 6. 3). Chlorites from the Shigar valley pegmatites are rich in FeO and very poor in MgO, therefore, they qualify as daphnite, a variety of chlorite in which FeO wt. % is more than 40 and MgO is very low (1 wt. %) but the chemical analyses of chlorites from the Indus-Gilgit Confluence pegmatites are in agreement with the standard analyses of chlorites (Table 6. 3). In addition, it is also noted that the chlorites from the Indus-Gilgit Confluence pegmatites are relatively rich in their titanium contents and in one analysis the $TiO_2$ is even up to 7 wt. %. Another prominent difference between the chlorites from Indus-Gilgit Confluence pegmatites and Shigar valley pegmatites is that the chlorites from the ICP are relatively rich in MnO (0.85 - 1.37 wt. %). The chlorites from the Shengus pegmatites are similar in their chemistry to the Indus-Gilgit Confluence pegmatites, as majority of the constituents of their chlorites are very close.

**Zircon**

The minute crystals of zircon, present as inclusion, in the pegmatites from Indus-Gilgit Confluence and Shengus are analyzed by the Electron Probe Microanalyzer and the results are given in Tables 6. 2 and 6. 3. These analyses are discussed in comparison with that of the Shigar valley pegmatites. The Shigar valley pegmatites, especially of Nyit, are relatively enriched in Y, Yb and P than the zircons of the Indus-Gilgit Confluence pegmatites. In the presence of REEs, especially yttrium group, the phosphorous may replace some of the Si (Correia, et al., 1974). In the zircons from Shigar valley pegmatites, the $P_2O_5$ has replaced the $SiO_2$ to some extent. But the zircons from the Indus-Gilgit Confluence pegmatites are poor both in REEs and in $P_2O_5$, therefore, no

substitution or replacement has taken place in these zircons. The hafnium contents of Indus-Gilgit Confluence zircons are also lower than the zircons from the Shigar valley pegmatites (Table 6. 1). As already discussed in the zircons from the Shigar valley pegmatites that the hafnon rich zircons are either reported from the Li-bearing or Ta-bearing pegmatites but like the Shigar valley pegmatites, the ICP are also poor in these elements, therefore, the zircons from the Indus-Gilgit Confluence pegmatites are also poor in their hafnon contents.

The most common range for Hf / Zr ratio in zircons is 0.02 – 0.04, the zircons from the Indus-Gilgit Confluence pegmatites fall in this range (Table 6. 3). The Indus-Gilgit Confluence pegmatites are less differentiated than the Shigar valley pegmatites because according to Vorma and Passivirta (1979) Hf in zircons becomes progressively enriched as the differentiation of the granite increases. The results show that the Shigar valley pegmatites are relatively more enriched in $HfO_2$ and therefore, more differentiated than the Indus-Gilgit Confluence pegmatites (Tables 6. 1 and 6. 3). Although, $UO_3$, $ThO_2$ along with certain other cations may be present in the zircons but as the total is very near to 100 wt. % that minimizes the presence of these elements in the studied zircons.

**Ilmenite**

Ilmenite being a common accessory mineral of many igneous and metamorphic rocks is also occasionally found in massive veins. The formula of ilmenite is generally expressed as (Fe, Mg, Mn) $TiO_3$ with a very limited amount of Mg and Mn but the Mn-rich varieties may reach up to 20 wt. % (Deer et al., 1966).

The ilmenite grains from the Indus-Gilgit Confluence pegmatites are analyzed by the Electron Probe Microanalyzer and the results are presented in Table 6. 3. This indicates that these are enriched in their manganese contents (up to 19 wt. %) and are characterized as manganese ilmenite. The $Fe_2O_3$ content may be up to 6 wt. % in the solid solution of ilmenites but in the studied ilmenites from the Indus-Gilgit Confluence pegmatites, it ranges from 0.75 – 2.02 wt. %. Howie (1955) and Gjelsvik (1957) have

reported that ilmenite and magnetite occur in association in certain rocks and in such type of association the ilmenites are preferentially enriched in manganese. The present work shows that the magnetites and ilmenites are crystallized together in the Indus-Gilgit Confluence pegmatites (Table 6. 3) and the ilmenites are enriched in Mn. It is the well known that these oxide minerals are formed at very high temperatures, therefore, these must be formed before the other common major and accessory minerals of the Indus-Gilgit Confluence pegmatites. A notable difference is also noticed in the compositions of ilmenites of the Indus-Gilgit Confluence pegmatites. The ilmenites of sample number 114 (Table 6. 3) are rich in titanium and manganese and poor in ferrous iron, while it is reverse in sample number 111, where ilmenites are rich in ferrous iron and poor in titanium and manganese. In certain cases the $Fe^{+2}$ is completely replaced either by Mg or Mn and as a result the two end-members geikielite ($MgTiO_3$) and pyrophanite ($MnTiO_3$) are formed. This occurs in rare cases and the $Fe^{+2}$ is partially replaced by Mn to form manganese ilmenites as is proved in the ilmenites from Indus-Gilgit Confluence pegmatites.

**Magnetite**

The magnetite grains of the Indus-Gilgit Confluence are analyzed by the Electron Probe Microanalyzer and the results are given in Table 6. 3. These magnetite have $Fe_2O_3$ ranging from 67.52 to 68.21 wt. % and FeO from 30.38 to 30.44 wt. %. This indicates that these magnetites are pure. One analysis contains $TiO_2$ up to 13.98 wt. % which can be the titanomagnetite. The occurrence of both titanomagnetite and ilmenite is very useful in both the igneous and metamorphic thermometry (Buddington et al., 1955). According to Buddington et al. (1955), the magnetites of metamorphic paragenesis have lower $TiO_2$ than those of igneous paragenesis, especially in the more siliceous rocks. The replacements on small scale may occur in the structures of magnetite where Al is replaced by $Fe^{+3}$ and Ca, Mn, Mg may replace some amount of $Fe^{+2}$. However, no such replacement has been noticed in the studied magnetites. Sometimes, the $SiO_2$ may be present in small amounts in the magnetites that may be due to the contamination by certain silicate phases or it may be due to the presence of some non-opaque minerals as

an inclusion (Vincent and Phillips, 1954). But the studied magnetites are pure and there is no contribution of silica component in the structure of these magnetites. In addition to the above-mentioned replacements that occur in the magnetite at divalent site; the Cr and V may also substitute for $Fe^{+3}$ in considerable amounts in the trivalent group (Howie, 1955). But again the magnetites from the Indus-Gilgit Confluence pegmatites are pure and there is no replacement of these trivalent ions in the studied magnetites.

## Gemstones from the Shigar valley pegmatites and their mineral chemistry

In addition to the above mentioned common rock-forming minerals, a variety of gem-quality minerals i.e., beryl (aquamarine), topaz (both colorless and yellow), garnet, fluorite, apatite, tourmaline (schorl) etc are found in the gem-bearing class of pegmatites of the Shigar valley area (Fig. 6. 9). In addition to these gemstones, other gemstones, either of metamorphic or metasomatic paragenesis, are found in the different localities of the Shigar valley. These are epidote, zoisite, clinozoisite and axinite etc (Fig. 6. 9). To identify and confirm these gemstones, the XRD and Electron Probe Microanalyzer techniques are used. By these techniques different gemstones can be properly identified and the results of these two techniques in the context of paragenesis of these gemstones are described below:

### Topaz ($Al_2SiO_4(OH, F)_2$

Topaz is most commonly found in cavities and druses in granites, granite pegmatites, rhyolites and also in contact zones. The formation of topaz in plutonic rocks especially in granitic pegmatites is mostly associated with the late-stage pneumatolytic action. The common mineral associations for topaz are cassiterite, beryl, fluorite, tourmaline and muscovite (Rosenberg, 1972).

The colorless and yellow topaz have been found from gem-bearing class of pegmatites from various localities (Yuno, Kashmol, Dassu, Nyit Bruk, Goyungo areas) of the Shigar valley (Fig. 6. 9). Two colorless crystals of topaz (1x 3 cm), one from

Kashmol and another from Yuno were collected during the fieldwork (Plate 6.1). The crystals are composed of two types of faces: tetragonal prisms and c-pinacoid. The topaz crystals are generally associated with albite-quartz-muscovite matrix in the pegmatitic body.

The chemical composition of the topaz is stoichiometrically similar to that of standard topaz (Table 6. 5). No significant variation in the chemistry of the topaz is noticed from core to margin of the crystals and is, therefore, homogenous in composition. Trace elements in the topaz play an important role in the color of the topaz for example, the yellow varieties are relatively enriched in Cr, Mn, Co, and V, while the Ni is characteristic for blue topaz (Rosenberg, 1972). On the basis of trace element geochemistry, Haapala (1974) differentiated the topaz-bearing granites from the normal and Rapakivi granites. According to him, the topaz-bearing granites have relatively high values of F, Be, Li, Rb, Sn, Ga and Nb and low values of Fe, Mg, Ti, Ba, Sr, and Zr. Though Be, Sn and Li are not determined in the Shigar valley pegmatites, however, these pegmatites are rich in Rb, F and Nb and poor in Fe, Mg, Ti, Ba, Sr and Zr. Therefore, these pegmatites host gem-quality tourmalines, topazes, axinites as these are saturated in volatiles such as the F, B, $H_2O$. Some crystals of topaz in a pegmatite near Yuno (Shigar valley) are noticed at the base of core-margin zone, suggesting a gravitational settling of topaz in the melt. This type of situation has also been reported by Rosenberg (1972) for Brown Derby granitic pegmatite, Gunnison County, Colorado. The fluorine contents of the studied topaz crystals (Table 6. 5) are similar to that of Brown Derby granitic pegmatites, which are formed at about 750°c and 2000 Kbar pressure (Rosenberg (1972).

**Garnet**

Although, large garnet crystals of gem-quality are scarce in the pegmatites of the Shigar valley but small crystals (~ 2 cm) are present in these pegmatite bodies. These garnet crystals are analyzed by the Electron Probe Microanalyzer and the results are given in Table 6. 5. Though, small crystals of garnet are present in the gem-bearing class of pegmatites in every locality of the Shigar valley but these are generally found in higher concentration in the pegmatites from Dassu and Yuno. These pegmatites are extensively mined for well-developed euhedral crystals of garnet along with other gemstones (Plate 6. 2). The garnets are generally concentrate (either at the border or wall zones) of the pegmatites. The gem-quality garnets collected during field are 1 - 2 cm in diameter, translucent and reddish-brown in color with dodecahedron habbit (Plate 6. 3).

In the garnet isomorphous series, no member occurs as a separate pure phase but it always caries molecules of another end-member. Therefore, according to the classification scheme of Sobolov (1965), the garnets of the Shigar valley pegmatites, including gem-quality garnet, are not pure but contain considerable quantities of different end-members. The end-members of the studied garnets are calculated by the method of Deer et al. (1992) and are given in Table 6. 5. According to the molecular proportions of the end-members, the studied garnets are generally almandine-spessartine but one garnet analysis has a composition of spessartine-almandine (Table 6. 5). The molecular formula of the gem-quality garnet end-members can be written as $Alm_{51.97 - 52.87}$ $Sp_{46.36 - 46.48}$ $Gro_{.97}$ $Py_{0.57 - 0.63}$ and $Sp_{55.51}$ $Alm_{43.68}$ $Gro_{0.60}$

The Electron Probe Microanalyzer analyses of the garnets from the polished thin sections of pegmatites and the gem-quality garnets are almost identical and no major differences are noted in the chemical compositions of these two types of garnets. The calculated end-members indicate that the gem-quality garnets of the studied pegmatites are rich in almandine-spessartine and spessartine-almandine molecules and are not either pure almandine or spessartine, although pure spessartine has been reported from various

pegmatites elsewhere in the world (Strock, 1930; Hall, 1965; Gresens, 1966; Fajklewicz, 1969). Moreover, the XRD pattern and d-values (Fig. 6. 1 and Table 6. 6) of the studied garnets from the Shigar valley pegmatites are very near to the almandine but some of the peaks common in spessartine and almandine are also present, which also confirm that these are almandine-spessartine garnets with major input of almandine. The proportions of other end-members are very insignificant (Tables 6. 1 and 6. 5). According to Hall (1965), if the micas mainly muscovite, are poor in their MnO (0.06 - 0.08 wt. %) content either in granitic aplites or pegmatites then the manganese apparently concentrated in the residual magma until almandine-spessartine forms. As the majority of analyses of muscovite from these pegmatites (Table 6. 1) indicate that the MnO contents of these muscovites are ranging from 0.03 to 0.09 wt. %, so it is probable that the manganese has been retained in the residual magma until these garnets have been formed near the core-margin zone.

**Beryl ($Be_3Al_2Si_6O_{18}$)**

Beryl is a group of minerals having a variety of gemstones such as emerald, aquamarine, morganite and goshenite. Various varieties of beryl found during this study from Shigar valley pegmatites are light to dark blue colored aquamarines and colorless variety known as goshenite. The transparent and colorless to pale blue aquamarine crystals (5 - 15cm x 1 - 7.5 cm) have been reported by Middlemiss and Parshad (1918) from the Dassu pegmatites. According to Kazmi et al. (1985) aquamarine crystals up to 16 cm long and 7 cm wide from the Dassu pegmatites have been reported in the James A. Gibbs collection. The colorless and transparent variety goshenite and light bluish aquamarine crystals of gem-quality ranging in size from 2 to 12 cm are common in the gem-bearing class of the Shigar valley pegmatites (Plate 6. 4). These are mainly concentrated in the specified cavities and vugs present either near the core-margin zone or in the coarse-grained intermediate zone (Plate 6. 5). The form of these crystals is open, i.e. prismatic and c- pinacoid are present at a time in one crystal and their crystal system is hexagonal with no cleavage and conchoidal fracture. Some crystals are also twinned with aquamarine itself and with tourmaline. Albite, muscovite and tourmaline are

commonly associated with aquamarine but at places calcite is also seen in association with aquamarine as matrix material. In this connection, Gubelin, (1981) reported goshenite, a colorless to white variety of beryl from the pegmatites of the Dassu area. According to the local miners, morganite (pink-beryl) is also present in these pegmatites but when these light-pink colored gemstones are tested on XRD and analyzed on Electron Probe Microanalyzer, it has been found that these pink-colored gemstones are not morganite (beryl) but are characterized as apatite (Tables 6. 5 and 6. 6).

Beryl crystals of gem-quality collected during the present field work are analyzed by the Scanning Electron Microscope, X-Ray Diffractometer, and the Electron Probe Microanalyzer. The results of these three techniques are presented in Tables 6. 4, 6. 5 and 6. 6 and Figure 6. 2. The data of these three techniques show that the analyzed crystals are pure beryls. There are only slight differences between the chemical compositions and d-values of the aquamarines and goshenite, otherwise the analyses are stoichiometrically close to the standard beryl analyses (Tables 6. 5 and 6. 6; Fig. 6. 2). In the analyzed beryls, both the $SiO_2$ and $Al_2O_3$ are in range to the standard beryl analyses, while BeO being the lightest element is below the detection limit of Electron Probe Microanalyzer, therefore, the total is less than 100 wt. %. Besides, the water molecule is also not determined, which in certain beryl analyses ranges up to 2 wt. %. Normally beryl and its varieties contain some of the alkalis such as Na, Li, K, Cs and Rb. In case of the studied beryls, only in sample number 16 - D the $Cs_2O$ is present up to 1.5 wt. %, while Na and K are not more than 0.51 wt. %. As discussed in the previous sections that the pegmatites of the Shigar valley are Li-poor, therefore, the lithium contents of certain minerals is also very low. Other trace elements (Sc, Y, Nb, P, W, Zr) may occur in considerable quantities in the structures of beryls and are useful for the characterization of beryl as well as pegmatites but these are not determined in the studied beryls. There is always a close relationship between the type of beryl and their parent pegmatite. Therefore, the beryls and their parent pegmatites can be classified on the basis of alkali variation (Beus, 1966; Hawt.horne and Ćerný, 1977). These are classified as alkali-free beryl, alkali-poor beryl, sodic beryl, sodic-lithian beryl, and lithian-caesian beryl. This classification is dependant on the wt. % of corresponding alkalis. According to this classification, the

beryls of the Shigar valley pegmatites belong either to the alkali- free or sodic-beryl category and such type of beryls are characteristic of graphic pegmatites and pegmatites containing high albite assemblages and poor rare alkalis contents as is noted in these pegmatites (Hawt.horne and Ćerný, 1977).

There is always a close relationship between the chemical composition of a mineral and its physical as well as optical properties. In case of beryl, as the alkali content increases, the refractive indices also increase (Schaller et al., 1962; Watters, 1963; Ćerný and Simpson, 1977). In this connection Pavlova (1963) has related the refractive indices of beryls with their paragenesis. According to him beryls occurring in basic rocks have higher refractive indices relative to those, which occur in acid granitic rocks. Ćerný and Hawthorne (1976) in their studies on beryl have proposed various substitutions either at tetrahedral or octahedral sites by which the refractive indices of beryls may raise. Like other physical properties, the color of gemstones is also dependant on the chemical composition along with the internal structure of atoms. In case of aquamarines, which are mostly pale-blue to sky-blue in color; Wood and Nassau (1968) relate this color of aquamarines with the presence of ferrous iron in the range of 0.1 to 0.3 wt. % at site B. In this regard, the ferrous iron of the analyzed aquamarines from the Shigar valley pegmatites is also in this range with some exceptions.

Although, the beryl mineralization most commonly found near the core-margin zone, also occurs from the wall zone to inward but in this paragenesis, the habit of crystals may change from prismatic to equant to tabular. In such type of paragenesis the sodium, lithium and cesium contents of beryl generally increase from the wall zone to core, while the beryllium decreases (Jahns and Ewing, 1977). The beryl mineralization in granitic pegmatites mostly occurs in the complex or zoned pegmatites but it is not true for all pegmatites. The beryl mineralization may even occur in the simple pegmatites, if the metasomatic replacement has been occurred. The studied beryls are very poor in rare alkalis because their parent pegmatites are poor in Li-contents. The alkali content of beryl from Li pegmatites is higher than those of non-lithium pegmatites (Gallagher, 1975). This is the reason that the beryls of the Shigar valley pegmatites have low concentration of

alkalis because these pegmatites are poor in their Li-contents. However, both the normal as well as the alkali-rich beryls may occur simultaneously in the same pegmatite (Erametsa et al., 1973).

**Schorl-foitite [$NaFe_3^{+2}Al_6(BO_3)_3Si_6O_{18}(OH)_4$]**

The schorl "black tourmaline" is a ubiquitous phase in the gem-bearing pegmatites of the Shigar valley (Fig. 6. 9). Although, it is scattered in the whole groundmass of the pegmatitic dykes and veins but mostly either concentrate at the border zone or in the core-margin zone in the associations of other gemstones. The schorl is not as attractive as the other gem-varieties of tourmalines such as dravites, rubellite, indicolite, achroite and bi and tri-colored tourmalines, but still it is used as a gemstone and is also famous among the mineral collectors. The sizes of the schorls in the pegmatites of the Shigar valley are variable. Although, we could not collect best specimen during the fieldwork but one crystal of the gem-quality was collected from a pegmatite of Kashmol village measuring 3.5 ×1 cm (Plate 6. 6) along with certain other minute crystals from the different localities in the Shigar valley. The base of this crystal is broken and the top is terminated. Numerous striations are present along the long prismatic faces of the crystal. Good specimens of this kind are generally associated with aquamarine, albite, muscovite and quartz.

The main compositional varieties found in tourmaline group of minerals are the magnesian tourmalines or dravites, the iron tourmalines or schorl and the alkali tourmalines or elbaites. In these varieties, the Y-sites are predominantly composed of Mg, $Fe^{2+}$ and Li respectively. Although, various studies have shown that different types of tourmalines may be present even in a single pegmatitic body as is reported by Laurs et al. (1998) from Stak Nala pegmatites and Shearer et al. (1984) from the Black Hills, South Dakota; while on the other hand, some specific types of tourmalines may be present in a specific type of a pegmatite. As, already discussed in chapter 5 that the pegmatites of the Shigar valley are broadly classified into two main categories i.e., gem-bearing and gem-barren pegmatites. The schorl is the ubiquitous constituent of the gem-

bearing class of pegmatites. The tourmalines of the Shigar valley appear to be of two genetic types. Those, formed during the main pegmatitic evolution are the primary, while those formed during the pneumatolytic or hydrothermal action are secondary in origin. Optically it is observed that some of these schorls are zoned tourmalines (Plates 5. 14, 15, 16 and 17) and Quensel (1956) reported that such types of zoned tourmalines belong to the sodium replacement unit within the pegmatite body and are of pneumatogenic stage. Tourmalines in the Shigar valley pegmatites are most commonly associated with beryl, quartz, albite and muscovite and not with biotite because biotite is almost absent in the gem-bearing class of pegmatites.

The tourmaline is analyzed by Scanning Electron Microscope, X-Ray Diffractometer and Electron Probe Microanalyzer and the results are given in Table 6. 4, 6. 5 and 6. 6 and Fig. 6. 3. According to the Electron Probe Microanalyzer data, these tourmalines are the iron-rich variety known as schorl but the XRD data supports another iron rich variety known as foitite (Table 6. 6 and Fig. 6. 3). Although on the basis of major oxides there is no significant difference between these two iron-rich tourmalines but only slight differences of MnO, $Al_2O_3$ exist between these two varieties. The foitites are slightly enriched in these oxides relative to schorls (Mac Donald et al., 1993). The analyzed tourmalines are also rich in their MnO contents, indicating that these tourmalines can be classified as foitites instead of schorl. The $SiO_2$ is ranging from 33.08 to 35.93 wt. %, while the $Al_2O_3$ is ranging from 32.80 to 35.10 wt. %. On the basis of XRD data and patterns, the main three intensive d-values are according to the patterns of either foitite or foitite-schorl (Table 6. 6 and Fig. 7. 3). In case of foitite, the main d-value is 3.45 that is present in all the analyzed tourmalines along with the second highest peak of 2.57, which is almost common in all the varieties of tourmalines. The third intensive peak, a characteristic of foitites is 6.33 and this is also present in the analyzed tourmalines. A fourth intensive peak of 2.96 is present in some of the tourmalines, which shows that the end-member is foitite-schorl. It is important to mention that not only the Shigar valley pegmatites have foitites but the Shengus pegmatites also contain foitites but these are not pure because, XRD patterns also show a highest peak of 2.96 that is the characteristic of dravites, therefore, these tourmalines are foitite-dravites (Table 6. 6).

The analyzed tourmalines are also in agreement with the work of Mac Donald et al., (1993) and Milan and Taylor, (2000).

**Zoisite [$Ca_2$ (Al, Fe)$_3$ (OH) ($SiO_4$)$_3$]**

In case of Shigar valley gemstones, as it is already described in chapter 3 that the gemstones found from this valley are not all of pegmatitic origin but some of them are either the product of metasomatic or thermal and regional metamorphism. The gemstones such as the zoisites, clinozoisites, and axinite are the products of the above-mentioned processes and are being mined from those localities of the Shigar valley, where the pegmatites are not exposed such as the Alchuri and Hashupa areas (Fig. 6. 9). Although, these gemstones are present in the best museums of the world, in the world gem-market and are being related with the pegmatites of this valley but it is not true because no work has been done on the paragenesis of these gemstones before. To know the mineralization and paragenesis of these gemstones, the mines of these areas were visited during the field work and the samples both of the gemstones as well as their host rocks are collected for further analytical work to ascertain their paragenesis.

Zoisite belongs to the epidote group of minerals and like other members of this group does also occur in a variety of parageneses from igneous to metamorphic. Some of its varieties are of gem-quality and are world-famous in the gemstone market, for example tanzanite. Another variety of zoisite, which sometimes used as a gemstone, is the thulite. The sapphire blue color of tanzanite is due to the vanadium content, while the pinkish variety thulite is due to the manganese (Kumskova, and Khostova., 1964).

The x-ray pattern and Electron Probe Microanalyzer analyses were conducted on the zoisite and the results are given in Tables 6. 5 and 6. 6; Fig. 6. 4. A colorless to light-green gem-variety of zoisite is identified from the Shigar valley area. Although, on the basis of physical properties, it was very difficult to identify this mineral, because the crystals collected during field work are very small in size (Plate 6. 7), but on the basis of XRD data and Electron Probe Microanalyzer analyses, it is observed that these are

stoichiometrically zoisites (Tables 6. 5 and 6. 6; Fig. 6. 4). However, this variety of gemstone is known as tanzanite among the local miners. As gem-quality zoisite is not associated with pegmatites but are usually present along the margins of the metamorphosed mafic veins within the greenschist to amphibolite grade facies metamorphosed rocks in the Shigar valley, therefore, this mineralization could be the result of metasomatic or metamorphic reaction in the host rocks.

**Axinite [(Ca, Fe, Mn, Mg)$_3$ $Al_2BO_3Si_4O_{12}$ (OH)]**

Although before 1968, the term axinite was used only for the axinite mineral but after the detailed work of Sanero and Gottardi (1968), Milton et al., (1953), Kurshakova (1976) and Jobbins et al. (1975), the axinite is nowadays used as a group of minerals with the members such as magnesioaxinite, ferroaxinite, manganaxinite, and tinzenite.

The gemstone variety of axinite is collected from Alchuri and Hashupa areas (Fig. 6. 9), where the pegmatites are not exposed and these axinites are mined from the local veins within the greenschist to epidote-amphibolite grade facies rocks. These axinite grains are analyzed for both x-ray patterns and chemical composition by X-Ray Diffractometer and Electron Probe Microanalyzer respectively and the results are given in Tables 6. 5 and 6. 6; Fig. 6. 5.

The EPMA results of the analyzed axinites indicate that these are ferroaxinite because these are rich in iron and poor in manganese and magnesium (Table 6. 5). Moreover, the XRD data and x-ray pattern (Table 6. 6 and Fig. 6. 5) are also very close to the ferroaxinite instead of magnesio or manganoaxinites. The color of these axinites is light-pink to brown (Plate 6. 8) and chemically these resemble the axinites reported from Sri Lanka (Hanni and Gunawardene, 1982). In addition, the studied ferroaxinites are also very close in compositions to the ferroaxintes reported from New Melones Lake, California (Cummings, 1983) and New Jersey (Pohl et al., 1982).

Axinite is most commonly formed either by contact metamorphism and metasomatism (Hanni, and Gunawardene, 1982). Among the boron-bearing calc-silicate minerals, it is the commonest and found in the altered calcareous sediments. The presence of boron in axinites is either related to the acidic magmas or to the primary sedimentary deposits, which generate boron during the metamorphism (Sanero, and Gottardi, 1968). Therefore, the suitable rocks required for the formation of axinite are present in the Shigar valley. In case of calcareous rocks, the huge marble beds up to 15 m are seen and mapped in the Daltumbore and the Bauma Harel Formations, so it is probable that the formation of axinites have been taken place at the margin of these carbonate rocks. The formation of these axinites can be attributed to the contact metamorphism or metasomatism in the area, which has been probably caused by the pegmatites. Due to this intrusion, the carbonate rocks are metasomatized which, resulted in the formation of skarn and the axinite could be related to this skarn.

**Fluorite ($CaF_2$)**

Fluorite is found in various parageneses from vein mineralization to pneumatolytic origin as in granites and pegmatites and also as a metasomatic mineral (Deer et al., 1966). The gem-quality fluorites found from the Shigar valley are of pneumatolytic origin and are present in the cavities with other gemstones in the studied pegmatitic bodies. Fluorite usually occurs in a variety of colors (i.e., colorless, yellow, green, white, blue etc). These colors are generally caused by variety of mechanisms, these are the defect structures, radioactive inclusions, traces of rare earth elements, the presence of inclusions of carbonaceous material and also emanations from nearby radioactive material (Bill et al., 1967). To know the relationship of REE and the color of fluorites, Naldrett et al. (1987) conducted detailed study on various colored fluorites and concluded that the color of fluorite is not due the presence of REE but the REEs may increase the intensity of color. However, according to Feofilov (1956) and Bill et al. (1967), the green color of some fluorites is due to the presence of either Sm or Dy. Bellanca et al. (1981) are of the opinion that the green colored fluorites are rich in Sm and Eu relative to violet, blue, or white varieties. In a comparative study, Stolynova

(1993) concluded that the green fluorite have higher contents of REE, Co, Fe, U, and Hf than violet fluorites. Fluorite in the pegmatites of Shigar valley is pale to dark-green in color and is reported in various localities such as Yuno, Nyit Bruk, Mungo, Kashmol and Baha. The average size of these crystals is 2 x 3 cm and these are usually associated with muscovite, tourmaline, beryl, quartz and topaz in the studied pegmatites (Plate 6. 9). Gem-quality fluorite crystals are analyzed for the x-ray pattern and the chemical composition by the XRD and Electron Probe Microanalyzer respectively. The results are presented in Table 6. 5 and 6. 6 and Figure 6. 6. The data show that like the minute crystals of fluorite observed in the thin sections, the large gem-quality green colored fluorites are also stoichiometrically pure $CaF_2$ (Plates 6. 10 and 11). According to the Electron Probe Microanalyzer data, these are pure fluorites because the total sum is very near to 100 wt. % but on the basis of XRD data some of the fluorites are yttrian (Table 6. 6 and Fig. 6. 6). Although some amounts of Si, Al, and Mg may be present in the fluorites either as impurities or inclusions or may replace some of the Ca as reported by Saito (1950). In the studied fluorites no signs either of inclusion or replacement and substitution are noted and the fluorites are almost pure $CaF_2$ with very small amount of $SiO_2$ (0.30 wt. %). As already mentioned, that the hydrothermal activity is usually associated with the Shigar valley pegmatites. The presence of fluorite is another evidence for this activity because the fluorite is probably formed in the last stages of hydrothermal activity within the pegmatites at the time of saturation of fluids.

**Apatite [$Ca_5 (PO_4)_3 (OH, F, Cl)$]**

Pink and light-pink colored apatites occurring in the Shigar valley pegmatites are of gem-quality apatite (Plate 6. 12). These light pink-colored apatites are generally known as morganite (a variety of beryl) among the local miners and gem-dealers. The gem-quality apatites are analyzed both for x-ray pattern and chemical composition by using XRD and Electron Probe Microanalyzer and the results are given in Tables 6. 5 and 6. 6; Fig. 6. 7. The data clearly show that these are stoichiometrically pure apatites and not the morganite. In addition to the pink-colored apatites, the colorless apatites are also reported from the Shigar valley area but the colorless apatite crystals could not be

obtained during this study. The best specimens containing apatite and other gemstones from the Shigar valley are exported in the world gem-market. For example a best specimen is shown in plate 6. 13, taken from the Alpine Mineral Company website, in which fluorite, garnet and pink apatite are present on pericline. Gem-quality apatites are only present within the gem-bearing class of pegmatites, but small crystals are also observed in the gem-barren class of pegmatites under microscopic study (Table 5. 2). Electron Probe Microanalyzer data show that the total sum of the cations is about 100 % without the chlorine, fluorine, carbonate and hydroxyl ions; suggesting that these ions may be present in traces (Table 6. 5). Some of these apatites are, however, enriched in MnO (up to 7.36 wt. %) and are, therefore, classified as manganapatite (Table 6. 5). The apatites have also been analyzed on Electron Scanning Microscope (SEM) and it is noticed that some of these apatites contain up to 4.90 wt. % fluorine and are, therefore, classified as fluorapatite. However, the apatites collected from the pegmatites of Yuno area show x-ray pattern similar to a variety of apatite known as dahlite (Fig. 6. 7 and Table 6. 6). There could be replacements and substitutions of Sr, Ba, Mn, Na and the REEs in the apatites. But the studied apatites have no such replacement except Mn. Apatites may occur in various associations (Stromer et al., 1993). Similarly in Shigar valley pegmatites, the apatite is generally associated with topaz, beryl, schorl, fluorite and muscovite.

**Clinozoisite [$Ca_2Al_3Si_3O_{12}$ (OH)]**

The gem-quality zoisite, clinozoisite, titanite (sphene) and diopside are being mined from those localities in the Shigar valley, where pegmatites are not exposed (Fig. 6. 9). The most productive and famous localities for these gemstones and fine mineral specimens in the Shigar valley area are the Alchuri and Hashupa areas. The mineralization of epidote-clinozoisite is also variable in these localities. It is either in the form of veins or it occurs at the contact zones of epidote-amphibolites or greenschists (Plate 6. 14). Different varieties of gem-quality epidote are collected from the Alchuri and Hashupa areas. The color as well as the size of these epidotes is variable. The majority of these are dark-brown and opaque but transparent to translucent greenish-

brown to light-brown varieties are also being mined from these areas (Plates 6.15 and 6.16). These varieties of epidote are known as Zabarjad (peridote) by the local miners and gem-dealers. These epidotes are analyzed by the SEM, XRD and EPMA and the results are given in (Tables 6.4, 6. 5 and 6. 6 and Fig. 6. 8). The data suggest that the studied epidotes are stoichiometrically similar to clinozoisites (Tables 6. 5, 6. 6 and Fig. 6. 8). The x-ray patterns (Table 6. 6) have also confirmed that these epidotes are clinozoisites. The clinozoisite contain $SiO_2$ in the range of 37.75 to 40.78 wt. %, $Al_2O_3$ from 25.89 to 28.92 wt. %, FeO from 5.07 to 8.73 wt. %, and CaO from 20.58 to 24.68 wt. %, while rest of the oxides are present in negligible amount. The total sum is less than 100% because the $H_2O^+$ molecule is not analyzed, which is generally 3 wt. % in the clinozoisites. Some replacements and substitutions such as of Mn and Mg may also occur in clinozoisite but in the studied clinozoisites these components are very low and no signs of these kinds of substitutions are noted.

### Economics of the Gemstones of the Shigar Valley area

Gemstones, being the beauty of museums, are mostly used in jewellery and are commonly considered as the symbols of beauty and power. Some areas of the world are famous among the people of various schools of thought merely due to the occurrence of certain gemstones. In this context, before 1970 Pakistan was not present on the world gemstone map but after the discoveries of certain world-famous gemstones from different regions of Pakistan, especially the northern areas, now it has a prominent position in the world gemstone map. Not only this, but the Pakistani gemstones have also a great market value in the international gem-trade.

Though, Pakistan government has not given a proper attention to this sector but in 1979, it established the Gemstone Corporation of Pakistan to explore and boost up this industry. The main objective of this corporation was to effectively explore Pakistan's own share of wealth in minerals and to facilitate gemstone mining and business in Pakistan. It had worked a lot and had some valuable influence but ultimately was liquidated in 1997 and hence abandoned. Not only the Gemstone Corporation of Pakistan

but various other geological organizations have also worked a lot to explore this wealth. Due to these efforts, now various gemstones and their varieties have been explored from different localities of the northern areas of Pakistan.

Some of the rock suits have a specific type of gemstone but the granitic pegmatite is such type of rocks, which holds a variety of gemstones such as aquamarine, goshenite, morganite to topaz, fluorite, different varieties of tourmaline and quartz etc. In this regard, the granitic pegmatites of northern areas of Pakistan in general and of the Shigar valley in particular are world-famous among the mineral and gem collectors. The Shigar valley area of Baltistan is not only famous for its gemstones of pegmatitic origin but gemstones and mineral specimens such as the epidote, zoisite, clinozoisite, axinite, sphene are also found and restricted to this valley. The Shigar valley pegmatites also hold a variety of gemstones such as the dark-blue to pale-blue aquamarine, colorless goshenite, colorless to yellow topaz, pink-apatite, light-green to pink-green apatites and colorless to rose quartz (Fig. 6. 9). Though a variety of pegmatites is exposed at various localities of the Shigar valley but the gemstones are generally confined to the zoned pegmatites and are present in cavities or vugs either at the core-margin zone or in the intermediate zone.

The Shigar valley pegmatites have great potential for the occurrence of various gemstones and mineral specimens and these gemstones have every type of quality that a gemstone should possess. These are free of flaws and are very attractive both in size and color as well as in different associations. The pink apatite of this valley is so attractive in color that sometimes even the gem-collectors become confused that either it is apatite or morganite. The local miners also call this pink-colored apatite as a morganite. The light-blue colored aquamarines are also very attractive when they are in association with their host minerals. In addition to this, the light-green colored fluorites are also pure and free of flaws; therefore, these may be cut and polished as gemstones. The colorless quartz crystals of the central core zone are so big in size and clarity that nowadays these are the beauty of various museums of national and international repute.

It was observed during the field work that obsolete mining methods such as the blasting have been carried out by the local people. It also came in observation that local people have occupied certain mines, which are near to their villages and never allow anyone to go there and do the mining. It was also observed that the gem-dealers come here and purchase these gemstones at very lowest prices from the local miners and sell these at very high prices in the international gem-market. The socio-economic conditions of the people of this valley are very miserable.

In the following section certain suggestions / recommendations are made in order to improve the exploration, mining, cutting and polishing of gemstones and their business in Pakistan, particularly in the context of northern areas, especially the Shigar valley:

**Exploration and evaluation of gemstones**

Pakistan is endowed with great mineral wealth, especially the gemstones, but its proper exploration and evaluation is still lacking. The mineral sector organizations are not playing their role in exploring this hidden wealth. So far limited exploration work has been done on local scale but no detail large scale exploration has ever been conducted. There is a great need to explore many areas in the northern Pakistan, including Shigar valley, where there is a great potential for the occurrence of various types of gemstones. The proper identification and evaluation of the gemstones at the mining sites are very important. For this purpose the government should provided expertise to the local people so that they cannot be deceived by the gem traders. In this way the trust should be established between the local gem dealers and international gem trades so that this business can flourish without any mistrust. This will certainly help in the socio-economic uplift of the country in general and the northern areas in particular.

**Mining of gemstones**

It has been noticed in every gemstone province of Pakistan and especially in the Shigar valley that the mining is rudimentary and unscientific. Unscientific blasting and

mining techniques destroy the precious gemstone and mineral specimens and hence make them valueless in the gems market. The mining activity in Pakistan is facing great problems; therefore, special measures are needed to be taken to improve the quality of mining.

The gemstones mining involves substantial funds in order to successfully operate a project, which should be procured by the governmental and private sector entrepreneurship. The private sector should be encouraged with the backing of the government to take up mining activity. Technical expertise in the form of joint ventures with the private sector should be encouraged. Modernization of mining techniques and infrastructure is needed in order to get the better results. The procedures for the grant of mining leases/licenses should be simplified. The small scale mining should be encouraged by (1) granting mining lease to the local people already engaged in the mining and the illicit mining should be legalized for some time, (2) the local miners should be trained, (3) machineries should be provided to the local miners on reduce prices and (4) illicit gems trafficking should be stopped in the area.

**Lapidary work**

Precision in cutting and polishing of gemstones is very important because it is increasing the value of gem to greater extent. In Pakistan, the gemstone cutting and polishing is done by inexperienced people on obsolete machinery and tools, which is degrading the precious commodity to manifold. This is the reason that most of the gemstones in Pakistan, especially from Shigar valley, are exported as rough stones without value addition because our cutting and polishing are not up to the international standards and, therefore, are not accepted in the export market. This sector of the industry needs particular attention in order to get maximum benefits from our rough stones. In this regard the following measures should be taken: (1) Government of Pakistan should import the sophisticated cutting and polishing machineries and provide the same to the local industry on subsidized rates or loan basis, (2) The local craftsmen should be trained on these machines, (3) gem cutting and polishing training centers should be established in

the gemstone provinces, especially in northern areas, to train the local people involved in gem industry and (4) computer designing and modeling of the gems and jewelry should be encouraged for value-addition of the gems and jewelry.

In order to further strengthen the gemstone business in Pakistan, certain specific recommendations are given below:

- Gems trade should be given amnesty from taxes for a period of certain time in order to bring it from clandestine trade to mainstream trade.

- Gem industrial states should be established to provide space for establishment of lapidaries in the country. Soft term loans may be provided for these cutting and polishing units.

- Import of rough gem stones may be allowed without any duty.

- Financial support for gems' export should be provided on mark up against confirmed export orders in order to encourage exporters.

- Modern training institutes may be set up in major cities by the government-private partnership, where training facilities should be provided for identification and evaluation of gems and in related lapidary work.

- In academia and R and D institutions, a major part of the research may be devoted to gemological studies where the gem traders should have an easy excess.

- Geological research with regards to exploration, mining, economic viability and uses in today's business may be made available on common website jointly and / or independently developed by various geological organizations, agencies, academic and R and D institutions to provide day to day and long term awareness to the business, research and other related communities.

**ALBITE**

| Sample # | KSH-63 | | KSH-67 | | KSH - 68 | | KSH-74 | |
|---|---|---|---|---|---|---|---|---|
| Grain # | 1 | 1 | 1 | 2 | 1 | 2 | 1 | 2 |
| Analysis # | 1 | 1 | 1 | 1 | 1 | 1 | 1 | 1 |
| $SiO_2$ | 66.74 | 66.67 | 66.30 | 66.48 | 68.69 | 69.48 | 68.70 | 68.03 |
| $TiO_2$ | 0.00 | 0.00 | 0.00 | 0.00 | 0.00 | 0.00 | 0.00 | 0.00 |
| $Al_2O_3$ | 21.34 | 20.95 | 21.10 | 21.42 | 19.44 | 19.38 | 19.47 | 24.65 |
| $Cr_2O_3$ | 0.00 | 0.00 | 0.00 | 0.00 | 0.00 | 0.00 | 0.01 | 0.00 |
| FeO | 0.00 | 0.00 | 0.01 | 0.01 | 0.04 | 0.01 | 0.01 | 0.85 |
| MnO | 0.00 | 0.00 | 0.00 | 0.02 | 0.00 | 0.00 | 0.00 | 0.01 |
| MgO | 0.01 | 0.00 | 0.00 | 0.01 | 0.01 | 0.00 | 0.00 | 0.09 |
| CaO | 2.37 | 2.09 | 2.01 | 2.39 | 0.17 | 0.08 | 0.29 | 0.34 |
| $Na_2O$ | 10.39 | 11.01 | 11.15 | 10.98 | 12.24 | 12.08 | 12.12 | 8.30 |
| $K_2O$ | 0.25 | 0.09 | 0.21 | 0.20 | 0.13 | 0.15 | 0.21 | 0.39 |
| NiO | 0.00 | 0.01 | 0.00 | 0.00 | 0.00 | 0.01 | 0.03 | 0.00 |
| **Total** | **101.10** | **100.82** | **100.78** | **101.51** | 100.72 | **101.19** | **100.84** | **102.66** |

Structural formulas calculated on the basis of 32 oxygen.

| | | | | | | | | |
|---|---|---|---|---|---|---|---|---|
| Si | 11.61 | 11.64 | 11.59 | 11.55 | 11.95 | 12.01 | 11.94 | 11.53 |
| Ti | 0.00 | 0.00 | 0.00 | 0.00 | 0.00 | 0.00 | 0.00 | 0.00 |
| Al | 4.37 | 4.31 | 4.35 | 4.39 | 3.99 | 3.95 | 3.99 | 4.93 |
| Cr | 0.00 | 0.00 | 0.00 | 0.00 | 0.00 | 0.00 | 0.00 | 0.00 |
| $Fe_2$ | 0.00 | 0.00 | 0.00 | 0.00 | 0.01 | 0.00 | 0.00 | 0.12 |
| Mn | 0.00 | 0.00 | 0.00 | 0.00 | 0.00 | 0.00 | 0.00 | 0.00 |
| Mg | 0.00 | 0.00 | 0.00 | 0.00 | 0.00 | 0.00 | 0.00 | 0.02 |
| Ca | 0.44 | 0.39 | 0.38 | 0.45 | 0.03 | 0.02 | 0.05 | 0.06 |
| Na | 3.50 | 3.73 | 3.78 | 3.70 | 4.13 | 4.05 | 4.09 | 2.73 |
| K | 0.06 | 0.02 | 0.05 | 0.05 | 0.03 | 0.03 | 0.05 | 0.08 |
| Ni | 0.00 | 0.00 | 0.00 | 0.00 | 0.00 | 0.00 | 0.00 | 0.00 |

(Table 6. 1 continued)

**ORTHOCLASE**

| Sample # | KSH - 68 | | | | | NYT-32 | KSH-74 | | | | |
|---|---|---|---|---|---|---|---|---|---|---|---|
| Grain # | 1 | 2 | 2 | 3 | 4 | 1 | 1 | 1 | 2 | 2 | 3 |
| Analysis # | 1 | 1 | 2 | 1 | 1 | 1 | 1 | 2 | 1 | 2 | 1 |
| $SiO_2$ | 64.28 | 64.38 | 64.45 | 64.88 | 64.84 | 64.60 | 64.82 | 65.16 | 64.89 | 64.42 | 64.05 |
| $TiO_2$ | 0.00 | 0.00 | 0.00 | 0.00 | 0.00 | 0.00 | 0.00 | 0.01 | 0.00 | 0.00 | 0.00 |
| $Al_2O_3$ | 18.44 | 18.34 | 18.13 | 18.23 | 18.27 | 18.16 | 18.17 | 18.28 | 18.20 | 18.42 | 18.14 |
| $Cr_2O_3$ | 0.03 | 0.00 | 0.00 | 0.04 | 0.03 | 0.04 | 0.04 | 0.00 | 0.00 | 0.00 | 0.02 |
| FeO | 0.03 | 0.00 | 0.00 | 0.00 | 0.01 | 0.04 | 0.03 | 0.14 | 0.00 | 0.01 | 0.02 |
| MnO | 0.02 | 0.00 | 0.01 | 0.01 | 0.00 | 0.00 | 0.00 | 0.02 | 0.00 | 0.02 | 0.01 |
| MgO | 0.00 | 0.00 | 0.00 | 0.00 | 0.00 | 0.00 | 0.00 | 0.00 | 0.00 | 0.00 | 0.00 |
| CaO | 0.01 | 0.01 | 0.00 | 0.00 | 0.00 | 0.00 | 0.00 | 0.00 | 0.00 | 0.02 | 0.00 |
| $Na_2O$ | 0.76 | 1.76 | 1.00 | 0.68 | 0.95 | 1.03 | 0.95 | 0.89 | 0.62 | 1.09 | 0.44 |
| $K_2O$ | 15.69 | 14.75 | 15.92 | 16.25 | 15.99 | 15.67 | 15.80 | 16.02 | 16.17 | 15.70 | 16.34 |
| NiO | 0.00 | 0.03 | 0.00 | 0.00 | 0.00 | 0.00 | 0.01 | 0.00 | 0.04 | 0.00 | 0.03 |
| **Total** | **99.26** | **99.27** | **99.51** | **100.09** | **100.09** | **99.54** | **99.82** | **100.52** | **99.92** | **99.68** | **99.05** |

Structural formulas calculated on the basis of 32 oxygen.

| | | | | | | | | | | | |
|---|---|---|---|---|---|---|---|---|---|---|---|
| Si | 11.96 | 11.95 | 11.98 | 12.00 | 11.98 | 11.99 | 12.00 | 11.99 | 12.01 | 11.95 | 11.98 |
| Ti | 0.00 | 0.00 | 0.00 | 0.00 | 0.00 | 0.00 | 0.00 | 0.00 | 0.00 | 0.00 | 0.00 |
| Al | 4.04 | 4.01 | 3.97 | 3.97 | 3.98 | 3.97 | 3.96 | 3.97 | 3.97 | 4.03 | 4.00 |
| Cr | 0.00 | 0.00 | 0.00 | 0.01 | 0.00 | 0.01 | 0.01 | 0.00 | 0.00 | 0.00 | 0.00 |
| $Fe_2$ | 0.00 | 0.00 | 0.00 | 0.00 | 0.00 | 0.01 | 0.01 | 0.02 | 0.00 | 0.00 | 0.00 |
| Mn | 0.00 | 0.00 | 0.00 | 0.00 | 0.00 | 0.00 | 0.00 | 0.00 | 0.00 | 0.00 | 0.00 |
| Mg | 0.00 | 0.00 | 0.00 | 0.00 | 0.00 | 0.00 | 0.00 | 0.00 | 0.00 | 0.00 | 0.00 |
| Ca | 0.00 | 0.00 | 0.00 | 0.00 | 0.00 | 0.00 | 0.00 | 0.00 | 0.00 | 0.00 | 0.00 |
| Na | 0.28 | 0.63 | 0.36 | 0.24 | 0.34 | 0.37 | 0.34 | 0.32 | 0.22 | 0.39 | 0.16 |
| K | 3.72 | 3.50 | 3.78 | 3.83 | 3.77 | 3.71 | 3.73 | 3.76 | 3.82 | 3.72 | 3.90 |
| Ni | 0.00 | 0.00 | 0.00 | 0.00 | 0.00 | 0.00 | 0.00 | 0.00 | 0.01 | 0.00 | 0.01 |

**MUSCOVITE**

| Sample | NYT-32 | | | | | | | | KSH-74 | | | | | | | |
|---|---|---|---|---|---|---|---|---|---|---|---|---|---|---|---|---|
| Grain | 1 | 2 | 3 | 3 | 3 | 3 | 3 | 4 | 1 | 2 | 3 | 4 | 5 | 5 | 6 | 6 |
| Analysis | 1 | 1 | 1 | 2 | 3 | 4 | 5 | 1 | 1 | 1 | 1 | 1 | 1 | 2 | 1 | 2 |
| $SiO_2$ | 45.97 | 46.11 | 45.67 | 45.54 | 45.68 | 45.48 | 45.91 | 47.53 | 45.94 | 46.99 | 46.33 | 47.23 | 46.09 | 46.36 | 47.08 | 47.20 |
| $TiO_2$ | 0.14 | 0.11 | 0.15 | 0.10 | 0.13 | 0.17 | 0.13 | 0.33 | 0.05 | 0.02 | 0.13 | 0.00 | 0.01 | 0.00 | 0.03 | 0.18 |
| $Al_2O_3$ | 34.01 | 34.07 | 34.16 | 34.11 | 34.02 | 34.13 | 34.05 | 27.69 | 35.97 | 31.92 | 34.63 | 32.74 | 35.79 | 34.45 | 34.31 | 34.46 |
| $Cr_2O_3$ | 0.01 | 0.00 | 0.00 | 0.00 | 0.03 | 0.00 | 0.00 | 0.02 | 0.01 | 0.00 | 0.00 | 0.00 | 0.00 | 0.02 | 0.00 | 0.01 |
| FeO | 2.80 | 2.84 | 2.85 | 2.80 | 2.83 | 2.73 | 2.98 | 7.60 | 1.42 | 5.00 | 1.88 | 3.72 | 1.48 | 1.65 | 1.78 | 1.95 |
| MnO | 0.08 | 0.04 | 0.01 | 0.03 | 0.07 | 0.02 | 0.02 | 0.05 | 0.00 | 0.08 | 0.05 | 0.07 | 0.01 | 0.02 | 0.00 | 0.04 |
| MgO | 0.19 | 0.19 | 0.19 | 0.20 | 0.17 | 0.16 | 0.18 | 0.70 | 0.12 | 0.00 | 0.22 | 0.00 | 0.12 | 0.17 | 0.29 | 0.29 |
| CaO | 0.00 | 0.01 | 0.01 | 0.00 | 0.00 | 0.00 | 0.01 | 0.01 | 0.02 | 0.00 | 0.00 | 0.00 | 0.00 | 0.00 | 0.00 | 0.00 |
| $Na_2O$ | 0.71 | 0.69 | 0.79 | 0.80 | 0.69 | 0.70 | 0.67 | 0.06 | 0.68 | 0.13 | 0.49 | 0.07 | 0.66 | 0.40 | 0.69 | 0.64 |
| $K_2O$ | 10.65 | 10.20 | 10.28 | 10.30 | 10.38 | 10.52 | 10.55 | 10.87 | 9.95 | 10.85 | 10.67 | 11.09 | 10.04 | 10.23 | 10.64 | 10.56 |
| NiO | 0.00 | 0.00 | 0.00 | 0.00 | 0.01 | 0.04 | 0.04 | 0.03 | 0.00 | 0.03 | 0.00 | 0.01 | 0.00 | 0.00 | 0.06 | 0.00 |
| **Total** | **94.56** | **94.26** | **94.11** | **93.88** | **93.99** | **94.01** | **94.54** | **94.89** | **94.16** | **95.02** | **94.40** | **94.93** | **94.20** | **93.30** | **94.88** | **95.33** |

Structural formulas calculated on the basis of 22 oxygen.

| | | | | | | | | | | | | | | | | |
|---|---|---|---|---|---|---|---|---|---|---|---|---|---|---|---|---|
| Si | 6.23 | 6.24 | 6.20 | 6.20 | 6.21 | 6.19 | 6.22 | 6.58 | 6.17 | 6.39 | 6.24 | 6.39 | 6.19 | 6.29 | 6.30 | 6.29 |
| Ti | 0.01 | 0.01 | 0.02 | 0.01 | 0.01 | 0.02 | 0.01 | 0.03 | 0.00 | 0.00 | 0.01 | 0.00 | 0.00 | 0.00 | 0.00 | 0.02 |
| Al | 5.43 | 5.44 | 5.47 | 5.48 | 5.46 | 5.48 | 5.44 | 4.52 | 5.69 | 5.12 | 5.50 | 5.22 | 5.66 | 5.51 | 5.42 | 5.41 |
| Cr | 0.00 | 0.00 | 0.00 | 0.00 | 0.00 | 0.00 | 0.00 | 0.00 | 0.00 | 0.00 | 0.00 | 0.00 | 0.00 | 0.00 | 0.00 | 0.00 |
| $Fe_2$ | 0.32 | 0.32 | 0.32 | 0.32 | 0.32 | 0.31 | 0.34 | 0.88 | 0.16 | 0.57 | 0.21 | 0.42 | 0.17 | 0.19 | 0.20 | 0.22 |
| Mn | 0.01 | 0.00 | 0.00 | 0.00 | 0.01 | 0.00 | 0.00 | 0.01 | 0.00 | 0.01 | 0.01 | 0.01 | 0.00 | 0.00 | 0.00 | 0.00 |
| Mg | 0.04 | 0.04 | 0.04 | 0.04 | 0.03 | 0.03 | 0.04 | 0.14 | 0.02 | 0.00 | 0.04 | 0.00 | 0.02 | 0.03 | 0.06 | 0.06 |
| Ca | 0.00 | 0.00 | 0.00 | 0.00 | 0.00 | 0.00 | 0.00 | 0.00 | 0.00 | 0.00 | 0.00 | 0.00 | 0.00 | 0.00 | 0.00 | 0.00 |
| Na | 0.19 | 0.18 | 0.21 | 0.21 | 0.18 | 0.19 | 0.18 | 0.02 | 0.18 | 0.03 | 0.13 | 0.02 | 0.17 | 0.11 | 0.18 | 0.17 |
| K | 1.84 | 1.76 | 1.78 | 1.79 | 1.80 | 1.83 | 1.82 | 1.92 | 1.70 | 1.88 | 1.83 | 1.91 | 1.72 | 1.77 | 1.82 | 1.80 |
| Ni | 0.00 | 0.00 | 0.00 | 0.00 | 0.00 | 0.00 | 0.00 | 0.00 | 0.00 | 0.00 | 0.00 | 0.00 | 0.00 | 0.00 | 0.01 | 0.00 |

**(Table 6. 1 continued)**

**MUSCOVITE**

| Sample | KSH-67 | | | | | | | | | KSH-63 | | | | | | | |
|---|---|---|---|---|---|---|---|---|---|---|---|---|---|---|---|---|---|
| Grain | 1 | 2 | 3 | 3 | 4 | 5 | 6 | 7 | 8 | 1 | 2 | 2 | 3 | 4 | 5 | 6 | 7 |
| Analysis | 1 | 1 | 1 | 2 | 1 | 1 | 1 | 1 | 1 | 1 | 1 | 2 | 1 | 1 | 1 | 1 | 1 |
| $SiO_2$ | 46.74 | 47.33 | 46.65 | 46.26 | 47.60 | 46.71 | 47.08 | 46.62 | 46.86 | 46.06 | 45.98 | 45.29 | 45.55 | 45.85 | 45.49 | 46.21 | 46.45 |
| $TiO_2$ | 0.26 | 0.17 | 0.20 | 0.18 | 0.23 | 0.17 | 0.19 | 0.11 | 0.18 | 0.12 | 0.08 | 0.00 | 0.05 | 0.07 | 0.08 | 0.12 | 0.14 |
| $Al_2O_3$ | 31.93 | 31.62 | 31.45 | 30.66 | 29.50 | 31.42 | 31.81 | 31.42 | 32.09 | 32.39 | 32.79 | 33.39 | 32.52 | 31.86 | 32.06 | 32.16 | 32.17 |
| $Cr_2O_3$ | 0.02 | 0.00 | 0.00 | 0.00 | 0.03 | 0.02 | 0.00 | 0.00 | 0.00 | 0.00 | 0.00 | 0.00 | 0.01 | 0.00 | 0.06 | 0.00 | 0.00 |
| FeO | 4.62 | 4.76 | 4.79 | 4.84 | 5.44 | 4.71 | 4.44 | 4.53 | 3.82 | 4.67 | 3.78 | 3.76 | 4.70 | 5.03 | 4.73 | 4.59 | 4.99 |
| MnO | 0.19 | 0.18 | 0.20 | 0.16 | 0.20 | 0.19 | 0.18 | 0.17 | 0.15 | 0.17 | 0.10 | 0.12 | 0.12 | 0.14 | 0.16 | 0.11 | 0.14 |
| MgO | 0.38 | 0.38 | 0.39 | 0.41 | 0.50 | 0.34 | 0.32 | 0.32 | 0.26 | 0.09 | 0.03 | 0.03 | 0.09 | 0.08 | 0.08 | 0.15 | 0.12 |
| CaO | 0.00 | 0.00 | 0.00 | 0.02 | 0.03 | 0.01 | 0.00 | 0.01 | 0.00 | 0.02 | 0.00 | 0.00 | 0.01 | 0.00 | 0.00 | 0.00 | 0.01 |
| $Na_2O$ | 0.56 | 0.52 | 0.48 | 0.46 | 0.49 | 0.52 | 0.47 | 0.49 | 0.40 | 0.59 | 0.44 | 0.68 | 0.51 | 0.47 | 0.51 | 0.61 | 0.47 |
| $K_2O$ | 10.51 | 10.68 | 10.74 | 10.71 | 10.68 | 10.79 | 10.55 | 10.86 | 11.02 | 10.36 | 10.71 | 10.35 | 10.54 | 10.50 | 10.56 | 10.45 | 10.50 |
| NiO | 0.00 | 0.03 | 0.01 | 0.02 | 0.00 | 0.01 | 0.00 | 0.00 | 0.01 | 0.00 | 0.01 | 0.03 | 0.02 | 0.00 | 0.00 | 0.03 | 0.00 |
| **Total** | **95.21** | **95.67** | **94.91** | **93.72** | **94.70** | **94.89** | **95.04** | **94.53** | **94.79** | **94.47** | **93.92** | **93.65** | **94.12** | **94.00** | **93.73** | **94.43** | **94.99** |

Structural formulas calculated on the basis of 22 oxygen.

| | | | | | | | | | | | | | | | | | |
|---|---|---|---|---|---|---|---|---|---|---|---|---|---|---|---|---|---|
| Si | 6.34 | 6.39 | 6.36 | 6.40 | 6.52 | 6.37 | 6.39 | 6.38 | 6.37 | 6.30 | 6.30 | 6.22 | 6.26 | 6.31 | 6.28 | 6.32 | 6.32 |
| Ti | 0.03 | 0.02 | 0.02 | 0.02 | 0.02 | 0.02 | 0.02 | 0.01 | 0.02 | 0.01 | 0.01 | 0.00 | 0.00 | 0.01 | 0.01 | 0.01 | 0.01 |
| Al | 5.10 | 5.03 | 5.06 | 5.00 | 4.77 | 5.05 | 5.09 | 5.07 | 5.14 | 5.22 | 5.29 | 5.40 | 5.27 | 5.17 | 5.22 | 5.18 | 5.16 |
| Cr | 0.00 | 0.00 | 0.00 | 0.00 | 0.00 | 0.00 | 0.00 | 0.00 | 0.00 | 0.00 | 0.00 | 0.00 | 0.00 | 0.00 | 0.01 | 0.00 | 0.00 |
| $Fe_2$ | 0.52 | 0.54 | 0.55 | 0.56 | 0.62 | 0.54 | 0.50 | 0.52 | 0.43 | 0.53 | 0.43 | 0.43 | 0.54 | 0.58 | 0.55 | 0.52 | 0.57 |
| Mn | 0.02 | 0.02 | 0.02 | 0.02 | 0.02 | 0.02 | 0.02 | 0.02 | 0.02 | 0.02 | 0.01 | 0.01 | 0.01 | 0.02 | 0.02 | 0.01 | 0.02 |
| Mg | 0.08 | 0.08 | 0.08 | 0.08 | 0.10 | 0.07 | 0.07 | 0.06 | 0.05 | 0.02 | 0.01 | 0.01 | 0.02 | 0.02 | 0.02 | 0.03 | 0.02 |
| Ca | 0.00 | 0.00 | 0.00 | 0.00 | 0.00 | 0.00 | 0.00 | 0.00 | 0.00 | 0.00 | 0.00 | 0.00 | 0.00 | 0.00 | 0.00 | 0.00 | 0.00 |
| Na | 0.15 | 0.14 | 0.13 | 0.12 | 0.13 | 0.14 | 0.12 | 0.13 | 0.10 | 0.16 | 0.12 | 0.18 | 0.14 | 0.12 | 0.14 | 0.16 | 0.12 |
| K | 1.82 | 1.84 | 1.87 | 1.89 | 1.87 | 1.88 | 1.83 | 1.90 | 1.91 | 1.81 | 1.87 | 1.81 | 1.85 | 1.85 | 1.86 | 1.82 | 1.82 |
| Ni | 0.00 | 0.00 | 0.00 | 0.00 | 0.00 | 0.00 | 0.00 | 0.00 | 0.00 | 0.00 | 0.00 | 0.00 | 0.00 | 0.00 | 0.00 | 0.00 | 0.00 |

(Table 6.1 continued)

**MUSCOVITE**

| Sample | KSH-67 | | | | | | | | | | KSH-63 | | | | |
|---|---|---|---|---|---|---|---|---|---|---|---|---|---|---|---|
| Grain | 1 | 1 | 2 | 2 | 3 | 4 | 5 | 6 | 7 | 8 | 1 | 2 | 3 | 4 | 4 |
| Analysis | 1 | 2 | 1 | 2 | 1 | 1 | 1 | 1 | 1 | 1 | 1 | 1 | 1 | 1 | 2 |
| $SiO_2$ | 48.01 | 48.16 | 48.20 | 47.85 | 48.37 | 49.13 | 47.50 | 47.26 | 47.53 | 47.86 | 47.84 | 47.67 | 47.33 | 47.94 | 47.63 |
| $TiO_2$ | 0.24 | 0.29 | 0.36 | 0.11 | 0.19 | 0.09 | 0.10 | 0.06 | 0.15 | 0.13 | 0.09 | 0.10 | 0.08 | 0.11 | 0.13 |
| $Al_2O_3$ | 31.74 | 31.29 | 31.61 | 31.88 | 29.45 | 30.58 | 35.05 | 34.20 | 34.94 | 35.10 | 33.38 | 32.77 | 32.62 | 32.21 | 32.08 |
| $Cr_2O_3$ | 0.00 | 0.00 | 0.00 | 0.04 | 0.02 | 0.02 | 0.04 | 0.03 | 0.00 | 0.00 | 0.00 | 0.01 | 0.01 | 0.00 | 0.00 |
| FeO | 4.78 | 4.86 | 4.73 | 4.75 | 7.04 | 5.62 | 2.88 | 3.01 | 1.66 | 1.83 | 4.44 | 4.65 | 5.18 | 4.90 | 4.75 |
| MnO | 0.21 | 0.20 | 0.17 | 0.17 | 0.13 | 0.06 | 0.06 | 0.01 | 0.05 | 0.00 | 0.15 | 0.16 | 0.20 | 0.13 | 0.16 |
| MgO | 0.40 | 0.39 | 0.41 | 0.30 | 0.39 | 0.31 | 0.11 | 0.14 | 0.24 | 0.27 | 0.07 | 0.05 | 0.06 | 0.17 | 0.16 |
| CaO | 0.00 | 0.02 | 0.00 | 0.00 | 0.00 | 0.00 | 0.00 | 0.01 | 0.01 | 0.00 | 0.00 | 0.01 | 0.02 | 0.00 | 0.00 |
| $Na_2O$ | 0.46 | 0.41 | 0.42 | 0.49 | 0.12 | 0.18 | 0.58 | 0.62 | 0.51 | 0.46 | 0.32 | 0.37 | 0.39 | 0.40 | 0.44 |
| $K_2O$ | 10.87 | 10.97 | 10.93 | 10.69 | 11.06 | 11.10 | 10.53 | 10.47 | 10.88 | 10.83 | 10.76 | 10.80 | 10.65 | 10.78 | 10.72 |
| NiO | 0.01 | 0.01 | 0.01 | 0.00 | 0.00 | 0.00 | 0.00 | 0.00 | 0.04 | 0.00 | 0.00 | 0.00 | 0.00 | 0.00 | 0.00 |
| F | 1.89 | 2.03 | 1.85 | 1.63 | 1.50 | 1.26 | 0.84 | 1.01 | 0.41 | 0.43 | 1.30 | 1.64 | 1.39 | 1.59 | 1.47 |
| -O=F | 0.80 | 0.85 | 0.78 | 0.69 | 0.63 | 0.53 | 0.36 | 0.43 | 0.17 | 0.18 | 0.55 | 0.69 | 0.59 | 0.67 | 0.62 |
| Cl | 0.00 | 0.01 | 0.03 | 0.01 | 0.00 | 0.02 | 0.01 | 0.03 | 0.01 | 0.01 | 0.00 | 0.02 | 0.00 | 0.03 | 0.00 |
| -O=Cl | 0.00 | 0.00 | 0.01 | 0.00 | 0.00 | 0.00 | 0.00 | 0.01 | 0.00 | 0.00 | 0.00 | 0.01 | 0.00 | 0.01 | 0.00 |
| $SO_3$ | 0.01 | 0.00 | 0.06 | 0.00 | 0.01 | 0.01 | 0.02 | 0.03 | 0.00 | 0.00 | 0.03 | 0.05 | 0.00 | 0.00 | 0.01 |
| **Total** | 97.83 | 97.77 | 97.99 | 97.24 | 97.64 | 97.83 | 97.36 | 96.45 | 96.24 | 96.72 | 97.83 | 97.60 | 97.34 | 97.57 | 96.92 |

Structural formulas calculated on the basis of 22 oxygens.

| | | | | | | | | | | | | | | | |
|---|---|---|---|---|---|---|---|---|---|---|---|---|---|---|---|
| Si | 6.53 | 6.58 | 6.54 | 6.52 | 6.63 | 6.63 | 6.30 | 6.36 | 6.31 | 6.32 | 6.42 | 6.46 | 6.43 | 6.50 | 6.49 |
| Ti | 0.02 | 0.03 | 0.04 | 0.01 | 0.02 | 0.01 | 0.01 | 0.01 | 0.02 | 0.01 | 0.01 | 0.01 | 0.01 | 0.01 | 0.01 |
| Al | 5.09 | 5.04 | 5.06 | 5.12 | 4.76 | 4.87 | 5.48 | 5.42 | 5.47 | 5.46 | 5.28 | 5.24 | 5.22 | 5.15 | 5.15 |
| Cr | 0.00 | 0.00 | 0.00 | 0.00 | 0.00 | 0.00 | 0.00 | 0.00 | 0.00 | 0.00 | 0.00 | 0.00 | 0.00 | 0.00 | 0.00 |
| $Fe_2$ | 0.54 | 0.56 | 0.54 | 0.54 | 0.81 | 0.63 | 0.32 | 0.34 | 0.18 | 0.20 | 0.50 | 0.53 | 0.59 | 0.56 | 0.54 |
| Mn | 0.02 | 0.02 | 0.02 | 0.02 | 0.02 | 0.01 | 0.01 | 0.00 | 0.01 | 0.00 | 0.02 | 0.02 | 0.02 | 0.01 | 0.02 |
| Mg | 0.08 | 0.08 | 0.08 | 0.06 | 0.08 | 0.06 | 0.02 | 0.03 | 0.05 | 0.05 | 0.01 | 0.01 | 0.01 | 0.04 | 0.03 |
| Ca | 0.00 | 0.00 | 0.00 | 0.00 | 0.00 | 0.00 | 0.00 | 0.00 | 0.00 | 0.00 | 0.00 | 0.00 | 0.00 | 0.00 | 0.00 |
| Na | 0.12 | 0.11 | 0.11 | 0.13 | 0.03 | 0.05 | 0.15 | 0.16 | 0.13 | 0.12 | 0.08 | 0.10 | 0.10 | 0.11 | 0.12 |
| K | 1.89 | 1.91 | 1.89 | 1.86 | 1.93 | 1.91 | 1.78 | 1.80 | 1.84 | 1.82 | 1.84 | 1.87 | 1.84 | 1.86 | 1.86 |
| Ni | 0.00 | 0.00 | 0.00 | 0.00 | 0.00 | 0.00 | 0.00 | 0.00 | 0.00 | 0.00 | 0.00 | 0.00 | 0.00 | 0.00 | 0.00 |
| F | 0.81 | 0.87 | 0.79 | 0.70 | 0.65 | 0.54 | 0.35 | 0.43 | 0.17 | 0.18 | 0.55 | 0.70 | 0.60 | 0.68 | 0.63 |
| Cl | 0.00 | 0.00 | 0.01 | 0.00 | 0.00 | 0.00 | 0.00 | 0.01 | 0.00 | 0.00 | 0.00 | 0.01 | 0.00 | 0.01 | 0.00 |
| S | 0.00 | 0.00 | 0.01 | 0.00 | 0.00 | 0.00 | 0.00 | 0.00 | 0.00 | 0.00 | 0.00 | 0.00 | 0.00 | 0.00 | 0.00 |

(Table 6. 1 continued)

| MUSCOVITE | | | | | | | | | | | BIOTITE | | | | |
|---|---|---|---|---|---|---|---|---|---|---|---|---|---|---|---|
| Sample | KSH-63 | | NYT-32 | | | | | | | | | | | | |
| Grain | 4 | 5 | 1 | 2 | 3 | 4 | 4 | 5 | 5 | 6 | 1 | 1 | 1 | 2 | 2 |
| Analysis | 3 | 1 | 1 | 1 | 1 | 1 | 2 | 1 | 2 | 1 | 1 | 2 | 3 | 1 | 2 |
| $SiO_2$ | 47.65 | 46.42 | 45.97 | 47.23 | 47.87 | 47.33 | 47.84 | 46.08 | 46.43 | 49.09 | 34.67 | 34.28 | 34.50 | 34.47 | 34.30 |
| $TiO_2$ | 0.15 | 0.10 | 0.10 | 0.13 | 0.00 | 0.14 | 0.10 | 0.13 | 0.10 | 0.06 | 1.12 | 1.08 | 1.10 | 1.19 | 1.15 |
| $Al_2O_3$ | 32.21 | 31.50 | 33.82 | 34.30 | 35.10 | 34.66 | 34.47 | 34.02 | 33.50 | 30.96 | 20.90 | 20.60 | 20.63 | 20.60 | 20.59 |
| $Cr_2O_3$ | 0.03 | 0.01 | 0.01 | 0.01 | 0.00 | 0.00 | 0.01 | 0.03 | 0.00 | 0.00 | 0.00 | 0.00 | 0.00 | 0.00 | 0.03 |
| FeO | 4.75 | 4.76 | 2.86 | 2.94 | 1.77 | 2.90 | 2.96 | 3.10 | 2.90 | 4.81 | 28.15 | 28.26 | 28.62 | 28.53 | 28.57 |
| MnO | 0.21 | 0.15 | 0.05 | 0.03 | 0.12 | 0.05 | 0.09 | 0.05 | 0.06 | 0.10 | 0.66 | 0.66 | 0.63 | 0.65 | 0.66 |
| MgO | 0.18 | 0.08 | 0.16 | 0.20 | 0.00 | 0.24 | 0.24 | 0.15 | 0.18 | 0.27 | 0.61 | 0.63 | 0.65 | 0.72 | 0.71 |
| CaO | 0.02 | 0.02 | 0.00 | 0.01 | 0.00 | 0.00 | 0.00 | 0.00 | 0.00 | 0.00 | 0.03 | 0.04 | 0.01 | 0.00 | 0.00 |
| $Na_2O$ | 0.35 | 0.41 | 0.62 | 0.62 | 0.24 | 0.62 | 0.58 | 0.66 | 0.61 | 0.24 | 0.06 | 0.09 | 0.09 | 0.16 | 0.15 |
| $K_2O$ | 10.89 | 10.63 | 10.87 | 10.53 | 11.47 | 10.73 | 10.81 | 10.76 | 10.98 | 11.33 | 9.74 | 9.79 | 9.79 | 9.75 | 9.67 |
| NiO | 0.00 | 0.00 | 0.03 | 0.00 | 0.00 | 0.00 | 0.01 | 0.03 | 0.00 | 0.01 | 0.02 | 0.01 | 0.00 | 0.00 | 0.00 |
| F | 1.49 | 1.22 | 0.91 | 1.01 | 0.52 | 1.16 | 1.09 | 0.97 | 0.69 | 1.08 | 0.68 | 0.67 | 0.75 | 1.40 | 1.31 |
| -O=F | 0.63 | 0.52 | 0.38 | 0.43 | 0.22 | 0.49 | 0.46 | 0.41 | 0.29 | 0.45 | 0.29 | 0.28 | 0.32 | 0.59 | 0.55 |
| Cl | 0.02 | 0.02 | 0.00 | 0.01 | 0.02 | 0.01 | 0.02 | 0.01 | 0.00 | 0.00 | 0.03 | 0.05 | 0.06 | 0.03 | 0.04 |
| -O=Cl | 0.01 | 0.00 | 0.00 | 0.00 | 0.00 | 0.00 | 0.01 | 0.00 | 0.00 | 0.00 | 0.01 | 0.01 | 0.01 | 0.01 | 0.01 |
| $SO_3$ | 0.01 | 0.02 | 0.00 | 0.00 | 0.00 | 0.00 | 0.00 | 0.03 | 0.00 | 0.00 | 0.00 | 0.00 | 0.00 | 0.02 | 0.04 |
| **Total** | **97.60** | **94.80** | **95.02** | **96.59** | **96.89** | **97.34** | **97.75** | **95.60** | **95.16** | **97.50** | **96.36** | **95.88** | **96.49** | **96.94** | **96.65** |

Structural formulas calculated on the basis of 22 oxygens.

| | | | | | | | | | | | | | | | |
|---|---|---|---|---|---|---|---|---|---|---|---|---|---|---|---|
| Si | 6.48 | 6.46 | 6.29 | 6.34 | 6.34 | 6.33 | 6.36 | 6.28 | 6.33 | 6.61 | 5.52 | 5.50 | 5.51 | 5.54 | 5.53 |
| Ti | 0.02 | 0.01 | 0.01 | 0.01 | 0.00 | 0.01 | 0.01 | 0.01 | 0.01 | 0.01 | 0.13 | 0.13 | 0.13 | 0.14 | 0.14 |
| Al | 5.16 | 5.16 | 5.46 | 5.43 | 5.48 | 5.46 | 5.40 | 5.46 | 5.38 | 4.92 | 3.92 | 3.90 | 3.89 | 3.90 | 3.91 |
| Cr | 0.00 | 0.00 | 0.00 | 0.00 | 0.00 | 0.00 | 0.00 | 0.00 | 0.00 | 0.00 | 0.00 | 0.00 | 0.00 | 0.00 | 0.00 |
| $Fe_2$ | 0.54 | 0.55 | 0.33 | 0.33 | 0.20 | 0.32 | 0.33 | 0.35 | 0.33 | 0.54 | 3.75 | 3.80 | 3.83 | 3.84 | 3.85 |
| Mn | 0.02 | 0.02 | 0.01 | 0.00 | 0.01 | 0.01 | 0.01 | 0.01 | 0.01 | 0.01 | 0.09 | 0.09 | 0.09 | 0.09 | 0.09 |
| Mg | 0.04 | 0.02 | 0.03 | 0.04 | 0.00 | 0.05 | 0.05 | 0.03 | 0.04 | 0.05 | 0.14 | 0.15 | 0.15 | 0.17 | 0.17 |
| Ca | 0.00 | 0.00 | 0.00 | 0.00 | 0.00 | 0.00 | 0.00 | 0.00 | 0.00 | 0.00 | 0.00 | 0.01 | 0.00 | 0.00 | 0.00 |
| Na | 0.09 | 0.11 | 0.16 | 0.16 | 0.06 | 0.16 | 0.15 | 0.17 | 0.16 | 0.06 | 0.02 | 0.03 | 0.03 | 0.05 | 0.05 |
| K | 1.89 | 1.89 | 1.90 | 1.80 | 1.94 | 1.83 | 1.83 | 1.87 | 1.91 | 1.95 | 1.98 | 2.01 | 2.00 | 2.00 | 1.99 |
| Ni | 0.00 | 0.00 | 0.00 | 0.00 | 0.00 | 0.00 | 0.00 | 0.00 | 0.00 | 0.00 | 0.00 | 0.00 | 0.00 | 0.00 | 0.00 |
| F | 0.64 | 0.54 | 0.39 | 0.43 | 0.22 | 0.49 | 0.46 | 0.42 | 0.30 | 0.46 | 0.34 | 0.34 | 0.38 | 0.71 | 0.67 |
| Cl | 0.00 | 0.00 | 0.00 | 0.00 | 0.00 | 0.00 | 0.01 | 0.00 | 0.00 | 0.00 | 0.01 | 0.01 | 0.02 | 0.01 | 0.01 |
| S | 0.00 | 0.00 | 0.00 | 0.00 | 0.00 | 0.00 | 0.00 | 0.00 | 0.00 | 0.00 | 0.00 | 0.00 | 0.00 | 0.00 | 0.00 |

(Table 6. 1 continued)

**BIOTITE**

| Sample | NYT-32 | | | | | KSH-63 | | MUN-16 | |
|---|---|---|---|---|---|---|---|---|---|
| Grain | 1 | 2 | 3 | 3 | 4 | 1-core | 1-rim | 1-core | 1-rim |
| Analysis | 1 | 1 | 1 | 2 | 1 | 1 | 1 | 1 | 1 |
| SiO2 | 32.75 | 33.73 | 33.65 | 32.24 | 33.66 | 35.71 | 34.97 | 34.43 | 34.33 |
| TiO2 | 1.21 | 1.17 | 1.25 | 1.21 | 0.99 | 1.07 | 1.02 | 3.91 | 3.87 |
| Al2O3 | 25.15 | 21.09 | 20.71 | 20.77 | 22.00 | 21.39 | 20.90 | 15.23 | 15.00 |
| Cr2O3 | 0.00 | 0.02 | 0.02 | 0.00 | 0.04 | 0.04 | 0.00 | 0.01 | 0.00 |
| FeO | 27.13 | 28.63 | 28.72 | 31.55 | 26.40 | 27.67 | 28.34 | 28.53 | 27.30 |
| MnO | 0.51 | 0.69 | 0.62 | 0.57 | 0.63 | 0.66 | 0.67 | 0.18 | 0.26 |
| MgO | 0.56 | 0.73 | 0.62 | 0.72 | 0.65 | 0.41 | 0.35 | 5.78 | 5.17 |
| CaO | 0.05 | 0.00 | 0.00 | 0.01 | 0.00 | 0.00 | 0.00 | 0.00 | 0.00 |
| Na2O | 0.05 | 0.19 | 0.19 | 0.09 | 0.21 | 0.10 | 0.12 | 0.09 | 0.06 |
| K2O | 8.09 | 9.65 | 9.70 | 7.72 | 10.22 | 10.14 | 10.38 | 10.32 | 10.50 |
| NiO | 0.02 | 0.00 | 0.00 | 0.01 | 0.03 | 0.00 | 0.07 | 0.06 | 0.00 |
| **Total** | **95.52** | **95.90** | **95.48** | **94.89** | **94.83** | **97.19** | **96.82** | **98.54** | **96.49** |

Structural formulas calculated on the basis of 22 oxygens.

| | | | | | | | | | |
|---|---|---|---|---|---|---|---|---|---|
| Si | 5.20 | 5.36 | 5.38 | 5.22 | 5.36 | 5.54 | 5.49 | 5.37 | 5.45 |
| Ti | 0.14 | 0.14 | 0.15 | 0.15 | 0.12 | 0.13 | 0.12 | 0.46 | 0.46 |
| Al | 4.71 | 3.95 | 3.90 | 3.96 | 4.13 | 3.91 | 3.87 | 2.80 | 2.81 |
| Cr | 0.00 | 0.00 | 0.00 | 0.00 | 3.52 | 3.59 | 3.73 | 3.72 | 3.63 |
| $Fe_2$ | 3.61 | 3.80 | 3.84 | 4.27 | 0.09 | 0.09 | 0.09 | 0.02 | 0.03 |
| Mn | 0.07 | 0.09 | 0.08 | 0.08 | 0.15 | 0.10 | 0.08 | 1.34 | 1.22 |
| Mg | 0.13 | 0.17 | 0.15 | 0.17 | 0.00 | 0.00 | 0.00 | 0.00 | 0.00 |
| Ca | 0.01 | 0.00 | 0.00 | 0.00 | 0.06 | 0.03 | 0.04 | 0.03 | 0.02 |
| Na | 0.02 | 0.06 | 0.06 | 0.03 | 2.08 | 2.01 | 2.08 | 2.06 | 2.13 |
| K | 0.83 | 1.95 | 1.98 | 1.59 | 0.01 | 0.01 | 0.00 | 0.00 | 0.00 |
| Ni | 0.00 | 0.00 | 0.00 | 0.00 | 0.00 | 0.00 | 0.01 | 0.01 | 0.00 |

(Table 6. 1 continued)

**SCHORL**

| Sample | KSH-74 | | | | | | | | | | | |
|---|---|---|---|---|---|---|---|---|---|---|---|---|
| Grain | 1 | 1 | 1 | 1 | 2 | 3 | 4 | 4 | 5 | 6 | 6 | 7 |
| Analysis | 1 | 2 | 3 | 4 | 1 | 1 | 1 | 2 | 1 | 1 | 2 | 1 |
| $SiO_2$ | 35.23 | 35.12 | 35.45 | 35.10 | 34.87 | 35.59 | 35.56 | 35.14 | 30.71 | 34.78 | 34.99 | 34.23 |
| $TiO_2$ | 0.07 | 0.25 | 0.05 | 0.06 | 0.08 | 0.40 | 0.71 | 0.69 | 0.52 | 0.31 | 0.28 | 0.30 |
| $Al_2O_3$ | 33.11 | 33.33 | 33.04 | 32.97 | 33.25 | 32.43 | 32.46 | 32.56 | 29.12 | 32.33 | 32.12 | 31.24 |
| $Cr_2O_3$ | 0.00 | 0.04 | 0.04 | 0.02 | 0.01 | 0.00 | 0.00 | 0.00 | 0.03 | 0.01 | 0.00 | 0.00 |
| FeO | 14.78 | 14.04 | 14.85 | 14.37 | 13.84 | 13.65 | 11.55 | 12.20 | 13.13 | 14.26 | 14.03 | 13.99 |
| MnO | 0.26 | 0.15 | 0.25 | 0.23 | 0.23 | 0.20 | 0.09 | 0.14 | 0.22 | 0.31 | 0.23 | 0.13 |
| MgO | 0.81 | 1.31 | 0.83 | 1.28 | 1.13 | 1.89 | 3.22 | 2.74 | 1.49 | 1.58 | 1.55 | 1.75 |
| CaO | 0.05 | 0.08 | 0.06 | 0.07 | 0.08 | 0.17 | 0.21 | 0.20 | 0.23 | 0.28 | 0.31 | 0.19 |
| $Na_2O$ | 2.32 | 2.54 | 2.61 | 2.52 | 2.50 | 2.20 | 2.52 | 2.56 | 1.84 | 2.53 | 2.43 | 2.08 |
| $K_2O$ | 0.05 | 0.08 | 0.05 | 0.06 | 0.05 | 0.05 | 0.06 | 0.03 | 0.04 | 0.09 | 0.07 | 0.03 |
| NiO | 0.00 | 0.02 | 0.00 | 0.00 | 0.00 | 0.00 | 0.01 | 0.00 | 0.00 | 0.00 | 0.00 | 0.03 |
| **Total** | **86.68** | **86.96** | **87.23** | **86.68** | **86.04** | **86.58** | **86.39** | **86.26** | **77.33** | **86.48** | **86.01** | **83.97** |

Structural formulas calculated on the basis of 24.5 oxygen.

| | | | | | | | | | | | | |
|---|---|---|---|---|---|---|---|---|---|---|---|---|
| Si | 5.94 | 5.89 | 5.95 | 5.92 | 5.91 | 5.98 | 5.93 | 5.90 | 5.82 | 5.89 | 5.95 | 5.96 |
| Ti | 0.01 | 0.03 | 0.01 | 0.01 | 0.01 | 0.05 | 0.09 | 0.09 | 0.07 | 0.04 | 0.04 | 0.04 |
| Al | 6.58 | 6.59 | 6.54 | 6.55 | 6.64 | 6.42 | 6.38 | 6.44 | 6.51 | 6.46 | 6.43 | 6.41 |
| Cr | 0.00 | 0.01 | 0.01 | 0.00 | 0.00 | 0.00 | 0.00 | 0.00 | 0.00 | 0.00 | 0.00 | 0.00 |
| $Fe_2$ | 2.09 | 1.97 | 2.09 | 2.03 | 1.96 | 1.92 | 1.61 | 1.71 | 2.08 | 2.02 | 1.99 | 2.04 |
| Mn | 0.04 | 0.02 | 0.04 | 0.03 | 0.03 | 0.03 | 0.01 | 0.02 | 0.04 | 0.04 | 0.03 | 0.02 |
| Mg | 0.20 | 0.33 | 0.21 | 0.32 | 0.28 | 0.47 | 0.80 | 0.69 | 0.42 | 0.40 | 0.39 | 0.45 |
| Ca | 0.01 | 0.01 | 0.01 | 0.01 | 0.01 | 0.03 | 0.04 | 0.04 | 0.05 | 0.05 | 0.06 | 0.04 |
| Na | 0.76 | 0.83 | 0.85 | 0.82 | 0.82 | 0.72 | 0.81 | 0.83 | 0.68 | 0.83 | 0.80 | 0.70 |
| K | 0.01 | 0.02 | 0.01 | 0.01 | 0.01 | 0.01 | 0.01 | 0.01 | 0.01 | 0.02 | 0.02 | 0.01 |
| Ni | 0.00 | 0.00 | 0.00 | 0.00 | 0.00 | 0.00 | 0.00 | 0.00 | 0.00 | 0.00 | 0.00 | 0.00 |

**(Table 6. 1 continued)**

| **SCHORL** | | | | | | **SCHORL-FOITITE** | | | | | **CHLORITE** | | |
|---|---|---|---|---|---|---|---|---|---|---|---|---|---|
| Sample | NYT-32 | | | | | | | | KSH-74 | | NYT-32 | | |
| Grain | 1 | 1 | 2 | 3 | 3 | 1 | 2 | 3 | 1 | 2 | 1 | 1 | 2 |
| Analysis | 1 | 2 | 1 | 1 | 2 | 1 | 1 | 1 | 1 | 1 | 1 | 2 | 1 |
| $SiO_2$ | 34.90 | 34.96 | 34.73 | 34.80 | 34.65 | 34.38 | 34.53 | 34.26 | 34.12 | 34.23 | 23.16 | 23.05 | 22.50 |
| $TiO_2$ | 0.36 | 0.32 | 0.26 | 0.10 | 0.25 | 0.15 | 0.11 | 0.27 | 0.07 | 0.48 | 0.12 | 0.07 | 0.07 |
| $Al_2O_3$ | 32.83 | 33.19 | 32.85 | 33.56 | 33.18 | 34.01 | 33.51 | 33.86 | 33.71 | 33.05 | 20.51 | 20.87 | 21.60 |
| $Cr_2O_3$ | 0.00 | 0.00 | 0.00 | 0.02 | 0.00 | 0 | 0.02 | 0 | 0.02 | 0 | 0.02 | 0.00 | 0.02 |
| FeO | 14.96 | 15.15 | 15.73 | 15.08 | 15.59 | 15.82 | 15.88 | 14.97 | 14.06 | 12.65 | 43.42 | 42.65 | 41.11 |
| MnO | 0.07 | 0.11 | 0.11 | 0.13 | 0.08 | 0.11 | 0.16 | 0.09 | 0.38 | 0.18 | 0.68 | 0.72 | 0.87 |
| MgO | 0.50 | 0.54 | 0.48 | 0.52 | 0.53 | 0.57 | 0.4 | 0.54 | 0.74 | 2.65 | 0.58 | 0.43 | 0.70 |
| CaO | 0.29 | 0.29 | 0.31 | 0.33 | 0.35 | 0.39 | 0.36 | 0.37 | 0.04 | 0.2 | 0.01 | 0.02 | 0.08 |
| $Na_2O$ | 1.99 | 1.98 | 2.02 | 1.93 | 1.94 | 1.75 | 1.82 | 1.77 | 1.83 | 2.33 | 0.04 | 0.02 | 0.05 |
| $K_2O$ | 0.04 | 0.04 | 0.07 | 0.05 | 0.05 | 0.07 | 0.08 | 0.02 | 0.02 | 0.06 | 0.00 | 0.00 | 0.02 |
| NiO | 0.00 | 0.00 | 0.00 | 0.00 | 0.00 | 0.02 | 0.12 | 0.02 | 0 | 0 | 0.00 | 0.00 | 0.00 |
| **Total** | **85.94** | **86.58** | **86.56** | **86.52** | **86.62** | **87.27** | **86.99** | **86.17** | **84.99** | **85.83** | **88.54** | **87.83** | **87.02** |

Structural formulas calculated on the basis of 24.5 and 28 oxygens for schorl and chlorite respectively.

| | | | | | | | | | | | | | |
|---|---|---|---|---|---|---|---|---|---|---|---|---|---|
| Si | 5.94 | 5.91 | 5.90 | 5.89 | 5.88 | 5.79 | 5.84 | 5.82 | 5.85 | 5.79 | 5.38 | 5.38 | 5.27 |
| Ti | 0.05 | 0.04 | 0.03 | 0.01 | 0.03 | 0.02 | 0.02 | 0.03 | 0.01 | 0.06 | 0.02 | 0.01 | 0.01 |
| Al | 6.58 | 6.61 | 6.58 | 6.69 | 6.63 | 6.75 | 6.68 | 6.77 | 6.8 | 6.59 | 5.61 | 5.74 | 5.96 |
| Cr | 0.00 | 0.00 | 0.00 | 0.00 | 0.00 | 0 | 0 | 0 | 0 | 0 | 0.00 | 0.00 | 0.00 |
| $Fe_2$ | 2.13 | 2.14 | 2.23 | 2.13 | 2.21 | 2.23 | 2.25 | 2.13 | 2.01 | 1.79 | 8.43 | 8.32 | 8.05 |
| Mn | 0.01 | 0.02 | 0.02 | 0.02 | 0.01 | 0.02 | 0.02 | 0.01 | 0.06 | 0.03 | 0.13 | 0.14 | 0.17 |
| Mg | 0.13 | 0.14 | 0.12 | 0.13 | 0.13 | 0.14 | 0.1 | 0.14 | 0.19 | 0.67 | 0.20 | 0.15 | 0.25 |
| Ca | 0.05 | 0.05 | 0.06 | 0.06 | 0.06 | 0.07 | 0.07 | 0.07 | 0.01 | 0.04 | 0.00 | 0.00 | 0.02 |
| Na | 0.66 | 0.65 | 0.67 | 0.63 | 0.64 | 0.57 | 0.6 | 0.58 | 0.61 | 0.76 | 0.02 | 0.01 | 0.02 |
| K | 0.01 | 0.01 | 0.02 | 0.01 | 0.01 | 0.02 | 0.02 | 0.01 | 0.01 | 0.01 | 0.00 | 0.00 | 0.01 |
| Ni | 0.00 | 0.00 | 0.00 | 0.00 | 0.00 | 0 | 0.02 | 0 | 0 | 0 | 0.00 | 0.00 | 0.00 |

(Table 6. 1 continued)

**SCHORL**

| Sample | KSH-74 | | | | | KSH-67 | | | | |
|---|---|---|---|---|---|---|---|---|---|---|
| Grain | 1 | 1 | 2 | 2 | 3 | 1 | 1 | 2 | 3 | 4 |
| Analysis | 1 | 2 | 1 | 2 | 1 | 1 | 2 | 1 | 1 | 1 |
| $SiO_2$ | 35.76 | 36.23 | 35.85 | 36.24 | 35.92 | 36.59 | 36.16 | 35.14 | 35.17 | 34.76 |
| $TiO_2$ | 0.06 | 0.06 | 0.35 | 0.69 | 0.29 | 0.14 | 0.08 | 0.25 | 0.26 | 0.25 |
| $Al_2O_3$ | 33.49 | 33.25 | 32.61 | 32.45 | 33.04 | 34.62 | 34.20 | 33.74 | 34.19 | 34.50 |
| $Cr_2O_3$ | 0.00 | 0.01 | 0.00 | 0.04 | 0.00 | 0.00 | 0.02 | 0.02 | 0.00 | 0.00 |
| FeO | 14.15 | 14.01 | 13.06 | 11.22 | 13.18 | 13.80 | 14.23 | 14.56 | 14.97 | 15.33 |
| MnO | 0.28 | 0.34 | 0.21 | 0.10 | 0.17 | 0.07 | 0.10 | 0.11 | 0.10 | 0.08 |
| MgO | 0.94 | 0.92 | 2.04 | 3.33 | 1.85 | 0.32 | 0.28 | 0.41 | 0.41 | 0.47 |
| CaO | 0.09 | 0.10 | 0.10 | 0.24 | 0.08 | 0.16 | 0.15 | 0.32 | 0.46 | 0.36 |
| $Na_2O$ | 2.27 | 2.04 | 2.50 | 2.43 | 2.47 | 1.58 | 1.57 | 1.79 | 1.92 | 1.82 |
| $K_2O$ | 0.04 | 0.04 | 0.09 | 0.05 | 0.10 | 0.06 | 0.07 | 0.06 | 0.07 | 0.08 |
| NiO | 0.00 | 0.01 | 0.00 | 0.00 | 0.04 | 0.03 | 0.00 | 0.00 | 0.00 | 0.00 |
| F | 0.33 | 0.29 | 0.35 | 0.40 | 0.32 | 0.24 | 0.48 | 0.61 | 0.52 | 0.69 |
| -O=F | 0.14 | 0.12 | 0.15 | 0.17 | 0.14 | 0.10 | 0.20 | 0.26 | 0.22 | 0.29 |
| Cl | 0.00 | 0.00 | 0.03 | 0.00 | 0.00 | 0.00 | 0.01 | 0.01 | 0.00 | 0.03 |
| -O=Cl | 0.00 | 0.00 | 0.01 | 0.00 | 0.00 | 0.00 | 0.00 | 0.00 | 0.00 | 0.01 |
| $SO_3$ | 0.00 | 0.00 | 0.00 | 0.01 | 0.00 | 0.00 | 0.00 | 0.01 | 0.00 | 0.03 |
| **Total** | **87.26** | **87.16** | **87.03** | **87.02** | **87.33** | **87.49** | **87.15** | **86.76** | **87.84** | **88.10** |

Structural formulas calculated on the basis of 24.5 oxygens.

| | | | | | | | | | | |
|---|---|---|---|---|---|---|---|---|---|---|
| Si | 6.00 | 6.06 | 6.01 | 6.02 | 6.00 | 6.06 | 6.06 | 5.96 | 5.90 | 5.85 |
| Ti | 0.01 | 0.01 | 0.04 | 0.09 | 0.04 | 0.02 | 0.01 | 0.03 | 0.03 | 0.03 |
| Al | 6.62 | 6.56 | 6.45 | 6.36 | 6.51 | 6.75 | 6.75 | 6.75 | 6.76 | 6.84 |
| Cr | 0.00 | 0.00 | 0.00 | 0.01 | 0.00 | 0.00 | 0.00 | 0.00 | 0.00 | 0.00 |
| $Fe_2$ | 1.98 | 1.96 | 1.83 | 1.56 | 1.84 | 1.91 | 1.99 | 2.07 | 2.10 | 2.16 |
| Mn | 0.04 | 0.05 | 0.03 | 0.01 | 0.02 | 0.01 | 0.01 | 0.02 | 0.01 | 0.01 |
| Mg | 0.24 | 0.23 | 0.51 | 0.82 | 0.46 | 0.08 | 0.07 | 0.10 | 0.10 | 0.12 |
| Ca | 0.02 | 0.02 | 0.02 | 0.04 | 0.01 | 0.03 | 0.03 | 0.06 | 0.08 | 0.06 |
| Na | 0.74 | 0.66 | 0.81 | 0.78 | 0.80 | 0.51 | 0.51 | 0.59 | 0.62 | 0.60 |
| K | 0.01 | 0.01 | 0.02 | 0.01 | 0.02 | 0.01 | 0.01 | 0.01 | 0.01 | 0.02 |
| Ni | 0.00 | 0.00 | 0.00 | 0.00 | 0.01 | 0.00 | 0.00 | 0.00 | 0.00 | 0.00 |
| F | 0.18 | 0.15 | 0.19 | 0.21 | 0.17 | 0.13 | 0.25 | 0.33 | 0.28 | 0.37 |
| Cl | 0.00 | 0.00 | 0.01 | 0.00 | 0.00 | 0.00 | 0.00 | 0.00 | 0.00 | 0.01 |
| S | 0.00 | 0.00 | 0.00 | 0.00 | 0.00 | 0.00 | 0.00 | 0.00 | 0.00 | 0.00 |

(Table 6. 1 continued)

**FLUORITE**

| Sample | KSH-63 | | | | | | | | | | | | | | |
|---|---|---|---|---|---|---|---|---|---|---|---|---|---|---|---|
| Grain | 1 | 2 | 2 | 3 | 4 | 5 | 6 | 6 | 6 | 7 | 8 | 9 | 9 | 10 | 11 |
| Analysis | 1 | 1 | 2 | 1 | 1 | 1 | 1 | 2 | 3 | 1 | 1 | 1 | 2 | 1 | 1 |
| $SiO_2$ | 0.00 | 0.00 | 0.00 | 0.00 | 0.00 | 0.00 | 0.00 | 0.00 | 0.00 | 0.01 | 0.00 | 0.02 | 0.01 | 0.61 | 0.07 |
| $TiO_2$ | 0.00 | 0.00 | 0.00 | 0.01 | 0.00 | 0.01 | 0.00 | 0.00 | 0.02 | 0.00 | 0.00 | 0.00 | 0.00 | 0.00 | 0.00 |
| $Al_2O_3$ | 0.02 | 0.13 | 0.05 | 0.03 | 0.07 | 0.00 | 0.02 | 0.01 | 0.00 | 0.02 | 0.29 | 0.02 | 0.02 | 0.74 | 0.03 |
| $Cr_2O_3$ | 0.00 | 0.00 | 0.00 | 0.00 | 0.00 | 0.00 | 0.03 | 0.00 | 0.00 | 0.00 | 0.03 | 0.02 | 0.01 | 0.00 | 0.05 |
| FeO | 0.03 | 0.09 | 0.10 | 0.01 | 0.04 | 0.04 | 0.02 | 0.01 | 0.03 | 0.10 | 0.09 | 0.07 | 0.11 | 0.13 | 0.00 |
| MnO | 0.06 | 0.01 | 0.02 | 0.00 | 0.00 | 0.00 | 0.04 | 0.00 | 0.00 | 0.04 | 0.01 | 0.00 | 0.01 | 0.00 | 0.00 |
| MgO | 0.02 | 0.01 | 0.00 | 0.00 | 0.01 | 0.02 | 0.00 | 0.00 | 0.00 | 0.00 | 0.00 | 0.00 | 0.00 | 0.02 | 0.00 |
| CaO | 78.61 | 78.90 | 78.85 | 76.88 | 77.10 | 79.51 | 78.32 | 78.53 | 77.43 | 82.90 | 82.47 | 82.85 | 83.24 | 82.99 | 84.37 |
| $Na_2O$ | 0.00 | 0.02 | 0.00 | 0.05 | 0.05 | 0.01 | 0.01 | 0.00 | 0.01 | 0.01 | 0.01 | 0.02 | 0.03 | 0.02 | 0.02 |
| $K_2O$ | 0.08 | 0.07 | 0.13 | 0.02 | 0.02 | 0.03 | 0.00 | 0.00 | 0.00 | 0.12 | 0.10 | 0.09 | 0.10 | 0.32 | 0.01 |
| NiO | 0.00 | 0.02 | 0.00 | 0.00 | 0.00 | 0.00 | 0.00 | 0.00 | 0.01 | 0.03 | 0.00 | 0.00 | 0.00 | 0.03 | 0.03 |
| F | 45.02 | 44.77 | 44.22 | 44.99 | 44.93 | 46.41 | 44.94 | 44.81 | 44.92 | 44.54 | 42.08 | 44.12 | 43.13 | 42.58 | 42.69 |
| -O=F | 18.96 | 18.85 | 18.62 | 18.94 | 18.92 | 19.54 | 18.92 | 18.87 | 18.91 | 18.75 | 17.72 | 18.58 | 18.16 | 17.93 | 17.98 |
| Cl | 0.01 | 0.04 | 0.02 | 0.04 | 0.00 | 0.01 | 0.02 | 0.02 | 0.00 | 0.01 | 0.00 | 0.01 | 0.00 | 0.00 | 0.01 |
| -O=Cl | 0.00 | 0.01 | 0.00 | 0.01 | 0.00 | 0.00 | 0.00 | 0.00 | 0.00 | 0.00 | 0.00 | 0.00 | 0.00 | 0.00 | 0.00 |
| $SO_3$ | 0.00 | 0.00 | 0.02 | 0.00 | 0.02 | 0.01 | 0.03 | 0.01 | 0.00 | 0.00 | 0.01 | 0.02 | 0.01 | 0.02 | 0.02 |
| **Total** | **97.79** | **98.15** | **97.81** | **95.99** | **96.23** | **99.18** | **97.42** | **97.45** | **96.41** | **101.99** | **100.73** | **101.70** | **101.69** | **102.81** | **102.59** |

(Table 6. 1 continued)

**FLUORITE**

| Sample | NYT-32 | | | | | | | | | | KSH-67 | | |
|---|---|---|---|---|---|---|---|---|---|---|---|---|---|
| Grain | 1 | 2 | 3 | 4 | 5 | 6 | 7 | 8 | 9 | 10 | 1 | 2 | 3 |
| Analysis | 1 | 1 | 1 | 1 | 1 | 1 | 1 | 1 | 1 | 1 | 1 | 1 | 1 |
| $SiO_2$ | 0.00 | 0.00 | 0.00 | 0.00 | 4.07 | 0.00 | 0.00 | 4.07 | 0.00 | 0.00 | 0.15 | 0.00 | 0.08 |
| $TiO_2$ | 0.00 | 0.00 | 0.01 | 0.00 | 0.00 | 0.00 | 0.00 | 0.00 | 0.00 | 0.00 | 0.00 | 0.03 | 0.00 |
| $Al_2O_3$ | 0.00 | 0.00 | 0.01 | 0.00 | 1.29 | 0.01 | 0.90 | 1.29 | 0.01 | 0.90 | 0.08 | 0.01 | 0.04 |
| $Cr_2O_3$ | 0.00 | 0.04 | 0.01 | 0.00 | 0.00 | 0.01 | 0.00 | 0.00 | 0.01 | 0.00 | 0.02 | 0.00 | 0.00 |
| FeO | 0.04 | 0.02 | 0.01 | 0.00 | 0.00 | 0.01 | 0.00 | 0.00 | 0.01 | 0.00 | 0.11 | 0.00 | 0.05 |
| MnO | 0.00 | 0.00 | 0.03 | 0.00 | 0.00 | 0.00 | 0.00 | 0.00 | 0.00 | 0.00 | 0.02 | 0.03 | 0.02 |
| MgO | 0.00 | 0.01 | 0.00 | 0.00 | 0.00 | 0.00 | 0.01 | 0.00 | 0.00 | 0.01 | 0.01 | 0.00 | 0.00 |
| CaO | 82.98 | 84.08 | 85.17 | 84.74 | 73.96 | 78.86 | 76.74 | 73.96 | 78.86 | 76.74 | 84.53 | 84.43 | 82.39 |
| $Na_2O$ | 0.00 | 0.02 | 0.01 | 0.03 | 0.89 | 0.00 | 0.03 | 0.89 | 0.00 | 0.03 | 0.02 | 0.03 | 0.00 |
| $K_2O$ | 0.00 | 0.00 | 0.04 | 0.01 | 0.00 | 0.01 | 0.01 | 0.00 | 0.01 | 0.01 | 0.23 | 0.00 | 0.06 |
| NiO | 0.04 | 0.01 | 0.00 | 0.01 | 0.03 | 0.06 | 0.01 | 0.03 | 0.06 | 0.01 | 0.04 | 0.00 | 0.00 |
| F | 43.32 | 42.71 | 44.07 | 43.29 | 42.67 | 44.53 | 42.46 | 42.67 | 44.53 | 42.46 | 39.93 | 44.32 | 43.99 |
| -O=F | 18.24 | 17.98 | 18.56 | 18.23 | 17.97 | 18.75 | 17.88 | 17.97 | 18.75 | 17.88 | 16.81 | 18.66 | 18.52 |
| Cl | 0.00 | 0.01 | 0.00 | 0.00 | 0.01 | 0.02 | 0.02 | 0.01 | 0.02 | 0.02 | 0.02 | 0.00 | 0.00 |
| -O=Cl | 0.00 | 0.00 | 0.00 | 0.00 | 0.00 | 0.01 | 0.01 | 0.00 | 0.01 | 0.01 | 0.00 | 0.00 | 0.00 |
| $SO_3$ | 0.00 | 0.00 | 0.02 | 0.00 | 0.00 | 0.04 | 0.00 | 0.00 | 0.04 | 0.00 | 0.00 | 0.00 | 0.00 |
| **Total** | **101.30** | **102.17** | **103.87** | **103.02** | **98.23** | **97.78** | **95.59** | **98.22** | **97.78** | **95.61** | **101.99** | **103.19** | **101.16** |

**(Table 6. 1 continued)**

| | SPESSARTINE | | | | ALMANDINE | | | GARNET | | | | |
|---|---|---|---|---|---|---|---|---|---|---|---|---|
| Sample # | KSH-63 | | | | SIL-79 | | | MUN-16 | | KSH-63 | | |
| Grain # | 1-core | 1-rim | 2-core | 2-rim | 1-rim | 1-core | 2-rim | 1-core | 1-rim | 1 | 2 | 3 |
| Analysis # | 1 | 1 | 1 | 1 | 1 | 1 | 1 | 1 | 1 | 1 | 1 | 1 |
| SiO2 | 37.08 | 36.38 | 36.58 | 37.47 | 37.66 | 37.58 | 38.25 | 37.64 | 37.37 | 36.68 | 36.96 | 36.64 |
| TiO2 | 0.00 | 0.01 | 0.00 | 0.01 | 0.03 | 0.08 | 0.04 | 0.05 | 0.11 | 0.04 | 0.00 | 0.00 |
| Al2O3 | 21.21 | 21.09 | 21.39 | 21.68 | 22.02 | 22.12 | 22.13 | 21.27 | 21.48 | 21.04 | 21.03 | 20.87 |
| FeO | 25.45 | 29.74 | 29.75 | 27.01 | 35.26 | 34.35 | 36.48 | 26.94 | 26.91 | 25.94 | 29.39 | 25.55 |
| MnO | 16.83 | 13.65 | 13.55 | 15.02 | 0.02 | 0.08 | 0.07 | 1.94 | 1.82 | 16.26 | 13.50 | 17.11 |
| MgO | 0.01 | 0.01 | 0.09 | 0.04 | 3.39 | 1.58 | 3.35 | 1.10 | 1.09 | 0.01 | 0.03 | 0.01 |
| CaO | 0.76 | 0.58 | 0.69 | 0.83 | 3.47 | 6.75 | 3.30 | 11.56 | 11.54 | 0.82 | 0.65 | 0.77 |
| Na2O | 0.01 | 0.00 | 0.02 | 0.00 | 0.04 | 0.02 | 0.02 | 0.02 | 0.02 | 0.02 | 0.00 | 0.00 |
| K2O | 0.00 | 0.01 | 0.01 | 0.01 | 0.02 | 0.00 | 0.02 | 0.00 | 0.00 | 0.00 | 0.00 | 0.00 |
| Cr2O3 | 0.01 | 0.04 | 0.00 | 0.00 | 0.00 | 0.02 | 0.08 | 0.05 | 0.04 | 0.01 | 0.00 | 0.00 |
| NiO | 0.00 | 0.00 | 0.00 | 0.00 | 0.00 | 0.00 | 0.00 | 0.00 | 0.00 | 0.01 | 0.00 | 0.00 |
| **Total** | **101.36** | **101.51** | **102.08** | **102.07** | **101.91** | **102.58** | **103.74** | **100.57** | **100.38** | **100.83** | **101.56** | **100.95** |
| Structural formulas are calculated on the basis of 24 oxygens. | | | | | | | | | | | | |
| Si | 6.03 | 5.92 | 5.91 | 6.04 | 5.91 | 5.89 | 5.91 | 5.96 | 5.93 | 5.99 | 6.00 | 5.99 |
| Al | 4.06 | 4.04 | 4.07 | 4.12 | 4.07 | 4.08 | 4.03 | 3.97 | 4.01 | 0.00 | 0.00 | 0.00 |
| Ti | 0.00 | 0.00 | 0.00 | 0.00 | 0.00 | 0.01 | 0.00 | 0.01 | 0.01 | 4.05 | 4.02 | 4.02 |
| Fe2 | 3.46 | 4.05 | 4.02 | 3.64 | 4.63 | 4.50 | 4.71 | 3.57 | 3.57 | 3.54 | 3.99 | 3.49 |
| Mn | 2.32 | 1.88 | 1.85 | 2.05 | 0.00 | 0.01 | 0.01 | 0.26 | 0.25 | 2.25 | 1.86 | 2.37 |
| Mg | 0.00 | 0.00 | 0.02 | 0.01 | 0.79 | 0.37 | 0.77 | 0.26 | 0.26 | 0.00 | 0.01 | 0.00 |
| Ca | 0.13 | 0.10 | 0.12 | 0.14 | 0.58 | 1.13 | 0.55 | 1.96 | 1.96 | 0.14 | 0.11 | 0.14 |
| Na | 0.00 | 0.00 | 0.01 | 0.00 | 0.01 | 0.01 | 0.01 | 0.01 | 0.01 | 0.01 | 0.00 | 0.00 |
| K | 0.00 | 0.00 | 0.00 | 0.00 | 0.00 | 0.00 | 0.00 | 0.00 | 0.00 | 0.00 | 0.00 | 0.00 |
| Cr | 0.00 | 0.01 | 0.00 | 0.00 | 0.00 | 0.00 | 0.01 | 0.01 | 0.01 | 0.00 | 0.00 | 0.00 |
| Ni | 0.00 | 0.00 | 0.00 | 0.00 | 0.00 | 0.00 | 0.00 | 0.00 | 0.00 | 0.00 | 0.00 | 0.00 |
| Recalculated by the method of Deer et al., 1992. | | | | | | | | | | | | |
| Alm | 58.47 | 67.11 | 66.74 | 62.29 | 69.554 | 74.81 | 77.96 | 58.93 | 59.11 | | | |
| And | 0.00 | 0.00 | 0.00 | 0.00 | 0 | 0.00 | 0.00 | 0.00 | 0.00 | | | |
| Gross | 2.21 | 1.54 | 1.98 | 2.45 | 12.883 | 18.77 | 8.78 | 32.22 | 32.37 | | | |
| Pyrope | 0.06 | 0.02 | 0.37 | 0.17 | 17.502 | 6.11 | 12.77 | 4.30 | 4.27 | | | |
| Spess | 39.17 | 31.19 | 30.79 | 35.07 | 0.062 | 0.17 | 0.15 | 4.30 | 4.06 | | | |
| Uvaro | 0.03 | 0.14 | 0.00 | 0.00 | 0 | 0.05 | 0.24 | 0.17 | 0.11 | | | |

**(Table 6. 1 continued)**

**GARNET**

| Sample | KSH-63 | | | | | |
|---|---|---|---|---|---|---|
| Grain | 1 | 2 | 3 | 4 | 5 | 6 |
| Analysis | 1 | 1 | 1 | 1 | 1 | 1 |
| $SiO_2$ | 37.83 | 37.19 | 37.82 | 37.58 | 37.64 | 37.81 |
| $TiO_2$ | 0.01 | 0.03 | 0.03 | 0.05 | 0.02 | 0.02 |
| $Al_2O_3$ | 21.11 | 20.88 | 20.89 | 21.04 | 20.92 | 21.04 |
| $Cr_2O_3$ | 0.03 | 0.00 | 0.00 | 0.00 | 0.00 | 0.00 |
| FeO | 27.00 | 24.81 | 24.86 | 24.95 | 30.21 | 25.59 |
| MnO | 14.91 | 17.32 | 17.33 | 17.60 | 11.88 | 16.57 |
| MgO | 0.00 | 0.01 | 0.01 | 0.02 | 0.03 | 0.01 |
| CaO | 0.68 | 0.78 | 0.83 | 0.86 | 0.81 | 0.78 |
| $Na_2O$ | 0.02 | 0.03 | 0.04 | 0.02 | 0.06 | 0.00 |
| $K_2O$ | 0.00 | 0.01 | 0.00 | 0.00 | 0.01 | 0.00 |
| NiO | 0.00 | 0.00 | 0.00 | 0.00 | 0.01 | 0.00 |
| F | 0.08 | 0.13 | 0.07 | 0.14 | 0.01 | 0.06 |
| -O=F | 0.03 | 0.05 | 0.03 | 0.06 | 0.00 | 0.02 |
| Cl | 0.02 | 0.00 | 0.00 | 0.00 | 0.02 | 0.00 |
| -O=Cl | 0.00 | 0.00 | 0.00 | 0.00 | 0.01 | 0.00 |
| **Total** | **101.72** | **101.24** | **101.91** | **102.32** | **101.63** | **101.90** |
| Structural formulas are calculated on the basis of 24 oxygens. | | | | | | |
| Si | 6.10 | 6.05 | 6.09 | 6.06 | 6.08 | 6.08 |
| Ti | 0.00 | 0.00 | 0.00 | 0.01 | 0.00 | 0.00 |
| Al | 4.01 | 4.00 | 3.97 | 4.00 | 3.98 | 3.99 |
| Cr | 0.00 | 0.00 | 0.00 | 0.00 | 0.00 | 0.00 |
| $Fe_2$ | 3.64 | 3.38 | 3.35 | 3.36 | 4.08 | 3.44 |
| Mn | 2.04 | 2.39 | 2.36 | 2.40 | 1.63 | 2.26 |
| Mg | 0.00 | 0.00 | 0.00 | 0.01 | 0.01 | 0.00 |
| Ca | 0.12 | 0.14 | 0.14 | 0.15 | 0.14 | 0.13 |
| Na | 0.00 | 0.01 | 0.01 | 0.01 | 0.02 | 0.00 |
| K | 0.00 | 0.00 | 0.00 | 0.00 | 0.00 | 0.00 |
| Ni | 0.00 | 0.00 | 0.00 | 0.00 | 0.00 | 0.00 |
| F | 0.04 | 0.06 | 0.03 | 0.07 | 0.01 | 0.03 |
| Cl | 0.00 | 0.00 | 0.00 | 0.00 | 0.01 | 0.00 |
| Alm | 62.83 | 57.20 | 57.16 | 56.82 | 69.73 | 58.99 |
| And | 0.00 | 0.00 | 0.00 | 0.00 | 0.00 | 0.00 |
| Gross | 1.94 | 2.31 | 2.44 | 2.50 | 2.39 | 2.29 |
| Pyrope | 0.00 | 0.05 | 0.05 | 0.09 | 0.11 | 0.03 |
| Spess | 35.14 | 40.45 | 40.36 | 40.59 | 27.78 | 38.68 |

**(Table 6. 1 continued)**

| ZIRCON | | | | | | COLUMBITE | | | APATITE | | | | |
|---|---|---|---|---|---|---|---|---|---|---|---|---|---|
| Sample # | NYT-32 | | | KSH-63 | KSH-67 | KSH-63 | | | KSH-67 | | | | |
| Grain # | 1 | 2 | 3 | 1 | 1 | 1 | 2 | 3 | 1 | 1 | 3 | 3 | 4 |
| Analysis | 1 | 1 | 1 | 1 | 1 | 1 | 1 | 1 | 1 | 2 | 1 | 2 | 1 |
| $SiO_2$ | 28.83 | 27.71 | 33.58 | 32.04 | 32.33 | 1.44 | 0.50 | 0.39 | 0.00 | 0.00 | 0.00 | 0.00 | 0.00 |
| $TiO_2$ | 0.09 | 0.00 | 0.00 | 0.03 | 0.01 | 0.71 | 0.90 | 1.11 | 0.01 | 0.00 | 0.00 | 0.01 | 0.00 |
| $Al_2O_3$ | 0.00 | 0.11 | 0.00 | 0.12 | 0.00 | 0.01 | 0.00 | 0.00 | 0.00 | 0.00 | 0.00 | 0.00 | 0.00 |
| FeO | 0.02 | 0.00 | 0.10 | 0.06 | 0.26 | 15.23 | 16.28 | 16.96 | 0.16 | 0.14 | 0.12 | 0.16 | 0.15 |
| MnO | 0.00 | 0.00 | 0.00 | 0.00 | 0.00 | 3.74 | 4.52 | 3.68 | 0.75 | 0.71 | 0.78 | 0.77 | 0.78 |
| MgO | 0.03 | 0.04 | 0.00 | 0.01 | 0.02 | 0.00 | 0.00 | 0.00 | 0.01 | 0.00 | 0.00 | 0.00 | 0.00 |
| CaO | 0.00 | 0.00 | 0.01 | 0.02 | 0.00 | 0.00 | 0.00 | 0.00 | 56.41 | 56.42 | 56.56 | 55.40 | 55.66 |
| $ZrO_2$ | 51.14 | 51.93 | 66.15 | 62.09 | 63.12 | 0.21 | 0.04 | 0.17 | 0.13 | 0.11 | 0.18 | 0.17 | 0.11 |
| $HfO_2$ | 1.72 | 2.09 | 2.15 | 5.47 | 3.90 | 0.00 | 0.09 | 0.06 | 0.02 | 0.04 | 0.14 | 0.00 | 0.07 |
| $La_2O_3$ | 0.12 | 0.10 | 0.01 | 0.00 | 0.06 | 0.04 | 0.00 | 0.00 | 0.02 | 0.08 | 0.00 | 0.26 | 0.00 |
| $Ce_2O_3$ | 0.00 | 0.06 | 0.00 | 0.21 | 0.00 | 0.11 | 0.01 | 0.00 | 0.22 | 0.29 | 0.13 | 0.21 | 0.16 |
| $Nb_2O_5$ | 0.00 | 0.00 | 0.00 | 0.00 | 0.00 | 50.99 | 67.40 | 67.44 | 0.00 | 0.00 | 0.00 | 0.00 | 0.00 |
| $Ta_2O_5$ | 0.04 | 0.00 | 0.00 | 0.00 | 0.00 | 26.84 | 10.78 | 9.82 | 0.05 | 0.05 | 0.16 | 0.00 | 0.00 |
| $Y_2O_3$ | 4.43 | 5.69 | 0.04 | 0.52 | 0.48 | 0.00 | 0.00 | 0.07 | 0.60 | 0.40 | 0.54 | 0.57 | 0.37 |
| $Yb_2O_3$ | 1.31 | 1.20 | 0.05 | 0.13 | 0.28 | 0.03 | 0.04 | 0.00 | 0.01 | 0.15 | 0.00 | 0.00 | 0.00 |
| $P_2O_5$ | 2.82 | 3.99 | 0.11 | 0.34 | 0.30 | 0.00 | 0.00 | 0.00 | 41.31 | 40.97 | 41.72 | 42.02 | 41.16 |
| **Total** | **90.55** | **92.92** | **102.20** | **101.04** | **100.76** | **99.35** | **100.56** | **99.70** | **99.70** | **99.36** | **100.33** | **99.57** | **98.46** |

Structural formulas calculated on the basis of 16. 24 and 26 oxygen for zircon, columbite and apatite respectively.

| | | | | | | | | | | | | | |
|---|---|---|---|---|---|---|---|---|---|---|---|---|---|
| Si | 3.88 | 3.66 | 4.03 | 3.96 | 3.98 | 0.36 | 0.12 | 0.09 | 0.00 | 0.00 | 0.00 | 0.00 | 0.00 |
| Ti | 0.01 | 0.00 | 0.00 | 0.00 | 0.00 | 0.13 | 0.16 | 0.19 | 0.00 | 0.00 | 0.00 | 0.00 | 0.00 |
| Al | 0.00 | 0.02 | 0.00 | 0.02 | 0.00 | 0.00 | 0.00 | 0.00 | 0.00 | 0.00 | 0.00 | 0.00 | 0.00 |
| $Fe_2$ | 0.00 | 0.00 | 0.01 | 0.01 | 0.03 | 3.18 | 3.16 | 3.31 | 0.02 | 0.02 | 0.02 | 0.02 | 0.02 |
| Mn | 0.00 | 0.00 | 0.00 | 0.00 | 0.00 | 0.79 | 0.89 | 0.73 | 0.11 | 0.10 | 0.11 | 0.11 | 0.12 |
| Mg | 0.01 | 0.01 | 0.00 | 0.00 | 0.00 | 0.00 | 0.00 | 0.00 | 0.00 | 0.00 | 0.00 | 0.00 | 0.00 |
| Ca | 0.00 | 0.00 | 0.00 | 0.00 | 0.00 | 0.00 | 0.00 | 0.00 | 10.51 | 10.57 | 10.47 | 10.29 | 10.47 |
| Zr | 3.36 | 3.34 | 3.87 | 3.74 | 3.79 | 0.03 | 0.00 | 0.02 | 0.01 | 0.01 | 0.02 | 0.01 | 0.01 |
| Hf | 0.07 | 0.08 | 0.07 | 0.19 | 0.14 | 0.00 | 0.01 | 0.00 | 0.00 | 0.00 | 0.01 | 0.00 | 0.00 |
| La | 0.01 | 0.01 | 0.00 | 0.00 | 0.00 | 0.00 | 0.00 | 0.00 | 0.00 | 0.01 | 0.00 | 0.02 | 0.00 |
| Ce | 0.00 | 0.00 | 0.00 | 0.01 | 0.00 | 0.01 | 0.00 | 0.00 | 0.01 | 0.02 | 0.01 | 0.01 | 0.01 |
| Nb | 0.00 | 0.00 | 0.00 | 0.00 | 0.00 | 5.76 | 7.07 | 7.11 | 0.00 | 0.00 | 0.00 | 0.00 | 0.00 |
| Ta | 0.00 | 0.00 | 0.00 | 0.00 | 0.00 | 1.82 | 0.68 | 0.62 | 0.00 | 0.00 | 0.01 | 0.00 | 0.00 |
| Y | 0.32 | 0.40 | 0.00 | 0.03 | 0.03 | 0.00 | 0.00 | 0.01 | 0.06 | 0.04 | 0.05 | 0.05 | 0.03 |
| Yb | 0.05 | 0.05 | 0.00 | 0.00 | 0.01 | 0.00 | 0.00 | 0.00 | 0.00 | 0.01 | 0.00 | 0.00 | 0.00 |
| P | 0.32 | 0.45 | 0.01 | 0.04 | 0.03 | 0.00 | 0.00 | 0.00 | 6.08 | 6.07 | 6.10 | 6.17 | 6.12 |

| | OLIGICLASE | | BIOTITE | | | | | | | | | | MUSCOVITE | |
|---|---|---|---|---|---|---|---|---|---|---|---|---|---|---|
| Sample # | SHN-102 | | SHN-102 | | | | SHN-102 | | | | | | SHN-102 | |
| Grain # | 1 | 1 | 1 | 2-rim | 2core | 2-rim | 1 | 1 | 1 | 2 | 2 | 3 | 1 | 1 |
| Analysis # | 1 | 2 | 1 | 2 | 2 | 3 | 1 | 2 | 3 | 1 | 2 | 1 | 1 | 2 |
| $SiO_2$ | 65.18 | 65.62 | 33.85 | 34.24 | 34.99 | 35.01 | 34.21 | 34.69 | 35.13 | 34.93 | 34.61 | 35.40 | 46.72 | 47.39 |
| $TiO_2$ | 0.01 | 0.02 | 2.48 | 2.86 | 2.56 | 2.25 | 2.63 | 2.71 | 2.53 | 2.86 | 2.79 | 2.79 | 0.02 | 0.03 |
| $Al_2O_3$ | 22.44 | 22.17 | 21.98 | 19.13 | 19.74 | 20.11 | 19.19 | 19.46 | 19.50 | 19.24 | 19.46 | 19.90 | 37.95 | 37.03 |
| $Cr_2O_3$ | 0.01 | 0.02 | 0 | 0.04 | 0.04 | 0 | 0.01 | 0.01 | 0.00 | 0.00 | 0.01 | 0.00 | 0.01 | 0.00 |
| FeO | 0.00 | 0.07 | 21.27 | 22.77 | 22.46 | 22.87 | 22.59 | 22.27 | 22.43 | 22.67 | 22.67 | 22.30 | 0.55 | 0.85 |
| MnO | 0.00 | 0.02 | 0.47 | 0.41 | 0.44 | 0.47 | 0.45 | 0.45 | 0.50 | 0.47 | 0.46 | 0.46 | 0.04 | 0.05 |
| MgO | 0.00 | 0.00 | 5.22 | 6 | 6.14 | 5.68 | 5.69 | 5.77 | 6.10 | 5.79 | 5.76 | 5.99 | 0.08 | 0.15 |
| CaO | 3.71 | 3.37 | 0 | 0 | 0 | 0 | 0.00 | 0.00 | 0.01 | 0.00 | 0.00 | 0.00 | 0.00 | 0.00 |
| $Na_2O$ | 9.54 | 9.89 | 0.21 | 0.11 | 0.21 | 0.1 | 0.18 | 0.19 | 0.22 | 0.16 | 0.18 | 0.20 | 0.52 | 0.50 |
| $K_2O$ | 0.40 | 0.32 | 8.80 | 10.03 | 9.94 | 9.76 | 9.91 | 9.84 | 9.87 | 9.85 | 9.93 | 9.86 | 10.40 | 10.43 |
| NiO | 0.00 | 0.00 | 0.09 | 0.02 | 0.01 | 0.01 | 0.02 | 0.02 | 0.03 | 0.00 | 0.01 | 0.01 | 0.01 | 0.02 |
| **Total** | **101.29** | **101.50** | **94.37** | **95.61** | **96.53** | **96.26** | **94.88** | **95.41** | **96.32** | **95.97** | **95.88** | **96.91** | **96.30** | **96.45** |

Structural formulas calculated on the basis of 32 and 22 oxygens for oligoclase and biotite, muscovite respectively.

| | | | | | | | | | | | | | | |
|---|---|---|---|---|---|---|---|---|---|---|---|---|---|---|
| Si | 11.36 | 11.42 | 5.24 | 5.32 | 5.36 | 5.38 | 5.35 | 5.38 | 5.39 | 5.39 | 5.35 | 5.38 | 6.11 | 6.19 |
| Ti | 0.00 | 0.00 | 0.29 | 0.33 | 0.3 | 0.26 | 0.31 | 0.32 | 0.29 | 0.33 | 0.32 | 0.32 | 0.00 | 0.00 |
| Al | 4.61 | 4.55 | 4.01 | 3.5 | 3.56 | 3.64 | 3.54 | 3.55 | 3.53 | 3.50 | 3.55 | 3.57 | 5.85 | 5.70 |
| Cr | 0.00 | 0.00 | 0 | 0 | 0 | 0 | 0.00 | 0.00 | 0.00 | 0.00 | 0.00 | 0.00 | 0.00 | 0.00 |
| $Fe_2$ | 0.00 | 0.01 | 2.75 | 2.96 | 2.88 | 2.94 | 2.96 | 2.89 | 2.88 | 2.93 | 2.93 | 2.84 | 0.06 | 0.09 |
| Mn | 0.00 | 0.00 | 0.06 | 0.03 | 0.06 | 0.03 | 0.06 | 0.06 | 0.06 | 0.06 | 0.06 | 0.06 | 0.00 | 0.01 |
| Mg | 0.00 | 0.00 | 1.21 | 1.39 | 1.4 | 1.3 | 1.33 | 1.33 | 1.40 | 1.33 | 1.33 | 1.36 | 0.02 | 0.03 |
| Ca | 0.69 | 0.63 | 0 | 0 | 0 | 0 | 0.00 | 0.00 | 0.00 | 0.00 | 0.00 | 0.00 | 0.00 | 0.00 |
| Na | 3.22 | 3.34 | 0.06 | 0.03 | 0.06 | 0.03 | 0.06 | 0.06 | 0.07 | 0.05 | 0.05 | 0.06 | 0.13 | 0.13 |
| K | 0.09 | 0.07 | 1.74 | 1.99 | 1.94 | 1.91 | 1.98 | 1.95 | 1.93 | 1.94 | 1.96 | 1.91 | 1.73 | 1.74 |
| Ni | 0.00 | 0.00 | 0.01 | 0 | 0 | 0 | 0.00 | 0.00 | 0.00 | 0.00 | 0.00 | 0.00 | 0.00 | 0.00 |

**(Table 6. 2 continued)**

| **BIOTITE** | | | | **CHLORITE** | |
|---|---|---|---|---|---|
| Sample | SHN-102 | | | | |
| Grain | 1 | 2 | 3 | 1 | 2 |
| Analysis | 1 | 1 | 1 | 1 | 1 |
| $SiO_2$ | 35.82 | 35.36 | 34.99 | 27.26 | 29.91 |
| $TiO_2$ | 2.55 | 3.39 | 3.64 | 0.10 | 0.88 |
| $Al_2O_3$ | 19.97 | 18.80 | 18.45 | 20.64 | 19.14 |
| $Cr_2O_3$ | 0.00 | 0.00 | 0.00 | 0.00 | 0.00 |
| FeO | 18.93 | 22.64 | 23.08 | 29.60 | 22.20 |
| MnO | 0.43 | 0.52 | 0.49 | 0.61 | 0.43 |
| MgO | 5.77 | 5.85 | 5.92 | 8.85 | 5.54 |
| CaO | 0.00 | 0.00 | 0.00 | 0.10 | 0.55 |
| $Na_2O$ | 0.20 | 0.11 | 0.15 | 0.10 | 0.21 |
| $K_2O$ | 9.14 | 9.79 | 9.97 | 0.15 | 2.53 |
| NiO | 0.03 | 0.00 | 0.04 | 0.02 | 0.00 |
| F | 0.67 | 0.50 | 0.44 | 0.10 | 0.48 |
| -O=F | 0.28 | 0.21 | 0.19 | 0.04 | 0.20 |
| Cl | 0.05 | 0.04 | 0.02 | 0.01 | 0.06 |
| -O=Cl | 0.01 | 0.01 | 0.00 | 0.00 | 0.01 |
| $SO_3$ | 0.00 | 0.03 | 0.04 | 0.00 | 0.00 |
| **Total** | **93.27** | **96.80** | **97.04** | **87.48** | **83.05** |

| **APATITE** | | | | |
|---|---|---|---|---|
| Sample = | SHN-102 | | | |
| Grain = | 1 | 2 | 3 | 3 |
| Analysis = | 1 | 1 | 1 | 2 |
| $SiO_2$ | 0.00 | 0.00 | 0.00 | 0.00 |
| $TiO_2$ | 0.00 | 0.00 | 0.00 | 0.00 |
| $Al_2O_3$ | 0.00 | 0.00 | 0.00 | 0.00 |
| FeO | 0.35 | 0.38 | 0.41 | 0.39 |
| MnO | 1.23 | 1.26 | 1.22 | 1.27 |
| MgO | 0.04 | 0.03 | 0.02 | 0.02 |
| CaO | 56.44 | 55.48 | 56.21 | 56.00 |
| $ZrO_2$ | 0.15 | 0.24 | 0.20 | 0.10 |
| $HfO_2$ | 0.09 | 0.00 | 0.10 | 0.05 |
| $La_2O_3$ | 0.00 | 0.08 | 0.00 | 0.08 |
| $Ce_2O_3$ | 0.09 | 0.03 | 0.14 | 0.05 |
| $Nb_2O_5$ | 0.00 | 0.00 | 0.00 | 0.00 |
| $Ta_2O_5$ | 0.02 | 0.01 | 0.00 | 0.17 |
| $Y_2O_3$ | 0.13 | 0.20 | 0.15 | 0.21 |
| $Yb_2O_3$ | 0.00 | 0.06 | 0.08 | 0.00 |
| $P_2O_5$ | 38.96 | 41.75 | 42.41 | 42.14 |
| Total | **97.49** | **99.51** | **100.94** | **100.48** |

Structural formulas calculated on the basis of 22, 28 and 26 oxygens for biotite, chlorite and apatite respectively.

| | | | | | |
|---|---|---|---|---|---|
| Si | 5.61 | 5.45 | 5.40 | 5.88 | 6.60 |
| Ti | 0.30 | 0.39 | 0.42 | 0.02 | 0.15 |
| Al | 3.69 | 3.41 | 3.36 | 5.25 | 4.98 |
| Cr | 0.00 | 0.00 | 0.00 | 0.00 | 0.00 |
| $Fe_2$ | 2.48 | 2.92 | 2.98 | 5.34 | 4.10 |
| Mn | 0.06 | 0.07 | 0.06 | 0.11 | 0.08 |
| Mg | 1.35 | 1.34 | 1.36 | 2.85 | 1.82 |
| Ca | 0.00 | 0.00 | 0.00 | 0.02 | 0.13 |
| Na | 0.06 | 0.03 | 0.05 | 0.04 | 0.09 |
| K | 1.82 | 1.93 | 1.96 | 0.04 | 0.71 |
| Ni | 0.00 | 0.00 | 0.00 | 0.00 | 0.00 |
| F | 0.33 | 0.24 | 0.22 | 0.07 | 0.33 |
| Cl | 0.01 | 0.01 | 0.01 | 0.00 | 0.02 |
| S | 0.00 | 0.00 | 0.00 | 0.00 | 0.00 |

| | | | | |
|---|---|---|---|---|
| Si | 0.00 | 0.00 | 0.00 | 0.00 |
| Ti | 0.00 | 0.00 | 0.00 | 0.00 |
| Al | 0.00 | 0.00 | 0.00 | 0.00 |
| $Fe_2$ | 0.05 | 0.06 | 0.06 | 0.06 |
| Mn | 0.19 | 0.19 | 0.18 | 0.18 |
| Mg | 0.01 | 0.01 | 0.01 | 0.01 |
| Ca | 10.87 | 10.32 | 10.31 | 10.32 |
| Zr | 0.01 | 0.02 | 0.02 | 0.01 |
| Hf | 0.00 | 0.00 | 0.00 | 0.00 |
| La | 0.00 | 0.00 | 0.00 | 0.00 |
| Ce | 0.01 | 0.00 | 0.01 | 0.00 |
| Nb | 0.00 | 0.00 | 0.00 | 0.00 |
| Ta | 0.00 | 0.00 | 0.00 | 0.01 |
| Y | 0.01 | 0.02 | 0.01 | 0.02 |
| Yb | 0.00 | 0.00 | 0.00 | 0.00 |
| P | 5.93 | 6.14 | 6.15 | 6.14 |

**Table 6. Electron Probe Microanalyses analyses of various minerals from pegmatites.**

**OLIGICLASE**

| Sample # | ICP-111 | | | | | | | | | | | |
|---|---|---|---|---|---|---|---|---|---|---|---|---|
| Grain # | 1 | 1 | 1 | 2 | 2 | 3 | 3 | 3 | 4 | 4 | 5 | 5 |
| Analysis # | 1 | 2 | 3 | 1 | 2 | 1 | 2 | 3 | 1 | 2 | 1 | 2 |
| $SiO_2$ | 62.24 | 62.23 | 61.62 | 61.51 | 62.05 | 62.40 | 62.52 | 62.08 | 62.41 | 62.50 | 66.10 | 62.24 |
| $TiO_2$ | 0.00 | 0.00 | 0.00 | 0.00 | 0.02 | 0.00 | 0.00 | 0.00 | 0.00 | 0.03 | 0.00 | 0.02 |
| $Al_2O_3$ | 22.59 | 22.48 | 22.82 | 22.84 | 22.73 | 22.57 | 22.53 | 22.62 | 22.70 | 22.46 | 20.78 | 23.10 |
| $Cr_2O_3$ | 0.01 | 0.00 | 0.01 | 0.03 | 0.01 | 0.00 | 0.03 | 0.03 | 0.00 | 0.01 | 0.00 | 0.01 |
| FeO | 0.07 | 0.05 | 0.02 | 0.05 | 0.04 | 0.07 | 0.05 | 0.02 | 0.03 | 0.06 | 0.01 | 0.02 |
| MnO | 0.00 | 0.01 | 0.00 | 0.00 | 0.00 | 0.02 | 0.00 | 0.02 | 0.02 | 0.00 | 0.02 | 0.02 |
| MgO | 0.00 | 0.00 | 0.01 | 0.00 | 0.00 | 0.00 | 0.00 | 0.00 | 0.00 | 0.00 | 0.00 | 0.00 |
| CaO | 4.51 | 4.52 | 4.87 | 5.09 | 4.81 | 4.38 | 4.27 | 4.50 | 4.34 | 4.30 | 2.94 | 4.95 |
| $Na_2O$ | 9.07 | 8.80 | 8.77 | 8.74 | 8.90 | 9.13 | 9.31 | 9.04 | 9.08 | 9.09 | 9.92 | 8.85 |
| $K_2O$ | 0.19 | 0.50 | 0.26 | 0.23 | 0.23 | 0.32 | 0.29 | 0.23 | 0.21 | 0.29 | 0.11 | 0.10 |
| NiO | 0.00 | 0.01 | 0.00 | 0.00 | 0.01 | 0.00 | 0.00 | 0.04 | 0.00 | 0.04 | 0.03 | 0.00 |
| **Total** | **98.68** | **98.60** | **98.38** | **98.72** | **98.80** | **98.89** | **99.00** | **98.58** | **99.49** | **98.78** | **99.91** | **99.29** |

Structural formulas calculated on the basis of 32 oxygens.

| | | | | | | | | | | | | |
|---|---|---|---|---|---|---|---|---|---|---|---|---|
| Si | 11.18 | 11.19 | 11.11 | 11.09 | 11.14 | 11.18 | 11.19 | 11.16 | 11.18 | 11.21 | 11.63 | 11.11 |
| Ti | 0.00 | 0.00 | 0.00 | 0.00 | 0.00 | 0.00 | 0.00 | 0.00 | 0.00 | 0.00 | 0.00 | 0.00 |
| Al | 4.78 | 4.77 | 4.85 | 4.85 | 4.81 | 4.77 | 4.75 | 4.79 | 4.79 | 4.75 | 4.31 | 4.86 |
| Cr | 0.00 | 0.00 | 0.00 | 0.00 | 0.00 | 0.00 | 0.00 | 0.00 | 0.00 | 0.00 | 0.00 | 0.00 |
| $Fe_2$ | 0.01 | 0.01 | 0.00 | 0.01 | 0.01 | 0.01 | 0.01 | 0.00 | 0.01 | 0.01 | 0.00 | 0.00 |
| Mn | 0.00 | 0.00 | 0.00 | 0.00 | 0.00 | 0.00 | 0.00 | 0.00 | 0.00 | 0.00 | 0.00 | 0.00 |
| Mg | 0.00 | 0.00 | 0.00 | 0.00 | 0.00 | 0.00 | 0.00 | 0.00 | 0.00 | 0.00 | 0.00 | 0.00 |
| Ca | 0.87 | 0.87 | 0.94 | 0.98 | 0.92 | 0.84 | 0.82 | 0.87 | 0.83 | 0.83 | 0.55 | 0.95 |
| Na | 3.16 | 3.07 | 3.07 | 3.05 | 3.10 | 3.17 | 3.23 | 3.15 | 3.15 | 3.16 | 3.39 | 3.06 |
| K | 0.04 | 0.11 | 0.06 | 0.05 | 0.05 | 0.07 | 0.07 | 0.05 | 0.05 | 0.07 | 0.02 | 0.02 |
| Ni | 0.00 | 0.00 | 0.00 | 0.00 | 0.00 | 0.00 | 0.00 | 0.01 | 0.00 | 0.01 | 0.00 | 0.00 |

**(Table 6. 3 continued)**

| **ALBITE** | | | | | | | **ANDESINE** |
|---|---|---|---|---|---|---|---|
| Sample # | ICP-111 | | | | | | |
| Grain # | 1 | 2 | 2 | 3 | 4 | 4 | 1 |
| Analysis # | 1 | 1 | 2 | 1 | 1 | 2 | 1 |
| $SiO_2$ | 68.52 | 67.45 | 67.30 | 69.92 | 68.66 | 67.33 | 58.46 |
| $TiO_2$ | 0.00 | 0.00 | 0.00 | 0.00 | 0.02 | 0.00 | 0.01 |
| $Al_2O_3$ | 19.28 | 19.10 | 19.53 | 19.71 | 19.48 | 19.35 | 24.86 |
| $Cr_2O_3$ | 0.04 | 0.00 | 0.03 | 0.00 | 0.03 | 0.00 | 0.00 |
| FeO | 0.00 | 0.00 | 0.04 | 0.04 | 0.07 | 0.03 | 0.05 |
| MnO | 0.00 | 0.00 | 0.02 | 0.01 | 0.00 | 0.00 | 0.02 |
| MgO | 0.00 | 0.00 | 0.01 | 0.00 | 0.00 | 0.00 | 0.00 |
| CaO | 0.27 | 0.22 | 0.48 | 0.28 | 0.22 | 0.44 | 7.46 |
| $Na_2O$ | 11.51 | 11.60 | 11.41 | 11.52 | 11.55 | 11.43 | 7.41 |
| $K_2O$ | 0.16 | 0.14 | 0.12 | 0.18 | 0.15 | 0.11 | 0.17 |
| NiO | 0.06 | 0.00 | 0.02 | 0.03 | 0.03 | 0.01 | 0.00 |
| **Total** | **99.84** | **98.51** | **98.96** | **101.69** | **100.21** | **98.70** | **98.44** |

Structural formulas calculated on the basis of 32 oxygens.

| | | | | | | | |
|---|---|---|---|---|---|---|---|
| Si | 12.00 | 11.98 | 11.91 | 12.01 | 11.98 | 11.93 | 10.62 |
| Ti | 0.00 | 0.00 | 0.00 | 0.00 | 0.00 | 0.00 | 0.00 |
| Al | 3.98 | 4.00 | 4.07 | 3.99 | 4.01 | 4.04 | 5.32 |
| Cr | 0.01 | 0.00 | 0.00 | 0.00 | 0.00 | 0.00 | 0.00 |
| $Fe_2$ | 0.00 | 0.00 | 0.01 | 0.01 | 0.01 | 0.00 | 0.01 |
| Mn | 0.00 | 0.00 | 0.00 | 0.00 | 0.00 | 0.00 | 0.00 |
| Mg | 0.00 | 0.00 | 0.00 | 0.00 | 0.00 | 0.00 | 0.00 |
| Ca | 0.05 | 0.04 | 0.09 | 0.05 | 0.04 | 0.08 | 1.45 |
| Na | 3.91 | 3.99 | 3.91 | 3.83 | 3.91 | 3.93 | 2.61 |
| K | 0.04 | 0.03 | 0.03 | 0.04 | 0.03 | 0.02 | 0.04 |
| Ni | 0.01 | 0.00 | 0.00 | 0.00 | 0.00 | 0.00 | 0.00 |

**MICROCLINE**

| Sample # | ICP-111 | | | | | | | | | | | | | | ICP-114 | | |
|---|---|---|---|---|---|---|---|---|---|---|---|---|---|---|---|---|---|
| Grain # | 1 | 2 | 3 | 3 | 3 | 3 | 4 | 4 | 5 | 5 | 6 | 6 | 7 | 8 | 1 | 1 | 2 |
| Analysis | 1 | 1 | 1 | 2 | 3 | 4 | 1 | 2 | 1 | 2 | 1 | 2 | 1 | 1 | 1 | 1 | 1 |
| $SiO_2$ | 63.29 | 63.47 | 63.39 | 63.92 | 63.94 | 63.68 | 62.76 | 63.66 | 63.56 | 63.91 | 63.48 | 63.66 | 64.68 | 65.20 | 63.90 | 63.93 | 64.08 |
| $TiO_2$ | 0.00 | 0.01 | 0.01 | 0.00 | 0.01 | 0.01 | 0.00 | 0.02 | 0.01 | 0.00 | 0.00 | 0.00 | 0.04 | 0.01 | 0.01 | 0.02 | 0.02 |
| $Al_2O_3$ | 17.99 | 17.98 | 18.12 | 18.08 | 18.20 | 17.98 | 17.82 | 17.92 | 17.97 | 18.06 | 17.93 | 17.91 | 18.45 | 18.05 | 18.14 | 18.24 | 18.29 |
| $Cr_2O_3$ | 0.01 | 0.01 | 0.01 | 0.05 | 0.00 | 0.00 | 0.00 | 0.01 | 0.02 | 0.04 | 0.00 | 0.00 | 0.00 | 0.00 | 0.04 | 0.01 | 0.00 |
| FeO | 0.01 | 0.05 | 0.11 | 0.12 | 0.10 | 0.13 | 0.16 | 0.05 | 0.03 | 0.06 | 0.04 | 0.26 | 0.06 | 0.05 | 0.11 | 0.20 | 0.06 |
| MnO | 0.00 | 0.00 | 0.00 | 0.00 | 0.00 | 0.00 | 0.00 | 0.02 | 0.00 | 0.00 | 0.03 | 0.00 | 0.01 | 0.01 | 0.00 | 0.00 | 0.02 |
| MgO | 0.00 | 0.00 | 0.00 | 0.00 | 0.00 | 0.00 | 0.00 | 0.00 | 0.00 | 0.00 | 0.00 | 0.00 | 0.00 | 0.00 | 0.00 | 0.00 | 0.00 |
| CaO | 0.00 | 0.00 | 0.00 | 0.01 | 0.01 | 0.00 | 0.00 | 0.01 | 0.00 | 0.00 | 0.00 | 0.00 | 0.28 | 0.00 | 0.03 | 0.00 | 0.00 |
| $Na_2O$ | 0.85 | 0.97 | 0.99 | 0.91 | 0.98 | 0.88 | 0.66 | 0.76 | 1.01 | 1.09 | 0.95 | 0.72 | 1.12 | 0.98 | 0.82 | 0.80 | 1.05 |
| $K_2O$ | 16.49 | 15.82 | 15.93 | 15.99 | 15.89 | 16.16 | 16.39 | 16.44 | 15.80 | 15.77 | 15.95 | 16.25 | 15.36 | 15.91 | 16.31 | 16.19 | 15.87 |
| NiO | 0.00 | 0.03 | 0.00 | 0.01 | 0.00 | 0.00 | 0.00 | 0.00 | 0.00 | 0.00 | 0.00 | 0.00 | 0.00 | 0.00 | 0.00 | 0.00 | 0.01 |
| **Total** | **98.64** | **98.34** | **98.56** | **99.09** | **99.13** | **98.84** | **97.79** | **98.89** | **98.40** | **98.93** | **98.38** | **98.80** | **100.00** | **100.21** | **99.36** | **99.39** | **99.40** |

Structural formulas calculated on the basis of 32 oxygens.

| | | | | | | | | | | | | | | | | | |
|---|---|---|---|---|---|---|---|---|---|---|---|---|---|---|---|---|---|
| Si | 11.93 | 11.96 | 11.93 | 11.96 | 11.95 | 11.96 | 11.94 | 11.96 | 11.96 | 11.96 | 11.96 | 11.96 | 12.00 | 12.03 | 11.94 | 11.93 | 11.94 |
| Ti | 0.00 | 0.00 | 0.00 | 0.00 | 0.00 | 0.00 | 0.00 | 0.00 | 0.00 | 0.00 | 0.00 | 0.00 | 0.01 | 0.00 | 0.00 | 0.00 | 0.00 |
| Al | 4.00 | 3.99 | 4.02 | 3.99 | 4.01 | 3.98 | 3.99 | 3.97 | 3.99 | 3.98 | 3.98 | 3.97 | 4.11 | 3.92 | 4.00 | 4.01 | 4.02 |
| Cr | 0.00 | 0.00 | 0.00 | 0.01 | 0.00 | 0.00 | 0.00 | 0.00 | 0.00 | 0.01 | 0.00 | 0.00 | 0.00 | 0.00 | 0.01 | 0.00 | 0.00 |
| $Fe_2$ | 0.00 | 0.01 | 0.02 | 0.02 | 0.02 | 0.02 | 0.03 | 0.01 | 0.00 | 0.01 | 0.01 | 0.04 | 0.01 | 0.01 | 0.02 | 0.03 | 0.01 |
| Mn | 0.00 | 0.00 | 0.00 | 0.00 | 0.00 | 0.00 | 0.00 | 0.00 | 0.00 | 0.00 | 0.00 | 0.00 | 0.00 | 0.00 | 0.00 | 0.00 | 0.00 |
| Mg | 0.00 | 0.00 | 0.00 | 0.00 | 0.00 | 0.00 | 0.00 | 0.00 | 0.00 | 0.00 | 0.00 | 0.00 | 0.00 | 0.00 | 0.00 | 0.00 | 0.00 |
| Ca | 0.00 | 0.00 | 0.00 | 0.00 | 0.00 | 0.00 | 0.00 | 0.00 | 0.00 | 0.00 | 0.00 | 0.00 | 0.06 | 0.00 | 0.01 | 0.00 | 0.00 |
| Na | 0.31 | 0.35 | 0.36 | 0.33 | 0.35 | 0.32 | 0.24 | 0.28 | 0.37 | 0.40 | 0.35 | 0.26 | 0.41 | 0.35 | 0.30 | 0.29 | 0.38 |
| K | 3.97 | 3.80 | 3.82 | 3.82 | 3.79 | 3.87 | 3.98 | 3.94 | 3.79 | 3.77 | 3.83 | 3.90 | 3.70 | 3.74 | 3.89 | 3.86 | 3.77 |
| Ni | 0.00 | 0.00 | 0.00 | 0.00 | 0.00 | 0.00 | 0.00 | 0.00 | 0.00 | 0.00 | 0.00 | 0.00 | 0.00 | 0.00 | 0.00 | 0.00 | 0.00 |

**(Table 6. 3 continued)**

**BIOTITE**

| Sample # | ICP-111 | | | | | | | | | | |
|---|---|---|---|---|---|---|---|---|---|---|---|
| Grain # | 1 | 1 | 2 | 2 | 3 | 3 | 4 | 5 | 6 | 7 | 8 |
| Analysis # | 1 | 2 | 1 | 2 | 1 | 2 | 1 | 1 | 1 | 1 | 1 |
| $SiO_2$ | 32.34 | 35.68 | 35.16 | 35.60 | 35.36 | 35.78 | 35.82 | 35.97 | 35.82 | 35.90 | 35.10 |
| $TiO_2$ | 2.63 | 3.08 | 2.93 | 2.99 | 3.04 | 2.93 | 3.06 | 2.66 | 3.06 | 2.98 | 3.29 |
| $Al_2O_3$ | 14.13 | 15.45 | 15.42 | 15.48 | 15.76 | 15.56 | 15.66 | 15.79 | 15.83 | 15.40 | 15.18 |
| $Cr_2O_3$ | 0.01 | 0.01 | 0.02 | 0.04 | 0.01 | 0.03 | 0.05 | 0.00 | 0.00 | 0.01 | 0.00 |
| FeO | 19.77 | 21.73 | 21.63 | 21.87 | 21.93 | 22.18 | 21.53 | 22.41 | 22.04 | 20.04 | 22.35 |
| MnO | 0.49 | 0.64 | 0.54 | 0.59 | 0.67 | 0.60 | 0.64 | 0.60 | 0.61 | 0.50 | 0.47 |
| MgO | 7.47 | 8.17 | 8.09 | 8.22 | 7.92 | 8.29 | 8.26 | 8.06 | 8.10 | 7.84 | 7.63 |
| CaO | 4.72 | 0.00 | 0.01 | 0.03 | 0.00 | 0.00 | 0.00 | 0.01 | 0.00 | 0.00 | 0.01 |
| $Na_2O$ | 0.05 | 0.07 | 0.08 | 0.08 | 0.10 | 0.06 | 0.09 | 0.06 | 0.11 | 0.05 | 0.06 |
| $K_2O$ | 8.94 | 10.25 | 10.34 | 10.17 | 9.70 | 9.98 | 10.25 | 10.15 | 9.92 | 9.14 | 9.83 |
| NiO | 0.00 | 0.01 | 0.06 | 0.01 | 0.01 | 0.00 | 0.03 | 0.03 | 0.00 | 0.00 | 0.00 |
| Total | 90.55 | 95.09 | 94.28 | 95.08 | 94.50 | 95.41 | 95.39 | 95.74 | 95.49 | 91.86 | 93.92 |

Structural formulas calculated on the basis of 23 oxygens.

| | | | | | | | | | | | |
|---|---|---|---|---|---|---|---|---|---|---|---|
| Si | 5.61 | 5.83 | 5.80 | 5.82 | 5.80 | 5.82 | 5.82 | 5.84 | 5.81 | 5.97 | 5.82 |
| Ti | 0.34 | 0.38 | 0.36 | 0.37 | 0.37 | 0.36 | 0.37 | 0.32 | 0.37 | 0.37 | 0.41 |
| Al | 2.89 | 2.97 | 3.00 | 2.98 | 3.05 | 2.98 | 3.00 | 3.02 | 3.03 | 3.02 | 2.97 |
| Cr | 0.00 | 0.00 | 0.00 | 0.00 | 0.00 | 0.00 | 0.01 | 0.00 | 0.00 | 0.00 | 0.00 |
| $Fe_2$ | 2.87 | 2.97 | 2.99 | 2.99 | 3.01 | 3.02 | 2.93 | 3.04 | 2.99 | 2.79 | 3.10 |
| Mn | 0.07 | 0.09 | 0.08 | 0.08 | 0.09 | 0.08 | 0.09 | 0.08 | 0.08 | 0.07 | 0.07 |
| Mg | 1.93 | 1.99 | 1.99 | 2.00 | 1.94 | 2.01 | 2.00 | 1.95 | 1.96 | 1.94 | 1.88 |
| Ca | 0.88 | 0.00 | 0.00 | 0.00 | 0.00 | 0.00 | 0.00 | 0.00 | 0.00 | 0.00 | 0.00 |
| Na | 0.02 | 0.02 | 0.03 | 0.02 | 0.03 | 0.02 | 0.03 | 0.02 | 0.03 | 0.02 | 0.02 |
| K | 1.98 | 2.14 | 2.18 | 2.12 | 2.03 | 2.07 | 2.12 | 2.10 | 2.06 | 1.94 | 2.08 |
| Ni | 0.00 | 0.00 | 0.01 | 0.00 | 0.00 | 0.00 | 0.00 | 0.00 | 0.00 | 0.00 | 0.00 |

(Table 6. 3 continued)

**BIOTITE**

| Sample # | ICP-114 | | | | | | | | | | | |
|---|---|---|---|---|---|---|---|---|---|---|---|---|
| Grain # | 1 | 1 | 1 | 2 | 2 | 3 | 3 | 4 | 5 | 6 | 7 | 8 |
| Analysis # | 1 | 2 | 3 | 1 | 2 | 1 | 2 | 1 | 1 | 1 | 1 | 1 |
| $SiO_2$ | 35.50 | 35.63 | 34.98 | 34.10 | 36.25 | 35.46 | 35.32 | 35.33 | 35.65 | 35.22 | 35.56 | 35.68 |
| $TiO_2$ | 3.05 | 2.94 | 2.83 | 2.84 | 3.15 | 3.16 | 4.06 | 3.03 | 2.96 | 2.99 | 3.05 | 3.20 |
| $Al_2O_3$ | 16.42 | 16.52 | 16.19 | 16.41 | 16.07 | 16.28 | 15.82 | 16.14 | 16.23 | 16.29 | 16.42 | 17.14 |
| $Cr_2O_3$ | 0.00 | 0.00 | 0.00 | 0.03 | 0.05 | 0.00 | 0.03 | 0.00 | 0.02 | 0.00 | 0.04 | 0.01 |
| FeO | 23.62 | 23.71 | 24.58 | 23.21 | 21.93 | 24.23 | 23.99 | 24.29 | 24.13 | 24.28 | 24.14 | 23.11 |
| MnO | 1.01 | 1.00 | 0.96 | 0.78 | 0.60 | 0.60 | 0.57 | 0.62 | 0.64 | 0.77 | 0.70 | 0.57 |
| MgO | 5.76 | 5.83 | 6.32 | 7.61 | 7.53 | 6.39 | 6.38 | 6.23 | 6.32 | 6.74 | 6.23 | 6.35 |
| CaO | 0.00 | 0.00 | 0.07 | 0.09 | 0.00 | 0.00 | 0.27 | 0.10 | 0.01 | 0.13 | 0.00 | 0.04 |
| $Na_2O$ | 0.07 | 0.06 | 0.08 | 0.07 | 0.08 | 0.06 | 0.07 | 0.09 | 0.03 | 0.12 | 0.07 | 0.08 |
| $K_2O$ | 10.05 | 9.96 | 8.99 | 8.60 | 10.13 | 9.99 | 9.36 | 9.99 | 10.07 | 9.00 | 10.12 | 9.75 |
| NiO | 0.03 | 0.03 | 0.00 | 0.00 | 0.01 | 0.00 | 0.00 | 0.00 | 0.06 | 0.00 | 0.00 | 0.00 |
| **Total** | **95.50** | **95.68** | **94.99** | **93.74** | **95.80** | **96.17** | **95.87** | **95.81** | **96.12** | **95.54** | **96.33** | **95.93** |

Structural formulas calculated on the basis of 22 oxygen.

| | | | | | | | | | | | | |
|---|---|---|---|---|---|---|---|---|---|---|---|---|
| Si | 5.57 | 5.57 | 5.52 | 5.41 | 5.60 | 5.53 | 5.51 | 5.53 | 5.56 | 5.51 | 5.53 | 5.52 |
| Ti | 0.36 | 0.35 | 0.34 | 0.34 | 0.37 | 0.37 | 0.48 | 0.36 | 0.35 | 0.35 | 0.36 | 0.37 |
| Al | 3.03 | 3.04 | 3.01 | 3.07 | 2.93 | 2.99 | 2.91 | 2.98 | 2.98 | 3.00 | 3.01 | 3.13 |
| Cr | 0.00 | 0.00 | 0.00 | 0.00 | 0.01 | 0.00 | 0.00 | 0.00 | 0.00 | 0.00 | 0.01 | 0.00 |
| $Fe_2$ | 3.10 | 3.10 | 3.24 | 3.08 | 2.84 | 3.16 | 3.13 | 3.18 | 3.15 | 3.17 | 3.14 | 2.99 |
| Mn | 0.13 | 0.13 | 0.13 | 0.10 | 0.08 | 0.08 | 0.07 | 0.08 | 0.08 | 0.10 | 0.09 | 0.07 |
| Mg | 1.35 | 1.36 | 1.49 | 1.80 | 1.74 | 1.48 | 1.48 | 1.46 | 1.47 | 1.57 | 1.44 | 1.47 |
| Ca | 0.00 | 0.00 | 0.01 | 0.02 | 0.00 | 0.00 | 0.05 | 0.02 | 0.00 | 0.02 | 0.00 | 0.01 |
| Na | 0.02 | 0.02 | 0.02 | 0.02 | 0.02 | 0.02 | 0.02 | 0.03 | 0.01 | 0.04 | 0.02 | 0.02 |
| K | 2.01 | 1.99 | 1.81 | 1.74 | 2.00 | 1.99 | 1.86 | 2.00 | 2.00 | 1.79 | 2.01 | 1.93 |
| Ni | 0.00 | 0.00 | 0.00 | 0.00 | 0.00 | 0.00 | 0.00 | 0.00 | 0.01 | 0.00 | 0.00 | 0.00 |

**BIOTITE**

| Sample | ICP-111 | | | | | | | | ICP-114 | | | | |
|---|---|---|---|---|---|---|---|---|---|---|---|---|---|
| Grain | 1 | 1 | 1 | 2 | 3 | 3 | 3 | 4 | 1 | 2 | 3 | 3 | 4 |
| Analysis | 1 | 2 | 3 | 1 | 1 | 2 | 3 | 1 | 1 | 1 | 1 | 2 | 1 |
| $SiO_2$ | 35.50 | 36.16 | 36.11 | 36.78 | 36.50 | 36.74 | 36.45 | 36.36 | 36.11 | 36.45 | 30.62 | 36.64 | 36.48 |
| $TiO_2$ | 2.86 | 3.24 | 3.20 | 3.23 | 2.75 | 2.92 | 3.37 | 3.22 | 2.98 | 3.00 | 1.49 | 3.07 | 3.08 |
| $Al_2O_3$ | 15.34 | 15.56 | 15.82 | 16.58 | 15.76 | 15.40 | 15.46 | 15.30 | 16.69 | 16.58 | 16.52 | 16.33 | 16.13 |
| $Cr_2O_3$ | 0.03 | 0.00 | 0.01 | 0.00 | 0.00 | 0.03 | 0.02 | 0.03 | 0.00 | 0.01 | 0.02 | 0.00 | 0.00 |
| FeO | 20.72 | 20.24 | 21.29 | 20.14 | 21.09 | 21.96 | 21.73 | 22.20 | 23.36 | 23.39 | 27.91 | 22.53 | 23.91 |
| MnO | 0.57 | 0.60 | 0.64 | 0.72 | 0.57 | 0.54 | 0.59 | 0.62 | 0.98 | 0.96 | 0.89 | 0.66 | 0.60 |
| MgO | 7.76 | 7.62 | 7.74 | 7.45 | 8.01 | 8.25 | 7.65 | 7.71 | 5.72 | 5.73 | 7.16 | 7.59 | 6.41 |
| CaO | 0.42 | 0.25 | 0.00 | 0.02 | 0.00 | 0.00 | 0.01 | 0.03 | 0.01 | 0.00 | 0.43 | 0.03 | 0.00 |
| $Na_2O$ | 0.14 | 0.17 | 0.06 | 0.06 | 0.14 | 0.09 | 0.04 | 0.04 | 0.04 | 0.07 | 0.06 | 0.04 | 0.09 |
| $K_2O$ | 9.11 | 9.57 | 10.05 | 10.25 | 9.84 | 9.94 | 10.06 | 10.09 | 10.13 | 10.05 | 3.37 | 9.81 | 10.15 |
| NiO | 0.00 | 0.00 | 0.00 | 0.02 | 0.00 | 0.00 | 0.00 | 0.00 | 0.02 | 0.00 | 0.00 | 0.00 | 0.04 |
| F | 0.18 | 0.10 | 0.10 | 0.13 | 0.19 | 0.10 | 0.04 | 0.13 | 0.05 | 0.04 | 0.08 | 0.02 | 0.01 |
| -O=F | 0.08 | 0.04 | 0.04 | 0.05 | 0.08 | 0.04 | 0.02 | 0.06 | 0.02 | 0.02 | 0.03 | 0.01 | 0.00 |
| Cl | 0.05 | 0.03 | 0.04 | 0.01 | 0.02 | 0.04 | 0.03 | 0.03 | 0.03 | 0.00 | 0.01 | 0.03 | 0.03 |
| -O=Cl | 0.01 | 0.01 | 0.01 | 0.00 | 0.01 | 0.01 | 0.01 | 0.01 | 0.01 | 0.00 | 0.00 | 0.01 | 0.01 |
| $SO_3$ | 0.58 | 0.53 | 0.06 | 0.06 | 0.04 | 0.05 | 0.02 | 0.06 | 0.13 | 0.11 | 0.01 | 0.08 | 0.11 |
| Total | 93.17 | 94.02 | 95.06 | 95.37 | 94.81 | 95.99 | 95.46 | 95.76 | 96.23 | 96.37 | 88.52 | 96.79 | 97.04 |

Structural formulas calculated on the basis of 22 oxygens.

| | | | | | | | | | | | | | |
|---|---|---|---|---|---|---|---|---|---|---|---|---|---|
| Si | 5.61 | 5.64 | 5.62 | 5.66 | 5.69 | 5.67 | 5.65 | 5.65 | 5.60 | 5.63 | 5.18 | 5.60 | 5.61 |
| Ti | 0.34 | 0.38 | 0.37 | 0.37 | 0.32 | 0.34 | 0.39 | 0.38 | 0.35 | 0.35 | 0.19 | 0.35 | 0.36 |
| Al | 2.86 | 2.86 | 2.90 | 3.01 | 2.89 | 2.80 | 2.83 | 2.80 | 3.05 | 3.02 | 3.29 | 2.94 | 2.92 |
| Cr | 0.00 | 0.00 | 0.00 | 0.00 | 0.00 | 0.00 | 0.00 | 0.00 | 0.00 | 0.00 | 0.00 | 0.00 | 0.00 |
| $Fe_2$ | 2.74 | 2.64 | 2.77 | 2.59 | 2.75 | 2.83 | 2.82 | 2.88 | 3.03 | 3.02 | 3.95 | 2.88 | 3.08 |
| Mn | 0.08 | 0.08 | 0.08 | 0.09 | 0.08 | 0.07 | 0.08 | 0.08 | 0.13 | 0.13 | 0.13 | 0.08 | 0.08 |
| Mg | 1.83 | 1.77 | 1.80 | 1.71 | 1.86 | 1.90 | 1.77 | 1.79 | 1.32 | 1.32 | 1.81 | 1.73 | 1.47 |
| Ca | 0.07 | 0.04 | 0.00 | 0.00 | 0.00 | 0.00 | 0.00 | 0.01 | 0.00 | 0.00 | 0.08 | 0.00 | 0.00 |
| Na | 0.04 | 0.05 | 0.02 | 0.02 | 0.04 | 0.03 | 0.01 | 0.01 | 0.01 | 0.02 | 0.02 | 0.01 | 0.03 |
| K | 1.84 | 1.90 | 2.00 | 2.01 | 1.96 | 1.96 | 1.99 | 2.00 | 2.01 | 1.98 | 0.73 | 1.91 | 1.99 |
| Ni | 0.00 | 0.00 | 0.00 | 0.00 | 0.00 | 0.00 | 0.00 | 0.00 | 0.00 | 0.00 | 0.00 | 0.00 | 0.01 |
| F | 0.09 | 0.05 | 0.05 | 0.06 | 0.09 | 0.05 | 0.02 | 0.07 | 0.02 | 0.02 | 0.04 | 0.01 | 0.00 |
| Cl | 0.01 | 0.01 | 0.01 | 0.00 | 0.01 | 0.01 | 0.01 | 0.01 | 0.01 | 0.00 | 0.00 | 0.01 | 0.01 |
| S | 0.07 | 0.06 | 0.01 | 0.01 | 0.00 | 0.01 | 0.00 | 0.01 | 0.01 | 0.01 | 0.00 | 0.01 | 0.01 |

**(Table 6. 3 continued)**

**EPIDOTE**

| Sample # | ICP-114 | | | | | | | ICP-111 | | | | | | |
|---|---|---|---|---|---|---|---|---|---|---|---|---|---|---|
| Grain # | 1 | 1 | 1 | 2 | 2 | 3 | 3 | 1 | 1 | 2 | 3 | 4 | 5 | 5 |
| Analysis # | 1 | 2 | 3 | 1 | 2 | 1 | 2 | 1 | 2 | 1 | 1 | 1 | 1 | 2 |
| $SiO_2$ | 35.37 | 37.18 | 37.43 | 35.13 | 35.12 | 34.58 | 36.96 | 37.60 | 37.44 | 37.25 | 37.88 | 37.71 | 37.53 | 37.56 |
| $TiO_2$ | 0.09 | 0.12 | 0.11 | 0.09 | 0.14 | 0.08 | 0.18 | 0.12 | 0.13 | 0.22 | 0.16 | 0.13 | 0.14 | 0.12 |
| $Al_2O_3$ | 21.06 | 22.30 | 23.09 | 21.04 | 20.80 | 20.18 | 22.73 | 23.69 | 23.54 | 23.32 | 23.77 | 23.48 | 23.31 | 23.74 |
| $Cr_2O_3$ | 0.00 | 0.05 | 0.00 | 0.00 | 0.02 | 0.00 | 0.00 | 0.00 | 0.01 | 0.00 | 0.04 | 0.01 | 0.00 | 0.00 |
| FeO | 12.01 | 11.68 | 11.76 | 11.88 | 11.95 | 12.16 | 12.01 | 11.05 | 11.21 | 11.29 | 11.10 | 11.29 | 11.19 | 11.17 |
| MnO | 0.59 | 0.44 | 0.40 | 0.52 | 0.59 | 0.75 | 0.42 | 0.54 | 0.34 | 0.45 | 0.35 | 0.39 | 0.53 | 0.33 |
| MgO | 0.15 | 0.05 | 0.00 | 0.13 | 0.19 | 0.21 | 0.04 | 0.04 | 0.04 | 0.02 | 0.03 | 0.01 | 0.02 | 0.02 |
| CaO | 20.40 | 22.47 | 23.81 | 20.17 | 19.86 | 18.63 | 23.02 | 23.60 | 23.72 | 23.50 | 23.18 | 23.34 | 23.58 | 23.92 |
| $Na_2O$ | 0.01 | 0.03 | 0.00 | 0.00 | 0.01 | 0.01 | 0.00 | 0.01 | 0.02 | 0.00 | 0.02 | 0.02 | 0.00 | 0.02 |
| $K_2O$ | 0.00 | 0.00 | 0.00 | 0.00 | 0.05 | 0.00 | 0.01 | 0.00 | 0.00 | 0.01 | 0.00 | 0.01 | 0.01 | 0.00 |
| NiO | 0.01 | 0.01 | 0.01 | 0.01 | 0.01 | 0.05 | 0.00 | 0.00 | 0.01 | 0.00 | 0.00 | 0.02 | 0.02 | 0.00 |
| **Total** | **89.69** | **94.33** | **96.61** | **88.97** | **88.74** | **86.65** | **95.37** | **96.65** | **96.46** | **96.06** | **96.53** | **96.40** | **96.33** | **96.88** |

Structural formulas calculated on the basis of 12 oxygen.

| | | | | | | | | | | | | | | |
|---|---|---|---|---|---|---|---|---|---|---|---|---|---|---|
| Si | 3.02 | 3.01 | 2.96 | 3.02 | 3.02 | 3.05 | 2.97 | 2.96 | 2.96 | 2.96 | 2.98 | 2.98 | 2.97 | 2.95 |
| Ti | 0.01 | 0.01 | 0.01 | 0.01 | 0.01 | 0.01 | 0.01 | 0.01 | 0.01 | 0.01 | 0.01 | 0.01 | 0.01 | 0.01 |
| Al | 2.12 | 2.13 | 2.15 | 2.13 | 2.11 | 2.10 | 2.15 | 2.20 | 2.19 | 2.18 | 2.20 | 2.19 | 2.17 | 2.20 |
| Cr | 0.00 | 0.00 | 0.00 | 0.00 | 0.00 | 0.00 | 0.00 | 0.00 | 0.00 | 0.00 | 0.00 | 0.00 | 0.00 | 0.00 |
| $Fe_2$ | 0.86 | 0.79 | 0.78 | 0.85 | 0.86 | 0.90 | 0.81 | 0.73 | 0.74 | 0.75 | 0.73 | 0.75 | 0.74 | 0.73 |
| Mn | 0.04 | 0.03 | 0.03 | 0.04 | 0.04 | 0.06 | 0.03 | 0.04 | 0.02 | 0.03 | 0.02 | 0.03 | 0.04 | 0.02 |
| Mg | 0.02 | 0.01 | 0.00 | 0.02 | 0.02 | 0.03 | 0.00 | 0.01 | 0.01 | 0.00 | 0.00 | 0.00 | 0.00 | 0.00 |
| Ca | 1.86 | 1.95 | 2.02 | 1.86 | 1.83 | 1.76 | 1.98 | 1.99 | 2.01 | 2.00 | 1.95 | 1.97 | 2.00 | 2.02 |
| Na | 0.00 | 0.01 | 0.00 | 0.00 | 0.00 | 0.00 | 0.00 | 0.00 | 0.00 | 0.00 | 0.00 | 0.00 | 0.00 | 0.00 |
| K | 0.00 | 0.00 | 0.00 | 0.00 | 0.01 | 0.00 | 0.00 | 0.00 | 0.00 | 0.00 | 0.00 | 0.00 | 0.00 | 0.00 |
| Ni | 0.00 | 0.00 | 0.00 | 0.00 | 0.00 | 0.00 | 0.00 | 0.00 | 0.00 | 0.00 | 0.00 | 0.00 | 0.00 | 0.00 |

**EPIDOTE**

| Sample # | | ICP-111 | | | | | | | | | | | |
|---|---|---|---|---|---|---|---|---|---|---|---|---|---|
| Grain # | 1 | 1 | 2 | 2 | 2 | 3 | 3 | 4 | 5 | 6 | 7 | 8 | 8 |
| Analysis # | 1 | 2 | 1 | 2 | 3 | 1 | 2 | 1 | 1 | 1 | 1 | 1 | 2 |
| $SiO_2$ | 37.52 | 37.89 | 38.09 | 38.15 | 38.04 | 38.16 | 38.16 | 38.08 | 37.63 | 36.05 | 38.19 | 37.66 | 37.94 |
| $TiO_2$ | 0.11 | 0.12 | 0.12 | 0.19 | 0.22 | 0.18 | 0.14 | 0.11 | 0.15 | 0.20 | 0.13 | 0.12 | 0.11 |
| $Al_2O_3$ | 23.66 | 23.31 | 22.79 | 22.57 | 22.52 | 22.63 | 22.42 | 22.36 | 22.21 | 22.50 | 22.64 | 22.19 | 22.14 |
| FeO | 10.97 | 11.06 | 11.10 | 11.52 | 11.05 | 10.94 | 11.06 | 10.96 | 10.90 | 11.14 | 11.18 | 11.24 | 10.85 |
| MnO | 0.38 | 0.47 | 0.36 | 0.47 | 0.42 | 0.40 | 0.35 | 0.40 | 0.35 | 0.37 | 0.38 | 0.44 | 0.38 |
| MgO | 0.06 | 0.04 | 0.01 | 0.02 | 0.04 | 0.02 | 0.03 | 0.04 | 0.02 | 0.12 | 0.03 | 0.04 | 0.04 |
| CaO | 23.14 | 23.51 | 23.33 | 23.11 | 23.30 | 23.28 | 23.10 | 23.22 | 23.16 | 23.03 | 23.17 | 23.32 | 23.56 |
| $ZrO_2$ | 0.00 | 0.00 | 0.00 | 0.04 | 0.00 | 0.03 | 0.04 | 0.00 | 0.00 | 0.00 | 0.00 | 0.05 | 0.02 |
| $HfO_2$ | 0.09 | 0.09 | 0.00 | 0.06 | 0.00 | 0.00 | 0.13 | 0.00 | 0.00 | 0.00 | 0.11 | 0.00 | 0.02 |
| $La_2O_3$ | 0.00 | 0.00 | 0.04 | 0.03 | 0.00 | 0.10 | 0.00 | 0.10 | 0.00 | 0.00 | 0.04 | 0.04 | 0.00 |
| $Ce_2O_3$ | 0.18 | 0.04 | 0.03 | 0.06 | 0.01 | 0.07 | 0.00 | 0.12 | 0.00 | 0.08 | 0.03 | 0.05 | 0.07 |
| $Nb_2O_5$ | 0.00 | 0.00 | 0.00 | 0.00 | 0.00 | 0.00 | 0.06 | 0.03 | 0.00 | 0.00 | 0.00 | 0.00 | 0.02 |
| $Ta_2O_5$ | 0.00 | 0.00 | 0.08 | 0.00 | 0.00 | 0.00 | 0.19 | 0.00 | 0.04 | 0.00 | 0.00 | 0.00 | 0.00 |
| $Y_2O_3$ | 0.52 | 0.27 | 0.00 | 0.02 | 0.11 | 0.00 | 0.01 | 0.11 | 0.00 | 0.07 | 0.07 | 0.02 | 0.00 |
| $Yb_2O_3$ | 0.00 | 0.15 | 0.01 | 0.00 | 0.05 | 0.00 | 0.01 | 0.00 | 0.03 | 0.11 | 0.06 | 0.00 | 0.01 |
| $P_2O_5$ | 0.04 | 0.03 | 0.00 | 0.00 | 0.03 | 0.02 | 0.04 | 0.02 | 0.03 | 0.01 | 0.03 | 0.00 | 0.03 |
| **Total** | **96.67** | **96.98** | **95.96** | **96.24** | **95.79** | **95.83** | **95.74** | **95.55** | **94.52** | **93.68** | **96.06** | **95.17** | **95.19** |
| Structural formulas calculated on the basis of 12 oxygens. | | | | | | | | | | | | | |
| Si | 2.961 | 2.982 | 3.020 | 3.022 | 3.022 | 3.028 | 3.035 | 3.035 | 3.028 | 2.946 | 3.028 | 3.019 | 3.03 |
| Ti | 0.006 | 0.007 | 0.007 | 0.012 | 0.013 | 0.011 | 0.008 | 0.007 | 0.009 | 0.012 | 0.008 | 0.007 | 0.01 |
| Al | 2.201 | 2.162 | 2.129 | 2.108 | 2.109 | 2.117 | 2.101 | 2.100 | 2.107 | 2.168 | 2.115 | 2.097 | 2.09 |
| $Fe_2$ | 0.724 | 0.728 | 0.736 | 0.763 | 0.734 | 0.726 | 0.736 | 0.730 | 0.733 | 0.761 | 0.741 | 0.753 | 0.73 |
| Mn | 0.025 | 0.032 | 0.024 | 0.032 | 0.028 | 0.027 | 0.023 | 0.027 | 0.024 | 0.025 | 0.025 | 0.030 | 0.03 |
| Mg | 0.007 | 0.004 | 0.001 | 0.002 | 0.005 | 0.002 | 0.004 | 0.005 | 0.003 | 0.015 | 0.003 | 0.005 | 0.01 |
| Ca | 1.956 | 1.982 | 1.982 | 1.962 | 1.984 | 1.979 | 1.968 | 1.983 | 1.997 | 2.017 | 1.968 | 2.003 | 2.02 |
| Zr | 0.000 | 0.000 | 0.000 | 0.002 | 0.000 | 0.001 | 0.002 | 0.000 | 0.000 | 0.000 | 0.000 | 0.002 | 0.00 |
| Hf | 0.002 | 0.002 | 0.000 | 0.001 | 0.000 | 0.000 | 0.003 | 0.000 | 0.000 | 0.000 | 0.003 | 0.000 | 0.00 |
| La | 0.000 | 0.000 | 0.001 | 0.001 | 0.000 | 0.003 | 0.000 | 0.003 | 0.000 | 0.000 | 0.001 | 0.001 | 0.00 |
| Ce | 0.005 | 0.001 | 0.001 | 0.002 | 0.000 | 0.002 | 0.000 | 0.003 | 0.000 | 0.002 | 0.001 | 0.002 | 0.00 |
| Nb | 0.000 | 0.000 | 0.000 | 0.000 | 0.000 | 0.000 | 0.002 | 0.001 | 0.000 | 0.000 | 0.000 | 0.000 | 0.00 |
| Ta | 0.000 | 0.000 | 0.002 | 0.000 | 0.000 | 0.000 | 0.004 | 0.000 | 0.001 | 0.000 | 0.000 | 0.000 | 0.00 |
| Y | 0.022 | 0.011 | 0.000 | 0.001 | 0.005 | 0.000 | 0.000 | 0.005 | 0.000 | 0.003 | 0.003 | 0.001 | 0.00 |
| Yb | 0.000 | 0.003 | 0.000 | 0.000 | 0.001 | 0.000 | 0.000 | 0.000 | 0.001 | 0.003 | 0.002 | 0.000 | 0.00 |
| P | 0.002 | 0.002 | 0.000 | 0.000 | 0.002 | 0.002 | 0.003 | 0.001 | 0.002 | 0.001 | 0.002 | 0.000 | 0.00 |

| Sample # | ICP-111 | | | | ICP-114 | | | | | | | |
|---|---|---|---|---|---|---|---|---|---|---|---|---|
| Grain # | 1 | 2 | 3 | 3 | 1 | 1 | 1 | 2 | 2 | 3 | 3 | 4 |
| Analysis # | 1 | 1 | 1 | 2 | 1 | 2 | 3 | 1 | 2 | 1 | 2 | 1 |
| $SiO_2$ | 38.43 | 39.01 | 37.94 | 37.89 | 38.39 | 38.26 | 38.10 | 36.84 | 38.24 | 38.33 | 38.15 | 38.32 |
| $TiO_2$ | 0.18 | 0.13 | 0.12 | 0.16 | 0.11 | 0.15 | 0.11 | 0.06 | 0.12 | 0.17 | 0.23 | 0.13 |
| $Al_2O_3$ | 22.24 | 22.45 | 22.37 | 22.61 | 23.05 | 22.76 | 22.76 | 22.17 | 22.08 | 21.88 | 22.03 | 22.24 |
| FeO | 11.90 | 12.16 | 11.10 | 10.74 | 11.52 | 11.53 | 11.84 | 11.56 | 11.39 | 11.60 | 12.27 | 11.36 |
| MnO | 0.59 | 0.58 | 0.47 | 0.38 | 0.37 | 0.49 | 0.43 | 0.36 | 0.38 | 0.45 | 0.52 | 0.38 |
| MgO | 0.01 | 0.01 | 0.06 | 0.03 | 0.02 | 0.04 | 0.02 | 0.02 | 0.02 | 0.03 | 0.03 | 0.04 |
| CaO | 22.61 | 22.97 | 22.79 | 23.31 | 23.10 | 22.81 | 23.35 | 23.48 | 23.02 | 22.98 | 23.16 | 22.95 |
| $ZrO_2$ | 0.01 | 0.09 | 0.07 | 0.08 | 0.00 | 0.03 | 0.00 | 0.00 | 0.00 | 0.00 | 0.05 | 0.00 |
| $HfO_2$ | 0.00 | 0.20 | 0.08 | 0.09 | 0.00 | 0.00 | 0.06 | 0.01 | 0.00 | 0.05 | 0.08 | 0.00 |
| $La_2O_3$ | 0.08 | 0.00 | 0.00 | 0.04 | 0.04 | 0.13 | 0.07 | 0.02 | 0.00 | 0.00 | 0.00 | 0.00 |
| $Ce_2O_3$ | 0.01 | 0.11 | 0.12 | 0.06 | 0.00 | 0.09 | 0.05 | 0.09 | 0.01 | 0.01 | 0.01 | 0.09 |
| $Nb_2O_5$ | 0.10 | 0.00 | 0.00 | 0.00 | 0.00 | 0.03 | 0.01 | 0.04 | 0.00 | 0.02 | 0.00 | 0.00 |
| $Ta_2O_5$ | 0.03 | 0.00 | 0.00 | 0.07 | 0.10 | 0.00 | 0.00 | 0.04 | 0.07 | 0.05 | 0.00 | 0.00 |
| $Y_2O_3$ | 0.00 | 0.00 | 0.32 | 0.04 | 0.11 | 0.18 | 0.07 | 0.10 | 0.04 | 0.09 | 0.05 | 0.06 |
| $Yb_2O_3$ | 0.01 | 0.00 | 0.01 | 0.09 | 0.07 | 0.07 | 0.03 | 0.00 | 0.20 | 0.02 | 0.03 | 0.00 |
| $P_2O_5$ | 0.00 | 0.00 | 0.03 | 0.00 | 0.02 | 0.01 | 0.00 | 0.06 | 0.00 | 0.03 | 0.04 | 0.01 |
| **Total** | **96.20** | **97.71** | **95.48** | **95.59** | **96.80** | **96.58** | **96.80** | **94.84** | **95.57** | **95.71** | **96.65** | **95.58** |

Structural formulas calculated on the basis of 12 oxygens.

| | | | | | | | | | | | | |
|---|---|---|---|---|---|---|---|---|---|---|---|---|
| Si | 3.05 | 3.05 | 3.03 | 3.02 | 3.02 | 3.02 | 3.01 | 2.98 | 3.05 | 3.05 | 3.02 | 3.05 |
| Ti | 0.01 | 0.01 | 0.01 | 0.01 | 0.01 | 0.01 | 0.01 | 0.00 | 0.01 | 0.01 | 0.01 | 0.01 |
| Al | 2.08 | 2.07 | 2.10 | 2.12 | 2.14 | 2.12 | 2.12 | 2.11 | 2.08 | 2.06 | 2.06 | 2.09 |
| $Fe_2$ | 0.79 | 0.80 | 0.74 | 0.72 | 0.76 | 0.76 | 0.78 | 0.78 | 0.76 | 0.77 | 0.81 | 0.76 |
| Mn | 0.04 | 0.04 | 0.03 | 0.03 | 0.02 | 0.03 | 0.03 | 0.02 | 0.03 | 0.03 | 0.03 | 0.03 |
| Mg | 0.00 | 0.00 | 0.01 | 0.00 | 0.00 | 0.00 | 0.00 | 0.00 | 0.00 | 0.00 | 0.00 | 0.00 |
| Ca | 1.92 | 1.92 | 1.95 | 1.99 | 1.95 | 1.93 | 1.97 | 2.03 | 1.97 | 1.96 | 1.97 | 1.96 |
| Zr | 0.00 | 0.00 | 0.00 | 0.00 | 0.00 | 0.00 | 0.00 | 0.00 | 0.00 | 0.00 | 0.00 | 0.00 |
| Hf | 0.00 | 0.00 | 0.00 | 0.00 | 0.00 | 0.00 | 0.00 | 0.00 | 0.00 | 0.00 | 0.00 | 0.00 |
| La | 0.00 | 0.00 | 0.00 | 0.00 | 0.00 | 0.00 | 0.00 | 0.00 | 0.00 | 0.00 | 0.00 | 0.00 |
| Ce | 0.00 | 0.00 | 0.00 | 0.00 | 0.00 | 0.00 | 0.00 | 0.00 | 0.00 | 0.00 | 0.00 | 0.00 |
| Nb | 0.00 | 0.00 | 0.00 | 0.00 | 0.00 | 0.00 | 0.00 | 0.00 | 0.00 | 0.00 | 0.00 | 0.00 |
| Ta | 0.00 | 0.00 | 0.00 | 0.00 | 0.00 | 0.00 | 0.00 | 0.00 | 0.00 | 0.00 | 0.00 | 0.00 |
| Y | 0.00 | 0.00 | 0.01 | 0.00 | 0.00 | 0.01 | 0.00 | 0.00 | 0.00 | 0.00 | 0.00 | 0.00 |
| Yb | 0.00 | 0.00 | 0.00 | 0.00 | 0.00 | 0.00 | 0.00 | 0.00 | 0.00 | 0.00 | 0.00 | 0.00 |
| P | 0.00 | 0.00 | 0.00 | 0.00 | 0.00 | 0.00 | 0.00 | 0.00 | 0.00 | 0.00 | 0.00 | 0.00 |

**ALLANITE**

| Sample # | ICP-114 | | | | | | | | | | | | ICP-111 | | | |
|---|---|---|---|---|---|---|---|---|---|---|---|---|---|---|---|---|
| Grain # | 1 | 1 | 2 | 3 | 3 | 4 | 5 | 6 | 7 | 7 | 8 | 9 | 1 | 1 | 2 | 3 |
| Analysis | 1 | 2 | 1 | 1 | 2 | 1 | 1 | 1 | 1 | 2 | 1 | 1 | 1 | 2 | 1 | 1 |
| $SiO_2$ | 34.35 | 34.83 | 33.85 | 34.01 | 33.68 | 33.73 | 34.53 | 33.58 | 34.08 | 34.12 | 33.95 | 34.05 | 33.60 | 33.69 | 33.95 | 34.09 |
| $TiO_2$ | 0.12 | 0.17 | 0.12 | 0.13 | 0.14 | 0.14 | 0.19 | 0.08 | 0.16 | 0.14 | 0.16 | 0.15 | 0.14 | 0.16 | 0.18 | 0.12 |
| $Al_2O_3$ | 18.52 | 18.44 | 18.40 | 18.42 | 18.27 | 17.55 | 18.11 | 17.16 | 17.69 | 17.78 | 17.85 | 18.02 | 17.34 | 17.86 | 17.97 | 18.18 |
| FeO | 12.53 | 12.79 | 12.46 | 12.70 | 12.54 | 12.94 | 13.33 | 12.61 | 12.88 | 12.72 | 12.55 | 12.89 | 12.43 | 12.44 | 12.43 | 12.64 |
| MnO | 0.42 | 0.42 | 0.42 | 0.40 | 0.45 | 0.52 | 0.60 | 0.30 | 0.60 | 0.48 | 0.39 | 0.47 | 0.59 | 0.84 | 0.86 | 0.40 |
| MgO | 0.50 | 0.51 | 0.45 | 0.45 | 0.44 | 0.48 | 0.33 | 0.49 | 0.41 | 0.46 | 0.43 | 0.46 | 0.53 | 0.50 | 0.45 | 0.48 |
| CaO | 15.08 | 15.16 | 15.36 | 15.62 | 15.16 | 14.93 | 16.14 | 14.77 | 15.18 | 15.29 | 15.39 | 14.92 | 14.97 | 15.31 | 15.69 | 15.20 |
| $ZrO_2$ | 0.04 | 0.00 | 0.06 | 0.00 | 0.00 | 0.04 | 0.04 | 0.02 | 0.00 | 0.00 | 0.01 | 0.00 | 0.00 | 0.05 | 0.00 | 0.00 |
| $HfO_2$ | 0.00 | 0.06 | 0.06 | 0.02 | 0.02 | 0.01 | 0.14 | 0.00 | 0.00 | 0.00 | 0.01 | 0.00 | 0.05 | 0.00 | 0.16 | 0.00 |
| $La_2O_3$ | 2.77 | 2.99 | 2.67 | 3.03 | 3.11 | 3.30 | 2.69 | 2.81 | 2.83 | 2.95 | 3.27 | 3.06 | 3.01 | 2.69 | 2.19 | 3.16 |
| $Ce_2O_3$ | 5.16 | 6.07 | 5.81 | 5.78 | 6.09 | 5.88 | 5.31 | 5.91 | 6.00 | 5.97 | 6.17 | 6.25 | 5.30 | 5.23 | 4.61 | 5.86 |
| $Nb_2O_5$ | 0.00 | 0.00 | 0.00 | 0.00 | 0.05 | 0.00 | 0.00 | 0.05 | 0.05 | 0.02 | 0.08 | 0.08 | 0.00 | 0.01 | 0.05 | 0.03 |
| $Ta_2O_5$ | 0.05 | 0.00 | 0.00 | 0.02 | 0.00 | 0.02 | 0.14 | 0.02 | 0.00 | 0.22 | 0.00 | 0.00 | 0.06 | 0.00 | 0.00 | 0.12 |
| $Y_2O_3$ | 0.11 | 0.10 | 0.11 | 0.10 | 0.13 | 0.02 | 0.20 | 0.08 | 0.09 | 0.08 | 0.07 | 0.10 | 0.05 | 0.30 | 0.50 | 0.03 |
| $Yb_2O_3$ | 0.05 | 0.03 | 0.09 | 0.00 | 0.07 | 0.00 | 0.00 | 0.07 | 0.00 | 0.07 | 0.00 | 0.06 | 0.00 | 0.00 | 0.06 | 0.07 |
| $P_2O_5$ | 0.00 | 0.09 | 0.04 | 0.05 | 0.10 | 0.19 | 0.15 | 0.12 | 0.03 | 0.04 | 0.09 | 0.11 | 0.11 | 0.06 | 0.04 | 0.04 |
| **Total** | **89.70** | **91.66** | **89.90** | **90.73** | **90.25** | **89.75** | **91.90** | **88.07** | **90.00** | **90.34** | **90.42** | **90.62** | **88.18** | **89.14** | **89.14** | **90.41** |

Structural formulas calculated on the basis of 12 oxygens.

| | | | | | | | | | | | | | | | | |
|---|---|---|---|---|---|---|---|---|---|---|---|---|---|---|---|---|
| Si | 3.08 | 3.08 | 3.05 | 3.04 | 3.04 | 3.06 | 3.05 | 3.09 | 3.08 | 3.07 | 3.06 | 3.06 | 3.08 | 3.06 | 3.06 | 3.06 |
| Ti | 0.01 | 0.01 | 0.01 | 0.01 | 0.01 | 0.01 | 0.01 | 0.01 | 0.01 | 0.01 | 0.01 | 0.01 | 0.01 | 0.01 | 0.01 | 0.01 |
| Al | 1.96 | 1.92 | 1.95 | 1.94 | 1.94 | 1.88 | 1.88 | 1.86 | 1.88 | 1.89 | 1.90 | 1.91 | 1.88 | 1.91 | 1.91 | 1.92 |
| $Fe_2$ | 0.94 | 0.94 | 0.94 | 0.95 | 0.95 | 0.98 | 0.98 | 0.97 | 0.97 | 0.96 | 0.95 | 0.97 | 0.95 | 0.94 | 0.94 | 0.95 |
| Mn | 0.03 | 0.03 | 0.03 | 0.03 | 0.03 | 0.04 | 0.05 | 0.02 | 0.05 | 0.04 | 0.03 | 0.04 | 0.05 | 0.06 | 0.07 | 0.03 |
| Mg | 0.07 | 0.07 | 0.06 | 0.06 | 0.06 | 0.06 | 0.04 | 0.07 | 0.06 | 0.06 | 0.06 | 0.06 | 0.07 | 0.07 | 0.06 | 0.06 |
| Ca | 1.45 | 1.43 | 1.48 | 1.50 | 1.46 | 1.45 | 1.53 | 1.46 | 1.47 | 1.48 | 1.49 | 1.44 | 1.47 | 1.49 | 1.52 | 1.46 |
| Zr | 0.00 | 0.00 | 0.00 | 0.00 | 0.00 | 0.00 | 0.00 | 0.00 | 0.00 | 0.00 | 0.00 | 0.00 | 0.00 | 0.00 | 0.00 | 0.00 |
| Hf | 0.00 | 0.00 | 0.00 | 0.00 | 0.00 | 0.00 | 0.00 | 0.00 | 0.00 | 0.00 | 0.00 | 0.00 | 0.00 | 0.00 | 0.00 | 0.00 |
| La | 0.09 | 0.10 | 0.09 | 0.10 | 0.10 | 0.11 | 0.09 | 0.10 | 0.09 | 0.10 | 0.11 | 0.10 | 0.10 | 0.09 | 0.07 | 0.10 |
| Ce | 0.17 | 0.20 | 0.19 | 0.19 | 0.20 | 0.20 | 0.17 | 0.20 | 0.20 | 0.20 | 0.20 | 0.21 | 0.18 | 0.17 | 0.15 | 0.19 |
| Nb | 0.00 | 0.00 | 0.00 | 0.00 | 0.00 | 0.00 | 0.00 | 0.00 | 0.00 | 0.00 | 0.00 | 0.00 | 0.00 | 0.00 | 0.00 | 0.00 |
| Ta | 0.00 | 0.00 | 0.00 | 0.00 | 0.00 | 0.00 | 0.00 | 0.00 | 0.00 | 0.01 | 0.00 | 0.00 | 0.00 | 0.00 | 0.00 | 0.00 |
| Y | 0.01 | 0.00 | 0.01 | 0.00 | 0.01 | 0.00 | 0.01 | 0.00 | 0.00 | 0.00 | 0.00 | 0.00 | 0.00 | 0.01 | 0.02 | 0.00 |
| Yb | 0.00 | 0.00 | 0.00 | 0.00 | 0.00 | 0.00 | 0.00 | 0.00 | 0.00 | 0.00 | 0.00 | 0.00 | 0.00 | 0.00 | 0.00 | 0.00 |
| P | 0.00 | 0.01 | 0.00 | 0.00 | 0.01 | 0.01 | 0.01 | 0.01 | 0.00 | 0.00 | 0.01 | 0.01 | 0.01 | 0.00 | 0.00 | 0.00 |

| Sample # | ICP-114 | | | | | | | | | | | | | | |
|---|---|---|---|---|---|---|---|---|---|---|---|---|---|---|---|
| Grain # | 1 | 2 | 3 | 3 | 4 | 4 | 4 | 5 | 6 | 7 | 8 | 8 | 9 | 9 | 10 |
| Analysis | 1 | 1 | 1 | 2 | 1 | 2 | 3 | 1 | 1 | 1 | 1 | 2 | 1 | 2 | 1 |
| $SiO_2$ | 31.93 | 32.59 | 32.96 | 32.71 | 31.78 | 32.21 | 31.87 | 32.41 | 32.36 | 32.66 | 34.34 | 31.77 | 32.44 | 31.82 | 32.12 |
| $TiO_2$ | 0.13 | 0.09 | 0.13 | 0.07 | 0.13 | 0.17 | 0.12 | 0.19 | 0.17 | 0.11 | 0.11 | 0.11 | 0.11 | 0.10 | 0.16 |
| $Al_2O_3$ | 17.60 | 17.84 | 18.12 | 18.02 | 17.34 | 17.61 | 17.11 | 17.62 | 17.28 | 17.90 | 19.83 | 17.11 | 17.54 | 17.27 | 17.44 |
| $Cr_2O_3$ | 0.00 | 0.00 | 0.00 | 0.00 | 0.00 | 0.00 | 0.00 | 0.00 | 0.00 | 0.00 | 0.00 | 0.00 | 0.00 | 0.00 | 0.00 |
| FeO | 13.03 | 12.95 | 13.13 | 12.71 | 12.63 | 13.10 | 13.37 | 12.95 | 13.47 | 12.91 | 12.07 | 13.39 | 12.86 | 12.74 | 12.99 |
| MnO | 0.43 | 0.34 | 0.49 | 0.41 | 0.31 | 0.30 | 0.41 | 0.46 | 0.49 | 0.34 | 0.68 | 0.54 | 0.42 | 0.42 | 0.37 |
| MgO | 0.46 | 0.41 | 0.41 | 0.43 | 0.38 | 0.41 | 0.39 | 0.45 | 0.41 | 0.38 | 0.22 | 0.39 | 0.46 | 0.44 | 0.42 |
| CaO | 15.57 | 16.00 | 15.75 | 15.96 | 15.87 | 15.50 | 15.31 | 15.56 | 15.64 | 16.00 | 18.67 | 15.31 | 15.71 | 15.60 | 15.65 |
| $Na_2O$ | 0.03 | 0.00 | 0.00 | 0.00 | 0.00 | 0.01 | 0.00 | 0.02 | 0.03 | 0.01 | 0.02 | 0.00 | 0.00 | 0.01 | 0.03 |
| $K_2O$ | 0.00 | 0.00 | 0.00 | 0.00 | 0.01 | 0.00 | 0.00 | 0.00 | 0.01 | 0.00 | 0.01 | 0.00 | 0.00 | 0.00 | 0.02 |
| NiO | 0.00 | 0.02 | 0.02 | 0.00 | 0.03 | 0.04 | 0.00 | 0.03 | 0.01 | 0.00 | 0.00 | 0.04 | 0.00 | 0.00 | 0.00 |
| **Total** | **79.18** | **80.24** | **81.01** | **80.31** | **78.48** | **79.35** | **78.58** | **79.69** | **79.87** | **80.31** | **85.95** | **78.66** | **79.54** | **78.40** | **79.20** |

Structural formulas calculated on the basis of 12 oxygens.

| | | | | | | | | | | | | | | | |
|---|---|---|---|---|---|---|---|---|---|---|---|---|---|---|---|
| Si | 3.09 | 3.11 | 3.11 | 3.11 | 3.10 | 3.11 | 3.12 | 3.11 | 3.12 | 3.11 | 3.56 | 3.05 | 3.11 | 3.12 | 2.97 |
| Ti | 0.01 | 0.01 | 0.01 | 0.01 | 0.01 | 0.01 | 0.01 | 0.01 | 0.01 | 0.01 | 0.00 | 0.01 | 0.01 | 0.01 | 0.01 |
| Al | 2.01 | 2.01 | 2.02 | 2.02 | 2.00 | 2.00 | 1.97 | 2.00 | 1.96 | 2.01 | 2.58 | 2.08 | 1.97 | 1.99 | 2.16 |
| Cr | 0.00 | 0.00 | 0.00 | 0.00 | 0.00 | 0.00 | 0.00 | 0.00 | 0.00 | 0.00 | 0.00 | 0.00 | 0.00 | 0.00 | 0.00 |
| $Fe_2$ | 1.06 | 1.03 | 1.04 | 1.01 | 1.03 | 1.06 | 1.09 | 1.04 | 1.09 | 1.03 | 0.92 | 0.90 | 1.10 | 1.04 | 0.77 |
| Mn | 0.04 | 0.03 | 0.04 | 0.03 | 0.03 | 0.02 | 0.03 | 0.04 | 0.04 | 0.03 | 0.03 | 0.05 | 0.04 | 0.03 | 0.03 |
| Mg | 0.07 | 0.06 | 0.06 | 0.06 | 0.06 | 0.06 | 0.06 | 0.06 | 0.06 | 0.05 | 0.00 | 0.03 | 0.06 | 0.07 | 0.00 |
| Ca | 1.62 | 1.64 | 1.59 | 1.63 | 1.66 | 1.60 | 1.60 | 1.60 | 1.61 | 1.63 | 2.44 | 1.78 | 1.60 | 1.62 | 2.02 |
| Na | 0.01 | 0.00 | 0.00 | 0.00 | 0.00 | 0.00 | 0.00 | 0.00 | 0.01 | 0.00 | 0.00 | 0.00 | 0.00 | 0.00 | 0.00 |
| K | 0.00 | 0.00 | 0.00 | 0.00 | 0.00 | 0.00 | 0.00 | 0.00 | 0.00 | 0.00 | 0.00 | 0.00 | 0.00 | 0.00 | 0.00 |
| Ni | 0.00 | 0.00 | 0.00 | 0.00 | 0.00 | 0.00 | 0.00 | 0.00 | 0.00 | 0.00 | 0.00 | 0.00 | 0.00 | 0.00 | 0.00 |

(Table 6. 3 continued)

**ILMENITE**

| Sample # | ICP-114 | | | | | | | ICP-111 | |
|---|---|---|---|---|---|---|---|---|---|
| Grain # | 1 | 2 | 3 | 4 | 5 | 6 | 7 | 1 | 2 |
| Analysis # | 1 | 1 | 1 | 1 | 1 | 1 | 1 | 1 | 1 |
| $SiO_2$ | 0.00 | 0.00 | 0.00 | 0.03 | 0.00 | 0.00 | 0.00 | 0.02 | 0.00 |
| $TiO_2$ | 51.72 | 51.44 | 50.13 | 50.60 | 49.90 | 51.14 | 52.16 | 47.84 | 47.68 |
| $Al_2O_3$ | 0.05 | 0.03 | 0.03 | 0.09 | 0.10 | 0.04 | 0.04 | 0.05 | 0.06 |
| FeO | 27.44 | 26.82 | 26.54 | 33.10 | 31.75 | 33.06 | 32.58 | 44.36 | 43.77 |
| MnO | 19.34 | 20.13 | 19.24 | 16.36 | 15.57 | 15.31 | 15.56 | 4.56 | 4.50 |
| MgO | 0.00 | 0.00 | 0.01 | 0.08 | 0.06 | 0.09 | 0.10 | 0.02 | 0.00 |
| CaO | 0.04 | 0.01 | 0.05 | 0.00 | 0.00 | 0.00 | 0.00 | 0.05 | 0.06 |
| $ZrO_2$ | 0.00 | 0.00 | 0.00 | 0.00 | 0.00 | 0.00 | 0.00 | 0.00 | 0.00 |
| $HfO_2$ | 0.00 | 0.00 | 0.00 | 0.01 | 0.08 | 0.00 | 0.04 | 0.00 | 0.00 |
| $La_2O_3$ | 0.03 | 0.00 | 0.00 | 0.00 | 0.00 | 0.00 | 0.00 | 0.06 | 0.00 |
| $Ce_2O_3$ | 0.00 | 0.00 | 0.02 | 0.10 | 0.01 | 0.01 | 0.00 | 0.00 | 0.00 |
| $Nb_2O_5$ | 0.00 | 0.10 | 0.00 | 0.00 | 0.00 | 0.07 | 0.00 | 0.19 | 0.26 |
| $Ta_2O_5$ | 0.02 | 0.13 | 0.00 | 0.00 | 0.08 | 0.00 | 0.00 | 0.00 | 0.13 |
| $Y_2O_3$ | 0.02 | 0.06 | 0.00 | 0.00 | 0.01 | 0.02 | 0.00 | 0.02 | 0.00 |
| $Yb_2O_3$ | 0.00 | 0.06 | 0.02 | 0.00 | 0.00 | 0.00 | 0.00 | 0.00 | 0.00 |
| $P_2O_5$ | 0.02 | 0.02 | 0.00 | 0.00 | 0.00 | 0.00 | 0.00 | 0.00 | 0.00 |
| Total | 98.68 | 98.80 | 96.04 | 100.37 | 97.56 | 99.74 | 100.48 | 97.17 | 96.44 |
| Structural formulas calculated on the basis of 6 oxygens. | | | | | | | | | |
| Si | 0.00 | 0.00 | 0.00 | 0.00 | 0.00 | 0.00 | 0.00 | 0.00 | 0.00 |
| Ti | 1.99 | 1.98 | 1.98 | 1.93 | 1.95 | 1.96 | 1.98 | 1.90 | 1.91 |
| Al | 0.00 | 0.00 | 0.00 | 0.01 | 0.01 | 0.00 | 0.00 | 0.00 | 0.00 |
| $Fe_2$ | 1.17 | 1.15 | 1.17 | 1.41 | 1.38 | 1.41 | 1.37 | 1.96 | 1.95 |
| Mn | 0.84 | 0.87 | 0.86 | 0.70 | 0.69 | 0.66 | 0.66 | 0.20 | 0.20 |
| Mg | 0.00 | 0.00 | 0.00 | 0.01 | 0.00 | 0.01 | 0.01 | 0.00 | 0.00 |
| Ca | 0.00 | 0.00 | 0.00 | 0.00 | 0.00 | 0.00 | 0.00 | 0.00 | 0.00 |
| Zr | 0.00 | 0.00 | 0.00 | 0.00 | 0.00 | 0.00 | 0.00 | 0.00 | 0.00 |
| Hf | 0.00 | 0.00 | 0.00 | 0.00 | 0.00 | 0.00 | 0.00 | 0.00 | 0.00 |
| La | 0.00 | 0.00 | 0.00 | 0.00 | 0.00 | 0.00 | 0.00 | 0.00 | 0.00 |
| Ce | 0.00 | 0.00 | 0.00 | 0.00 | 0.00 | 0.00 | 0.00 | 0.00 | 0.00 |
| Nb | 0.00 | 0.00 | 0.00 | 0.00 | 0.00 | 0.00 | 0.00 | 0.00 | 0.01 |
| Ta | 0.00 | 0.00 | 0.00 | 0.00 | 0.00 | 0.00 | 0.00 | 0.00 | 0.00 |
| Y | 0.00 | 0.00 | 0.00 | 0.00 | 0.00 | 0.00 | 0.00 | 0.00 | 0.00 |
| Yb | 0.00 | 0.00 | 0.00 | 0.00 | 0.00 | 0.00 | 0.00 | 0.00 | 0.00 |
| P | 0.00 | 0.00 | 0.00 | 0.00 | 0.00 | 0.00 | 0.00 | 0.00 | 0.00 |

(Table 6. 3 continued)

| ILMENITE | | | | | | MAGNETITE | | | |
|---|---|---|---|---|---|---|---|---|---|
| Sample # | ICP-114 | | | | | | | | |
| Grain # | 1 | 2 | 2 | 3 | 3 | 1 | 1 | 1 | 2 |
| Analysis # | 1 | 1 | 2 | 1 | 2 | 1 | 2 | 3 | 1 |
| $SiO_2$ | 0.00 | 0.07 | 0.00 | 0.00 | 0.00 | 0.00 | 0.02 | 0.00 | 0.05 |
| $TiO_2$ | 50.89 | 51.84 | 51.76 | 51.48 | 50.78 | 0.06 | 0.08 | 0.03 | 13.98 |
| $Al_2O_3$ | 0.00 | 0.01 | 0.02 | 0.01 | 0.02 | 0.03 | 0.04 | 0.03 | 0.05 |
| $Cr_2O_3$ | 0.00 | 0.00 | 0.04 | 0.01 | 0.00 | 0.00 | 0.00 | 0.00 | 0.00 |
| $Fe_2O_3$ | 2.02 | 0.75 | 1.12 | 0.95 | 2.02 | 68.21 | 67.52 | 67.57 | 37.74 |
| FeO | 25.85 | 27.48 | 28.56 | 27.61 | 27.96 | 30.39 | 30.44 | 30.38 | 41.71 |
| MnO | 19.44 | 19.66 | 18.62 | 19.74 | 19.59 | 0.17 | 0.11 | 0.10 | 0.35 |
| MgO | 0.01 | 0.00 | 0.00 | 0.00 | 0.00 | 0.01 | 0.01 | 0.00 | 0.00 |
| CaO | 0.06 | 0.15 | 0.04 | 0.03 | 0.04 | 0.00 | 0.00 | 0.00 | 0.13 |
| $Na_2O$ | 0.02 | 0.02 | 0.03 | 0.02 | 0.01 | 0.04 | 0.00 | 0.00 | 0.00 |
| $K_2O$ | 0.00 | 0.00 | 0.00 | 0.00 | 0.03 | 0.01 | 0.00 | 0.00 | 0.00 |
| NiO | 0.02 | 0.00 | 0.00 | 0.00 | 0.00 | 0.00 | 0.03 | 0.00 | 0.03 |
| **Total** | **98.31** | **99.98** | **100.19** | **99.85** | **100.45** | **98.92** | **98.25** | **98.11** | **94.04** |

Structural formulas calculated on the basis of 6 and 32 oxygen for mangano-ilmenite and magnetite respectively.

| | | | | | | | | | |
|---|---|---|---|---|---|---|---|---|---|
| Si | 0.00 | 0.00 | 0.00 | 0.00 | 0.00 | 0.00 | 0.01 | 0.00 | 0.02 |
| Ti | 1.97 | 1.98 | 1.98 | 1.98 | 1.97 | 0.02 | 0.02 | 0.01 | 3.39 |
| Al | 0.00 | 0.00 | 0.00 | 0.00 | 0.00 | 0.01 | 0.01 | 0.01 | 0.02 |
| Cr | 0.00 | 0.00 | 0.00 | 0.00 | 0.00 | 0.00 | 0.00 | 0.00 | 0.00 |
| $Fe_3$ | 0.04 | 0.01 | 0.02 | 0.02 | 0.04 | 15.99 | 15.94 | 15.98 | 9.16 |
| $Fe_2$ | 1.20 | 1.17 | 1.22 | 1.18 | 1.20 | 7.92 | 7.98 | 7.98 | 11.26 |
| Mn | 0.85 | 0.85 | 0.80 | 0.86 | 0.85 | 0.04 | 0.03 | 0.03 | 0.10 |
| Mg | 0.00 | 0.00 | 0.00 | 0.00 | 0.00 | 0.00 | 0.00 | 0.00 | 0.00 |
| Ca | 0.00 | 0.01 | 0.00 | 0.00 | 0.00 | 0.00 | 0.00 | 0.00 | 0.05 |
| Na | 0.00 | 0.00 | 0.00 | 0.00 | 0.00 | 0.02 | 0.00 | 0.00 | 0.00 |
| K | 0.00 | 0.00 | 0.00 | 0.00 | 0.00 | 0.00 | 0.00 | 0.00 | 0.00 |
| Ni | 0.00 | 0.00 | 0.00 | 0.00 | 0.00 | 0.00 | 0.01 | 0.00 | 0.01 |

**APATITE**

| Sample # | ICP-111 | | | | | | | | | | | |
|---|---|---|---|---|---|---|---|---|---|---|---|---|
| Grain # | 1 | 1 | 1 | 2 | 3 | 3 | 4 | 4 | 4 | 5 | 6 | 6 |
| Analysis # | 1 | 2 | 3 | 1 | 1 | 2 | 1 | 2 | 3 | 1 | 1 | 2 |
| $SiO_2$ | 0.02 | 0.00 | 0.02 | 0.17 | 0.02 | 0.01 | 0.07 | 0.02 | 0.10 | 0.17 | 0.04 | 0.01 |
| $TiO_2$ | 0.00 | 0.03 | 0.01 | 0.00 | 0.00 | 0.00 | 0.00 | 0.01 | 0.00 | 0.04 | 0.00 | 0.00 |
| $Al_2O_3$ | 0.00 | 0.00 | 0.01 | 0.12 | 0.00 | 0.00 | 0.00 | 0.01 | 0.00 | 1.79 | 0.00 | 0.01 |
| FeO | 0.37 | 0.36 | 0.05 | 0.01 | 0.11 | 0.21 | 0.49 | 0.42 | 0.39 | 0.66 | 0.09 | 0.12 |
| MnO | 0.09 | 0.08 | 0.08 | 0.07 | 0.05 | 0.07 | 0.10 | 0.13 | 0.15 | 0.07 | 0.06 | 0.09 |
| MgO | 0.01 | 0.00 | 0.00 | 0.00 | 0.02 | 0.00 | 0.01 | 0.00 | 0.00 | 0.02 | 0.00 | 0.01 |
| CaO | 56.70 | 56.76 | 56.02 | 56.50 | 55.91 | 56.50 | 57.81 | 57.33 | 58.07 | 54.94 | 58.24 | 58.15 |
| $ZrO_2$ | 0.16 | 0.20 | 0.19 | 0.17 | 0.21 | 0.17 | 0.20 | 0.15 | 0.27 | 0.14 | 0.25 | 0.18 |
| $HfO_2$ | 0.00 | 0.00 | 0.00 | 0.08 | 0.01 | 0.17 | 0.17 | 0.00 | 0.01 | 0.00 | 0.00 | 0.08 |
| $La_2O_3$ | 0.00 | 0.00 | 0.02 | 0.03 | 0.00 | 0.02 | 0.08 | 0.01 | 0.08 | 0.00 | 0.00 | 0.08 |
| $Ce_2O_3$ | 0.06 | 0.00 | 0.06 | 0.00 | 0.08 | 0.14 | 0.14 | 0.07 | 0.04 | 0.04 | 0.01 | 0.11 |
| $Nb_2O_5$ | 0.02 | 0.00 | 0.00 | 0.00 | 0.00 | 0.00 | 0.00 | 0.00 | 0.00 | 0.00 | 0.00 | 0.00 |
| $Ta_2O_5$ | 0.00 | 0.00 | 0.00 | 0.05 | 0.00 | 0.00 | 0.09 | 0.02 | 0.07 | 0.13 | 0.11 | 0.00 |
| $Y_2O_3$ | 0.04 | 0.03 | 0.05 | 0.22 | 0.05 | 0.00 | 0.10 | 0.03 | 0.21 | 0.16 | 0.02 | 0.02 |
| $Yb_2O_3$ | 0.10 | 0.02 | 0.04 | 0.05 | 0.02 | 0.00 | 0.00 | 0.00 | 0.01 | 0.00 | 0.00 | 0.00 |
| $P_2O_5$ | 42.25 | 42.69 | 42.05 | 41.85 | 41.74 | 41.85 | 42.19 | 42.76 | 42.28 | 40.28 | 42.07 | 42.69 |
| **Total** | **99.82** | **100.18** | **98.60** | **99.32** | **98.22** | **99.14** | **101.45** | **100.96** | **101.68** | **98.43** | **100.89** | **101.47** |

Structural formulas calculated on the basis of 26 oxygens.

| | | | | | | | | | | | | |
|---|---|---|---|---|---|---|---|---|---|---|---|---|
| Si | 0.00 | 0.00 | 0.00 | 0.03 | 0.00 | 0.00 | 0.01 | 0.00 | 0.02 | 0.03 | 0.01 | 0.00 |
| Ti | 0.00 | 0.00 | 0.00 | 0.00 | 0.00 | 0.00 | 0.00 | 0.00 | 0.00 | 0.01 | 0.00 | 0.00 |
| Al | 0.00 | 0.00 | 0.00 | 0.02 | 0.00 | 0.00 | 0.00 | 0.00 | 0.00 | 0.37 | 0.00 | 0.00 |
| $Fe_2$ | 0.05 | 0.05 | 0.01 | 0.00 | 0.02 | 0.03 | 0.07 | 0.06 | 0.06 | 0.10 | 0.01 | 0.02 |
| Mn | 0.01 | 0.01 | 0.01 | 0.01 | 0.01 | 0.01 | 0.01 | 0.02 | 0.02 | 0.01 | 0.01 | 0.01 |
| Mg | 0.00 | 0.00 | 0.00 | 0.00 | 0.00 | 0.00 | 0.00 | 0.00 | 0.00 | 0.00 | 0.00 | 0.00 |
| Ca | 10.47 | 10.42 | 10.44 | 10.48 | 10.47 | 10.51 | 10.57 | 10.46 | 10.58 | 10.29 | 10.68 | 10.57 |
| Zr | 0.01 | 0.02 | 0.02 | 0.01 | 0.02 | 0.01 | 0.02 | 0.01 | 0.02 | 0.01 | 0.02 | 0.01 |
| Hf | 0.00 | 0.00 | 0.00 | 0.00 | 0.00 | 0.01 | 0.01 | 0.00 | 0.00 | 0.00 | 0.00 | 0.00 |
| La | 0.00 | 0.00 | 0.00 | 0.00 | 0.00 | 0.00 | 0.00 | 0.00 | 0.00 | 0.00 | 0.00 | 0.00 |
| Ce | 0.00 | 0.00 | 0.00 | 0.00 | 0.01 | 0.01 | 0.01 | 0.00 | 0.00 | 0.00 | 0.00 | 0.01 |
| Nb | 0.00 | 0.00 | 0.00 | 0.00 | 0.00 | 0.00 | 0.00 | 0.00 | 0.00 | 0.00 | 0.00 | 0.00 |
| Ta | 0.00 | 0.00 | 0.00 | 0.00 | 0.00 | 0.00 | 0.00 | 0.00 | 0.00 | 0.01 | 0.01 | 0.00 |
| Y | 0.00 | 0.00 | 0.00 | 0.02 | 0.00 | 0.00 | 0.01 | 0.00 | 0.02 | 0.02 | 0.00 | 0.00 |
| Yb | 0.01 | 0.00 | 0.00 | 0.00 | 0.00 | 0.00 | 0.00 | 0.00 | 0.00 | 0.00 | 0.00 | 0.00 |
| P | 6.16 | 6.19 | 6.19 | 6.13 | 6.18 | 6.15 | 6.09 | 6.16 | 6.09 | 5.96 | 6.09 | 6.13 |

| APATITE | | | | | | | | | BIOTITE | |
|---|---|---|---|---|---|---|---|---|---|---|
| Sample # | ICP-114 | | | | | | | | ICP-111 | |
| Grain # | 1 | 1 | 2 | 3 | 3 | 3 | 4 | 4 | 1 | 1 |
| Analysis # | 1 | 2 | 1 | 1 | 2 | 3 | 1 | 2 | 1 | 2 |
| $SiO_2$ | 0.00 | 0.00 | 0.00 | 0.00 | 0.00 | 0.01 | 0.04 | 0.02 | 36.48 | 36.90 |
| $TiO_2$ | 0.00 | 0.00 | 0.00 | 0.00 | 0.01 | 0.00 | 0.00 | 0.00 | 3.03 | 2.59 |
| $Al_2O_3$ | 0.00 | 0.00 | 0.00 | 0.07 | 0.00 | 0.00 | 0.01 | 0.00 | 15.81 | 14.91 |
| FeO | 0.05 | 0.06 | 0.11 | 0.04 | 0.00 | 0.07 | 0.00 | 0.04 | 22.34 | 22.27 |
| MnO | 0.12 | 0.10 | 0.05 | 0.13 | 0.12 | 0.12 | 0.10 | 0.10 | 0.57 | 0.61 |
| MgO | 0.01 | 0.00 | 0.00 | 0.01 | 0.00 | 0.00 | 0.02 | 0.00 | 8.05 | 8.44 |
| CaO | 57.66 | 57.89 | 58.22 | 57.47 | 57.74 | 57.94 | 57.70 | 57.64 | 0.04 | 0.03 |
| $ZrO_2$ | 0.12 | 0.11 | 0.16 | 0.18 | 0.23 | 0.17 | 0.18 | 0.08 | 0.02 | 0.04 |
| $HfO_2$ | 0.00 | 0.07 | 0.05 | 0.04 | 0.00 | 0.00 | 0.05 | 0.00 | 0.00 | 0.10 |
| $La_2O_3$ | 0.00 | 0.00 | 0.00 | 0.00 | 0.11 | 0.02 | 0.14 | 0.02 | 0.00 | 0.00 |
| $Ce_2O_3$ | 0.01 | 0.00 | 0.00 | 0.00 | 0.04 | 0.05 | 0.15 | 0.04 | 0.07 | 0.12 |
| $Nb_2O_5$ | 0.00 | 0.00 | 0.00 | 0.00 | 0.00 | 0.00 | 0.00 | 0.00 | 0.02 | 0.03 |
| $Ta_2O_5$ | 0.00 | 0.09 | 0.08 | 0.07 | 0.00 | 0.01 | 0.01 | 0.10 | 0.00 | 0.00 |
| $Y_2O_3$ | 0.08 | 0.01 | 0.14 | 0.10 | 0.15 | 0.09 | 0.09 | 0.04 | 0.00 | 0.10 |
| $Yb_2O_3$ | 0.09 | 0.04 | 0.00 | 0.00 | 0.00 | 0.00 | 0.00 | 0.07 | 0.00 | 0.00 |
| $P_2O_5$ | 41.50 | 42.09 | 42.39 | 41.87 | 41.40 | 41.66 | 42.00 | 42.12 | 0.00 | 0.02 |
| **Total** | **99.64** | **100.45** | **101.20** | **99.98** | **99.80** | **100.14** | **100.48** | **100.27** | **86.43** | **86.16** |

Structural formulas calculated on the basis of 26 and 22 oxygens for apatite and biotite respectively.

| | | | | | | | | | | |
|---|---|---|---|---|---|---|---|---|---|---|
| Si | 0.00 | 0.00 | 0.00 | 0.00 | 0.00 | 0.00 | 0.01 | 0.00 | 5.87 | 5.96 |
| Ti | 0.00 | 0.00 | 0.00 | 0.00 | 0.00 | 0.00 | 0.00 | 0.00 | 0.37 | 0.31 |
| Al | 0.00 | 0.00 | 0.00 | 0.01 | 0.00 | 0.00 | 0.00 | 0.00 | 3.00 | 2.84 |
| $Fe_2$ | 0.01 | 0.01 | 0.02 | 0.01 | 0.00 | 0.01 | 0.00 | 0.01 | 3.01 | 3.01 |
| Mn | 0.02 | 0.01 | 0.01 | 0.02 | 0.02 | 0.02 | 0.01 | 0.01 | 0.08 | 0.08 |
| Mg | 0.00 | 0.00 | 0.00 | 0.00 | 0.00 | 0.00 | 0.00 | 0.00 | 1.93 | 2.03 |
| Ca | 10.71 | 10.65 | 10.63 | 10.62 | 10.72 | 10.71 | 10.62 | 10.61 | 0.01 | 0.01 |
| Zr | 0.01 | 0.01 | 0.01 | 0.02 | 0.02 | 0.01 | 0.02 | 0.01 | 0.00 | 0.00 |
| Hf | 0.00 | 0.00 | 0.00 | 0.00 | 0.00 | 0.00 | 0.00 | 0.00 | 0.00 | 0.00 |
| La | 0.00 | 0.00 | 0.00 | 0.00 | 0.01 | 0.00 | 0.01 | 0.00 | 0.00 | 0.00 |
| Ce | 0.00 | 0.00 | 0.00 | 0.00 | 0.00 | 0.00 | 0.01 | 0.00 | 0.00 | 0.01 |
| Nb | 0.00 | 0.00 | 0.00 | 0.00 | 0.00 | 0.00 | 0.00 | 0.00 | 0.00 | 0.00 |
| Ta | 0.00 | 0.00 | 0.00 | 0.00 | 0.00 | 0.00 | 0.00 | 0.00 | 0.00 | 0.00 |
| Y | 0.01 | 0.00 | 0.01 | 0.01 | 0.01 | 0.01 | 0.01 | 0.00 | 0.00 | 0.01 |
| Yb | 0.00 | 0.00 | 0.00 | 0.00 | 0.00 | 0.00 | 0.00 | 0.00 | 0.00 | 0.00 |
| P | 6.09 | 6.12 | 6.11 | 6.11 | 6.07 | 6.08 | 6.11 | 6.13 | 0.00 | 0.00 |

**CHLORITE**

| Sample | ICP-114 | | | | | | | SHN-102 | |
|---|---|---|---|---|---|---|---|---|---|
| Grain | 1 | 2 | 2 | 3 | 4 | 5 | 6 | 1 | 2 |
| Analysis | 1 | 1 | 2 | 1 | 1 | 1 | 1 | 1 | 1 |
| $SiO_2$ | 25.94 | 25.76 | 25.77 | 27.05 | 23.84 | 26.46 | 25.22 | 27.26 | 29.91 |
| $TiO_2$ | 0.19 | 0.08 | 0.11 | 1.13 | 7.76 | 0.51 | 0.16 | 0.10 | 0.88 |
| $Al_2O_3$ | 17.32 | 16.93 | 16.74 | 17.38 | 16.87 | 17.37 | 18.84 | 20.64 | 19.14 |
| $Cr_2O_3$ | 0.00 | 0.00 | 0.00 | 0.00 | 0.02 | 0.01 | 0.04 | 0.00 | 0.00 |
| FeO | 31.72 | 30.05 | 29.95 | 28.99 | 28.01 | 29.69 | 31.90 | 29.60 | 22.20 |
| MnO | 0.89 | 0.85 | 0.88 | 1.17 | 1.33 | 1.04 | 1.37 | 0.61 | 0.43 |
| MgO | 8.71 | 10.03 | 9.98 | 8.63 | 8.94 | 9.60 | 8.70 | 8.85 | 5.54 |
| CaO | 0.32 | 0.32 | 0.24 | 0.23 | 0.15 | 0.22 | 0.16 | 0.10 | 0.55 |
| $Na_2O$ | 0.09 | 0.06 | 0.07 | 0.06 | 0.05 | 0.04 | 0.08 | 0.10 | 0.21 |
| $K_2O$ | 0.14 | 0.07 | 0.08 | 0.53 | 0.15 | 0.13 | 0.08 | 0.15 | 2.53 |
| NiO | 0.02 | 0.01 | 0.00 | 0.00 | 0.00 | 0.03 | 0.00 | 0.02 | 0.00 |
| **Total** | **85.34** | **84.16** | **83.82** | **85.17** | **87.12** | **85.1** | **86.55** | **87.43** | **81.39** |

Structural formulas calculated on the basis of 28 oxygen.

| | | | | | | | | | |
|---|---|---|---|---|---|---|---|---|---|
| Si | 5.88 | 5.87 | 5.90 | 6.05 | 5.24 | 5.94 | 5.64 | 5.88 | 6.60 |
| Ti | 0.03 | 0.01 | 0.02 | 0.19 | 1.28 | 0.09 | 0.03 | 0.02 | 0.15 |
| Al | 4.63 | 4.55 | 4.52 | 4.58 | 4.37 | 4.59 | 4.97 | 5.25 | 4.98 |
| Cr | 0.00 | 0.00 | 0.00 | 0.00 | 0.00 | 0.00 | 0.01 | 0.00 | 0.00 |
| $Fe_2$ | 6.01 | 5.73 | 5.73 | 5.42 | 5.15 | 5.57 | 5.97 | 5.34 | 4.10 |
| Mn | 0.17 | 0.16 | 0.17 | 0.22 | 0.25 | 0.20 | 0.26 | 0.11 | 0.08 |
| Mg | 2.94 | 3.41 | 3.40 | 2.88 | 2.93 | 3.21 | 2.90 | 2.85 | 1.82 |
| Ca | 0.08 | 0.08 | 0.06 | 0.05 | 0.04 | 0.05 | 0.04 | 0.02 | 0.13 |
| Na | 0.04 | 0.03 | 0.03 | 0.03 | 0.02 | 0.02 | 0.04 | 0.04 | 0.09 |
| K | 0.04 | 0.02 | 0.02 | 0.15 | 0.04 | 0.04 | 0.02 | 0.04 | 0.71 |
| Ni | 0.00 | 0.00 | 0.00 | 0.00 | 0.00 | 0.00 | 0.00 | 0.00 | 0.00 |

(Table 3 continued)

**ZIRCON**

| Sample # | ICP-114 | | | | | | |
|---|---|---|---|---|---|---|---|
| Grain # | 1 | 2 | 3 | 3 | 4 | 4 | 4 |
| Analysis # | 1 | 1 | 1 | 2 | 1 | 2 | 3 |
| $SiO_2$ | 33.81 | 34.44 | 33.56 | 33.98 | 33.90 | 33.81 | 33.60 |
| $TiO_2$ | 0.03 | 0.01 | 0.02 | 0.00 | 0.00 | 0.00 | 0.00 |
| $Al_2O_3$ | 0.00 | 0.00 | 0.00 | 0.06 | 0.02 | 0.00 | 0.00 |
| FeO | 0.05 | 1.73 | 0.00 | 0.33 | 0.02 | 0.05 | 0.07 |
| MnO | 0.00 | 0.02 | 0.01 | 0.02 | 0.01 | 0.00 | 0.00 |
| MgO | 0.00 | 0.01 | 0.01 | 0.01 | 0.03 | 0.00 | 0.00 |
| CaO | 0.00 | 0.00 | 0.01 | 0.02 | 0.03 | 0.02 | 0.00 |
| $ZrO_2$ | 64.20 | 64.86 | 62.16 | 62.90 | 64.62 | 63.77 | 63.51 |
| $HfO_2$ | 1.57 | 1.81 | 1.36 | 1.40 | 1.30 | 1.49 | 1.40 |
| $La_2O_3$ | 0.06 | 0.04 | 0.06 | 0.00 | 0.00 | 0.00 | 0.00 |
| $Ce_2O_3$ | 0.07 | 0.03 | 0.12 | 0.01 | 0.11 | 0.00 | 0.03 |
| $Nb_2O_5$ | 0.00 | 0.00 | 0.00 | 0.00 | 0.00 | 0.00 | 0.00 |
| $Ta_2O_5$ | 0.00 | 0.07 | 0.00 | 0.00 | 0.00 | 0.00 | 0.01 |
| $Y_2O_3$ | 0.87 | 0.33 | 1.20 | 0.61 | 0.83 | 0.51 | 0.93 |
| $Yb_2O_3$ | 0.27 | 0.03 | 0.23 | 0.12 | 0.29 | 0.20 | 0.24 |
| $P_2O_5$ | 0.34 | 0.13 | 0.35 | 0.28 | 0.28 | 0.17 | 0.28 |
| **Total** | **101.27** | **103.51** | **99.09** | **99.74** | **101.44** | **100.02** | **100.07** |
| Structural formulas calculated on the basis of 16 oxygens. | | | | | | | |
| Si | 4.07 | 4.07 | 4.12 | 4.13 | 4.07 | 4.11 | 4.09 |
| Ti | 0.00 | 0.00 | 0.00 | 0.00 | 0.00 | 0.00 | 0.00 |
| Al | 0.00 | 0.00 | 0.00 | 0.01 | 0.00 | 0.00 | 0.00 |
| $Fe_2$ | 0.01 | 0.17 | 0.00 | 0.03 | 0.00 | 0.00 | 0.01 |
| Mn | 0.00 | 0.00 | 0.00 | 0.00 | 0.00 | 0.00 | 0.00 |
| Mg | 0.00 | 0.00 | 0.00 | 0.00 | 0.00 | 0.00 | 0.00 |
| Ca | 0.00 | 0.00 | 0.00 | 0.00 | 0.00 | 0.00 | 0.00 |
| Zr | 3.77 | 3.74 | 3.72 | 3.73 | 3.79 | 3.78 | 3.77 |
| Hf | 0.05 | 0.06 | 0.05 | 0.05 | 0.04 | 0.05 | 0.05 |
| La | 0.00 | 0.00 | 0.00 | 0.00 | 0.00 | 0.00 | 0.00 |
| Ce | 0.00 | 0.00 | 0.01 | 0.00 | 0.00 | 0.00 | 0.00 |
| Nb | 0.00 | 0.00 | 0.00 | 0.00 | 0.00 | 0.00 | 0.00 |
| Ta | 0.00 | 0.00 | 0.00 | 0.00 | 0.00 | 0.00 | 0.00 |
| Y | 0.06 | 0.02 | 0.08 | 0.04 | 0.05 | 0.03 | 0.06 |
| Yb | 0.01 | 0.00 | 0.01 | 0.00 | 0.01 | 0.01 | 0.01 |
| P | 0.03 | 0.01 | 0.04 | 0.03 | 0.03 | 0.02 | 0.03 |
| Hf / Zr | 0.02 | 0.03 | 0.02 | 0.02 | 0.02 | 0.02 | 0.02 |

| | BERYL | | | | | SCHORL | | | | AUGITE | DIOP. | ALBITE | AXINITE | Cl.Zoisite |
|---|---|---|---|---|---|---|---|---|---|---|---|---|---|---|
| Sample | 16 | 40 | 46 | 54 | 58 | 29C | 38E | 49 | 57 | 24 | 25 | 29A | 12A | 22 |
| Grain | 1 | 1 | 1 | 1 | 1 | 1 | 1 | 1 | 1 | 1 | 1 | 1 | 1 | 1 |
| Analysis | KSH | MUN | DASS | GOY | BASH | SHN | YUN | DASS | BASH | ALCH | BASH | SHN | ALCH | HASH |
| $SiO_2$ | 64.40 | 62.29 | 62.46 | 63.84 | 62.72 | 33.54 | 34.15 | 34.67 | 35.03 | 51.62 | 53.27 | 66.79 | 42.97 | 41.00 |
| $TiO_2$ | 0.00 | 0.00 | 0.00 | 0.00 | 0.00 | 0.00 | 0.63 | 0.00 | 0.00 | 0.00 | 0.00 | 0.00 | 0.00 | 0.00 |
| $Al_2O_3$ | 18.10 | 17.89 | 18.23 | 18.23 | 16.76 | 32.77 | 33.85 | 32.89 | 32.29 | 2.53 | 2.04 | 19.48 | 17.42 | 27.73 |
| FeO | 4.79 | 0.00 | 0.74 | 0.00 | 0.00 | 14.67 | 15.81 | 14.44 | 14.58 | 14.11 | 5.92 | 0.06 | 10.18 | 8.51 |
| MnO | 0.00 | 0.00 | 0.00 | 0.00 | 0.00 | 1.14 | 1.28 | 0.00 | 0.00 | 0.00 | 0.00 | 0.00 | 1.11 | 0.00 |
| MgO | 0.00 | 0.00 | 0.00 | 0.00 | 0.00 | 0.00 | 0.00 | 0.00 | 0.00 | 8.49 | 18.77 | 0.00 | 1.38 | 0.00 |
| CaO | 0.00 | 0.87 | 0.00 | 0.00 | 0.00 | 0.46 | 0.00 | 0.00 | 0.00 | 22.99 | 20.21 | 1.16 | 22.22 | 23.87 |
| $Na_2O$ | 0.80 | 1.85 | 0.00 | 0.00 | 0.00 | 1.67 | 2.04 | 1.43 | 1.27 | 0.50 | 0.00 | 11.25 | 0.00 | 0.00 |
| $K_2O$ | 0.80 | 0.85 | 0.60 | 0.00 | 0.55 | 0.59 | 0.86 | 1.61 | 0.59 | 0.00 | 0.00 | 0.34 | 0.00 | 0.45 |
| **Total** | **88.89** | **83.75** | **82.03** | **82.07** | **80.03** | **84.84** | **88.62** | **85.04** | **83.76** | **100.24** | **100.21** | **99.08** | **95.28** | **101.56** |
| | | | | | | | | | | | | | | |
| Si | 11.63 | 11.72 | 11.85 | 11.98 | 12.11 | 5.84 | 5.73 | 5.98 | 6.09 | 1.97 | 1.93 | 11.85 | 9.04 | 3.13 |
| Ti | 0.00 | 0.00 | 0.00 | 0.00 | 0.00 | 0.00 | 0.08 | 0.00 | 0.00 | 0.00 | 0.00 | 0.00 | 0.00 | 0.00 |
| Al | 3.85 | 3.96 | 4.07 | 4.03 | 3.81 | 6.72 | 6.69 | 6.68 | 6.61 | 0.11 | 0.09 | 4.07 | 4.32 | 2.49 |
| $Fe_2$ | 0.72 | 0.00 | 0.12 | 0.00 | 0.00 | 2.14 | 2.22 | 2.08 | 2.12 | 0.45 | 0.18 | 0.01 | 1.79 | 0.54 |
| Mn | 0.00 | 0.00 | 0.00 | 0.00 | 0.00 | 0.17 | 0.18 | 0.00 | 0.00 | 0.00 | 0.00 | 0.00 | 0.20 | 0.00 |
| Mg | 0.00 | 0.00 | 0.00 | 0.00 | 0.00 | 0.00 | 0.00 | 0.00 | 0.00 | 0.48 | 1.02 | 0.00 | 0.43 | 0.00 |
| Ca | 0.00 | 0.18 | 0.00 | 0.00 | 0.00 | 0.09 | 0.00 | 0.00 | 0.00 | 0.94 | 0.79 | 0.22 | 5.01 | 0.00 |
| Na | 0.28 | 0.67 | 0.00 | 0.00 | 0.00 | 0.56 | 0.66 | 0.48 | 0.43 | 0.04 | 0.00 | 3.87 | 0.00 | 1.95 |
| K | 0.18 | 0.20 | 0.15 | 0.00 | 0.14 | 0.13 | 0.18 | 0.35 | 0.13 | 0.00 | 0.00 | 0.08 | 0.00 | 0.04 |

**BERYL**

| Sample | 4-A | 4-B | 4-C | 4-D | 4-E | 4-F | 8M | 8M | 8M | 16B | 16C | 16C | 16C | 16D | 16D |
|---|---|---|---|---|---|---|---|---|---|---|---|---|---|---|---|
| Grain | 1 | 1 | 1 | 1 | 1 | 1 | 1 | 2 | 3 | 1 | 1 | 2 | 3 | 1 | 2 |
| Analysis | YUN | | | | | | | | | KSH | | | | | |
| $SiO_2$ | 65.13 | 65.35 | 65.16 | 64.45 | 65.80 | 64.88 | 65.35 | 64.41 | 64.09 | 65.02 | 63.91 | 63.56 | 63.45 | 63.55 | 63.80 |
| $TiO_2$ | 0.00 | 0.00 | 0.02 | 0.00 | 0.01 | 0.00 | 0.00 | 0.00 | 0.02 | 0.00 | 0.00 | 0.00 | 0.01 | 0.00 | 0.00 |
| $Al_2O_3$ | 17.98 | 18.24 | 18.39 | 18.25 | 18.23 | 17.91 | 17.47 | 17.44 | 17.40 | 18.00 | 17.31 | 17.37 | 17.55 | 17.28 | 17.47 |
| FeO | 0.14 | 0.28 | 0.23 | 0.38 | 0.35 | 0.31 | 0.04 | 0.06 | 0.47 | 0.20 | 0.69 | 0.56 | 0.66 | 0.77 | 0.32 |
| MnO | 0.12 | 0.00 | 0.04 | 0.00 | 0.00 | 0.00 | 0.00 | 0.00 | 0.00 | 0.00 | 0.04 | 0.03 | 0.06 | 0.01 | 0.12 |
| MgO | 0.00 | 0.01 | 0.00 | 0.00 | 0.03 | 0.04 | 0.00 | 0.00 | 0.00 | 0.04 | 0.00 | 0.00 | 0.00 | 0.00 | 0.00 |
| CaO | 0.00 | 0.01 | 0.00 | 0.00 | 0.01 | 0.00 | 0.00 | 0.00 | 0.00 | 0.01 | 0.00 | 0.00 | 0.00 | 0.00 | 0.00 |
| $Na_2O$ | 0.12 | 0.09 | 0.12 | 0.21 | 0.12 | 0.10 | 0.00 | 0.00 | 0.00 | 0.12 | 0.00 | 0.00 | 0.00 | 0.38 | 0.49 |
| $K_2O$ | 0.02 | 0.01 | 0.02 | 0.00 | 0.00 | 0.03 | 0.11 | 0.10 | 0.04 | 0.00 | 0.04 | 0.00 | 0.00 | 0.04 | 0.05 |
| $Cr_2O_3$ | 0.00 | 0.04 | 0.00 | 0.00 | 0.00 | 0.03 | 0.00 | 0.00 | 0.00 | 0.03 | 0.01 | 0.03 | 0.00 | 0.00 | 0.00 |
| NiO | 0.00 | 0.05 | 0.02 | 0.03 | 0.03 | 0.00 | 0.00 | 0.00 | 0.01 | 0.03 | 0.00 | 0.00 | 0.04 | 0.00 | 0.00 |
| **Total** | **83.51** | **84.08** | **84** | **83.32** | **84.58** | **83.3** | **82.97** | **82.01** | **82.03** | **83.45** | **82** | **81.55** | **81.77** | **82.03** | **82.25** |

Structural formulas calculated on the basis of 36 oxygens.

| | | | | | | | | | | | | | | | |
|---|---|---|---|---|---|---|---|---|---|---|---|---|---|---|---|
| Si | 12.03 | 12.00 | 11.98 | 11.96 | 12.01 | 12.02 | 12.12 | 12.09 | 12.05 | 12.02 | 12.04 | 12.03 | 11.99 | 11.98 | 11.98 |
| Ti | 0.00 | 0.00 | 0.00 | 0.00 | 0.00 | 0.00 | 0.00 | 0.00 | 0.00 | 0.00 | 0.00 | 0.00 | 0.00 | 0.00 | 0.00 |
| Al | 3.91 | 3.95 | 3.98 | 3.99 | 3.92 | 3.91 | 3.82 | 3.86 | 3.85 | 3.92 | 3.84 | 3.87 | 3.91 | 3.84 | 3.86 |
| $Fe_2$ | 0.02 | 0.04 | 0.04 | 0.06 | 0.05 | 0.05 | 0.01 | 0.01 | 0.07 | 0.03 | 0.10 | 0.08 | 0.09 | 0.11 | 0.05 |
| Mn | 0.00 | 0.00 | 0.00 | 0.00 | 0.01 | 0.01 | 0.00 | 0.00 | 0.00 | 0.01 | 0.01 | 0.01 | 0.01 | 0.00 | 0.02 |
| Mg | 0.02 | 0.00 | 0.01 | 0.00 | 0.00 | 0.00 | 0.00 | 0.00 | 0.00 | 0.00 | 0.00 | 0.00 | 0.00 | 0.00 | 0.00 |
| Ca | 0.00 | 0.00 | 0.00 | 0.00 | 0.00 | 0.00 | 0.00 | 0.00 | 0.00 | 0.00 | 0.00 | 0.00 | 0.00 | 0.00 | 0.00 |
| Na | 0.04 | 0.03 | 0.04 | 0.08 | 0.04 | 0.04 | 0.00 | 0.00 | 0.00 | 0.04 | 0.00 | 0.00 | 0.00 | 0.14 | 0.18 |
| K | 0.00 | 0.00 | 0.01 | 0.00 | 0.00 | 0.01 | 0.03 | 0.02 | 0.01 | 0.00 | 0.01 | 0.00 | 0.00 | 0.01 | 0.01 |
| Cr | 0.00 | 0.01 | 0.00 | 0.00 | 0.00 | 0.00 | 0.00 | 0.00 | 0.00 | 0.00 | 0.00 | 0.00 | 0.00 | 0.00 | 0.00 |
| Ni | 0.00 | 0.01 | 0.00 | 0.00 | 0.00 | 0.00 | 0.00 | 0.00 | 0.00 | 0.00 | 0.00 | 0.00 | 0.01 | 0.00 | 0.00 |

**BERYL**

| Sample | 16D | 16-E | 27 | 27 | 27 | 30 | 30 | 31 | 31 | 31 | 50 | 50 | 50 |
|---|---|---|---|---|---|---|---|---|---|---|---|---|---|
| Grain | 3 | 1 | 1 | 2 | 3 | 1 | 2 | 1 | 2 | 3 | 1 | 2 | 3 |
| Analysis | | | SHN | | | | | | | | NYT | | |
| $SiO_2$ | 64.68 | 65.79 | 65.16 | 65.13 | 64.13 | 64.90 | 65.01 | 64.50 | 64.66 | 64.74 | 63.64 | 65.33 | 65.45 |
| $TiO_2$ | 0.00 | 0.00 | 0.00 | 0.00 | 0.00 | 0.00 | 0.00 | 0.12 | 0.00 | 0.00 | 0.15 | 0.07 | 0.00 |
| $Al_2O_3$ | 17.43 | 18.45 | 17.57 | 19.58 | 20.67 | 18.54 | 20.44 | 18.31 | 20.59 | 20.59 | 17.63 | 19.91 | 17.87 |
| FeO | 0.48 | 0.26 | 0.00 | 0.00 | 0.00 | 0.32 | 0.25 | 0.52 | 0.31 | 0.40 | 3.92 | 0.50 | 0.57 |
| MnO | 0.00 | 0.06 | 0.00 | 0.00 | 0.00 | 0.15 | 0.00 | 0.27 | 0.00 | 0.00 | 0.13 | 0.06 | 0.16 |
| MgO | 0.00 | 0.04 | 0.00 | 0.12 | 0.13 | 0.00 | 0.03 | 0.00 | 0.09 | 0.01 | 0.01 | 0.11 | 0.00 |
| CaO | 0.00 | 0.01 | 0.07 | 0.02 | 0.01 | 0.00 | 0.00 | 0.00 | 0.00 | 0.00 | 2.34 | 0.48 | 0.00 |
| $Na_2O$ | 0.51 | 0.15 | 0.00 | 0.00 | 0.04 | 0.00 | 0.26 | 0.00 | 0.26 | 0.19 | 0.00 | 0.16 | 0.00 |
| $K_2O$ | 0.03 | 0.01 | 0.21 | 0.03 | 0.02 | 0.03 | 0.00 | 0.15 | 0.09 | 0.06 | 0.14 | 0.42 | 0.00 |
| $Cr_2O_3$ | 0.00 | 0.01 | 0.00 | 0.00 | 0.00 | 0.00 | 0.00 | 0.10 | 0.00 | 0.00 | 0.02 | 0.00 | 0.00 |
| NiO | 0.00 | 0.03 | 0.00 | 0.00 | 0.00 | 0.00 | 0.00 | 0.00 | 0.00 | 0.00 | 0.00 | 0.00 | 0.00 |
| **Total** | **83.13** | **84.81** | **83.01** | **84.88** | **85.00** | **83.94** | **85.99** | **83.97** | **86.00** | **85.99** | **87.98** | **87.04** | **84.05** |

Structural formulas calculated on the basis of 36 oxygens.

| | | | | | | | | | | | | | |
|---|---|---|---|---|---|---|---|---|---|---|---|---|---|
| Si | 12.01 | 11.98 | 12.10 | 11.84 | 11.66 | 11.94 | 11.70 | 11.90 | 11.65 | 11.66 | 11.51 | 11.69 | 12.03 |
| Ti | 0.00 | 0.00 | 0.00 | 0.00 | 0.00 | 0.00 | 0.00 | 0.02 | 0.00 | 0.00 | 0.02 | 0.01 | 0.00 |
| Al | 3.81 | 3.96 | 3.84 | 4.19 | 4.42 | 4.02 | 4.33 | 3.98 | 4.37 | 4.37 | 3.76 | 4.20 | 3.87 |
| $Fe_2$ | 0.07 | 0.04 | 0.00 | 0.00 | 0.00 | 0.04 | 0.03 | 0.07 | 0.04 | 0.05 | 0.53 | 0.07 | 0.08 |
| Mn | 0.00 | 0.01 | 0.00 | 0.00 | 0.00 | 0.02 | 0.00 | 0.04 | 0.00 | 0.00 | 0.02 | 0.01 | 0.03 |
| Mg | 0.00 | 0.01 | 0.00 | 0.03 | 0.04 | 0.00 | 0.01 | 0.00 | 0.02 | 0.00 | 0.00 | 0.03 | 0.00 |
| Ca | 0.00 | 0.00 | 0.01 | 0.00 | 0.00 | 0.00 | 0.00 | 0.00 | 0.00 | 0.00 | 0.45 | 0.09 | 0.00 |
| Na | 0.18 | 0.05 | 0.00 | 0.00 | 0.01 | 0.00 | 0.09 | 0.00 | 0.09 | 0.07 | 0.00 | 0.06 | 0.00 |
| K | 0.01 | 0.00 | 0.05 | 0.01 | 0.01 | 0.01 | 0.00 | 0.04 | 0.02 | 0.01 | 0.03 | 0.10 | 0.00 |
| Cr | 0.00 | 0.00 | 0.00 | 0.00 | 0.00 | 0.00 | 0.00 | 0.02 | 0.00 | 0.00 | 0.00 | 0.00 | 0.00 |
| Ni | 0.00 | 0.00 | 0.00 | 0.00 | 0.00 | 0.00 | 0.00 | 0.00 | 0.00 | 0.00 | 0.00 | 0.00 | 0.00 |

**CLINOZOISITE**

| Sample | 10-C | 10-F | 10-G | 10-H | 10-I | 10-J | 10-K | 13A | 13A | 13B | 13B | 13B | 13C |
|---|---|---|---|---|---|---|---|---|---|---|---|---|---|
| Grain | 1 | 1 | 1 | 1 | 1 | 1 | 1 | 1 | 2 | 1 | 2 | 3 | 1 |
| Analysis | ALCH | | | | | | | | | | | | |
| $SiO_2$ | 38.39 | 38.64 | 38.05 | 38.59 | 37.75 | 38.51 | 38.30 | 40.36 | 39.65 | 40.72 | 40.22 | 40.78 | 39.48 |
| $TiO_2$ | 0.13 | 0.23 | 0.08 | 0.12 | 0.06 | 0.04 | 0.13 | 0.09 | 0.06 | 0.21 | 0.07 | 0.11 | 0.14 |
| $Al_2O_3$ | 28.92 | 28.26 | 26.51 | 28.74 | 25.89 | 26.96 | 28.24 | 27.78 | 27.19 | 27.55 | 27.83 | 26.74 | 27.48 |
| FeO | 5.54 | 5.07 | 7.68 | 5.37 | 7.42 | 7.93 | 5.27 | 7.44 | 7.43 | 6.88 | 7.07 | 7.64 | 7.29 |
| MnO | 0.06 | 0.00 | 0.02 | 0.07 | 0.14 | 0.08 | 0.05 | 0.15 | 0.04 | 0.02 | 0.16 | 0.15 | 0.05 |
| MgO | 0.05 | 0.07 | 0.06 | 0.08 | 0.09 | 0.12 | 0.03 | 0.00 | 0.01 | 0.05 | 0.09 | 0.05 | 0.10 |
| CaO | 21.60 | 20.66 | 20.58 | 21.52 | 20.45 | 21.31 | 20.92 | 22.30 | 24.67 | 22.59 | 22.90 | 23.31 | 23.44 |
| $Na_2O$ | 0.02 | 0.01 | 0.01 | 0.03 | 0.00 | 0.01 | 0.00 | 0.00 | 0.00 | 0.00 | 0.01 | 0.05 | 0.01 |
| $K_2O$ | 0.00 | 0.00 | 0.00 | 0.00 | 0.00 | 0.00 | 0.00 | 0.00 | 0.00 | 0.00 | 0.00 | 0.00 | 0.00 |
| $Cr_2O_3$ | 0.04 | 0.18 | 0.00 | 0.00 | 0.00 | 0.08 | 0.05 | 0.00 | 0.04 | 0.06 | 0.00 | 0.00 | 0.00 |
| NiO | 0.17 | 0.06 | 0.00 | 0.00 | 0.06 | 0.07 | 0.00 | 0.00 | 0.01 | 0.00 | 0.10 | 0.07 | 0.04 |
| **Total** | **94.92** | **93.18** | **92.99** | **94.52** | **91.86** | **95.11** | **92.99** | **98.12** | **99.10** | **98.08** | **98.45** | **98.90** | **98.03** |

Structural formulas calculated on the basis of 13 oxygens.

| | | | | | | | | | | | | | |
|---|---|---|---|---|---|---|---|---|---|---|---|---|---|
| Si | 3.07 | 3.13 | 3.14 | 3.09 | 3.15 | 3.11 | 3.12 | 3.23 | 3.17 | 3.26 | 3.22 | 3.25 | 3.18 |
| Ti | 0.01 | 0.01 | 0.01 | 0.01 | 0.00 | 0.00 | 0.01 | 0.01 | 0.00 | 0.01 | 0.00 | 0.01 | 0.01 |
| Al | 2.73 | 2.70 | 2.57 | 2.71 | 2.54 | 2.57 | 2.71 | 2.62 | 2.56 | 2.59 | 2.62 | 2.51 | 2.61 |
| $Fe_2$ | 0.37 | 0.34 | 0.53 | 0.36 | 0.52 | 0.54 | 0.36 | 0.45 | 0.45 | 0.41 | 0.43 | 0.46 | 0.44 |
| Mn | 0.00 | 0.00 | 0.00 | 0.01 | 0.01 | 0.01 | 0.00 | 0.01 | 0.00 | 0.00 | 0.01 | 0.01 | 0.00 |
| Mg | 0.01 | 0.01 | 0.01 | 0.01 | 0.01 | 0.02 | 0.00 | 0.00 | 0.00 | 0.01 | 0.01 | 0.01 | 0.01 |
| Ca | 1.85 | 1.79 | 1.82 | 1.85 | 1.83 | 1.85 | 1.82 | 1.91 | 2.12 | 1.94 | 1.96 | 1.99 | 2.02 |
| Na | 0.00 | 0.00 | 0.00 | 0.01 | 0.00 | 0.00 | 0.00 | 0.00 | 0.00 | 0.00 | 0.00 | 0.01 | 0.00 |
| K | 0.00 | 0.00 | 0.00 | 0.00 | 0.00 | 0.00 | 0.00 | 0.00 | 0.00 | 0.00 | 0.00 | 0.00 | 0.00 |
| Cr | 0.00 | 0.01 | 0.00 | 0.00 | 0.00 | 0.01 | 0.00 | 0.00 | 0.00 | 0.00 | 0.00 | 0.00 | 0.00 |
| Ni | 0.01 | 0.00 | 0.00 | 0.00 | 0.00 | 0.00 | 0.00 | 0.00 | 0.00 | 0.00 | 0.01 | 0.00 | 0.00 |

**CLINOZOISITE**

| Sample | 13C | 13C | 13D | 13D | 13D | 13E | 13E | 13E | 22 | 22 | 22 |
|---|---|---|---|---|---|---|---|---|---|---|---|
| Grain | 2 | 3 | 1 | 2 | 3 | 1 | 2 | 3 | 1 | 2 | 3 |
| Analysis | ALCH | | | | | | | | HAS | | |
| $SiO_2$ | 39.88 | 39.45 | 39.57 | 39.91 | 39.68 | 38.98 | 39.13 | 39.25 | 39.11 | 39.21 | 39.18 |
| $TiO_2$ | 0.09 | 0.11 | 0.07 | 0.04 | 0.13 | 0.18 | 0.11 | 0.06 | 0.15 | 0.14 | 0.06 |
| $Al_2O_3$ | 27.65 | 27.21 | 27.77 | 27.32 | 27.77 | 26.08 | 27.17 | 27.88 | 27.57 | 26.85 | 27.07 |
| FeO | 7.17 | 8.45 | 7.66 | 7.04 | 7.29 | 8.73 | 7.74 | 7.65 | 7.54 | 7.49 | 8.60 |
| MnO | 0.09 | 0.23 | 0.05 | 0.01 | 0.19 | 0.23 | 0.12 | 0.12 | 0.14 | 0.14 | 0.19 |
| MgO | 0.09 | 0.00 | 0.10 | 0.05 | 0.08 | 0.00 | 0.10 | 0.12 | 0.14 | 0.00 | 0.06 |
| CaO | 22.97 | 22.86 | 22.74 | 22.86 | 22.42 | 24.68 | 23.21 | 23.52 | 23.30 | 23.98 | 23.26 |
| $Na_2O$ | 0.01 | 0.00 | 0.00 | 0.00 | 0.01 | 0.00 | 0.00 | 0.02 | 0.00 | 0.04 | 0.00 |
| $K_2O$ | 0.00 | 0.00 | 0.00 | 0.00 | 0.00 | 0.00 | 0.00 | 0.00 | 0.00 | 0.00 | 0.00 |
| $Cr_2O_3$ | 0.00 | 0.00 | 0.02 | 0.00 | 0.00 | 0.00 | 0.00 | 0.00 | 0.00 | 0.00 | 0.00 |
| NiO | 0.06 | 0.02 | 0.00 | 0.02 | 0.06 | 0.02 | 0.05 | 0.08 | 0.07 | 0.00 | 0.08 |
| **Total** | **98.01** | **98.33** | **97.98** | **97.25** | **97.63** | **98.90** | **97.63** | **98.70** | **98.02** | **97.85** | **98.50** |

Structural formulas calculated on the basis of 13 oxygens.

| | | | | | | | | | | | |
|---|---|---|---|---|---|---|---|---|---|---|---|
| Si | 3.21 | 3.18 | 3.18 | 3.23 | 3.20 | 3.15 | 3.17 | 3.15 | 3.16 | 3.18 | 3.16 |
| Ti | 0.01 | 0.01 | 0.00 | 0.00 | 0.01 | 0.01 | 0.01 | 0.00 | 0.01 | 0.01 | 0.00 |
| Al | 2.62 | 2.58 | 2.63 | 2.60 | 2.64 | 2.48 | 2.59 | 2.63 | 2.62 | 2.56 | 2.57 |
| $Fe_2$ | 0.43 | 0.51 | 0.46 | 0.43 | 0.44 | 0.53 | 0.47 | 0.46 | 0.46 | 0.46 | 0.52 |
| Mn | 0.01 | 0.02 | 0.00 | 0.00 | 0.01 | 0.02 | 0.01 | 0.01 | 0.01 | 0.01 | 0.01 |
| Mg | 0.01 | 0.00 | 0.01 | 0.01 | 0.01 | 0.00 | 0.01 | 0.01 | 0.02 | 0.00 | 0.01 |
| Ca | 1.98 | 1.97 | 1.96 | 1.98 | 1.94 | 2.14 | 2.02 | 2.02 | 2.02 | 2.08 | 2.01 |
| Na | 0.00 | 0.00 | 0.00 | 0.00 | 0.00 | 0.00 | 0.00 | 0.00 | 0.00 | 0.01 | 0.00 |
| K | 0.00 | 0.00 | 0.00 | 0.00 | 0.00 | 0.00 | 0.00 | 0.00 | 0.00 | 0.00 | 0.00 |
| Cr | 0.00 | 0.00 | 0.00 | 0.00 | 0.00 | 0.00 | 0.00 | 0.00 | 0.00 | 0.00 | 0.00 |
| Ni | 0.00 | 0.00 | 0.00 | 0.00 | 0.00 | 0.00 | 0.00 | 0.01 | 0.00 | 0.00 | 0.01 |

(Table 6. 5 continued)

| GARNET | | | | | ZOISITE | | | | | | | | |
|---|---|---|---|---|---|---|---|---|---|---|---|---|---|
| Sample | 5 | 5 | 5 | 20-H | 11A-M | 11A-C | 11A-M | 11B-M | 11B-M | 11C | 11D-M | 11D-C | 11D-M |
| Grain | 1 | 2 | 3 | 1 | 1 | 2 | 3 | 1 | 2 | 1 | 1 | 2 | 3 |
| Analysis | YUN | | | DASS | ALCH | | | | | | | | |
| $SiO_2$ | 37.77 | 37.61 | 36.28 | 35.83 | 39.89 | 39.67 | 39.61 | 39.88 | 39.34 | 39.14 | 39.65 | 39.07 | 39.65 |
| $TiO_2$ | 0.00 | 0.00 | 0.00 | 0.05 | 0.06 | 0.04 | 0.06 | 0.00 | 0.00 | 0.11 | 0.03 | 0.07 | 0.20 |
| $Al_2O_3$ | 23.72 | 23.42 | 24.95 | 20.73 | 31.17 | 30.09 | 31.09 | 32.64 | 32.67 | 32.01 | 32.54 | 33.65 | 32.61 |
| FeO | 21.55 | 21.37 | 21.32 | 20.42 | 1.89 | 2.23 | 1.80 | 2.40 | 2.29 | 1.54 | 2.16 | 1.65 | 2.03 |
| MnO | 16.80 | 16.76 | 16.94 | 23.05 | 0.00 | 0.00 | 0.00 | 0.02 | 0.02 | 0.02 | 0.11 | 0.03 | 0.00 |
| MgO | 0.13 | 0.31 | 0.12 | 0.00 | 0.02 | 0.00 | 0.01 | 0.09 | 0.07 | 0.00 | 0.00 | 0.09 | 0.00 |
| CaO | 0.00 | 0.27 | 0.28 | 0.23 | 25.28 | 26.93 | 25.65 | 24.56 | 24.54 | 24.71 | 25.42 | 23.55 | 26.12 |
| $Na_2O$ | 0.02 | 0.17 | 0.00 | 0.02 | 0.05 | 0.00 | 0.00 | 0.00 | 0.00 | 0.00 | 0.00 | 0.00 | 0.00 |
| $K_2O$ | 0.03 | 0.00 | 0.00 | 0.00 | 0.00 | 0.00 | 0.00 | 0.00 | 0.00 | 0.00 | 0.00 | 0.00 | 0.00 |
| $Cr_2O_3$ | 0.00 | 0.00 | 0.00 | 0.03 | 0.03 | 0.03 | 0.00 | 0.00 | 0.03 | 0.00 | 0.00 | 0.00 | 0.05 |
| NiO | 0.00 | 0.00 | 0.00 | 0.00 | 0.06 | 0.00 | 0.02 | 0.00 | 0.08 | 0.00 | 0.05 | 0.08 | 0.02 |
| **Total** | **100.02** | **99.91** | **99.89** | 100.36 | **98.45** | **98.99** | **98.24** | **99.57** | **99.04** | **97.53** | **99.96** | **98.19** | **100.68** |
| Structural formulas calculated on the basis of 24 and 13 oxygens for garnet and zoisite respectively. | | | | | | | | | | | | | |
| Si | 6.27 | 6.23 | 6.01 | 5.90 | 3.03 | 3.02 | 3.02 | 2.99 | 2.97 | 3.01 | 2.97 | 2.96 | 2.96 |
| Ti | 0.00 | 0.00 | 0.00 | 0.01 | 0.00 | 0.00 | 0.00 | 0.00 | 0.00 | 0.01 | 0.00 | 0.00 | 0.01 |
| Al | 4.64 | 4.57 | 4.87 | 4.02 | 2.79 | 2.70 | 2.79 | 2.88 | 2.91 | 2.89 | 2.87 | 3.00 | 2.86 |
| $Fe_2$ | 2.69 | 2.66 | 2.66 | 2.81 | 0.11 | 0.13 | 0.10 | 0.14 | 0.13 | 0.10 | 0.12 | 0.09 | 0.11 |
| Mn | 2.36 | 2.35 | 2.38 | 3.21 | 0.00 | 0.00 | 0.00 | 0.00 | 0.00 | 0.00 | 0.01 | 0.00 | 0.00 |
| Mg | 0.03 | 0.08 | 0.03 | 0.00 | 0.00 | 0.00 | 0.00 | 0.01 | 0.01 | 0.00 | 0.00 | 0.01 | 0.00 |
| Ca | 0.00 | 0.05 | 0.05 | 0.04 | 2.06 | 2.20 | 2.10 | 1.97 | 1.99 | 2.03 | 2.04 | 1.91 | 2.09 |
| Na | 0.01 | 0.05 | 0.00 | 0.01 | 0.01 | 0.00 | 0.00 | 0.00 | 0.00 | 0.00 | 0.00 | 0.00 | 0.00 |
| K | 0.00 | 0.00 | 0.00 | 0.00 | 0.00 | 0.00 | 0.00 | 0.00 | 0.00 | 0.00 | 0.00 | 0.00 | 0.00 |
| Cr | 0.00 | 0.00 | 0.00 | 0.00 | 0.00 | 0.00 | 0.00 | 0.00 | 0.00 | 0.00 | 0.00 | 0.00 | 0.00 |
| Ni | 0.00 | 0.00 | 0.00 | 0.00 | 0.00 | 0.00 | 0.00 | 0.00 | 0.00 | 0.00 | 0.00 | 0.00 | 0.00 |
| Alm | 52.86 | 52.54 | 51.97 | 43.68 | | | | | | | | | |
| And | 0.00 | 0.00 | 0.00 | 0.00 | | | | | | | | | |
| Gross | 0.00 | 0.97 | 0.97 | 0.60 | | | | | | | | | |
| Pyrope | 0.63 | 0.57 | 0.58 | 0.00 | | | | | | | | | |
| Spess | 46.38 | 46.36 | 46.48 | 55.51 | | | | | | | | | |
| Uvaro | 0.00 | 0.00 | 0.00 | 0.09 | | | | | | | | | |

(Table 6. 5 continued)

**APATITE**

| Sample | 3-M | 3-M | 3-C | 9A | 9A | 9A | 9A | 9A | 9A | 9B | 9B | 9B | 9B | 9B | 9B | 32-M | 32-C | 32-M |
|---|---|---|---|---|---|---|---|---|---|---|---|---|---|---|---|---|---|---|
| Grain | 1 | 2 | 3 | 1 | 2 | 3 | 4 | 5 | 6 | 1 | 2 | 3 | 4 | 5 | 6 | 1 | 2 | 3 |
| Analysis | YUN | | | KSH | | | | | | | | | | | | SHN | | |
| $SiO_2$ | 0.34 | 0.21 | 0.18 | 0.31 | 0.55 | 0.29 | 0.18 | 0.14 | 0.41 | 0.37 | 0.25 | 0.33 | 0.37 | 0.00 | 0.38 | 0.62 | 0.31 | 0.40 |
| $TiO_2$ | 0.01 | 0.26 | 0.00 | 0.00 | 0.05 | 0.00 | 0.00 | 0.01 | 0.03 | 0.04 | 0.02 | 0.02 | 0.11 | 0.00 | 0.00 | 0.00 | 0.17 | 0.01 |
| $Al_2O_3$ | 0.03 | 0.00 | 0.01 | 0.00 | 0.05 | 0.00 | 0.00 | 0.02 | 0.00 | 0.02 | 0.00 | 0.04 | 0.45 | 0.00 | 0.16 | 0.04 | 0.03 | 0.00 |
| FeO | 0.04 | 0.03 | 0.04 | 0.11 | 0.28 | 0.28 | 0.03 | 0.13 | 0.17 | 0.16 | 0.10 | 0.13 | 0.00 | 0.08 | 0.09 | 0.12 | 0.00 | 0.08 |
| MnO | 0.75 | 0.20 | 1.07 | 6.41 | 7.36 | 6.84 | 6.47 | 6.98 | 6.77 | 0.42 | 2.04 | 1.56 | 0.29 | 2.08 | 0.96 | 0.46 | 0.26 | 2.09 |
| MgO | 0.00 | 0.00 | 0.00 | 0.00 | 0.00 | 0.01 | 0.02 | 0.00 | 0.01 | 0.00 | 0.00 | 0.03 | 0.00 | 0.01 | 0.05 | 0.01 | 0.00 | 0.00 |
| CaO | 56.77 | 58.33 | 57.83 | 49.96 | 49.64 | 50.18 | 51.92 | 52.23 | 50.65 | 57.13 | 57.83 | 55.10 | 58.39 | 55.95 | 56.93 | 55.76 | 57.21 | 56.75 |
| $Na_2O$ | 0.26 | 0.08 | 0.07 | 0.07 | 0.13 | 0.06 | 0.12 | 0.14 | 0.12 | 0.05 | 0.03 | 0.07 | 0.00 | 0.06 | 0.01 | 0.00 | 0.06 | 0.03 |
| $K_2O$ | 0.00 | 0.00 | 0.00 | 0.00 | 0.00 | 0.00 | 0.00 | 0.00 | 0.00 | 0.00 | 0.00 | 0.00 | 0.00 | 0.00 | 0.00 | 0.00 | 0.00 | 0.00 |
| $Cr_2O_3$ | 0.00 | 0.00 | 0.00 | 0.05 | 0.00 | 0.05 | 0.03 | 0.03 | 0.12 | 0.02 | 0.01 | 0.00 | 0.00 | 0.00 | 0.00 | 0.05 | 0.01 | 0.03 |
| NiO | 0.05 | 0.00 | 0.03 | 0.07 | 0.03 | 0.04 | 0.11 | 0.05 | 0.00 | 0.07 | 0.08 | 0.11 | 0.00 | 0.09 | 0.17 | 0.07 | 0.00 | 0.02 |
| $P_2O_5$ | 41.76 | 39.90 | 40.76 | 43.01 | 41.91 | 42.26 | 41.11 | 40.26 | 41.71 | 41.73 | 39.65 | 42.60 | 40.39 | 41.72 | 41.25 | 40.88 | 40.94 | 40.57 |
| **Total** | **100.01** | **99.01** | **99.99** | **99.99** | **100.00** | **100.01** | **99.99** | **99.99** | **99.99** | **100.01** | **100.01** | **99.99** | **100.00** | **99.99** | **100.00** | **98.01** | **98.99** | **99.98** |

Structural formulas calculated on the basis of 26 oxygens.

| | | | | | | | | | | | | | | | | | | |
|---|---|---|---|---|---|---|---|---|---|---|---|---|---|---|---|---|---|---|
| Si | 0.06 | 0.04 | 0.03 | 0.05 | 0.10 | 0.05 | 0.03 | 0.03 | 0.07 | 0.06 | 0.04 | 0.06 | 0.06 | 0.00 | 0.07 | 0.11 | 0.05 | 0.07 |
| Ti | 0.00 | 0.03 | 0.00 | 0.00 | 0.01 | 0.00 | 0.00 | 0.00 | 0.00 | 0.01 | 0.00 | 0.00 | 0.01 | 0.00 | 0.00 | 0.00 | 0.02 | 0.00 |
| Al | 0.01 | 0.00 | 0.00 | 0.00 | 0.01 | 0.00 | 0.00 | 0.00 | 0.00 | 0.00 | 0.00 | 0.01 | 0.09 | 0.00 | 0.03 | 0.01 | 0.01 | 0.00 |
| $Fe_2$ | 0.01 | 0.00 | 0.01 | 0.01 | 0.04 | 0.04 | 0.00 | 0.02 | 0.02 | 0.02 | 0.01 | 0.02 | 0.00 | 0.01 | 0.01 | 0.02 | 0.00 | 0.01 |
| Mn | 0.11 | 0.03 | 0.16 | 0.94 | 1.08 | 1.00 | 0.96 | 1.04 | 1.00 | 0.06 | 0.30 | 0.23 | 0.04 | 0.31 | 0.14 | 0.07 | 0.04 | 0.31 |
| Mg | 0.00 | 0.00 | 0.00 | 0.00 | 0.00 | 0.00 | 0.01 | 0.00 | 0.00 | 0.00 | 0.00 | 0.01 | 0.00 | 0.00 | 0.01 | 0.00 | 0.00 | 0.00 |
| Ca | 10.48 | 10.98 | 10.77 | 9.22 | 9.23 | 9.32 | 9.72 | 9.85 | 9.43 | 10.54 | 10.86 | 10.12 | 10.84 | 10.37 | 10.54 | 10.48 | 10.68 | 10.58 |
| Na | 0.09 | 0.03 | 0.02 | 0.02 | 0.04 | 0.02 | 0.04 | 0.05 | 0.04 | 0.02 | 0.01 | 0.02 | 0.00 | 0.02 | 0.00 | 0.00 | 0.02 | 0.01 |
| K | 0.00 | 0.00 | 0.00 | 0.00 | 0.00 | 0.00 | 0.00 | 0.00 | 0.00 | 0.00 | 0.00 | 0.00 | 0.00 | 0.00 | 0.00 | 0.00 | 0.00 | 0.00 |
| Cr | 0.00 | 0.00 | 0.00 | 0.01 | 0.00 | 0.01 | 0.00 | 0.00 | 0.02 | 0.00 | 0.00 | 0.00 | 0.00 | 0.00 | 0.00 | 0.01 | 0.00 | 0.00 |
| Ni | 0.01 | 0.00 | 0.00 | 0.01 | 0.00 | 0.01 | 0.02 | 0.01 | 0.00 | 0.01 | 0.01 | 0.02 | 0.00 | 0.01 | 0.02 | 0.01 | 0.00 | 0.00 |
| **P** | 6.09 | 5.93 | 6.00 | 6.27 | 6.16 | 6.20 | 6.08 | 6.00 | 6.14 | 6.08 | 5.88 | 6.18 | 5.93 | 6.11 | 6.03 | 6.07 | 6.04 | 5.98 |

**SCHORL-FOITITE**

| Sample | 15-M | 15-M | 15-C | 20-A | 20C | 20C | 20C | 20D | 20D | 20D | 20E | 20E | 20E |
|---|---|---|---|---|---|---|---|---|---|---|---|---|---|
| Grain | 1 | 2 | 3 | 1 | 1 | 2 | 3 | 1 | 2 | 3 | 1 | 2 | 3 |
| Analysis | KSH | | | DASS | | | | | | | | | |
| $SiO_2$ | 33.51 | 33.08 | 34.75 | 35.06 | 34.52 | 34.82 | 34.68 | 33.16 | 34.01 | 34.17 | 33.47 | 34.32 | 34.41 |
| $TiO_2$ | 0.26 | 0.28 | 0.29 | 0.22 | 0.08 | 0.14 | 0.09 | 0.07 | 0.20 | 0.11 | 0.01 | 0.09 | 0.10 |
| $Al_2O_3$ | 32.80 | 33.22 | 33.11 | 33.79 | 34.30 | 34.24 | 34.67 | 34.92 | 34.81 | 34.70 | 34.64 | 34.48 | 34.18 |
| FeO | 13.52 | 14.18 | 14.66 | 14.37 | 13.05 | 14.30 | 13.66 | 14.02 | 14.74 | 14.35 | 13.78 | 14.02 | 14.43 |
| MnO | 1.05 | 1.19 | 1.00 | 0.58 | 0.67 | 0.73 | 0.49 | 0.54 | 0.74 | 0.43 | 0.71 | 0.66 | 0.64 |
| MgO | 0.13 | 0.00 | 0.00 | 0.21 | 0.00 | 0.00 | 0.00 | 0.00 | 0.00 | 0.00 | 0.00 | 0.00 | 0.00 |
| CaO | 0.66 | 0.07 | 0.17 | 0.04 | 0.04 | 0.06 | 0.01 | 0.16 | 0.03 | 0.03 | 0.05 | 0.00 | 0.04 |
| $Na_2O$ | 2.16 | 1.98 | 1.86 | 1.88 | 1.31 | 1.44 | 1.18 | 0.97 | 1.31 | 1.04 | 1.27 | 1.44 | 1.13 |
| $K_2O$ | 0.05 | 0.02 | 0.10 | 0.02 | 0.01 | 0.10 | 0.00 | 0.03 | 0.06 | 0.01 | 0.03 | 0.00 | 0.03 |
| $Cr_2O_3$ | 0.00 | 0.00 | 0.00 | 0.03 | 0.03 | 0.00 | 0.00 | 0.00 | 0.00 | 0.00 | 0.00 | 0.00 | 0.00 |
| NiO | 0.01 | 0.00 | 0.05 | 0.07 | 0.04 | 0.16 | 0.22 | 0.11 | 0.12 | 0.15 | 0.04 | 0.00 | 0.04 |
| **Total** | **84.15** | **84.02** | **85.99** | **86.27** | **84.05** | **85.99** | **85.00** | **83.98** | **86.02** | **84.99** | **84.00** | **85.01** | **85.00** |

Structural formulas calculated on the basis of 24.5 oxygens.

| | | | | | | | | | | | | | |
|---|---|---|---|---|---|---|---|---|---|---|---|---|---|
| Si | 5.68 | 5.61 | 5.75 | 5.80 | 5.77 | 5.73 | 5.74 | 5.58 | 5.61 | 5.67 | 5.63 | 5.70 | 5.72 |
| Ti | 0.03 | 0.04 | 0.04 | 0.03 | 0.01 | 0.02 | 0.01 | 0.01 | 0.02 | 0.01 | 0.00 | 0.01 | 0.01 |
| Al | 6.54 | 6.64 | 6.46 | 6.59 | 6.76 | 6.64 | 6.76 | 6.92 | 6.76 | 6.78 | 6.86 | 6.74 | 6.69 |
| $Fe_2$ | 1.72 | 1.81 | 1.83 | 1.99 | 1.64 | 1.77 | 1.70 | 1.77 | 1.83 | 1.79 | 1.74 | 1.75 | 1.80 |
| Mn | 0.15 | 0.17 | 0.14 | 0.08 | 0.10 | 0.10 | 0.07 | 0.08 | 0.10 | 0.06 | 0.10 | 0.09 | 0.09 |
| Mg | 0.03 | 0.00 | 0.00 | 0.05 | 0.00 | 0.00 | 0.00 | 0.00 | 0.00 | 0.00 | 0.00 | 0.00 | 0.00 |
| Ca | 0.12 | 0.01 | 0.03 | 0.01 | 0.01 | 0.01 | 0.00 | 0.03 | 0.01 | 0.01 | 0.01 | 0.00 | 0.01 |
| Na | 0.71 | 0.65 | 0.60 | 0.60 | 0.43 | 0.46 | 0.38 | 0.32 | 0.42 | 0.34 | 0.41 | 0.46 | 0.36 |
| K | 0.01 | 0.00 | 0.02 | 0.00 | 0.00 | 0.02 | 0.00 | 0.01 | 0.01 | 0.00 | 0.01 | 0.00 | 0.01 |
| Cr | 0.00 | 0.00 | 0.00 | 0.00 | 0.00 | 0.00 | 0.00 | 0.00 | 0.00 | 0.00 | 0.00 | 0.00 | 0.00 |
| Ni | 0.00 | 0.00 | 0.01 | 0.01 | 0.01 | 0.02 | 0.03 | 0.01 | 0.02 | 0.02 | 0.01 | 0.00 | 0.01 |

(Table 6. 5 continued)

**SCHORL-FOITITE**

| Sample | 20F | 20F | 20F | 20G | 20G | 20G | 23 | 23 | 23 |
|---|---|---|---|---|---|---|---|---|---|
| Grain | 1 | 2 | 3 | 1 | 2 | 3 | 1 | 2 | 3 |
| Analysis | DASS | | | | | | | | |
| $SiO_2$ | 34.25 | 33.98 | 34.48 | 33.55 | 34.11 | 34.07 | 35.93 | 34.85 | 34.59 |
| $TiO_2$ | 0.08 | 0.09 | 0.05 | 0.27 | 0.37 | 0.20 | 0.18 | 0.20 | 0.02 |
| $Al_2O_3$ | 34.50 | 35.22 | 34.68 | 34.87 | 33.89 | 34.88 | 34.71 | 34.76 | 35.10 |
| FeO | 15.03 | 13.57 | 15.01 | 15.02 | 14.49 | 14.64 | 13.31 | 14.01 | 13.77 |
| MnO | 0.80 | 0.69 | 0.62 | 0.68 | 0.62 | 0.67 | 0.27 | 0.64 | 0.25 |
| MgO | 0.01 | 0.00 | 0.00 | 0.06 | 0.00 | 0.05 | 0.11 | 0.02 | 0.04 |
| CaO | 0.06 | 0.13 | 0.03 | 0.11 | 0.06 | 0.15 | 0.00 | 0.05 | 0.00 |
| $Na_2O$ | 1.24 | 1.16 | 1.28 | 1.39 | 1.39 | 1.28 | 1.21 | 1.24 | 1.17 |
| $K_2O$ | 0.02 | 0.01 | 0.00 | 0.02 | 0.07 | 0.04 | 0.00 | 0.00 | 0.02 |
| $Cr_2O_3$ | 0.00 | 0.00 | 0.02 | 0.00 | 0.00 | 0.00 | 0.00 | 0.00 | 0.03 |
| NiO | 0.02 | 0.14 | 0.00 | 0.02 | 0.00 | 0.01 | 0.00 | 0.04 | 0.00 |
| **Total** | **86.01** | **84.99** | **86.17** | **85.99** | **85.00** | **85.99** | **85.72** | **85.81** | **84.99** |

Structural formulas calculated on the basis of 24.5 oxygens.

| | | | | | | | | | |
|---|---|---|---|---|---|---|---|---|---|
| Si | 5.65 | 5.64 | 5.66 | 5.54 | 5.68 | 5.61 | 5.86 | 5.73 | 5.72 |
| Ti | 0.01 | 0.01 | 0.01 | 0.03 | 0.05 | 0.02 | 0.02 | 0.02 | 0.00 |
| Al | 6.70 | 6.88 | 6.71 | 6.79 | 6.65 | 6.77 | 6.67 | 6.72 | 6.83 |
| $Fe_2$ | 1.86 | 1.69 | 1.85 | 1.87 | 1.82 | 1.81 | 1.63 | 1.73 | 1.71 |
| Mn | 0.11 | 0.10 | 0.09 | 0.10 | 0.09 | 0.09 | 0.04 | 0.09 | 0.04 |
| Mg | 0.00 | 0.00 | 0.00 | 0.02 | 0.00 | 0.01 | 0.03 | 0.01 | 0.01 |
| Ca | 0.01 | 0.02 | 0.01 | 0.02 | 0.01 | 0.03 | 0.00 | 0.01 | 0.00 |
| Na | 0.40 | 0.37 | 0.41 | 0.45 | 0.45 | 0.41 | 0.38 | 0.40 | 0.38 |
| K | 0.00 | 0.00 | 0.00 | 0.00 | 0.02 | 0.01 | 0.00 | 0.00 | 0.00 |
| Cr | 0.00 | 0.00 | 0.00 | 0.00 | 0.00 | 0.00 | 0.00 | 0.00 | 0.00 |
| Ni | 0.00 | 0.02 | 0.00 | 0.00 | 0.00 | 0.00 | 0.00 | 0.01 | 0.00 |

**(Table 6. 5 continued)**

**AXINITE**

| Sample | 12A | 12A | 12A | 12B | 12B | 12B | 12D | 12D | 12D | 12E | 12E | 12E | 12F | 12F |
|---|---|---|---|---|---|---|---|---|---|---|---|---|---|---|
| Grain | 1 | 2 | 3 | 1 | 2 | 3 | 1 | 2 | 3 | 1 | 2 | 3 | 1 | 2 |
| Analysis | ALCH | | | | | | | | | | | | | |
| $SiO_2$ | 43.93 | 42.48 | 44.46 | 42.58 | 43.04 | 43.15 | 42.58 | 43.07 | 42.07 | 43.30 | 42.35 | 42.67 | 43.04 | 42.52 |
| $TiO_2$ | 0.00 | 0.10 | 0.00 | 0.00 | 0.00 | 0.09 | 0.07 | 0.05 | 0.12 | 0.00 | 0.04 | 0.00 | 0.00 | 0.00 |
| $Al_2O_3$ | 17.89 | 17.88 | 19.36 | 17.05 | 17.39 | 17.79 | 17.40 | 17.40 | 17.72 | 17.99 | 17.19 | 17.27 | 17.34 | 17.62 |
| FeO | 10.10 | 11.03 | 9.26 | 10.46 | 10.81 | 10.80 | 9.25 | 10.80 | 10.90 | 10.68 | 12.09 | 12.13 | 11.02 | 10.53 |
| MnO | 0.38 | 0.21 | 0.00 | 0.28 | 0.27 | 0.39 | 0.21 | 0.60 | 0.61 | 0.65 | 0.83 | 0.50 | 0.80 | 0.52 |
| MgO | 0.82 | 0.73 | 1.41 | 0.92 | 1.14 | 0.90 | 1.13 | 0.83 | 0.91 | 1.08 | 0.99 | 0.82 | 0.99 | 0.85 |
| CaO | 19.75 | 20.25 | 20.81 | 20.54 | 19.36 | 19.90 | 21.33 | 20.15 | 20.43 | 19.41 | 20.19 | 20.53 | 20.84 | 19.82 |
| $Na_2O$ | 0.00 | 0.00 | 0.00 | 0.00 | 0.00 | 0.00 | 0.00 | 0.00 | 0.00 | 0.00 | 0.00 | 0.00 | 0.00 | 0.00 |
| $K_2O$ | 0.00 | 0.00 | 0.00 | 0.00 | 0.00 | 0.00 | 0.00 | 0.00 | 0.00 | 0.00 | 0.00 | 0.00 | 0.00 | 0.00 |
| $Cr_2O_3$ | 0.00 | 0.09 | 0.00 | 0.06 | 0.00 | 0.00 | 0.03 | 0.00 | 0.09 | 0.00 | 0.00 | 0.07 | 0.00 | 0.10 |
| NiO | 0.02 | 0.15 | 0.00 | 0.11 | 0.00 | 0.03 | 0.00 | 0.00 | 0.15 | 0.02 | 0.31 | 0.00 | 0.00 | 0.02 |
| **Total** | **92.89** | **92.92** | **95.30** | **92.00** | **92.01** | **93.05** | **92.00** | **92.90** | **93.00** | **93.13** | **93.99** | **93.99** | **94.03** | **91.98** |

Structural formulas calculated on the basis of 32 oxygens.

| | | | | | | | | | | | | | | |
|---|---|---|---|---|---|---|---|---|---|---|---|---|---|---|
| Si | 9.15 | 8.92 | 9.00 | 9.03 | 9.08 | 9.02 | 9.01 | 9.04 | 8.86 | 9.03 | 8.87 | 8.91 | 8.96 | 9.00 |
| Ti | 0.00 | 0.02 | 0.00 | 0.00 | 0.00 | 0.01 | 0.01 | 0.01 | 0.02 | 0.00 | 0.01 | 0.00 | 0.00 | 0.00 |
| Al | 4.39 | 4.42 | 4.62 | 4.26 | 4.32 | 4.38 | 4.34 | 4.30 | 4.39 | 4.42 | 4.24 | 4.25 | 4.25 | 4.39 |
| $Fe_2$ | 1.58 | 1.74 | 1.41 | 1.67 | 1.71 | 1.70 | 1.47 | 1.70 | 1.73 | 1.67 | 1.90 | 1.90 | 1.73 | 1.68 |
| Mn | 0.07 | 0.04 | 0.00 | 0.05 | 0.05 | 0.07 | 0.04 | 0.11 | 0.11 | 0.11 | 0.15 | 0.09 | 0.14 | 0.09 |
| Mg | 0.25 | 0.23 | 0.43 | 0.29 | 0.36 | 0.28 | 0.36 | 0.26 | 0.29 | 0.34 | 0.31 | 0.26 | 0.31 | 0.27 |
| Ca | 4.41 | 4.56 | 4.52 | 4.67 | 4.38 | 4.46 | 4.84 | 4.53 | 4.61 | 4.34 | 4.53 | 4.59 | 4.65 | 4.50 |
| Na | 0.00 | 0.00 | 0.00 | 0.00 | 0.00 | 0.00 | 0.00 | 0.00 | 0.00 | 0.00 | 0.00 | 0.00 | 0.00 | 0.00 |
| K | 0.00 | 0.00 | 0.00 | 0.00 | 0.00 | 0.00 | 0.00 | 0.00 | 0.00 | 0.00 | 0.00 | 0.00 | 0.00 | 0.00 |
| Cr | 0.00 | 0.01 | 0.00 | 0.01 | 0.00 | 0.00 | 0.01 | 0.00 | 0.01 | 0.00 | 0.00 | 0.01 | 0.00 | 0.02 |
| Ni | 0.00 | 0.03 | 0.00 | 0.02 | 0.00 | 0.01 | 0.00 | 0.00 | 0.03 | 0.00 | 0.05 | 0.00 | 0.00 | 0.00 |

**(Table 6. 5 continued)**

| | AXINITE | | | | | | AUGITE | | | | | | | |
|---|---|---|---|---|---|---|---|---|---|---|---|---|---|---|
| Sample | 12G | 12G | 12G | 12 H | 12 H | 12 H | 10-A | 10-B | 10-D | 10-E | 10-L | 24 | 24 | 24 |
| Grain | 1 | 2 | 3 | 1 | 2 | 3 | 1 | 1 | 1 | 1 | 1 | 1 | 2 | 3 |
| Analysis | ALCH | | | | | | ALCH | | | | | | | |
| $SiO_2$ | 42.90 | 43.12 | 42.71 | 44.64 | 42.57 | 43.19 | 52.97 | 53.23 | 52.99 | 52.44 | 53.51 | 52.57 | 52.71 | 52.91 |
| $TiO_2$ | 0.11 | 0.02 | 0.01 | 0.00 | 0.09 | 0.00 | 0.01 | 0.03 | 0.00 | 0.02 | 0.02 | 0.02 | 0.01 | 0.04 |
| $Al_2O_3$ | 17.34 | 17.09 | 17.29 | 17.56 | 17.58 | 17.47 | 0.98 | 0.94 | 0.17 | 0.20 | 0.68 | 2.55 | 2.91 | 3.05 |
| FeO | 10.84 | 10.21 | 11.54 | 9.24 | 9.49 | 8.74 | 9.74 | 8.26 | 8.80 | 9.65 | 4.91 | 8.26 | 7.79 | 8.78 |
| MnO | 0.40 | 0.63 | 0.55 | 1.04 | 0.66 | 0.69 | 0.17 | 0.21 | 0.24 | 0.28 | 0.13 | 0.13 | 0.11 | 0.12 |
| MgO | 0.86 | 0.93 | 0.82 | 1.58 | 1.56 | 1.55 | 11.95 | 13.00 | 11.97 | 12.29 | 15.12 | 13.46 | 13.32 | 12.44 |
| CaO | 21.47 | 19.92 | 19.68 | 21.91 | 22.03 | 21.12 | 21.53 | 21.60 | 22.05 | 21.09 | 21.70 | 22.16 | 22.78 | 22.55 |
| $Na_2O$ | 0.00 | 0.00 | 0.00 | 0.00 | 0.00 | 0.00 | 0.58 | 0.44 | 0.19 | 0.16 | 0.32 | 0.00 | 0.14 | 0.00 |
| $K_2O$ | 0.00 | 0.00 | 0.00 | 0.00 | 0.00 | 0.00 | 0.00 | 0.00 | 0.00 | 0.00 | 0.00 | 0.00 | 0.00 | 0.00 |
| $Cr_2O_3$ | 0.00 | 0.00 | 0.06 | 0.00 | 0.00 | 0.00 | 0.09 | 0.07 | 0.05 | 0.02 | 0.00 | 0.00 | 0.00 | 0.01 |
| NiO | 0.06 | 0.05 | 0.17 | 0.08 | 0.00 | 0.22 | 0.00 | 0.14 | 0.00 | 0.01 | 0.04 | 0.09 | 0.08 | 0.13 |
| **Total** | **93.98** | **91.97** | **92.83** | **96.05** | **93.98** | **92.98** | **98.02** | **97.92** | **96.46** | **96.16** | **96.43** | **99.24** | **99.85** | **100.03** |

Structural formulas calculated on the basis of 32 and 6 oxygens for axinite and augite respectively.

| | | | | | | | | | | | | | | |
|---|---|---|---|---|---|---|---|---|---|---|---|---|---|---|
| Si | 8.94 | 9.12 | 8.99 | 9.07 | 8.87 | 9.04 | 2.03 | 2.03 | 2.07 | 2.05 | 2.04 | 1.99 | 1.98 | 2.00 |
| Ti | 0.02 | 0.00 | 0.00 | 0.00 | 0.01 | 0.00 | 0.00 | 0.00 | 0.00 | 0.00 | 0.00 | 0.00 | 0.00 | 0.00 |
| Al | 4.26 | 4.26 | 4.29 | 4.20 | 4.31 | 4.31 | 0.04 | 0.04 | 0.01 | 0.01 | 0.03 | 0.01 | 0.02 | 0.00 |
| $Fe_2$ | 1.70 | 1.62 | 1.83 | 1.41 | 1.49 | 1.38 | 0.31 | 0.26 | 0.29 | 0.32 | 0.16 | 0.24 | 0.22 | 0.25 |
| Mn | 0.07 | 0.11 | 0.10 | 0.18 | 0.12 | 0.12 | 0.01 | 0.01 | 0.01 | 0.01 | 0.00 | 0.00 | 0.00 | 0.00 |
| Mg | 0.27 | 0.29 | 0.26 | 0.48 | 0.48 | 0.48 | 0.68 | 0.74 | 0.70 | 0.72 | 0.86 | 0.66 | 0.67 | 0.62 |
| Ca | 4.79 | 4.51 | 4.44 | 4.77 | 4.92 | 4.74 | 0.88 | 0.88 | 0.92 | 0.88 | 0.89 | 0.90 | 0.92 | 0.91 |
| Na | 0.00 | 0.00 | 0.00 | 0.00 | 0.00 | 0.00 | 0.04 | 0.03 | 0.01 | 0.01 | 0.02 | 0.00 | 0.01 | 0.00 |
| K | 0.00 | 0.00 | 0.00 | 0.00 | 0.00 | 0.00 | 0.00 | 0.00 | 0.00 | 0.00 | 0.00 | 0.00 | 0.00 | 0.00 |
| Cr | 0.00 | 0.00 | 0.01 | 0.00 | 0.00 | 0.00 | 0.00 | 0.00 | 0.00 | 0.00 | 0.00 | 0.00 | 0.00 | 0.00 |
| Ni | 0.01 | 0.01 | 0.03 | 0.01 | 0.00 | 0.04 | 0.00 | 0.00 | 0.00 | 0.00 | 0.00 | 0.00 | 0.00 | 0.00 |

**TOPAZ**

| Sample | 6 | 6 | 6 | 19-M | 19-C | 19-M | 29 | 29 | 29 |
|---|---|---|---|---|---|---|---|---|---|
| Grain | 1 | 2 | 3 | 1 | 1 | 1 | 1 | 2 | 3 |
| Analysis | YUN | | | KSH | | | SHN | | |
| $SiO_2$ | 32.37 | 32.13 | 32.25 | 32.25 | 31.82 | 32.45 | 31.87 | 31.75 | 31.65 |
| $TiO_2$ | 0.00 | 0.00 | 0.03 | 0.00 | 0.00 | 0.00 | 0.00 | 0.00 | 0.04 |
| $Al_2O_3$ | 55.12 | 55.45 | 55.18 | 57.16 | 55.12 | 57.03 | 56.73 | 56.65 | 55.98 |
| FeO | 0.00 | 0.02 | 0.00 | 0.00 | 0.00 | 0.00 | 0.00 | 0.00 | 0.00 |
| MnO | 0.00 | 0.00 | 0.00 | 0.00 | 0.00 | 0.00 | 0.00 | 0.00 | 0.00 |
| MgO | 0.06 | 0.03 | 0.04 | 0.07 | 0.00 | 0.10 | 0.00 | 0.01 | 0.01 |
| CaO | 0.00 | 0.00 | 0.02 | 0.11 | 0.00 | 0.00 | 0.00 | 0.00 | 0.00 |
| $Na_2O$ | 0.02 | 0.00 | 0.00 | 0.03 | 0.00 | 0.00 | 0.00 | 0.00 | 0.00 |
| $K_2O$ | 0.05 | 0.01 | 0.02 | 0.13 | 0.06 | 0.09 | 0.01 | 0.02 | 0.00 |
| $Cr_2O_3$ | 0.00 | 0.00 | 0.00 | 0.00 | 0.00 | 0.00 | 0.00 | 0.00 | 0.00 |
| NiO | 0.00 | 0.00 | 0.00 | 0.00 | 0.00 | 0.00 | 0.00 | 0.00 | 0.00 |
| F | 18.77 | 19.46 | 19.25 | 20.15 | 19.28 | 20.18 | 20.17 | 20.25 | 20.15 |
| O ≡ F | 7.90 | 8.19 | 8.10 | 8.48 | 8.12 | 8.50 | 8.49 | 8.53 | 8.48 |
| **Total** | **95.52** | **95.83** | **95.64** | **98.23** | **95.12** | **98.17** | **97.10** | **96.96** | **96.16** |

Structural formulas calculated on the basis of 24 oxygens.

| | | | | | | | | | |
|---|---|---|---|---|---|---|---|---|---|
| Si | 4.79 | 4.75 | 4.77 | 4.67 | 4.74 | 4.69 | 4.66 | 4.65 | 4.68 |
| Ti | 0.00 | 0.00 | 0.00 | 0.00 | 0.00 | 0.00 | 0.00 | 0.00 | 0.00 |
| Al | 9.60 | 9.65 | 9.61 | 9.74 | 9.67 | 9.71 | 9.77 | 9.78 | 9.74 |
| $Fe_2$ | 0.00 | 0.00 | 0.00 | 0.00 | 0.00 | 0.00 | 0.00 | 0.00 | 0.00 |
| Mn | 0.00 | 0.00 | 0.00 | 0.00 | 0.00 | 0.00 | 0.00 | 0.00 | 0.00 |
| Mg | 0.01 | 0.01 | 0.01 | 0.02 | 0.00 | 0.02 | 0.00 | 0.00 | 0.00 |
| Ca | 0.00 | 0.00 | 0.00 | 0.02 | 0.00 | 0.00 | 0.00 | 0.00 | 0.00 |
| Na | 0.01 | 0.00 | 0.00 | 0.01 | 0.00 | 0.00 | 0.00 | 0.00 | 0.00 |
| K | 0.01 | 0.00 | 0.00 | 0.02 | 0.01 | 0.02 | 0.00 | 0.00 | 0.00 |
| Cr | 0.00 | 0.00 | 0.00 | 0.00 | 0.00 | 0.00 | 0.00 | 0.00 | 0.00 |
| Ni | 0.00 | 0.00 | 0.00 | 0.00 | 0.00 | 0.00 | 0.00 | 0.00 | 0.00 |
| F | 7.39 | 7.66 | 7.58 | 7.76 | 7.65 | 7.77 | 7.86 | 7.91 | 7.93 |

**Fluorite**

| Sample | 1C-M | 1C-C | 1C-M | 1D-M | 1D-M | 1D-C | 7-M | 7-M | 7-C | 18A-M |
|---|---|---|---|---|---|---|---|---|---|---|
| Grain | 1 | 2 | 3 | 1 | 2 | 3 | 1 | 2 | 3 | 1 |
| Analysis | YUN | | | | | | | | | KSH |
| $SiO_2$ | 0.28 | 0.14 | 0.18 | 0.21 | 0.14 | 0.13 | 0.37 | 0.30 | 0.26 | 0.20 |
| $TiO_2$ | 0.11 | 0.00 | 0.12 | 0.11 | 0.15 | 0.09 | 0.19 | 0.08 | 0.09 | 0.07 |
| $Al_2O_3$ | 0.00 | 0.00 | 0.00 | 0.00 | 0.00 | 0.00 | 0.04 | 0.00 | 0.00 | 0.00 |
| FeO | 0.00 | 0.02 | 0.00 | 0.00 | 0.00 | 0.00 | 0.00 | 0.00 | 0.00 | 0.00 |
| MnO | 0.03 | 0.06 | 0.13 | 0.02 | 0.00 | 0.01 | 0.11 | 0.00 | 0.00 | 0.04 |
| MgO | 0.00 | 0.00 | 0.00 | 0.01 | 0.00 | 0.00 | 0.00 | 0.01 | 0.02 | 0.00 |
| CaO | 52.12 | 51.42 | 51.77 | 51.91 | 51.66 | 50.29 | 51.12 | 52.83 | 52.85 | 51.71 |
| $Na_2O$ | 0.01 | 0.00 | 0.00 | 0.00 | 0.00 | 0.04 | 0.00 | 0.05 | 0.05 | 0.02 |
| $K_2O$ | 0.00 | 0.00 | 0.00 | 0.00 | 0.00 | 0.00 | 0.00 | 0.00 | 0.00 | 0.00 |
| NiO | 0.00 | 0.05 | 0.00 | 0.00 | 0.00 | 0.00 | 0.00 | 0.00 | 0.00 | 0.00 |
| $Cr_2O_3$ | 0.04 | 0.01 | 0.03 | 0.02 | 0.10 | 0.06 | 0.00 | 0.03 | 0.05 | 0.00 |
| F | 48.41 | 48.25 | 47.67 | 48.62 | 48.77 | 47.38 | 48.11 | 48.71 | 47.68 | 48.63 |
| **Total** | **101.00** | **99.95** | **99.90** | **100.90** | **100.82** | **98.00** | **99.94** | **102.01** | **101.00** | **100.67** |

**Fluorite**

| Sample | 18A-C | 18A-M | 18B-M1 | 18B-M2 | 18B-M3 | 21-C | 21-M | 26-M | 26-M | 26-C |
|---|---|---|---|---|---|---|---|---|---|---|
| Grain | 2 | 3 | 1 | 2 | 3 | 1 | 2 | 1 | 2 | 3 |
| Analysis | KSH | | | | | | | SHN | | |
| $SiO_2$ | 0.26 | 0.25 | 0.32 | 0.17 | 0.18 | 0.34 | 0.18 | 0.30 | 0.29 | 0.17 |
| $TiO_2$ | 0.10 | 0.09 | 0.03 | 0.03 | 0.07 | 0.00 | 0.17 | 0.09 | 0.02 | 0.10 |
| $Al_2O_3$ | 0.07 | 0.00 | 0.05 | 0.00 | 0.00 | 0.00 | 0.04 | 0.10 | 0.00 | 0.00 |
| FeO | 0.00 | 0.04 | 0.00 | 0.00 | 0.00 | 0.00 | 0.00 | 0.01 | 0.01 | 0.00 |
| MnO | 0.01 | 0.06 | 0.00 | 0.00 | 0.00 | 0.00 | 0.04 | 0.00 | 0.00 | 0.00 |
| MgO | 0.00 | 0.00 | 0.00 | 0.00 | 0.00 | 0.00 | 0.00 | 0.00 | 0.02 | 0.02 |
| CaO | 52.61 | 51.10 | 51.88 | 52.46 | 51.33 | 51.29 | 51.71 | 51.75 | 52.05 | 52.42 |
| $Na_2O$ | 0.02 | 0.09 | 0.00 | 0.00 | 0.00 | 0.00 | 0.00 | 0.00 | 0.00 | 0.02 |
| $K_2O$ | 0.00 | 0.00 | 0.00 | 0.00 | 0.00 | 0.00 | 0.00 | 0.00 | 0.00 | 0.00 |
| NiO | 0.00 | 0.00 | 0.00 | 0.07 | 0.00 | 0.00 | 0.00 | 0.00 | 0.00 | 0.00 |
| $Cr_2O_3$ | 0.00 | 0.00 | 0.00 | 0.00 | 0.04 | 0.00 | 0.00 | 0.04 | 0.00 | 0.03 |
| F | 47.91 | 48.61 | 48.72 | 47.27 | 48.36 | 48.35 | 48.84 | 48.69 | 48.68 | 48.24 |
| **Total** | **100.98** | **100.24** | **101.00** | **100.00** | **99.98** | **99.98** | **100.98** | **100.98** | **101.07** | **101.00** |

**Table 6. 6. XRD data of the Shigar valley gemstones with three major d - values.**

| S. No. | Sample # | Name of the Locality | d - 1 | d - 2 | d - 3 | Gemstone |
|---|---|---|---|---|---|---|
| 1 | 23 | Dassu | 3.45 | 2.56 | 6.33 | Foitite |
| 2 | 20B | Dassu | 3.45 | 2.56 | 6.32 | Foitite |
| 3 | 15 | Kashmol | 3.45 | 2.57 | 6.32 | Foitite-schorl |
| 4 | 29C | Shengus | 3.46 | 2.97 | 2.59 | Foitite-dravite |
| 5 | 10A | Alchuri | 2.94 | 3.22 | 2.97 | Augite |
| 6 | 24 | Alchuri | 3.21 | 2.93 | 2.97 | Augite |
| 7 | 29A | Shengus | 3.18 | 2.12 | 6.32 | Albite |
| 8 | 13D | Alchuri | 2.87 | 2.78 | 2.65 | Clinozoisite |
| 9 | 10C | Alchuri | 2.88 | 2.66 | 2.59 | Clinozoisite |
| 10 | 22 | Hashupa | 2.57 | 3.96 | 2.88 | Clinozoisite |
| 11 | 11A | Alchuri | 2.68 | 2.02 | 4.03 | Zoisite |
| 12 | 19 | Kashmol | 2.91 | 3.17 | 3.65 | Topaz |
| 13 | 6 | Yuno | 2.92 | 3.02 | 3.65 | Topaz |
| 14 | 29B | Shengus | 2.31 | 3.21 | 3.74 | Topaz |
| 15 | 3 | Yuno | 2.78 | 3.41 | 2.71 | Dahlite |
| 16 | 9A | Alchuri | 2.77 | 2.24 | 2.68 | apatite |
| 17 | 9B | Alchuri | 2.78 | 2.76 | 3.41 | apatite |
| 18 | 32 | Shengus | 2.71 | 2.81 | 3.46 | apatite |
| 19 | 7 | Yuno | 3.13 | 1.92 | 1.64 | Fluorite, |
| 20 | 21 | Kashmol | 3.13 | 1.96 | 1.64 | Fluorite,Yttrian |
| 21 | 18 | Kashmol | 3.13 | 1.92 | 1.64 | Fluorite,Yttrian |
| 22 | 26 | Shengus | 3.13 | 1.92 | 1.64 | Fluorite, |
| 23 | 4A | Yuno | 2.85 | 3.24 | 7.89 | Beryl |
| 24 | 8 | Yuno | 2.84 | 3.22 | 7.89 | Beryl |
| 25 | 46 | Dassu | 2.85 | 3.23 | 7.89 | Beryl |
| 26 | 54 | Goyungo | 2.85 | 3.23 | 7.86 | Beryl |
| 27 | 50 | Nyit | 2.88 | 3.27 | 7.92 | Beryl |
| 28 | 53 | Nyit | 2.85 | 3.24 | 7.93 | Beryl |
| 29 | 27 | Shengus | 2.85 | 3.24 | 7.89 | Beryl |
| 30 | 31 | Shengus | 2.86 | 3.25 | 8.75 | Beryl |
| 31 | 30 | Shengus | 2.87 | 3.26 | 8.04 | Beryl |
| 32 | 58 | Basha | 2.85 | 3.24 | 7.89 | Beryl |
| 33 | 48 | Dassu | 2.56 | 1.56 | 1.54 | Almandine |
| 34 | 5 | Yuno | 2.54 | 2.83 | 1.51 | Almandine |

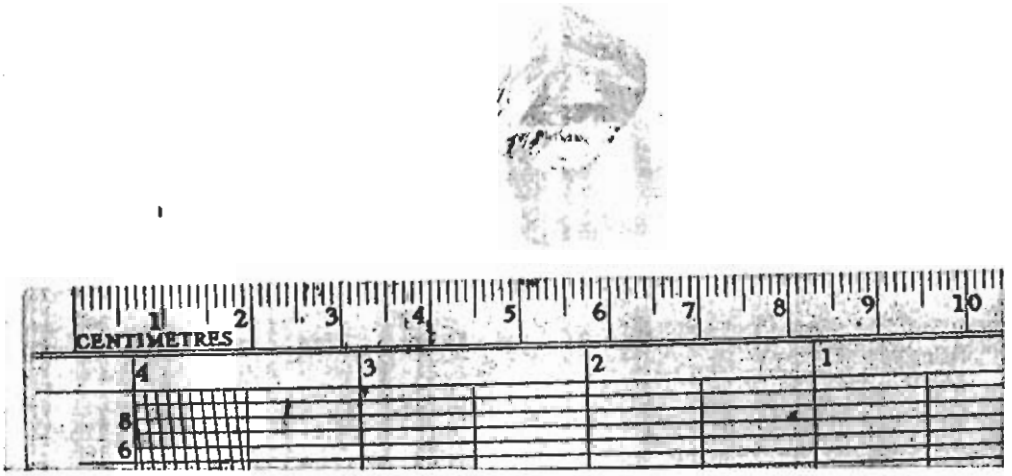


**Plate 6. 1.** Colorless and transparent crystal of topaz from Kashmol pegmatite. The size of crystals is about 1 to 2 cm across. Tetragonal prisms along with c- pinacoid are also present.

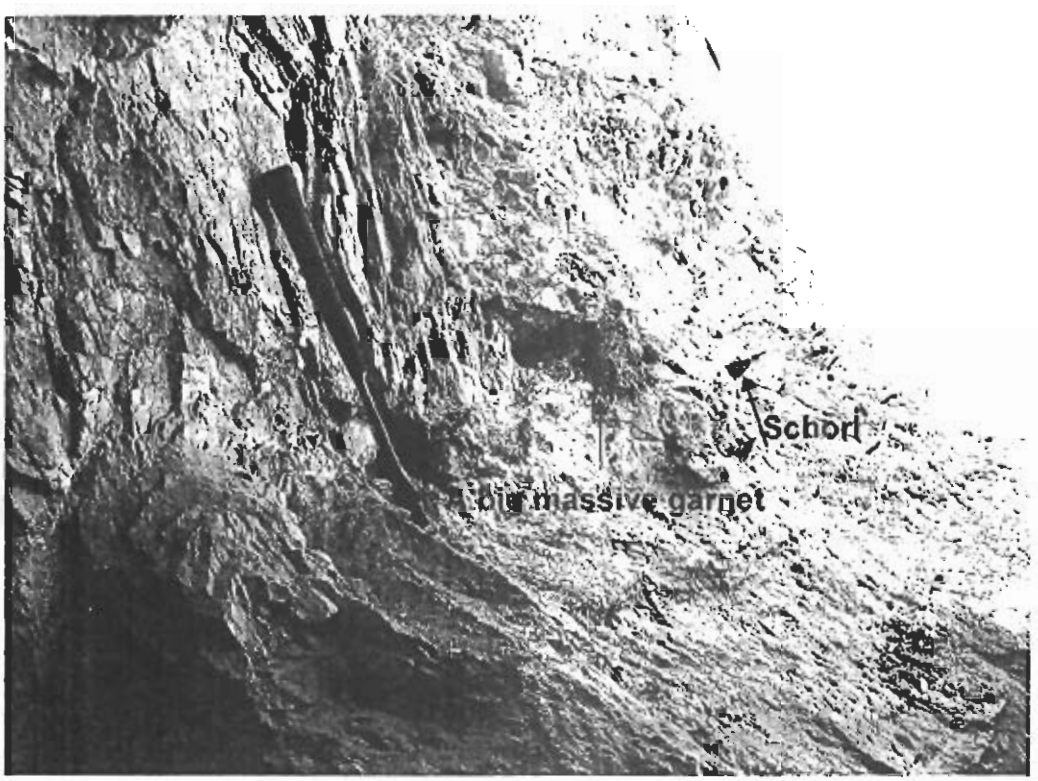


**Plate 6. 2.** A zoned pegmatite near Dassu from which certain gemstones have been excavated and the empty cavities are very clear. A garnet crystal about 6 cm in massive form is very prominent near the cavities. The black-colored schorl is also visible.

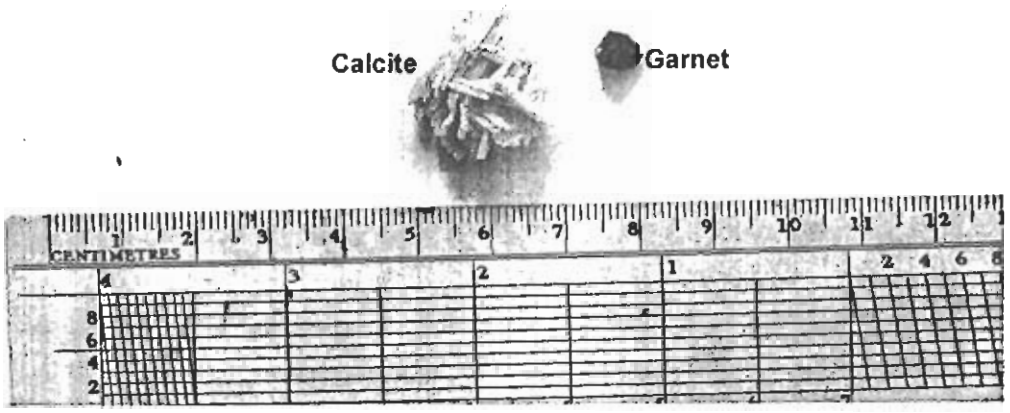


**Plate 6. 3.** A reddish-brown garnet (small grain) from Yuno pegmatite, Shigar valley. An aggregate of white colored calcite crystals is also visible.

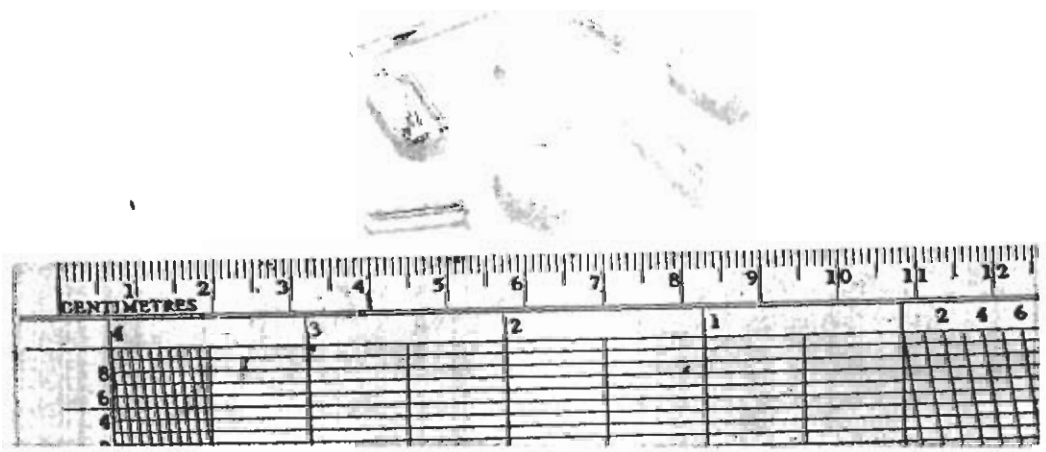


**Plate 6. 4.** Colorless to pale-blue and transparent aquamarine crystals with rectangular prismatic faces of the hexagonal crystal system from various pegmatites of the Shigar valley area. The average size of these crystals is about 1.5 - 3 cm.

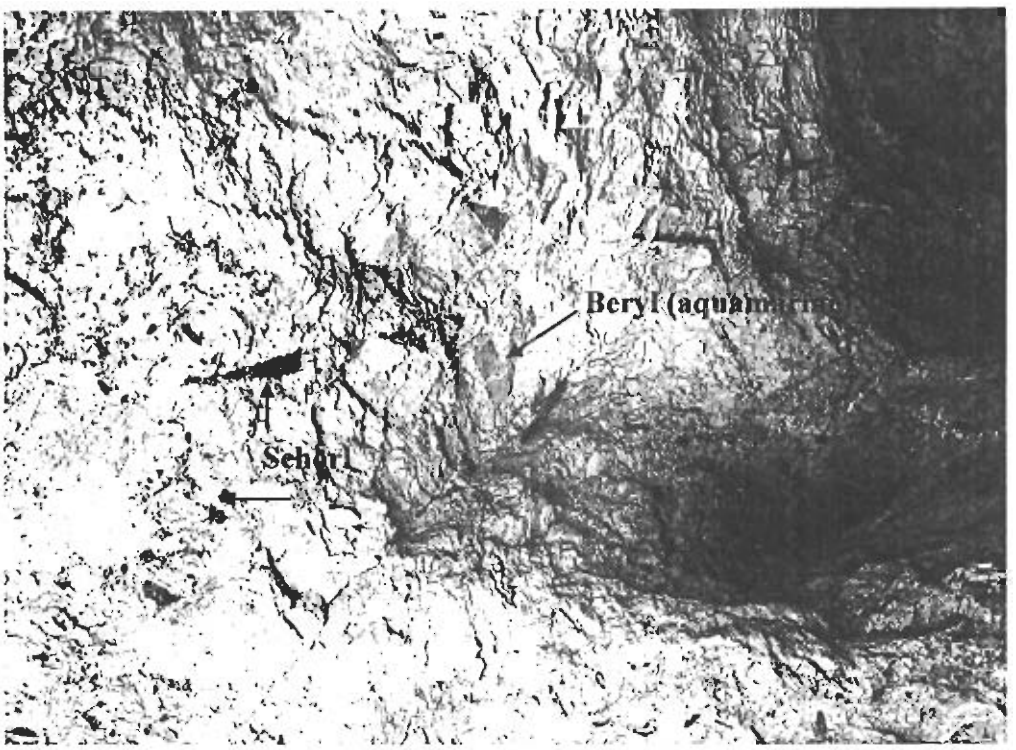


**Plate 6. 5.** A coarse-grained pegmatite near Dassu containing two light blue-colored aquamarine crystals along with certain schorl needles are present in the coarse grained intermediate zone.

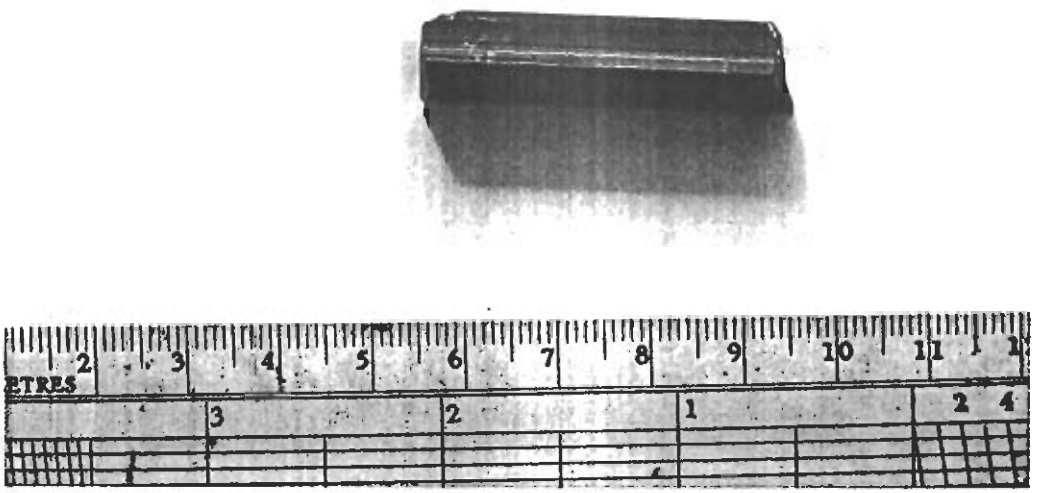

**Plate 6. 6.** Black-coloured tourmaline (Schorl) from Kashmol pegmatite, Shigar valley. The size of crystal is ~ 4 x 1 cm. Numerous striations can also be seen along the hexagonal prismatic faces.

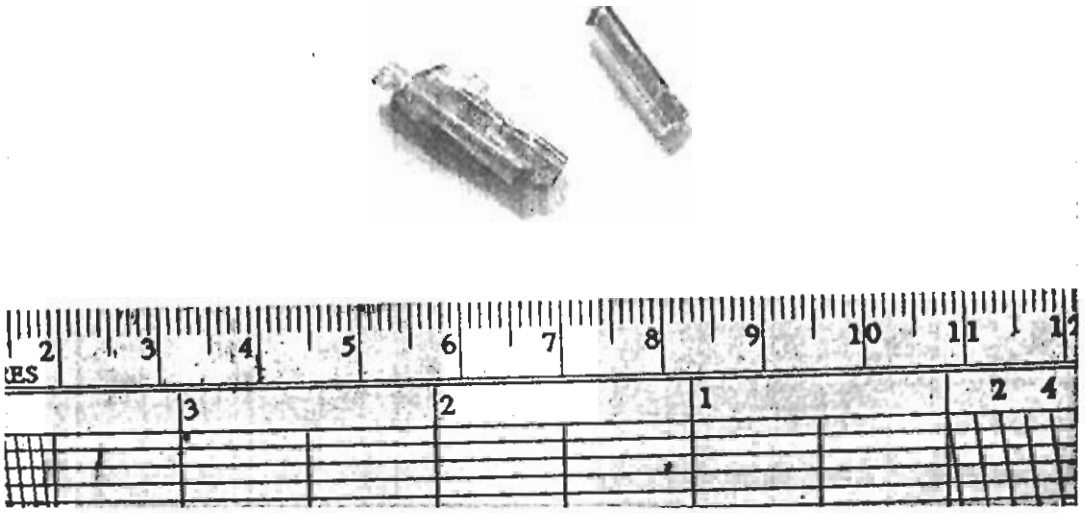

**Plate 6. 7.** Two zoisite crystals from Alchuri, Shigar valley area.

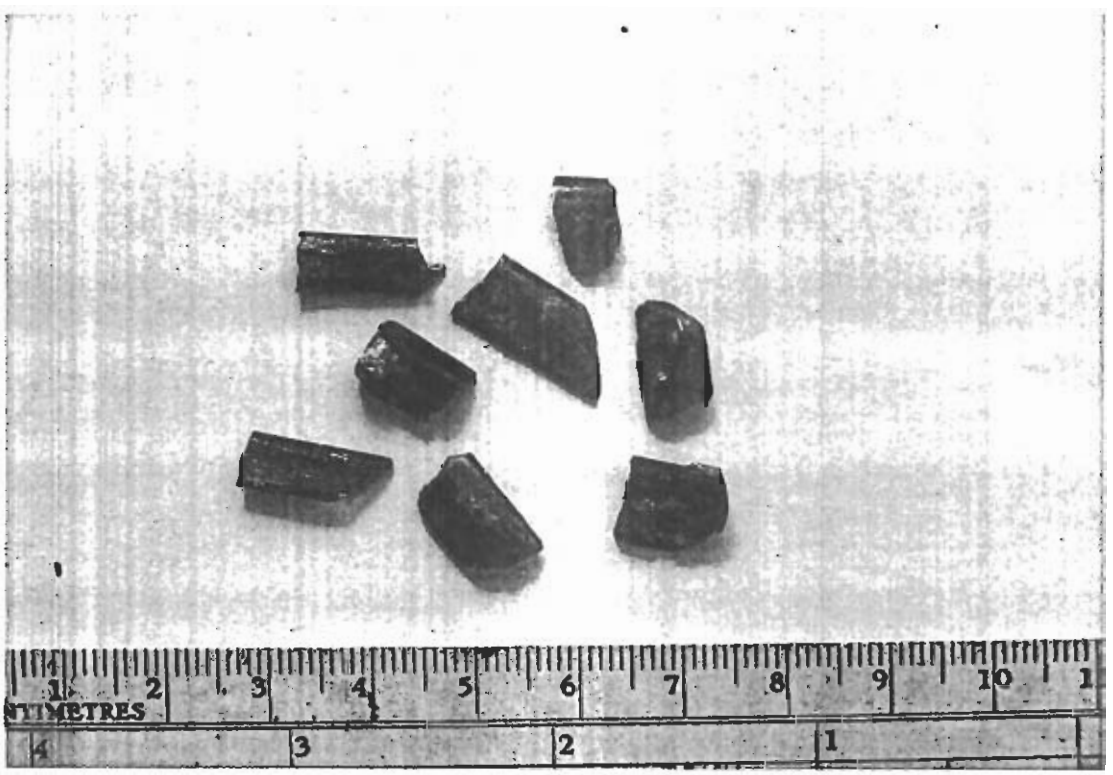

**Plate 6. 8.** Brown colored axinites from the Alchuri, Shigar valley.

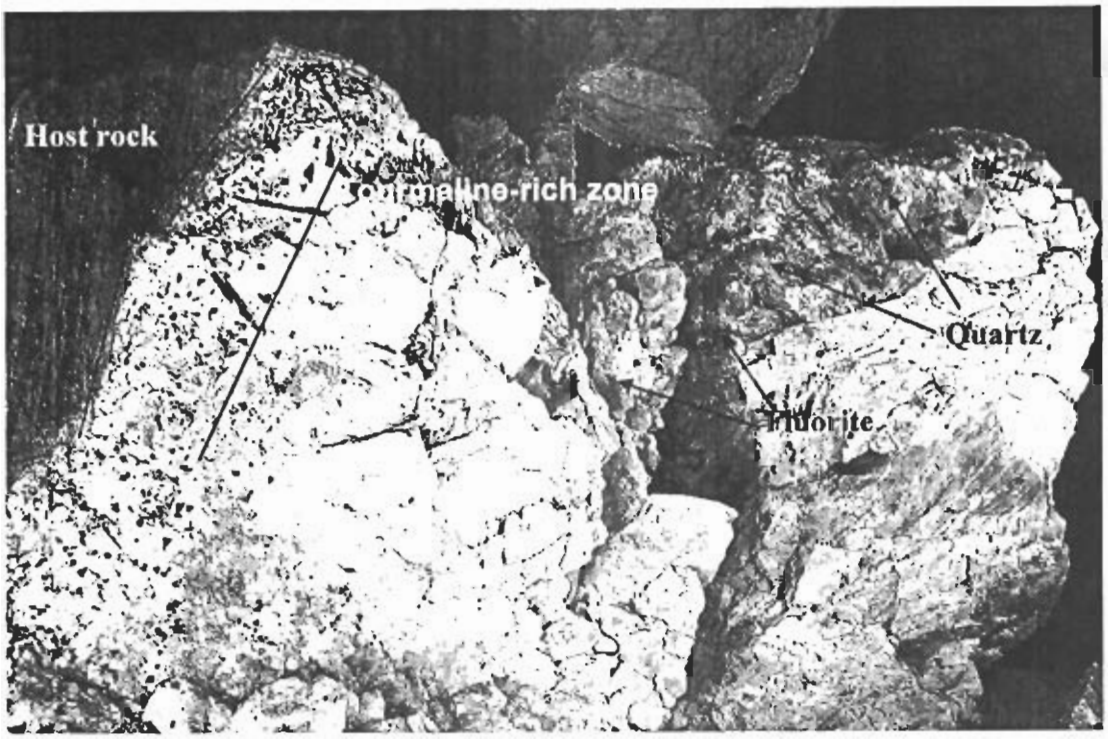


**Plate 6. 9.** A zoned and coarse-grained pegmatite near Yuno, Shigar valley. Numerous radiating and comb structured tourmalines are present at the border zone near the contact with the host rock, while three euhedral green-colored fluorite along with quartz are present into the coarse-grained intermediate zone.

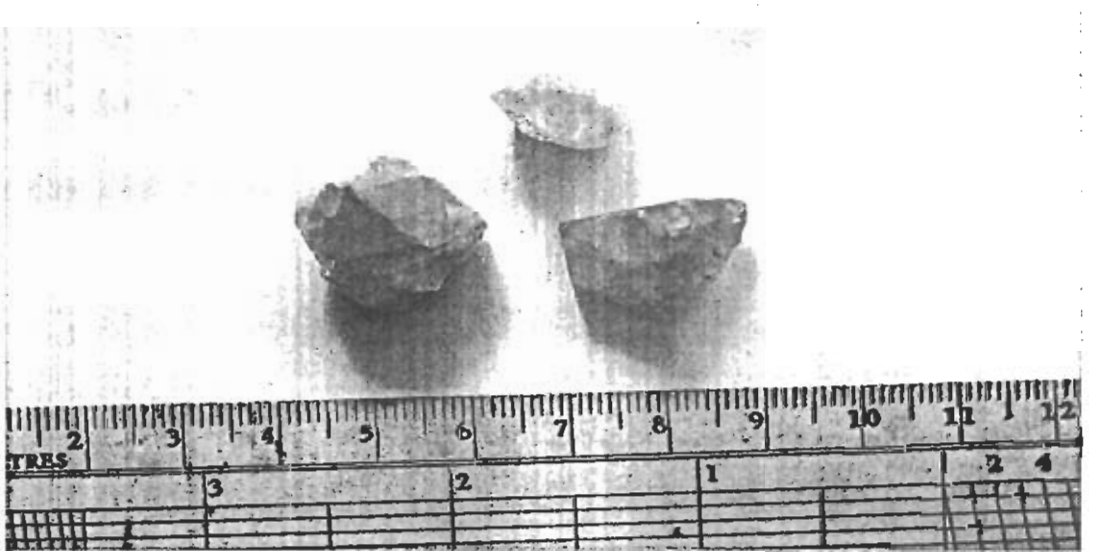

**Plate 6. 10.** Three light-green to dark-green fluorites collected from the pegmatite mines in the Kashmol area, Shigar valley.

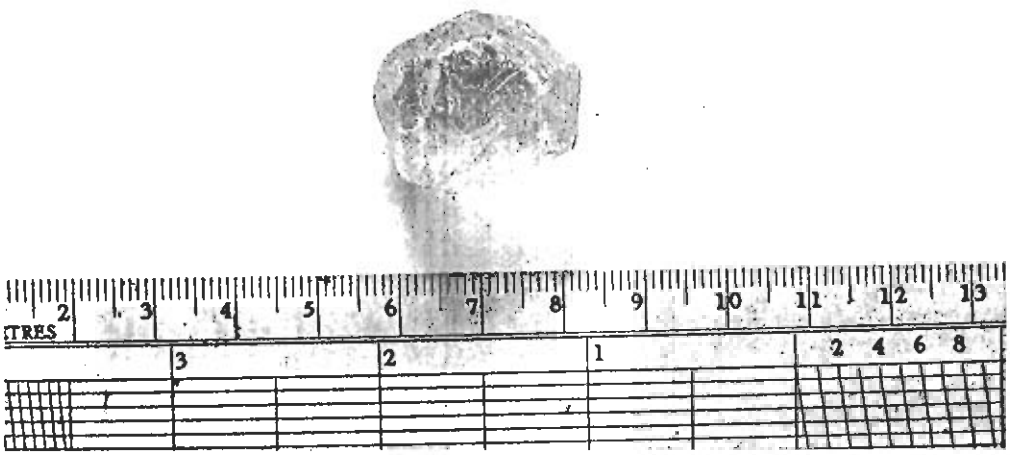

**Plate 6. 11.** Light-green colored fluorite crystal (2cm across) from the Yuno mine, Shigar valley.

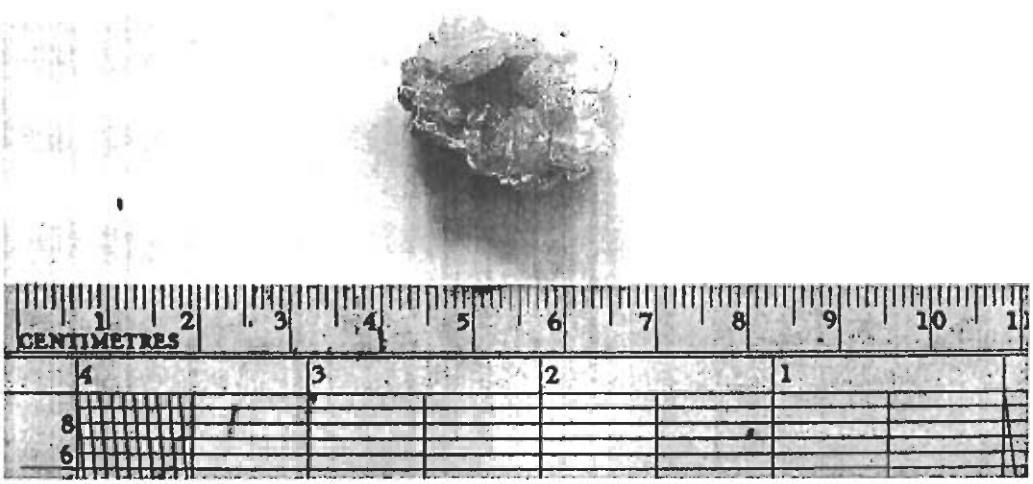

**Plate 6. 12.** An aggregate of light-pink colored apatite crystals from Yuno mine, Shigar valley.

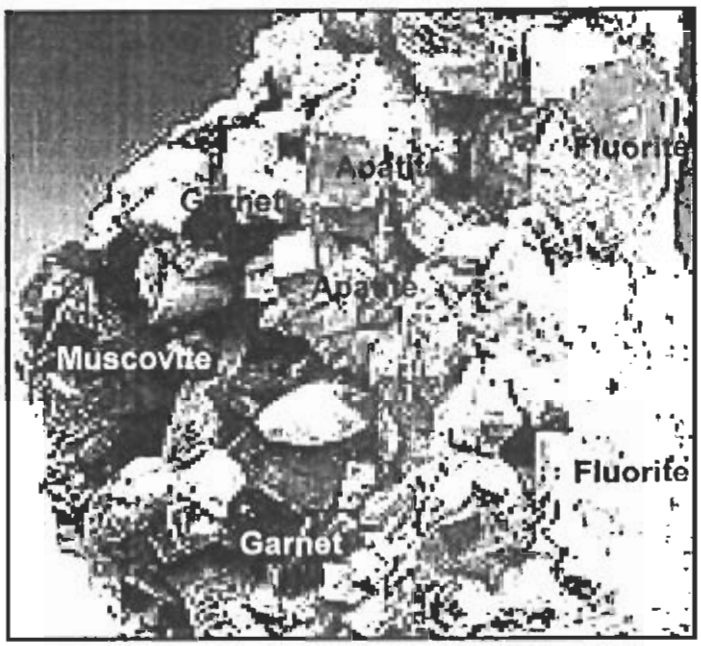


**Plate 6. 13.** An aggregate of light-pink colored apatite, fluorite, garnet and large books of muscovite crystals from Yuno mine, Shigar valley.

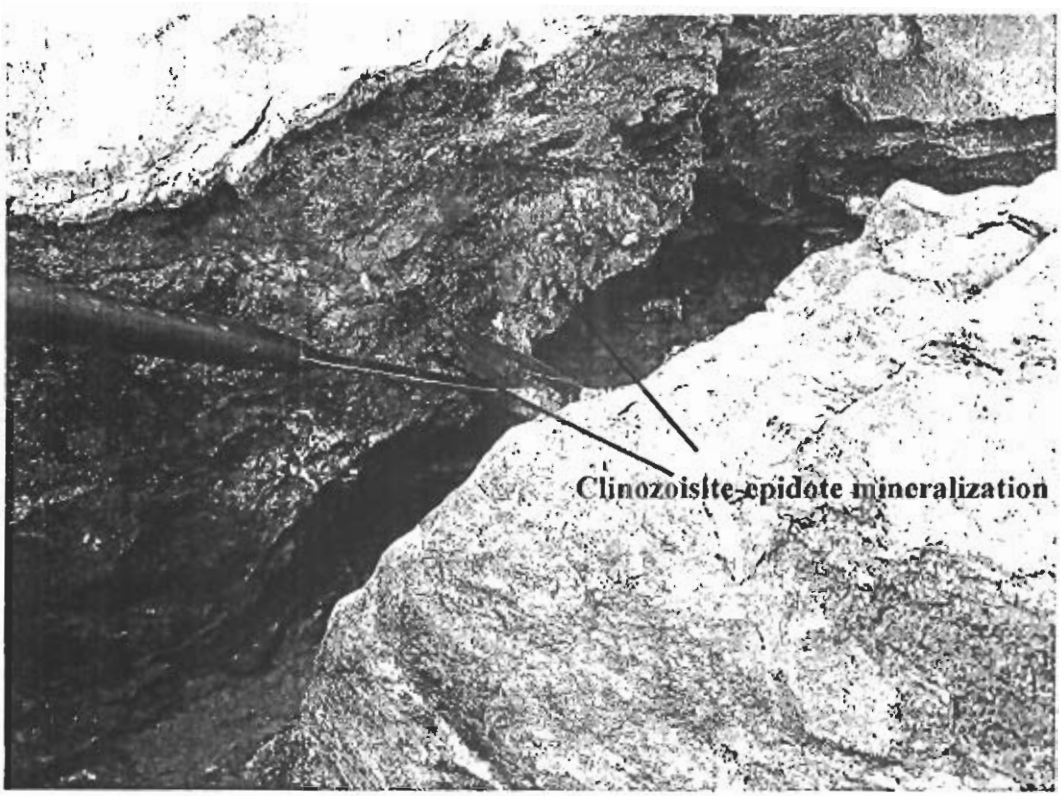


**Plate 6. 14.** The clinozoisite-epidote mineralization is visible in the greenschists at Alchuri, Shigar valley.

**Plate 6. 15.** Light brown-greenish brown clinozoisites (epidote) from Alchuri, Shigar valley. In the bottom, the black euhedral prismatic crystal is augite. At the top twinned clinozoisite crystal is seen.

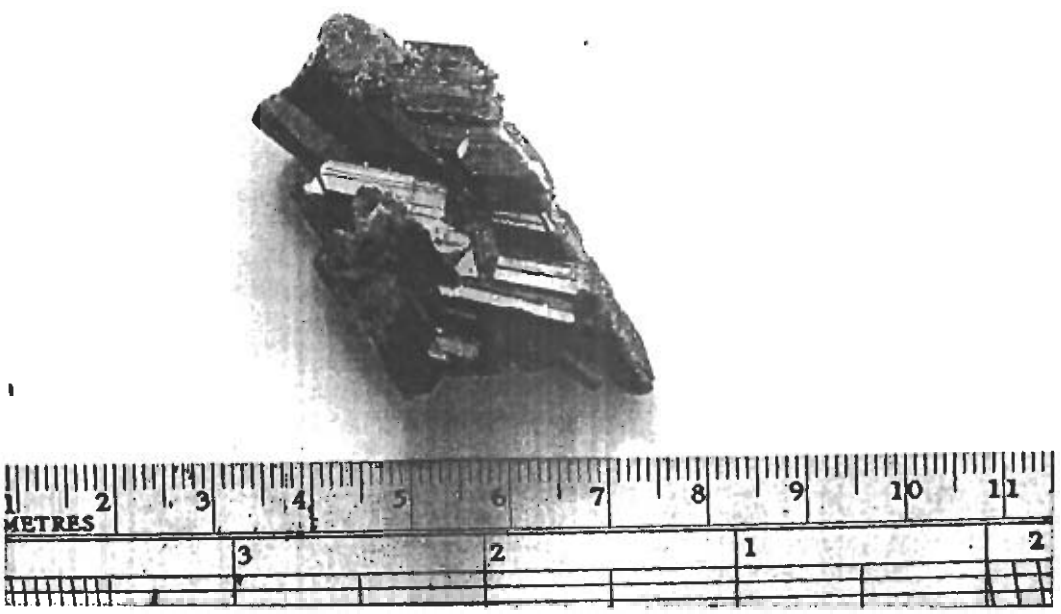


**Plate 6. 16.** An aggregate of dark brown clinozoisite from the Hashupa, Shigar valley.

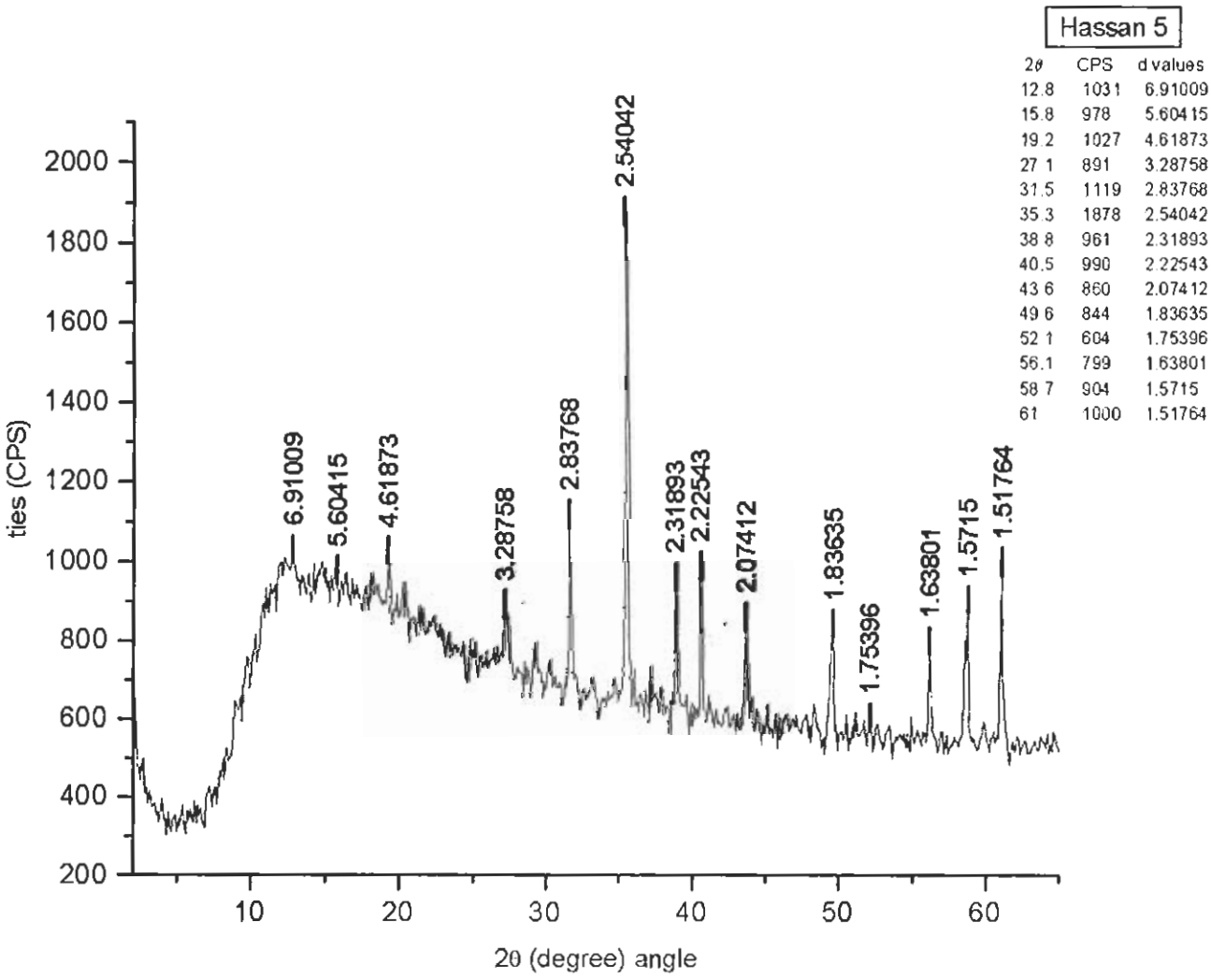


**Fig. 6. 1.** X-ray powder diffraction pattern and data of the garnet from a pegmatite, Yuno, Shigar valley.

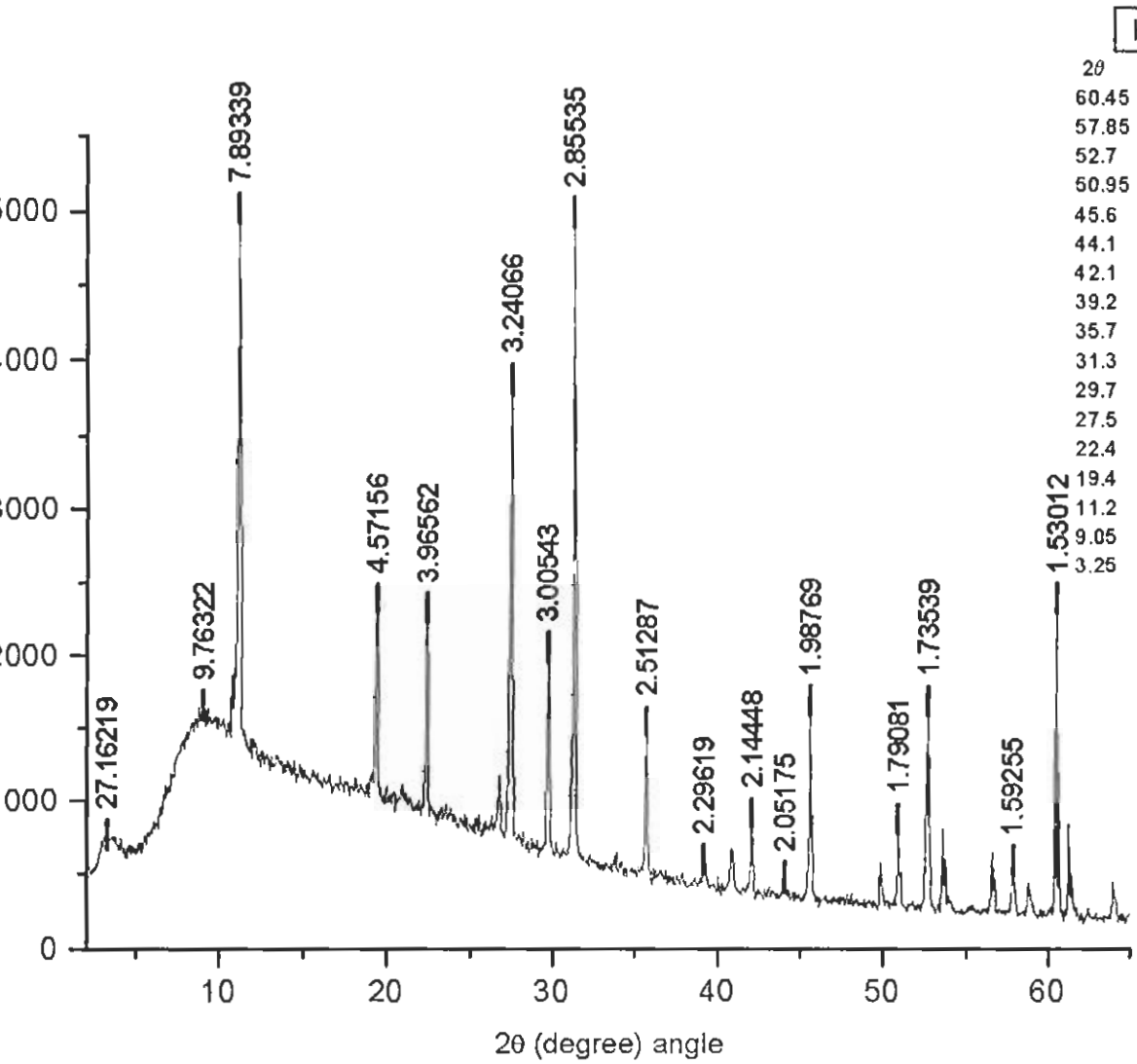


Hassan.23

| 2θ | CPS | d values |
|---|---|---|
| 60.45 | 2394 | 1.53012 |
| 57.85 | 587 | 1.59255 |
| 52.7 | 1686 | 1.73539 |
| 50.95 | 873 | 1.79081 |
| 45.6 | 1689 | 1.98769 |
| 44.1 | 477 | 2.05175 |
| 42.1 | 914 | 2.14448 |
| 39.2 | 597 | 2.29619 |
| 35.7 | 1546 | 2.51287 |
| 31.3 | 4988 | 2.85535 |
| 29.7 | 2060 | 3.00543 |
| 27.5 | 3873 | 3.24066 |
| 22.4 | 2329 | 3.96562 |
| 19.4 | 2397 | 4.57156 |
| 11.2 | 5019 | 7.89339 |
| 9.05 | 1666 | 9.76322 |
| 3.25 | 770 | 27.16219 |

**Fig. 6. 2.** X-ray powder diffraction pattern and data of the beryl (var. aquamarine) from a pegmatite, Dassu, Shigar valley.

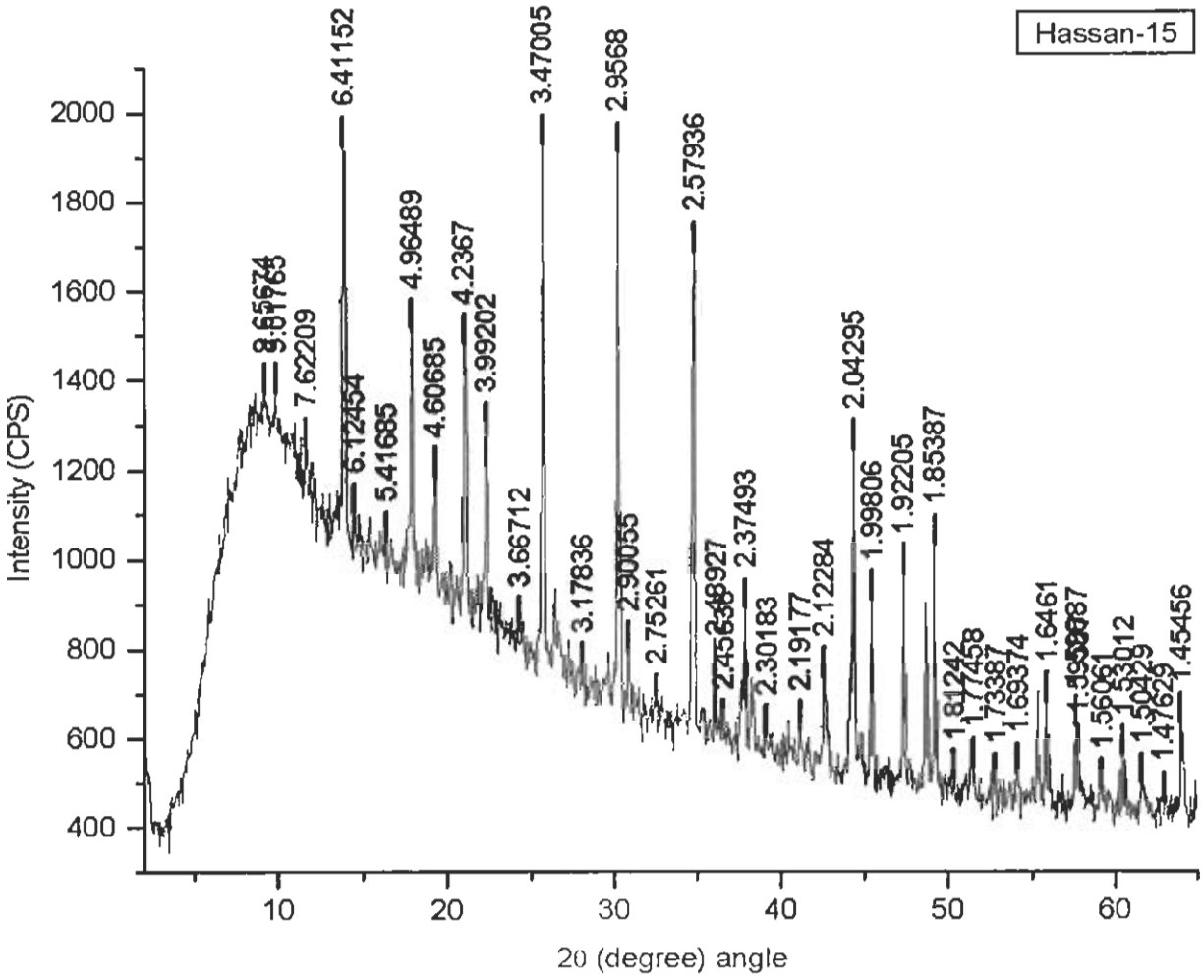


**Fig. 6. 3.** X-ray powder diffraction pattern of the tourmaline (var. schorl-foitite) from a pegmatite, Kashmol, Shigar valley.

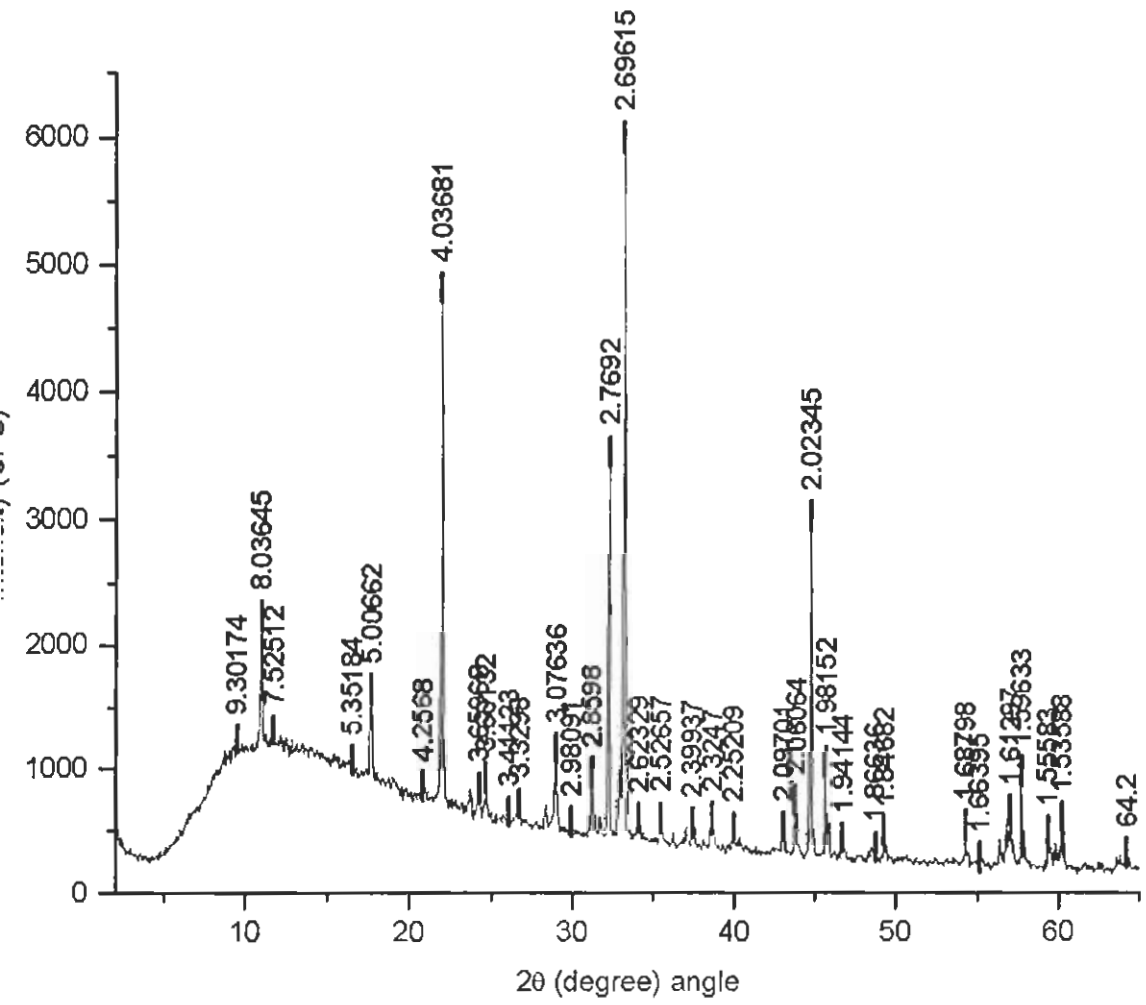


Hassan-11

| 2θ | CPS | d v |
|---|---|---|
| 9.5 | 1244 | 9.3 |
| 11 | 2240 | 8.0 |
| 11.75 | 1319 | 7.5 |
| 16.55 | 1075 | 5.3 |
| 17.7 | 1657 | 5.0 |
| 20.85 | 862 | 4.2 |
| 22 | 4820 | 4.0 |
| 24.3 | 848 | 3.6 |
| 24.7 | 932 | 3.6 |
| 26.1 | 655 | 3.4 |
| 26.75 | 720 | 3.3 |
| 29 | 1170 | 3.0 |
| 29.95 | 577 | 2.9 |
| 31.25 | 970 | 2.8 |
| 32.3 | 3537 | 2.7 |
| 33.2 | 6000 | 2.6 |
| 34.15 | 601 | 2.6 |
| 35.5 | 607 | 2.5 |
| 37.45 | 568 | 2.3 |
| 38.7 | 610 | 2.3 |
| 40 | 523 | 2.2 |
| 43.1 | 535 | 2.0 |
| 43.9 | 753 | 2.0 |
| 44.75 | 3032 | 2.0 |
| 45.75 | 1061 | 1.9 |
| 46.75 | 447 | 1.9 |
| 48.75 | 367 | 1.8 |
| 49.3 | 500 | 1.8 |
| 54.3 | 545 | 1.6 |
| 55.15 | 289 | 1.6 |
| 57.05 | 670 | 1.6 |
| 57.7 | 980 | 1.5 |
| 59.35 | 499 | 1.5 |
| 60.2 | 612 | 1.5 |
| 64.2 | 327 | 64 |

**Fig. 6. 4.** X-ray powder diffraction pattern and data of the epidote (var. zoisite) from Alchuri, Shigar valley.

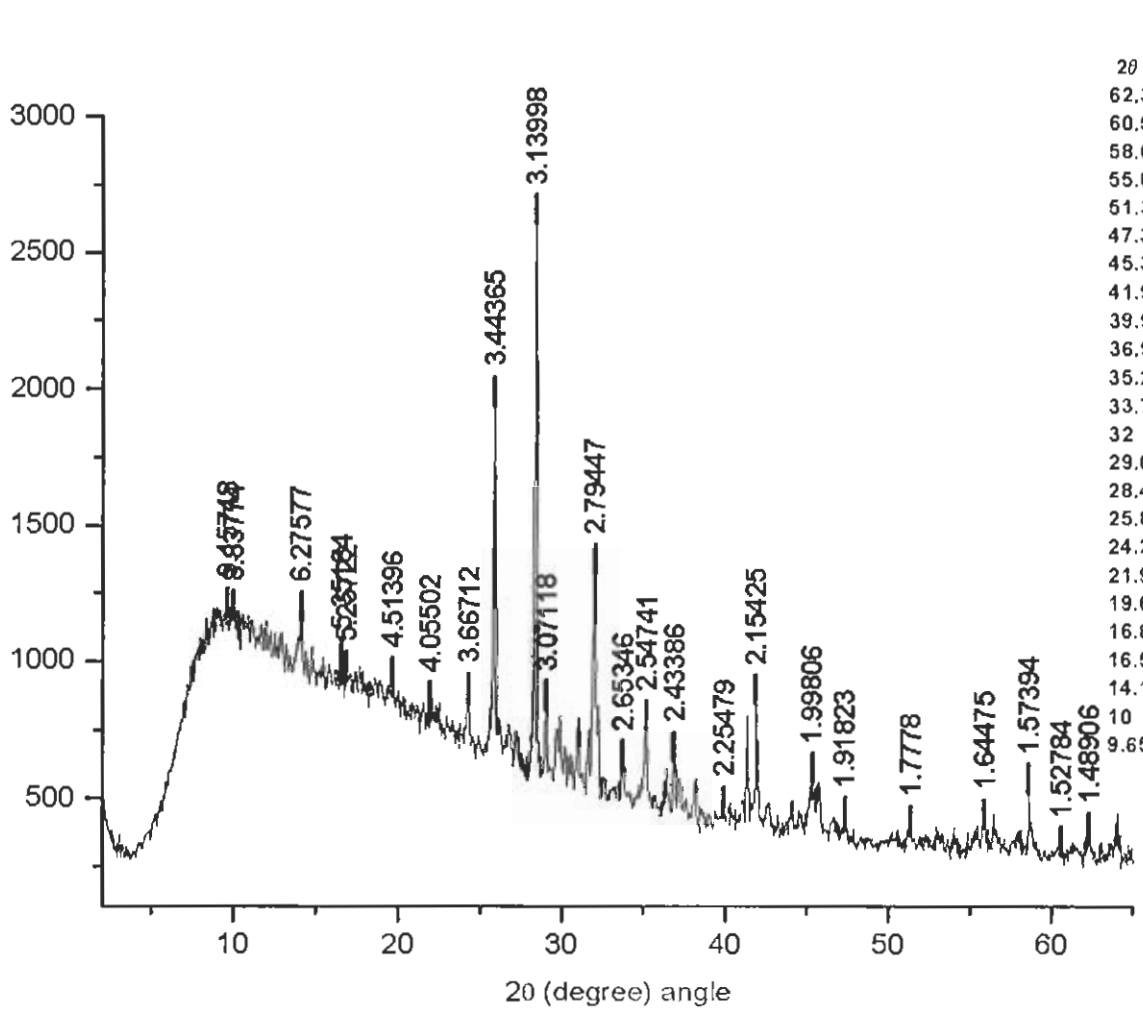


Hassan-12

| 2θ | CPS | d values |
|---|---|---|
| 62.3 | 396 | 1.48906 |
| 60.55 | 344 | 1.52784 |
| 58.6 | 576 | 1.57394 |
| 55.85 | 446 | 1.64475 |
| 51.35 | 420 | 1.7778 |
| 47.35 | 452 | 1.91823 |
| 45.35 | 612 | 1.99806 |
| 41.9 | 896 | 2.15425 |
| 39.95 | 490 | 2.25479 |
| 36.9 | 689 | 2.43386 |
| 35.2 | 801 | 2.54741 |
| 33.75 | 658 | 2.65346 |
| 32 | 1376 | 2.79447 |
| 29.05 | 875 | 3.07118 |
| 28.4 | 2659 | 3.13998 |
| 25.85 | 1990 | 3.44365 |
| 24.25 | 902 | 3.66712 |
| 21.9 | 871 | 4.05502 |
| 19.65 | 960 | 4.51396 |
| 16.85 | 982 | 5.25722 |
| 16.55 | 1023 | 5.35184 |
| 14.1 | 1201 | 6.27577 |
| 10 | 1205 | 8.83774 |
| 9.65 | 1216 | 9.15748 |

**Fig. 6. 5.** X-ray powder diffraction pattern and data of the axinite (var. ferroaxinite) from Alchuri, Shigar valley.

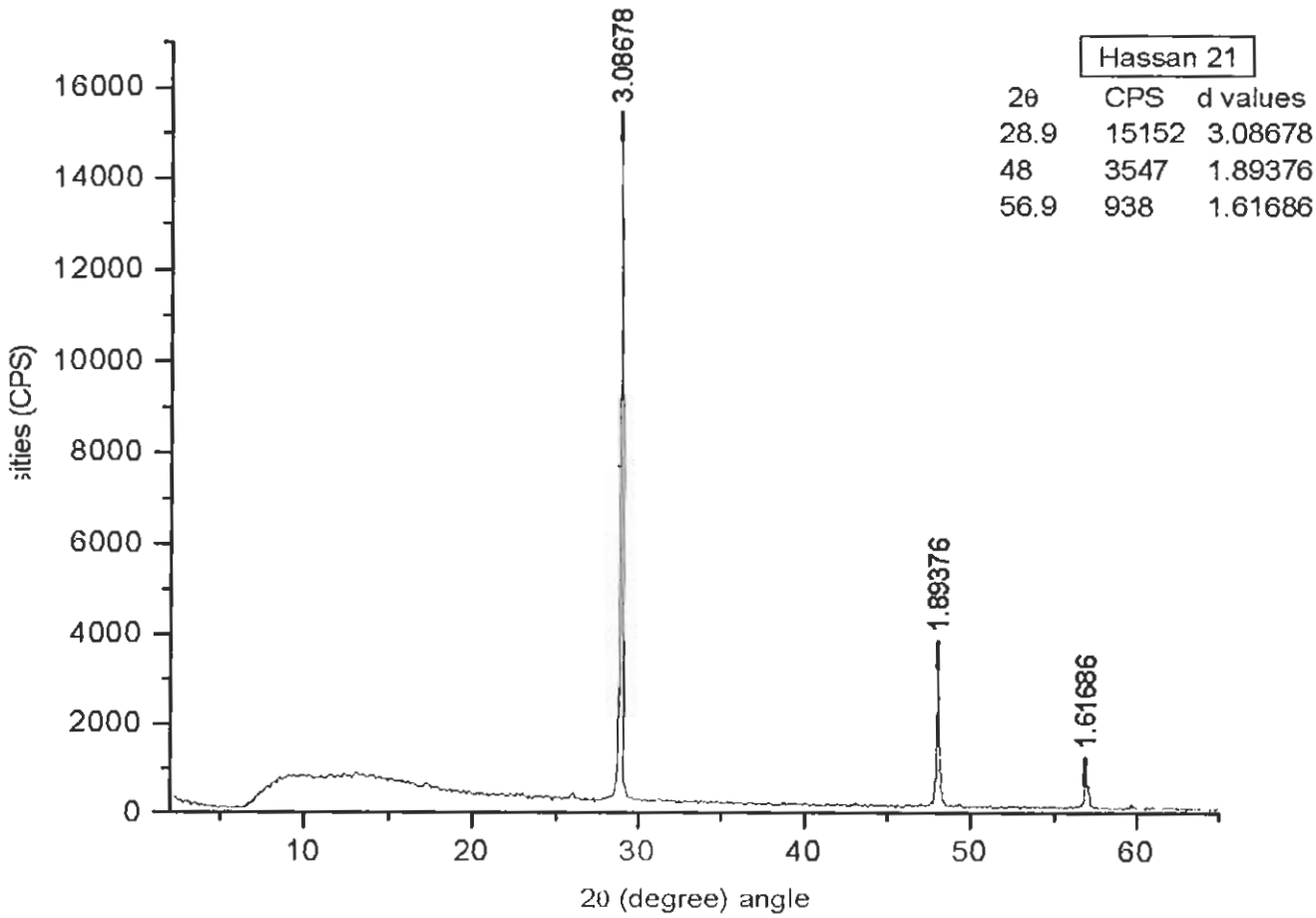


**Fig. 6. 6.** X-ray powder diffraction pattern and data of the fluorite from Kashmol mine, Shigar valley.

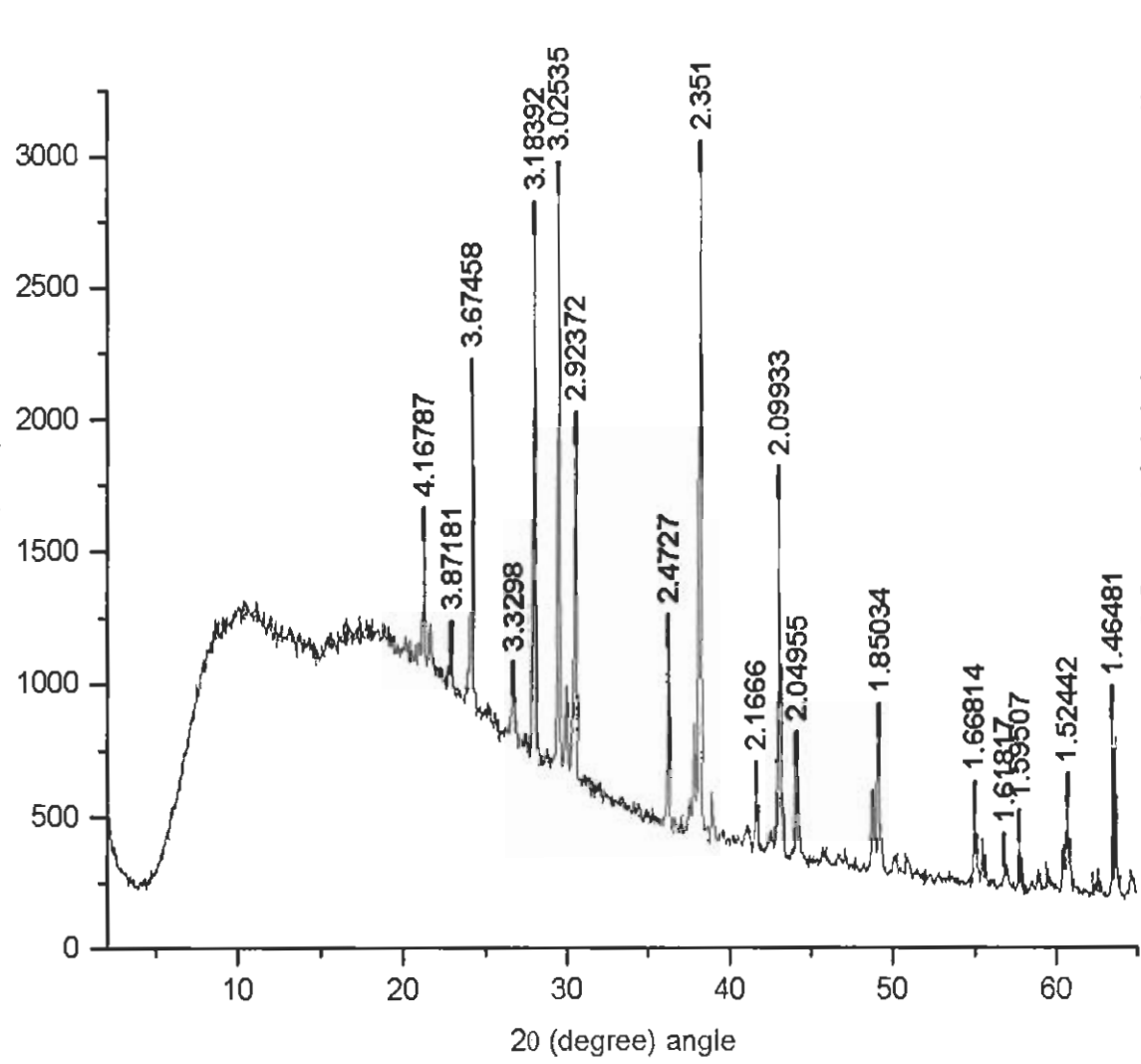


Hassan-3

| 2θ | CPS | d valu |
|---|---|---|
| 21.3 | 1605.5 | 4.167 |
| 22.95 | 1177 | 3.871 |
| 24.2 | 2169 | 3.674 |
| 26.75 | 1023 | 3.329 |
| 28 | 2764.5 | 3.183 |
| 29.5 | 2917.5 | 3.025 |
| 30.55 | 1968 | 2.923 |
| 36.3 | 1201 | 2.472 |
| 38.25 | 2995.5 | 2.351 |
| 41.65 | 647.5 | 2.166 |
| 43.05 | 1761 | 2.099 |
| 44.15 | 759.5 | 2.049 |
| 49.2 | 866 | 1.850 |
| 55 | 572 | 1.668 |
| 56.85 | 376 | 1.618 |
| 57.75 | 466.5 | 1.595 |
| 60.7 | 601.5 | 1.524 |
| 63.45 | 929.5 | 1.464 |

**Fig. 6. 7.** X-ray powder diffraction pattern and data of the apatite (var. dahlite) from Yuno mine, Shigar valley.

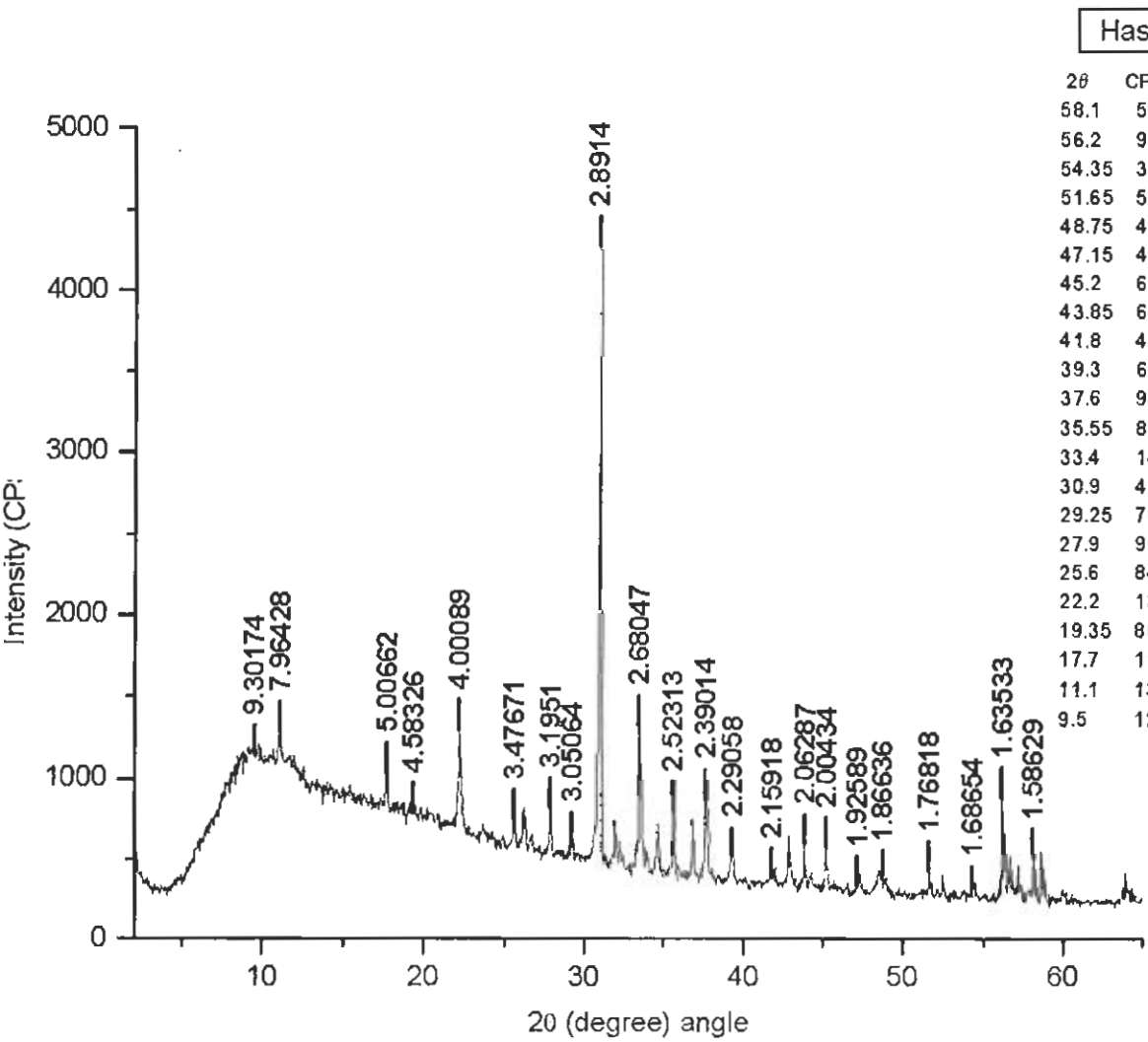


Hassan-13D

| 2θ | CPS | d values |
|---|---|---|
| 58.1 | 598 | 1.58629 |
| 56.2 | 974 | 1.63533 |
| 54.35 | 367 | 1.68654 |
| 51.65 | 520 | 1.76818 |
| 48.75 | 464 | 1.86636 |
| 47.15 | 426 | 1.92589 |
| 45.2 | 669 | 2.00434 |
| 43.85 | 688 | 2.06287 |
| 41.8 | 477 | 2.15918 |
| 39.3 | 611 | 2.29058 |
| 37.6 | 965 | 2.39014 |
| 35.55 | 892 | 2.52313 |
| 33.4 | 1414 | 2.68047 |
| 30.9 | 4365 | 2.8914 |
| 29.25 | 700 | 3.05064 |
| 27.9 | 913 | 3.1951 |
| 25.6 | 840 | 3.47671 |
| 22.2 | 1387 | 4.00089 |
| 19.35 | 881 | 4.58326 |
| 17.7 | 1125 | 5.00662 |
| 11.1 | 1372 | 7.96428 |
| 9.5 | 1231 | 9.30174 |

**Fig. 6. 8.** X-ray powder diffraction pattern and data of the epidote (var. elinozoisite) from Yuno mine, Shigar valley area.

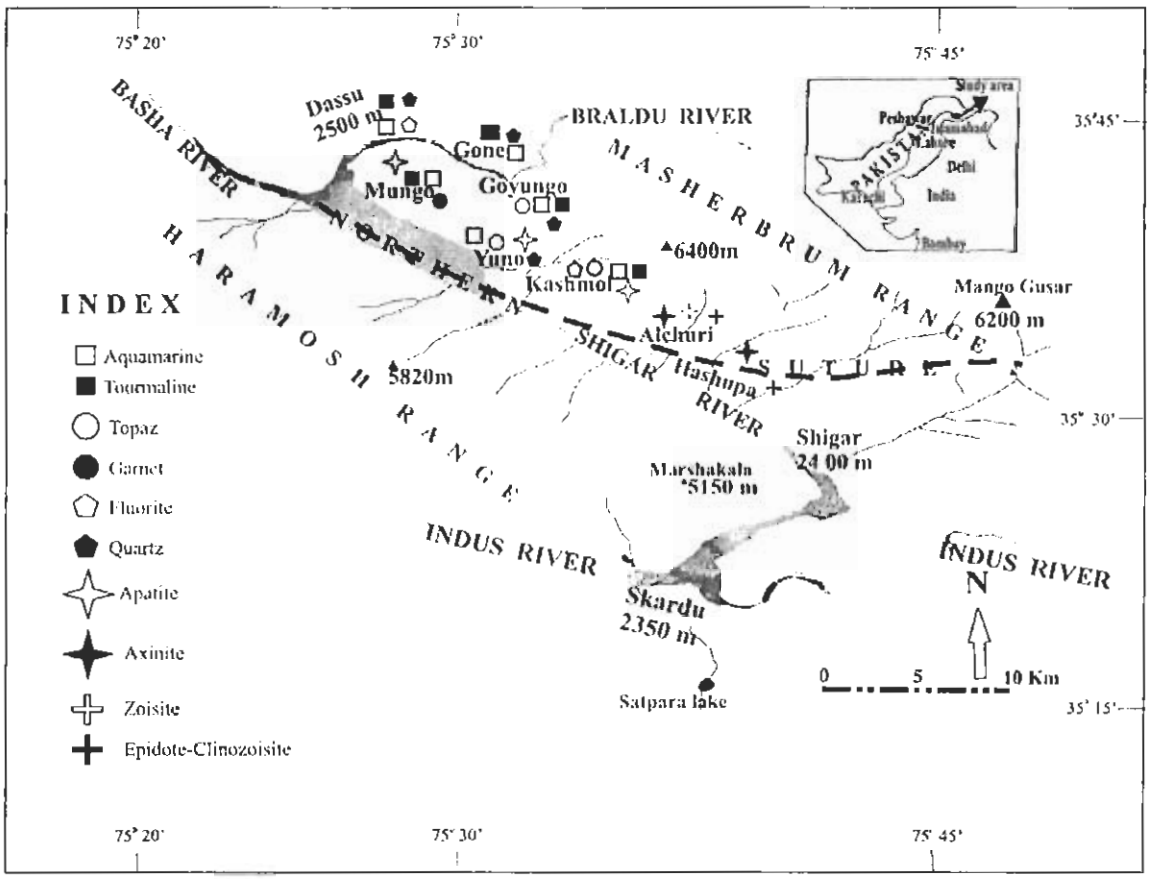


**Fig. 6. 9.** Map showing gemstone occurrences in the Shigar valley area.

# CHAPTER 7

## WHOLE ROCK GEOCHEMISTRY

A total of sixty two representative samples (43 of pegmatites and 19 host rocks) from Shigar, Shengus and Indus-Gilgit pegmatites were analyzed for the whole rock geochemistry including major, trace and rare earth elements. In order to discuss and decipher the petrogenesis and the classification on the basis of major, trace and rare earth elements data for Shigar valley pegmatites. A brief introduction of the genetic types and classifications of pegmatites, especially granitic-pegmatites is discussed here. Genetically, pegmatites have been classified on various parameters such as the depth of consolidation or emplacement, type of mineralization, relations to the parent plutons and the metamorphic environment in which they have been frequently found (Ginsburg et al. 1979; Ćerný, 1982b).

In addition to the above-mentioned criteria of classification, the pegmatites have also been classified as gabbroic-pegmatites, syenite-pegmatite, and granitic-pegmatites depending on the major mineral constituents and whole rock geochemistry. Among these the granitic-pegmatites are the most abundant pegmatites. Moreover, the granitic-pegmatites can be further subdivided into various types and subtypes or sub-classes (e.g., petalite-quartz subtype, spodumene-quartz subtype, lithium-cesium-tantalum- subtype etc) depending on the presence of accessory minerals and metals, which are present in them (Ćerný, 1982a, b). All the subtypes of granitic-pegmatites almost maintain the granite composition because the accessory components are mostly restricted to a fraction of a percent (Stewart 1963, 1978; London and Burt 1982; Ćerný, 1982a, b). There are two schools of thought regarding the origin of granitic-pegmatites. One is of the opinion that the granitic-pegmatites are the result of supercritical fluids, hydrothermal solutions and / or aqueous vapor phase in the absence of a melt, while the other is suggesting a volatile rich melt for the formation of pegmatites (Ćerný, 1982b). Majority of the petrologists (e.g., Bakumenko, 1968; Bazarov and Motorina 1969; Zakharchenko 1976; Roedder, 1979) supports the latter opinion. There are two other openions, regarding the

origin of pegmatites, i.e., igneous versus metamorphic (Ćerný, 1982a, b). Majority of petrologists supports the igneous origin (Ćerný, 1982a, b; Baker, 1998; Burnham and Jahns, 1961) while some authors are in favor that the pegmatites are the direct product of anataxis (Brisbin, 1986; Ginsberg et al., 1979). This mode of origin can be generally applied to mica-bearing pegmatites (Sokolov et al., 1975), but this concept is also being applied to the rare element pegmatites where they acquire rare-element accumulation from the source lithologies (Norton, 1973; Stewart, 1978).

### Major element characteristics and classification of pegmatites

The major element data of the pegmatites from Shigar valley, Indus-Gilgit confluence and Shengus have been given in Tables 7.1 to 7.5 and graphically presented in Figures 7.1 to 7.7. The major element data is generally used for the nomenclature, classification and petrogenesis of various rock-suits. On the basis of mineralogy, the studied pegmatites have been classified as granitic in composition rather than syenitic or gabbroic because of their leucocratic character. However, certain chemical classification schemes and discrimination diagrams are also used to further confirm and classify these pegmatites. At present various schemes have been proposed and are in use for the classification and nomenclature of granitoid rocks and each classification scheme has its own merits and demerits but these are still very useful to fulfill the purpose. Because of the granitic character of these pegmatites only those classification schemes were used, which have been developed for the classification of granitoid rocks. Although, Cox et al. (1979) have given a classification of volcanic rocks on the basis of silica versus alkalis but it is also equally used for the plutonic rocks. According to this classification scheme, all the proposed sub-classes of Shigar valley pegmatites, the Indus-Gilgit confluence and Shengus pegmatites plot in the rhyolites field (i. e., granites) (Fig. 7. 1), which further confirm the granitic character of the studied pegmatites and these can be considered as leucogranitic-pegmatites. Another classification scheme suggested for granitoid rocks is of O' Connor, (1965) and Barker, (1979), in this scheme, the normative anorthite, albite and orthoclase are used. When the normative albite, anorthite and orthoclase of the studied pegmatites plotted on this diagram, the majority of the rocks from the three

pegmatite fields (i.e., Shigar, Shengus, and Indus-Gilgit Confluence pegmatites) plot in the granite field (Fig. 7. 2). The granite pegmatites have further divided into rare-element class and miarolitic class by Ginsberg et al. (1979).

The major element geochemistry, as well as the major and accessory mineral assemblages of the studied pegmatites from Shigar valley, Shengus and Indus-Gilgit confluence indicates that these are granitic in composition, so for this reason these pegmatites are granitic-pegmatites. Moreover, the pegmatites of the Shigar valley probably are either classified as the rare element class or miarolitic pegmatite class (Ginsburg et al., 1979). This classification is based on the depth of emplacement and metamorphic environment in which the pegmatites are now exposed, and is hence known as the geological classification of pegmatites. Because of the scarcity of rare elements (i.e., Li, Nb, Ta, Sn etc) in the Shigar valley pegmatites, these pegmatites can be classified as the miarolitic pegmatites rather than rare element pegmatites (Ginsberg et al., 1979).

The major element data of the studied pegmatites from the Shigar valley is plotted on the Harker diagram (i.e., $SiO_2$ versus major oxides (Fig. 7. 3). It is clear from this diagram that no well-defined trend has been observed for various oxides against $SiO_2$ indicating that the fractional crystallization has not played a major role in the formation of these pegmatites. However, the role of partial melting not be ruled out in this regard. The major element data of the pegmatites from Indus-Gilgit confluence and Shengus are plotted in the Figure 7. 4. This figure shows that the Indus-Gilgit confluence pegmatites have vaguely defined positive trend against $SiO_2$ for $Fe_2O_3$, $TiO_2$, CaO, MgO, MnO, $P_2O_5$ and $K_2O$, while the $Al_2O_3$ and $K_2O$ are showing negative trend. This is suggesting the fractionation behaviour for these pegmatites. However, due to the scarcity of the samples from Shengus pegmatites, no conclusion can be made in this regard.

The major element data of the pegmatites from the Shigar valley in Tables 7.1 to 7.4 show that the muscovite-schorl-beryl-garnet pegmatites have the wt. % of $SiO_2$ in the range of 73.23 to 77.3, $Al_2O_3$ 12.8 to 14.9, $Fe_2O_3$ 0.01 to 1.05, CaO 0.43 to 1.87, $Na_2O$

2.12 to 9.12, $K_2O$ 1.09 to 7.32 and $P_2O_5$ 0.04 to 0.28; the muscovite-schorl pegmatites have $SiO_2$ wt. % in the range of 73.02 to 75.13, $Al_2O_3$ 12.67 to 14.13, $Fe_2O_3$ 0.53 to 0.69, CaO 0.56 to 1.62, $Na_2O$ 4.78 to 7.56, $K_2O$ 2.02 to 4.23 and $P_2O_5$ 0.04 to 0.28; biotite ± garnet ± muscovite pegmatites the $SiO_2$ in the range of 74.32 to 76.5, $Al_2O_3$ 12.2 to 13.12, $Fe_2O_3$ 1.52 to 1.61, CaO 0.40 to 0.78, $Na_2O$ 2.17 to 2.56, $K_2O$ 6.12 to 6.38 and $P_2O_5$ 0.06 to 0.16 and the muscovite-biotite ± garnet pegmatites have $SiO_2$ content in the range of 73.45 to 76.20, $Al_2O_3$ 13.1 to 14.32, $Fe_2O_3$, 0.28 to 0.87, CaO 0.93 to 1.68, $Na_2O$ 2.34 to 6.21, $K_2O$ 3.16 to 6.56 and $P_2O_5$ 0.03 to 0.26. The Shengus pegmatites have $SiO_2$ ranging from 72.98 to 73.12, $Al_2O_3$ 14.89 to 14.99, $Fe_2O_3$ 0.88 to 0.89, CaO 0.56 to 0.65, $Na_2O$ 5.45 to 5.59, $K_2O$ 2.99 to 3.12 and $P_2O_5$ 0.06 to 0.07 (Table 7. 5). The major element data of the Indus-Gilgit confluence pegmatites in the Table 7.5 indicate that the $SiO_2$ varies from 71.52 to 74.41, $Al_2O_3$ 13.43 to 15.05, $Fe_2O_3$ 0.30 to 1.35, CaO 0.42 to 1.85, $Na_2O$ 2.56 to 6.32, $K_2O$ 2.34 to 9.55 and $P_2O_5$ 0.01 to 0.10.

It is clear from the Tables 7. 1 to 7. 5 and the Figures 7.3 and 7.4 that the biotite ± garnet ± muscovite sub-class of pegmatites is relatively poor in $Al_2O_3$ and $Na_2O$ and rich in $Fe_2O_3$ and $TiO_2$ as compared to the other sub-classes of pegmatites in the Shigar valley and to the Indus-Gilgit confluence and Shengus pegmatites. The relatively higher concentrations of the $Fe_2O_3$ and $TiO_2$ are due to the presence of biotite in this sub-class of pegmatites, which is also evident from the petrographic studies (Table 5. 2) and the mineral chemistry data of the biotites of this sub-class contain higher concentrations of $TiO_2$ (Table 6.1). In addition to this, the biotite ± garnet ± muscovite sub-class of pegmatites of the Shigar valley are enriched in their $K_2O$ contents relative to $Na_2O$ and this is also evident from their CIPW norms that the percentage of orthoclase is greater than the albite in these pegmatites (Table 7. 3). Besides this, the muscovite-biotite ± garnet sub-class of pegmatites shows similar characteristics as that of the biotite ± garnet ± muscovite pegmatites sub-class. However, the other oxides are more or less similar in all the sub-classes of these pegmatites. Some of the Indus-Gilgit confluence pegmatites are relatively rich in their CaO and $K_2O$ contents as compared to the Shigar valley and Shengus pegmatites (Table 7. 5 and Fig. 7. 4). Due to this reason, some of the Indus-Gilgit confluence pegmatites have very higher contents of orthoclase and anorthite as is

evident in their CIPW norms that is consistent with the petrographic studies mentioned in chapter 5. The studied pegmatites from all the three fields are granitic in character, therefore, they have relatively higher values of $SiO_2$, $Na_2O$, $K_2O$ and lower contents of $Fe_2O_3$, MgO, and CaO. In addition, these pegmatites are also depleted in $TiO_2$ content except the biotite ± garnet ± muscovite sub-class of pegmatites.

The leucocratic character of all the studied pegmatites is also clear from their CIPW norms that the percentage of silicic phases such as quartz, albite, and orthoclase in almost all the samples is > 95 % (Tables 7.1 to 7. 5). The other components such as diopside, hypersthene, corundum, magnetite, hematite, apatite, etc. are not greater that 5 %. The anorthite contents in almost all the pegmatite groups are < 9%, indicating that most of the plagioclase in the Shigar valley pegmatites is albitic in composition. This is consistent with the observations already made during the petrographic studies and mineral chemistry of these pegmatites (chapter 5 and 6 respectively). The modal mineralogy and CIPW norms of the same sub-classes of the Shigar valley pegmatites are very identical but at places, variation occurs where the samples have been collected from different zones of these pegmatites. Such types of observations have also been noted within the world famous pegmatites, e.g., Tin Mountain pegmatite of Black Hills, South Dakota (Walker et al., 1986).

In order to check the nature of granitoids (including pegmatites) in terms of their alkaline affinity, the most frequently used diagram is of Maniar and Piccoli (1989) that is the modification of Shand's (1927). Shand, (1927) classified the rocks into three main types on the basis of alumina-saturation such as (1) peraluminous ($Al_2O_3 > CaO + Na_2O + K_2O$), (2) metaluminous ($Al_2O_3 > Na_2O + K_2O$) and (3) peralkaline ($Al_2O_3 < Na_2O + K_2O$). By using these parameters, Maniar and Piccoli (1989) established a discrimination diagram in which they redefined the boundaries in the Shand's diagram. By using this discrimination diagram, all the groups of the Shigar valley pegmatites along with the Indus-Gilgit confluence and Shengus pegmatites follow a continuous trend from peralkaline to peraluminous (Fig. 7. 5). This is also clear from the CIPW norms that majority (~ 85 %) of samples contain corundum (Tables 7. 1 - 7. 5) and therefore plot in

the peraluminous field, while less number (15 %) of samples plot below the unity 1 in the peralkaline field. It is suggesting that the protolith of these pegmatites is probably of metasedimentary in character. If this is the case, then the pre-existing metasediments have been melted by the processes of thrusting and crustal thickening after the collision of India with the Eurasian plate and are, therefore, considered as post-collisional pegmatites like those of the Hunza valley and Baltoro leucogranites (Crawford, 1988; Fraser et al., 2001).

The major element data of the granitoid rocks is not only used for their classification and nomenclature but at the same time it is also important for their petrogenetic evolution. Different workers (e.g., Petro et al., 1979; Pearce et al., 1984; Maniar and Piccoli, 1989) have proposed different discrimination diagrams based on major element chemistry for various tectonic environments. Maniar and Piccoli (1989) have differentiated granitoids belonging to various tectonic environments as post orogenic granitoids (POG), rift-related granitoids (RRG), continental epeiorogenic uplifted granitoids (CEUG), continental-collision granitoids (CCG), and oceanic plagiogranites (OP) by using different major oxides versus silica such as $Al_2O_3$ versus $SiO_2$ and FeO(t) / FeO(t) + MgO versus $SiO_2$ diagrams (Figs. 7.6 and 7.7). In addition to this, they have also grouped all these tectonic environments into three groups such as IAG + CAG + CCG into group I, RRG + CEUG into group II and the POG into group III (Figs. 7.6 and 7.7). To know the tectonic environment of the studied pegmatites, the data from the three pegmatite fields are plotted in the $Al_2O_3$ versus $SiO_2$ diagram (Fig. 7. 6), the majority of the data plot in the fields defined for group I (IAG + CAG + CCG) and group II (POG) by Maniar and Piccoli, (1989). Moreover, when the same data is plotted in another diagram FeO (t) / FeO (t) + MgO versus $SiO_2$ of Maniar and Piccoli (1989), majority of the data plot in the field of IAG + CAG + CCG but some of the samples plot in the field of POG (Fig. 7. 7). As the continental arc and continental collisional granitoids (CCG) are characterized by lower FeO(t) / FeO(t) + MgO ratios (~ 0.55 – 0.8), while the rift-related and continental epeirogenic uplift granitoids have higher FeO(t) / FeO(t) + MgO ratios at the same silica levels. Majority of pegmatites plot in the field of continental collisional granitoids because they have very low values of this ratio.

Some of the samples have higher the FeO(t) / FeO(t) + MgO ratio (0.9) and, therefore, plot at the margin of post orogenic granites (POG). As all the studied pegmatites plot in the fields of IAG + CAG + CCG and POG, therefore, these pegmatites are of orogenic and compressional tectonic environments. In this respect the Shigar valley and Shengus pegmatites can be correlated with the continental collisional granitoids as the collisional events between India and Eurasia are still continue and the Indus-Gilgit confluence pegmatites can be correlated with the island arc granitoids (IAG) because of their existence in the Kohistan island arc.

## Trace element characteristics and tectonic environments

After emerging the plate tectonic theory in 1960s, the emphasis on geochemistry has been increased. Various new sophisticated analytical techniques have been devised to improve the quality of data and as a result various discrimination diagrams have been constructed to constrain and discriminate the rock suits belonging to different tectonic settings. In this connection, the most important and the noteworthy works are of Chayes (1964), Dickinson and Hathorton (1967), Dickinson (1968), Pearce and Cann (1973), Flyod and Winchester (1975), Wood et al. (1975), Shervais (1982), Pearce et al. (1984), Maniar and Piccoli (1989). Geochemically, all the elements of the periodic table have been classified into major, minor, trace and rare earth elements and each of these groups have their own importance for the classification, nomenclature, and petrogenesis of igneous rocks. In addition to these broad divisions, the major, minor and trace elements have also been geochemically divided as mobile and immobile elements and these elements play an important role in the various geological processes. Majority of these elements are more or less mobile as is suggested by Cann (1969), Hart et al. (1970), Hart (1962) and Hatori et al. (1972). Therefore, many workers have used mainly immobile and compatible elements to constrain the petrogenesis, because mobile elements are not suitable for the petrogenesis.

Various discrimination diagrams based on major elements were suggested to determine the tectonic setting of the different rocks (Pearce, 1975, 1976; Pearce and Cann, 1973; Flyod and Winchester, 1975; Wood et al. 1975; Shervais, 1982). The discrimination diagrams based on major elements ($SiO_2$, $Na_2O$, $K_2O$) and mobile elements are sometimes not very effective, when the rocks are subjected to metamorphism and alteration due to tectonism and plutonism. In these conditions, discrimination diagrams based on immobile and compatible elements are proposed to further confirm their tectonic affinity (Flyod and Winchester, 1975; 1978; Winchester and Flyod, 1977; Shervais, 1982; Harris, 1982; Pearce et al., 1984). These diagrams are not only helpful in understanding the tectonic setting but also useful to determine the type of magma responsible for the formation of rocks, particularly pegmatites and granites of the present study area.

In order to know the tectonic environment of the studied pegmatites, the trace element data is plotted in the Nb versus Y diagram of Pearce et al. (1984). Majority of data plot in the field of syn-collisional granites (SYN-COLG) and volcanic arc granites (VAG) but some of the samples also plot at the boundary line between the SYN – COLG, VAG and WPG (Fig. 7. 8 and Tables 7. 6 to 7. 10). Like wise, when the same data is plotted on the Rb versus Y + Nb diagram, all the pegmatite sub-classes of Shigar valley and the Shengus pegmatites except few samples clearly plot in the filed of syn-collisional granites (SYN-COLG), while the Indus-Gilgit Confluence pegmatites plot clearly in the field of volcanic arc granites (VAG) (Fig. 7. 9). The data of all the studied three pegmatite fields are further plotted in the $SiO_2$ versus Rb discrimination diagram of Pearce et al. (1984) it is found that all the samples from the Shigar valley and the Shengus pegmatites clearly plot in the field of syn-collisional granites "SYN-COLG", while the pegmatites of the Indus-Gilgit confluence plot in the field of island arc granites "IAG" (Fig. 7. 10 and Tables 7. 6 to 7. 10). The selective Rb enrichment in these pegmatites (especially the Shigar valley and Shengus pegmatites) shows the crustal involvement as is suggested by Harris et al. (1983).

When the trace element data of the different groups of the Shigar valley pegmatites are plotted on the primitive-mantle normalized spider diagram (Fig. 7. 11) of Sun and Mc Donald (1989), it became evident that almost all of the groups show very similar patterns. The large ion lithophile elements (LILEs) such as the Ba and Sr are depleted (Fig. 7. 11), while the Rb and K (Tables 7. 6 and 7. 10) are rich in almost all of the groups or sub-classes of the Shigar valley pegmatites. The gem-bearing pegmatite class (muscovite-schorl-beryl-garnet pegmatite and the muscovite-schorl pegmatite sub-classes) is relatively depleted in Sr and Ba (Tables 7. 6 and 7. 7) as compare to the other groups or sub-classes of pegmatites in the Shigar valley (Fig. 7. 11). In case of high field strength elements (HFSEs), all of the groups are generally depleted in the Ti and enriched in Nb. The positive Rb and negative Ba and Sr anomalies in all the studied groups or sub-classes of pegmatites indicate that these pegmatites are not the last product of any primary magma generated by the input of upper mantle but have been formed from the partial melts of the continental crust from a metasedimentary protolith and are, therefore, considered as S-type granites.

When the trace element and the REE data of the pegmatite fields of Shengus and Indus-Gilgit confluence are compared with the different groups of the Shigar valley pegmatites (Figs. 7. 12 to 7. 16), it became evident that the Shengus pegmatites, which are also the gem-bearing pegmatites have almost similar trace element characteristics as that of the different groups of the Shigar valley pegmatites (Fig. 7. 13) but the Indus-Gilgit confluence pegmatites show completely different characteristics (Fig. 7. 14). Although, the Shengus pegmatites show very similar patterns on the spider diagrams but they are relatively depleted in the Nb and Zr as compare to the Shigar valley pegmatites (Tables 7. 6 to 7. 10). Like the Shigar valley pegmatites, the Shengus pegmatites are also enriched in Rb and depleted in the Sr and Ba (Fig. 7 13), which indicate that the Shengus pegmatites have also been originated from the metasedimentary protolith. The Indus-Gilgit Confluence pegmatites are completely different from the Shigar valley as well as of the Shengus pegmatites in their trace and REE characteristics and patterns (Figs. 7. 14, 15 and 16).

## Characteristics of the Rare Earth Elements (REEs)

The Rare Earth Elements (REEs) patterns of the studied pegmatites are presented in Figures 7.12, 7.15 and 7. 16. It is clear from Figure 7.12 that the REE characteristics of the different sub-classes of the Shigar valley pegmatites are generally similar. All the sub-classes show very smooth patterns from the light rare earth elements (LREEs) to heavy rare earth elements (HREEs) with a characteristic negative Eu anomaly. In addition to these similarities, some minute differences are also noted between different sub-classes of these pegmatites. The gem-bearing pegmatite sub-class (muscovite-schorl-beryl-garnet pegmatite) is enriched in both the light rare earth elements (LREEs) and heavy rare earth elements (HREEs) as compare to other pegmatites from the Shigar valley area. The biotite ± garnet ± muscovite pegmatite sub-class and the muscovite-biotite ± garnet sub-class have almost similar patterns but the biotite ± garnet ± muscovite pegmatite sub-class is relatively depleted in the light rare earth elements (LREEs) especially La, Ce, and Pr and enriched in heavy rare earth elements (HREEs) such as the Er, Yb, and Lu (Tables 7. 6 to 7. 10). The muscovite-biotite ± garnet pegmatite sub-class is showing similar patterns like the other sub-classes but is distinctively depleted in the heavy rare earth elements (HREEs), especially in Er, Yb, and Lu. The broad negative Eu anomaly indicates that the melting of the source rock would have involved feldspar and the biotite of the pelites.

No rare earth element-bearing minerals (e.g., allanite, monazite, etc.) are found from all the three pegmatite fields as evident from the low concentrations of LREEs in these pegmatites. However, apatite in Shigar and Shengus pegmatites and allanite from the Indus-Gilgit confluence pegmatites are found in traces. These phases are also having negligible amount of LREEs (see Tables 6.1 to 6.3). The occurrence of lesser amount of allanite in these pegmatites is because of peraluminous and granitic nature of the studied pegmatites as the allanite is most commonly found in alkaline rocks such as alkaline granites or alkaline pegmatites (Halleran and Russell, 1996).

**Possible source of magma for the Shigar valley pegmatites**

Various sources such as partial melting of immature graywakes, fractional crystallization of basaltic magma, partial melting of eclogites or basic granulites, partial melting of amphibolites with or without garnet, have been suggested for the formation of granitoid rocks (Martin, 1987). As discussed earlier in this context, that the partial melting of the metasedimentary rock may have formed the Shigar valley pegmatites. However, Searle and Fryer (1986) suggested the igneous protolith for the formation of Indus-Gilgit confluence pegmatites. Although, the Shigar valley pegmatites are different in their mineralogy and major element characteristics from the granitoids those of the Baltoro Plutonic Unit (BPU) but they show similar characteristics in terms of trace and REE patterns, which indicates that the source of these is same and these may be co-magmatic. As the main lithology of the BPU are monzogranites and according to Crawford, (1988) and Searle, (1991) the BPU leucogranites are the fractionating products of these monzogranites. In addition, they also proposed that the monzogranites represent a primary melt, generated from the lower Karakoram crust. On the basis of some characteristics such as the Sr isotope ratios, moderate $\partial^{18}O$ values and negative Nb anomaly, they have also suggested that the source of these monzogranites and their associated leucogranites could be the metapelites (or tonalites). Crawford (1988) suggested that these metapelites have been undergone anhydrous melting via dehydration of biotite ± hornblende to generate a hot, under-saturated magma. In addition to this, the quartz, feldspar, muscovite, garnet, sillimanite ± sphene could be the other likely sources of BPU granitoids. The Sr and Ba of the BPU monzogranites are high enough, which create some ambiguity to be a crustal source but it is possible that some contamination may have been occurred from the mantle input due to which Ba and Sr are high. So, it is probable that the source rock of the Shigar valley pegmatites (except the muscovite-schorl-beryl-garnet sub-class) could be the same as is suggested for the Baltoro Plutonic Unit by Crawford, (1988) and Searle, (1991), if these pegmatites are the off shoots of BPU. But the mineralogy and trace element data of the Shigar valley pegmatites suggest a purely crustal-derived melt saturated in volatiles such as water, fluorine and boron and such type of melt may be generated from the metapelites. The peraluminous character

and the Rb enrichment of the Shigar valley pegmatites also suggest a crustal- derived melt. Clemens and Wall (1981) have suggested that the dehydration partial melting of quartz-alkali feldspar-muscovite will occur below 700°C and between 4 - 10 kb pressure to produce extremely $H_2O$ - rich and strongly peraluminous melts and will crystallize muscovite, garnet, cordierite and tourmaline depending on the pressure. Such types of partial melts could be suggested for the formation of Shigar valley pegmatites because these pegmatites also contain the same mineral assemblages as suggested by Clemens and Wall, (1981).

The leucogranites and peraluminous granites with near-eutectic composition are common in collisional belts and there is a general agreement that the leucogranites are the anatectic products of pelitic crustal sources but the heat sources for their production have remain controversial. Thickened orogens do not become sufficiently hot to cause water-absent melting of pelites without additional heat input from the mantle or crustal processes, such as shear-heating or accretion of rocks with high concentrations of radioactive isotopes (Royden, 1993; Thompson and Connolly, 1995). The dominant collisional leucogranites are two mica granites and muscovite-tourmaline granites. Muscovite dehydration melting (MDM) of metapelites that includes the breakdown of tourmaline explains the chemical characteristics of muscovite-tourmaline granites and granite pegmatites, including the necessary boron concentrations (Wike et al., 2002). The mineral assemblages, very low concentrations of light rare earth elements (LREEs) and low concentrations of other high field strength elements (HFSEs) of the Shigar valley pegmatites indicate that the muscovite dehydration melting (MDM) has been occurred in the source rock. These low concentrations are due to the result of lack of equilibrium between the melts and the accessory minerals, such as monazite and zircon in residues. This disequilibrium may be ascribed to the rapid removal of melts from the source regions as is described by Watt and Harley, (1993) and Nabelek and Glascock, (1995), and Nabelek, (2004) for the granite and granite pegmatites of the Black Hills, South Dakota, USA. The very low concentrations of the light rare earth elements (LREEs) also indicate that monazite may remain armoured by biotite, which does not partake in the

melting reaction, thus preventing equilibration of monazite with the partial melt as suggested by Nabelek and Glascock, (1995).

Although, on the basis of alumina saturation index (ASI), the Shigar valley pegmatites are mildly peraluminous and show a sedimentary protolith as a source rock but according to Chappell and White, (2001) the alumina saturation index is not enough to classify the granitoid rocks in either as I-and S - type granites. According to them the alumina saturation indices mostly converge, especially in the silicic rocks and this is not enough for the classification of granitoid rocks in I-and S - types. So for this reason they have recommended that the isotopic studies, especially the oxygen isotope compositions are more suitable instead of initial Sr-isotopic compositions (because there is also overlap between the two types of granites) for the classification of granitoid rocks into I-and S-types.

The oxygen isotope compositions of any granitoid rock are very helpful for its petrogenesis, especially for their source rocks and the oxygen isotopic compositions of a magma does not affected by the magmatic processes such as the fractional crystallization and according to Taylor, (1978) the oxygen isotope fractionation between the silicate liquids and minerals at magmatic temperatures is very small. As the $\partial^{18}O$ values are very good discriminant between the I-and S - type granites and according to Halliday et al., (1981) and Blattner et al., (1983), the $\partial^{18}O$ values of S- type granites are generally greater than 10 ‰, while those of I - type granites are lower than 10 ‰.

**Mineralogical and chemical characteristics of collisional leucogranites and the Shigar valley pegmatites**

On the basis of color index, mineral assemblages and chemical characteristics, the Shigar valley pegmatites are also leucocratic granites and these share many mineralogical and chemical characteristics with the continental collisional leucogranites. Commonly, collisional leucogranites are characterized by their peraluminous character and very low concentrations (< 1 wt. %) CaO, MgO, and FeO) (Nabelek and Glascock, 1995; Nabelek, 2004). Muscovite is the characteristic mineral of the leucogranites along with tourmaline and biotite, while almandine-spessartine garnet and minor sillimanite can also occur in eertain cases (Nabelek and Liu, 2004). In the gem-bearing pegmatites of Shigar valley muscovite, tourmaline, beryl and garnet occur as accessories, while biotite is generally absent in this sub-class of pegmatites. Moreover, biotite is usually found in those rocks which have more than ~ 0.06 wt. % $TiO_2$, whereas tourmaline occurs in those rocks which have less $TiO_2$ concentration. This is the reason that biotite is mainly present in that sub-class of Shigar valley pegmatites, which is having high contents of $TiO_2$ as compare to other sub-classes. Tourmaline and biotite-bearing granites and leucogranites often exist but within different parts of composite plutons, such as in the Badrinath-Gangotri plutons in India and in the Harney Peak Granite and its satellite plutons in the Black Hills, South Dakota (Scaillet et al., 1990; Nabelek et al., 1992a). The relationship between tourmaline and biotite-bearing leucogranites has been attributed to fractional crystallization (Scaillet et al., 1990; Guillot and Le Fort, 1995) or production by muscovite versus biotite-dehydration-melting reactions (Nabelek et al., 1992a). The latter alternative is based often on distinct isotopic compositions of the two-leucogranite types in a given region (Nabelek and Glascock, 1995; Nabelek, 2004). In this connection it is suggested that at least the gem-bearing sub-class of Shigar valley pegmatites mainly composed of muscovite, tourmaline, beryl and garnet as accessories may have been developed from the biotite ± muscovite ± garnet sub-class of the Shigar valley pegmatites through fractional crystallization.

Various mechanisms have been proposed for the generation and emplacement of leucogranites as for example leucogranite plutons are generally formed by intrusion of multitudes of dykes and sills in ballooning magma chambers (Duke et al., 1988; Searle, et al., 1997; Brown and Solar, 1998). Magma batches migrate from source regions in dilatant portions of the shear-zone systems in crustal sequences, which are undergoing contractional or compressional deformation (Brown and Solar, 1998). Moreover, the shear-zone systems are integral to leucogranite magma generation, ascent and emplacement. After emplacement, the individual melt sheets often locally differentiate in aplite-pegmatite couples, giving wide ranges in plagioclase/ K-feldspar ratios within the sheets or dykes (Nabelek et al., 1992a; Nabelek, 2004). The same phenomenon may have occurred into the Shigar valley area, where different sub-classes of these pegmatites have been formed and are discussed in the chapter 5. This, in turn, may leads to wide ranges in Ba, Sr and other trace elements that are fractionated by feldspars (Duke et al., 1992) but as the trace elements of these feldspars are not determined, therefore, the fractionation of Ba and Sr in the feldspars of these pegmatites could not be further explained.

**Chemical characteristics of Indus-Gilgit confluence pegmatites**

Petterson and Windley (1985; 1986; 1991) and Petterson et al. (1990b) have mapped the Kohistan batholith in the Gilgit area and described the magmatism in Kohistan batholith in three stages. Later on Khan (1994) has also mapped certain parts of this batholith and proposed multi-phase magmatism from subduction-related calc-alkaline to collisional granites of peraluminous affinity. According to these authors, the magmatism in the Kohistan batholith records several episodes that possibly spanned some 70 Ma (from Late Cretaceous to Pliocene). They have also proposed that such type of large batholith could not have been formed from a single body by differentiation, however, it is possible that the differentiation may have played local role in the evolution of the independent plutons. The final stage of this magmatism is present as garnet-muscovite or garnet-biotite leucogranite or pegmatite intrusions in the form of sheets or dykes. These dykes or sheets are exposed along the Gilgit river and near the confluence of Gilgit and Indus river, are called as Parri and Indus-Gilgit confluence acid sheets

respectively. As the majority of Indus-Gilgit confluence acid sheets is coarse grained and are in the form of dykes, therefore, it is more suitable to call these bodies as Indus-Gilgit confluence pegmatite dykes instead of Indus-Gilgit confluence acid sheets. These bodies are rich in Rb and K and depleted in LREE and most HFSE relative to the stage two granitoids of the Kohistan batholith (Petterson and Windley, 1985). The Indus-Gilgit confluence pegmatite dykes are extremely enriched in Ba and Sr and to a lesser extent in Zr. Such types of characteristics are also reported from the Ladakh segment of the Trans-Himalayan batholith by Honnegger et al. (1982) and from Baltoro plutonic unit in the Karakoram terrane by Rex et al. (1988).

Petterson and Windley (1985; 1986; 1991) have reported very low $^{87}Sr$ / $^{86}Sr$ ratios for the Kohistan batholith in relation to the Ladakh batholith and according to them this ratio has been increased with the time. This is the reason that the $^{87}Sr$ / $^{86}Sr$ ratios for the last third stage of magmatism in Kohistan are greater than the initial two stages. The Parri aplite acid sheets have a significantly higher $^{87}Sr$ / $^{86}Sr$ initial ratios, which suggests a higher crustal component involvement to the melting source. On the basis of strontium isotopic data, the source for the Kohistan granites could be the upper mantle or the lower crust, which is depleted in Rb and has Rb/Sr ratios similar to the mantle, or it could be the middle-upper crust, which has also low initial ratios and a short crustal residence time (Petterson and Windley, 1985). The High Himalayan leucogranites from Nepal (Vidal et al., 1982) and Zanskar (Searle and Fryer, 1986) have higher $^{87}Sr$ / $^{86}Sr$ initial ratios (> 0.7550) than the Indus-Gilgit confluence and Parri leucogranites from the Kohistan area. In addition to this, the source as well as mechanism of magma generation of these two leucogranites is also different. According to Searle and Fryer (1986) the source of the High Himalayan leucogranites was the Precambrian-Palaeozoic continental crustal rock and these have been formed by anatexis, while the source for the Kohistan leucogranite sheets is Mesozoic-Early Tertiary material of the Kohistan micro plate itself. This is the reason that they have lower strontium initial ratios.

The third and last phase of magmatism that is suggested by Petterson and Windley (1985; 1986; 1991) is spanned between 15 to 20 Ma but leucogranites as young as 2.3 Ma have also been described by Zeitler and Chamberlain (1991) in the Nanga Parbat-Haramosh Massif area.

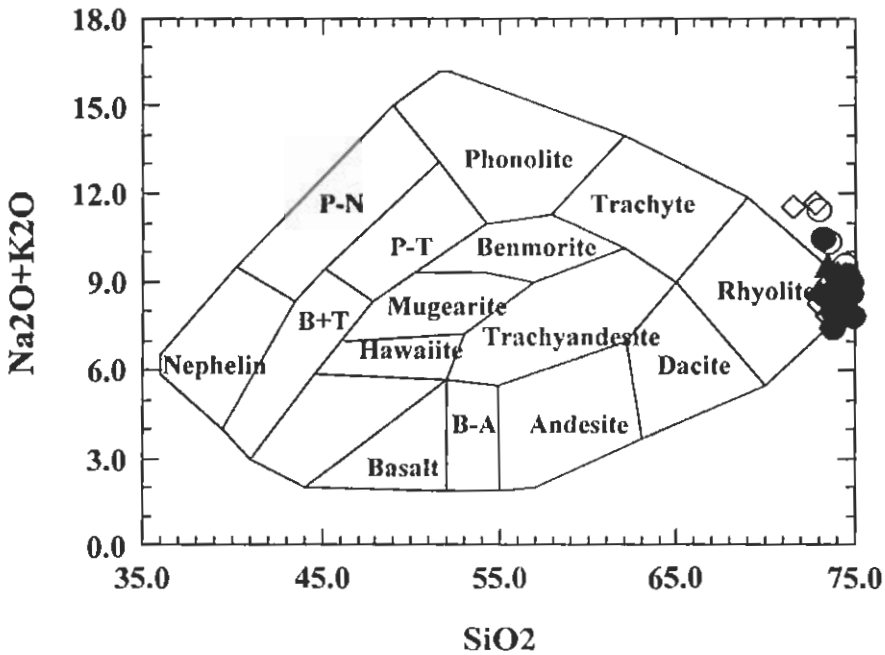


**Fig. 7. 1.** $Na_2O + K_2O$ versus $SiO_2$ plot for the classification of Shigar valley, Shengus and Indus-Gilgit Confluence Pegmatites (after Cox et al., 1979).

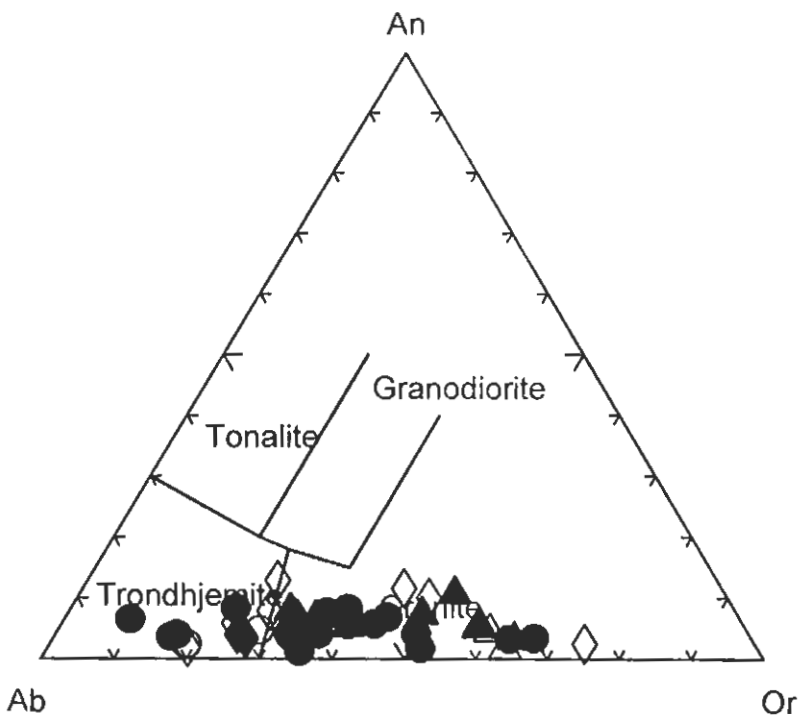


**Fig. 7. 2.** An-Ab-Or normative plot for the Shigar valley, Shengus and Indus-Gilgit Confluence pegmatites (after O' Connor, 1965 and Barker, 1979).

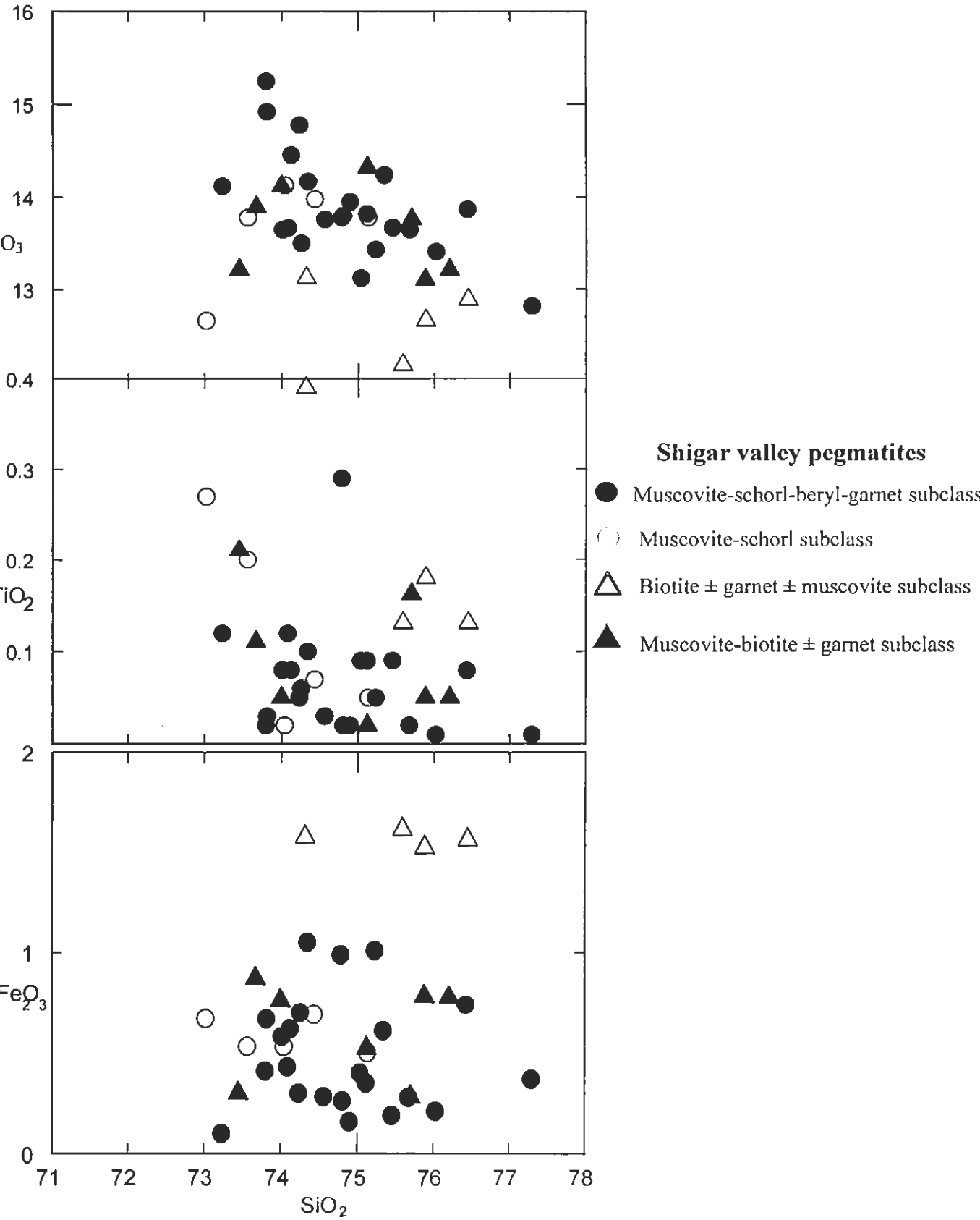


**Fig. 7. 3.** Harker-type binary diagrams for the Shigar valley pegmatites.

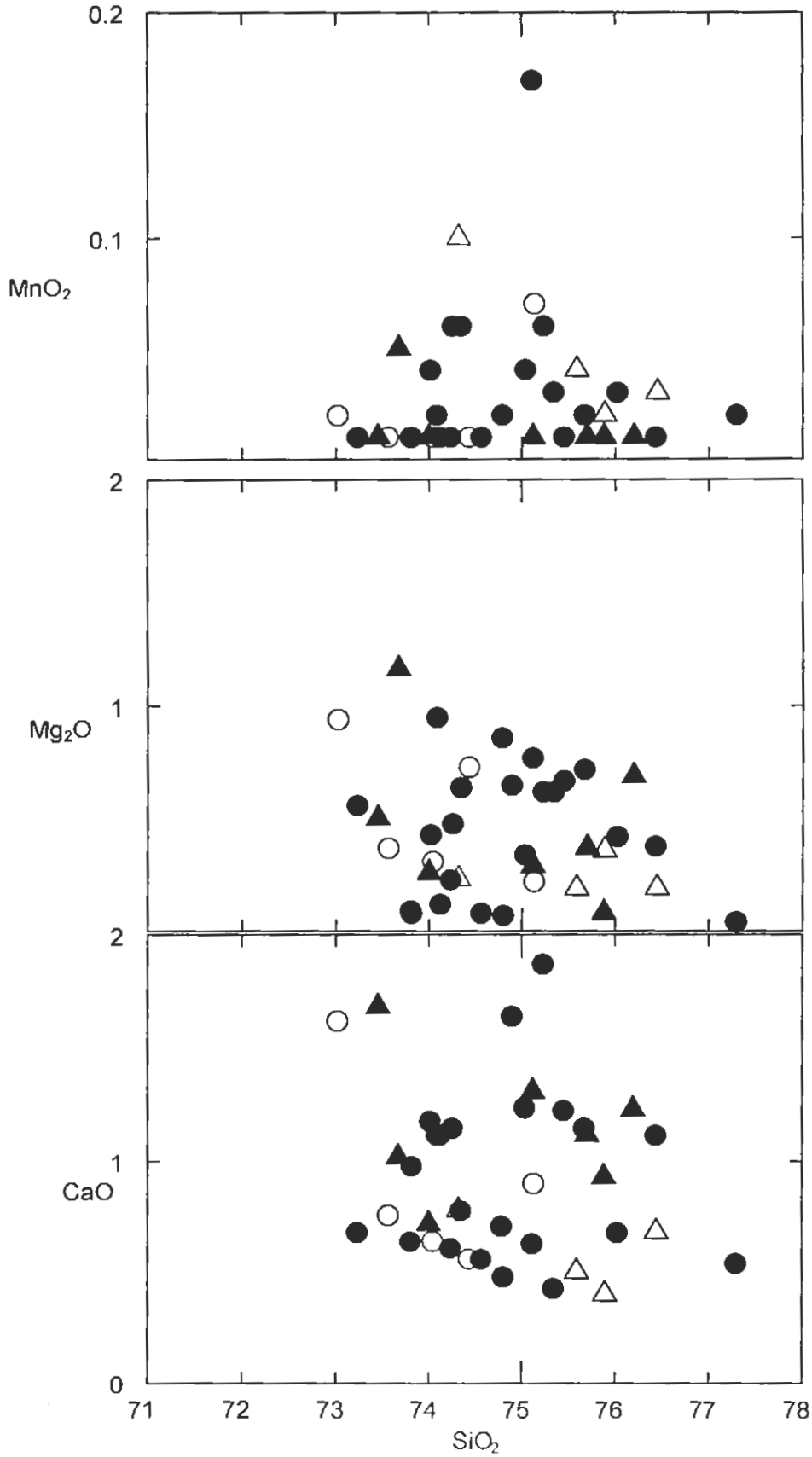


**Fig. 7. 3:** continued:

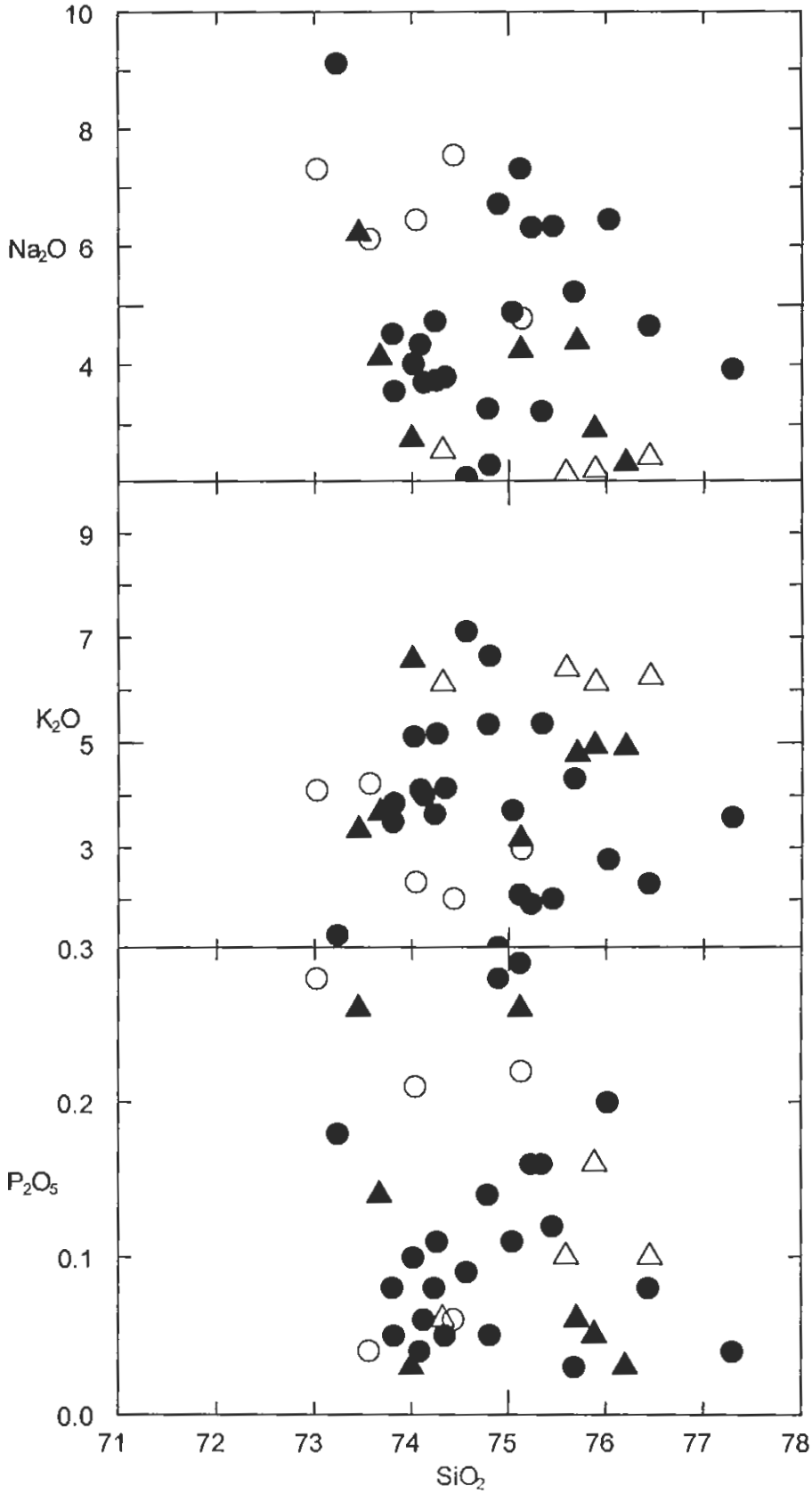


**Fig. 7. 3:** continued:

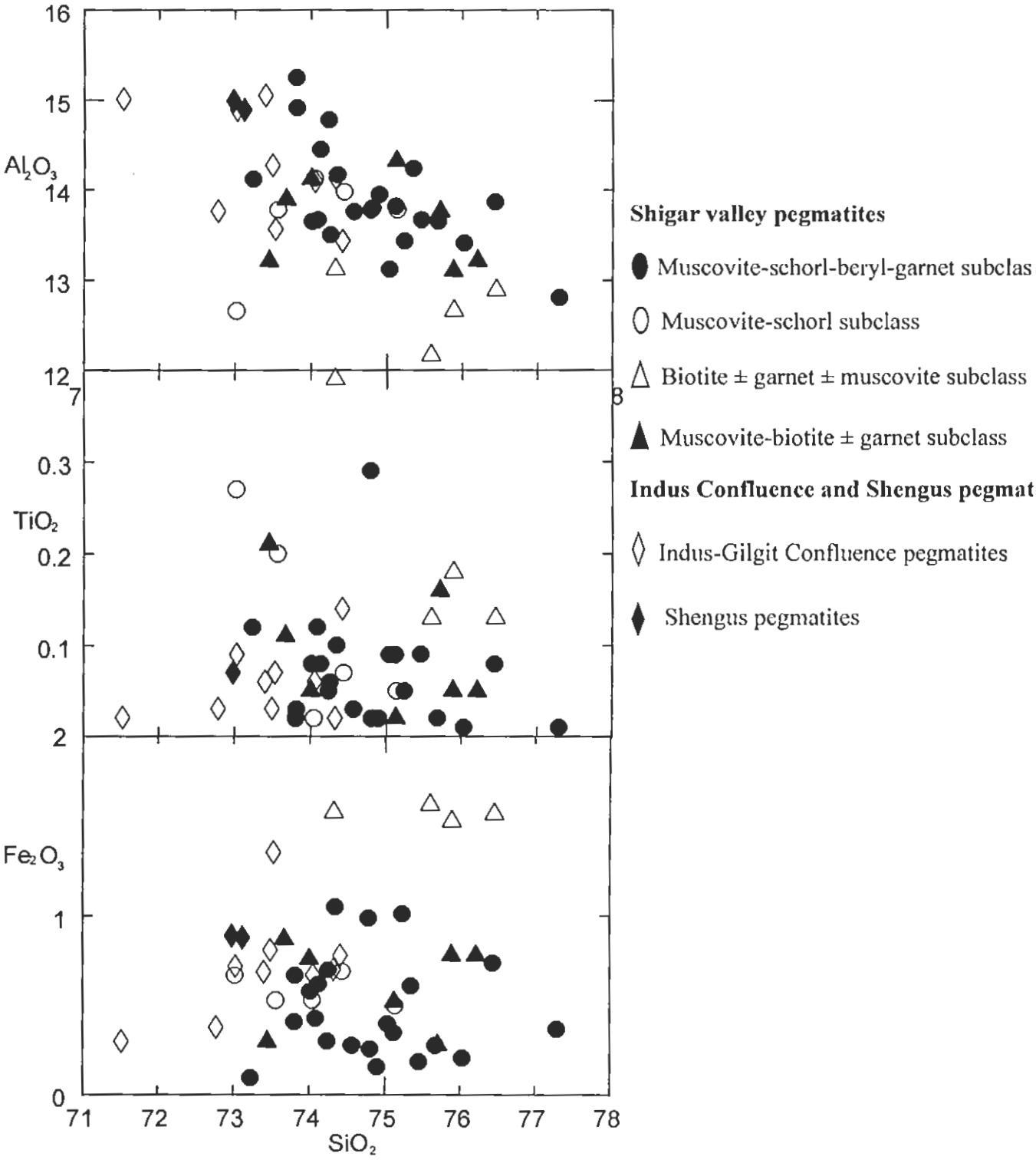


**Fig. 7. 4.** Binary diagrams for the Shengus and the Indus-Gilgit Confluence pegmatites.

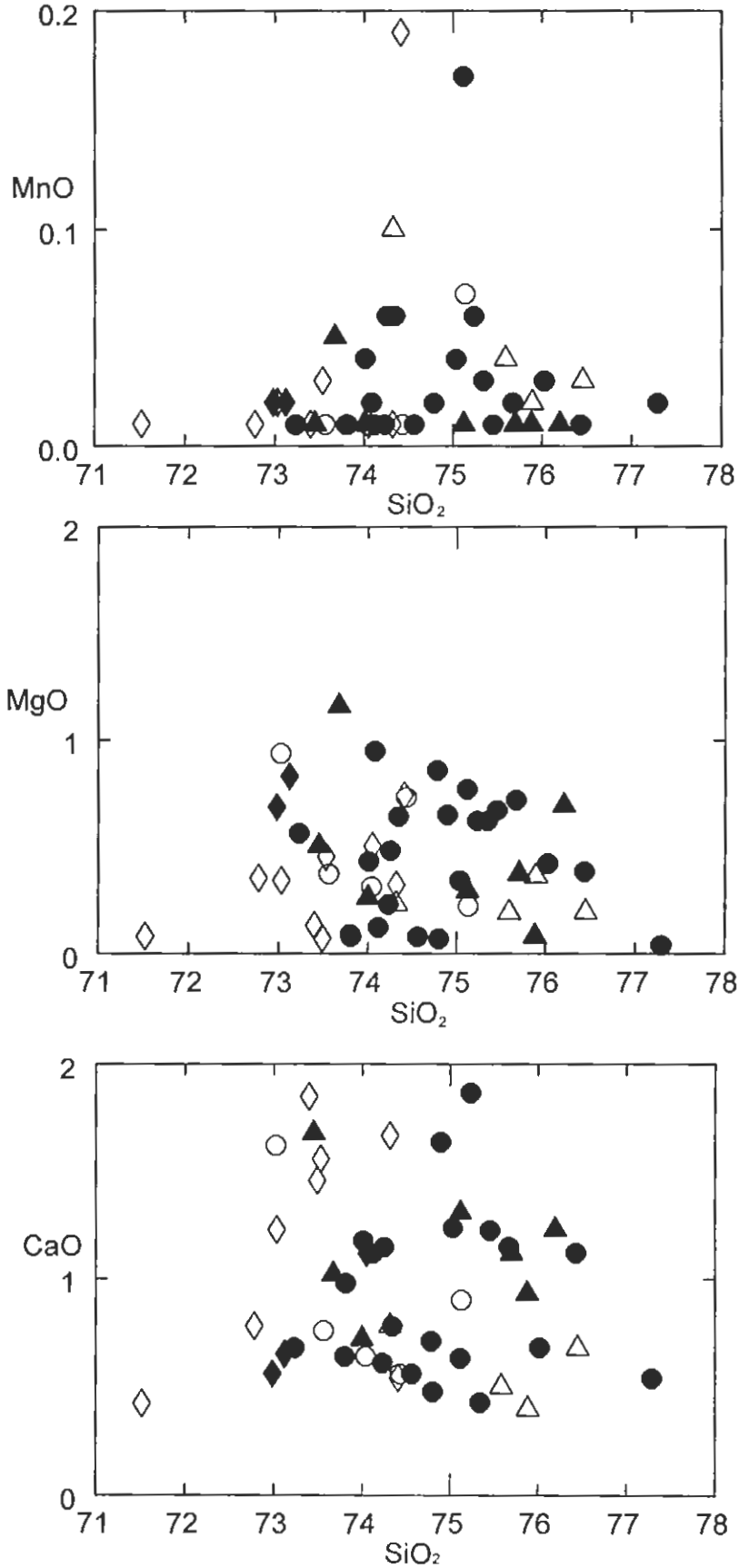


**Fig. 7. 4:** continued:

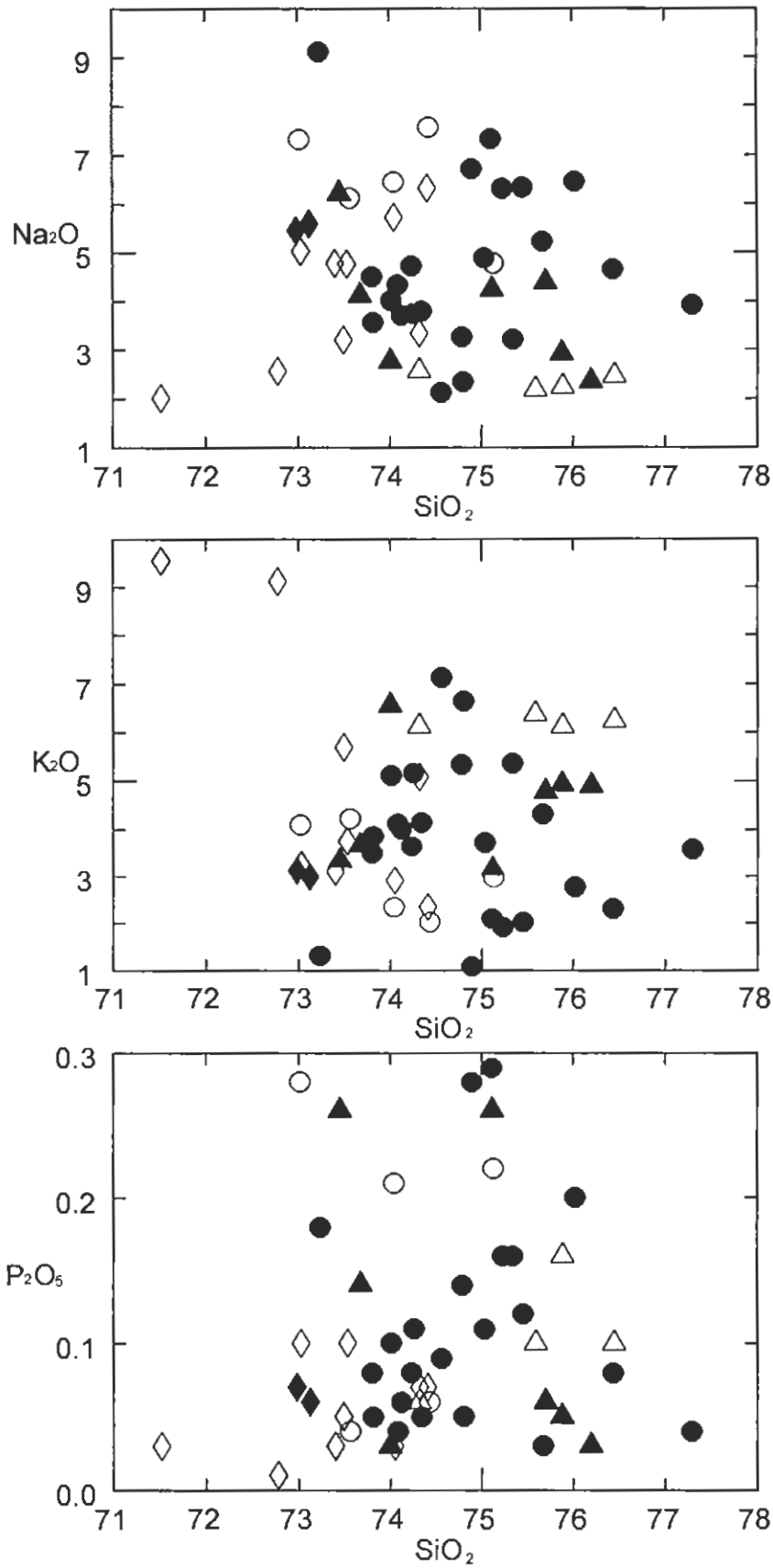


**Fig. 7. 4:** continued:

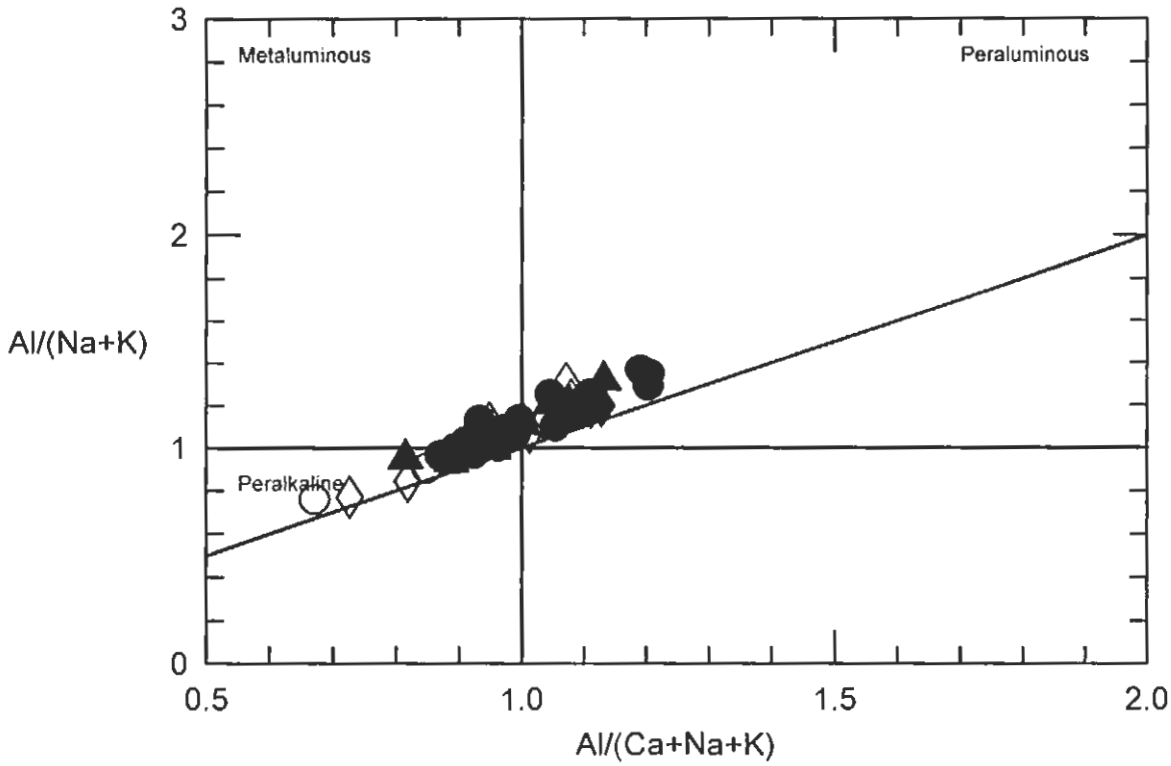


**Fig. 7. 5.** Classification of Shigar valley, Shengus and Indus-Gilgit Confluence pegmatites on the basis of Shands agapaitic (ANK = molar $Al_2O_3$ / ($Na_2O$ + $K_2O$) and miaskitic (ACNK = molar $Al_2O_3$ / (CaO+ $Na_2O$ + $K_2O$) indices (after Maniar and Piccoli, 1989). Symbols as in Figs. 7.3 and 7.4.

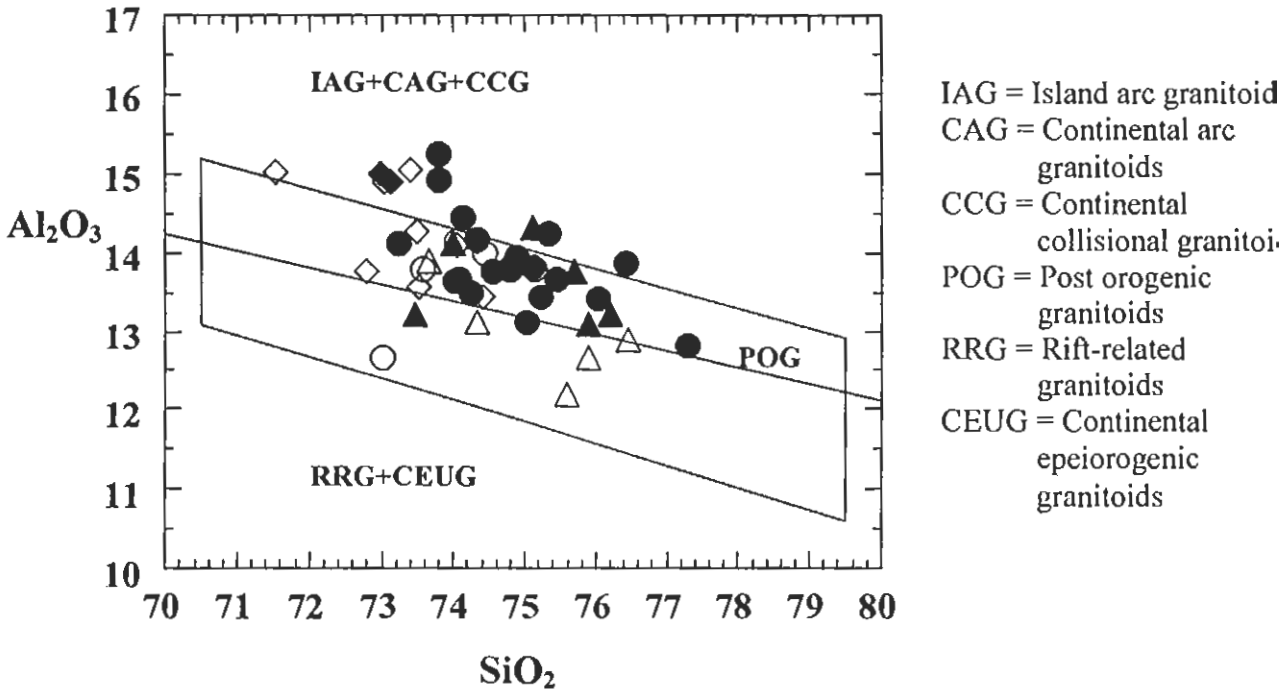


**Fig. 7. 6.** The $SiO_2$ vs $Al_2O_3$ plot for the Shigar valley, Shengus and Indus Confluence Pegmatites (after Maniar and Piccoli, 1989). Symbols as in Figs. 7.3 and 7.4.

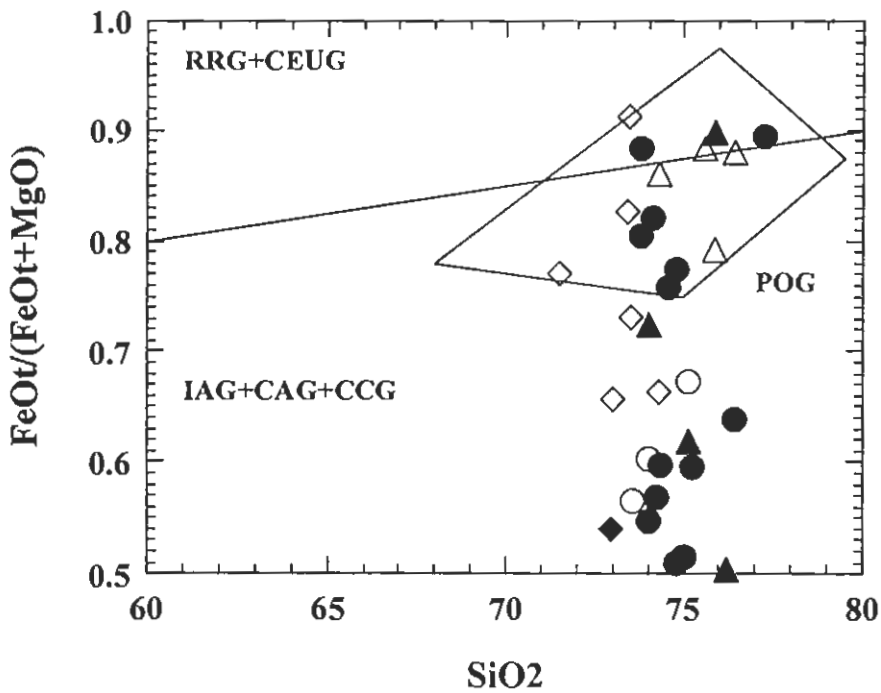


**Fig. 7. 7.** FeO (t) / FeO (t) + MgO vs. $SiO_2$ plot for the pegmatites from Shigar valley, Shengus and Indus-Gilgit confluence (after Maniar and Piccoli, 1989). Symbols as in Figs. 7.3 and 7.4.

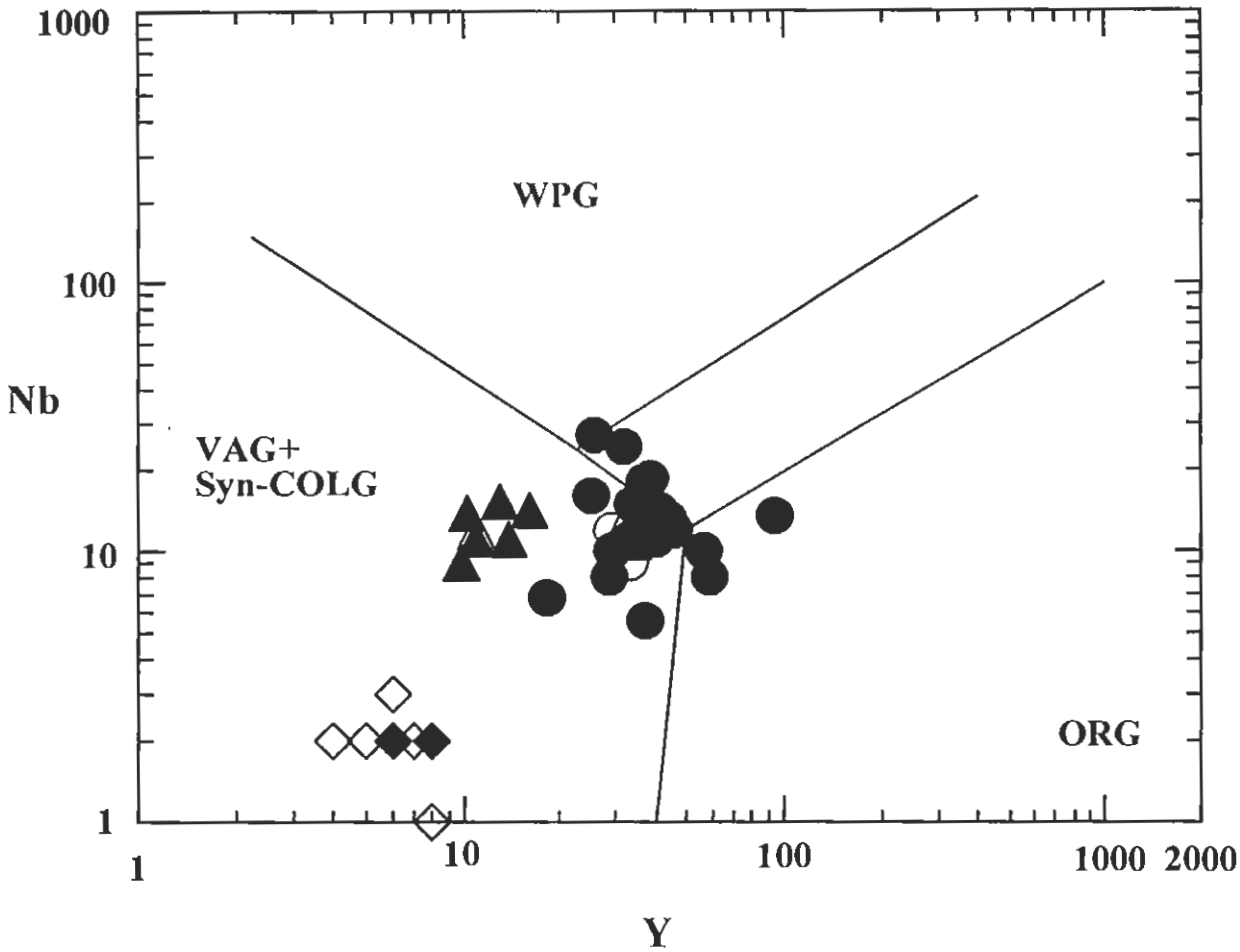


**Fig. 7. 8.** Nb-Y discrimination diagram for the Shigar valley, Shengus and Indus Confluence pegmatites (after Pearce et al., 1984). Symbols as in Figs. 7.3 and 7.4.

WPG = within plate granitoids
VAG = volcanic arc granitoids
Syn-COLG = syn-collisional granitoids
ORG = oceanic ridge granitoids

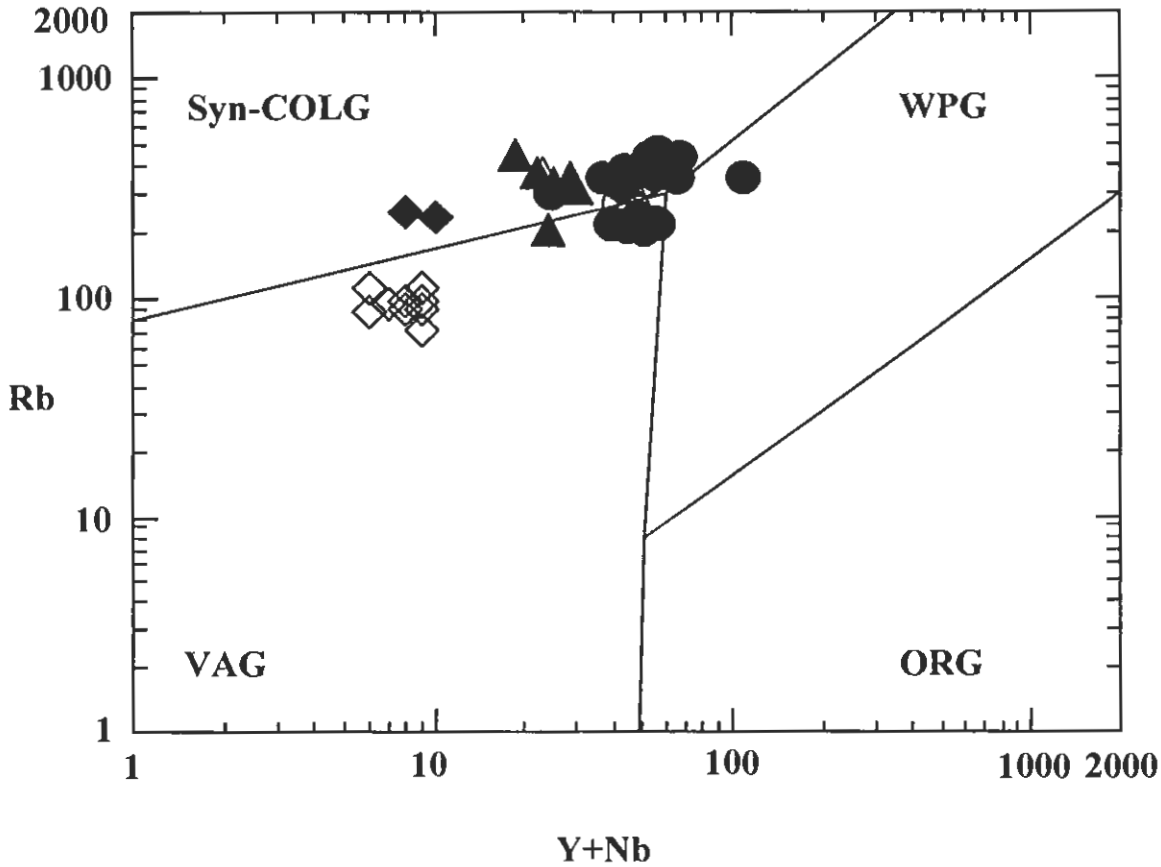


**Fig. 7. 9.** Rb-(Y + Nb) discrimination diagram for the Shigar Valley, Shengus and Indus-Gilgit Confluence pegmatites (after Pearce et al., 1984). Symbols as in Figs. 7.3 and 7. 4.

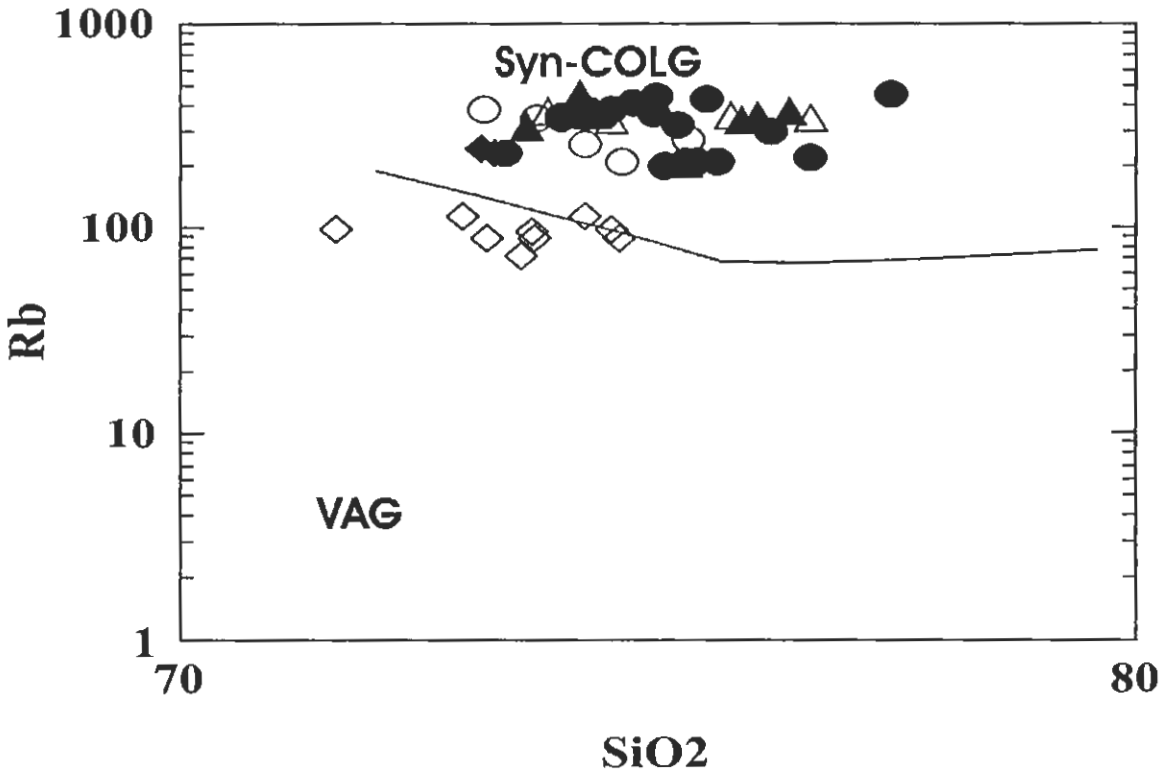


**Fig. 7. 10.** Tectonic discrimination for the Shigar valley, Indus-Gilgit confluence and the Shengus pegmatites (after Pearce et al., 1984). Symbols as in Figs. 7. 3 and 7. 4.

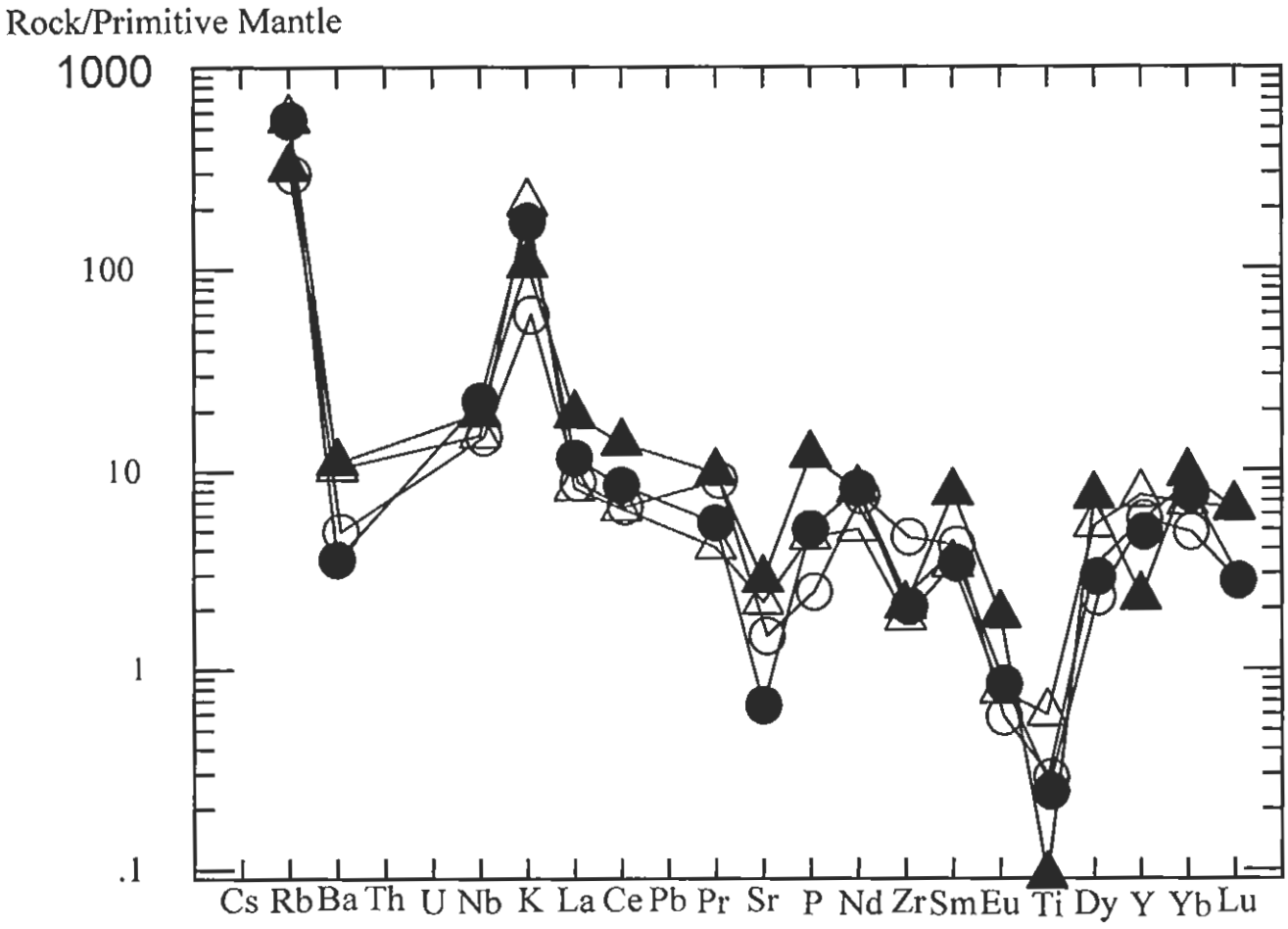


**Fig. 7. 11.** Primitive mantle normalized spider diagram for the different classes/groups of the Shigar valley pegmatites. (after Sun and Mc Don, 1989). Symbols as in Fig. 7.3.

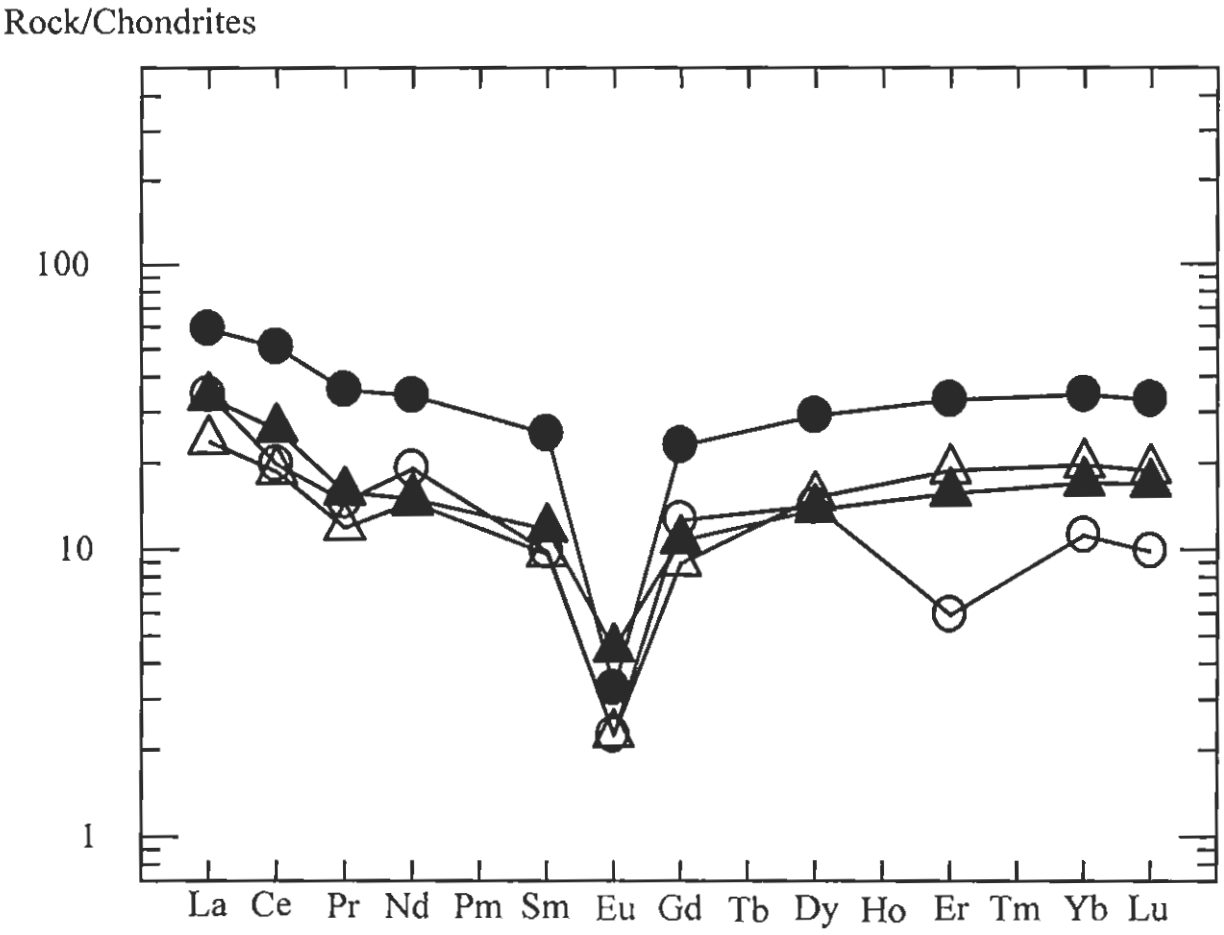


**Fig. 7. 12.** Chondrite-normalized REE patterns for the different groups of the Shigar valley pegmatites (after Sun and Mc Don, 1989). Symbols as in Fig. 7.3.

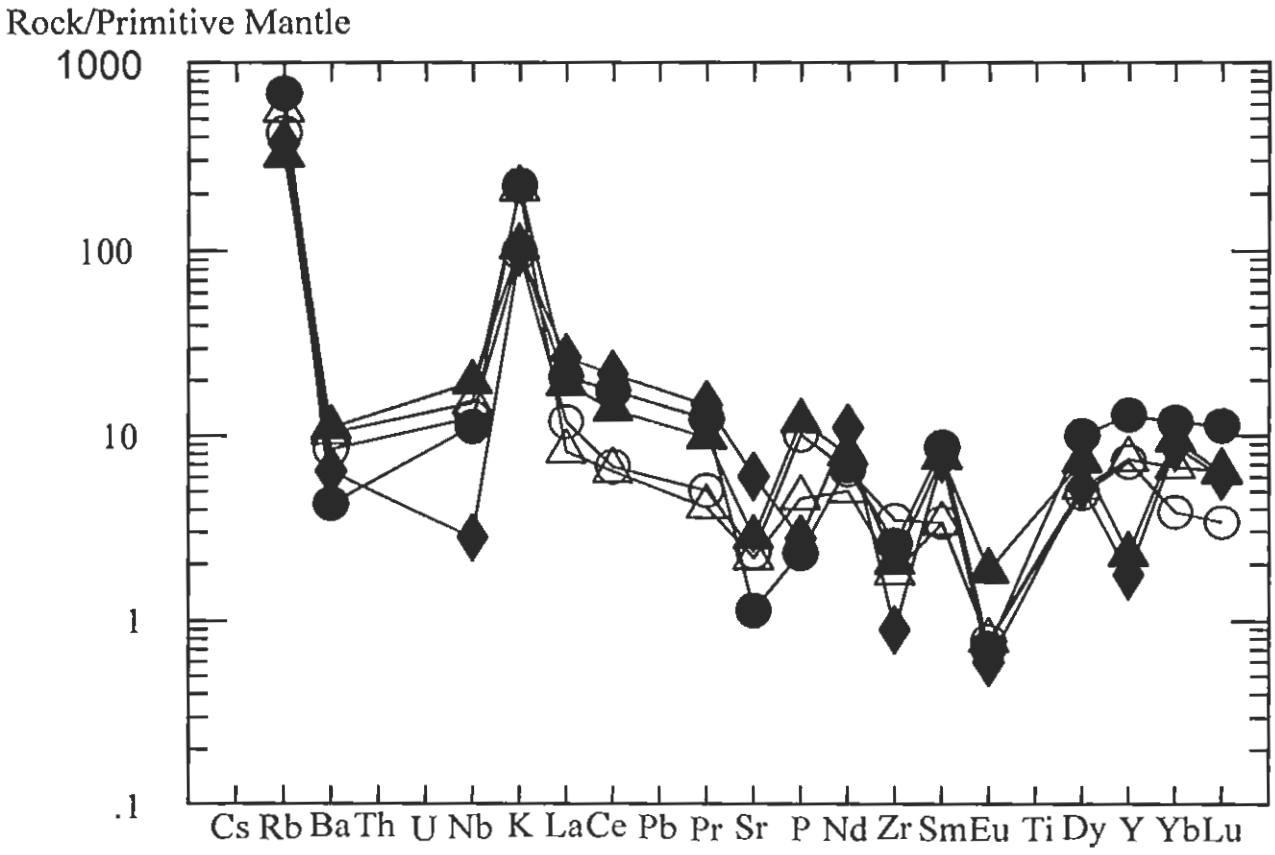


**Fig. 7. 13.** Primitive mantle normalized spidergram for comparison of the post-collisional pegmatites of the Shengus and Shigar valley (after Sun and Mc Don, 1989). Symbols as used for Figs. 7.3 and 7.4.

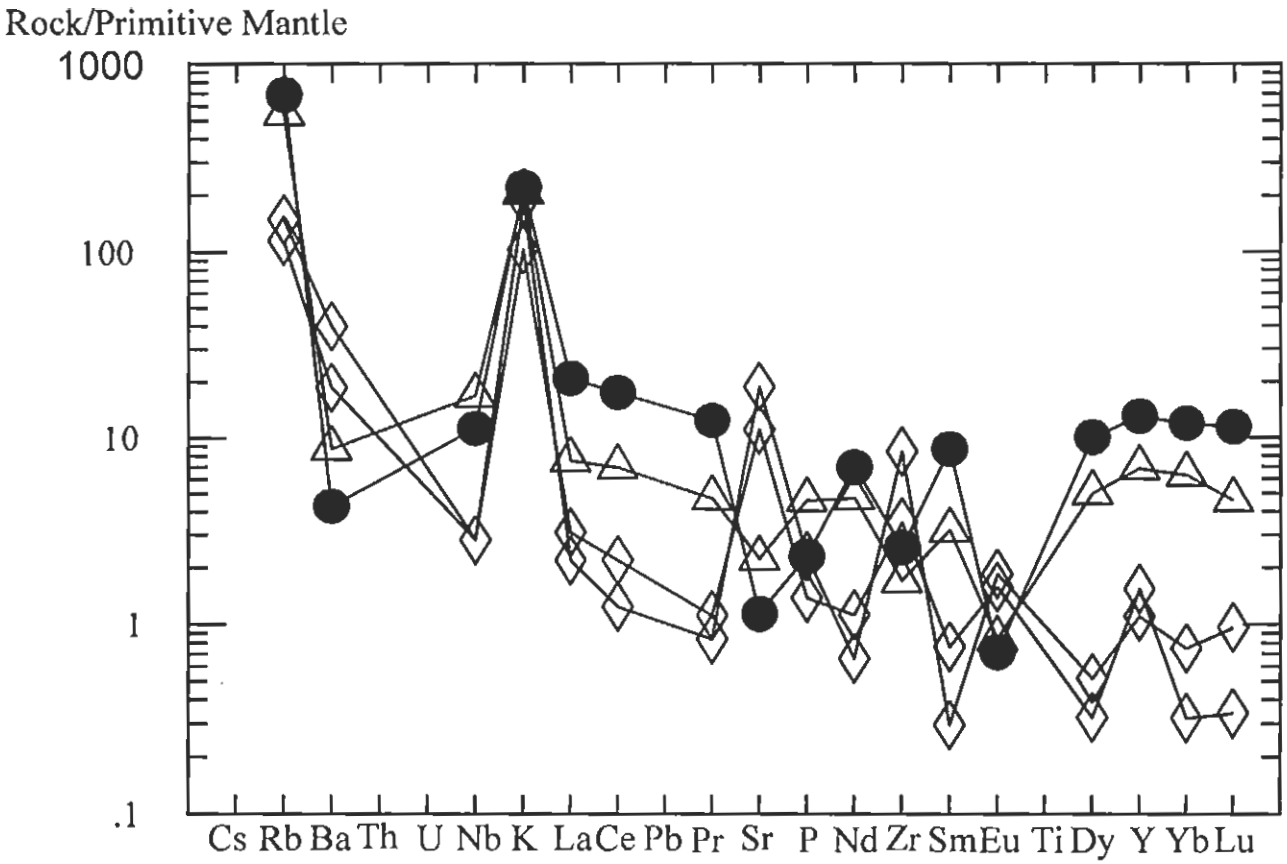


**Fig. 7. 14.** Primitive mantle normalized spidergram for comparison of the post-collisional pegmatites of the Indus-Gilgit Confluence and the Shigar valley (after Sun and Mc Don, 1989). Symbols as in Figs. 7.3 and 7.4.

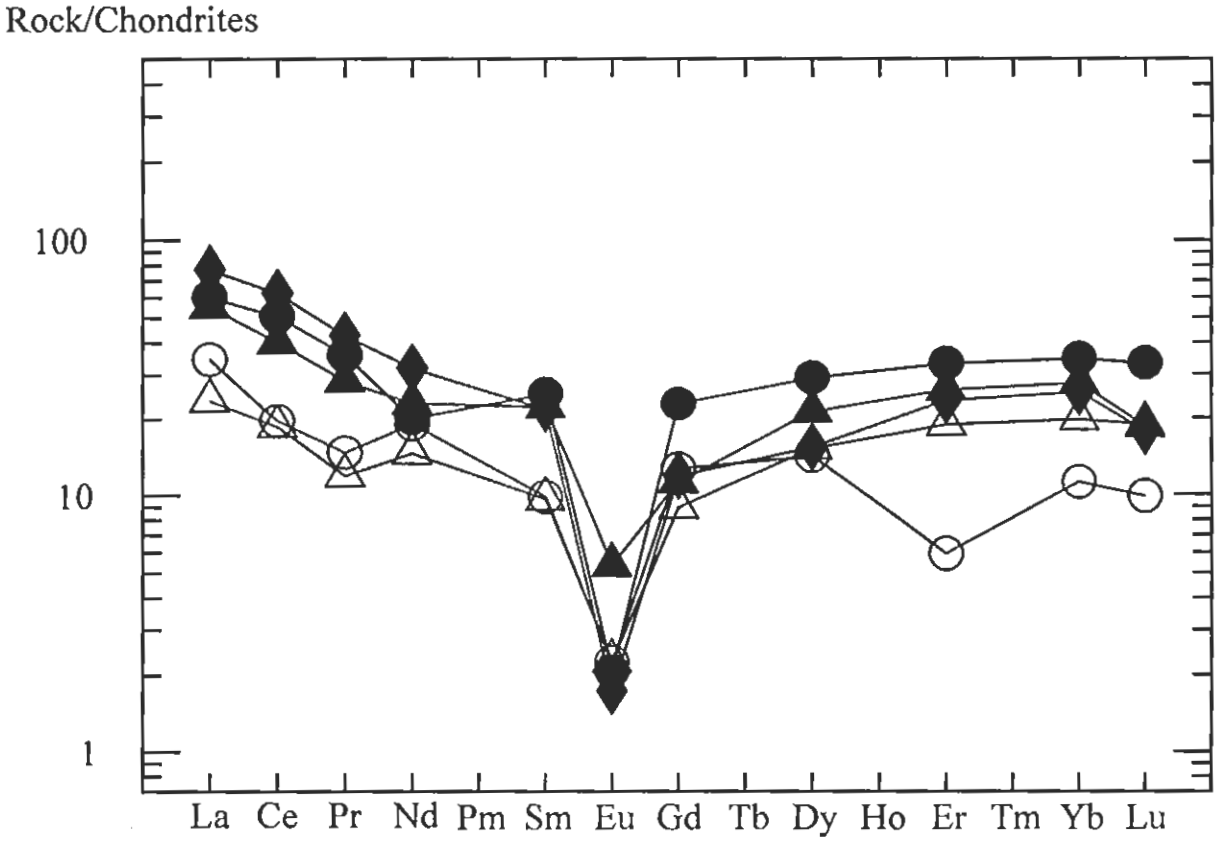


**Fig. 7. 15.** Comparison of the Chondrite-normalized REE patterns of the Shigar valley and the Shengus pegmatites (after Sun and Mc Don, 1989). Symbols as in Figs. 7.3 and 7.4.

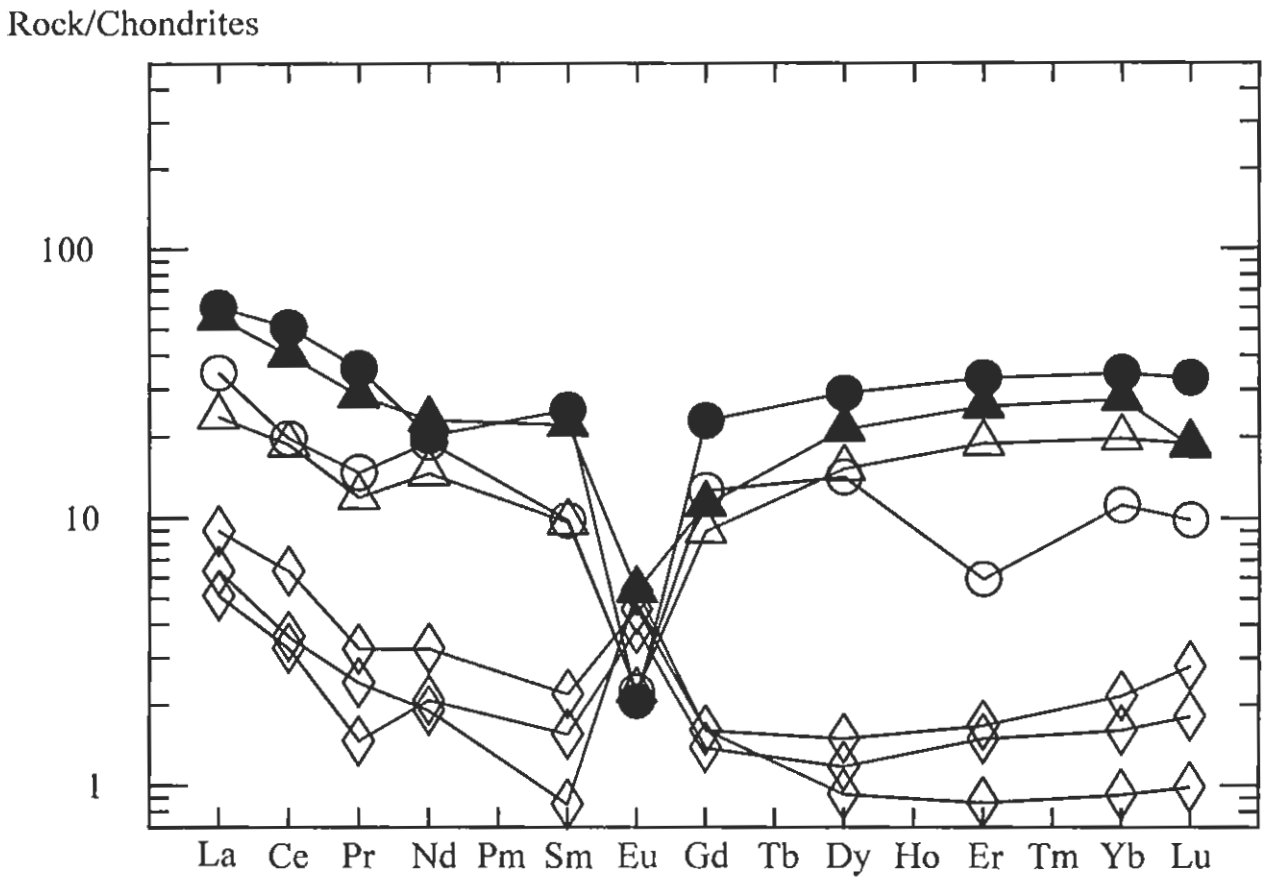


**Fig. 7. 16.** Comparison of the chondrite-normalized REE patterns of the Shigar valley and the Indus Confluence pegmatites (after Sun and Mc Don, 1989). Symbols as in Figs. 7.3 and 7.4.

**Table 7. 1. The major element chemical analyses along with C. I. P. W. norms of muscovite-schorl-beryl-garnet pegmatite sub-class of Shigar valley.**

| Sample # | 19 | 22A | 22B | 22C | 23 | 26 | 28 | 28 | 29 | 32 | 33 |
|---|---|---|---|---|---|---|---|---|---|---|---|
| $SiO_2$ | 75.34 | 76.02 | 74.78 | 75.11 | 75.45 | 73.23 | 74.23 | 73.8 | 75.03 | 76.43 | 74.89 |
| $TiO_2$ | 0.00 | 0.01 | 0.29 | 0.09 | 0.09 | 0.12 | 0.05 | 0.024 | 0.09 | 0.08 | 0.02 |
| $Al_2O_3$ | 14.24 | 13.41 | 13.78 | 13.82 | 13.67 | 14.12 | 14.78 | 15.2 | 13.12 | 13.87 | 13.95 |
| $Fe_2O_3$ | 0.61 | 0.21 | 0.99 | 0.35 | 0.19 | 0.10 | 0.30 | 0.41 | 0.40 | 0.74 | 0.16 |
| MnO | 0.03 | 0.03 | 0.02 | 0.17 | 0.01 | 0.01 | 0.01 | 0.011 | 0.04 | 0.01 | 0.00 |
| MgO | 0.62 | 0.42 | 0.86 | 0.77 | 0.67 | 0.56 | 0.23 | 0.09 | 0.34 | 0.38 | 0.65 |
| CaO | 0.43 | 0.68 | 0.71 | 0.63 | 1.23 | 0.68 | 0.61 | 0.64 | 1.24 | 1.12 | 1.64 |
| $Na_2O$ | 3.22 | 6.45 | 3.27 | 7.32 | 6.34 | 9.12 | 4.73 | 4.51 | 4.89 | 4.65 | 6.72 |
| $K_2O$ | 5.37 | 2.78 | 5.34 | 2.10 | 2.02 | 1.32 | 3.65 | 3.50 | 3.73 | 2.31 | 1.09 |
| $P_2O_5$ | 0.16 | 0.20 | 0.14 | 0.29 | 0.12 | 0.18 | 0.08 | 0.08 | 0.11 | 0.08 | 0.28 |
| LOI | 0.74 | 0.55 | 0.62 | 0.43 | 0.50 | 0.20 | 0.54 | 1.03 | 0.45 | 0.65 | 0.80 |
| **Total** | **100.76** | **100.76** | **100.80** | **101.09** | **100.29** | **99.64** | **99.21** | **99.35** | **99.44** | **100.33** | **100.20** |
| ANK | 1.28 | 0.98 | 1.24 | 0.97 | 1.08 | 0.86 | 1.26 | 1.36 | 1.09 | 1.37 | 1.14 |
| ACNK | 1.20 | 0.90 | 1.11 | 0.89 | 0.92 | 0.80 | 1.15 | 1.23 | 0.92 | 1.14 | 0.92 |
| FeO (t) | 0.55 | 0.19 | 0.89 | 0.32 | 0.17 | 0.09 | 0.27 | 0.37 | 0.36 | 0.67 | 0.15 |
| FeO (t) / (FeO(t)+MgO) | 0.47 | 0.31 | 0.51 | 0.29 | 0.20 | 0.14 | 0.54 | 0.80 | 0.51 | 0.64 | 0.18 |
| CaO / ($Na_2O$ +$K_2O$) | 0.05 | 0.07 | 0.08 | 0.07 | 0.15 | 0.07 | 0.07 | 0.08 | 0.14 | 0.16 | 0.21 |
| | | | | | **CIPW norms** | | | | | | |
| Q | 35.82 | 27.87 | 34.44 | 25.37 | 29.34 | 21.60 | 32.18 | 33.65 | 30.96 | 38.65 | 29.63 |
| Or | 31.94 | 16.47 | 31.78 | 12.45 | 12.04 | 7.89 | 21.91 | 21.07 | 22.35 | 13.75 | 6.52 |
| Ab | 27.42 | 53.63 | 26.87 | 57.57 | 54.13 | 66.03 | 40.66 | 38.88 | 41.96 | 38.63 | 57.59 |
| An | 1.09 | 0.00 | 2.63 | 0.00 | 2.90 | 0.00 | 2.54 | 2.70 | 2.87 | 5.07 | 4.74 |
| C | 2.75 | 0.00 | 1.68 | 0.00 | 0.00 | 0.00 | 2.16 | 3.08 | 0.00 | 1.89 | 0.00 |
| Ac | 0.00 | 0.61 | 0.00 | 1.02 | 0.00 | 0.29 | 0.00 | 0.00 | 0.00 | 0.00 | 0.00 |
| D | 0.00 | 1.64 | 0.00 | 0.85 | 1.80 | 1.56 | 0.00 | 0.00 | 1.99 | 0.00 | 1.27 |
| Hy | 1.36 | 0.58 | 1.84 | 2.01 | 0.85 | 0.71 | 0.73 | 0.00 | 0.22 | 1.75 | 1.18 |
| Ti | 0.00 | 0.02 | 0.00 | 0.22 | 0.22 | 0.30 | 0.00 | | 0.22 | 0.00 | 0.05 |
| Ru | 0.00 | 0.00 | 0.29 | 0.00 | | 0.00 | 0.05 | 0.02 | 0.00 | 0.08 | 0.00 |
| Mt | 0.14 | - | 0.28 | - | 0.06 | - | 0.10 | | 0.12 | 0.18 | 0.04 |
| Hm | 0.61 | 0.00 | 1.00 | 0.00 | 0.19 | 0.00 | 0.30 | 0.42 | 0.41 | 0.75 | 0.16 |
| Il | - | 0.02 | 0.55 | 0.17 | 0.17 | - | 0.05 | | 0.17 | 0.15 | 0.04 |
| Ap | 0.37 | 0.46 | 0.33 | 0.67 | 0.28 | 0.42 | 0.19 | 0.19 | 0.26 | 0.19 | 0.66 |
| NMS | 0.00 | 0.09 | 0.00 | 0.33 | | 2.72 | 0.00 | | 0.00 | | 0.00 |
| Colour Index | 2.50 | 2.24 | 3.67 | 3.16 | 3.00 | 2.45 | 0.87 | 0.85 | 2.64 | 2.08 | 2.55 |
| Diff. Index | 93.29 | 96.94 | 91.72 | 95.36 | 93.83 | 94.13 | 93.15 | 93.12 | 94.24 | 90.78 | 92.08 |
| %AN | 3.84 | 0.00 | 8.61 | | 5.09 | 0.00 | 5.89 | 6.50 | 6.41 | 11.34 | 7.60 |
| % of Q+Ab+Or | 95.18 | 97.97 | 93.09 | 95.39 | 95.51 | 95.52 | 94.75 | 93.60 | 95.28 | 91.03 | 93.74 |

(Table 7. 1 continued)

| Sample # | 43 | 44A | 44 | 47A | 47 | 62 | 63 | 66 | 67 | 68 | 68 |
|---|---|---|---|---|---|---|---|---|---|---|---|
| $SiO_2$ | 74.08 | 74.56 | 74.8 | 74.12 | 73.8 | 74.25 | 74.01 | 75.23 | 74.34 | 75.67 | 77.3 |
| $TiO_2$ | 0.12 | 0.03 | 0.022 | 0.08 | 0.034 | 0.06 | 0.08 | 0.05 | 0.10 | 0.02 | 0.015 |
| $Al_2O_3$ | 13.67 | 13.76 | 13.8 | 14.45 | 14.9 | 13.50 | 13.65 | 13.43 | 14.17 | 13.65 | 12.8 |
| $Fe_2O_3$ | 0.43 | 0.28 | 0.26 | 0.62 | 0.67 | 0.70 | 0.58 | 1.01 | 1.05 | 0.28 | 0.37 |
| MnO | 0.02 | 0.01 | 0.004 | 0.01 | 0.009 | 0.06 | 0.04 | 0.06 | 0.06 | 0.02 | 0.024 |
| MgO | 0.95 | 0.08 | 0.07 | 0.12 | 0.08 | 0.48 | 0.43 | 0.62 | 0.64 | 0.72 | 0.04 |
| CaO | 1.12 | 0.56 | 0.48 | 1.12 | 0.98 | 1.15 | 1.18 | 1.87 | 0.78 | 1.15 | 0.54 |
| $Na_2O$ | 4.34 | 2.12 | 2.33 | 3.72 | 3.57 | 3.75 | 4.02 | 6.32 | 3.80 | 5.23 | 3.92 |
| $K_2O$ | 4.12 | 7.12 | 6.65 | 4.01 | 3.86 | 5.17 | 5.12 | 1.92 | 4.15 | 4.34 | 3.59 |
| $P_2O_5$ | 0.04 | 0.09 | 0.05 | 0.06 | 0.05 | 0.11 | 0.10 | 0.16 | 0.05 | 0.03 | 0.04 |
| LOI | 0.45 | 0.67 | 0.88 | 1.25 | 1.09 | 0.55 | 0.65 | 0.50 | 0.62 | 0.45 | 0.81 |
| **Total** | **99.33** | **99.27** | **99.34** | **99.56** | **99.09** | **99.78** | **99.86** | **101.18** | **99.76** | **101.56** | **99.48** |
| ANK | 1.18 | 1.23 | 1.25 | 1.38 | 1.49 | 1.15 | 1.12 | 1.08 | 1.32 | 1.03 | 1.24 |
| ACNK | 1.00 | 1.13 | 1.16 | 1.16 | 1.26 | 0.97 | 0.95 | 0.85 | 1.17 | 0.89 | 1.13 |
| FeO (t) | 0.38 | 0.25 | 0.24 | 0.55 | 0.61 | 0.63 | 0.52 | 0.91 | 0.95 | 0.25 | 0.34 |
| FeO (t) / (FeO(t)+MgO) | 0.29 | 0.76 | 0.78 | 0.82 | 0.88 | 0.57 | 0.55 | 0.60 | 0.60 | 0.26 | 0.88 |
| CaO / ($Na_2O$ +$K_2O$) | 0.13 | 0.06 | 0.05 | 0.14 | 0.13 | 0.13 | 0.13 | 0.23 | 0.10 | 0.12 | 0.07 |
| | | | | | **CIPW norms** | | | | | | |
| Q | 30.44 | 34.55 | 35.48 | 35.56 | 37.10 | 29.45 | 29.40 | 28.79 | 34.38 | 27.15 | 40.29 |
| Or | 24.87 | 42.71 | 39.94 | 24.14 | 23.31 | 30.69 | 30.64 | 11.35 | 24.91 | 25.55 | 21.52 |
| Ab | 36.51 | 18.21 | 20.04 | 32.06 | 30.87 | 34.02 | 33.45 | 53.49 | 31.67 | 44.09 | 33.65 |
| An | 5.41 | 2.22 | 2.09 | 5.26 | 4.63 | 4.05 | 4.13 | 2.61 | 3.60 | 0.95 | 2.45 |
| C | 0.13 | 1.79 | 2.05 | 2.14 | 3.26 | 0.00 | 0.00 | 0.00 | 2.16 | 0.00 | 1.60 |
| Ae | 0.00 | 0.00 | 0.00 | 0.00 | 0.00 | 0.00 | 0.00 | 0.00 | 0.00 | 0.00 | 0.00 |
| D | 0.00 | 0.00 | 0.00 | 0.00 | 0.00 | 0.00 | 0.81 | 2.55 | 0.00 | 1.87 | 0.00 |
| Hy | 2.72 | 0.52 | 0.48 | 0.96 | 1.02 | 0.77 | 1.26 | 0.53 | 2.84 | 0.58 | 0.35 |
| Ti | 0.00 | 0.00 | | 0.00 | | 0.21 | 0.20 | 0.12 | 0.00 | 0.05 | 0.03 |
| Ru | 0.12 | 0.03 | 0.02 | 0.08 | 0.03 | 0.00 | 0.00 | 0.00 | 0.10 | 0.00 | 0.02 |
| Mt | 0.13 | 0.07 | 0.06 | 0.16 | 0.16 | 0.13 | 0.15 | 0.24 | 0.27 | 0.09 | 0.05 |
| Hm | 0.44 | 0.28 | 0.26 | 0.63 | 0.68 | 0.45 | 0.59 | 1.01 | 1.07 | 0.28 | 0.38 |
| Il | 0.23 | 0.06 | 0.04 | 0.15 | 0.07 | 0.00 | 0.15 | 0.09 | 0.19 | 0.03 | |
| Ap | 0.09 | 0.21 | 0.12 | 0.14 | 0.12 | 0.20 | 0.23 | 0.37 | 0.12 | 0.07 | 0.09 |
| NMS | 0.00 | 0.00 | | 0.00 | | 0.00 | 0.00 | 0.00 | 0.00 | 0.00 | |
| Colour Index | 3.08 | 0.65 | 0.58 | 1.27 | 1.25 | 2.43 | 2.50 | 5.48 | 3.30 | 0.70 | 0.65 |
| Diff. Index | 91.32 | 95.12 | 95.16 | 91.19 | 90.74 | 93.08 | 93.15 | 91.56 | 90.84 | 95.14 | 95.12 |
| %AN | 12.60 | 10.88 | 9.44 | 14.09 | 13.05 | 10.65 | 10.71 | 4.65 | 9.92 | 2.10 | 6.79 |
| % of Q+Ab+Or | 91.81 | 95.47 | 95.46 | 91.76 | 91.28 | 94.16 | 93.50 | 93.62 | 90.96 | 96.79 | 95.47 |

**Table 7. 2. The major element chemical analyses along with C. I. P. W. norms of muscovite-schorl pegmatite sub-class of Shigar valley.**

| Sample # | 54 | 74 | 81 | 97 | 98 |
|---|---|---|---|---|---|
| $SiO_2$ | 73.56 | 74.04 | 75.13 | 74.43 | 73.02 |
| $TiO_2$ | 0.20 | 0.02 | 0.05 | 0.07 | 0.27 |
| $Al_2O_3$ | 13.78 | 14.13 | 13.78 | 13.98 | 12.67 |
| $Fe_2O_3$ | 0.53 | 0.53 | 0.50 | 0.69 | 0.67 |
| MnO | 0.01 | 0.01 | 0.07 | 0.01 | 0.02 |
| MgO | 0.37 | 0.31 | 0.22 | 0.73 | 0.94 |
| CaO | 0.76 | 0.64 | 0.90 | 0.56 | 1.62 |
| $Na_2O$ | 6.12 | 6.45 | 4.78 | 7.56 | 7.32 |
| $K_2O$ | 4.23 | 2.34 | 2.97 | 2.02 | 4.10 |
| $P_2O_5$ | 0.04 | 0.21 | 0.22 | 0.06 | 0.28 |
| LOI | 0.55 | 0.70 | 0.60 | 0.55 | 0.75 |
| **Total** | **100.16** | **99.38** | **99.23** | **100.66** | **101.66** |
| ANK | 0.94 | 1.08 | 1.24 | 0.96 | 0.77 |
| ACNK | 0.86 | 0.99 | 1.08 | 0.89 | 0.65 |
| FeO (t) | 0.48 | 0.47 | 0.45 | 0.62 | 0.61 |
| FeO (t) / (FeO(t)+MgO) | 0.56 | 0.60 | 0.67 | 0.46 | 0.39 |
| CaO / ($Na_2O$ +$K_2O$) | 0.07 | 0.07 | 0.12 | 0.06 | 0.14 |
| | | **CIPW norms** | | | |
| Q | 23.15 | 27.24 | 35.24 | 23.48 | 23.89 |
| Or | 25.19 | 14.06 | 17.85 | 12.01 | 24.24 |
| Ab | 47.70 | 55.49 | 41.14 | 60.05 | 40.37 |
| An | 0.00 | 1.83 | 3.08 | 0.00 | 0.00 |
| C | 0.00 | 0.33 | 1.62 | 0.00 | 0.00 |
| Ac | 1.55 | 0.00 | 0.00 | 2.01 | 1.94 |
| D | 2.54 | 0.00 | 0.00 | 1.83 | 3.51 |
| Hy | - | 1.44 | 1.20 | 1.73 | 0.47 |
| Ti | 0.49 | 0.00 | 0.00 | 0.17 | 0.66 |
| Ru | 0.00 | 0.02 | 0.05 | 0.00 | 0.00 |
| Mt | - | 0.12 | 0.14 | - | - |
| Hm | 0.00 | 0.54 | 0.51 | 0.00 | 0.00 |
| Il | 0.38 | 0.04 | 0.10 | 0.13 | 0.51 |
| Ap | 0.09 | 0.49 | 0.52 | 0.14 | 0.65 |
| NMS | 0.64 | 0.00 | 0.00 | 0.24 | 4.05 |
| Colour Index | 3.15 | 1.60 | 1.44 | 3.79 | 5.84 |
| Diff. Index | 95.45 | 95.73 | 93.35 | 95.03 | 88.66 |
| %AN | 0.00 | 3.20 | 6.96 | 0.00 | 0.00 |
| % of Q+Ab+Or | 96.05 | 96.79 | 94.23 | 95.54 | 88.50 |

**Table 7. 3. The major element chemical analyses along with C. I. P. W. norms of biotite ± garnet ± muscovite pegmatite sub-class of Shigar valley.**

| Sample # | 3A | 3 | 6 | 48 |
|---|---|---|---|---|
| $SiO_2$ | 76.5 | 75.6 | 74.32 | 75.89 |
| $TiO_2$ | 0.13 | 0.13 | 0.39 | 0.18 |
| $Al_2O_3$ | 12.9 | 12.2 | 13.12 | 12.67 |
| $Fe_2O_3$ | 1.56 | 1.61 | 1.57 | 1.52 |
| MnO | 0.03 | 0.04 | 0.10 | 0.02 |
| MgO | 0.19 | 0.19 | 0.23 | 0.36 |
| CaO | 0.68 | 0.50 | 0.78 | 0.40 |
| $Na_2O$ | 2.45 | 2.17 | 2.56 | 2.23 |
| $K_2O$ | 6.23 | 6.38 | 6.12 | 6.12 |
| $P_2O_5$ | 0.10 | 0.10 | 0.06 | 0.16 |
| LOI | 0.48 | 0.77 | 0.40 | 0.50 |
| **Total** | **101.18** | **99.66** | **99.65** | **100.04** |
| ANK | 0.72 | 0.73 | 0.71 | 0.73 |
| ACNK | 0.67 | 0.69 | 0.66 | 0.70 |
| FeO (t) | 1.40 | 1.45 | 1.41 | 1.37 |
| FeO (t) / (FeO(t)+MgO) | 0.88 | 0.89 | 0.86 | 0.79 |
| CaO / ($Na_2O$ +$K_2O$) | 0.08 | 0.06 | 0.09 | 0.05 |
| | | **CIPW norms** | | |
| Q | 36.03 | 37.28 | 33.89 | 38.42 |
| Or | 35.62 | 3720 | 35.56 | 35.47 |
| Ab | 20.62 | 18.61 | 21.90 | 19.03 |
| An | 2.71 | 1.85 | 3.52 | 0.95 |
| C | 1.12 | 1.07 | 1.02 | 2.05 |
| Ac | 0.00 | 0.00 | 0.00 | 0.00 |
| D | 0.00 | 0.00 | 0.00 | 0.00 |
| Hy | 2.24 | 2.36 | 1.96 | 2.52 |
| Ti | | | 0.00 | 0.00 |
| Ru | 0.13 | 0.13 | 0.39 | 0.18 |
| Mt | 0.37 | 0.39 | 0.45 | 0.38 |
| Hm | 1.55 | 1.63 | 1.59 | 1.53 |
| Il | 0.25 | 0.25 | 0.75 | 0.34 |
| Ap | 0.23 | 0.23 | 0.14 | 0.37 |
| NMS | | | 0.00 | 0.00 |
| Colour Index | 2.85 | 3.00 | 3.15 | 3.24 |
| Diff. Index | 93.08 | 93.84 | 92.17 | 93.39 |
| %AN | 11.60 | 9.05 | 13.83 | 4.74 |
| % of Q+Ab+Or | 92.27 | 93.09 | 91.35 | 92.92 |

**Table 7. 4. The major element chemical analyses along with C. I. P. W. norms of muscovite-biotite ± garnet pegmatite sub-class of Shigar valley.**

| Sample # | 1 | 5 | 7 | 21 | 38A | 38 | 41 |
|---|---|---|---|---|---|---|---|
| $SiO_2$ | 73.45 | 75.12 | 75.70 | 74.00 | 76.20 | 75.9 | 73.67 |
| $TiO_2$ | 0.21 | 0.02 | 0.16 | 0.05 | 0.05 | 0.049 | 0.11 |
| $Al_2O_3$ | 13.21 | 14.32 | 13.76 | 14.12 | 13.21 | 13.1 | 13.89 |
| $Fe_2O_3$ | 0.30 | 0.52 | 0.28 | 0.76 | 0.78 | 0.78 | 0.87 |
| MnO | 0.01 | 0.01 | 0.01 | 0.01 | 0.01 | 0.005 | 0.05 |
| MgO | 0.50 | 0.29 | 0.37 | 0.26 | 0.69 | 0.08 | 1.16 |
| CaO | 1.68 | 1.31 | 1.12 | 0.72 | 1.23 | 0.93 | 1.02 |
| $Na_2O$ | 6.21 | 4.23 | 4.38 | 2.76 | 2.34 | 2.91 | 4.12 |
| $K_2O$ | 3.34 | 3.16 | 4.78 | 6.56 | 4.90 | 4.93 | 3.67 |
| $P_2O_5$ | 0.26 | 0.26 | 0.06 | 0.03 | 0.03 | 0.05 | 0.14 |
| LOI | 0.32 | 0.15 | 0.70 | 0.60 | 0.50 | 0.86 | 0.40 |
| **Total** | **99.49** | **99.39** | **101.32** | **99.88** | **99.93** | **99.58** | **99.10** |
| ANK | 0.96 | 1.38 | 1.11 | 1.21 | 1.44 | 1.30 | 1.29 |
| ACNK | 0.01 | 0.02 | 0.01 | 0.01 | 0.02 | 0.01 | 0.02 |
| FeO (t) | 0.27 | 0.47 | 0.25 | 0.68 | 0.70 | 0.70 | 0.78 |
| FeO (t) / (FeO(t)+MgO) | 0.35 | 0.62 | 0.41 | 0.72 | 0.50 | 0.90 | 0.40 |
| CaO / ($Na_2O$ +$K_2O$) | 0.18 | 0.18 | 0.12 | 0.08 | 0.17 | 0.12 | 0.13 |
| | | | | **CIPW norms** | | | |
| Q | 24.94 | 36.74 | 29.93 | 31.70 | 40.82 | 38.78 | 33.74 |
| Or | 20.01 | 18.87 | 28.18 | 39.16 | 28.33 | 29.53 | 21.25 |
| Ab | 48.03 | 36.18 | 36.98 | 23.59 | 20.05 | 24.96 | 34.76 |
| An | 0.00 | 4.85 | 3.76 | 3.41 | 5.98 | 4.35 | 4.25 |
| C | 0.00 | 2.21 | 0.00 | 1.25 | 1.92 | 1.42 | 1.66 |
| Ac | 0.88 | 0.00 | 0.00 | 0.00 | 0.00 | 0.00 | 0.00 |
| D | 4.92 | 0.00 | 0.86 | 0.00 | 0.00 | 0.00 | 0.00 |
| Hy | - | 1.38 | 0.45 | 1.54 | 2.64 | 1.12 | 3.90 |
| Ti | 0.52 | 0.00 | 0.39 | 0.00 | 0.00 | | 0.00 |
| Ru | 0.00 | 0.02 | 0.00 | 0.05 | 0.05 | 0.05 | 0.11 |
| Mt | - | 0.12 | 0.10 | 0.18 | 0.18 | 0.18 | 0.23 |
| Hm | 0.00 | 0.53 | 0.28 | 0.77 | 0.79 | 0.79 | 0.89 |
| Il | 0.40 | 0.04 | 0.30 | 0.10 | 0.10 | 0.09 | 0.21 |
| Ap | 0.61 | 0.61 | 0.14 | 0.07 | 0.07 | 0.12 | 0.33 |
| NMS | 0.52 | 0.00 | 0.00 | 0.00 | 0.00 | | 0.00 |
| Colour Index | 4.48 | 1.53 | 1.95 | 1.82 | 2.92 | 1.40 | 4.33 |
| Diff. Index | 93.96 | 90.81 | 94.17 | 93.45 | 89.15 | 92.71 | 89.47 |
| %AN | 0.00 | 11.83 | 9.23 | 12.63 | 22.97 | 14.83 | 10.63 |
| % of Q+Ab+Or | 92.97 | 91.79 | 95.09 | 94.45 | 89.20 | 93.28 | 89.75 |

**Table 7. 5. The major element chemical analyses along with C. I. P. W. norms of the Indus-Gilgit Confluence and the Shengus pegmatites.**

| Sample # | 107 | 109A | 109 | 110A | 110 | 111 | 113 | 114A | 114 | 102SN | 103SN |
|---|---|---|---|---|---|---|---|---|---|---|---|
| $SiO_2$ | 74.41 | 72.78 | 71.52 | 73.03 | 73.40 | 73.53 | 74.05 | 74.32 | 73.49 | 73.12 | 72.98 |
| $TiO_2$ | 0.14 | 0.03 | 0.02 | 0.09 | 0.06 | 0.07 | 0.06 | 0.02 | 0.03 | 0.00 | 0.07 |
| $Al_2O_3$ | 13.43 | 13.76 | 15.01 | 14.89 | 15.05 | 13.56 | 14.09 | 14.13 | 14.27 | 14.89 | 14.99 |
| $Fe_2O_3$ | 0.78 | 0.38 | 0.30 | 0.72 | 0.69 | 1.35 | 0.67 | 0.70 | 0.81 | 0.88 | 0.89 |
| MnO | 0.19 | 0.01 | 0.01 | 0.02 | 0.01 | 0.03 | 0.01 | 0.01 | 0.00 | 0.02 | 0.02 |
| MgO | 0.74 | 0.35 | 0.08 | 0.34 | 0.13 | 0.45 | 0.50 | 0.32 | 0.07 | 0.83 | 0.68 |
| CaO | 0.54 | 0.78 | 0.42 | 1.23 | 1.85 | 1.56 | 1.12 | 1.67 | 1.46 | 0.65 | 0.56 |
| $Na_2O$ | 6.32 | 2.56 | 2.00 | 5.02 | 4.77 | 4.76 | 5.71 | 3.34 | 3.20 | 5.59 | 5.45 |
| $K_2O$ | 2.34 | 9.12 | 9.55 | 3.25 | 3.10 | 3.75 | 2.91 | 5.08 | 5.69 | 2.99 | 3.12 |
| $P_2O_5$ | 0.07 | 0.01 | 0.03 | 0.10 | 0.03 | 0.10 | 0.03 | 0.07 | 0.05 | 0.06 | 0.07 |
| LOI | 0.40 | 0.54 | 0.73 | 0.67 | 0.54 | 0.35 | 0.65 | 0.15 | 0.56 | 0.15 | 0.34 |
| **Total** | **99.36** | **100.31** | **99.66** | **99.35** | **99.63** | **99.51** | **99.81** | **99.81** | **99.64** | **99.16** | **99.17** |
| ANK | 1.04 | 0.98 | 1.10 | 1.27 | 1.34 | 1.14 | 1.12 | 1.29 | 1.25 | 1.20 | 1.21 |
| ACNK | 0.97 | 0.89 | 1.04 | 1.06 | 1.03 | 0.92 | 0.97 | 1.01 | 1.01 | 1.09 | 1.12 |
| FeO (t) | 0.70 | 0.34 | 0.27 | 0.65 | 0.62 | 1.22 | 0.61 | 0.63 | 0.73 | 0.79 | 0.80 |
| FeO (t) / (FeO(t)+MgO) | 0.49 | 0.50 | 0.78 | 0.66 | 0.82 | 0.73 | 0.55 | 0.66 | 0.91 | 0.49 | 0.54 |
| CaO / ($Na_2O$ +$K_2O$) | 0.06 | 0.07 | 0.04 | 0.15 | 0.23 | 0.18 | 0.13 | 0.20 | 0.16 | 0.08 | 0.07 |
| | | | | | | **CIPW norms** | | | | | |
| Q | 27.48 | 22.82 | 22.77 | 29.53 | 30.22 | 29.37 | 27.01 | 32.29 | 30.42 | 27.46 | 28.88 |
| Or | 14.11 | 54.21 | 57.11 | 19.53 | 18.51 | 22.46 | 17.43 | 30.22 | 33.95 | 18.00 | 18.79 |
| Ab | 53.56 | 20.12 | 17.13 | 43.20 | 40.77 | 40.82 | 47.99 | 28.45 | 27.34 | 47.18 | 47.00 |
| An | 1.39 | 0.00 | 1.91 | 5.54 | 9.07 | 4.62 | 4.28 | 7.88 | 6.98 | 2.89 | 2.37 |
| C | 0.00 | 0.00 | 0.69 | 1.14 | 0.61 | 0.00 | 0.00 | 0.27 | 0.35 | 1.45 | 1.83 |
| Ac | 0.00 | 1.11 | 0.00 | 0.00 | 0.00 | 0.00 | 0.00 | 0.00 | 0.00 | 0.00 | 0.00 |
| D | 0.50 | 3.05 | 0.00 | 0.00 | 0.00 | 2.05 | 0.85 | 0.00 | 0.00 | 0.00 | 0.00 |
| Hy | 2.51 | 0.00 | 0.56 | 1.12 | 0.00 | 1.70 | 1.54 | 1.18 | 0.00 | 3.25 | 0.00 |
| Ti | 0.35 | 0.07 | | 0.00 | | 0.17 | 0.15 | 0.00 | | 0.00 | 0.00 |
| Ru | 0.00 | 0.00 | 0.02 | 0.09 | 0.06 | 0.00 | 0.00 | 0.02 | 0.03 | 0.00 | 0.07 |
| Mt | 0.25 | - | 0.07 | 0.17 | | 0.32 | 0.16 | 0.19 | | 0.20 | 0.00 |
| Hm | 0.80 | 0.00 | 0.30 | 0.73 | 0.70 | 1.37 | 0.68 | 0.70 | 0.82 | 0.90 | 0.91 |
| Il | 0.27 | 0.06 | 0.03 | 0.11 | | 0.13 | 0.11 | 0.06 | | - | 0.00 |
| Ap | 0.17 | 0.02 | 0.07 | 0.24 | 0.07 | 0.23 | 0.07 | 0.16 | 0.12 | 0.14 | 0.17 |
| NMS | 0.00 | 0.10 | | 0.00 | | 0.00 | 0.00 | 0.00 | | 0.00 | 0.00 |
| Colour Index | 3.74 | 3.01 | 0.67 | 1.40 | 1.35 | 4.30 | 2.77 | 1.41 | 1.39 | 3.45 | 3.30 |
| Diff. Index | 94.71 | 96.42 | 96.65 | 88.85 | 89.75 | 90.86 | 92.89 | 91.13 | 91.12 | 92.10 | 91.80 |
| %AN | 2.49 | 0.00 | 10.03 | 11.37 | 18.20 | 10.17 | 8.03 | 21.69 | 20.35 | 5.65 | 4.79 |
| % of Q+Ab+Or | 95.15 | 97.15 | 97.01 | 92.27 | 89.50 | 92.64 | 92.43 | 90.97 | 91.71 | 92.64 | 94.67 |

**Table 7. 6. The trace and rare earth element chemical analyses of muscovite-schorl-beryl-garnet pegmatite sub-class of Shigar valley.**

**Trace elements**

| Sample # | 19 | 22A | 22B | 22C | 23 | 26 | 28 | 28 | 29 | 32 | 33 |
|---|---|---|---|---|---|---|---|---|---|---|---|
| Ba | 32 | 16 | 26 | 41 | 41 | 17 | 32 | 16 | 32 | 18 | 32 |
| Cr | 7 | 5 | 4 | 5 | 7 | 6 | 3 | 2 | 6 | 4 | 6 |
| Nb | 27 | 7 | 25 | 10 | 13 | 15 | 8 | 8 | 6 | 14 | 12 |
| Ni | 3 | 2 | 3 | 5 | 5 | 4 | 3 | 2 | 3 | 3 | 4 |
| Rb | 434 | 295 | 364 | 212 | 212 | 232 | 334 | 348 | 318 | 222 | 201 |
| Sr | 16 | 22 | 17 | 26 | 34 | 27 | 29 | 16 | 18 | 21 | 24 |
| V | 2 | 2 | 2 | 4 | 2 | 2 | 4 | 6 | 0 | 4 | 2 |
| Y | 26 | 18 | 32 | 29 | 44 | 34 | 32 | 29 | 37 | 41 | 39 |
| Zn | 23 | 20 | 25 | 24 | 23 | 22 | 25 | 21 | 19 | 12 | 20 |
| Zr | 17 | 32 | 22 | 39 | 37 | 52 | 42 | 23 | 37 | 28 | 21 |
| Sc | 13 | 2 | 9 | 3 | 3 | 3 | 3 | 3 | 4 | 2 | 4 |
| Rb / Sr | 28 | 14 | 21 | 8 | 6 | 9 | 12 | 21 | 17 | 11 | 8 |

**Rare Earth elements**

| | | | | | | | | | | | |
|---|---|---|---|---|---|---|---|---|---|---|---|
| La | 9.2 | 12.7 | 11.9 | 14.9 | 6.5 | 14.0 | 13.0 | 10.5 | 8.5 | 7.9 | 6.8 |
| Ce | 13.1 | 18.1 | 14.0 | 17.4 | 13.8 | 21.0 | 21.0 | 25.5 | 16.8 | 13.0 | 14.7 |
| Pr | 2.4 | 1.8 | 3.2 | 2.7 | 1.7 | 2.3 | 3.5 | 3.0 | 1.8 | 1.6 | 1.2 |
| Nd | 8.5 | 12.7 | 9.7 | 8.8 | 7.6 | 9.7 | 11.2 | 12 | 8.9 | 8.8 | 9.6 |
| Sm | 4.8 | 3.8 | 3.4 | 5.2 | 1.9 | 3.9 | 3.8 | 7.0 | 1.8 | 1.6 | 2 |
| Eu | 0.11 | 0.12 | 0.4 | 0.16 | 0.18 | 0.28 | 0.12 | 0.18 | 0.13 | 0.19 | 0.24 |
| Gd | 2.3 | 3.2 | 1.7 | 1.4 | 1.5 | 3.2 | 2.3 | 3.9 | 2.8 | 1.9 | 1.5 |
| Dy | 3.4 | 2.9 | 3.7 | 3.3 | 3.9 | 4.6 | 4.2 | 4.6 | 1.9 | 3.2 | 4.8 |
| Er | 1.8 | 1.2 | 0.99 | 1.7 | 4.1 | 3.4 | 1.2 | 1.6 | 0.95 | 3.8 | 3.7 |
| Yb | 1.5 | 1.3 | 2.7 | 2.5 | 4.2 | 3.5 | 1.8 | 3.3 | 2.9 | 3.9 | 3.6 |
| Lu | 0.23 | 0.35 | 0.21 | 0.13 | 0.45 | 0.43 | 0.34 | 0.47 | 0.19 | 0.53 | 0.42 |

(Table 7. 1 continued)

**Trace elements**

| Sample # | 43 | 44A | 44 | 47A | 47 | 62 | 63 | 66 | 67 | 68 | 68 |
|---|---|---|---|---|---|---|---|---|---|---|---|
| Ba | 71 | 38 | 30 | 17 | 18 | 25 | 32 | 6 | 42 | 80 | 13 |
| Cr | 5 | 3 | 2 | 2 | 2 | 4 | 3 | 5 | 5 | 8 | 2 |
| Nb | 11 | 12 | 8 | 10 | 13 | 16 | 18 | 11 | 11 | 13 | 19 |
| Ni | 5 | 2 | 2 | 2 | 2 | 2 | 3 | 5 | 4 | 7 | 2 |
| Rb | 376 | 412 | 436 | 354 | 349 | 350 | 356 | 211 | 376 | 323 | 457 |
| Sr | 23 | 22 | 24 | 19 | 16 | 14 | 12 | 23 | 21 | 51 | 27 |
| V | 5 | 3 | 4 | 5 | 6 | 3 | 5 | 6 | 8 | 2 | 3 |
| Y | 39 | 46 | 59 | 56 | 95 | 25 | 37 | 34 | 33 | 43 | 38 |
| Zn | 29 | 29 | 10 | 31 | 25 | 28 | 31 | 31 | 28 | 36 | 20 |
| Zr | 39 | 36 | 29 | 31 | 48 | 26 | 33 | 34 | 28 | 39 | 40 |
| Sc | 6 | 3 | 3 | 5 | 10 | 1 | 3 | 4 | 1 | 3 | 1 |
| Rb / Sr | 16 | 19 | 18 | 19 | 22 | 25 | 30 | 9 | 18 | 6 | 17 |

**Rare Earth elements**

| | | | | | | | | | | | |
|---|---|---|---|---|---|---|---|---|---|---|---|
| La | 14.3 | 12.4 | 14.3 | 11.8 | 15.3 | 8.0 | 9.4 | 8.5 | 11.0 | 8.0 | 14.2 |
| Ce | 18.9 | 23.2 | 31.1 | 19.2 | 32.1 | 15.0 | 16.3 | 13.7 | 12.0 | 33.1 | 32.7 |
| Pr | 3.1 | 3.2 | 3.4 | 4.1 | 6.2 | 1.5 | 1.6 | 1.8 | 2.2 | 1.9 | 4.0 |
| Nd | 13.1 | 12.3 | 9.4 | 11.4 | 15.5 | 11.0 | 12.1 | 6.9 | 9.8 | 13.5 | 17 |
| Sm | 3.9 | 2.8 | 3.9 | 4.3 | 4.6 | 1.7 | 1.9 | 1.9 | 2.8 | 3.3 | 4.8 |
| Eu | 0.13 | 0.11 | 0.12 | 0.11 | 0.12 | 0.16 | 0.14 | 0.23 | 0.17 | 0.16 | 0.10 |
| Gd | 3.9 | 3.2 | 4.7 | 2.8 | 4.2 | 3.5 | 3.8 | 1.8 | 2.3 | 1.9 | 4.3 |
| Dy | 5.8 | 6.8 | 7.4 | 6.6 | 6 | 2.4 | 2.1 | 4.6 | 2.1 | 3.9 | 5.0 |
| Er | 5.1 | 4.90 | 5.5 | 5.2 | 5.4 | 1.8 | 1.6 | 3.8 | 2.10 | 4.5 | 2.9 |
| Yb | 5.4 | 5.8 | 5.9 | 6.2 | 6.4 | 4.2 | 3.4 | 4.2 | 1.6 | 4.2 | 4.1 |
| Lu | 0.68 | 0.86 | 0.84 | 0.56 | 0.3 | 0.23 | 0.2 | 0.34 | 0.16 | 0.37 | 0.60 |

**Table 7. 7. The trace and rare earth element chemical analyses of muscovite-schorl pegmatite sub-class of Shigar valley.**

**Trace elements**

| Sample # | 54 | 74 | 81 | 97 | 98 |
|---|---|---|---|---|---|
| Ba | 76 | 38 | 59 | 39 | 74 |
| Cr | 2 | 3 | 2 | 4 | 7 |
| Nb | 11 | 12 | 9 | 12 | 13 |
| Ni | 2 | 2 | 2 | 3 | 5 |
| Rb | 344 | 254 | 267 | 212 | 377 |
| Sr | 42 | 38 | 49 | 35 | 52 |
| V | 4 | 4 | 3 | 5 | 4 |
| Y | 40 | 35 | 33 | 29 | 39 |
| Zn | 20 | 19 | 43 | 38 | 27 |
| Zr | 21 | 26 | 39 | 58 | 48 |
| Sc | 3 | 2 | 2 | 3 | 1 |
| Rb / Sr | 8 | 7 | 5 | 6 | 7 |

**Rare Earth elements**

| | | | | | |
|---|---|---|---|---|---|
| La | 5.6 | 7.6 | 8.2 | 6.8 | 8.3 |
| Ce | 15.4 | 10.4 | 12.1 | 13.2 | 11.1 |
| Pr | 2.3 | 1.6 | 1.4 | 2.8 | 3.1 |
| Nd | 5.6 | 7.6 | 8.9 | 11.4 | 4.9 |
| Sm | 3.5 | 2.5 | 1.5 | 2.1 | 2.5 |
| Eu | 0.11 | 0.12 | 0.13 | 0.11 | 0.12 |
| Gd | 3.8 | 2.8 | 2.6 | 3.9 | 2.1 |
| Dy | 2.7 | 2.1 | 3.6 | 1.9 | 2.1 |
| Er | 1.01 | 1.1 | 0.98 | 0.67 | 1.6 |
| Yb | 2.3 | 1.7 | 1.9 | 2.7 | 1.6 |
| Lu | 0.32 | 0.12 | 0.25 | 0.23 | 0.29 |

**Table 7. 8. The trace and rare earth element chemical analyses of biotite ± garnet ± muscovite pegmatite sub-class of Shigar valley.**

**Trace elements**

| Sample # | 3A | 3 | 6 | 48 |
|---|---|---|---|---|
| Ba | 61 | 72 | 75 | 52 |
| Cr | 5 | 4 | 6 | 3 |
| Nb | 12 | 11 | 11 | 13 |
| Ni | 4 | 4 | 5 | 2 |
| Rb | 345 | 353 | 339 | 340 |
| Sr | 47 | 46 | 48 | 37 |
| V | 8 | 8 | 7 | 7 |
| Y | 31 | 34 | 33 | 37 |
| Zn | 25 | 27 | 25 | 32 |
| Zr | 19 | 20 | 22 | 25 |
| Sc | 4 | 4 | 3 | 3 |
| Rb / Sr | 7 | 8 | 7 | 9 |
| **Rare Earth elements** | | | | |
| La | 5.2 | 5.6 | 6.3 | 7.4 |
| Ce | 12.3 | 11.4 | 12.2 | 11.4 |
| Pr | 1.3 | 1.1 | 1.3 | 1.5 |
| Nd | 6.4 | 6.8 | 7.4 | 6.8 |
| Sm | 1.4 | 1.5 | 1.7 | 1.9 |
| Eu | 0.14 | 0.13 | 0.16 | 0.18 |
| Gd | 1.7 | 1.8 | 1.9 | 2.1 |
| Dy | 3.7 | 3.9 | 4.1 | 4.3 |
| Er | 3.2 | 3.1 | 3.7 | 3.9 |
| Yb | 3.1 | 3.4 | 3.8 | 4.1 |
| Lu | 0.34 | 0.48 | 0.51 | 0.34 |

**Table 7. 9. The trace and rare earth element chemical analyses of muscovite – biotite ± garnet pegmatite sub-class of Shigar valley.**

**Trace elements**

| Sample # | 1 | 5 | 7 | 21 | 38A | 38 | 41 |
|---|---|---|---|---|---|---|---|
| **Ba** | 94 | 77 | 86 | 126 | 76 | 89 | 92 |
| **Cr** | 5 | 5 | 3 | 5 | 6 | 4 | 5 |
| **Nb** | 14 | 14 | 11 | 9 | 11 | 15 | 12 |
| **Ni** | 4 | 3 | 2 | 3 | 5 | 2 | 4 |
| **Rb** | 312 | 203 | 334 | 451 | 367 | 354 | 367 |
| **Sr** | 54 | 59 | 39 | 49 | 52 | 41 | 45 |
| **V** | 3 | 5 | 2 | 1 | 2 | 5 | 6 |
| **Y** | 16 | 10 | 14 | 10 | 11 | 13 | 11 |
| **Zn** | 26 | 20 | 20 | 21 | 28 | 32 | 34 |
| **Zr** | 29 | 23 | 32 | 22 | 21 | 18 | 20 |
| **Sc** | 3 | 6 | 4 | 1 | 3 | 3 | 5 |
| **Rb / Sr** | 6 | 3 | 9 | 9 | 7 | 9 | 8 |

**Rare Earth elements**

| | | | | | | | |
|---|---|---|---|---|---|---|---|
| **La** | 11.6 | 13.1 | 12.3 | 10.9 | 12.0 | 8.6 | 12.6 |
| **Ce** | 18.2 | 24.6 | 28.1 | 16.3 | 19.4 | 17.4 | 21.4 |
| **Pr** | 3.1 | 2.7 | 4 | 2.5 | 2.5 | 1.8 | 2.9 |
| **Nd** | 9.5 | 10.8 | 12.5 | 10.4 | 14.2 | 8.2 | 12.8 |
| **Sm** | 3.1 | 3.4 | 3.6 | 2.8 | 2.8 | 2.4 | 3.7 |
| **Eu** | 0.23 | 0.31 | 0.21 | 0.05 | 0.12 | 0.18 | 0.14 |
| **Gd** | 1.8 | 2.3 | 2.8 | 2.7 | 1.7 | 3.3 | 3.8 |
| **Dy** | 4.8 | 5.4 | 4.9 | 2.8 | 4.3 | 5.8 | 4.9 |
| **Er** | 3.2 | 4.3 | 3.6 | 1.5 | 4.3 | 4.5 | 4.8 |
| **Yb** | 3.5 | 4.7 | 4.8 | 1.6 | 4.7 | 5.0 | 4.9 |
| **Lu** | 0.45 | 0.47 | 0.56 | 0.43 | 0.58 | 0.72 | 0.56 |

**Table 7. 10. The trace and rare earth element chemical analyses of the Indus-Gilgit Confluence and the Shengus pegmatites.**

**Trace elements**

| Sample # | 107 | 109A | 109 | 110A | 110 | 111 | 113 | 114A | 114 | 102SN | 103SN |
|---|---|---|---|---|---|---|---|---|---|---|---|
| Ba | 191 | 158 | 157 | 143 | 130 | 178 | 165 | 188 | 278 | 45 | 54 |
| Cr | 4 | 6 | 4 | 3 | 2 | 3 | 3 | 3 | 2 | 5 | 7 |
| Nb | 3 | 1 | 2 | 2 | 2 | 2 | 2 | 2 | 2 | 2 | 2 |
| Ni | 3 | 5 | 3 | 2 | 2 | 3 | 2 | 2 | 2 | 3 | 3 |
| Rb | 89 | 112 | 98 | 88 | 73 | 89 | 112 | 97 | 94 | 234 | 243 |
| Sr | 345 | 298 | 289 | 218 | 231 | 298 | 267 | 323 | 394 | 127 | 143 |
| V | 2 | 3 | 2 | 4 | 2 | 5 | 3 | 4 | 4 | 3 | 2 |
| Y | 6 | 8 | 7 | 4 | 7 | 6 | 4 | 6 | 5 | 8 | 6 |
| Zn | 23 | 21 | 13 | 19 | 23 | 21 | 18 | 12 | 10 | 10 | 9 |
| Zr | 45 | 43 | 39 | 36 | 39 | 43 | 58 | 49 | 94 | 10 | 10 |
| Sc | 2 | 2 | 2 | 1 | 2 | 1 | 1 | 1 | 2 | 1 | 1 |

**Rare Earth elements**

| | | | | | | | | | | | |
|---|---|---|---|---|---|---|---|---|---|---|---|
| La | 1.2 | 1.5 | 1.2 | 1.8 | 2.1 | 1.6 | 0.89 | 1.3 | 1.5 | 18.3 | 14.5 |
| Ce | 2.1 | 3.2 | 2.0 | 2.7 | 3.9 | 1.8 | 1.6 | 2.4 | 2.2 | 38.3 | 21.5 |
| Pr | 0.13 | 0.15 | 0.14 | 0.11 | 0.31 | 0.23 | 0.21 | 0.14 | 0.23 | 4.1 | 3.6 |
| Nd | 0.87 | 0.75 | 0.97 | 1.2 | 1.5 | 0.89 | 1.1 | 0.56 | 0.89 | 14.9 | 13.8 |
| Sm | 0.21 | 0.22 | 0.24 | 0.18 | 0.34 | 0.19 | 0.25 | 0.17 | 0.13 | 3.4 | 3.7 |
| Eu | 0.23 | 0.26 | 0.22 | 0.32 | 0.26 | 0.21 | 0.26 | 0.32 | 0.31 | 0.10 | 0.09 |
| Gd | 0.29 | 0.21 | 0.28 | 0.27 | 0.33 | 0.31 | 0.15 | 0.35 | 0.33 | 2.4 | 3.5 |
| Dy | 0.31 | 0.28 | 0.30 | 0.29 | 0.24 | 0.32 | 0.19 | 0.23 | 0.38 | 3.9 | 4.5 |
| Er | 0.25 | 0.21 | 0.25 | 0.22 | 0.14 | 0.18 | 0.15 | 0.21 | 0.28 | 3.9 | 3.8 |
| Yb | 0.21 | 0.22 | 0.27 | 0.31 | 0.16 | 0.19 | 0.22 | 0.19 | 0.37 | 4.3 | 3.9 |
| Lu | 0.04 | 0.02 | 0.05 | 0.03 | 0.03 | 0.3 | 0.02 | 0.05 | 0.07 | 0.45 | 0.34 |

# Chapter 8

## DISCUSSION

In case of pegmatite evolution, there are various theories such that the pegmatites may be the last product of primary granitic magmas by the processes of differentiation and fractional crystallization or they may also be formed by direct anataxis or partial melting of metasedimentary rocks, mostly in the metamorphic terrains. In the vicinity of the Shigar valley, there are various plutons such as the Baltoro plutonic unit, Mango Gusar pluton and the Chinkang La pluton (Searle et al., 1989; Searle, 1991; Fraser et al., 2001). The most extensive of these plutons, particularly the Baltoro pluton unit in the vicinity of the Shigar valley is suggesting that these may probably have certain correlations with pegmatites of the Shigar valley. Therefore, the Shigar valley pegmatites may be genetically very close to the Baltoro plutonic unit in the central Karakoram but the occurrence of tourmaline as ubiquitous phase in the muscovite-tourmaline-beryl-garnet sub-class of the Shigar valley pegmatites is suggesting that these may have been formed by a separate pulse of magma by the direct anatexis of a metasedimentary protolith. However, according to Searle (1991) tourmaline is absent in the leucogranites and the monzogranites of the Baltoro plutonic unit. So at this stage it could be said that the Shigar valley pegmatites are either the off shoots of the Baltoro plutonic unit (BPU) resulted due to fractional crystallization or these may be the separate magmatic pulses formed by the partial melting of a metasedimentary protolith due to crustal thickening and thrusting after the collision of Indian and Eurasian plates. Searle (1991) has shown that the Precambrian-Palaeozoic crust is the source rock for the BPU but on the basis of similar isotopic characteristics he suggested that there is a possibility of the high-grade metamorphic rocks in the lower crust of the Karakoram Metamorphic Complex. In addition to this, on the basis of lead isotope signatures Scharer et al. (1986) and Searle (1991) have described that the BPU has a strong affinity to the South Tibetan crust.

As Searle (1989 and1991) has described numerous leucogranite dykes emerging at the margin of BPU along the course of upper Braldu river and on the basis of

geochronological data these dykes are contemporaneous with the emplacement age of BPU (Parrish and Tirrul, 1989). It is, therefore, probable that the process of differentiation/fractionation continued after the formation of these leucogranite dykes and as a result the remaining magma became more saturated in fluids, volatiles, and incompatible elements. It resulted in the formation of the more differentiated and more evolved Shigar valley pegmatites. It is because of this that as the process of differentiation and fractional crystallization continues and the remaining melt become enriched in incompatible elements, volatiles and fluids. The presence of tourmaline in the Shigar valley pegmatites suggests a separate source as well as the magma rather being the more evolved phases of the BPU. From the occurrence point of view, it is generally observed that the leucogranites and pegmatites are more commonly formed in the continental collisional tectonic settings due to the crustal thickening, thrusting and as a result of partial melting of the metasediments (Nabelek and Liu, 2004). As the process of subduction has been closed after the collision of Indo-Pakistan plate with the Eurasia around some ~ 50 Ma and as a result of this collision, the magmatism that occurred all along the entire length of Himalayas is the result of crustal thrusting and thickening rather than the subduction related magmatism. So, it is suggested that all the leucogranite bodies from NW Himalayas in Pakistan up to eastern Himalayas in Nepal are collisional instead of subduction-related magmatism (Also see Searle, 1991; Kazmi and Jan, 1997; Le Fort et al., 1987; Zeitler and Chamberlain, 1991). Following this collision of Indian and Eurasian plates (ca. 50 Ma) the processes of crustal thickening, thrusting, and denudation have occurred all along the entire length of the High Himalaya and is still continue and in the result several leucogranites and pegmatites have been formed due to the partial melting of the metasediments (Searle, 1991; Le Fort et al., 1987). So, it is more appropriate to discuss the origin of these High Himalayan leucogranites in the regional scenario to put some light and constrain the petrogenesis and evolution of the leucogranites in general and the Shigar valley pegmatites in particular. It is because of this that the evolution of the Shigar valley pegmatites is of similar nature as the other High Himalayan leucogranites. Like the Shigar valley pegmatites, the tourmaline is also the ubiquitous mineral of the High Himalayan leucogranites. Before discussing the

leucogranites of the High Himalaya, a brief description for the generation of the leucogranites is also given below.

## Leucogranites

The leucogranites including pegmatites are most commonly regarded as the products of collisional orogenies. They are found in orogenic terranes from Proterozoic such as the Trans - Hudson orogen as exemplified in the Black Hills, South Dakota, and the Appalachian orogen in Maine, USA to the ongoing Himalayan orogeny. Characteristics of these collisional leucogranites show that they were derived from predominantly pelitic sources at the veining stages of deformation and metamorphism in upper parts of thickened crusts. Once generated, the leucogranite magmas ascended as dykes and were emplaced within shallower parts of their source sequences. In these orogenic belts, there was strong connection between deformation, metamorphism and granite generation. However, the heat sources needed for partial melting of the source rocks remain controversial. Lack of evidence for significant intrusion of mafic magmas necessary to cause melting of upper plate source rocks suggests that leucogranite generation in collisional orogens is mainly a crustal process (See also Le Fort, 1981; Le Fort et al., 1987; Strong and Hanmer, 1981; Nabelek and Liu, 2004).

Various models have been proposed for the generation of leucogranites in collisional belts (Le Fort, 1981; Strong and Hanmer, 1981; Nabelek and Liu, 2004). The most suitable models capable of raising the crustal temperatures sufficiently to initiate partial melting of metapelites in thickened crust are: 1) thick sequences of sedimentary rocks with high amounts of internal radioactive heat production, 2) decompression melting, 3) thinning of mantle lithosphere and 4) shear-heating. According to Nabelek and Liu, (2004), the shear-heating model is very suitable for the generation of leucogranites and they have described that for reasonable boundary conditions, shear-heating along crustal-scale shear zones is the most possible process to induce melting in upper plates of collisional orogens, where pelitic source lithologies are usually present.

The shear-heating model directly links partial melting to the deformation and metamorphism that typically precede leucogranite generation.

Whilst the Himalayas provide an example of recent leucogranite petrogenesis, extensive leucogranites also occur in ancient collisional belts, including the 270 - 400 Ma leucogranites of Maine, USA, which were generated during the Appalachian orogeny (Tomascak et al., 1996; Pressley and Brown, 1999) and the leucogranites of the Black Hills, South Dakota, USA, which are the products of melting in the southern part of the Trans-Hudson orogen (Redden et al., 1990; Nabelek et al., 1992a; Nabelek and Bartlett, 1998). The chemistry, mineralogy, character of occurrence and differentiation, and the relationships to the host rocks of these leucogranites bear many similarities to the Himalayan leucogranites. The Shigar valley pegmatites particularly have many similarities to the Black Hills, South Dakota pegmatite field. The continental collision and the crustal thrusting and thickening are the most suitable mechanisms for the crustal melting and the formation of leucogranites in the collisional tectonic settings. The classic model for leucogranite formation in collisional belts is that on the Manaslu pluton in the High Himalaya (Le Fort et al., 1975; 1981; 1987). As already discussed, the leucogranites may be the last product of a more basic magma in the calc-alkaline plutonism but the mineralogy of the Shigar valley pegmatites suggests that these pegmatites do not belong to the calc-alkaline magmatism and are post-collisional and have been formed by direct anatexis due to crustal thrusting and thickening.

## Himalayan leucogranites

The leucogranites are very important rock suits and mostly occur in many metamorphic terrains of collisional tectonic settings. The mechanisms of leucogranite emplacement can provide important information about tectonics and the metamorphic processes occurring during an orogeny. In case of High Himalaya, the leucogranites are exposed throughout the length of orogenic belt, mostly concentrate along the hanging wall of Main Central Thrust (MCT) or its structural analogs in the form of small plutons or dike swarms (Le Fort et al., (1975; 1981; 1987; Zeitler and Chamberlain, 1991).

Moreover, the postcollisional leucogranites and pegmatites do also occur in the Trans-Himalayan region such as the leucogranites and pegmatites of the Garam Chasma area, Chitral (Zafar et al., 2000). It is clear from the mineralogy and isotopic compositions of the Himalayan leucogranites that these have been derived from near-minimum melts of crustal rocks in which there was significant water activity. Although, the leucogranites are present along the entire length of the High Himalaya but most of the studies have been carried out only along the central portion of this orogeny (Scharer, 1984; Le Fort et al., 1987; Searle and Rex, 1989). The U-Pb zircon radiometric dating of these leucogranites ranges from 9 to 25 Ma, which indicates that these leucogranites have been emplaced after the Indian-Eurasian collision.

## The models and causes for the generation of the Himalayan leucogranites

The Himalayan Mountains are the best examples of the collisional tectonics, where the orogeny is still ongoing and the uplift of Nanga Parbat Haramosh Massif (NPHM) is the best example. Various workers have studied the Tertiary leucogranites of the High Himalayas and in the result different models and mechanisms have been proposed for the generation of these collisional Himalayan leucogranites. In this regard four models have been proposed. In these, Le Fort (1981), Le Fort, et al. (1987), Guillot and Le Fort (1995) have proposed that the Himalayan leucogranites have been generated by fluxing of hot hanging wall material due to the escape of volatiles from the dehydrating footwall of major crustal-scale fault complexes such as the Main Central Thrust, while Zeitler and Chamberlain (1991), Harris and Massey (1994) are in the favor of decompression melting. According to Huerta et al. (1998) and Jamieson et al. (1998), the deep accretion of rocks with high concentration of radioactive isotopes may be the melting mechanism for the generation of the High Himalayan leucogranites. Zhu and Shi (1990), Harrison et al. (1998) have proposed that the deformation-induced heating along the shear zones is the most suitable mechanism for the generation of Himalayan leucogranites.

## Classification of the Himalayan leucogranites

Crawford (1988) did work on leucogranites in the Hunza valley section and has proposed two types of leucogranites for the High Himalayas and the Karakoram regions. The two types are:

1) Type - a: Syn-tectonic crustal melts (Manaslu type): these are partial melts of a minimum melt composition
2) Type - b: Post-tectonic crustal melts (Baltoro type): such type of melts originates at the base of the crust, where the temperature has been elevated by crustal thickening and also by mantle promoting large-scale dehydration melting.

Tourmaline is the most common mineral in type - a leucogranites reflects higher concentrations of boron in the source, suggesting a metapelitic protolith. Tourmaline was also found in the type - b leucogranites but in small quantities as reported from some pegmatites in the Hunza area by Crawford (1988). The formation of tourmaline in such a fashion is due to the fractionation and the concentration of boron in the residual magma. In such conditions, the source of boron may be the small quantities of tourmaline in the source, or the contamination of magma by metapelitic country rocks as it rose through the crust. Crawford (1988) also differentiated the type - a leucogranites formed by the early crystallization of mica with high magmatic water content from the type - b leucogranites that are the last phases to crystallize. Crawford, (1988) also distinguishes these two leucogranite types on the basis of isotope systems. The type- b leucogranites of the Karakoram Axial batholith have low initial Sr ratios (0.71 to 0.72), while the High Himalayan type- a leucogranites have high values of Sr ranging from 0.74 to 0.82. These isotopic values along with many other characteristics are mainly dependant on the source. Therefore, the source with low Rb / Sr ratios could be fluxed by fluids to give type - a leucogranites with low Sr isotope values. The source characteristics may also be deduced from the Sumayar and Manaslu and Britanny leucogranites (Crawford, 1988). Though, the leucogranites of these plutons have been formed by the similar mechanisms of crustal anatexis due to fluid fluxing and regional metamorphism, but they have different strontium (Sr) isotope values because of different source materials. The Sumayar and the

Manaslu leucogranites have high initial Sr isotope values (0.74 to 0.78) due to metapelites being the source material (Le Fort et al., 1987), whilst the Britanny leucogranites have much lower values (0.708 to 0.71) due to a different source material (Strong and Hanmer, 1981). All these post-collisional leucogranites like the Shigar valley pegmatites show a peraluminous character, suggesting a metasedimentary protolith being the source material for melting.

## Comparison of the Shigar valley pegmatites with other post-collisional leucogranites and pegmatites of the Karakoram Axial batholith

As for as the pegmatite petrogenesis is concerned, it is generally accepted that the pegmatites are formed in the last stages from a silicic granitic magma rich in volatiles and fluids through the process of fractionation and these are commonly rich in those mineral phases and elements, which are incompatible in the initial stages of crystallization (Jahns, 1955; Černý, 1982a, b). Therefore, majority of the pegmatites hold valuable rare metals and a variety of gemstones. In addition, the leucogranites and pegmatites may occur in separate magmatic pulses in the form of sheets and dykes without being the off shoots of any parent plutonic unit. The High Himalayan leucogranites and pegmatites are considered to be of the same type. In order to know the possible genesis of the Shigar valley pegmatites, it is imperative to consider and correlate the nearby plutonic units of the Shigar valley pegmatites to see whether these are the off shoots of these plutons or the separate magmatic pulses generated by batch melting.

As in the central Karakoram Range (Fig. 2. 1), the post-collisional leucogranites and pegmatites are mainly exposed in the Hunza valley section, Baltoro Plutonic Unit, Masherbrum Migmatite Complex and in the Shigar valley area. Besides, the post-collisional leucogranites and pegmatites are also reported from the Garam Chasma in the Hindu Kush (Trans-Himalayas) region. The pegmatites of the Hunza valley section, Garam Chasma and Shigar valley areas are generally gem-bearing (but not all), while the

pegmatites of the Baltoro Plutonic Unit are gem-barren and the pegmatites of the Masherbrum Migmatite Complex are not yet studied in detail.

To know about any possible genetic linkage between the Shigar valley pegmatites and the nearby plutonic units, it is probable that the Shigar valley pegmatites may be the possible off shoots or satellites of either the Baltoro Plutonic Unit (BPU) or Mango Gusar Pluton (MGP), which are present to the northeast of the Shigar valley (Fig. 2. 2). In the following sections, the Shigar valley pegmatites are compared with the Baltoro Plutonic Unit (BPU) and Mango Gusar Pluton (MGP) to know the possible genetic relationship, if any, between them. In addition to this, the Shigar valley pegmatites are also compared with the other post-collisional granitoid rocks of the Hunza valley (Karakoram Mountains) to know the genetic relationships and similarities in a regional context.

**Baltoro Plutonic Unit: the possible parent magma of the Shigar valley pegmatites?**

Unlike the Manaslu leucogranites, which are purely crustal derived (Le Fort et al., 1987), the Baltoro Plutonic Unit leucogranites are formed through fractional crystallization after the formation of monzogranites, where the primary magma have been generated at the lower crust, where it may have been contaminated by some input of upper mantle (Searle, 1991; Crawford, 1988; Fraser et al., 2001). The Baltoro monzogranites have been formed after the dehydration melting under water-undersaturated conditions at the base of the crust, contaminated by an input from the mantle. Similarly, the leucogranite dykes of Baltoro Plutonic Unit (BPU) are correlated with the Baltoro monzogranites, which show that these leucogranites are not the separate magmatic pulses but have been formed by the process of fractional crystallization after the formation of Baltoro Plutonic Unit monzogranites (Crawford, 1988; Searle, 1991; and Searle et al., 1992) (Fig. 8.1). The monzogranites of the Baltoro Plutonic Unit (BPU) are deficient in the $SiO_2$ and enriched in $TiO_2$ and $Fe_2O_3$ contents, while the leucogranites are enriched in the $SiO_2$ and depleted in $TiO_2$ and $Fe_2O_3$ relative to the monzogranites.

This enrichment of $TiO_2$ and $Fe_2O_3$ in the monzogranites may be due to the relative abundance of biotite.

On the basis of present study, the Shigar valley pegmatites are grouped in four sub-classes on the basis of field features, mineralogy and petrographic studies but the trace and rare earth element patterns of these sub-classes are generally similar with minor differences. In this regard, various studies have shown that the evolution of pegmatites is either local or regional and the pegmatite bodies may be the off shoots of any nearby pluton or may be the separate magmatic pulses in the metamorphic terranes (Ćerný, 1982a, b; Nabelek and Liu, 2004). So the principles and models of regional zonation, differentiation and the evolution of the most-evolved pegmatites could be used for the Shigar valley pegmatites to relate them with the Baltoro Plutonic Unit, if these are the off shoots of BPU. Various studies on the evolution of granitic pegmatites have shown that the process of fractionation and zonation starts from the crystallization of normal granite in situ up to the most evolved rare-element pegmatites distal to their parent plutons (Jahns, 1953; Ćerný, 1982a, b). Besides this, various studies have also proved that the most distal pegmatite bodies are most-evolved in the sense of occurrence of rare-metals, while the pegmatites nearest to their parent are less-evolved (Mulja et al., 1995). The mode of occurrence, internal evolution, zonation, textures, and mineral assemblages of the Shigar valley pegmatites is somewhat problematic to relate them with the Baltoro Plutonic Unit because instead of rare-metal class these belong to the miarolitic pegmatite class. Although it is possible that some of the Shigar valley pegmatites such as the muscovite-tourmaline-beryl-garnet sub-class may belong to the BPU and is the last fractionated and most-evolved phase rich in volatiles such as the B, F, $H_2O$ and rare-elements (e.g., Be). But the simultaneously presence of other pegmatite sub-classes such as the biotite ± garnet ± muscovite sub-class, muscovite-biotite ± garnet pegmatite sub-class in the Shigar valley area creates some ambiguities. However, the local processes of fractional crystallization and differentiation may not be rejected to produce such types of pegmatites at one place either from the same magma or due to the batch melting of the similar source rock. In addition, most of the models for the generation of granitic pegmatites have revealed that the maximum distance of most-evolved pegmatite from its

parent pluton is approximately 10 -15 km (Baker, 1998). But the Shigar valley pegmatites are about 30 km away from the Baltoro Plutonic Unit (Fig. 2. 2). Therefore, the correlation of the Shigar valley pegmatites with the Baltoro Plutonic Unit may not be justified. However, there is a possibility that some of the pegmatites of the Shigar valley area may belong to the Baltoro Plutonic Unit. It is therefore suggested that the BPU leucogranites may have formed after the crystallization of the monzogranites of the BPU (Fig. 8.1). It is also possible that the process of differentiation and saturation of fluids and volatiles continued till the formation of Shigar valley pegmatites. But the major element characteristics of the Shigar valley pegmatites show that the process of differentiation has occurred on local scale within the Shigar valley pegmatites, resulted in the formation of the four groups of the pegmatites. But in terms of trace and rare earth elements modeling, the leucogranites of the BPU and the Shigar valley pegmatites show similar characteristics and patterns (Figs. 8. 2, 8. 3, and 8. 4), indicating a similar source rock for these. The REE patterns of the BPU, especially the monzogranites (Fig. 8. 4) show relatively enrichment in the LREE, which indicates the precipitation of small amounts of monazite because the La and Ce are present in significant quantities in its structures.

The Shigar valley pegmatites are unmetamorphosed and have intrusive contact with the Dassu orthogneiss, which is the host rock of most of these pegmatites. No geochronological data is present for the Shigar valley pegmatites; however, the dates on the host rock are available. The rocks of southern margin of the Asian plate (Karakoram Metamorphic Complex) record the four stages of metamorphism and deformation that have also been dated (Searle, et al., 1989; Searle 1991; Fraser et al., 2001). The last stage of this metamorphism and deformation is recorded on the Dassu orthogneiss (the host rock of the Shigar valley pegmatites). Searle, et al., (1989) and Searle (1991) have suggested that the last (M4) metamorphism has occurred up to sillimanite grade due to the emplacement of Dassu domal structure and they have determined the K-Ar biotite ages for the Dassu orthogneiss as 7.1 ± 0.3 and 4.7 ± 0.2 Ma, whereas, on the basis of U-Pb Fraser et al. (2001) have reported the metamorphic age of 5.4 ± 0.2 Ma for the Dassu orthogneiss. As the Shigar valley pegmatites have no metamorphic imprints, therefore, these are at least younger than metamorphic ages of the Dassu orthogneisses, which are

the host rock of the Shigar valley pegmatites. Therefore, the age relationship of the Shigar valley pegmatites is not favouring their direct correlation with the Baltoro Plutonic Unit as the age of emplacement of this unit has been reported as ca. 21- 26 Ma (Searle et al., 1989; Searle, 1991 and Fraser et al., 2001).

**Comparison of the Shigar valley pegmatites with the Hunza valley Post-collisional leucogranites**

In the Hunza valley section of the Karakoram Mountain Range, the plutons both of the pre-collision and post-collision are exposed, which indicates multiphase magmatism and hence, the name Hunza Plutonic Complex (HPC) has been used for these magmatic bodies by Crawford (1988). The pre-collisional magmatism is mainly in the form of granodiorite, while the monzogranite to leucogranite dykes along with the Sumayar pluton are the examples of post-collisional leucogranites. Crawford (1988) divided the Hunza dykes into two sets: as dykes of set -1 and set - 2. He considered these sets of dykes as post-collisional but Fraser et al. (2001) on the basis of U-Pb geochronological data (50-52 Ma) put the dykes of set- 1 in the pre-collisional granitoids, while the dykes of set -2 as post-collisional. Crawford, (1988) considered these two sets of dykes in the Hunza valley as equivalent of the Baltoro Plutonic Unit to the east but according to Fraser et al. (2001), the dykes of set - 1 are older than the Baltoro Plutonic Unit. However, the source rock of the monzogranites of both the Baltoro Plutonic Unit and Hunza Plutonic Complex is the same because both are formed by the lower crustal melts contaminated by mantle input (Crawford, 1988; Crawford and Windley, 1990; Searle, 1991). The Hunza post-collisional leucogranites have also been studied and classified into three lithologic groups (Crawford, 1988; Crawford and Windley, 1990; Crawford and Searle, 1993). The group one is comprised of large aplite sheets, which intruded the Hunza Plutonic Complex (HPC), the second group is mostly composed of monzogranite and pegmatitic leucogranite dykes and these also intrude the Hunza Plutonic Complex and the sillimanite grade country rocks to the south. The third group called Sumayar Pluton is the youngest phase of magmatic activity, exposed to the south of Hunza Plutonic Complex.

On the basis of petrogenesis, Crawford (1988) has broadly divided the post-collisional leucogranites of the Karakoram Axial batholith into two types. One of these belongs to the Manaslu-type leucogranites (Sumayar Pluton), which are mainly derived from a metasedimentary crustal component, while the other type derived from a metasedimentary protolith and contaminated by some mantle inputs is known as Baltoro-type leucogranite (Searle, et al., 1989; Searle, 1991; Searle et al., 1992; Fraser et al., 2001). According to Crawford, (1988) the post-collisional leucogranites of both of the above-mentioned types are present in the Hunza valley section of the Karakoram Axial Batholith. Among the above-mentioned three lithological groups of leucogranites, the first two groups of leucogranites belong to the Baltoro-type leucogranites, while the third type belongs to the Manaslu-type leucogranites of the High Himalayas (Crawford, 1988).

In case of the Shigar valley area, although the trace and REE characteristics of all the studied pegmatites are almost similar with some minor differences (Figs. 7. 11 and12) but on the basis of mineralogy, petrographic studies and partly on major element characteristics (Fig. 7. 3), the Shigar valley pegmatites are classified into four sub-classes. However, the trace and rare earth elements of these pegmatites show similar patterns, which indicate that genetically all the classified groups are comagmatic and derived from the same source rock. However, the relative enrichment and depletion of the constituent minerals, is mainly due to the local differentiation processes, which may have occurred during the emplacement of these pegmatites. But the process of batch melting can not be ignored. When the Shigar valley pegmatites were compared with the post-collisional Hunza valley granitic rocks in terms of their major, trace, and rare earth elements, they show many similarities (Figs. 8. 1, 8. 7, and 8. 8). As proposed by Crawford, (1988), Searle, (1991), Searle et al., (1992) and Fraser et al., (2001), the post-collisional leucogranites of both the Hunza valley and the Baltoro Plutonic Unit have been formed after the crystallization of biotite-rich monzogranites by a local process of fractional crystallization. Therefore, it is possible that similar fractionation processes may have occurred locally within the Shigar valley pegmatites at the time of their emplacement, which may resulted in such types of pegmatite formation. In the field no

cross cutting relationships between the proposed types or sub-classes of pegmatites are noted in the Shigar valley area, as described by Crawford, (1988) and Searle et al., (1992) in the Hunza valley section, where the dykes of set - 2 generally cross cut the dykes of set-1. Therefore, the Shigar valley pegmatites are discussed in the context of above-mentioned two types (i.e., Manaslu-type and Baltoro-type). The biotite along with traces of garnet is the only main accessory mineral of the biotite ± garnet ± muscovite sub-class of pegmatites in the Shigar valley area, therefore, it is probable that like the leucogranites of Hunza valley section and Baltoro Plutonic Unit which fractionated after the formation of monzogranites. The other three types of pegmatites in the Shigar valley area may have been formed through fractional crystallization after the formation of biotite ± garnet ± muscovite sub-class of pegmatites from the same melt because the trace and rare earth elements pattern of these pegmatites depict a similar pattern, indicating to be comagmatic (Figs. 7. 11 and 12). It is probable that the more fractionated muscovite-tourmaline-beryl-garnet type of Shigar valley pegmatites is the last product of this local fractional crystallization process. The fluids and other volatile materials have been concentrated in the residual melt and finally the crystallization of tourmaline, beryl, garnet, topaz, and other phases have occurred in the zoned and more fractionated sub-class of these pegmatites.

Among the Hunza post-collisional leucogranites, the Sumayar pluton which is ~ 4 km wide homogenous magmatic body with sharp intrusive contacts to the host garnet-staurolite schists and is considered to be the youngest magmatic activity in the Hunza valley area. This post-collisional magmatic plutonic body is similar not only in mineralogy but also in the major as well as the trace and REE characteristics to the Shigar valley pegmatites (Figs. 8. 5 and 8. 6). Like, the tourmaline-beryl-muscovite-garnet sub-class of pegmatites of the Shigar valley this leucogranite body also contains abundant tourmaline, garnet, and muscovite as the main accessory phases. Both the Shigar valley pegmatites and the Sumayar pluton are very similar to the High Himalayan Manaslu-type leucogranites. According to Fraser et al., (2001), the dykes of gem-bearing pegmatites around the Nagar and parts of the Haramosh region may be the off shoots or satellites of this youngest magmatic phase but they do also not reject the possibility that these gem-

bearing pegmatites may even be younger than the Sumayar pluton of the Hunza valley section. The Sumayar pluton is dated by U-Pb zircon and monazite techniques as 9.3 ± 0.1 Ma by Fraser et al. (2001). In this way, as the Shigar valley pegmatites are genetically very close to the Manaslu-type leucogranites of the High Himalayas as well as to the Sumayar pluton of the Hunza valley area and on the basis of (M4) metamorphism that occurred in the host rocks of the Shigar valley pegmatites. It is suggested that the Shigar valley pegmatites may be the time equivalent of the Sumayar pluton. Moreover, on the basis of Sr (0.8118) and Nd (0.51146) isotopic compositions Crawford, (1988) compared the Sumayar leucogranites with the High Himalayan Manaslu-type leucogranites and described a metapelitic source for these leucogranites. In this way, as the trace element spider diagrams, the rare earth element patterns (Figs. 8. 5 and 8. 6), and the high Rb / Sr ratio and the boron (B) content of both the Shigar valley pegmatites and the Sumayar leucogranites are very identical, therefore, it can be suggested that the source rock for the Shigar valley pegmatites may be the same as that of the Sumayar leucogranites. However, it is clear from the REEs patterns (Fig. 8. 6) that the Shigar valley pegmatites almost exhibit a smooth pattern from the LREE to HREE, while the Sumayar pluton is significantly poor in the HREEs.

## Classification of the Shigar valley pegmatites

Genetically, the pegmatites have been classified on various parameters such as the depth of consolidation or emplacement, the type of mineralization, relation to the igneous processes and the metamorphic environment, in which they are frequently found (Ginsburg et al. 1979; Ćerný, 1982a, b). In addition to the above-mentioned criteria of classification, the pegmatites have also been classified as gabbroic pegmatites, syenite pegmatite, and granitic pegmatite depending on the major mineral constituents and geochemistry. The major element geochemistry as well as the essential and the accessory mineral assemblages of the three studied pegmatite fields (i.e., Shigar valley, Shengus, and Indus Confluence-Gilgit Confluence pegmatites) indicates that these are granitic in composition. So for this reason, the pegmatites of these three fields are granitic-pegmatites. The granitic pegmatites are further subdivided into various types or subtypes or sub-classes (such as petalite-quartz subtype, spodumene-quartz subtype, lithium-cesium-tantalum subtype, beryl-subtype) depending on the presence of accessory minerals and metals (Ćerný, 1991a, b). All the above-mentioned subtypes of granitic pegmatites almost maintain the granite composition because the accessory components are mostly restricted to a fraction of a percent (Stewart 1963; 1978; London and Burt 1982; Ćerný, 1982a, b). There are two schools of thought regarding the origin of granitic-pegmatites. First, the granitic pegmatites are the result of supercritical fluids, hydrothermal solutions and / or aqueous vapor phase in the absence of a melt and the second is volatile rich melt (Ćerný, 1982a, b). Majority of the petrologist (e.g., Bakumenko, 1968; Bazarov and Motorina 1969; Zakharchenko, 1976; Roedder, 1979) supports the second opinion. Besides, there are two other points of view, regarding the origin of pegmatites, i.e., igneous versus. metamorphic. Majority of petrologist support the igneous genesis, while some are of opinion that the pegmatites are the direct product of anataxis. This mode of origin may probably be applied to the mica-bearing pegmatites (Sokolov et al., 1975). This concept can also be applied to the rare-element-bearing pegmatites, where they acquire rare-element accumulation from the source lithologies (Norton, 1973; Stewart, 1978). However, Ćerný (1982a, b) supported the geological classification of pegmatites given by Ginsburg et al. (1979).

The pegmatites of the Shigar valley probably fall in the miarolitic pegmatite sub-class of Ginsburg et al., (1979). This classification is based on the depth of emplacement and metamorphic environment in which the pegmatites are presently exposed, and this classification is known as the geological classification of pegmatites. The granitic-pegmatites of the Shigar valley are mostly miarolitic in character rather than the rare-element class because the rare-element-bearing minerals, if present, are very few. The field and the petrographic studies indicate that no mineral containing rare-elements such as Li, Nb, Ta, Sn W, etc was found from these pegmatites, but only Be is present in the differnt types of beryl, e.g., aquamarine, goshenite etc. The present studies indicate that the Shigar valley pegmatites are of miarolitic pegmatite class (because of the presence of miarolitic cavities or vugs) and not to the rare element pegmatite class according to the classification scheme of Ginsburg et al. (1979). But if igneous versus metamorphic origin of classification is considered then majority of Shigar valley pegmatites on the basis of their mica and tourmaline contents are considered to be of metamorphic origin and could be the product of direct anatexis rather than the product of the fractional crystallization of near by plutonic body. However, an igneous origin for these pegmatites can not be ruled out.

Various studies have been carried out on pegmatites regarding to their internal evolution, causes of zonation, relationship to their parental granitoids, the type of the host rock and formation of pockets or cavities where enormous euhedral gemstones are formed. However, there are very few studies to constrain the source rock of these pegmatites (Ćerný, 1982a, b; Ćerný, 1991a, b; Ginsburg et al. 1979; Norton, 1973; Stewart, 1978). For the classification of pegmatites, the above-mentioned parameters are most commonly used but most of the authors believed on the relative proportions of the diverse minerals that are present in the pegmatites. They proposed various classification schemes based on the presence or absence or relative proportion of the mineral phases present in the pegmatites. It has also been proved that the pegmatites present in the same pegmatitic field may be belonged to various classification schemes. Genetically they are similar but differences are only due to their internal evolution.

Fersman (1930) proposed ten types of granitic pegmatites on the basis of mineralogy in correspondence with seven genetic phases as: epimagamtic (700/ 800°C), pegmatitic (700/600°C), pegmatoid (600/500°C), hypercritic (500/400°C), high hydrothermal (400/300°C), medium hydrothermal (300/200°C), and low hydrothermal (200/100°C). This classification has strongly influenced the work of many later petrologists. After Fersman (1930), Cameron et al. (1949) established a sequence of mineralogical assemblages that reflects in a general way, the entire course of genetic process of pegmatite evolution. This classification scheme has been very useful in describing the zoning and paragenesis of individual pegmatites or groups of pegmatites belonging to the same genetic type. Furthermore, Solodov (1959) classified the rare metal-bearing granitic-pegmatites into four types based on the relative abundance of microcline, albite, and spodumene. This classification is fundamentally descriptive and does not consider the characteristics and relative abundance of the various phases of the genetic process (e.g., primary crystallization, replacement, etc). In this context, the classification of Ginsburg, (1960) is of great importance. He has grouped the pegmatites in three types that differ in mineralogy, structure, age and specific geochemical characteristics such as trace element content and mode of replacement. Although, this scheme of classification is mainly descriptive but also considers factors such as depth, age, type and composition of the associated intrusives, which vary considerably in different parts of the world.

The genetic classification given by Brotzen, (1959) for granitic pegmatites, is of great importance and is also being used nowadays. This scheme distinguishes four main stages within a continuous genetic process, each represented by a pegmatite type of characteristic mineralization, which is more or less regularly distributed in the zonal sequence. The paragenetic units proposed by Brotzen (1959) are: (1) granitoid zone (border), (2) graphic zone, (3) pegmatoid zone, (4) core-margin zone, (5) alkali replacements, (6) core margin mica and (7) alteration products.

The classifications of pegmatites are somewhat different from the other rock suits. As genetically similar pegmatites of a pluton have also been classified in various

types or subtypes depending on the regional zonation, internal structure, mineral assemblages and the occurrence of rare metals. For example, the pegmatites of the Black Hills, South Dakota, which are genetically similar but on the basis of above-mentioned criteria have been classified in various types. Besides, the processes for the formation of the genetically similar pegmatites may be different by which these types have been formed.

It is not necessary that only the zoned pegmatites belong to the rare element pegmatite class and will be economically important, but certain unzoned and massive pegmatites may also hold rare minerals as is the case of Black Hills, South Dakota (London, 1986). Although, the rare element and miarolitic pegmatites are the two separate pegmatite classes that hold both the gems and the rare minerals and are, therefore, known as gem-bearing miarolitic rare-element pegmatites such as the Tanco, Manitoba; Harding, New Mexico, San Diego County, California (Foord et al., 1986; Webber et al., 1999). In this context, the Shigar valley pegmatites generally hold gemstones in the cavities and vugs and no distinct rare metal-bearing phases have been identified in these pegmatites. Therefore, these are only gem-bearing miarolitic pegmatites, rather rare element pegmatites. The Little Three pegmatite-aplite layered intrusive, Ramona, California is an example of miarolitic pegmatite having tourmaline and topaz (Stern et al., 1986) and therefore, is comparable to the Shigar valley pegmatites. As no rare metal except the Be-bearing phase (beryl and its varieties) has been found in the Shigar valley pegmatites and these are mostly gem-bearing which are present in cavities and vugs, therefore, it is appropriate to classify the Shigar valley pegmatites as of miarolitic class instead of rare metal class of pegmatites.

## Causes of zonation and Shigar valley pegmatites

Various genetic models and mechanisms have been proposed for the zonation and internal evolution of the pegmatites (Staatz et al., 1955; Norton et al., 1962; Jahns and Burnham 1969; Stewart, 1978; Jahns, 1982; Norton, 1983). It is generally accepted that the crystallization sequence in the zoned pegmatites generally starts from the outer border zone and continue towards the inner core zone. It is also accepted that the aqueous fluid phase is mostly associated with the silicate pegmatitic melts. In case of pegmatites, the zonation is being described by two ways: one is the regional zonation and the other is the local internal zonation of the pegmatite body itself. The regional zonation starts from the parent rock and continue to the last crystallized phases of pegmatite that are intruded in the country rock. According to Trueman and Ćerný (1982) and Mulja et al. (1996) as the distance increases, the pegmatites will be more fractionated. It means that the farthest pegmatites from their parental rock will be more fractionated than those which are nearer to their parent rock. For example, Mulja et al., (1996) have described the zoned pegmatites of the Preissac-Lacorne batholith, Quebec, Canada in three assemblages, the least fractionated beryl type is found in the parental pluton through a transitional spodumene + beryl type at the edge of the plutons to a most fractionated spodumene type pegmatites in the country rocks. In this regard they have also mentioned that the beryl type pegmatites, which are emplaced in their parental pluton are least evolved, while the spodumene type which are emplaced some 2-3 km away from their parental pluton in the country rock are the most evolved. Such a regional zonation as an essential feature of the evolutionary model proposed for rare-element granitic pegmatites, is seldom encountered but is of great importance for the evolution of more-evolved and differentiated pegmatites.

In this context of regional zonation as described above, if we consider that the Shigar valley pegmatites are the most evolved and fractionated part of the Baltoro Plutonic Unit then it is probable that fractionation may have started from the monzogranites through leucogranites up to the formation of Shigar valley pegmatites. But

the geochronology of the Baltoro Plutonic Unit and the host rocks of the Shigar valley pegmatites does not allow to associate the pegmatites of the Shigar valley with the Baltoro Plutonic Unit because the Baltoro Plutonic Unit has been assigned an age of ~ 25 Ma (Searle, 1991), while the host rock of the Shigar valley pegmatites shows very youngest ages (~ 7 - 4 Ma) of metamorphism.

Various workers (Trueman and Černý, 1982; Mulja et al., 1996; Foord et al., 1986; Webber et al., 1999; Černý, 1982a, b; Černý, 1991a, b; Ginsburg et al. 1979; Jahns, 1953) have described in detail the formation of internal zonation in various types of pegmatites. According to them, the crystallization starts from the border zone towards the core zone and the proportion of the exsolved aqueous fluids increases inward. As a result, these fluids continuously concentrate in the remaining melts and take part in the last stages of crystallization in the form of late stage fracture-filling minerals, where all the incompatible elements take part in the crystallization and form the most important economic minerals and gemstones in the cavities or vugs. Sometimes, this internal fracturing stage is so intensive that the country rocks are also affected. Therefore, sometimes minerals of economic importance are also found in the fractures of the country rocks near the contact with pegmatite because the fluids as well as the incompatible elements of the interior zone migrate through these fractures. At the time of emplacement, the pegmatitic melts are not saturated in water and fluids but they become saturated at some point during their crystallization in order to form miarolitic cavities London et al. (1988) and London, (1990). The internal zonation and differentiation of pegmatitic magma takes place in a fashion similar to the process of differentiation commence from the basic towards acidic part. These conclusions have been supported by various studies based on radiogenic and stable isotope and trace element measurements (Taylor and Friedrichsen, 1983a; Černý et al., 1984).

Among the various sub-classes of the Shigar valley pegmatites, the muscovite-tourmaline-beryl-garnet pegmatite sub-class is symmetrically zoned having three or four zones, but at places, asymmetrical zones of this sub-class are also found at different localities of the Shigar valley. The zoning is gradational in almost all the dykes but in

some cases the intermediate zone pinches out in the wall zone and it is very difficult to differentiate between the wall and the intermediate zones. The border zone is mostly fine to medium-grained and is mainly composed of albite with accessory garnet and muscovite. In some of the symmetrically zoned dykes, the border zone is composed of cm-sized line-rock of garnet and muscovite along with albite. Texturally, the wall zone and the different types of the intermediate zone of the zoned pegmatites are coarse-grained and the grade of coarseness increases towards the center. In addition, the fracture-filling patterns are well developed in this sub-class of pegmatites at the localities of Dassu, Goyungo, Kashmol, and Yuno. Besides, the vugs and cavities are present near the core-margin zone, where gemstones usually occur. All the field observations and features suggest that the crystallization has started from the border zone towards the core zone. These features are very similar to the standard models proposed for the internal evolution of the world famous zoned pegmatites (Trueman and Černý, 1982; Mulja et al., 1996; Webber et al., 1999; Černý, 1982a, b; Černý, 1991a, b; Ginsburg et al. 1979; Jahns, 1953; Baker, 1998). The other three sub-classes of the Shigar valley pegmatites are unzoned, simple in their mineralogy and internal structure and are, therefore, classified as simple pegmatites.

The zoned miarolitic pegmatites of the Shigar valley have enormous similarities with the world-famous pegmatites. Like the San Diego County, California, pegmatites, (Webber, et al., 1999), some of the symmetrically zoned pegmatites of the Shigar valley (e.g., the Dassu and Kashmol pegmatites) have a fine-grained aplitic border zone, which shows a faster cooling, nucleation, and crystal growth. The intimately association of fine-grained aplites and coarse-grained pegmatites with large crystals is still debatable. The border-zoned aplites are sometimes layered but some of the dykes without aplitic layering are also noticed in the Shigar valley pegmatites. The alternative rhythmic layering in the aplitic zone is mostly of albite and garnet. The presence of garnet either in the border zone or in the wall zone is also favoring the crystallization from border zone towards the core zone. The changes in the grain sizes of the constituents of the different zones indicate that the crystallization parameters such as the nucleation and growth rates are not consistent during the crystallization history of these pegmatites. The behavior of

undercooling, volatiles and fluids is very critical to the development of textural features that characterize pegmatite dykes. Such types of zonations and textural features are also reportd by Webber, et al. (1999) from the Himalaya mine, George Ashley pegmatite, and Mission dykes from the Pala pegmatite district and the Mesa Grande Pegmatite Districts of the San Diego County, California. Some of the dykes at Dassu, Yuno, and Kashmol indicate asymmetrical zoning behaviour with a typically fine-grained footwall and coarse-grained hanging wall with a core zone having miarolitic cavities, which are generally holding gemstones.

The complex, zoned and simple pegmatites may occur and form simultaneously at one pegmatite field. A same pegmatite at the same time may be complex at its one end and simple towards the other side such as the Morefield pegmatite of Virginia, USA (Smerekaniez and Dudas, 1999). Although, mineralogically, the zoned pegmatites of the Shigar valley area are different from the Morefield pegmatite but in terms of internal structure and zonation both of these are identical and share many characteristics. Both of these have four zones (i.e., border zone, wall zone, intermediate zone, and the core zone). The border zone is very thin, discontinous, and somewhere it is even completely absent in the zoned pegmatites and the wall zone is in direct contact with the host rock. Therefore, instead of four zones, three zones are noticed at certain places in the Shigar valley pegmatites, especially at Dassu. Besides this, the Morefield pegmatite have very complex mineralogy from common minerals to rare minerals and metals to gemstones but the Shigar valley pegmatites are generally gem-bearing and have very minute amount of rare minerals and metals such as columbite-tantalite, cassiterite, lepidolite, microlite, etc.

The mineralogy and chemistry of the host rocks of pegmatites also play an important role in the evolution of pegmatites and several metasomatic mineral assemblages have been formed either at the margin of the pegmatite and its host rock or even distal to pegmatite within the country rock (Morgan and London, 1987). The host rock of the Shigar valley pegmatites is mainly Dassu orthogneiss but some of the dykes intrude the Palaeozoic metasediments of the Daltumbore formation. The contacts of the pegmatites with their host rocks are very sharp but in some of the zoned pegmatites, the

presence of tourmaline at the contact zone may show some metasomatic effects in the host orthogneiss. In some of the dykes (e.g., Dassu and Goyungo, Yuno) tourmaline is found at the contacts of pegmatites and their host rocks (Fig. 6. 9). So, it is possible that the tourmaline has been formed due to the interaction of boron from the pegmatitic melt with the Fe and Mg of the host rocks, as the host rocks are rich in biotite. Such types of observations were also noted at the Himalaya and George Ashley Block pegmatite (GAB) dike system (Foord et al., 1986; Kleck, and Foord, 1999), where the host rock is gabbroic in composition. The presence of tourmaline in such zoned pegmatite dykes indicates that the crystallization has been started from the footwall to the hanging wall of the dike and as the crystallization continue the concentration of volatiles (B, $H_2O$, F, Cl) become enriched inward and ultimately crystallized the tourmaline at the border zone by excavating Fe and Mg from its host rock (i.e., biotite orthogneiss). In addition to this, the presence of fluorite in the wall zone near the tourmaline crystals also supports the idea that the sequence of crystallization starts from footwall to hanging wall. In the internal zonation and crystallization sequence, the majority of the Shigar valley pegmatites are very identical to the GAB pegmatites. Both are symmetrically zoned but some variations do occur.

Not only the complex pegmatites are zoned but sometimes the simple pegmatites are also zoned (Norton and Redden, 1990). However, the simple pegmatites of the Shigar valley area are not zoned. The simple and zoned pegmatites may occur in one and same pegmatite field as is the case of Black Hills, South Dakota, pegmatites (Krogstad et al., 1991; Norton and Redden, 1990). Similarly, both the simple as well as the zoned pegmatites are also present in the Shigar valley area but the number of zoned and gem-bearing pegmatites is very limited as compared to the simple pegmatites. The zonation of the Shigar valley pegmatites indicates that due to the differentiation of the magma not only four sub-classes of pegmatites are formed but the process of differentiation has also produced the zonation along with other factors and processes.

It is generally supposed that the zoned pegmatites have always a quartz core zone but this supposition is not always true because in the pegmatites of the Black Hills, South

Dakota, only 20 % of the zoned pegmatites have quartz in the core zone (Norton and Redden, 1990). As such, the majority of the Shigar valley zoned pegmatites are also without the quartz-rich core zone. But some of the dykes (e.g., Dassu pegmatites) are mostly composed of central quartz zone with a very thin border or wall zone composed of albite, K-feldspar and quartz.

Like the Little Three aplite-pegmatite (Stern et al., 1986), some of the Shigar valley pegmatites are also asymmetrically zoned with a fine-grained aplite in the footwall and the coarse-grained pegmatite in the hanging wall. Furthermore, the Shigar valley pegmatites have also vertical contrast in texture, composition, and zoning patterns. The centrally located "pockets" host a giant-textured suite of granitic mineral assemblages as well as some unusual accessory minerals. The Shigar valley pegmatites are also following the similar distribution patterns of Na and K and zonation from border to intermediate and to core zones as that of the Little Three main pegmatites of Stern et al., (1986). It is observed that the wall zone of the Shigar valley pegmatites is rich in Na and poor in K, while the coarse-grained intermediate zone is K-rich and depleted in Na (Fig. 8. 10). The vertical zonation within the Shigar valley pegmatites is also from border to wall zone to intermediate and up to core zone. Besides, the aplitic border zone in some of the Shigar valley pegmatites is also massive like that of the Little Three main pegmatites, while in others it is layered. Moreover, some of the dykes are without the aplitic border zone. In the granitic pegmatites, the lithium minerals occur as lithium aluminosilicates. London (1986) has reported that these are formed at the last stages of pegmatite evolution and mostly associated with other pocket minerals. But the field observations and the petrographic studies show that no such type of Li-mineralization has been observed in the pegmatites from the Shigar valley area.

## Trace element fractionation

As already discussed, the crystallization sequence in the Shigar valley zoned pegmatites is generally from margin towards core. The trace element data, especially the Rb and Sr, also support this crystallization sequence. Though, the Rb and Sr are the good discriminant parameters to deduce the crystallization sequence of the zoned pegmatites (Černý, 1982a, b, c; Černý et al., 1985) but sometimes it became very difficult to know about the crystallization sequence, because in certain cases, the post crystallization processes of pegmatites such as the fracture-filling stage and the hydrothermal effect may produce ambiguities (Černý et al., 1985). This is the reason that at the last stage of crystallization of the pegmatite, the fracture-filling process may alter the previously crystallized assemblages and also their chemistry due to the mobility of certain elements. In such cases, it is very difficult to know the order of crystallization sequence in the zoned pegmatites. But, if the fracture-filling and hydrothermal stages are of minimal level then the Sr and Rb are good discriminant and may be used to understand the crystallization sequence (Černý et al., 1985). Therefore, if the above-mentioned processes are intensive, then sampling should be done from the less affected parts of the zoned pegmatites to find out the order of crystallization. This relationship can easily be achieved, if the minerals collected from the different zones are analysed for their trace elements. However, the whole rock chemistry of various zones may also play an important role in determining the sequence of crystallization. In the case of Shigar valley pegmatites, the whole rock geochemistry of various zones is used to understand the mode of crystallization within these pegmatites. In the Dassu area of Shigar valley, a complex zoned pegmatite is exposed and samples are collected from its different zones (sample No. 22C, 23, 26 from the wall zone and sample No. 19, 22B, 28 from the intermediate zone) to check the crystallization sequence within this pegmatite. The whole rock trace element data of these samples indicate that the samples taken from the wall zone are relatively depleted in Rb and enriched in Sr, while those taken from the intermediate zone show inverse behaviour of these elements (Fig. 8. 9). This behaviour of Rb and Sr in the wall and intermediate zones can be attributed to the relative high concentration of alkali-feldspar and plagioclase in the intermediate and wall zones respectively. So this mode of

fractionation of Rb and Sr indicates that the crystallization sequence starts from margin to core and such type of crystallization sequence and zonation has also been reported from the Tin Mountain pegmatite, Black Hills, South Dakota by Walker et al. (1986), although lithium mineralization has also been documented from Tin Mountain pegmatite. In addition to this, such type of differentiation of Rb and Sr from wall zone to core zone is also described by Shmakin (1979) and Ćerný et al., (1984).

## Petrogenesis of Shigar valley pegmatites

The various studies carried out so for on the petrogenesis of pegmatites are mostly confined to their internal evolution, causes of zonation, relationships to their parental granitoids, the host rock where pegmatite bodies have been intruded, exsolution of fluids, formation of pockets or cavities, where enormous euhedral gemstones are formed (London, 1986a, b), but few studies are carried out on the source lithologies of the pegmatites (Nabelek and Bartlett., 1998; Nabelek and Liu., 2004). On the basis of accessory minerals and zonation, the Shigar valley pegmatites are classified into four sub-classes and belong to the miarolitic class of pegmatites. The mineral chemistry, whole rock chemistry, petrography, classification and internal evolution of the Shigar valley pegmatites have already been discussed. Here, the possible petrogenetic evolution of the Shigar valley pegmatites in relation to the world-famous granitic pegmatites is described in the light of field features, mineral chemistry, petrographic studies, and whole rock geochemistry. Besides, the possible linkages between the granites and their associated pegmatites, stages of the evolution of fluids and volatiles, formation of cavities, types of mineralization and the composition of the source rock are also discussed.

The experimental studies have contributed a lot to understand the pegmatites and their petrogenesis. In this regard the basic work was provided by (Jahns and Burnham, 1969; Burnham and Jahns, 1961; Luth et al., 1964; Roering, 1966). Most petrologists are

agreed that the aqueous-fluid phase plays an important role in the generation of the pegmatites. The experimental work in the case of compositionally simple systems (silica-$H_2O$, albite-$H_2O$, haplogranite-$H_2O$) have led the petrologists to propose that pegmatitic aqueous fluids possess relatively low solute concentrations (Stewart, 1978; Roedder, 1981; Jahns, 1982). The rare-element bearing pegmatites contain minerals rich in Li, B, F. Addition of these hyperfusible components (possibly Be, Rb, Cs, P) to the granitic systems, alters partitioning coefficients for major and minor elements, lowers solidus and liquidus temperatures, and generally increases the silicate liquid-$H_2O$ miscibility (Wyllie and Tuttle, 1964; Koster and Wyllie, 1968; Chorlton and Martin, 1978; Manning, 1981; Benard et al., 1985). Several studies of fluid inclusions in pegmatite minerals already have presented empirical evidence for the existence of dense aqueous fluids or brines that contain up to 85 wt% dissolved silicate and salt components (London, 1986). These aqueous fluids in rare element pegmatites may have solute concentrations (especially with regard to aluminosilicates components) that are far greater than those generated in the simple silicate-$H_2O$ experiments on which existing pegmatite models are based (Norton, 1983). The most valuable means of tracing the evolution of pegmatitic fluids is through examination of the fluid inclusions that are abundant in pegmatite minerals.

It is generally accepted that the pegmatites originate through the crystallization of residual magmatic fluids (Herrera, 1968). The zonal sequence described in the previous sections would represent the general trend of evolution of the fluids. This process, although essentially continuous, does not proceed uniformly but rather continue by a succession of compositional steps. This may be the reason that the minerals like tourmaline, fluorite and topaz are found in the wall and the intermediate zones of the Shigar valley pegmatites. Crystal-melt fractionation seems to be the leading factor in the geochemical development from the parental granites to the highly differentiated pegmatites (London, et al., 1988; Černý, 1991a, b). In most areas, where several types of pegmatite are presumably associated with the intrusive body, a distinct zonal distribution related to the igneous body is mostly observed. As sodium or lithium rich bodies are nearly always peripheral, potassium-rich bodies are intermediate, while microcline-oligoclase bodies are closest to the intrusive (Herrera, 1968). In this way if the Shigar

valley pegmatites are considered as the off shoots of the Baltoro Plutonic Unit then these would have been more differentiated and fractionated. As already discussed, the possibility of associating the Shigar valley pegmatites with this pluton is minimum and further investigations are needed in this regard.

The granitic pegmatites belonging to different pegmatite fields of the world, have different characteristics but the pegmatites of a similar type or class share many characteristics. The models proposed for the granitic pegmatites of one pegmatite field can also be applied to other pegmatite fields (Baker, 1998; Černý, 1991a, b). In this regard, the Shigar valley pegmatites are correlated with the world-known granitic pegmatites to understand the petrogenesis of these pegmatites. In this context, the Shigar valley pegmatites share many characteristics with the San Diego, California pegmatites (e.g., internal zonation, lithologies, occurrence of gemstones etc). On the basis of fluid inclusion and various isotopic studies, Taylor et al. (1979), Jolliff et al. (1986), Foord, (1976) and Foord et al. (1986) have deduced the conditions of formation of the best-known gem-bearing pegmatites (the Himalaya Mine, the Tourmaline Queen, and the Stewart dike) of the San Diego, California. They also concluded that the pegmatitic magmas have been emplaced at temperatures of 700 - 730°C, with the formation of pockets/cavities at subsolidus conditions in the range of 525 - 565°C. They have also estimated the pressure as 2.1 - 2.2 kbars at the time of crystallization. Though the temperature and pressure estimates are not available for the Shigar valley pegmatites but on the basis of many similarities of the Shigar valley pegmatites with the gem-bearing pegmatites of San Diego, California, these conditions of emplacement of the pegmatites and the formation of miarolitic cavities/pockets can also be suitably applied for the Shigar valley pegmatites.

Miarolitic cavities/pockets provide incontrovertible evidence for the exsolution of comparatively low-density aqueous fluids from the silicate melt during the late stage of the pegmatite genesis (London, 1986a, b). Crystal-lined cavities such as those cited by Jahns (1982) are generally primary in nature. Gemstones like beryl, topaz, fluorite, and tourmaline are usually present in the pockets or cavities within the Shigar valley

pegmatites. These gemstones are formed at the last stages of pegmatite consolidation and the exsolution of the fluid phase from the aluminosilicates, indicate that the aqueous fluids were rich in B, F and Be. But some of the euhedral to subhedral crystals of the tourmaline and beryl are also found in the intermediate or even at the border zone, which suggest that the process of exsolution of fluids was not only occurred at the late stages but it started from the early stages and became more intensive during the last stages of the evolution of these pegmatites. As a result, the cavities or pockets developed in the core-margin zone. Besides, it is also notable that the tourmaline and beryl found either in the wall zone or the intermediate zone, are not as attractive in their size and color as those occurring in the core-margin zone.

Like the San Diego, California pegmatites, majority of the granitic pegmatites of the Afghanistan and Hindu Kush Range are also belong to the miarolitic and rare-element class of pegmatites (Rossoversuskii, 1981; London, 1986a, b). London (1986a, b) on the basis of experimental work and fluid inclusion studies on the pegmatites of Kulam, Afghanistan and San Diego, California has shown that both the miarolitic and massive rare-element pegmatites crystallize under similar pressure-temperature conditions. According to him, the magmatic-hydrothermal transition in miarolitic pegmatites occurs in the approximate ranges of 425 - 475°C and 2.4 - 2.8 kbars. He also suggested that in the miarolitic rare-element pegmatites, crystallization of tourmaline does not occur until the late stages of pegmatite consolidation. Crystallization of tourmaline consumes the alkali borate-fluxing component, which results in the deposition of other alkali aluminosilicates and oxide minerals and the consequent exsolution of large amounts of water. The deposition of tourmaline contributes directly to the pocket/cavity formation by promoting the exsolution of an aqueous fluid phase. As the Shigar valley pegmatites are comparable to the miarolitic pegmatites of the San Diego, California in several aspects but certain minor differences also exist. The pockets or cavities of gemstones are surrounded by various clay and carbonate minerals in the pegmatites of the San Diego, California (Foord, et al., 1986). They have related the zeolite-clay-carbonate pocket-filling assemblage with the host norite and the pocket minerals were deposited under moderate to low-temperature hydrothermal conditions after the crystallization of the

primary pocket minerals. By correlating the pockets/cavities assemblage of Shigar valley pegmatites with that of the pegmatites of San Diego, California, it is observed that both have different pocket mineral assemblages. In Shigar valley pegmatites the pocket mineral assemblages are mostly albite, orthoclase and muscovite, while those of San Diego pegmatites contain clay and carbonates. It can be assumed here that due to alteration and weathering with the passage of time the pocket mineral assemblages of the Shigar valley pegmatites may attain the same mineral assemblages (clay and carbonates) as that of the pegmatites of San Diego, California. As such, both types of the pegmatites may have similar phenomenon for the formation of their mineral assemblages in the pockets/cavities.

Most of the pegmatites are associated to their parent rocks as being their off shoots; for example the pegmatites of North Pilbara Craton, Australia (Sweetapple and Collins, 2002), Sierras Pampeanas pegmatites, Northwest Argentina (Morteani et al., 1995) and the pegmatites of Black Hills, South Dakota (Shearer et al., 1992), but the separate pegmatite bodies without a parent plutonic rock may also occur either in the intermediate or high grade metamorphic rocks, and known as metamorphic pegmatites (Cerny, 1982a, b; 1991a). It does not mean that these pegmatites are metamorphosed but only because of their presence in the metamorphic rocks, other wise these are of igneous origin but are not related to any parent plutonic body and are formed by separate magmatic pulses in the continental collisional tectonic settings due to crustal thickening. As the composition of the pegmatites is mainly dependant on the composition of the initial magma or their parental magma (Herrera, 1968), but there is significant difference between the Shigar valley pegmatites and the possible plutonic body Baltoro Plutonic Unit (BPU), which suggests that the Baltoro Plutonic Unit is not the possible source of the Shigar valley pegmatites. It is probable that the Shigar valley pegmatites are separate magmatic pulses rather than being the off shoots of any nearby plutonic body. The predominance of more or less "pure" types in most pegmatite districts of the world, however, indicates that there is an intimate relationship between the chemical differentiation and tectonic conditions. According to Herrera, (1968) most granite magmas are capable to produce a series of pegmatite types during their final phase of

crystallization. Whether part or all of the members of the series formed will be depend mostly on the tectonic conditions acting during the pegmatogenic period, rather than on initial chemical composition.

The processes of formation of pegmatites are so diverse that even the pegmatitic bodies of the same pegmatite field show considerable differences in their internal zonation and mineralogy, especially the accessory and pocket mineralogy. Not only this, but the same pegmatite body may even display variations along its every dimension. It is very clear from the Little Three pegmatites of Stern et al. (1986) that the pegmatites of similar asymmetrical zoning and composition have different pocket/cavity mineralogy. This suggests an independent mode of formation of cavities and the behaviour and exsolution of fluids. In this respect it is noted that the main Little Three pegmatite dike and the other associated pegmatite dykes of this area (e.g., Hercules - Spessartine "ledge", the Sinkankas dike, and the Hatfield Creek dike) have also variable pocket mineralogy. The variability of this kind of accessory and pocket mineralogy is also observed in the different pegmatite bodies of the Shigar valley area. It shows that to some extent very similar processes of exsolution of fluids and the formation of cavities may have occurred in same way as are described for the Little Three pegmatites. Though the pegmatites of the Little Three area show considerable similarities with the Shigar valley pegmatites but certain differences are noted in these fields. The Shigar valley pegmatites are devoid of columbite-tantalite minerals while the Little Three pegmatites show columbite-tantalite mineralogy along with microlite. Moreover, the Shigar valley pegmatites have produced enormous quantities of beryl but the Little Three pegmatites are not as rich in beryl as the Shigar valley pegmatites. The Shigar valley pegmatites have also produced fluorite, apatite, while these are not reported from the Little Three area. Rest of the minerals such as the tourmaline, topaz, garnet, and muscovite are common in the pegmatites of these localities. In this way, the pegmatites of the Little Three area are of dual nature as they belong to the miarolitic class as well as the rare-element pegmatitic class and are highly fractionated (Stern et al., 1986). The Shigar valley pegmatites are just miarolitic contaning only gemstones and are not fractionated for the rare-metals, as the Little Three pegmatites. The Shigar valley pegmatites are also comparable with the

pegmatites of the North Pilbara Craton, Western Australia (Sweetapple and Collins, 2002). The North Pilbara Craton, Western Australia is a pegmatite province where several pegmatite fields and groups of pegmatites with variable mineralogy are present. Although majority of the pegmatites in the North Pilbara Craton, Western Australia belongs to the rare metal class of pegmatites (Sweetapple and Collins, 2002), where world's major tantalum, cassiterite and other rare metals deposits are present but some of these pegmatites are of gem-bearing miarolitic pegmatite class. This indicates that the rare-element class and the miarolitic classes of pegmatites do occur at the same pegmatite field.

Pegmatites associated with granitic plutons typically display regional zonation from less-evolved compositions near the parental pluton to more evolved (rich in F , B , Li , Cs , Rb, P) compositions away from the parental plutons (Cameron et al., 1949; Heinrich, 1953; Černý 1982a, b). The plutons are commonly assumed to be parental to the pegmatites, however, the low temperatures (450 - 700°C) and high viscosities of pegmatite-forming melts make their extraction very difficult, if not impossible, from a granitic pluton near its solidus (Shaw, 1972; London, 1992; 1996). While describing the petrogenetic links between the granites and the pegmatites of the Black Hills, South Dakota; Shearer et al. (1992) have discussed that a fractionation trajectory from biotite granites to tourmaline granites does not represent an evolutionary path of a single magma, but most likely represents paths of fractional crystallization of similar batches of magma. Therefore, it is probable that the Shigar valley pegmatites have been formed from a separate batch of magma rather than being the product of fractional crystallization of the Baltoro Plutonic Unit in regional zonation context.

The whole rock compositions of zoned pegmatites of the Shigar valley area indicate that the samples taken from the wall zone, mostly composed of albite and quartz are relatively depleted in $K_2O$ and Rb, while the samples taken from the intermediate zone, composed of alkali feldspar and muscovite are enriched in $K_2O$ and Rb (Fig. 8. 11). This indicates that the crystallization sequence is from border to core zone. Similar observations are also documented by Shearer et al. (1992) for the pegmatites of the Black

Hills, South Dakota. Like the pegmatites of the Black Hills, South Dakota, the parent pluton (Harney Peak Granite) of these pegmatites also exhibits some mineralogical zonation. The southeastern part is tourmaline-rich granite, while the northwestern part is biotite granite. However, there is controversy over such type of zonation. Some of the authors (e.g., Nabelek et al. 1992a, b; Krogstad et al., 1991) favored a magma of two distinct batches, while Shearer et al. (1992) on the basis of field features, mineralogical and geochemical data suggested that the tourmaline-bearing granites have been formed through fractional crystallization and both of the types belong to one similar magma. Thus, it is possible that the Shigar valley pegmatites may be formed after the Baltoro Plutonic Unit monzogranites through fractional crystallization in the similar fashion as that of the tourmaline-rich granites after the formation of biotite-rich granites of the Harney Peak Granite of the Black Hills, South Dakota. It is also possible that the process of fractional crystallization may has occurred locally due to which the proposed types of pegmatites have been generated from a similar magma other than the BPU monzogranites. Although majority of the pegmatites of the Black Hills, South Dakota pegmatite field belongs to the rare element pegmatite class but some barren pegmatites are also exposed in this pegmatite field (Shearer et al., 1992). Therefore, it also certifies the simultaneous presence of both the gem-bearing and gem-barren pegmatites exposed in the Shigar valley area. Like the Harney Peak Granite of Black Hills, South Dakota, where the tourmaline-bearing granites are later in crystallization sequence than the biotite granites (Shearer et al., 1992). Similarly, the biotite ± garnet ± muscovite pegmatites sub-class of Shigar valley pegmatites may have formed earlier to the muscovite-schorl-beryl-garnet sub-class of pegmatites, which is the most evolved and differentiated sub-class of these pegmatites.

The Ba versus Rb plot shows that the Shigar valley pegmatites of the biotite ± garnet ± muscovite sub-class (probably fractionated earlier) have relatively higher concentrations of Ba and low concentrations of Rb, while the pegmatites of muscovite-schorl-beryl-garnet sub-class (later formed) are rich in Rb and poor in Ba (Fig. 8. 12). Such type of behaviour was also described by Shearer et al., (1992) from the pegmatites and granites of the Black Hills, South Dakota. It is evident from the Ba-Rb plot (Fig. 8.

12) that the Rb-enriched pegmatites are commonly biotite-bearing at high concentrations of Ba and the tourmaline-bearing at low concentrations of Ba. The presence of tourmaline itself indicates that the Shigar valley pegmatites are not highly enriched in Rb and Li. Because according to Shearer et al. (1992), the tourmaline is either absent or rare in those pegmatites which are enriched in Rb and Li. The Shigar valley pegmatites are intermediate in Rb and very poor in their Li-contents because no lithium-bearing minerals have been found in these pegmatites. The field as well as the chemical data indicates that the zoned pegmatites of the Shigar valley are tourmaline-bearing pegmatites.

Aplites are most commonly associated with the pegmatites and are generally present at the border zone but in some of the pegmatites these are also noticed in the core zone as is the case of Stak Nala pegmatites, northern Pakistan (Laurs et al., 1998). Aplites are also found in some of the zoned dykes of the Shigar valley pegmatites, where they are generally present near the border zone. There may be other reasons for the intimate association of applies and pegmatites, but the one most commonly quoted is that during the intrusion of the pegmatites some fractures are produced in their host rocks and some of the fluids are lost in these fractures and as a result fine textured minerals are developed due to rapid cooling at the border zone (Herrera, 1968). The pegmatitic fluids in the last stages of pegmatite evolution also react with the minerals present along these fractures and as a result metasomatic mineral assemblages developed along and in the contact of pegmatite and host rock (Shearer et al., 1984).

**Li-bearing source rock and the Shigar valley pegmatites**

The composition of magma is certainly dependant on the composition of its source rock. Apart from this, the prevailing temperature and pressure conditions are also play an important role. The same source rock may generate various batches of magma at different pressures and temperatures (Nabelek and Liu, 2004). It is possible that the metasomatically enriched metasedimentary rocks could be a protolith for some of the alkali-enriched magmas. Stewart (1978) and Shearer et al., (1987) reported that the melting of metasedimentary protoliths enriched in rare alkalis (Li, Rb, Cs) could potentially produce Li - and Rb-enriched granitic melts. Shearer et al. (1992) have described various mechanisms for the generation of magma of Harney Peak Granite and the associated pegmatites from a sedimentary protolith. Direct partial melting of the metasedimentary rocks through metasomatism and varying degrees of partial melting are the main mechanisms for the generation of magma of the Harney Peak Granite and the associated pegmatites (Shearer et al., 1992; Sirbescu and Nabelek, 2003a; Krogstad et al., 1991; Shearer and Papike, 1987).

The Shigar valley pegmatites are very poor in their Li-contents because no proper lithium-bearing mineral are found from these pegmatites and even the concentration of Li in either micas or feldspar is very low. It shows that the source rock of the Shigar valley pegmatites was poor in rare alkalis, particularly Li and Cs. Besides the lithium minerals, no cesium-rich mineral is found from these pegmatites. But only in some of the beryls from the Dassu zoned pegmatites, Cs is present up to 1 wt. %, and, therefore, these beryls may be called as cesium-rich beryls. If a magma is enriched in Li, this may be revealed by the presence of Li-enrichment in micas as well as the lithium-bearing minerals as is suggested by Kosals and Mazuror (1968) and Kozlov (1969). In addition, like the other volatiles or fluxing agents (e.g., $H_2O$, F, and B), Li is also accumulated in the residual melt (Wyllie and Tuttle, 1964; London, 1983) and will crystallize during the last stages, when the cavities or pockets are formed. This is the reason that most of the lithium-enriched minerals are commonly associated with the pocket minerals. If the lithium concentrations are high enough, then the proper lithium minerals (e.g., lepidolite,

zinnwaldite, spodumene etc) are formed, but if the Li concentrations are low, then the Li will be incorporated in the muscovite called as lithian muscovite (Stewart, 1963; 1978; Bazarov and Motorina, 1969; Gallagher, 1975; Laurs et al., 1998). Solodov (1971) documented that 5,000 ppm Li (1.01 wt. % $Li_2O$) is the minimal concentration required for precipitating Li- rich minerals in granitic pegmatites. In this way, the whole rock geochemical data of the Shigar valley pegmatites indicate that there are no chances of accommodating $Li_2O$ in such high amount, because the total sum of other oxides is already 100 %. In addition, the above threshold value is close to the lower limit of the bulk compositions of homogeneous spodumene and petalite-rich pegmatites, and of spodumene and petalite- rich inner zones of texturally heterogeneous zoned pegmatite bodies (1.0 - 1.2 wt. % $Li_2O$ (Stewart, 1978). As the Shigar valley pegmatites are mainly miarolitic gem- bearing class, therefore, the chances of lithium mineralization are very low.

In addition, the lithium aluminosilicates and phosphates are subordinate or entirely absent, where the higher activities of F and $H^+$ commonly lead to the precipitation of topaz, fluorite and microlite as suggested by Ćerný, (1985) and London, (1982). This is also the reason that the Shigar valley pegmatites contain topaz, tourmaline, fluorite, and beryl instead of any proper lithium rich mineral. But it is not a restrict rule, the miarolitic gem-bearing class of pegmatites may also hold lithium-mineralization as is evident from the miarolitic gem-bearing pegmatites: for example, the Afghanistan and Hindu Kush (Rossoversuskii, 1981), San Diego County, California (Jahns, 1969) and Minas Gerais, Brazil (Cassedanne and Cassedanne, 1981). In these pegmatites the lithium aluminosilicates minerals such as the spodumene is associated with quartz, albite, and also with other pocket constituents (London, 1986). As discussed, the Shigar valley pegmatites belong to the miarolitic gem-bearing class of pegmatites, and no lithium mineralization observed during the field as well as in the petrographic studies, which indicates that the source rock was deficient in rare alkalis particularly lithium.

Linnen (1998) has suggested that the Ta-mineralization is commonly associated with those granites and pegmatites that are invariably rich in lithium. As the Shigar valley pegmatites contain no obvious tantalum-mineralization, which further confirm that these pegmatites are poorer in their Li-contents.

**Mechanics of pegmatite intrusion**

The position, shape, orientation, and to some extent the size of pegmatite bodies are controlled by a complex interplay among pegmatite fluid pressures, rheologic state of the host rocks, lithostatic and directed stresses, pore-water pressures, strength and ductility anisotropies and dilational directions (Brisbin, 1986).

As commonly, the granitic pegmatites are related to the nearby plutonic bodies and various models have been proposed in this context. In this connection, Baker (1998) has proposed a model for the propagation of pegmatite bodies in the country rock and discussed the mechanism and extent to which the pegmatitic bodies may propagate to the country rock. According to him if a parent pluton is small in size, the pegmatite dykes will propagate to small distances, but in case of large plutons, the pegmatite dykes will cover maximum distance even several kilometers in the country rocks. According to his model, the pegmatites can rarely extend more than 10 km from their host or parental pluton. He further added that the more-evolved pegmatites can extend for greater distances from their host pluton as compared to the less-evolved pegmatites.

In the dike-propagation model of the Baker (1998), the estimated maximum distance of pegmatite-dike propagation is in the order of 10 km distance. This distance is commonly observed between the parental pluton and the most distal pegmatites emplaced within middle to upper crust (Cameron et al., 1949; Černý, 1982b; Shearer et al., 1992). In some regions, pegmatites are found even more than 10 km away from the exposed granite plutons. For example, the Harney Peak pegmatites which are exposed more than 10 km far away from their parental pluton which is the extension of the subsurface

Harney Peak granite (Shearer et al., 1992). This is in consistent with the model of the maximum distance of pegmatite dike propagation of Baker (1998).

The dike propagation model of the Baker (1998) also predicts that dykes formed early in the pluton's history should be close to the pluton. The early-formed dykes are less evolved mineral assemblages than those of later formed dykes found farther away from the pluton's margins, because the earlier-formed dykes are filled with higher-temperature magmas than the later-formed ones. This mechanism of zonation has also been observed in many other studies on pegmatites (e.g., Cameron et al., 1949; Heinrich, 1953; Černý, 1982b; Shearer et al., 1992; Mulja et al., 1995; Roda et al., 1995). Thus it appears that the frequently observed compositional zonation in pegmatite fields is due to a combination of magmatic evolution of the pluton, producing increasingly evolved pegmatite-forming melts while the heat lost from the pluton warms the country rocks sufficiently to lower the nearby thermal gradient to the point where dykes can propagate to significant distances away from the host pluton. According to the pegmatite dike propagation model proposed by Baker (1998), it is probable that the Shigar valley pegmatites may be the off shoots of the Baltoro Plutonic Unit, but the geochronology and metamorphism of the host rock of the Shigar valley pegmatites, as discussed earlier, do not allow associating these pegmatites with this plutonic unit, which is exposed more than 30 km northeast of the Shigar valley.

Pegmatite bodies are characterized by a variety of sizes, shapes, orientations, and structural relationships to host rocks. They may occur as single tabular bodies, multiple tabular bodies with a preferred orientation, or as multiple tabular bodies with a variety of orientations (Brisbin, 1986). In some cases these bodies are inter-connected, while in others these are not inter-connected. They occur as lenslike or podiform or irregular bulbous masses, or may be turnip-shaped bodies. In this regard, the Shigar valley pegmatites are mostly tabular in form with variable sizes. However, in some of the zoned pegmatite dykes, the irregular bulbous masses are also noticed especially in the pegmatites of Dassu area. Each pegmatite dike of the Shigar valley occurs as a separate single body and these dykes are neither cross-cutting nor interconnected with one another.

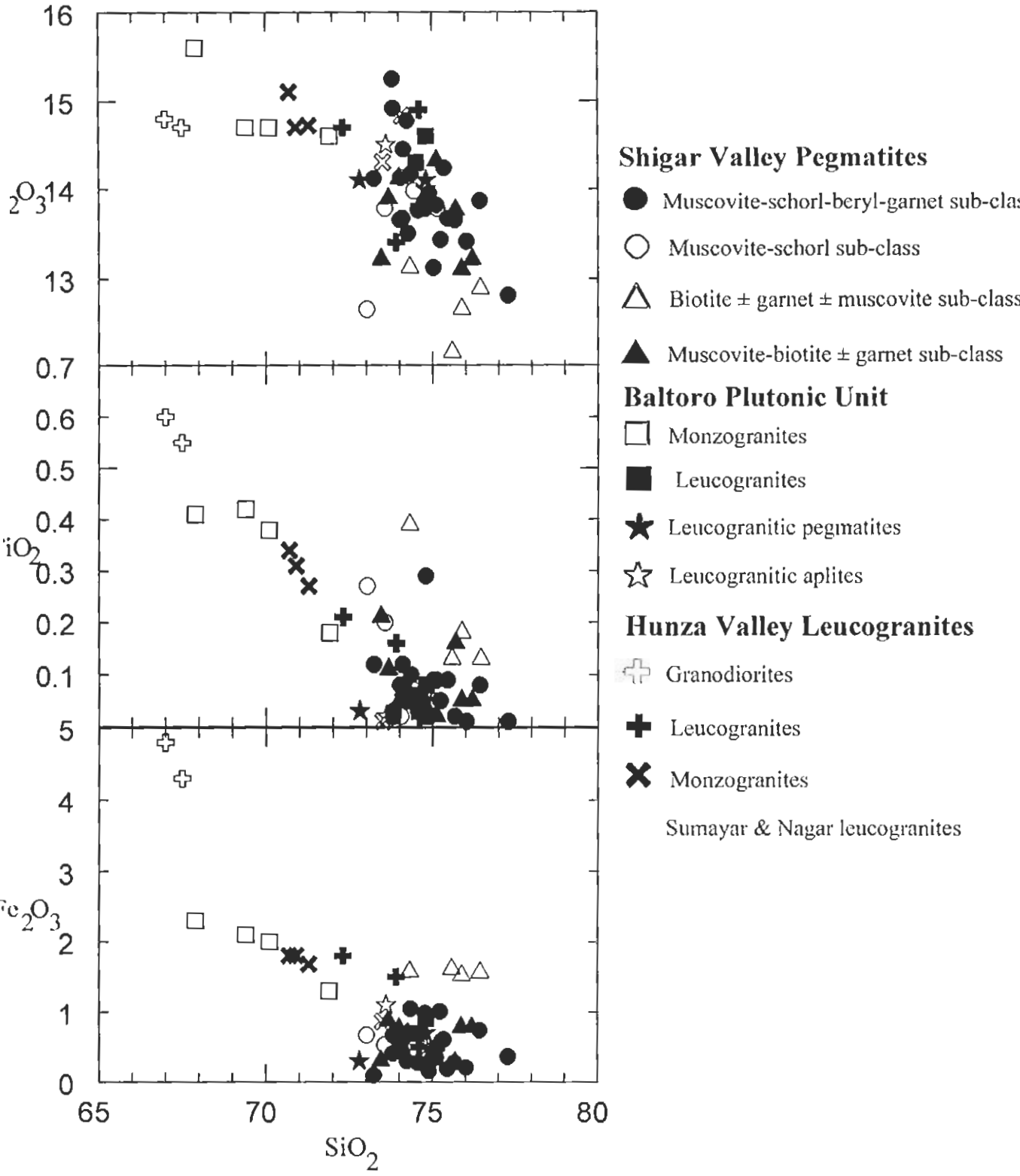


**Fig. 8. 1.** Harker-type binary diagrams showing comparison of Shigar valley pegmatites with the Baltoro and Hunza granitoid rocks.

ıg. 8. 1: continued:

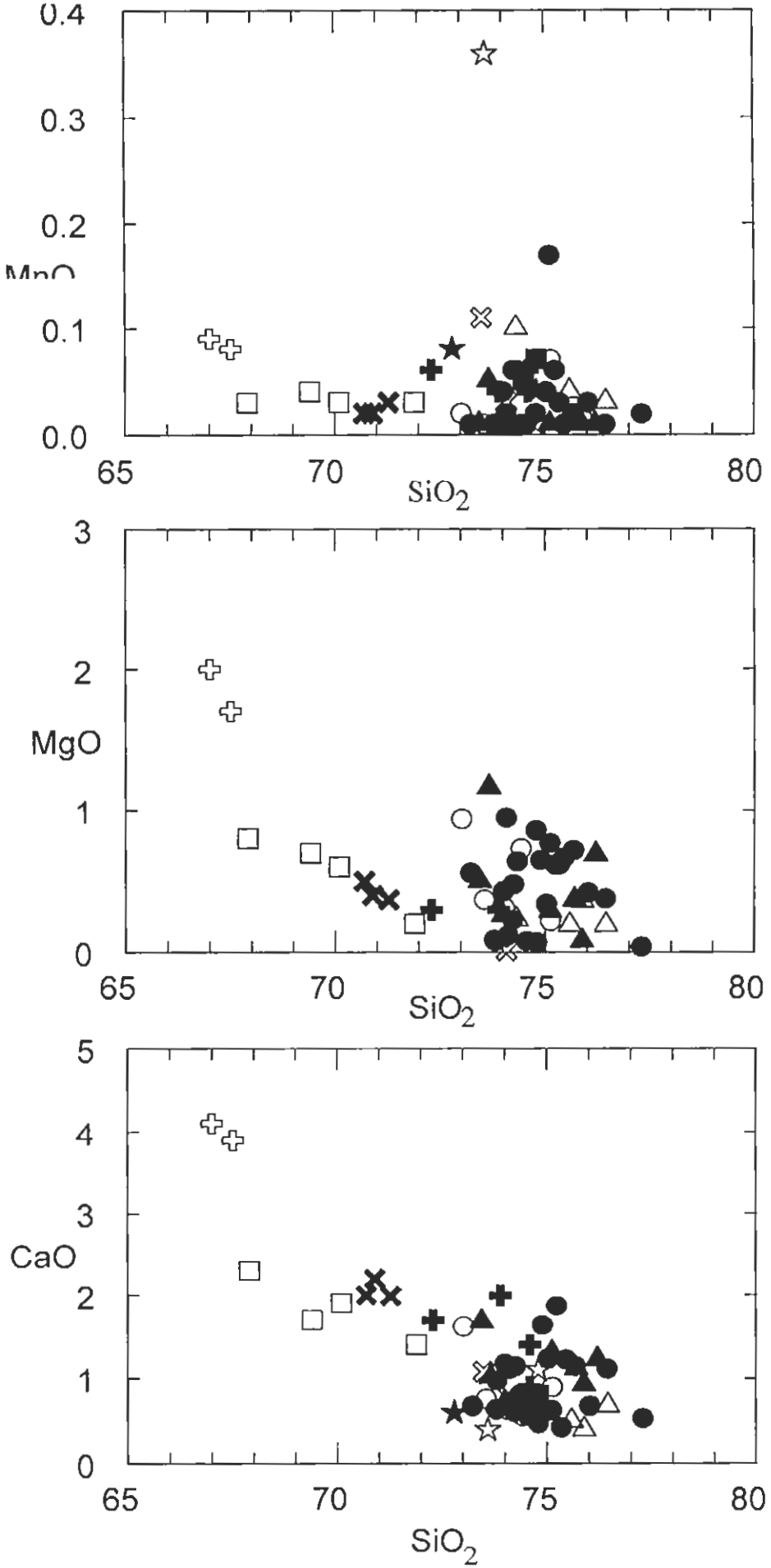

**Fig. 8. 1:** continued:

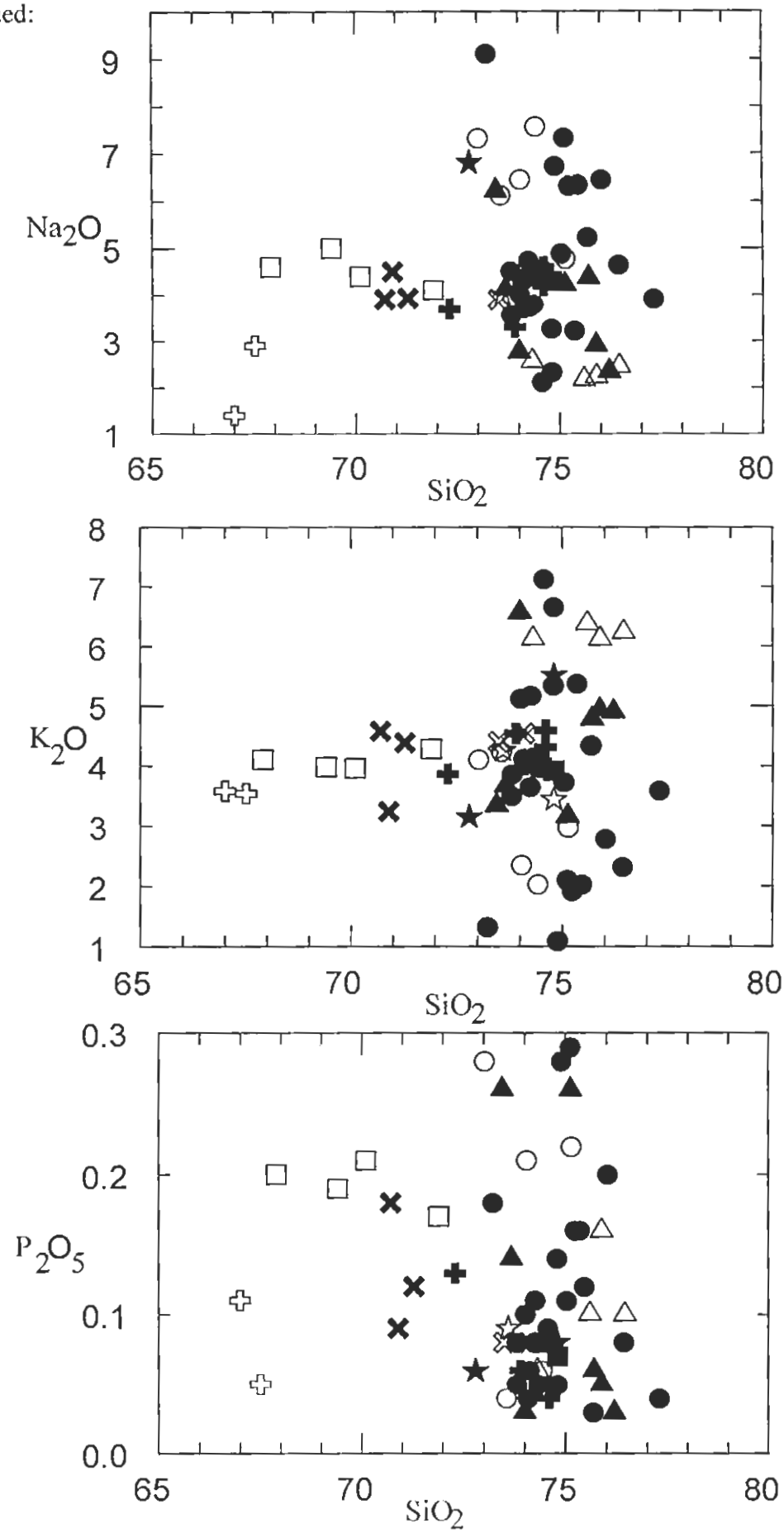

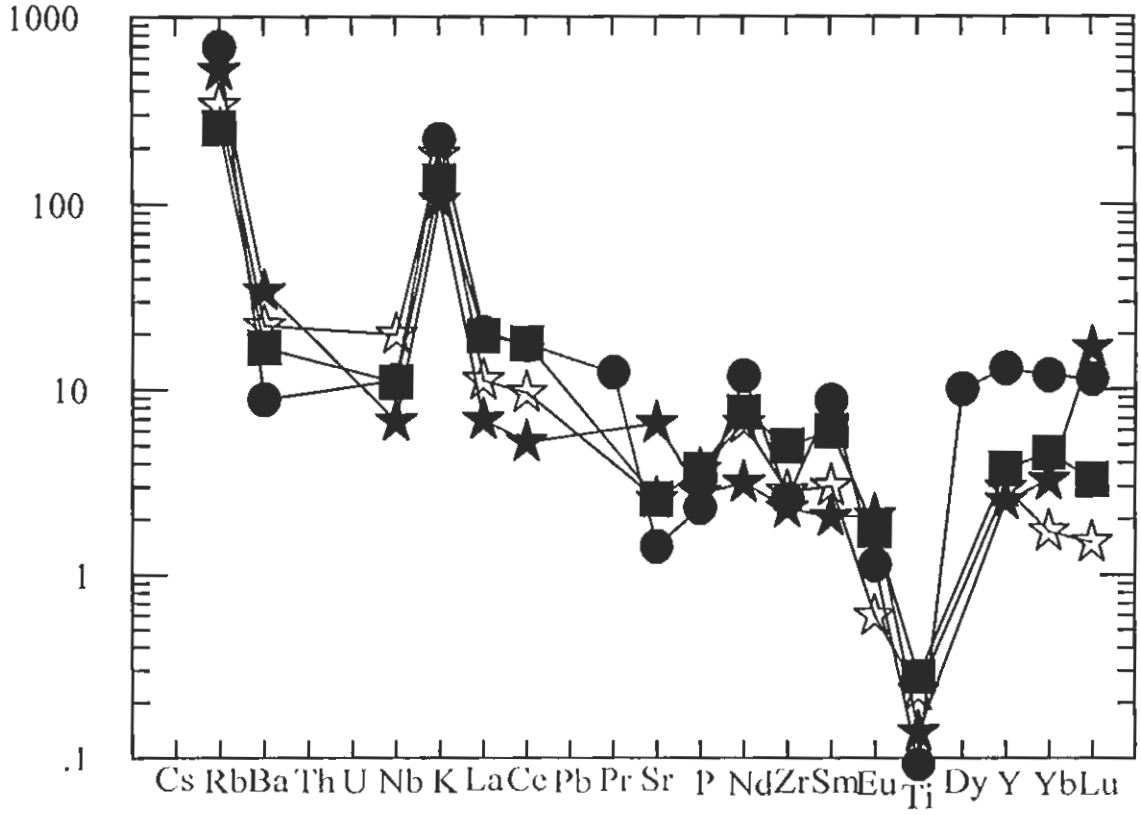


**Fig. 8. 2.** Primitive mantle spider diagram showing comparison of the different lithologies of the Baltoro Plutonic Unit and the Shigar valley pegmatites (after Sun and Mac Don., 1989). Symbols as in Fig. 8.1.

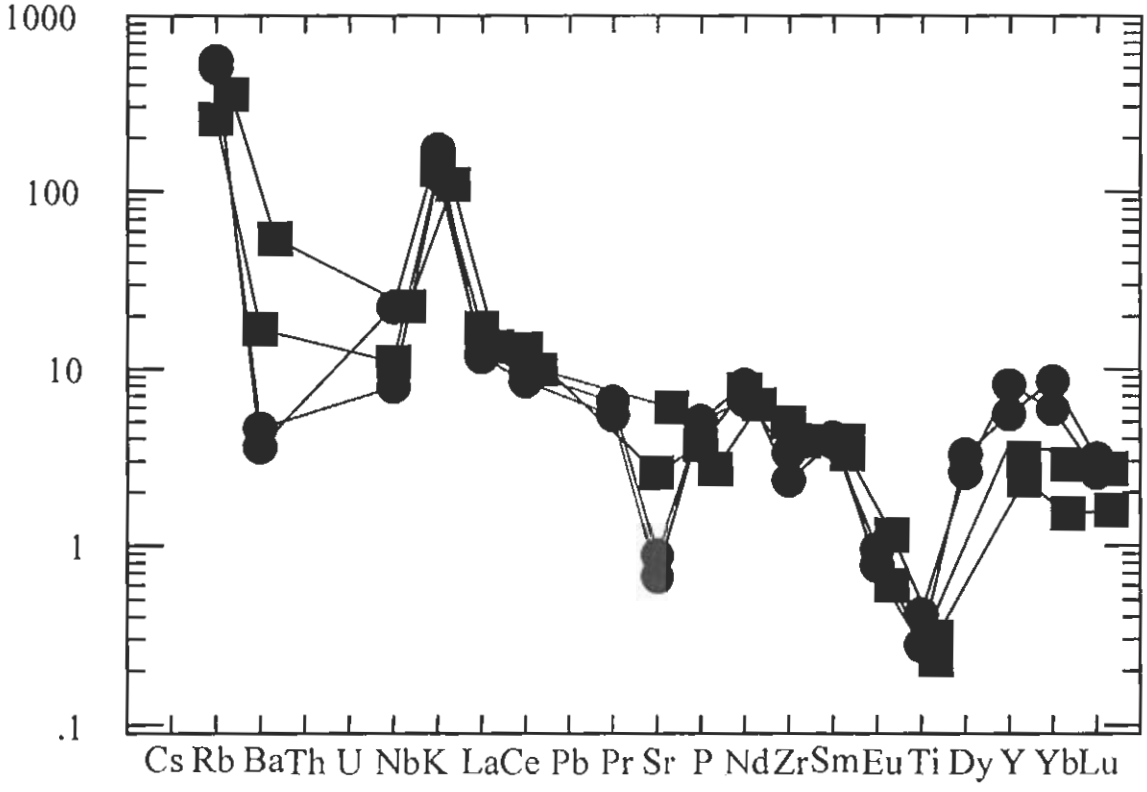


**Fig. 8. 3.** Spider diagram showing comparison of the leucogranites of the Baltoro Plutonic Unit and the Shigar valley pegmatites (after Sun and Mac Don., 1989). Symbols as in Fig. 8. 1.

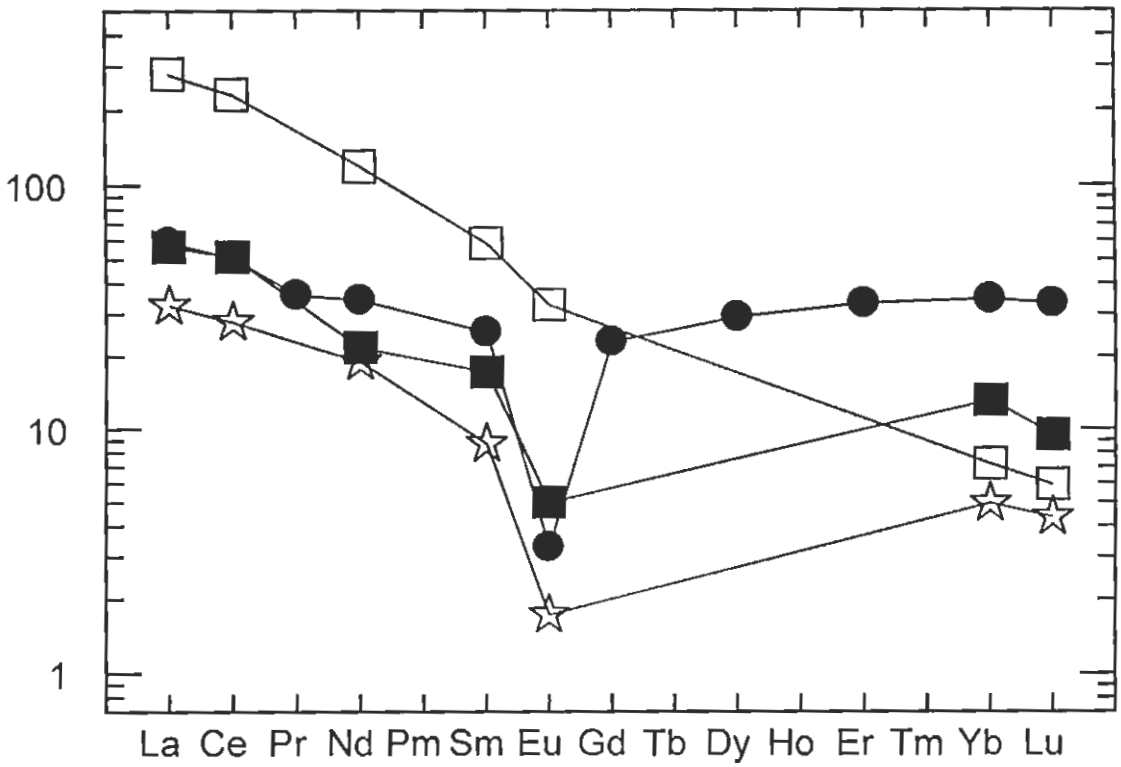


**Fig. 8. 4.** Chondrite normalized spider diagram for the lithologies of the Baltoro Plutonic Unit and Shigar valley pegmatites (after Sun and Mac Don., 1989). Symbols as in Fig. 8.1.

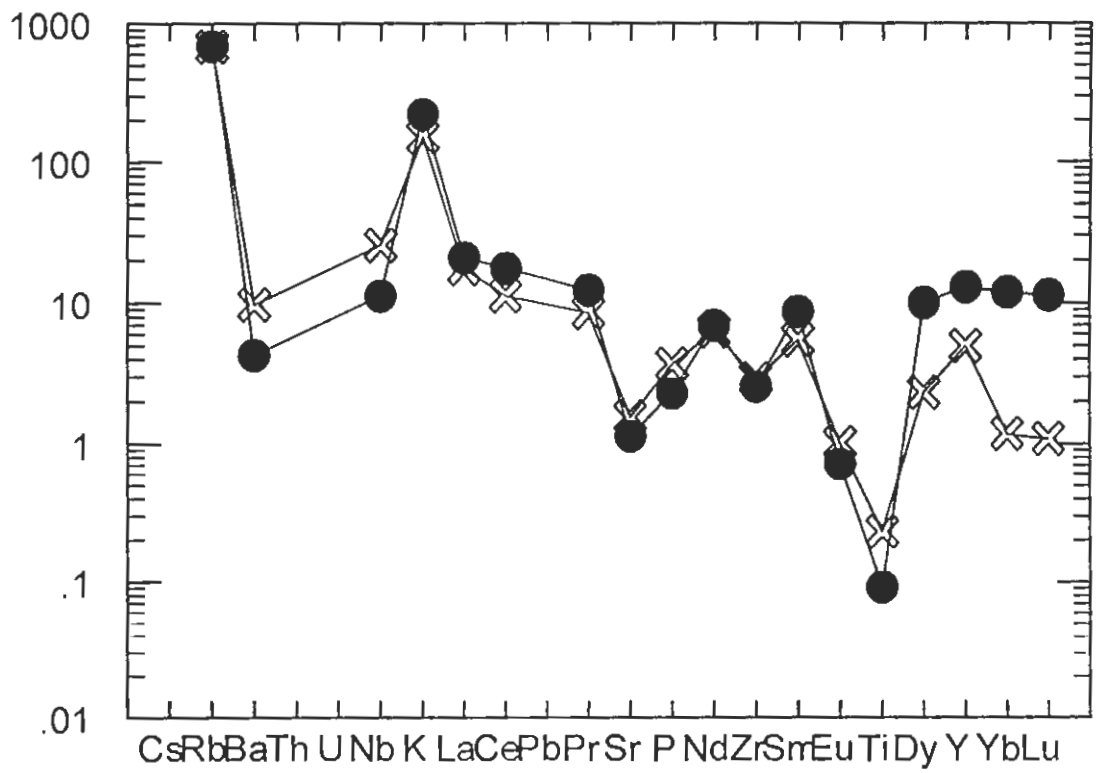


**Fig. 8. 5.** Spider diagram showing comparison of the Shigar valley pegmatites and the Sumayar leucogranite (after Sun and Mac Don., 1989). Symbols as in Fig. 8.1.

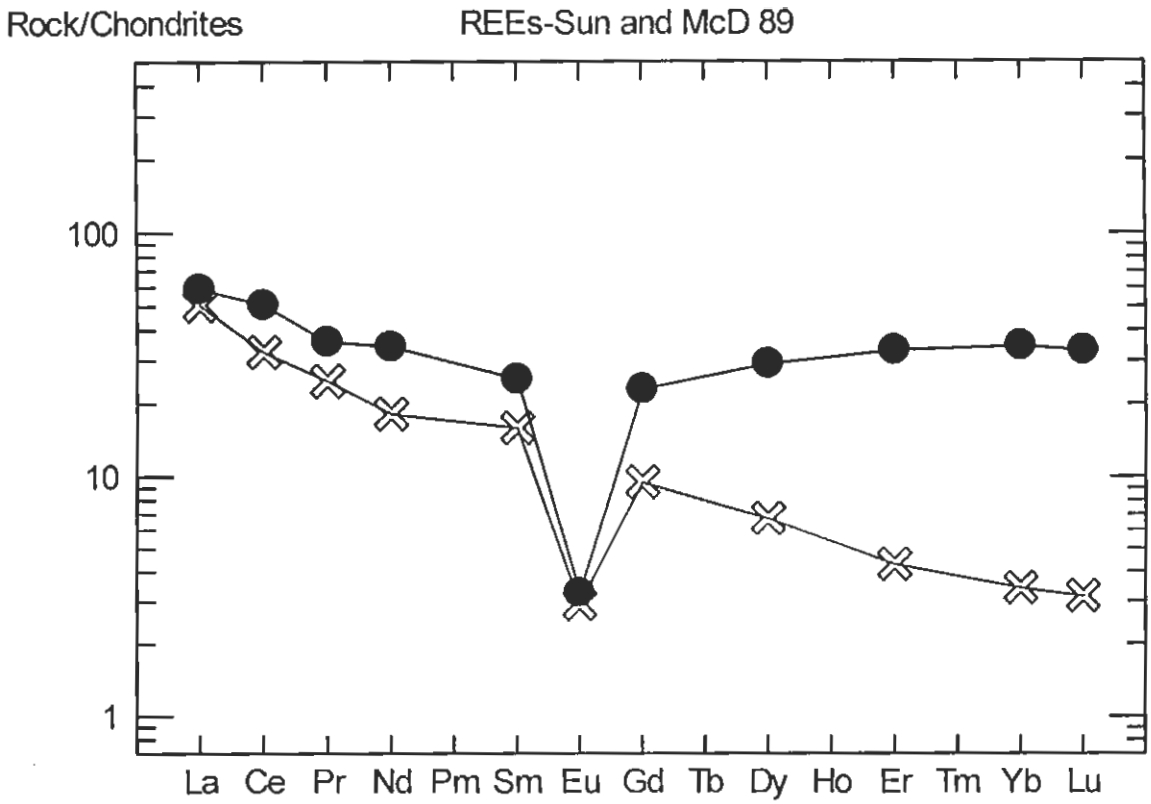


**Fig. 8. 6.** Chondrite-normalized REE pattern of Shigar valley pegmatites and the Sumayar pluton (after Sun and Mac Don., 1989). Symbols as in Fig. 8.1.

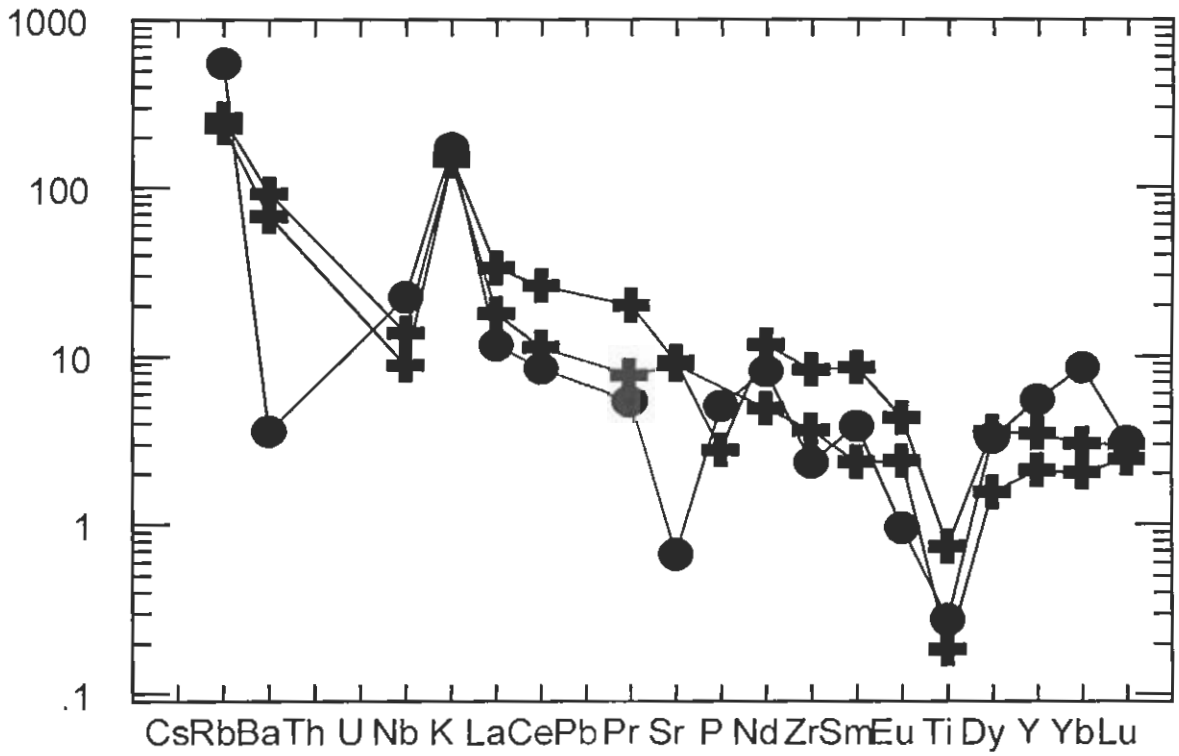


**Fig. 8. 7.** Primitive mantle normalized spider diagram for the leucogranites of the Hunza Plutonic Complex and the Shigar valley pegmatites (after Sun and Mac Don., 1989). Symbols as in Fig. 8.1.

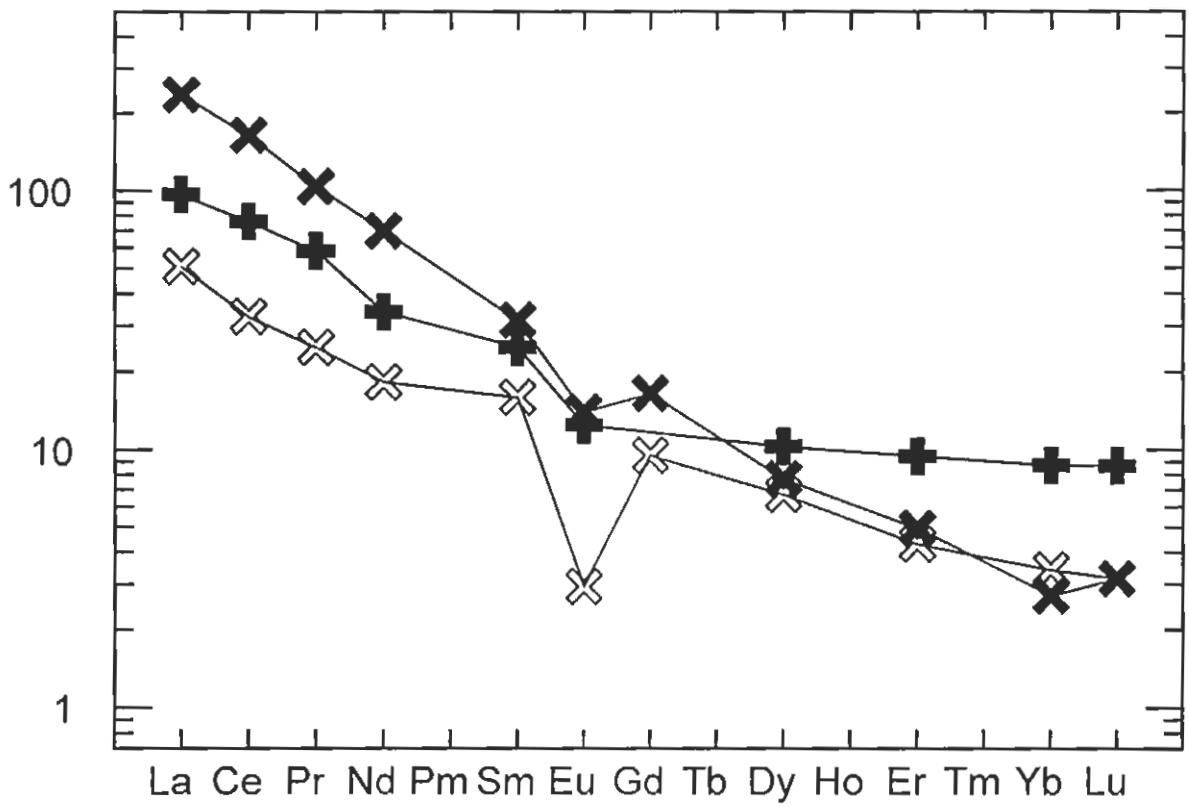


**Fig. 8. 8.** Chondrite-normalized REE - patterns of the different lithologies of the post-collisional Hunza Plutonic Complex (after Sun and Mac Don., 1989). Symbols as in Fig. 8.1.

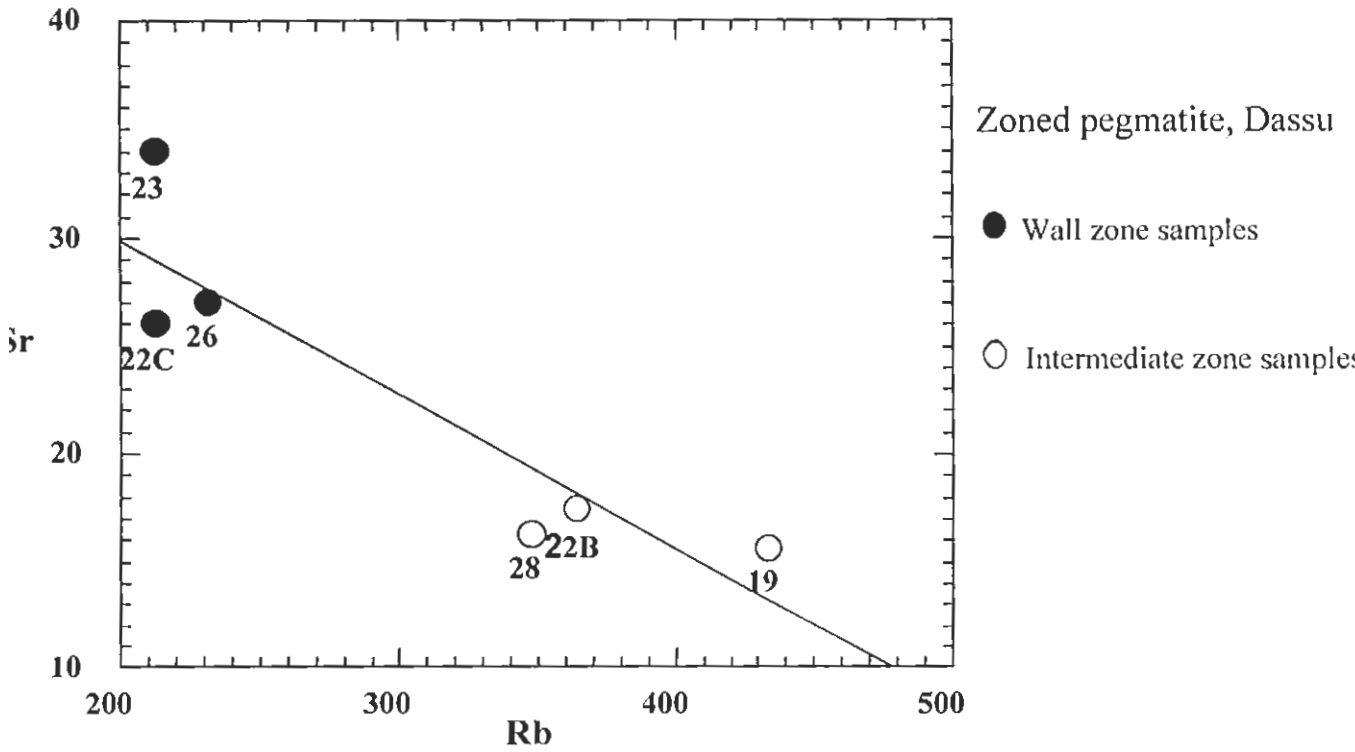


**Fig. 8. 9.** Rb vs Sr plot for different zones of the Shigar valley pegmatites.

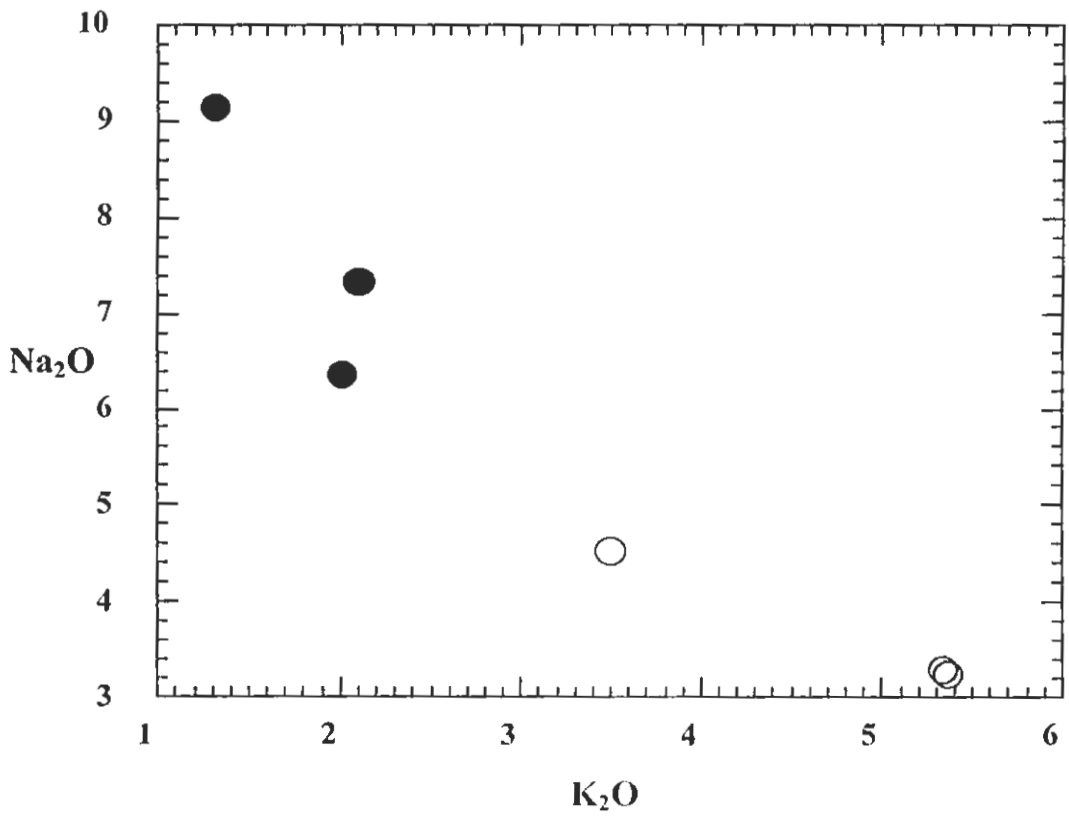


**Fig. 8. 10.** $K_2O$ vs. $Na_2O$ plot of wall zone and intermediate zone of the Shigar valley pegmatite. Symbols as in Fig. 8.9.

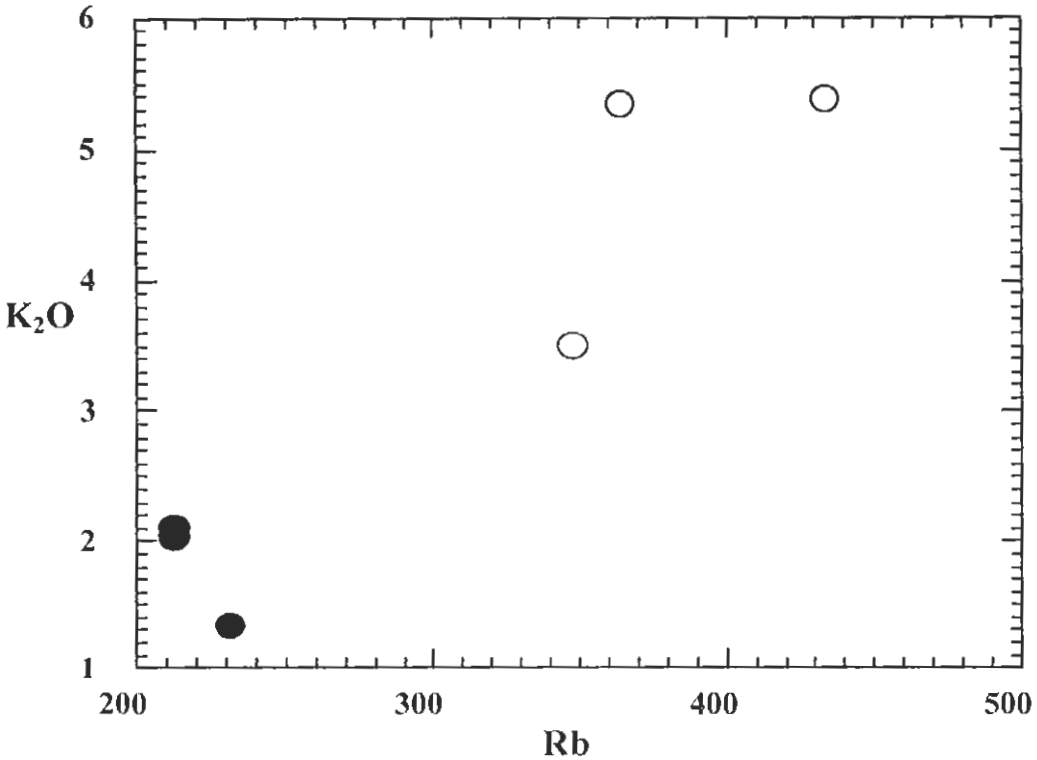


**Fig. 8. 11.** $K_2O$ vs. Rb plot for the wall and intermediate zones of the Shigar valley pegmatite. Symbols as in Fig. 8. 9.

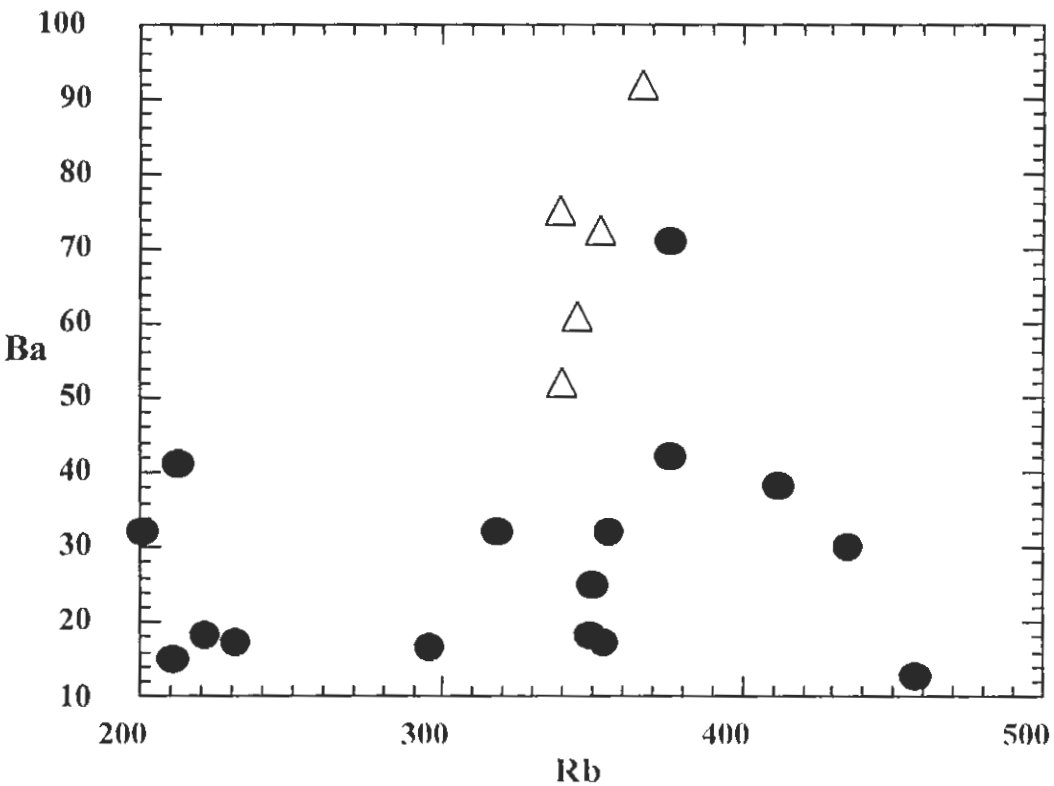


**Fig. 8. 12.** Rb vs. Ba plot for the tourmaline-rich and biotite-rich types of pegmatites of the Shigar valley area. Symbols as in Fig. 8.1.

# Chapter 9

## CONCLUSIONS

Keeping in view the field observations, petrographic studies, mineral chemistry, and whole rock geochemistry data, the following conclusions are made for the Shigar valley pegmatites:

1. The Shigar valley pegmatites are broadly classified into gem-bearing and gem-barren pegmatites. On the basis of mineralogy and internal structure, they are further classified as simple and zoned pegmatites. The zoned pegmatites are generally gem-bearing, while the simple pegmatites are mostly gem-barren. Besides, majority of the zoned pegmatites are symmetrically zoned, however, asymmetrically zoned pegmatites are also present. Moreover, some of the pegmatites are very ideal having four zones (border, wall, intermediate and core zones), while some of the pegmatites with three zones are also noticed. On the basis of field features and petrographic studies the Shigar valley pegmatites are further classified in four sub-classes: the muscovite-tourmaline-beryl-garnet rich, the muscovite rich, the biotite rich and the biotite-muscovite rich pegmatites.
2. Due to the occurrence of the gemstones in the cavities or pockets and the absence of certain rare metals, the Shigar valley pegmatites are also classified as miarolitic pegmatites rather than the rare-metal class of pegmatites.
3. Geochemically, all the groups of the Shigar valley pegmatites depict similar patterns/characteristics with minor differences, indicating to be co-magmatic. These minor differences may be due to the change in local fractional crystallization conditions. Further investigations such as the fluid inclusions and isotopic studies are required to determine the petrogenetic evolution of the pegmatites as well as of their host rocks.
4. In case of asymmetrically zoned pegmatites, the number of zones varies from three to six zones, where the intermediate zone is further divided into three zones.

5. In some of the dikes, the central quartz zone is very prominent containing euhedral quartz crystals ranging in size from 15 to 20 cm, while some of the dikes are without the central quartz core zone.
6. The mineralogical studies indicate, that no lithium and other rare minerals are observed in these pegmatites. Therefore, on the basis of mineralogy and standard classifications, these pegmatites as a whole belong to the gem-bearing miarolitic pegmatite class and simple pegmatites.
7. On the basis of mineralogy and whole rock geochemistry, the Shigar valley pegmatites are mainly peraluminous and are classified as S-type granitoids.
8. The Shigar valley pegmatites are geochemically compared with it's near by plutonic bodies (Baltoro Plutonic Unit and the Mungo Gusar pluton), which indicate that the Shigar valley pegmatites could not be the off shoots of any of these plutons but it is probable that they are the separate magmatic pulses. Moreover, in the light of the existing models of pegmatite generation, it is also concluded that there are minimal evidences to associate the Shigar valley pegmatites with the Baltoro Plutonic Unit.
9. The Shigar valley pegmatites share many geochemical characteristics in terms of major, trace, and rare earth elements with the pegmatites of Sumayar pluton in the Hunza valley and the Garam Chashma of the Trans-Himalaya, which shows that these three pegmatites may have been formed by the similar magmatic processes.
10. The post-collisional leucogranites of both the Hunza valley and the Baltoro Plutonic Unit are considered to be formed by local differentiation processes after the crystallization of the monzogranites. So, it is also suggested that such types of local differentiation processes may have also occurred during the formation of the Shigar valley pegmatites.
11. The Shigar valley pegmatites are unmetamorphosed and are intruded into the Dassu orthogneiss. Therefore, these pegmatites post-date the local metamorphism of 5.4 ± 0.2 Ma, suggesting a relatively younger age for the Shigar valley pegmatites.
12. In case of regional zonation, the Shigar valley pegmatites may be the most evolved and fractionated part of the Baltoro Plutonic Unit, where fractionation

started from the monzogranites through leucogranites and up to the evolution of pegmatites. The geochronology of the Baltoro Plutonic Unit (~ 25 Ma) and the host rock (~5 Ma) of the Shigar valley pegmatites suggest that the pegmatites of the Shigar valley could not be a part or equivalent to Baltoro Plutonic Unit.

13. The mechanisms of intrusions of pegmatites in the country rocks have been described in two ways: one is the internal pressure of the plutonic body itself and the fluids, because the pegmatites are formed in the last stages, while the other cause is the weaker zones that are produced in the active tectonic zones. In the case of Shigar valley pegmatites, both causes may be involved in the emplacement of the Shigar valley pegmatites. In this regard, if the Shigar valley pegmatites are the off shoots of Baltoro Plutonic Unit then definitely the internal fluid pressure at the last stages may have caused the propagation of both the leucogranite as well as the pegmatite dikes. But if the Shigar valley pegmatites are the separate magmatic pulses then it is probable that they have been injected through tectonic forces into the weaker zones or fractures, because tectonically this region is situated at the periphery of an active thrust zone (Main Karakoram Thrust).
14. The field data and the petrographic studies indicate that the source rocks of the Shigar valley pegmatites are poor in rare elements because except beryl no other rare element-bearing mineral having Li, Sn, Nb, Ta is found from these pegmatites. It may also be added here that almost all of the leucogranites and pegmatites of the Karakoram Axial Batholith are also poor in rare elements.
15. No lithium-bearing mineral is found in the Shigar valley pegmatites, which could be due to two reasons: first, the pegmatitic magma was poor in Li and the second reason is the presence of Be, because the Li and Be minerals rarely occur together.
16. On the basis of mineralogical and chemical data of the Shigar valley pegmatites and their host rocks, it is concluded that at least the host rocks (Dassu orthogneiss) are not the source rock of the Shigar valley pegmatites because tourmaline is a ubiquitous mineral of Shigar valley zoned pegmatites, while their host rock is devoid of tourmaline. Furthermore, the mineral assemblages of the

Shigar valley pegmatites suggest that the source rock of these pegmatites was significantly enriched in B, F, Cl, $H_2O$ and other volatiles because of the presence of tourmaline, topaz, fluorite. It was depleted in Li because no lithium-bearing mineral (e.g., lepidolite, zinnwaldite, spodumene) is identified in these pegmatites. Besides, the source rock is also depleted in other rare-metals because no significant rare-metal mineralization is noticed in these pegmatites.

17. The most common characteristic of all the post-collisional leucogranites including pegmatites of the High Himalayas and the Karakoram Mountains is that the source rock of these granitoids is very poor in lithium because no significant lithium mineralization as yet has been reportd from these.
18. The complex pegmatites are mostly found in the late orogenic or tectonic settings. In this context, the Shigar valley pegmatites are considered to be the product of continent-continent collision.
19. The compositions of the garnets from the pegmatites indicate that these are almandine-spessartine garnets, while their host rocks have very small molecular proportions of the spessartine, which indicates that the garnets of the Shigar valley pegmatites are magmatic in origin rather being xenocrystic due to assimilation from the host rock.
20. Petrographic studies indicate that the pegmatites of almost all the sub-classes are partially to completely altered showing intensive hydrothermal or weathering effect.
21. Petrographic and mineral chemistry data indicate that the main plagioclase of the gem-bearing class of pegmatites of the Shigar valley is albite, while oligoclase is the main constituent of the gem-barren class.
22. The XRD data of the black-colored tourmalines indicate that these tourmalines are the foitite instead of schorl and this is the first time that foitite is discovered from the pegmatites of the northern areas of Pakistan.
23. The hafnon rich zircons are either reported from the Li-bearing or Ta-bearing pegmatites but the Shigar valley pegmatites are poor in these elements. The zircons from the Shigar valley pegmatites are poor in their hafnon content but they contain higher hafnon values than the Indus-Gilgit Confluence pegmatites.

# REFERENCES


Ahmed, Z. and Chaudhry, M. N., 1976. Petrology of the Babusar area, Diamir District, Gilgit, Pakistan. Geol. Bull. Punjab Univ., 12, 67 - 78.

Allegre, C. and 34 others., 1984. Structure and evolution of the Himalaya-Tibet orogenic belt. Nature, 307, 17 - 22.

Allen, T. and Chamberlain, P. C., 1991. Metamorphic evidence for an inverted crustal section, with constraints on the Main Karakoram Thrust, Baltistan, Northern Pakistan. J. Metam. Geol., 9, 403 - 413.

Baker, D. R., 1998. The escape of pegmatite dikes from granitic plutons: constraints from new models of viscosity and dike propagation. Can. Min. 36, 255 - 263.

Bakumenko, I. T., 1968. On the formation of high temperature pegmatite zones. In: Mineralogical Thermometry and Barometry 1, 63-70; in Russian.

Baldwin, J. R. and von Knorring, O., 1983. Compositional range of Mn-garnet in zoned granitic pegmatites. Can. Min., 21, 683-688.

Bard, J. P., 1983. Metamorphic evolution of an obducted island arc: Examples of the Kohistan sequence (Pakistan) in the Himalayan collided range. Earth Planet. Sci. Lett., 65, 133 -144.

Bard, J. P., Maluski, H., Matte, P. and Proust, F., 1980. The Kohistan sequence: crust and mantle of an obducted island arc. Geol. Bull. Univ. Peshawar, 13, 87 - 94.

Barker, F., 1979. Trondhjemite; definition, environment, and hypothesis of origin. Trondhjemite, dacites, and related rocks edited by F. Barker, Elsevier, New York.

Bazarov, L. S. and Motorina, I. V., 1969. Physiochemical conditions during formation of rare-metal pegmatite of the sodium-lithium type. Doklady Acad. Sci. U. S. S. R., Engl. Transl. 188, 124-126.

Benard, F., Moutou, P. and Pichavant, M., 1985. Phase relations of tourmaline leucogranites and the significance of tourmaline in silicic magmas. J. Geol., 93, 271 - 291.

Bertrand, J. M., Kienast, J.R. and Pinardon, J. L., 1988. Structure and metamorphism of the Karakoram gneisses in the Braldu-Baltoro valley, N. Pakistan. Geodynam. Acta, 2, No. 3, 135 -150.

Beus, A. A., 1960. Geochemistry of beryllium and genetic types of beryllium deposits. Acad. Sci. U.S.S.R., Moscow; English translation (1966): Freeman and Co., San Francisco.

Beus, A. A., 1966. Geochemistry of beryllium and genetic types of beryllium deposits. (Trans. From Russian by F. Lachmann). W. H. Freeman and Co., San Francisco.

Bill, H. Sierro, J. and Lacroix, R., 1967. Origin of coloration in some fluorites. Am. Min., 52, 1003-8.

Blattner, P., Dietrich, V., and Gansser, A., 1983. Contrasting $^{18}O$ enrichment and origin of High Himalayan and Trans-Himalayan intrusives. Earth Planet. Sci. Lett., 65, 276 - 286.

Bostock, H. H., 1977. The composition of hornblende, grunerite, and garnet in Archean iron formation of the Itchen Lake area. District of Mackenize, Canada. Can. J. Earth Sci., 14, 1740-1752.

Brammall, A. and Harwood, H. F., 1925. Tourmalinization in the Dartmoor granite. Min. Mag., 20, 319-30.

Brisbin, W. C., 1986. Mechanics of pegmatite intrusion. Am. Min., 71, 644 - 651.

Brookfield, M. E., 1980. Reconnaissance geology of the Hushe and Saltoro - Kondus River valleys, Karakoram Mountains, Kashmir, Pakistan. Academia Nazion. dei Lincei, 69, 248 - 253.

Brookfield, M. E. and Andrews-Speed, C. P., 1984. Sedimentology, petrography, and tectonic significance of the shelf, flych and molasse clastic deposits across the Indus Suture Zone, Ladakh, NW India. Sediment. Geol., 40, 249 -286.

Brookfield, M.E. and Gupta, J., 1984. Permian fossils from the Shyok mélange, near Shigar, Baltistan, Pakistan, Bull. Indian Geol. Assoc., 17, 39 - 44.

Brotzen, O., 1959. Outline of mineralization in zoned granitic pegmatites: Geologiska Foreningers, Stockholm Forhandlingar, 496, 2 -98.

Brown, G. C., Thorpe, R. S. and Webb, P. C., 1984. The geochemical characteristics of granitoids in contrasting arcs and comments on magma sources. J. Geol. Soc., London, 141, 413 - 426.

Brown, M. and Solar, G. S., 1998. Shear-zone systems and melts: feedback relations and self-organization in orogenic belts. J. Struc. Geol., 20, 211 - 227.

Buddington, A. F., Fahey, J. and Vlisidis, A., 1955. Thermometric and petrogenetic significance of titaniferous magnetite. Am. J. Sci., 253, 497.

Burnham,C. W. and Jahns, R. H., 1961. Experimental studies of pegmatite genesis: The composition of pegmatite fluids. Geol. Soc. Am. Spec. Pap., 68, 143 - 144.

Burrard, S. G. and Heron, A. M., 1934. The Geography and geology of the Himalayan Mountains. 2nd Ed., Govt. of India. Press, Calcutta.

Burrard, S. G. and Hyden, H. H., 1908. A sketch of the geography and geology of the Himalaya Mountains and Tibet. Govt. India, Press, Calcutta, 308p.

Calkins, J., A., Jamiluddin, S., Kamaluddin, B., and Hussain, A., 1981. Geology and mineral resources of the Chitral - Partsan area, Hindu Kush Range, northern Pakistan. U S Geol. Surv. Prof. Pap., 716 - G, 33.

Cameron, E. N., Jahns, R. H., McNair, A. H. and Page, L. R., 1949. Internal structure of granitic pegmatites. Eco. Geol., Mongr. 2.

Cann, J. R., 1969. Spilites from the Carsberg Ridge, Indian Ocean. J. Petrol., 10, 1- 19.

Casnedi, R. and Ebblin, C., 1977. Geological notes on the area between Astor and Skardu (Kashmir); Rend. Accad. Naz., Lincei, 52, 662 - 668.

Casnedi, R., Desio, A., Forcella, F. Nicolette, M. and Petrucciani, C., 1978. Absolute age of some granitoid rocks between Hindu Raj and Gilgit (Karakoram), Rend. Accad. Naz., Lincei, 63, 8p.

Cassedanne, J. P. and Cassedanne, J. O., 1981. The Urubu pegmatite and vicinity. Min. Record, 12, 73 -77.

Ćerný P. 1982a. Anatomy and classification of granitic pegmatites. In: Granitic Pegmatites in Science and Industry (P. Ćerný, ed.). Min. Assoc. Can., Short Course Handbook 8, 1-39.

Ćerný, P. and Brisbin, W. C., 1982b. The Osis Lake pegmatitic granite, Winnipeg River district, southeastern Manitoba. In: Granitic Pegmatites in Science and Industry (P. Ćerný, ed.). Min. Assoc. Can., Short Course Handbook 8, 545 -555.

Ćerný, P. and Hawthorne, F. C., 1976. Refractive indices versus alkali contents in beryl: general limitations and applications to some pegmatitic types. Can. Min., 14, 491-97.

Ćerný, P. and Siivola, J., 1980. The Tanco pegmatite at Bernic Lake, Manitoba: X11. Hafnian zircons. Can. Min., 18, 313-321.

Ćerný, P., 1982b. Petrogenesis of granitic pegmatites. In: Granitic Pegmatites in Science and Industry (P. Ćerný, ed.). Min. Assoc. Can., Short Course Handbook 8, 405-461.

Ćerný, P., 1991a. Rare-element granitic pegmatites. Part 1: Anatomy and internal evolution of pegmatite deposits. Geoscience Canada, 18, 49 -67.

Ćerný, P. 1991b. Rare-element granitic pegmatites. Part 11: Regional to global environments and petrogenesis. Geoscience Canada, 18, 68 - 81.

Ćerný, P. and Simpson, F. M., 1977. The Tanco pegmatite at Bernic Lake, Manitoba. 1X. Beryl. Can. Mineral. 15, 489- 499.

Ćerný, P., 1975. Alkali variations in pegmatitic beryl and their petrogenetic implications. Neus Jaheb. Mineral. Abh. 123, 198-212.

Ćerný, P., 1982c. Mineralogy of rubidium and cesium. In: Granitic Pegmatites in Science and Industry (P. Ćerný, ed.). Min. Assoc. Can., Short Course Handbook 8, 149-162.

Ćerný, P. and Hawthorne, F. C., 1982. Selected peraluminous minerals. In: Granitic Pegmatites in Science and Industry (P. Ćerný, ed.). Min. Assoc. Can., Short Course Handbook 8, 163-186

Ćerný, P., Meintzer, R., E. and Anderson, A. J., 1985. Extreme fractionation in rare element granitic pegmatites: Selected examples of data and mechanisms. 23, 381-421.

Ćerný, P., Smith, J. V., Mason, R. A. and Delaney, J. S. 1984. Geochemistry and petrology of feldspar crystallization in the Vanza pegmatite, Czechoslovakia. Can. Min., 22, 631-651.

Cerveny, P.F., Naeser, C. W., Kelemen, P. B., Lieberman, J. E. and Zietler, P. K., 1989. Zircon fission-track ages from the Gasherbrum Diorite, Karakoram Range, northern Pakistan. Geol., 17, 1044 - 1048.

Chang, L. L. Y., Howie, R. A. and Zussman, J., 1998. Rock Forming Minerals, 2nd edition, Vol.,5B. Geol. Soc. London.

Chappell, B. W. and White, A.J.R., 2001. Two contrasting granite types: after 25 years later. Aust. J. Earth Sci., 48, 489 - 499.

Chaudhry, M. N., Kausar, A. B. and Lodhi, S. A. K., 1974. Geology of Timargara - Lal Qila area, Dir District, N. W. F. P. Geol. Bull. Punjab Univ., 11, 53 - 73.

Chayes, F., 1964. Variance - covariance relations in some published Harker diagrams of volcanic suits. J. Petrol., 5, 219 - 237.

Chorlton, L. B. and Martin, R. F. 1978. The effect of boron on the granite solidus. Can. Min., 16, 239 -244.

Clemens, J. D. and Wall, V. J., 1981. Origin and crystallization of some peraluminous (S-type) granitic magmas. Can. Min. 19, 111 - 131.

Correia Neves, J. M., Lopes Nunes, J. E. and Sahama, T. H. G., 1974. High hafnium members of the zircon-hafnon series from the granite pegmatites of Zambezia, Mozambique. Contrib. Mineral. Petrol., 48, 73-80.

Coward, M. P., Butler, R. W. H., Khan, M. A. and Knipe, R. J., 1987. The tectonic history of Kohistan and its implications for the Himalayan structure. J. Geol. Soc., London., 144, 377 - 391.

Coward, M. P., Jan, M. Q., Rex, D., Tarney, J., Thirlwall, M. and Windley, B. F., 1982. Geotectonic framework of the Himalaya of N. Pakistan. J. Geol. Soc. London., 139, 299 - 303.

Coward, M. P., Windley, B. F., Broughton, R. D., Luff, I. W., Petterson, M. G., Pudsey, C. J., Rex, D. C. and Khan, M. A., 1986. Collision tectonics in the NW Himalaya. In: Collision Tectonics (Coward, M. P. and Ries, A. C. eds.). Geol. Soc. London., Spec. Publ., 19, 203 -219.

Cox, K. J., Bell, J. D. and Pankhurst, R. J., 1979. The interpretation of igneous rocks. George, Allen and Unwin, London.

Crawford, M. B. and Searle, M. P., 1993. Collision-related granitoid magmatism and crustal structure of the Hunza Karakoram, north Pakistan. In: Himalayan Tectonics (Treloar, P. J. and Searle, M. P. eds.). Geol. Soc. London., Spec. Publ. 74, 53 - 68.

Crawford, M. B. and Searle, M. P., 1992. Field relationships and geochemistry of pre-collisional (India – Asia) granitoid magmatism in the central Karakoram, northern Pakistan. Tectonophysics., 206, 171 - 192.

Crawford, M. B. and Windley, B. F., 1990. Leucogranites of the Himalaya / Karakoram: implication for magmatic evolution within collisional belts and the study of the collision-related leucogranites petrogenesis. J. Volc. Geotherm. Res., 44, 1- 19.

Crawford, M. B., 1988. Leucogranites of the NW Himalayas: Crust - mantle interaction beneath the Karakoram and the magmatic evolution of the collisional belts. Unpubl. Ph. D. thesis, Univ. Leicester.

Cronin, V. S., 1982. The physical and magnetic polarity stratigraphy of the Skardu basin, Baltistan, northern Pakistan. Unpubl. M. A. thesis, Dartmouth College, 225 p.

Crouse, R. A. and Ćerný, P. 1972. The Tanco pegmatite at Bernic Lake, Manitoba. 1. Geology and paragenesis. Can. Min., 11, 511-608.

Cummings, W., 1983. Ferroaxinite from Bridgeville, New Jersey. Min. Rec., 14, 43 - 44.

De Terra, H., 1932. Geological studies in the Northwest Himalaya between the Kashmir and Indus valleys. Mem. Connecticut Acad. Arts and Sci., VII – II, 18 – 76.

Debon, F. and Le Fort, P., 1982. A chemical - mineralogical classification of common plutonic rocks and associations. Trans. R. Soc. Edinburgh, Earth Sci., 73, 135 - 149.

Debon, F., Le Fort, P., Dautel, D., Sonet, J. and Zimmermann, J. L. L., 1987. Granites of the western Karakoram and northern Kohistan (Pakistan): A composite Mid-Cretaceous to Upper Cenozoic magmatism. Lithos, 20, 19 - 40.

Debon, F., Le Fort, P., Sheppard, S. M. F. and Sonet, J., 1986. The four belts of the Transhimalaya - Himalaya: a chemical, mineralogical, isotopic, and chronological synthesis along a Tibet - Nepal section; J. Pet., 27, 219 - 250.

Debon, F., Zimmermann, J. L. and Le Fort, P., 1996. Upper Hunza granites (North Karakoram, Pakistan): a syn-collision bimodal plutonism of mid-Cretaceous age. Geomaterials. 323 11a, 381 - 388.

Deer, W. A., Howie, R. A. and Zussman, J., 1966. An Introduction to the Rock Forming Minerals. Longman, London.

Deer, W. A., Howie, R. A. and Zussman, J., 1962. Rock Forming Minerals, Sheet silicates, Vol., 3. Longman, London.

Deer, W. A., Howie, R. A. and Zussman, J., 1986. Rock Forming Minerals, 2nd edition, Vol., 1B. Geol. Soc. London.

Deer, W. A., Howie, R. A. and Zussman, J., 1997. Rock Forming Minerals, 2nd edition, Vol., 1A. Geol. Soc. London.

Desio, A., 1963. Review of the geological formations of the western Karakoram (Central Asia). Rivista Italiana de Paleontologia e Stratigraphia, 69, 475 - 501.

Desio, A., 1979. Geological evolution of the Karakoram. In: Geodynamics of Pakistan (Farah, A. and De Jong, K. A. eds.). Geol. Surv. Pakistan, Quetta, 111 -124.

Desio, A. and Zanettin, B., 1970. Geology of the Baltoro Basin. Italian Expeditions to the Karakoram (K2) and Hindu Kush (leader A. Desio), Scientific Reports, Section 11, vol. 2, Brill, Leiden, 308p.

Desio, A., 1964. Geological tentative map of the western Karakoram. Scale 1: 500,000. Inst. Geol., Univ. Milano.

Desio, A., 1978. On the geology of the Deosai Plateau. Atti della Academia nazionale dei Lincei (Rome). Memorie – Classe di Scienze fisiche, matematiche e naturali, serie VIII, vol. XV, sezione II, 1 -19.

Desio, A., Martina, E., Spadea, P. and Notarpietro, A., 1985. Geology of the Chogo Lungma - Biafo - Hispar area, Karakoram (NW Pakistan). Memorie - Classe di Scienze fisiche, matematiche e naturali, serie VIII, Academia nazionale dei Lincei, vol. XVIII, 1 -53.

Desio, A., Tongiorgi, E. and Ferrara, G., 1964. On the geological age of some granites of the Karakoram, Hindu Kush, and Badakhshan, Central Asia, 22nd Intern. Geol. Congr., New Delhi, 11, 479 - 496.

Dickinson, W. R., 1968. Circus - Pacific andesites types. J. Geophys. Res., 73, 22 - 61.

Dickinson, W. R. and Hatherton, T., 1967. Andesitic volcanism and seismicity around the Pacific. Sci., 157, 801.

Duke, E. F., Papike, J. J. and Laul, L. C., 1992. Geochemistry of a boron-rich peraluminous granite pluton: the Calamity Peak layered granite pegmatite complex, Black Hills, South Dakota, Can. Min. 30, 811 - 34.

Duke, E. F., Redden, J. A. and Papike, J. J., 1988. Calamity Peak layered granite-pegmatite complex, Black Hills, South Dakota: Part 1. Structure and emplacement. Bull. Geol. Soc. Am., 100, 825 - 40.

Duncan, R. A. and Pyle, D. G., 1988. Rapid extrusion of the Deccan flood basalts at the Cretaceous / Tertiary boundary. Nature, 333, 841 - 843.

Einfalt, H. C., Kaphle, K. P., and Joshe P. R., 1995. Trace element in muscovite as a guide to gem tourmaline bearing pegmatites in Nepal. J. Nepal Geol. Soc. Vol. 11, Spec. Issue, 141- 158.

Erametsa, O., Nieminen, K. and Niinisto, L., 1973. Two transparent beryl varieties from the Kaatiala pegmatite, Finland. Bull. Geol. Soc. Finland, 45, 125-130.

Exley, R. A., 1980. Microprobe studies of REE- rich accessory minerals: implications for Skye granite petrogenesis and REE mobility in hydrothermal systems. Earth Planet. Sci. Lett., 48, 97-110.

Feofilov, P. P., 1956. On the nature of the green color of fluorite. Mem. Soc. Russe Min., 85, 569-71.

Fersman, A. E., 1930. Les pegmatites: Acad. Cienc. USSR. (French translation Univ. of Louvana, Belgica), vol., 3.

Fleet, M. E., 2002. Rock Forming Minerals: Geol. Soc. London. Vol. 3A.

Flyod, P. A. and Winchester, J. A., 1975. Magma type and tectonic setting discrimination using immobile elements. Earth Planet. Sci. Lett., 27, 211 -218.

Flyod, P. A. and Winchester, J. A., 1978. Identification and discrimination of altered and metamorphosed volcanic rocks using immobile elements. Chem. Geol., 21, 291 - 306.

Foord, E. E., 1976. Mineralogy and petrogenesis of layered pegmatite-aplite dikes in the Mesa Grande District, San Diego County, California. Ph.D. thesis, Stanford Univ., Stanford, California.

Foord, E. E., Starkey, H. C. and Taggart, J. E., 1986. Mineralogy and paragenesis of "pocket" clays and associated minerals in complex granitic pegmatites, San Diego County, California. Am. Min., 71, 428 - 439.

Fraser, J. E., Searle, M. P., Parrish, R. R. and Noble, S. R., 2001. Chronology of deformation, metamorphism, and magmatism in the southern Karakoram Mountains. Bull. Geol. Soc. Am., 113, no. 11, 1443 -1455.

Frondel, J. W., 1964. Variation of some rare earths in allanite. Am. Min., 49, 1159-77.

Fuchs, G., 1977. Traverse of Zanskar from the Indus to the Valley of Kashmir - a preliminary note. Jahrbuch der Geologischen Bundesanstalt (Austria), 120 (2), 219 -229.

Fujiwara, S., Nagashima, K. and Chiba, M., 1965. A variety of zircon from Oro, Kyoto Prefecture, Japan. J. Chem. Soc. Japan (Pure Chem. Sect.), 86, 646-647 (in Japanese with English Summary).

Gaetani, M., Angiolini, L., Garzanti, E., Jadoul, F., Leven, E. Y., Nicora, A. and Sciunnach, D., 1995. Permian stratigraphy in the northern Karakoram, Pakistan, Riv. Ital. Pal. Strat., 101 (2), 107 -152.

Gaetani, M., 1997, The Karakoram block in Central Asia, from Ordovician to Cretaceous. *Sediment. Geol.*, 109, 339–359.

Gaetani, M., Casnedi, R., Fois, E., Garzanti, E., Jadoul, F., Nicora, A. and Tintori, A., 1985. Stratigraphy of the Tethys Himalayan in Zanskar, Ladakh. Rivista Italiana di Paleontologie e Stratigra., 91, 443 - 478.

Gaetani, M., Garzanti, E., Flavio, J., Nicora, A., Tintori, A., Pasini, M. and Sabir, A. K. K., 1990. The north Karakoram side of the Central Asia geopuzzle. Geol. Soc. Am. Bull., 102, 54 - 62.

Gallagher, M. J., 1975. Composition of some Rhodesian lithium-beryllium pegmatites. Trans. Geol. Soc. South Africa, 78, 35-41.

Gansser, A., 1964. Geology of the Himalayas. John Wiley, New York, 289p.

Gansser, A., 1979. The division between Himalaya and Karakoram, Proc. Intern.Commit. Geodynamics, Grp. 6, Mtg. Peshawar, Nov. 22 - 29, 1979. Spec, Issue, Geol. Bull. Univ. Peshawar.

Gee, E. R., 1989. Overview of the geology and structure of the Salt Range, with observations on related areas of northern Pakistan. In: Tectonics of the Western Himalaya (Maliconico, L.L. and Lillie. R. J., eds.), Geol. Soc. Am., Spec. Pap., 232, 95 -112.

George, M. T., Harris, N. B. W. and Butler, R. W. H., 1993. The tectonic implications of contrasting granite magmatism between the Kohistan island arc and the Nanga-Parbat Haramosh Massif, Pakistan Himalaya. . In: Himalayan Tectonics (Treloar, P. J. and Searle, M. P., eds.). Geol. Soc. London., Spec. Publ. 74, 173 -191.

Ghazanfar, M., Chaudhry, M. N. and Hussain, M. S., 1991. Geology and petrotectonics of southeast Kohistan, NW Himalaya, Pakistan. Kashmir J. Geol., 8 and 9, 67 - 97.

Ginsburg, A. I., Timofeyev, I. N. and Feldman, L. G., 1979. Principles of geology of the granitic pegmatites. Nedra Moscow, 296 pp., in Russian.

Gjelsvik, T., 1957. Geochemical and mineralogical investigations of titaniferous iron ores, west coast of Norway. Econ. Geol., 52, 482.

Green, T. H.,1977. Garnet in silicic liquids and its possible use as a P-T indicator. Contrib. Mineral. Petrol., 65, 59 -67.

Gresens, R. L., 1966. Dimensional and compositional control of garnet growth by mineralogical environment. Am. Min., 51, 524-528.

Gubelin, E., 1981. Pakistan enters the gem scene, Gems and Gemology, 17, 180-181.

Guillot, S., and Le Fort, P., 1995. Geochemical constraints on the bimodal origin of High Himalayan leucogranites. Lithos, 35, 221 - 234.

Hall, A., 1965. The origin of accessory garnet in the Donegal granite. Min. Mag., 35, 628-633.

Halleran, A. A. D. and Russell, J. K. 1996. REE-bearing alkaline pegmatites and associated light REE-enriched fenites at Mount Bisson, British Columbia. Econ. Geol., 91, 451 - 459.

Halliday, A. N., Stephens, W. E. and Harmon, R. S., 1981. Isotope and chemical constraints on the development of peraluminous Caledonian and Acadian granites. Can. Min., 19, 205 - 216.

Hamidullah, S. and Onslot, T. C., 1993. Ar / Ar evidence for Late Cretaceous formation of the Kohistan island arc, NW Pakistan. Kashmir J. Geol., 10, 105 - 122.

Hanni, H. A. and Gunawardene, M., 1982. Ferroaxinite: another new gem from Sri Lanka. J. Gemm., 18, 20-27.

Hanson, C. R., 1986. Bedrock geology of the Shigar valley area Skardu, Northern Pakistan. Unpubl. M.S. Thesis, Dartmouth College, New Hampshire, 124 p.

Hanson, C. R., 1989. The northern suture in the Shigar valley, Baltistan, Northern Pakistan. In: Tectonics of the Western Himalaya (Maliconico, L.L. and Lillie. R. J., eds.) Geol. Soc. Am., Spec. Pap., 232, 202 - 216.

Harker, A., 1909. The natural history of igneous rocks. Methuen, London.

Harris, N. and Massey, J. 1994. Decompression and anatexis of Himalayan metapelites. Tectonics 13, 1537 - 46.

Harrison, T. M., Grove, M., Lovera, O. M. and Catlos, E. J.,1998. A model for the origin of Himalayan anatexis and inverted metamorphism. J. Geophy. Research, 103, 27, 071 -32.

Hart, R. A., 1970. Chemical exchange between sea-water and deep ocean basalts. Earth Planet. Sci. Lett., 9, 269 – 279.

Hart, S. R., Brooks, C., Krogh, T. E., Davis, G. L. and Nava, D., 1970. Ancient and modern volcanic rocks; a trace element model. Earth Planet. Sci. Lett., 15, 17 -20.

Hasegawa, S., 1957. Chemical studies of allanites and their associated minerals from the pegmatites in the northern part of the Abukuma massif. Sci. Rept. Tohoku Univ., ser. 3, 5, 345- 371.

Hattori, H., Sugisaki, R. and Tanaka, T., 1972. Nature of hydration in Japanese Palaeozoic geosynclinal basalt. Earth Planet. Sci. Lett., 15, 271 - 285.

Hawthorne, F. C. and Černý, P., 1977. The alkali-metal positions in Cs-Li beryl. Can. Min., 15, 414 - 421.

Hayden, H. H., 1915. Notes on the geology of Chitral, Gilgit and the Pamirs. Geol. Surv. India, Rec., 45, 4: 271 -335.

Heinrich, E. W., 1946. Studies in the mica group; the biotite-phlogopite series. Am.. J. Sci., 244, 836.

Heinrich, E. W., 1953. Zoning in pegmatite districts. Amer. Min., 38, 68 -87.

Herrera, A. O., 1968. Geochemical evolution of zoned pegmatites of Argentina. Eco. Geol. 63, 13 – 29.

Honegger, K., Dietrich, V., Frank, W., Gansser, A., Thoni, M. and Trommsdorf, V., 1982. Magmatism and metamorphism in the Ladakh Himalayas (the Indus Tsangpo suture zone). Earth Planet. Sci. Lett., 60, 253 - 292.

Honegger, K., Le Fort, P., Mascle, G. and Zimmerman, J. L., 1989. The blueschists along the Indus Suture Zone in Ladakh, N. W. Himalaya. J. Metamor. Geol., 7, 57 - 72.

Honnegger, K., Dietrich, V., Frank, W., Gansser, A., Thoni, M. and Trommsdroff, V. 1982. Magmatism and metamorphism in the Ladakh Himalaya (the Indus Tsangpo suture zone). Earth Planet. Sci. Lett., 60, 253-293.

Howie, R. A. and Walsh, J. N., 1982. The geochemistry and mineralogy of an epidote glaucophanites from Hacava, Spissko-gemerske rudohorie mts., West Carpathians, Czechoslovakia. Geologicke Prace, 78, 59 - 64.

Howie, R. A., 1955. The geochemistry of the charnockite series of Madras, India. Trans. Roy. Soc. Edin., 62, 725.

Huerta, A. D., Royden, L. H. and Hodges, K. V., 1998. The thermal structure of the collisional orogens as a response to accretion, erosion, and radiogenic heat production. J. Geophy. Research, 103, 15, 287 - 302.

Hutton, C. O., 1951a. Allanite from Yosemite National Park, Tuolumne Co., California. Am. Min., 36, 233 - 48.

Hutton, C. O., 1951b. Allanite from Wilmot Pass, Fiordland, New Zealand. Am. J. Sci., 249, 208 -14.

Ito, J. and Frondel, C.1968. Synthetic zirconium and titanium garnets. Am. Min. 52, 773 - 81.

Ivanac, J. F., Traves, D. M. and King, D., 1956. The geology of the N. W. portion of the Gilgit Agency. Geol. Surv. Pakistan., Rec. 8 (2), 3 -26.

Ivanov, A. N., Shirayeva, V. A. and Shimakin, B. M., 1979. Again on the composition of allanite from West Cisbaikalia pegmatites. Geochemistry and endogenic processes. Acad. Sci. USSR, Sibrian Branch, Irkutsh, 178 - 82.

Jahns, R. H. and Tuttle, O. F. 1963. Layered pegmatite-aplite intrusions. Spec. Pap. Min. Soc. Am., 1, 78 - 92.

Jahns, R. H., 1953. The genesis of pegmatites. 1. Occurrence and origin of giant crystals. Am. Min., 38, 563 - 598.

Jahns, R. H., 1955. The study of pegmatites. Eco. Geol. 50th Anniv. vol. 1025 - 1130.

Jahns, R. H. and Burnham, 1969. Experimental studies of pegmatite genesis; 1. A model for the derivation and crystallization of granite pegmatites. Econ. Geol., 64, 843 - 864.

Jahns, R. H., 1982. Internal evolution of pegmatite bodies. In: Granitic pegmatites in science and industry (P. Ćerný, ed.). Min. Assoc. Can. Short Course Handbook, 8, 293 -327

Jahns, R.H. and Ewing, R. C., 1977. The Harding mine, Taos County, New Mexico. Min. Rec., 8, 115 -126.

Jamieson, R. A., Beaumont, C., Fullsack, P. and Lee, B., 1998. Barrovian regional metamorphism: where is the heat? In: What derives metamorphism and metamorphic reactions? (Treloar, P. J. and O' Brien, P. J., eds.) Geol. Soc., London, 23 - 51.

Jan, M. Q. and Howie, R. A., 1980. Ortho and clinopyroxenes from granulites of Swat Kohistan, northern Pakistan. Min. Mag., 43, 715 - 728.

Jan, M. Q. and Howie, R. A., 1981. The mineralogy and geochemistry of the metamorphosed basic and ultrabasic rocks of the Jigal complex, Kohistan, NW Pakistan. J. Petrol., 22, 85 - 126.

Jan, M. Q. and Karim, A., 1995. Coronas and high pressure veins in metagabbros of Kohistan island arc, N. Pakistan: evidence for crustal thickening during cooling. J. Metam. Geol., 13, 357 – 366.

Jan, M. Q. and Kempe, D. R. C., 1973. The petrology of the basic and intermediate rocks of Upper Swat, Pakistan. Geol. Mag., 110, 285 - 300.

Jan, M. Q. and Mian, I., 1971. Preliminary geology and petrography of Swat Kohistan, Geol. Bull. Univ. Peshawar, 6, 1 - 32.

Jan, M. Q., 1977. The mineralogy, Petrology, and Geochemistry of Swat Kohistan, NW Pakistan. Ph. D. Thesis. Univ. London, 349p.

Jan, M. Q., 1979. Petrography of the amphibolites of Swat and Kohistan. Geol. Bull. Univ. Peshawar, 11, 51 - 64.

Jan, M. Q., 1988. Geochemistry of amphibolites from the southern part of the Kohistan arc, N. Pakistan. Min. Mag., 52, 147 - 159.

Jan, M. Q., 1990. Petrology and geochemistry of the southern amphibolites of the Kohistan arc, N. Pakistan. Phys. Chem. Earth, 17, 71 - 92.

Jan, M. Q. and Khan, M. A., 1983. Geochemistry of tonalites and quartz diorites of the Kohistan - Ladakh (Trans-Himalayan) granitic belt in Swat, N. Pakistan. In: Granites of Himalayan, Karakoram and Hindu Kush (Shams, F. A., ed.). Inst. Geol., Punjab Univ., Lahore, 355 - 376.

Jan, M. Q., Asif, M., Tahirkheli, T. and Kamal, M., 1981. Tectonic subdivision of granitic rocks of north Pakistan. Geol. Bull. Univ. Peshawar, 14, 159 - 182.

Jan, M. Q., Banarass, M., Ghani, A. and Asif, M. 1983. The Tora Tigga ultramafic complex, southern Dir district. Geol. Bull. Univ. Peshawar, 16, 11 - 29.

Jan, M. Q., Khan, M. A. and Qazi, M. S., 1993. The Sapat mafic-ultramafic complex, Kohistan arc, North Pakistan. In: Himalayan Tectonics (Treloar, P. J. and Searle, M. P. eds.). Geol. Soc. London., Spec. Publ. 74, 113 -121.

Jan, M. Q., Khattak, M. U. K., Parvez, M. K. and Windley, B. F., 1984. The Chilas stratiform complex: field and mineralogical aspects. Geol. Bull. Univ. Peshawar, 17, 153 - 169.

Jobbins, E. A., Tresham, A. and Young, B. R., 1975. Pale blue axinite from East Africa. J. Gemm., 14, 368 - 75.

Johnson, B. D., Powell, C. M. A. and Veevers, J.J., 1976. Spreading history of the eastern Indian Ocean, and Greater India's northward flight from Antarctica and Australia. Bull. Geol. Am., 87, 1560 - 1566.

Johnson, N. M., Stix, J., Cerveny, P. F., and Tahirkheli, R. A. K., 1985. Paleomagnetic chronology, fluvial processes, and tectonic implications of the Siwaliks deposits near Chingi Village, Pakistan. J. Geol., 93, 27 - 40.

Jolliff, B. L, Papike, J. J. and Shearer, C. K., 1986. Tourmaline as a recorder of pegmatite evolution; Bob Ingersoll Pegmatite, Black Hills, South Dakota. Am. Min., 71, 472 - 500.

Jolliff, B. L., Papike, J. J. and Shearer, C. K., 1992. Petrogenetic relationships between pegmatite and granite based on the geochemistry of muscovite in pegmatitic wall zones, Black Hills, South Dakota. Geochim. Cosmochim. Acta, 56, 1915 -1939.

Kakar, S. K., Badshah, M. S. and Khan, J., 1971. The geology of the Jandul valley, Western Dir, Geol. Bull. Univ. Peshawar, 6, 54 - 73.

Kazmi, A. H. and Jan, M.Q., 1997. Geology and tectonics of Pakistan. Graphic Publishers, Karachi, 554p.

Kazmi, A. H. and O' Donoghue, M. 1990. Gemstones of Pakistan. Gemstone Corp. Pakistan, 146 p.

Kazmi, A. H., Lawrence, R. D., Dawood, H., Snee, L. W. and Hussain, S. S., 1984. Geology of the Indus Suture Zone in the Mingora-Shangla area of Swat, northern Pakistan. Geol. Bull. Univ. Peshawar.

Kazmi, A. H., Peters, J. J. and Obodda, H. P. 1985. Gem-pegmatites of the Shingus-Dassu area, Gilgit, Pakistan. Min. Rec., 16, 393 - 411.

Khan, M. A., 1997. Tectonic evolution of southeast Kohistan, Northwest Himalaya, Pakistan. Unpubl. Ph. D Thesis, Univ. Peshawar.

Khan, M. A. and Coward, M. P., 1990. Entrapment of an island arc in collision tectonics: A review of the structural history of the Kohistan arc complex, N. W. Himalayas. Phy. Chem. Earth, 17, 1 - 18.

Khan, M. A. and Jan, M. Q., 1992. Some fundamental field and petrographic aspects of the Chilas mafic-ultramafic complex, Kohistan arc, northern Pakistan. Acta Miner. Pak., 6, 126 - 147.

Khan, M. A. and Thirlwall, M. F., 1988. Babusar amphibolites: arc tholeiites from the southern Kohistan arc, N. Pakistan. Geol. Bull. Univ. Peshawar, 21, 147 -158.

Khan, M. A., 1988. Petrology and structure of the Chilas Ultramafic-mafic Complex, N. Pakistan. Unpubl. Ph. D. Thesis, Univ. London.

Khan, M. A., Jan, M. Q. and Weaver, B. L., 1993. Evolution of the lower arc crust in Kohistan, N. Pakistan. In: Himalayan Tectonics (Treloar, P. J. and Searle, M. P., eds.). Geol. Soc. London., Spec. Publ. 74, 123 -138.

Khan, M. A., Jan, M. Q., Winley, B. F., Tarney, J. and Thirlwall, M. F., 1989. The Chilas mafic-ultramafic igneous complex, the root of island arc in the Himalaya of northern Pakistan. In: Tectonics of the Western Himalaya (Maliconico, L.L. and Lillie, R. J., eds.). Geol. Soc. Am., Spec. Pap., 232, 75 - 94.

Khan, T. 1994. Evolution of the "Upper and middle crust in Kohistan island arc", northern Pakistan. Unpubl. Ph. D thesis. Univ. Peshawar. 225p.

Khan, T., Khan, M. A. and Jan, M. Q., 1994. Geology of a part of the Kohistan terrain between Gilgit and Chilas, northern areas, Pakistan. Geol. Bull. Univ. Peshawar. 27, 99 - 112.

Khan, T., Khan, M. A. Jan, M. Q., and Naseem, M., 1995. Back-arc basin assemblages in Kohistan, Northern Pakistan, Geodynam. Acta, 9(1), 30 - 40.

Kleck, W. D. and Foord E. E., 1999.The chemistry, mineralogy, and petrology of the George Ashley Block pegmatite body. Am. Min., 84, 695 - 707.

Klootwijk, C. T., Gee, J. S., Peirce, J. W. and Mc Fadden, P. L., 1992. An early India-Eurasia contact; Palaeomagnetic constraints from the Ninety East Ridge, ODP Leg 121. Geol., 20, 395 - 398.

Klootwijk, C. T., Sharma, M. L., Gergan, J., Tirkey, B., Shah, S. K. and Agarwal, V., 1979. The extent of Greater India, II. Palaeomagnetic data from the Ladakh intrusives at Kargil, northwestern Himalaya. Earth Planet. Sci. Lett., 44, 47 - 64.

Knorring, O. von. and Hornung, G., 1961. Hafnian zircons. Nature, 190, 1098 - 1099.

Kosals, Ya. A. and Mazurov, M. P., 1968. Behaviour of the rare alkalis, boron, fluorine, and beryllium during the emplacement of the Bitu-Dzhida granitic batholith, sourthwest Bakalia. Geochem. Int., 5, 1024-1034.

Koster, V. G. and Wyllie, P. J., 1968. Melting relationships in the system $NaAlSi_3O_8$-NaF- $H_2O$ to 4 kilobars. J. Geol. 76, 50 70.

Kozlov, V. D., 1969. Use of concentrator minerals in evaluation of rarer-element accumulation in the differentiation products of granitoid intrusions. Geochem. Int., 6, 269-280.

Krogstad, E. J., Walker, R. j., Nabelek, P. I. and Russ-Nabelek, C., 1991. Pb isotopic constraints on the origin of the Harney Peak Granite and spatially associated pegmatites, Black Hills, South Dakota. Trans. Am. Geophys. Union 72, 543 (abstr.)

Kumskova, N. M. and Khostova, V. A., 1964. X- ray study of the epidote-allanite group of minerals. Geochem. Intern., 4, 676-86.

Kuno, H., 1968. Differentiation of basaltic magmas. In: Basalts (Hess, H. H., and Poldervaart, A., eds.). The Poldervaart Treatise on rocks of basaltic composition, John Wiley and Sons, New York, 623 - 688.

Kurshakova, L. D., 1976. Physical-chemical conditions of formation of Skarn borosilicate deposits. Moscow (Nauka).

Larsen, E. S. Jr. and Draisin, W., 1950. Composition of the minerals in the rocks of the Southern California Batholith. Int. Geol. Congress, Report of 18th Session, Great Britain, 1948, Part 111, P. 66.

Laurs, B. M., Dilles, J. H., Wairrach, Y., Kausar, A. B. and Snee, L. W., 1998. Geological setting and petrogenesis of symmetrically zoned, miarolitic granitic pegmatites at Stak Nala, Nanga Parbat Haramosh Massif, Northern Pakistan. Can. Min. 36, 1- 47.

Le Fort, P., Cuney, M, Deneil, C., France- Lanord, Sheppard, S. M. F., Upreti, B. N. and Vidal, P.,1987. Crustal generation of Himalayan leucogranites, Tectnophysises, 134, 39 - 57.

Le Fort, P., 1975. Himalaya: the collided range; present knowledge of the continental arc. Am. J. Sci., 275A: 1- 44.

Le Fort, P., 1981. Manaslu leucogranite: A collisional signature of the Himalaya, a model for its genesis and emplacement, J. Geophys. Res., 86, 10545 - 10568.

Le Fort, P., Cuney, M., Deneil, C., France - Lenord, C., Sheppard, S. M. F., Upreti, B. N., and Vidal, P., 1987. Crustal generation of Himalayan leucogranites. Tectonophysics, 134, 39 - 57.

Le Fort, P., Debon, F. and Sonet, J., 1980. The "Lesser Himalayan" cordierite granite belt topology and age of the pluton of Mansehra (Pakistan). Geol. Bull. Univ. Peshawar.

Le Fort, P., Debon, F., and Sonet, J., 1983a. The Lower Palaeozoic "Lesser Himalayan Granitic Belt": Emphasis on the Simchar Pluton of the Central Nepal. In: Granites of Himalayan, Karakoram and Hindu Kush (Shams, F. A., ed.). Inst. Geol., Punjab Univ., Lahore, 217 - 255.

Le Fort, P., Lemennicierr, Y., Lombardo, B., Pecher, A., Pertusati, P., Pognante, H. and Rolfo, F., 1995. Preliminary geological map and description of the Himalayan-Karakoram junction in Chogo Lungma to Turmik area (Baltistan, northern Pakistan). J. Nepal Geol. Soc., 11, 17 - 38.

Le Fort, P., Tongiorgi, M. and Gaetani, M., 1994. Discovery of a crystalline basement and Early Ordovician marine transgression in the Karakoram Mountain Range, Pakistan, Geol., 22, 941 - 944.

Le Fort, P.,Michard, A., Sonet, J. and Zimmermann, J. L., 1983b. Petrography, geochemistry and geochronology of some samples from Karakoram axial batholith (northern Pakistan). In: Granites of Himalayas, Karakoram and Hindu Kush (Shams, F. A. ed.). Inst. Geol., Punjab Univ., Lahore, 377 - 387.

Leonova, V. A. and Galibin, V. A. 1963. Ratio of zirconium and hafnium in zircons from pegmatites and gneisses enclosing them in the White Sea region. Dokl. Acad. Sci. USSR, Earth Sci. Sec., 153, 163-166.

Linen, R. L., William- Jones, A. E. and Martin R. F. 1992. Evidence of magmatic cassiterite mineralization at the Nong Sua aplite-pegmatite complex, Thailand. Can. Min., 30, 739 - 61.

Linnen, L. R., 1998. The solubility of Nb – TA – Zr – Hf – W in granitic melts with Li and Li + F: constraints for mineralization in rare metal granites and pegmatites. Econ. Geol., 93, 1013 - 1025.

London, D., 1986a. Magmatic-hydrothermal transition in the Tanco Rare-element pegmatite: Evidence from fluid inclusions and phase-equilibrium experiments. Am. Min., 71, 376 -395.

London, D., 1982. Stability of spodumene in acidic and saline fluorine-rich environments. Carneigie Inst. Wash. Year Book, 81, 331-334.

London, D., 1983. The magmatic-hydrothermal transition in rare-element pegmatites: fluid inclusion evidence from the Tanco mine, Manitoba. Trans. Am. Geophys. Union, 65, 549 (abstr).

London, D., 1986b. Formation of tourmaline-rich gem pockets in miarolitic pegmatites, Am. Min., 71, 396 - 405.

London, D., 1992. The application of the experimental petrology to the genesis and crystallization of granitic pegmatites. Can. Min., 30, 499 - 540.

London, D., 1996. Granitic pegmatites. Trans. Roy. Soc. Edinburgh. Earth Sci. 87, 305 - 319.

London, D. and Burt, M. D., 1982. Lithium minerals in pegmatites. In: Granitic Pegmatites in Science and Industry (P. Černý, ed.). Min. Assoc. Can., Short Course Handbook 8, 99-133.

London, D., Hervig, R. L., and Morgan, G. B. 1988. Melt-vapor solubilities and element partitioning in peraluminous granite-pegmatite systems. Experimental results with Macusani glass at 200 Mpa. Contr. Min. Petro., 99, 360 - 373.

Luth, W. C., Jahns, R. H., and Tuttle, O. F. 1964. The granite system at pressures of 4 to 10 kilobars. J. Geophy. Res., 69, 759 - 773.

Lyakhovich, V. V. and Shevaleyevskii, I. D., 1962. Zr: Hf ratio in the accessory zircon of granitoids. Geochemistry, no. 5, 508-524.

Lyons, J. B., 1961. Uranium and thorium in the older pluton rocks of New Hampshire. Prof. Paper. US Geol. Surv., 424B, 69-71.

MacDonald, D. J, Hawthorne, F .C. and Grice, J .D. 1993 .Foitite, [$Fe_2$ (Al, Fe)] $Al_6Si_6O_{18}(BO_3)_3(OH)_4$, a new alkali-deficient tourmaline: Description and crystal structure. Am. Min., 78, 1299 -1303.

Maniar, P. D. and Piccoli, P. M., 1989. Tectonic discrimination of granitoids. Geol. Soc. Am., Bull., 101, 635- 643.

Manning, D. A. C., 1981. The effect of fluorine on liquidus phase relationships in the system Qz - Ab - Or with excess water at 1 kb. Contr. Min. Petrol., 76, 206 - 215.

Marcus T., Sweetapple, M. T. and Collins, P. L. F., 2002. Genetic framework for the classification and distribution of Archean Rare Metal Pegmatites in the North Pilbara Craton, Western Australia. Econ. Geol., 97, 873 - 895.

Martin, N. R., Siddique, S. F. A. and King, B. H., 1962. A geological reconnaissance of the region between the lower Swat and Indus river of Pakistan. Geol. Bull. Punjab Univ., 2, 1 -13.

Martin, H., 1987. Petrogenesis of Archean trondhjemites, tonalites, and granodiorites from Eastern Finland: major and trace element geochemistry. J. Petrol., 23, 921 – 953.

Martin, R. 1996. Evaluation and mining of the Pippingarra potash feldspar deposit: Perth.

Matsushita, S. and Huzita, K. (eds.), 1965. Geology of the Karakoram and Hindukush; Results of the Kyoto Univ. Sci. Exped. 1955, 160 p. Kyoto Univ., Japan.

Melentyev, G., B., 1961. The first finding of pollucite in the granitic pegmatites of Sayan. Dokl. Acad. Sci. U.S. S. R., Earth Sci. Sect. 141, 1287-1289.

Middlemiss, C.S. and Parshad, L.J. 1918. Note on the aquamarine mines of Dassu on the Braldu River, Shigar valley, Baltistan, Geol. Surv. India, Rec., 45, 160 - 172.

Milan, N. and Taylor, M. C., 2000. Foitite: formation during late stages of evolution of complex granitic pegmatites at Dobrá Voda, Czech Republic, and Pala, California, U.S.A. Can. Min. 38, 1399 - 408.

Miller, D. J., Loucks, R. R. and Ashraf, M., 1991. Platinum group element mineralization in the Jijal layered ultramafic - mafic complex, Pakistani Himalaya. Econ. Geol., 86, 1093 - 1102.

Milton, C., Hildebrand, F. A. and Sherwood, A. M., 1953. The identity of tinzenite with manganoan axinite. Am. Min., 38, 1148 - 58.

Misch, P., 1949. Metasomatic granitization of batholithic dimensions, Part I: syntectonic granitization in Nanga Parbat area, North West Himalaya. Am. J. Sci., 247, 209 - 245.

Molnar, P., 1988. A review of the geophysical constraints on the deep structure of the Tibetan Plateau, the Himalaya and Karakoram, and their tectonic implications. Phil. Trans. R. Soc., London., A. 326, 33 - 88.

Morgan, G. B. and London, D. 1999. Crystallization of the Little Three layered pegmatite- aplite dike, Ramona District, California. Contr. Min. Petrol., 136, 310-30.

Morgan, G. B. and London, D., 1987. Alteration of amphibolitic wallrocks around the Tanco rare-elemnt pegmatite, Bernic Lake, Manitoba. Am. Min, 72, 1097 - 1121.

Morteani, G., Preinfalk, C., Spiegel, W., and Bonalumi, A., 1995.The Achala granitic complex with the pegmatites of the Sierras Pampeanas (Northwest Argentina); a study of differentiation. Econ. Geol., 90: 636 - 647.

Mulja, T., Williams - Jones, A. E., Wood, S. A. and Boily, M., 1995. The Rare-element enriched monzogranite -pegmatite - quartz vein systems in the Preissac - Lacorne batholith, Quebec. 11. Geochemistry and petrogenesis. Can. Min., 33, 817 - 833.

Mulja, T., Williams-Jones, A., E., Martin, R. F. and Wood, S. A., 1996. Compositional variation and structural state of columbite-tantalite in rare-element granitic pegmatites of the Priessac-Lacorne batholith, Quebec, Canada. Am. Min., 81, 146 - 157.

Murthy, M. V. N., 1958. On the crystallization of accessory zircon in granitic rocks of magmatic origin. Can. Min., 6, 260-263.

Nabelek, P. I. and Glascock, M. D., 1995. REE - depleted leucogranites, Black Hills, South Dakota, USA: a consequence of disequilibrium melting of monazite-bearing schists. J. Petrol., 36, 1055 - 71.

Nabelek, P. I. and Liu, M., 2004. Petrologic and thermal constraints on the origin of leucogranites in collisional orogens. Trans. Royal Soc. Edinburgh: Earth Series, 95, 73 - 85.

Nabelek, P. I. and Bartlett, C. D., 1998. Petrologic and geochemical links between the post-collisional Proterozoic Harney Peak leucogranites, South Dakota, USA, and its source rocks, Lithos, 45, 71 - 85.

Nabelek, P. I., Russ - Nabelek, C. and Denison, J. R., 1992a. The generation and crystallization conditions of the Proterozoic Harney Peak leucogranite, Black Hills, South Dakota, USA: petrologic and geochemical constraints, Contr. Min. and Petrol., 110, 173 - 91.

Nabelek, P. I., Russ - Nabelek, C. and Hausseler, T., 1992b. Stable isotope evidence for the petrogenesis and fluid evolution in the Proterozoic Harney Peak leucogranite, Black Hills, South Dakota, USA: Geochim. Cosmochim. Acta 56, 403 - 417.

Nakata, T., 1989. Active faults of the Himalaya of India and Nepal. In: Tectonics of the Western Himalaya (Maliconico, L.L. and Lillie. R. J. eds.). Geol. Soc. Am., Spec. Pap., 232, 243 - 264.

Naldrett, D. L., Lachaine, A. and Naldrett, S. N., 1987. Rare earth elements, thermal history, and the color of natural fluorites. Can. J. Earth Sci., 24, 2082 - 8.

Norin, E., 1946. Geological Exploration in West Tibet: report on Sino-Swedish Expedition 29. Sweden Aktiebolaget Thule, Stockholm, 214p.

Norton, J. J. and Redden, J. A., 1990. Relations of zoned pegmatites to other pegmatites, granite, and metamorphic rocks in the southern Black Hills, South Dakota, Am. Min. 75, 631 - 55.

Norton, J. J., 1973. Lithium, cesium, and rubidium - the rare alkali metals. In: United States Mineral Resources (D.A. Brobst and W. P. Pratt, eds.). U.S. Geol. Surv. Prof. Pap. 820, 365 - 378.

Norton, J. J., 1983. Sequence of mineral assemblages in differentiated granitic pegmatites. Econ. Geol., 78, 854 – 874.

Norton, J. J., Page, L. R. and Brobst, D. A., 1962. Geology of the Hugo pegmatite, Keystne, South Dakota. U. S. Geol. Surv. Prof. Paper, 297 - B, 49 - 126.

O' Connor, J. T., 1965. A classification for quartz rich igneous rocks based on feldspar ratios. U. S. Geol. Surv., Prof. Paper- 525B, 79 - 84.

Parrish, R.R. and Tirrul, R. 1989. U-Pb age of the Baltoro granite, northwest Himalaya, and implications for zircon inheritance and monazite U-Pb systematics. J. Geol., 17, 1076 - 1079.

Patriat, P. and Achache, J., 1984. India-Eurasia collision chronology and its implications for crustal shortening and deriving mechanisms of plates. Nature, 311, 615 - 621.

Pavlova, I. G., 1963. Dependence of refractive indices of beryl on composition and mode of genesis. Dokl. Acad. Sci., USSR, Earth Sci. Sect., 150, 109-112.

Pearce, J. A., 1975. Basalt geochemistry used to investigate past tectonic environments on Cyprus. Tectonophysics, 25, 4 - 67.

Pearce, J. A. and Cann, J. R., 1973. Tectonic setting of basic volcanic rocks determined using trace element analysis. Earth Planet. Sci. Lett., 38, 211 -326.

Pearce, J. A., 1976. Statistical analysis of major element pattern in basalts. J. Petrol., 17, 15 - 43.

Pearce, J. A., Harris, N. B. W. and Tindle, A. G., 1984. Trace element discrimination diagrams for the tectonic interpretation of granitic rocks. J. Petrol., 25, 956-983.

Petro, W. L., Vogel, T. A. and Wilband, J. T., 1979. Major element chemistry of plutonic rock suits from compressional and extensional plate boundaries. Chem. Geol., 26, 217- 235.

Petterson, M. G. and Windley, B. F., 1986. Petrology and geochemical evolution of the Kohistan arc batholith, Gilgit, N. Pakistan. Geol. Bull. Univ. Peshawar, 19, 131-149.

Petterson, M. G. and Windley, B. F., 1991. Changing source regions of magmas and crustal growth in the Trans-Himalayas: Evidence from the Chalt volcanics and the Kohistan batholith, Kohistan, N. Pakistan. Earth Planet. Sci. Lett., 102, 326- 346.

Petterson, M. G., 1985. The structure, petrology and geochemistry of the Kohistan batholith, Gilgit, Kashmir, N. Pakistan. Unpubl. Ph. D. thesis, Univ. Leicester, UK.

Petterson, M. G., Windley, B. F. and Luff, I. W., 1990a. The Chalt volcanics, Kohistan, N. Pakistan; High-Mg tholeiitic and low-Mg clac-alkaline volcanism in a Cretaceous island arc. Phy. Chem. Earth, 17, 19 – 30.

Petterson, M. G., Windley, B. F. and Sullivan, M., 1990b. A petrological, chronological, structural, and geochemical review of Kohistan batholith and its relationship to regional tectonics. Phy. Chem. Earth, 17, 47-70.

Petterson, M. G. and Windley, B. F., 1985. Rb-Sr dating of the Kohistan arc batholith in the Trans-Himalaya of N. Pakistan, and tectonic implication. Earth Planet. Sci. Lett., 74, 54 - 75.

Pohl, D., Guillemette, R., Shigley, J. and Dunning, G., 1982. Ferroaxinite from new Melones Lake, Calaveras County, California, a remarkable new locality. Min. Rec, 13, 293-302.

Poldervaart, A., 1956. Zircon in rocks. 2. Igneous rocks. Amer. J. Sci., 254, 521-554.

Pollard P.J. 1995. Geology of rare metal deposits: An introduction and overview, Econ. Geol., 90, No. 3, 489 - 494.

Powell, C. Mc A., 1979. A speculative tectonic history of Pakistan and surroundings: Some constraints from the Indian Ocean. In: Farah, A. and De Jong, K. A. (eds.), Geodynamics of Pakistan, Geol. Surv. Pakistan, Quetta, 5 – 24.

Powell, C. Mc. A. 1979. A speculative tectonic history of Pakistan and surroundings: some constraints from the Indian Ocean. In: Geodynamics of Pakistan (Farah, A. and De Jong, K. A. eds.). Geol. Surv. Pakistan, Quetta, 5 - 24.

Powell, C. Mc. A. and Conaghan, P. J., 1973. Plate tectonics and the Himalayas. Earth Planet. Sci. Lett., 20, 1 -12.

Pressley, R. A. and Brown, M., 1999. The Phillips pluton, Maine, USA: evidence of heterogeneous crustal sources, and implication for granite ascent and emplacement mechanisms in convergent orogens, Lithos, 46, 335 - 366.

Pudsey, C. J., 1986. The northern suture, Pakistan: Margin of a Cretaceous island arc. Geol. Mag., 123, 405 - 423.

Pudsey, C. J., Coward, M. P., Luff, I. W., Shackleton, R. M., Windley, B. F. and Jan, M. Q., 1985. Collision zone between the Kohistan arc and the Asian plate in NW Pakistan. Trans. Royal. Soc. Edinburgh: Earth Sci, 76, 463 - 479.

Punjab University Expedition to Baltistan, 1985.

Quensel, P., 1956. The paragenesis of the Varutrask pegmatite. Ark. Mineral. Geol. 2, 9-125.

Rai, H. and Pandi, I. C., 1982. Study of norite from the Kargil igneous complex, Indus Suture Zone, Ladakh, India. In: Sinha, A. K. (ed.). Contemporary Geoscientific researches in Himalaya, 2, Shiva, Dehra Dun, 41- 47.

Rao, A. T., Rao, G. A. and Rao, P. P., 1979. Fluorian allanite from calc-granulite and pegmatite contacts at Garividi, Andhra Pardesh, India. Min. Mag., 43, 312.

Redden, J. A., Peterman, Z. E., Zaetman, R. E. and Dewitt, E., 1990. U-Th-Pb zircon and monazite ages and preliminary interpretation of the tectonic development of Precambrian rocks in the Black Hills, Geol. Assoc. Canada, Spec. Paper, 37, 229 - 51.

Rex, A. J., Searle, M. P., Tirrul, R., Crawford, M. B., Prior, D. J., Rex, D. C. and Barnicoat, A., 1988. The geochemical and tectonic evolution of the central Karakoram, north Pakistan, Phil. Trans. Roy. Soc. London, series A, 326, 229-255.

Richwood, P. C., 1968. On recasting analyses of garnet into end-member molecules. Contr. Min. Petrol., 18, 175-198.

Ringuette, L., Martingale, J. and Windley, B. F., 1999. Magmatic crystallization, isobaric cooling, and decompression of the garnet - bearing assemblages of the Jigal sequence (Kohistan terrane, Western Himalayas), Geol., 27, 139 -142.

Roberston, A. and Degnon, P., 1994. The Dras arc complex: Lithofacies and reconstruction of a Late Cretaceous oceanic volcanic arc in the Indus suture zone, Ladakh Himalaya. Sed. Geol., 92, 117 - 145.

Roda, E., Pesquera, A. and Velasco, F., 1995. Tourmaline in granitic pegmatites and their country rocks, Fregeneda area, Salamanca, Spain. Can. Min., 33, 835 - 848.

Roedder, E., 1981. Natural occurrence and significance of fluids indicating high temperature and pressure. Phy. Chem. Earth, 13, 9 -39.

Roedder, E., 1979. Natural occurrence and significance of fluids indicating high temperature and pressure. Nobel Symp. Chem. Geochem. Solutions at high temperature and pressure; lecture copy, 63p.

Roering, C., 1966. Aspects of the genesis and crystallization sequence of the Karbib pegmatites, South West Africa. Eco. Geol. 61, 1064 -1089.

Rosenberg, P. E., 1972. Paragenesis of the topaz-bearing portion of the Brown Derby no. 1 pegmatite, Gunnison County, Colorado. Am. Min., 57, 571-583.

Rossovskii, L, N., 1981. Rare element pegmatites with precious stones and conditions of their formation (Hindu Kush) (in Russian). Zapiski Vsesoyuznogo Mineralogicheskogo Obshchestva, 109, 301 - 311 (transl. Intern. Geol. Review, 23, 1312 - 1320, 1981).

Royden, L.H, 1993. The steady state thermal structure of eroding orogenic belts and accretionary prisms. J. Geophy. Res., 98, 4487 - 507.

Saito, T., 1950. Chemical composition of fluorites of Japan. J. Fac. Sci. Hokkaido Univ., Ser. 4, Geol. Min., 7, 307-314.

Sanero, E. and Gottardi, G., 1968. Nomenclature and crystal chemistry of axinites. Am. Min., 53, 1407-11.

Sano, S., Nakajima, T. and Khan, S. R., 1996. Geology and isotope geochemistry of the Jijal complex, Kohistan, northern Pakistan. Proc. Geosci. Colloq., 15, 127 - 135.

Scaillet, B., France - Lanord, C. and Le Fort, P., 1990. Badrinath - Gangtori plutons (Garhwal, India): petrological and geochemical evidence for fractionation processes in High Himalayan leucogranite. J. Vol. and Geotherm. Res., 44, 163 - 188.

Schaller., W. T., Stevens, R. E. and Jahns, R. H., 1962. An unusual beryl from Arizona. Am. Min., 11, 6 - 60.

Scharer, U. and Allegre, C. J., 1983. The Palung granite (Himalaya): high resolution U-Pb systematics in zircon and monazite. Earth Planet. Sci. Lett., 63, 423 - 432.

Scharer, U., Hamet, J. and Allegre, C. J.,1984b. The Trans-Himalaya (Gangdese) plutonic belt in the Ladakh region; a U-Pb and Rb-Sr study. Earth Planet. Sci. Lett., 67, 327 - 339.

Scharer, U., Xu, R. H. and Allegre, C. J.1986. U-(Th)-Pb systematics and ages of Himalayan leucogranites. Earth Planet. Sci. Lett., 77, 35 - 48.

Scharer, U., 1984a. The effect of initial $^{230}$Th disequilibrium on young U-Pb ages: The Makalu case, Himalaya, Earth Planet. Sci. Lett., 67, 191 - 204.

Schneider, H. J., 1957. Tektonik und magmatismus in N. W. Karakoram. Geol. Rundschau, 46, 426 - 476.

Schreyer, W. and Abraham, K., 1978. Prehnite / chlorite and actinolite / epidote mineral assemblages in the metamorphic igneous rocks of the la Helle and Challes, Venn-Stavelot-Massif, Belgium. Ann. Soc. Geol. Belgique, 101, 227 - 41.

Searle, M. P. and Fryer, B. J., 1986. Garnet, tourmaline and muscovite-bearing leucogranites, gneisses, and migmatites of the Higher Himalaya from Zanskar, Kulu, Lahoul and Kashmir. In: Collision Tectonics (Coward, M. P. and Ries, A. C. eds). Geol. Soc. London, Spec. Publ., 19, 185 - 201.

Searle, M. P. and Tirrul, R. 1991. Structural and thermal evolution of the Karakoram crust, J. Geol. Soc., London, 148, 65 – 82.

Searle, M. P. 1991. Geology and Tectonics of the Karakoram Mountains, John Willy and Sons, New York, 358 p.

Searle, M. P. and Khan, M. A., 1996. Geological map of north Pakistan and adjacent areas of northern Ladakh and western Tibet, scale 1: 650, 000, Oxford Univ., Oxford, England.

Searle, M. P. and Rex, A. J., 1989. Thermal model for the Zanskar Himalaya. J. Metam. Geol., 7, 127 - 134.

Searle, M. P., Crawford, M. B. and Rex, A. J., 1992. Field relations, geochemistry, origin and emplacement of the Baltoro granite, central Karakoram: Trans. Roy. Soc. Edinburgh. 83, 519 - 538.

Searle, M. P., Khan, M. A., Fraser, J. E. and Gough, S. J., 1999. The tectonic evolution of the Kohistan - Karakoram collision belt along the Karakoram Highway transect, north Pakistan. Tectonics, 18 (6), 929 - 949.

Searle, M. P., Parrish, R. R., Hodges, K. V., Hurford, A., Ayres, M. W. and Whitehouse, M, J., 1997. Shisha Pangma leucogranite, South Tibetan Himalaya; field relations, geochemistry, age, origin, and emplacement. J. Geol, 105, 295 -317.

Searle, M. P., Parrish, R. R., Tirrul, R. and Rex, D. C., 1990. Age of crystallization and cooling of the K2 gneiss in the Baltoro Karakoram. J. Geol. Soc., London, 147, 603 - 606.

Searle, M. P., Windley, B. F., Coward, M. P., Cooper, D. J. W., Rex, A. J., Rex, D., Tingdong, L., Xuchang, S. and Jan, M. Q., 1987. The closing of Tethys and the tectonics of the Himalayas. Bull. Geol. Soc. Am., 98, 678 - 701.

Searle, M. P., Rex, A. J., Tirrul, R., Rex, D.C, Barnicoat, A. and. Windley, B.F., 1989. Metamorphic, magmatic, and tectonic evolution of the Central Karakoram in the Biafo- Baltoro- Hushe regions of N. Pakistan, Geol. Soc. Am., Spec. Pap., 232,47-73.

Searle, M. P., Rex, A. J., Tirrul, R., Windley, B.F., St. Onge, M. and Hoffman, D. 1986. A geological profile across the Baltoro Karakoram Range, N- Pakistan, Geol. Bull. Univ. Peshawar, 19, 1- 12.

Shah, M. T., Majid, M., Hamidullah, S. and Shervais, J. W., 1992. Petrochemistry of amphibolites from the Shergarh Sar area, Allai Kohistan, N. Pakistan. Kashmir J. Geol., 10, 123 - 139.

Shah, M. T. and Majid, M., 1992. Petrology and chemistry of the ultramafic rocks from the Allai Kohistan section of the Indus Suture Zone in Hazara, N. Pakistan. Acta Miner. Pak., 6, 73 - 84.

Shah, M. T. and Ihtisham, 2002.

Shams, F. A.,1980. Origin of the Shangla blueschists, Swat Himalaya, Pakistan. Geol. Bull. Univ. Peshawar.

Shams, F. A. and Shafique, A., (eds.). 1984. Expedition to Baltistan. Geol. Bull. Univ. Punjab, 19, 1 - 67.

Shand, S. J., 1927. The eruptive rocks. Wiley, New York.
Shaw, H. R., 1972. Viscosities of magmatic silicate liquids: an empirical method of prediction. Amer. Jr. Sci., 272, 870 -893.
Shearer, C. K. and Papike, J. J., 1986. Distribution of boron in the Tip Top pegmatite, Black Hills, South Dakota. Geol. 14, 119 -123.
Shearer, C. K. & Papike, J. J., 1987. Mineralogical and chemical evolution of a Rare-element granite - pegmatite system: Harney Peak Granite Black, Hills, South Dakota. Geochim. Cosmochim. Acta, 51, 473 - 486.
Shearer, C. K., Papike, J. J. and Jollif, B. L., 1992. Petrogenetic links among granites and pegmatites in the Harney Peak Rare-element granite - pegmatite system, Black Hills, South Dakota. Can. Min., 30, 785 - 809.
Shearer, C. K., Papike, J. J. and Laul, J. C., 1985. Chemistry of potassium feldspars from three zoned pegmatites, Black Hills, South Dakota: Implications concerning pegmatite evolution. Geochim. Cosmochim. Acta, 49, 663 - 673.
Shearer, C. K., Papike, J. J., Simon, S. B., Laul, J. C., and Christian, R. P., 1984. Pegmatite/wallrock interactions, Black Hills, South Dakota: progressive boron metasomatism adjacent to the Tip Top pegmatite. Geochem. Cosmochim. Acta, 48, 2563-79.
Shervais, J. W., 1982. Ti-V plots and the petrogenesis of modern and ophiolitic lavas. Earth Planet. Sci. Lett., 59, 101 - 118.
Shmakin, B. M.,1979. Composition and structural state of K-feldspars from some U. S. pegmatites. Am. Min., 64, 49 -56.
Sinha, A. K., 1981. Geology and tectonics of the Himalayan region of Ladakh, Himachal, Garhwal - Kumaun and Arunachal Pradesh. In: Zagros - Hindu Kush - Himalaya, Geodynamic evolution (Gupta, H. K. and Delani, F. M., eds.). Am. Geophy. Union, Geodyn. Ser., 3, 122 - 148.
Sirbescu, M. L. C. and Nabelek, P. I., 2003a. Crystallization conditions and evolution of magmatic fluids in the Harney Peak Granite and associated pegmatites, Black Hills, South Dakota: evidence from fluid inclusions. Geochim. Cosmochim. Acta, 67, 2443 - 65.
Sirbescu, M. L. C. and Nabelek, P. I., 2003b. Crystal melts below 400°C, Geol., 31, 685-88.
Smerekanicz, J. R. and Dudas, F. Ö., 1999. Reconnaissance fluid inclusion study of the Morefield pegmatite, Amelia County, Virgenia. Am. Min. 84, 746 - 753.
Smith, A. G., Chamberlain, C. P. and Zeitler, P. K., 1992. Documentation of Neogene regional metamorphism in the Himalayas of Pakistan using U - Pb in monazite. Earth Planet. Sci. Lett., 113, 93 - 105.
Smith, W. L., Frank, M. L., and Sherwood, A. N., 1957. Uranium and thorium in the accessory allanite of igneous rocks. Am. Min., 42, 367-78.
Sobolov, N. V., 1965. Classification of rock - forming garnets. Dokl. Acad. Sci. USSR, Earth Sci. Sect., 157, 79-82.
Solodov, N. A., 1960. Distribution of alkali metals and beryllium in the minerals of zoned pegmatite in the Mongolian Altai. Geokhi., 726-735 (in Russia.).
Solodov, N. A., 1971. Scientific principles of perspective evaluation of rare- element pegmatites. Nauka, Moscow (in Russia).

Srimal, N., Basu, A. R. and Kyhser, R. K., 1987. Tectonic inferences from oxygen isotopes in volcano-plutonic complexes of the India-Asia collision zone. N. W. India. Tectonics, 6, 261 – 274.

Staatz, M. H., Murata, K. J. and Glass, J. J., 1955. Variation of composition and physical properties of tourmaline with its position in pegmatite. Am. Min. 40, 789 - 804.

Stauffer, K. W., 1968. Geology of the Gilgit-Hispar area, Gilgit Agency, West Pakistan. U. S. Geol. Surv. Rept. (IR) PK, 19, 42p.

Stern, L. A, Brown, G. E. Bird, D. K. Jahns, R. H. Foord, E E., Shigley, J. E. and Spaulding L. B., 1986. Mineralogy and geochemical evolution of the Little Three pegmatite-aplite layered intrusive, Ramona, California, Am. Min., 71: 406 - 427.

Stewart, D. B. 1963. Petrogenesis and mineral assemblages of lithium-rich pegmatites. Geol. Soc. Am. Spec. Pap. 76, 159, abstr.

Stewart, D. B. 1978. Petrogenesis of lithium-rich pegmatites. Am. Min. 63, 970 - 980.

Stolynova, M., 1993. Fluid inclusions and rare earths in the fluorite from some Bulgarian mineral deposits. Ann. Univ. Mining and Geol., 39(1), 29-32 (Bulgarian with English abstract).

Stormer, J. C., Pierson, M. L. and Tacker, R. C., 1993. Variation of F and Cl X-ray intensity due to the anisotropic diffusion in apatite during electron microprobe analysis. Am. Min., 78, 641- 648.

Strock, L. W., 1930. Spessartine from Avondale, Delaware County, Pennsylvania. Am. Min., 15, 40 - 42.

Strong, D. F. and Hanmer, S. K., 1981. The leucogranites of the southern Brittany: origin by faulting, frictional heating, fluid flux and fractional melting. Can. Min., 19, 163 - 176.

Sullivan, M. A., Windely, B. F., Saunders, A. D., Haynes, J. R. and Rex, D. C., 1993. A Palaeogeographic reconstruction of the Dir Group: Evidence for magmatic arc migration within Kohistan. N. Pakistan. In: Himalayan Tectonics (Treloar, P. J. and Searle, M. P. eds.). Geol. Soc. London., Spec. Publ. 74, 139 - 160.

Sullivan, M., 1992. The geology of the zone of the Kohistan batholith, northwestern Pakistan. Unpubl. Ph. D. Thesis, Univ. Leicester, UK.

Suwimonprecha, P., Černý, P. and Friederich, G., 1995. Rare metal mineralization related to the granites and pegmatites, Phuket, Thailand, Econ Geol., 90, 603 - 615.

Sweatman, T.R., Clavarino, J.G. and Dawney, R.L., 1995. Drainage geochemical exploration and mineral potential of Northern Pakistan. Third Report. Report by Rex Sweatman and Associates for Australian Agency for International Development. 91p.

Sweetapple, M. T. and Collins, P. L. F., 2002. Genetic framework for the classification and distribution of Archean rare metal pegmatites in the North Pilbara Craton, Western Australia. Econ. Geol. 97, 873 - 895.

Tahirkheli, R. A. K. 1967. Reconnaissance for radioactive minerals in Dardistan, Baltistan, and Haramosh in Gilgit Agency, West Pakistan. Geol. Surv. Pakistan, Inf. Rel. No. 33, 17 p.

Tahirkheli, R. A. K. and Jan, M. Q. (eds.), 1979. Geology of Kohistan, Karakoram Himalaya, northern Pakistan. Geol. Bull. Univ. Peshawar, 11, 187p.

Tahirkheli, R. A. K., 1979. Geology of Kohistan and adjoining Eurasian and Indo - Pakistan continents, Pakistan. Geol. Bull. Univ. Peshawar, 11, 1 - 30.

Tahirkheli, R. A. K., 1982. Geology of the Himalaya, Karakoram and Hindukush in Pakistan, Geol. Bull.Univ. Peshawar, 15, 51p.

Tahirkheli, R.A.K., Mattauer, M., Proust, F. and Tapponnier, P. 1979. The India - Eurasia suture zone in northern Pakistan; some new data interpretation at plate scale. In: Geodynamics of Pakistan, (Farah, A. and De Jong, K. A. eds.), Geol. Surv. Pakistan, Quetta, 125-130.

Taylor, H. P. Jr. 1978. Oxygen and hydrogen isotope studies of plutonic granitic rocks. Earth Planet. Sci. Lett., 38, 177 - 210.

Taylor, B. E. and Friedrichsen, Hans., 1983. Light stable isotope systematics of granitic pegmatites from North America and Norway. Isot. Geosci., 1, 127 -167.

Taylor, B. E., Foord, E. E. and Friedrichssen, H., 1979. Stable isotope and fluid inclusion studies of gem- bearing granitic pegmatite - aplite dikes, San Diego, California, Contr. Min. and Petrol. 68, 187 - 205.

Thakur, V. C. and Sharma, K. K. (eds.), 1983. Geology of the Indus Suture Zone of Ladakh, Wadia Inst. Himal. Geol., Dehra Dun, India, 250p.

Thakur, V. C., 1981. Regional framework and geodynamic evolution of the Indus-Tsangpo suture zone in the Ladakh Himalayas. Trans. Roy. Soc. Edinburgh, Earth Sci., 72, 89 -97.

Thompson, A. B. and Connolly, J. A. D., 1995. Melting of continental crust: some thermal and geological constraints on anatexis in continental collision zones and other tectonic settings. J. Geophy. Res., 100, 15, 565 -79.

Thomson, R. N., Morrison, M. A., Dickin, A. P., Hendry, G. L. and Parry, S. J., 1984. An assessment of the relative roles of crust and mantle in magma genesis: an elemental approach. Phil. Trans. Roy. Soc. London, Series A, 310, 549 -590.

Tomascak, P. B., Krogstad, E. J. and Walker, R. J., 1996. Nature of the crust in the Maine, USA: evidence from the Sebago batholith. Contr. Min. and Petrol. 125, 45 -59.

Tongiorgi, M., Di Milla, A., Le Fort, P. and Gaetani, M., 1994. Palynological dating (Arenig) of the sedimentary sequence overlying the Ishkarwaz granite (upper Yarkhun Valley, Chitral Pakistan). Terra Nova, 6, 595 - 607.

Treloar, P. J. and Izatt, C. N., 1993. Tectonics of the Himalayan collision zone between the Indian plate and the Afghan Block: a synthesis. In: Himalayan Tectonics (Treloar, P. J. and Searle, M. P. eds.). Geol. Soc. London., Spec. Publ. 74, 69 - 87.

Treloar, P. J., Petterson, M. G., Jan, M. Q. and Sullivan, M. A., 1996. A re - evaluation of the stratigraphy and evolution of the Kohistan arc sequence, Pakistan Himalaya; Implications for magmatic and tectonic arc - building processes, J. Geol. Soc. London, 153, 681 - 693.

Treloar, P. J., Rex, D. C., Guise, P. G., Coward, M. P., Windley, B. F., Petterson, M. G., Jan, M. Q. and Luff, I. W., 1989. K - Ar and Ar - Ar geochronology of the Himalayan collision in NW Pakistan: constraints on the timing of suturing, deformation, metamorphism and uplift. Tectonics. 8(4), 881 - 909.

Trueman, D. L. and Ćerný, P., 1982. Exploration for Rare-element granitic pegmatites. In: Granitic Pegmatites in Science and Industry (P. Ćerný, ed.). Min. Assoc. Can., Short Course Handbook 8, 463 - 491.

Vainstein, E. E., Tugarinov, A. I. and Turanskaya, N. V., 1956. On the regularity of distribution of rare earths in certain minerals. Geochemisrty. Publ. Acad. Sci., USSR, no. 2, 36-56.

Valdiya, K. S., 1989. Trans - Himadri intracrustal fault and basement upwarps south of Indus-Tsangpo suture zone. In: Tectonics of the Western Himalaya (Maliconico, L.L. and Lillie. R. J. eds.). Geol. Soc. Am., Spec. Paper, 232153 - 168.

Vidal, P. L., Cocherie, A. and Le Fort, P. 1982. Geochemical investigations of the origin of the Manaslu leucogranite (Himalaya, Nepal). Geochem. Cosmochim. Acta, 46, 2279 - 2292.

Vincent, E. A. and Phillips, R., 1954. Iron-titanium oxide minerals in layered gabbros of the Skaergaard intrusion, East Greenland. Geochem. Cosmochim. Acta, 6, p1.

Vorma, A. and Passivirta, T., 1979. Contribution to the mineralogy of rapakivi granites: 1. Zircon of the Latila Rapakivi, southwestern Finland. Bull. Geol. Surv. Finland, 303, 40 pp.

Wadia, D. N., 1937. The Cretaceous volcanic series of Astor, Deosai, Kashmir and its intrusions. Geol. Surv. India. Rec., 72, 151 -161.

Walker, R. J., Hanson, G. N., Papike, J. J., 1989. Trace element constraints on pegmatite genesis: Tin Mountain pegmatite, Black Hills, South Dakota. Contrib. Min. Petrol. 101, 290 -300.

Walker, R. J., Hanson, G. N., Papike, J. J., O' Neil, J. R. and Laul, J. C., 1986. Internal evolution of the Tin Mountain pegmatite, Black Hills, South Dakota. Amer. Min., 71, 440 - 459.

Watt, G. R. and Harley, S. L., 1993. Accessory phase controls on the geochemistry of the crustal melts and restites produced during water-undersaturated partial melting, Contr. Min. and Petro. 11, 550 - 66.

Watters, W. A., 1963. Zoned blue beryl from the Canaan area, Pikikiruna Range, Nelson, New Zealand. J. Geol. Geophys., 6, 715-717.

Webber, K. L., Simmons, W. B., Falster, A.U. and Foord, A. E., 1999. Cooling rates and crystallization dynamics of shallow level pegmatite - aplite dikes, San Diego County, California. Am. Min. 84, 708 - 717.

Wike, M., Nabelek, P. I. and Glascock, M. D., 2002. B and Li in metapelites from the Proterozoic Terrane in the Black Hills, South Dakota, USA: implications for the origin of leucogranitic magmas. Am. Min., 87, 491 -500.

Willemse, J. and Bensch, J. J. 1964. Inclusions of original carbonate rocks in gabbro and norite of the eastern part of the Bushveld complex. Trans. Geol. Soc. S. Africa, 67, 1- 87.

Winchester, J. A. and Flyod, P. A., 1977. Geochemical discrimination of the different magma series and their differentiation products using immobile elements. Chem. Geol., 20, 325 - 343.

Wood, D. A., Joront, J. L. and Frecil, M., 1979. A re-appraisal of the use of trace elements to classify and discriminate magma series emplaced in different tectonic settings. Earth Planet. Sci. Lett., 45, 326 - 336.

Wood, D. L. and Nassau, K., 1968. The characterization of beryl and emerald by visible and infrared absorption spectroscopy. Am. Min., 53, 777 - 800.

Wright, W. I., 1938. The composition and occurrence of garnets. Am. Min., 23, 436 - 449.

Tyllie, P. J. and Tuttle, O. F., 1964. Experimental investigation of silicate systems containing two volatiles components. 111. The effects of $SO_3$, $P_2O_5$, HCL, and $Li_2O$, in addition to $H_2O$, on the melting temperatures of albite and granite. Am. J. Sci. 262, 930-939.

Yamamoto, H. and Nakamura, E., 1996. Sm - Nd dating of garnet granulites from the Kohistan complex, northern Pakistan. J. Geol. Soc. London, 153, 965 - 969.

Yamamoto, H., 1993. Contrasting metamorphic P - T - time paths of the Kohistan granulites and tectonics of the Western Himalayas. J. Geol. Soc., London, 150, 843 - 856.

Zafar, M., Murata, M., Khan, T., Ozawa, H. and Nishimura, H., 2000. K-Ar biotite ages from Miocene post-collisional Garam Chasma leucogranite, eastern Hindukush Range (Trans-Himalayas), northwestern Pakistan. J. Min. Petrol. Sci., 95, 101-106.

Zakharchenko, A. I., 1976. Transition of melts into fluid solutions, the evolution of their composition, nature and metal content. 5th Internt. Sym. On Fluid Ind. Res. Sydney, Aust., Abstracts.

Zanchi, A., 1993. Structural evolution of the North Karakoram cover, North Pakistan. In: Himalayan Tectonics (Treloar, P. J. and Searle, M. P. eds.). Geol. Soc. London., Spec. Publ. 74, 21 - 38.

Zanettin, B., 1964. Geology and petrology of the Haramosh - Mango Gusar area, Italian expediations to the Karakoram 9K2) and Hindu Kush (leader A. Desio). Brill. Leiden, 301p.

Zeitler, P. K. and Chamberlain, C. P., 1991. Petrologic and tectonic significance of young leucogranites from the northwestern Himalaya, Pakistan. Tectonics, 10, 729 - 741.

Zhu, Y. and Shi, Y., 1990. Shear heating and partial melting of granite: thermal structure of overthrusted terrains in the Greater Himalaya, Pakistan. Chinese J. Geophy., 33, 341 -351.